# New phosphorus ligands for carbonylation catalysis


Alexandra M. Miles-Hobbs

A thesis submitted to the University of Bristol in accordance with the requirements for award of the degree of Doctor of Philosophy in the Faculty of Science

August 2019

## Abstract

A range of fluorophosphite, diphosphite and pyridylphosphine ligands have been prepared and their application in alkene hydroformylation or alkyne methoxycarbonylation catalysis explored. In addition, 9-phospha[3.3.1]bicyclononane (Phobane, PhobPH) derived ligands have been applied in Rh-catalysed asymmetric hydrogenation. The coordination chemistry of all the ligands has been investigated to probe their catalytic performance.

A series of cyclic fluorophosphites **L2.1-2.4**, containing 5- to 8-membered phosphacycles, derived from 1,2-catechol, 1,8-naphthalenediol, 2,2'-biphenol or bis(2-hydroxyphenyl)methane, have been synthesised and the effect of ring size on coordination has been probed. The 5- and 6-membered fluorophosphites **L2.6-2.8**, containing alkyl substituents on the catechol or naphthalene rings, have also been synthesised. The IR spectra of the *cis*-[$Mo(CO)_4L_2$] complexes (L = **L2.1-2.8**) show the π-acceptor properties of the fluorophosphites increase with decreasing ring size, and in terms of σ/π-bonding sit between $PF_3$ and P{$(OAr)_3$}. The effect of aryl substitution on the electronic properties of the ligand appear to be minimal. The IR data for *cis*-[$Mo(CO)_4$(**L2.5**)$_2$] (**L2.5** is the methoxy phosphite derived from 1,8-naphthalenediol) reflect the significant difference in electronics between ligands containing a P-F and P-OMe fragment. Reaction of the ligands **L2.2-2.8** with [$PtCl_2$(cod)] give the *cis*-[$PtCl_2L_2$] complexes. The reaction of [Pt(nbe)$_3$] with 4 equiv. of **L2.1-2.5** yields the [$PtL_4$] complexes. Whereas, using 2 equiv. of the ligand, equilibrium mixtures of [$PtL_x$(nbe)$_y$] species form. There is a trend in the CO substitution reactions of [$Rh_2Cl_2(CO)_4$] with **L2.1-2.8**: as the ring size and aryl substitution of the fluorophosphite increase, the properties move away from that of $PF_3$ towards phosphite **L2.5**.

Ligands **L2.1-2.8** have been tested in the Rh-catalysed hydroformylation of 1-hexene. The 5-membered fluorophosphites display no hydroformylation activity due to their high susceptibility to hydrolysis. Whereas, the other ligands display good catalyst performance; the 6-membered fluorophosphites, **L2.2** and **L2.8**, give the most active and *n*-selective catalysts. Upon increasing the concentration of the 6- and 7-membered fluorophosphites, the *n*-selectivity significantly increases, albeit with a diminution in activity. The selectivity and activity are also sensitive to the catalytic conditions used; the *n*-selectivity is higher under "concentrated-catalyst" conditions.

A novel route to cyclic chlorophosphites and aryl dichlorophosphites has been developed which involves a silicon-phosphorus exchange reaction. The novel 6-membered diphosphite **L4.2** derived from 1,8-naphthalenediol has been prepared. The ν(CO) value for *cis*-[$Mo(CO)_4$(**L4.2**)] shows **L4.2** is a significantly stronger π-acceptor than its monophosphite analogue, **L2.5**. Reaction of **L4.2** with [$PtMe_2$(cod)] gives the *cis*-[$PtMe_2$(**L4.2**)] complex. Diphosphites **L4.1-4.3**, containing 5- to 7-membered phosphacycles, have been tested in the Rh-catalysed hydroformylation of 1-hexene. The 6-membered **L4.2** shows promising catalyst performance, but high concentrations of ligand inhibit catalysis.

6-Chloro-2-(diphenylphosphino)pyridine, **L5.2**, has been synthesised and tested in the Pd-catalysed methoxycarbonylation of phenylacetylene, and produces a more active catalyst than $Ph_2P$(2-Py) (**L5.1**). The Pt(II) and Pd(II) coordination of **L5.2** show the ligand can adopt both $\kappa^1$-P and $\kappa^2$-P,N coordination modes, a feature that is key to the catalytic mechanism proposed. The dialkyl 2-pyridyl phosphines, $R_2P$(2-Py) (**L5.3-5.5**), have been prepared and tested in the Pd-catalysed methoxycarbonylation of phenylacetylene. When R = *t*Bu, the ligand **L5.3a** gives a highly active and branched-selective catalyst, comparable to that with **L5.1**. This reaction has been scaled up

successfully in collaboration with Lucite and in addition displays similar branched-selectivity to $\mathbf{L_{5.1}}$ in the catalytic methoxycarbonylation of propyne. In contrast, the $Cy_2P$ and *s*-PhobP (9-phospha[3.3.1]bicyclononane) derived ligands $\mathbf{L_{5.4\text{-}5.5}}$ display poor catalytic performance in the methoxycarbonylation of phenylacetylene. The $tBu_2P$ derived ligand $\mathbf{L_{5.3a}}$ displays the strongest preference for P,N-chelation to Pt, Pd and Rh. In addition, $\mathbf{L_{5.3a}}$ readily protonates at the pyridyl-N. Both of these properties are likely critical to the excellent catalyst performance of $\mathbf{L_{5.3a}}$.

The *cis*-[Rh(cod*)$L_2$][OTf] complexes, where L = PhobPR (R = *n*Bu or *t*Bu) $\mathbf{L_{5.1\text{-}5.5}}$, have been prepared. The chiral diene (bicyclo[3.3.1]nona-2,6-diene, cod*) is used in a successful resolution of the chiral *anti*-conformations (δ and λ) of the complexes (up to 96%). The enantiopure *cis*-[Rh((*S*,*S*)-cod*)($\mathbf{L_{6.1}}$)$_2$][OTf] complex has been tested in the Rh-catalysed asymmetric hydrogenation of MAA (methyl-2-acetamidoacrylate). No enantioselectivity is observed at -20 °C due to the lack of optical stability. Unfortunately, at lower temperatures (-40 °C), no conversion is detected. NMR studies of the catalysis show the hydrogenation of the catalyst precursor *cis*-[Rh(cod*)($\mathbf{L_{6.1}}$)$_2$]$^+$ is extremely slow. The crystal structure of *cis*-[Rh(cod*)($\mathbf{L_{6.1}}$)$_2$]$^+$ suggests this is due to the preorganised rigid structure of cod*, which results in stronger Rh-cod* binding.

## Declaration

I declare that the work in this thesis was carried out in accordance with the requirements of the University's Regulations and Code of Practice for Research Degree Programmes and that it has not been submitted for any other academic award. Except where indicated by specific reference in the text, the work is the candidate's own work. Work done in collaboration with, or with the assistance of others is indicated as such. Any views expressed in the dissertation are those of the author.

**Alexandra M. Miles-Hobbs**
University of Bristol
August 2019

**Acknowledgments**

Most importantly, I would like to thank Paul for being an amazing supervisor throughout my PhD, your continual guidance and support have been invaluable. It has been an honour to work for you and I will miss you, especially your infinite stories, vocabulary lessons and karaoke duets!

Of course a huge thank you to all of the members of the Pringle group, old and new, who have continued to make the lab such a joy to work in! Thank you to all the old Pringles who have put up with my endless questions and made me feel super welcome at the start: Drs. Clifton, Hazeland, Faradji, Bailey, Gorman, Papadouli and Mistry. And especially to Dr. Shuttleworth who taught me the ropes of the lab as an undergraduate at the very start! Also thanks to honorary Pringle, Georgia.

Thank you to the fabulous current Pringles: Hubert, Dan, Callum, Sarah, Rach, Rachel and Ashley (honorary Pringle) for making the lab the best place to work! And of course thank you to my library and lab neighbour Ailis – I couldn't have done it without you! I will really miss seeing you all every day. I've made endless memories as a Pringle… from conferences, Friday pub nights, Pringle ski trip (thank you Charly!), summer fun days and of course the Christmas parties (especially the lunging and karaoke)! Also thanks to non-Pringle members, particularly the 5$^{th}$ floor – the Bower girls and Wass group. Of course, thank you to all of you in Bristol outside of the department for the many needed distractions throughout – Emma (our mid-week dinners), the school gang (especially Chezz for our drink dates) and the best flatmate, Becky!

Thank you also to everyone who has contributed to this research. Particularly, Dr. Hazel Sparkes and Natalie Pridmore for their X-ray crystallography skills which have been invaluable. Thank you also to all the staff in NMR, particularly Paul Lawrence whose patience was crucial to the $^{195}$Pt NMR! Also thanks to all the staff in the mass spectrometry service. And thanks to Tony for his practical help in the department. Thank you to Paul Kamer and Christoph at LIKAT for hosting me in Rostock for an amazing two weeks and your helpful insights throughout the project. And thank you to Morag, Mark and Graham at Lucite for the testing my ligands and useful discussions.

Finally, a massive thank you to all my family and friends outside of Bristol for their continual support! Especially to my mum, Bo, for always being there, I couldn't have done it without you. And last but not least, Andrew, who has supported me all of the way!

Thank you!

## Collaborator acknowledgments and publications

Chapter 2 (excluding Sections 2.4 and 2.7) is reproduced from *'Ring-size effects in cyclic fluorophosphites: ligands that span the space between phosphites and $PF_3$'*, A. M Miles-Hobbs, E. Hunt, P. G. Pringle, H. A. Sparkes, *Dalton Trans.*, 2019, **48**, 9712-9724.

In Chapter 3, the testing of ligands $\mathbf{L}_{2.2}$ and $\mathbf{L}_{2.3}$ under "dilute-catalyst" conditions (Section 3.3) was carried out by the author and Dr. Christoph Kubis, in collaboration with Prof. Paul C. J. Kamer at the Leibniz Institute for Catalysis (Rostock, Germany).

In Chapter 4, the computational studies, initial discovery of the Si-P exchange reaction and testing of ligands $\mathbf{L}_{4.1\text{-}4.3}$ in catalysis was carried out by Tom A. Young, an MSci student who worked under the supervision of the author.

In Chapter 5, the testing of ligand $\mathbf{L}_{5.2}$ is reproduced from '*Palladium-catalysed alkyne alkoxycarbonylation with P,N-chelating ligands revisited: a density functional theory study*', S. Ahmad, A. Lockett, T. A. Shuttleworth, A. M. Miles-Hobbs, P. G. Pringle, M. Bühl, *Phys. Chem. Chem.*, 2019, **21**, 8543-8552. The synthesis of ligands $\mathbf{L}_{5.4\text{-}5.5}$, Pt(II) coordination of $\mathbf{L}_{5.4}$, Pd(II) and Rh(I) coordination of $\mathbf{L}_{5.3a}$ and $\mathbf{L}_{5.4\text{-}5.5}$ were carried out by Henry Smart, an MSci student who worked under the supervision of the author. The methoxycarbonylation of 3,3-dimethylbutyne was carried out by Lauren G. O'Neil, a PhD student who worked under the supervision of the author. The testing of ligands $\mathbf{L}_{5.1}$ and $\mathbf{L}_{5.3a}$ on a larger scale and in the methoxycarbonylation of propyne was carried out by Dr. Mark Waugh and Morag Nixon at Lucite.

All the work described in Chapter 6 was performed by the author and is yet unpublished.

Chapters 7 and 8 comprise of the experimental and supporting information for Chapters 2 – 6.

## Abbreviations

| General | |
|---|---|
| AcO | acetyl |
| Ar | aryl/ aromatic group |
| acac | acetylacetonate |
| cod | 1,5-cyclooctadiene |
| cod* | bicyclo[3.3.1]nona-2,6-diene |
| Cp | cyclopentadienyl |
| Cy | cyclohexyl |
| dppe | 1,2-bis(diphenylphosphino)ethane |
| dppm | 1,1-bis(diphenylphosphino)methane |
| DFT | density functional theory |
| eq | equivalents |
| Et | ethyl |
| h | hour(s) |
| HOMO | highest occupied molecular orbital |
| *i*Bu | iso-butyl |
| L | ligand |
| M | metal |
| MAA | methyl-2-acetamidoacrylate |
| me | methyl |
| min | minute(s) |
| MMA | methyl methacrylate |
| MsO | methane sulfonic |
| *n* | normal |
| nbe | norbornene |
| nbd | 2,5-norbornadiene |
| *n*Bu | normal-butyl |
| *p* | para |
| Ph | phenyl |
| Phob | 9-phospha[3.3.1]bicyclononane |
| Pr | propyl |
| py | pyridyl |
| R | aryl or alkyl substituent |
| *rac* | racemic |
| *t*Bu | tertiary-butyl |
| TfO | trifluoromethanesulfonic acid |
| THF | tetrahydrofuran |
| TOF | turnover frequency |
| TON | turnover number |

| Spectrochemical | |
|---|---|
| br. | broad |
| d | doublet |
| dd | doublet of doublets |
| dt | doublet of triplets |
| EI | electron ionisation |
| ESI | electronspray ionisation |
| GC | gas chromatography |
| HR-MS | high resolution mass spectrometry |
| IR | infra-red |
| *J* | coupling constant |
| m | multiplet |
| $M^+$ | molecular ion |
| MALDI | matrix-assisted laser desorption/ ionisation |
| m/z | mass/ charge ratio |
| NMR | nuclear magnetic resonance |
| ppm | parts per million |
| q | quintet |
| qq | quintet of quintets |
| vir. t | virtual triplet |
| tt | triplet of triplets |
| UV | ultraviolet |
| $\{^1H\}$ | proton decoupled |
| $\delta$ | chemical shift |
| $w_{1/2}$ | peak width at 50% intensity |

## Contents

## Table of Contents

# Chapter 1

# Introduction

The following chapter includes a brief introduction to the properties of phosphorus ligands and an overview of the coordination chemistry and catalytic applications of fluorophos ligands, including $PF_3$, fluorophosphines and fluorophosphites as ligands. This will put into context the research work described in succeeding Chapters 2 and 3. Chapters 4 – 6 are self-contained, since the areas of research discussed have been more recently reviewed.

## 1.1 Properties of phosphorus(III) ligands

Phosphorus ligands have found extensive application in late-transition metal homogeneous catalysis.[1,2] One of the crucial features of phosphorus ligands is their high level of tunability; changing the substituents at the phosphorus centre alter the σ-donor and π-acceptor properties as well as the steric properties of the ligand.[1] Factors that affect metal-phosphorus bonding and the reactivity of P-ligand complexes have been quantified, which facilitates the design and optimisation of new and existing catalysts.[1]

### 1.1.1 Electronic ligand parameters

Phosphorus-metal bonding is synergic with both σ-donor and π-acceptor components. The lone pair of the P-ligand can σ-donate into a vacant *d*-orbital on the metal with the correct symmetry (Figure 1.1a).[1,2] While an empty orbital on the P-ligand with π-symmetry can accept electron density from a filled *d*-orbital on the metal atom (Figure 1.1b).[1,3] There has been much debate about which empty P-ligand orbitals are involved in the π-bonding, but the prevailing view is that it involves the antibonding σ*-orbitals.[1,2] Experimental evidence presented by Orpen and Connelly suggested that this π-accepting orbital is a hybrid of the P-σ* and P-3*d* orbitals (Figure 1.2).[3,4]

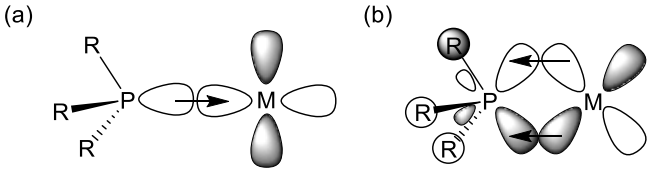


**Figure 1.1** Two components of metal phosphorus bonding: (a) σ-donation and (b) π-back donation.

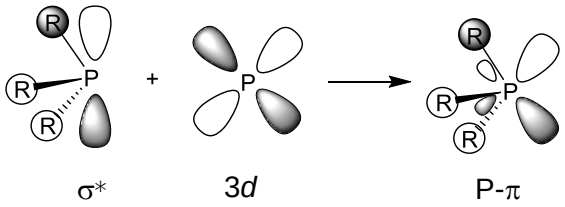


**Figure 1.2** Hybridisation of P-σ* orbitals, involved in the π-component of M-P bonding.

The σ-donor and π-accepting properties of a P(III)-ligand can be controlled by the electronics of the substituents bonded to the phosphorus: the σ-donor ability of the ligand increases when using electron-donating R-substituents (*e.g.* alkylphosphines). Whereas, electron-withdrawing R-substituents increase the π-accepting capacity of the ligand (*e.g.* fluorophosphines). The electronic properties of a ligand can be assessed by measuring the stretching frequency of coordinated carbonyl ligands (ν(CO), $A_1$) in transition metal complexes.[5,6] Tolman defined the electronic parameter, χ, which is based on the ν(CO) of nickel complexes of the type $[Ni(CO)_3L]$, with L = $t$Bu$_3$P as a reference.[5,7] The electronic parameter (χ) for other phosphorus ligands is defined as the difference between the ν(CO) ($A_1$) of $[Ni(CO)_3L]$ and $[Ni(CO)_3(t$Bu$_3$P)] (in cm$^{-1}$).[1,5] Alternatively, the ν(CO) ($A_1$) of *cis*-$[Mo(CO)_4L_2]$ complexes can be used since it is linearly related to Tolman's electronic parameter.[8] The ν(CO) stretch of *trans*-$[RhCl(CO)L_2]$ complexes has also been previously used.[6,9]

### 1.1.2 Steric ligand parameters

The steric properties of a phosphorus ligand can also greatly affect their donor properties. Tolman's cone angle (θ) is the most commonly used concept of measuring the steric bulk of monophosphine ligands (Figure 1.3a); it is defined as the angle at the metal centre formed by the cone which encompasses all the atoms in the ligand, where the phosphorus centre is located 2.28 Å away from the metal (a typical Ni-P bond distance).[1,7]

White *et al.* developed another approach to measure the steric bulk around the metal: the solid angles concept (Figure 1.3b).[1,10] The van der Waals radii of the ligand atoms are projected onto the van der Waals surface of the metal, constructed from either the crystal or calculated structures; the area of coverage on the metal centre is given by the solid angle.[1,10]

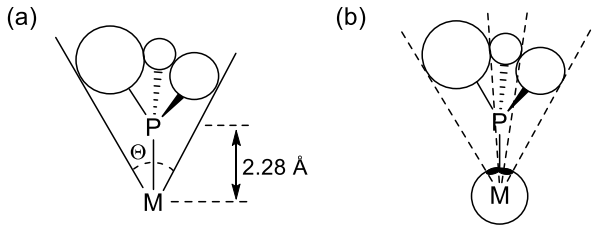


**Figure 1.3** Steric parameters of a phosphorus ligand: (a) Tolman's definition of a cone angle and (b) White's definition of the solid angle.

## 1.2 Coordination chemistry of $PF_3$

The first $PF_3$ transition metal complex dates back to 1890 and the synthesis of *cis*-$[PtF_2(PF_3)_2]$ by Moissan.[11] However, it was not until the 1950s, following the synthesis of *cis*-$[PtCl_2(PF_3)_2]$ and $[Pt_2Cl_4(PF_3)_2]$, that metal-$PF_3$ chemistry advanced mainly due to the extensive work of Kruck and Nixon.[12–15] The coordination chemistry of $PF_3$ has been reviewed up to the early 1990s.[11–13,16,17]

In the last 3 decades, the field of homoleptic metal complexes of $PF_3$ has received scant attention. This may be attributed to $PF_3$ being a poisonous and expensive gas which is difficult to obtain in large amounts and high purity.[18,19]

Herein, the transition metal chemistry of $PF_3$ since the 1990s will be summarised.

### 1.2.1 Metal-$PF_3$ bonding

Trifluorophosphine has an iconic status in coordination chemistry as a ligand that has π-acceptor properties that rival or exceed those of CO,[12] as demonstrated by their respective Tolman electronic parameters: 2111 $cm^{-1}$ for $PF_3$ and 2128 $cm^{-1}$ for CO.[20,21] Further evidence for this is that the complexes $[M(CO)_4]$ (M = Pd, Pt) only have fleeting existence in Ar matrices at <10 K, whereas the $PF_3$ analogues $[M(PF_3)_4]$ are relatively stable.[22–25] In addition, the $[Ni(PF_3)_4]$ complex is known to be more stable than the analogous $[Ni(CO)_4]$.[26] The strong back-bonding of $PF_3$ is related to the presence of three highly electronegative fluorine atoms.

### 1.2.2 More recent developments in the coordination chemistry of $PF_3$

Many of the current applications of $PF_3$ are found in materials science in photovoltaic devices and chemical vapour deposition (CVD) applications, specifically the use of $[Ni(PF_3)_4]$ and $[Pt(PF_3)_4]$ complexes.[27–30]

Although it has been frequently used in CVD, the chemistry of $[Pt(PF_3)_4]$ remained little developed.[19] However, Seppelt *et al.* have carried out a systematic study of the chemistry of $[Pt(PF_3)_4]$, where a large number of other Pt-$PF_3$ complexes were prepared and characterised by X-ray crystallography.[19] They further investigated the thermal decomposition of $[Pt(PF_3)_4]$ to $[Pt_4(PF_3)_8]$, which was first reported in 1997.[31]

The extensive research into the Pt coordination chemistry of $PF_3$ has been reviewed by Nixon and Heuer.[11,16] In 2013, Seppelt *et al.* synthesised the volatile complex *cis*-$[PtMe_2(PF_3)_2]$ (Scheme 1.1) alongside the analogous CO and dfmpe (dfmpe = $(CF_3)_2PC_2H_4P(CF_3)_2$) complexes.[32] Demethylation reactions using anhydrous HF were carried out in an attempt to obtain the partially stabilised "half-naked" $L_2Pt^{2+}$ complexes. However, this was not achieved with the $PF_3$ and CO analogues.[32] Reactions with $[PtMe_2(dfmpe)]$ were more successful due to its higher stability; the crystal structure of $[Pt(dfmpe)][Sb_2F_{11}]$ was obtained.[32] Nevertheless, HF was always bound to Pt in the presence of HF and xenon.[32] Recently, *trans*-$[PtF(PF_3)(Cy_3P)_2][PF_6]$ was synthesised by P-F bond activation of $PF_5$ using the Pt(0) complex, $[(Cy_3P)_2Pt]$ (where Cy = cyclohexyl); this was the first example of oxidative addition of a P-F bond to a transition metal.[33]

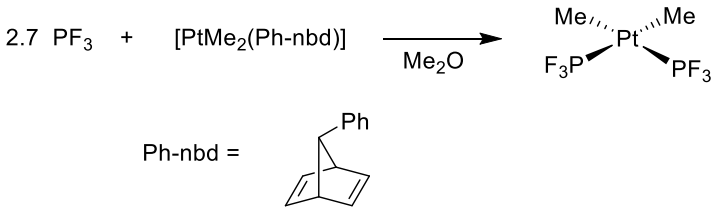


**Scheme 1.1** Synthesis of *cis*-$[PtMe_2(PF_3)_2]$.[32]

Since the 1990s there have been many reports of metal complexes containing both $PF_3$ and CO. In 1993, Huang *et al.* described the synthesis of the *cis*-$[W(CO)_4(Ph_3P)L]$ complexes, where L = $PF_3$ or other fluorophosphines, and studied their reactivity with $Me_3NO$ in MeCN.[34] For each complex, the fluorophosphine was eliminated instead of the CO ligand and the resulting complexes, *cis*-$[W(CO)_4(Ph_3P)(MeCN)]$, were identified.[34] This reactivity suggests that the CO ligands are less susceptible to nucleophilic attack by the amine oxide than the fluorophosphines.[34] They also reported the synthesis of the

novel complex $[W(PF_3)_4(dppe)]$ from the photolysis of $[W(CO)_4(dppe)]$ in the presence of a large excess of $PF_3$.[34] More recently, similar $[M(CO)_5(PX_3)]$ complexes (where M = Cr, Mo, W; X = H, Me, F, Cl) have been studied in order to assess the nature of the metal-ligand bonding.[35] It was shown that π-bonding contributes to approximately 50% of the total orbital interaction of the M-P bond in the $PF_3$ and $PCl_3$ analogues.[35] Complete analysis of the complicated NMR spectra of such complexes has also been carried out, for example for $[Mo(CO)_3(PF_3)_3]$.[36] The substitution of binuclear complexes, $[M_2(CO)_{10}]$ (M = Mn, Tc, Re), with $PF_3$ has also been investigated.[37,38] Incomplete substitution of the CO ligands with $PF_3$ was observed in all cases. When M = Mn, only four CO ligands were displaced by $PF_3$.[37] Whereas, for the Tc complex up to eight of the CO ligands were displaced, and up to ten for the Re analogue.[38]

Metal complexes containing bridging $PF_3$ groups are very rare relative to those containing terminal $PF_3$ groups and bridging CO groups, despite reports of complexes containing a $\mu_3$-$PF_3$ bridging ligand in the 1990s (*e.g.* **1.1**).[39,40] King *et al.* have recently presented several density functional theory studies on the reasons for the lack of binuclear transition metal complexes containing bridging $PF_3$ groups.[18,41–44] They have suggested that this is due to the energetically unfavourable hypervalent coordination of a bridging $PF_3$.[44] To facilitate this penta-coordinate P-centre, a high energy *d*-orbital or a three-centre four-electron system must be involved in the bonding.[44] In contrast, bridging CO ligands involve only a tri-coordinate carbon centre.[44]

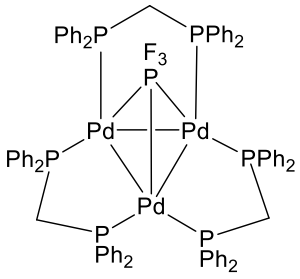


**1.1**

While there are abundant examples of transition metal complexes of $PF_3$, compounds containing homoleptic metal-$PF_3$ cations are rare.[45] In 1992, $[Au(PF_3)Cl]$ was first reported[46] and has recently been characterised by X-ray crystallography.[47] The $[Au(PF_3)Cl]$ complex was shown to be more stable than its CO analogue.[46] In addition, Kruck *et al.* reported the preparation of $[Au(PF_3)(CF_3)]$, but due to its thermal instability the complex was only characterised by mass spectrometry.[48] The complex, $[Au(PF_3)_2][Sb_2F_{11}]$, was the first example of a linear thermally stable metal $(PF_3)_2$ complex; it was prepared by CO

displacement of $[Au(CO)_2][Sb_2F_{11}]$ by $PF_3$.[45] The cation, $[Au(PF_3)_2]^+$, was also obtained in either $HSO_3F$ or $SO_2$ solution, from the reduction of $[Au(SO_3F)_3]$ with $PF_3$.[45]

In 2004, Jagirdar *et al.* reported the novel dicationic dihydrogen complexes, *trans*-$[M(\eta^2\text{-}H_2)(PF_3)(\text{diphosphane})_2]^{2+}$ (where M = Fe or Ru, diphosphane = dppe or dppm).[49] Only one other example of a dihydrogen complex with $PF_3$ is known.[50] The complex, *trans*-$[Ru(\eta^2\text{-}H_2)(PF_3)(dppe)_2]^{2+}$, displayed remarkable stability with respect to the loss of the bound $H_2$.[49]

In 1995, Howard *et al.* described the synthesis of the Al(0) species $[Al(PF_3)_2]$ and compared its magnetic properties to those of $[Al(CO)_2]$.[51] The magnetic parameters of $[Al(PF_3)_2]$ were similar to that of $[Al(CO)_2]$, suggesting that both complexes have similar structures with $C_{2V}$ symmetry and the same electronic ground state ($^2B_1$).[51]

## 1.3 Coordination chemistry of fluorophosphines

To the best of our knowledge, there are no reviews on the coordination chemistry of phosphorus-fluorine ligands. Therefore, a review of transition metal complexes of monofluorophosphine ($R_2PF$), difluorophosphine ($RPF_2$), fluorophosphite $\{(RO)_2PF\}$ and difluorophosphinite ($ROPF_2$) ligands will be presented herein. There are a few examples of metal complexes of bidentate difluorophosphines[32,52–54] and difluorophosphinites,[55–59] but these will not be discussed. Complexes of amino-fluorophosphine complexes are also known, but will not be discussed.[60]

### 1.3.1 Disproportionation of fluorophosphines

Unlike trifluorophosphine, the stereoelectronics of fluorophosphines, $R_xPF_y$ (x + y = 3), can be modified *via* substituent effects. Fluorophosphines can be readily prepared from their corresponding chlorophosphine, $R_xPCl_y$. In 1958, Brendel *et al.* reported the first synthesis of a fluorophosphine.[61] In general, fluorophosphines are strong π-acceptors due to the high electronegativity of the fluorine atoms (depending on the R substituent), but have rarely been explored as ligands for transition metals.[21] There are few reported applications of fluorophosphines in catalysis, perhaps due to their instability with respect to redox disproportionation in spite of their strong P-F bond (545 kJ mol$^{-1}$, *cf.* C-H = 418 kJ mol$^{-1}$) (Scheme 1.2).[62–64] This disproportionation reaction is well established and has been extensively studied by Schmutzler and others.[65–67] The following observations were made: (1) fluorophosphines such as $Ph_2PF$, $Me_2PF$ and $n$$Bu_2PF$ are highly susceptible to disproportionation; (2) fluorophosphines containing bulky substituents, such as $t$$Bu_2PF$,

or electron-withdrawing substituents, such as $(C_6F_5)_2PF$ or $(CF_3)_2PF$, are thermally stabilised to disproportionation.[61,68–70]

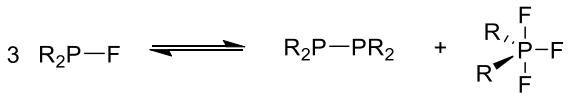

**Scheme 1.2** Disproportionation of fluorophosphines, $R_2PF$.

### 1.3.2 Ni coordination chemistry

Analogous to $PF_3$, some fluorophosphine ligands efficiently stabilise zerovalent metal complexes. In the late 1960s, Nixon *et al.* reported the synthesis of zerovalent $NiL_4$ complexes of several mono- and difluorophosphines, such as $(CF_3)_2PF$, $(CF_3)PF_2$ and $(CCl_3)PF_2$.[71,72] The complexes were synthesised by the reaction of Ni (formed from the decarboxylation of nickel oxalate) with the phosphine at 60 – 80 °C.[71] $[Ni\{(CF_3)PF_2\}_4]$ had been previously synthesised by Street *et al.* from $[Ni(CO)_4]$;[73] $NiL_4$ complexes were typically prepared *via* this route but would often produce mixed carbonyl phosphine complexes.[74] In 1961, Schmutzler reported the synthesis of the difluorophosphine complexes $[NiL_4]$, where L = $PhPF_2$ and $MePF_2$; these complexes have also been reported by other research groups.[75–79]

Nixon *et al.* have reported detailed analyses of the $^1H$, $^{19}F$ and $^{31}P$ NMR spectra of $[NiL_4]$ complexes, where L is a range of mono- and difluorophosphines such as $(CF_3)_2PF$, $(CF_3)PF_2$ and $(CCl_3)PF_2$; the corresponding coupling constants were calculated from the spectra.[72,74,80,81]

Schmutzler *et al.* have studied the $^{31}P$ and $^{19}F$ NMR spectra of $NiL_4$ complexes of numerous mono- and difluorophosphines and fluorophosphites (see Section 1.4.1); they observed that almost invariably, the $^1J_{P,F}$ value of the ligands decreased upon coordination.[82] Cassoux *et al.* also studied the $[NiL_4]$ complexes, where L = $Ph_2PF$ and $PhPF_2$.[83]

In 1971, Schmutzler reported the synthesis of the first stable dialkylfluorophosphine, $t$Bu$_2$PF.[84] To assess the electronic properties of $t$Bu$_2$PF and $t$BuPF$_2$ the corresponding $[Ni(CO)_3L]$ complexes were prepared and analysed by IR and NMR spectroscopy.[82,84] The stretching frequencies, $\nu$(CO) ($A_1$), were compared to the corresponding $PF_3$ and $t$Bu$_3$P complexes, and it was shown that the $\pi$-acceptor character increases in the order $PF_3$ > $t$BuPF$_2$ > $t$Bu$_2$PF > $t$Bu$_3$P.[84] This trend is also reflected in the change of NMR parameters.[84]

The 2-thienyldifluorophosphine ligand, **1.2**, was synthesised by Schmutzler *et al.* from the corresponding dichlorophosphine; the ligand was not entirely stable to redox disproportionation.[85] Nevertheless, the zerovalent [Ni(**1.2**)$_4$] complex was prepared from the reaction of [Ni(CO)$_4$] with **1.2**, this was also then oxidised to give the Ni(II) complex, [NiI$_2$(**1.2**)$_2$].[85]

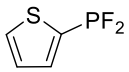


**1.2**

The Ni(II) complex, [NiBr$_2$(*t*Bu$_2$PF)$_2$], was first synthesised in 1973 from anhydrous nickel dibromide (Scheme 1.3) and its crystal structure confirmed the *trans*-square planar geometry around the Ni centre.[86] The molecular structure also provided evidence for a theoretical study reported by Crasnier *et al.*, where it was shown that the CPC angle was higher for the *t*Bu$_2$PF complex than in *t*Bu$_3$P.[87] The synthesis of [NiBr$_2$(*t*Bu$_2$PF)$_2$] was repeated in 1978 and its properties summarised.[88] The [NiX$_2$(*t*Bu$_2$PF)$_2$] complexes, where X = Cl or I, have been synthesised and the resulting NMR, IR and UV spectra confirmed their *trans*-square planar geometries.[86,89] For the chloro analogue, a *cis-trans* equilibrium existed in solution.[89]

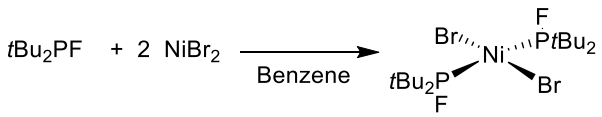


**Scheme 1.3** Synthesis of *trans*-[NiBr$_2$(*t*Bu$_2$PF)$_2$].[86]

### 1.3.3 Pt and Pd coordination chemistry

Stabilisation of low oxidation state transition metals by fluorophosphines has been further demonstrated through the synthesis of the zerovalent [PtL$_4$] complexes, where L = PF$_3$, (CF$_3$)PF$_2$, PhPF$_2$ and (CF$_3$)$_2$PF.[71,90,91] Nixon *et al.* prepared such complexes from the reaction of [PtCl$_2$] and an excess of fluorophosphine (Scheme 1.4); this reaction demonstrates the strong reducing nature of fluorophosphines as well as their coordinating ability.[71] In contrast to the PPh$_3$ analogue, the fluorophosphine Pt(0) complexes displayed remarkable stability to alkyl halides, hydrogen chloride, ethylene and carbon disulphide.[90] This difference in reactivity was attributed to fluorophosphines being significantly weaker σ-donors and stronger π-acceptors than PPh$_3$, which leads to reduced electron density at the metal centre, minimising its propensity to dissociate to more reactive intermediates.[90]

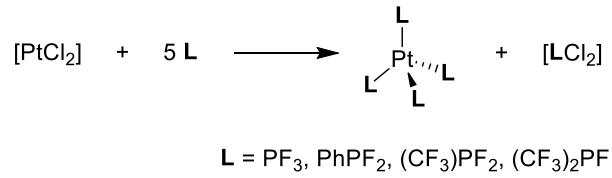


**Scheme 1.4** Synthesis of zerovalent $PtL_4$ complexes.

The $[PtL_4]$ complexes in Scheme 1.4 were stable to ligand dissociation, unlike many $[Pt(PR_3)_4]$ complexes. A series of [Pt(triphos)P'] complexes were synthesised by Meek[92] and later by Nixon[93] where triphos = $MeC(CH_2PPh_3)_3$ and P' = a range of phosphines including the fluorophosphines $(CF_3)_2PF$, $(PhO)PF_2$ and $(Cl_2CH)PF_2$. Meek and Nixon both carried out detailed analysis of the corresponding $^{31}P$ NMR spectra.[92,93]

More recently, in 2004 Perutz *et al.* showed that the reaction of the Pt(0) $[Pt(PR_3)_2]$ (R = *i*Pr, Cy) with pentafluoropyridine in THF gave the fluorophosphine complexes, $[Pt(R_2PF)(PR_3)(4\text{-}C_5NF_4)(R)]$, where R = *i*Pr or Cy (Scheme 1.5a).[94] The complexes were characterised by multinuclear ($^1H$, $^{31}P$, $^{19}F$ and $^{195}Pt$) NMR spectroscopy.[94] The Cy analogue was characterised by X-ray crystallography, which showed a square planar geometry about the Pt centre.[94] This reaction is an elegant example of both C-F and P-C activation.[94] On the other hand, when the reaction was carried out in hexane (where R = Cy), C-H activation occurred to form *cis*-$[Pt(H)(PCy_3)_2(4\text{-}C_5NF_4)]$, which isomerised to the *trans* isomer upon photolysis (Scheme 1.5b); it was suggested that the source of the hydride in the complex was one of the C-H bonds of $PCy_3$.[94] In contrast, upon reaction with the palladium analogues, $[Pd(PR_3)_2]$ (R = Cy, *i*Pr), C-F oxidation occurred to form the complexes, *trans*-$[Pd(F)(PR_3)_2(4\text{-}C_5NF_4)]$.[94]

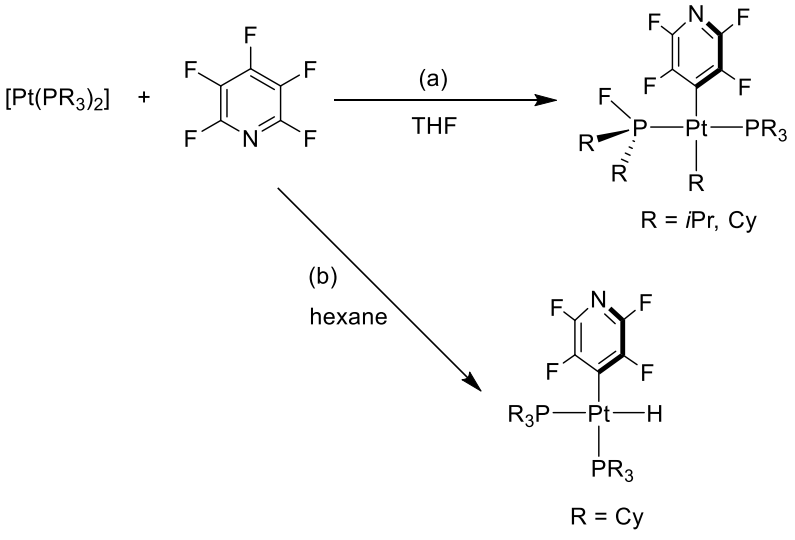


**Scheme 1.5** Reaction of pentafluoropyridyine at Pt(0) in different solvents.

Platinum(II) complexes of fluorophosphines were primarily investigated in the late 1980s and early 1990s by Schmutzler *et al.* In 1988, they synthesised several $ArPF_2$ (such as **1.3** – **1.5**); the substituents in the 2- and 6-position were shown to sterically protect the $PF_2$ centre from disproportionation.[95] The *cis*-$[PtCl_2L_2]$ complexes, where L = **1.3** – **1.5**, were synthesised and their NMR and mass spectra reported.[95] Schmutzler *et al.* also described the synthesis of a range of novel cyclopentadienyl-difluorophosphines (*e.g.* **1.6**) and the corresponding *cis*-$[PtCl_2L_2]$ complexes.[96] The analogous *cis*-$[PtCl_2L_2]$ complexes, where L = *t*Bu$PF_2$, Ad$PF_2$ and trt$PF_2$ and Ad = adamantyl, trt = triphenylmethyl, have also been reported;[97,98] the *t*Bu and Ad analogues were characterised by X-ray crystallography.[97]

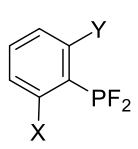


X, Y = OMe (**1.3**)
X, Y = OPh (**1.4**)
X = $CF_3$ Y = OMe (**1.5**)

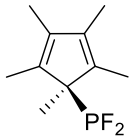


**1.6**

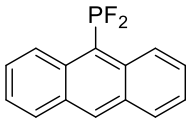


**1.7**

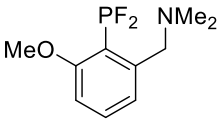


**1.8**

Schmutzler *et al.* synthesised the difluorophosphine derivative of anthracene (**1.7**) and its *cis*-$[PtCl_2L_2]$ complex.[99,100] The unusual aryldifluorophosphine **1.8** was also reported and an intramolecular interaction between the $NMe_2$ group and the phosphorus atom of $PF_2$ was suggested.[101] They synthesised the corresponding *cis*-$[PtCl_2(\mathbf{1.8})_2]$ complex, which was characterised by X-ray crystallography.[101] The crystal structure showed a pronounced distortion from tetrahedral to trigonal bipyramidal geometry around the P atom; it was suggested that this was as a result of the attractive interaction between the nitrogen and phosphorus atoms of **1.8**.[101]

Schmutzler *et al.* synthesised the *cis*-$[PtCl_2L_2]$ complexes, where L is the arylfluorophosphines, **1.9** and **1.10**.[102,103] The complexes were characterised by X-ray crystallography, which showed bond lengths in the expected range based on previously synthesised difluorophosphine Pt(II) complexes.[102–104] The crystal structures confirmed the *cis* geometry of fluorophosphines in a square planar arrangement around the Pt centre.[102,103]

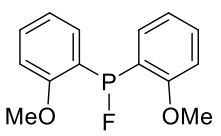


**1.9**

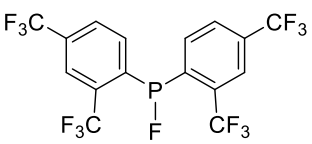


**1.10**

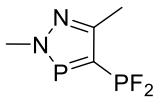


**1.11**

Cavell *et al.* reported the synthesis of the difluoro-diazophosphole **1.11** from the reaction of its corresponding dichlorophosphine and NaF.[105] Detailed analysis of the ligand's NMR spectra was carried out.[105] The coordination chemistry of **1.11** was investigated through the synthesis of *cis*-[$PtCl_2$(**1.11**)$_2$].[106] In addition, it was shown that the reaction of 2 equiv. of **1.11** to [PtClMe(cod)] gave the expected *cis*-[PtMeCl(**1.11**)$_2$] product.[106] However, using an excess of ligand **1.11** gave the zerovalent complex [Pt(**1.11**)$_4$], where the Pt(II) centre has been reduced to Pt(0).[106] The product was structurally characterised and showed the ligands coordinated *via* the exocyclic phosphine.[106]

More recently, the aryl fluorophosphine **1.12** was reacted with the chloro-dimer, *trans*-[$Pt_2Cl_2$(μ-Cl)$_2$($PEt_3$)$_2$] in a 2:1 ratio to give the mononuclear *trans*-[$PtCl_2$($PEt_3$)(**1.12**)] complex (Scheme 1.6); the large $^2J_{P,P}$ value of 567 Hz was consistent with a *trans*-geometry.[107]

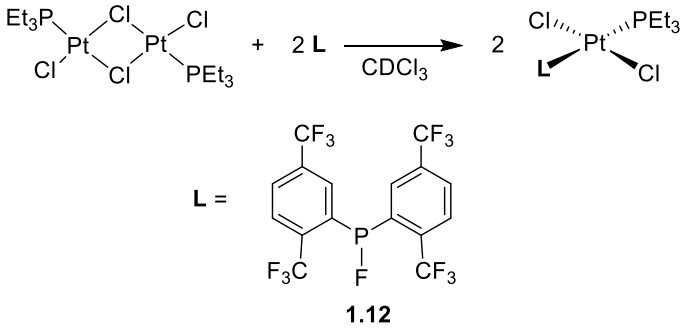


**Scheme 1.6** Synthesis of *trans*-[$PtCl_2$($PEt_3$)L], where L = **1.12**.[107]

In contrast to platinum, there are few reports of palladium complexes of fluorophosphines. Wild *et al.* achieved the first resolution of a free fluorophosphine, *rac*-Ph(*i*Pr)PF, through fractional crystallisation of the diastereomeric Pd binuclear complexes (Scheme 1.7), where the (*R*,$R_P$) diastereomer was less soluble than the (*R*,$S_P$) isomer.[108,109] Optically pure (*S*)-Ph(*i*Pr)PF was liberated from the (*R*,$R_P$) diastereomer and obtained in a good yield of 64%.[108,109]

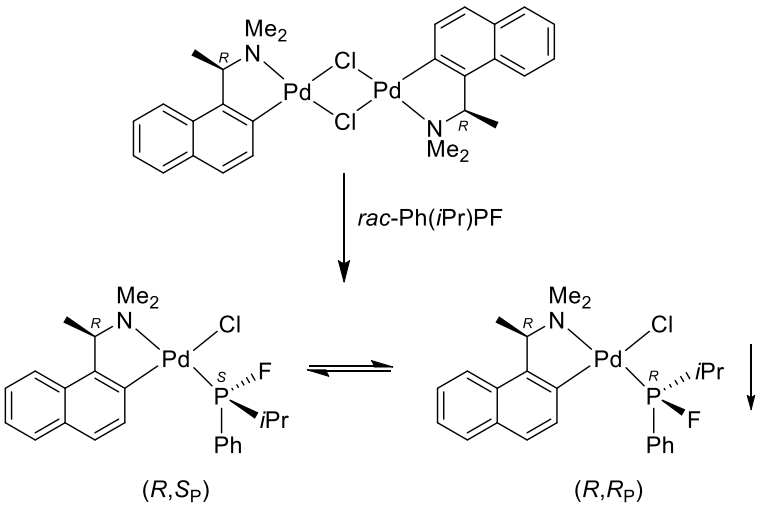


**Scheme 1.7** Resolution of Ph(*i*Pr)PF using Pd complexation.[108,109]

In 1992, the synthesis of the first fluorophosphine Pd(II) complex was described; the reaction of 2 equiv. of ligand with $[PdCl_2(cod)]$ gave the *cis*-$[PdCl_2L_2]$ complexes, where L = *t*BuPF$_2$ or AdPF$_2$.[97] The analogous reaction using L = trtPF$_2$ (trt = triphenylmethyl) to give *cis*-$[PdCl_2L_2]$ was reported in 1995.[98]

The coordination chemistry of the difluoro-diazophosphole **1.11** was extended to palladium by Cavell *et al.*[106] The reaction of ligand **1.11** with $[PdCl_2(cod)]$ gave a mixture of the zerovalent complex, $[Pd(\mathbf{1.11})_4]$ and the Pd(II) complex, $[PdCl_2(\mathbf{1.11})_2]$; $[Pd(\mathbf{1.11})_4]$ was also synthesised from $[Pd_2(dba)_3]$ (dba = dibenzylideneacetone) to confirm this assignment.[106]

### 1.3.4 Mo(0) coordination chemistry

Stelzer *et al.* have synthesised a range of *cis*-$[Mo(CO)_4L_2]$ complexes, where L = $R_{(3-n)}PX_n$ and X = Cl, F or H; their CO stretching frequencies and force constants were measured to assess the σ-donor and π-acceptor properties of the phosphine ligands.[110] The π-acceptor character of fluorophosphines, *t*Bu$_2$PF and *t*BuPF$_2$, has also been explored by Stelzer *et al.* through the synthesis of the corresponding $Mo(CO)_5L$, *cis*-$[Mo(CO)_4L_2]$ (Scheme 1.8) and *cis*-$[Mo(CO)_3L_3]$ complexes.[84,88] The IR data from each of these studies showed that the π-acceptor capacity of the phosphines increase in the order PF$_3$ > *t*BuPF$_2$ > *t*Bu$_2$PF > *t*Bu$_3$P.[84] Complete analysis of the NMR spectra was also carried out to obtain the spin coupling constants and was consistent with the observed trend in electronics.[84]

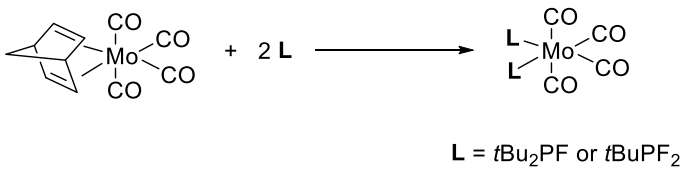


**Scheme 1.8** Synthesis of *cis*-[Mo(CO)$_4$L$_2$] complexes, where L = *t*Bu$_2$PF and *t*BuPF$_2$.[84]

The $^{31}$P and $^{19}$F NMR spectra of *cis*-[Mo(CO)$_4$L$_2$] and *fac*-[Mo(CO)$_3$L$_3$] complexes using numerous fluorophosphines (*e.g.* (CF$_3$)PF$_2$, (CF$_3$)$_2$PF, (ClCH$_2$)PF$_2$ and PhPF$_2$) have been analysed by Nixon and Schmutzler.[75,81,82,111] The coupling constants were accurately calculated and it was shown that the $^2J_{P,P}$ values increase with increasing electron-withdrawing power of the R substituent, *i.e.* PF$_3$ > (ClCH$_2$)PF$_2$.[111] As with the NiL$_4$ complexes, a decrease in the $^1J_{P,F}$ values upon coordination and a negative coordination shift was also observed.[82] Schmutzler *et al.* evaluated the changes in the $^{31}$P and $^{19}$F chemical shifts as a measure of the nature of the metal-ligand bond; one of the conclusions drawn from this was that for all complexes studied, there is an appreciable amount of π-bonding between the metal and the phosphorus atom.[82]

Nixon also presented the IR data, Raman data and calculated CO stretching force constants of such complexes, in conjunction with the analogous *fac*-[Mo(CO)$_3$L$_3$] complexes.[112] It was shown that the fluorophosphines have comparable π-accepting properties to CO. The trifluoromethyl fluorophosphines, (CF$_3$)PF$_2$ and (CF$_3$)$_2$PF, were shown to be stronger π-acceptors than PF$_3$.[112] This was rationalised by the competitive π-donor bonding between F and P and π-acceptor bonding between the metal and P.[112] The CF$_3$ group does not compete as much for the vacant π-orbitals of the P-atom, and so favours metal-phosphorus π-bonding.[112] Calculation of CO stretching force constants for a range of fluoro- and difluorophosphine Mo complexes has since been presented using rigorous algebraic procedures; the procedure was based on the Cotton and Kraihanzel force field.[113] It was shown that using interaction force constant relations did not improve the calculations.[113]

Several molybdenum-carbonyl complexes of other difluorophosphines have been reported.[77] The coordination chemistry of the difluoro-diazophosphole **1.11** (Section 1.3.3) has been extended to molybdenum by Cavell *et al.*; the *cis*-[Mo(CO)$_4$(**1.11**)$_2$] and *fac*-[Mo(CO)$_3$(**1.11**)$_3$] complexes were synthesised from [Mo(CO$_4$)(nbd)] and [Mo(CO)$_3$(MeCN)$_3$] respectively.[105] The *cis*-[Mo(CO)$_4$L$_2$] and *fac*-[Mo(CO)$_3$L$_3$] complexes of the 2-thienyldifluorophosphine ligand **1.2** (Section 1.3.2) have also been previously

synthesised.[85] The *cis*-$[Mo(CO)_4L_2]$ complex of the difluorophosphine, $trtPF_2$ (trt = triphenylmethyl), has also been reported; upon heating the *cis* complex isomerisation to the thermodynamically more stable *trans* complex occurred.[98]

### 1.3.5 Other Group 6 coordination chemistry

In contrast to molybdenum, there are few reports of other group 6 metal complexes of fluorophosphines. The synthesis of the $[M(CO)_5L]$ complexes, where L = $(CF_3)_2PF$ and M = Cr and W, has been described.[114] The high π-acidity of the fluorophosphine was demonstrated by the complexes' IR and NMR spectroscopic data.[114] The $[M(CO)_5L]$, *cis*-$[M(CO)_4L_2]$ and *fac*-$[M(CO)_3L_3]$ complexes of the bulky fluorophosphines, *t*$Bu_2PF$ and *t*$BuPF_2$ (where M = Cr and W), have been synthesised.[84] The complexes were evaluated and showed similar trends in ligand properties to their corresponding molybdenum complexes discussed in Section 1.3.4.[84]

Cavell *et al.* synthesised the $[Cr(CO)_5L]$ complex of the difluoro-diazophosphole **1.11** (Section 1.3.3) to evaluate its donor properties.[105] From the IR data for $[Cr(CO)_5$(**1.11**)], the stretching frequency of the $Ni(CO)_3L$ complex was estimated and the electronic parameter, χ, calculated; the calculated value of **1.11** was similar to that of $PF_3$ (51 $cm^{-1}$ vs. 55 $cm^{-1}$ respectively).[105]

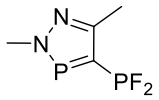


**1.11**

To the best of our knowledge, the only example of a group VII metal complex of a fluorophosphine is $[MnH(CO)_4\{(CF_3)_2PF\}]$, synthesised in 1971 by Dobbie.[115]

### 1.3.6 Group 8 coordination chemistry

In 1969, the first Fe complex of a fluorophosphine was reported by Haas *et al.*[116] The $[Fe(CO)_4L]$ complexes, where L = $(CF_3)_2PF$ and $(CF_3)PF_2$, were synthesised from the substitution reaction of $[Fe(CO)_5]$.[116] It was observed that an equatorial position was preferred by the fluorophosphines, in contrast to the fluorophosphites $(MeO)_{3-x}PF_x$ where a strong preference for an axial position was displayed.[116] $[Fe(CO)_4L]$ complexes of the aryl-fluorophosphines, **1.13** and **1.14**, have since been reported by Schmutzler *et al.*, and it was shown that **1.14** was stable to redox disproportionation.[103]

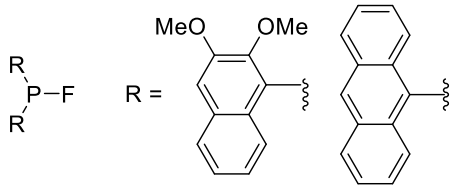


**1.13** **1.14**

In 2019, Wolf *et al.* reported the synthesis of [Cp*Fe{($C_5Ph_3H_2$)PF}] (**1.15**), which contains a fluorophosphinine.[117] Although there has recently been extensive research into phosphinines, metals complexes of halophosphinines have remained rare.[117] The crystal structure of complex **1.15** showed the P-F bond is covalent, in contrast to the Br and I analogues which displayed ionic structures.[117]

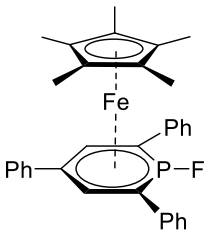


**1.15**

The binuclear species, [$Fe_2Cl_5(PhPF_2)_5$], was synthesised by Stezler *et al.* from the redox reaction of $PhPF_2$ and $FeCl_3$, and full spectroscopic data was reported.[118] X-ray crystallography identified the species as the mixed valence complex, [Fe(II)Cl($PhPF_2$)$_5$]-[Fe(III)$Cl_4$]; a distorted octahedral geometry was identified at the Fe(II) centre.[118] They also showed that the product from the reduction of the complex was dependent on the reducing agent used.[78] Using Zn/Hg afforded the Fe(0) complex, [Fe($PhPF_2$)$_5$], whereas using Fe powder as the reducing agent gave the Fe(II) complex, *cis*-[$FeCl_2(PhPF_2)_4$].[78]

There are only a few of examples of ruthenium complexes of fluorophosphines. Recently, Peruzzini *et al.* accessed desired fluorophosphines from the fluorination of phosphorus oxyacids, mediated by [RuClCp($PPh_3$)$_2$] (Scheme 1.9).[119] The commercial salt XtalFluor-E ([$Et_2NSF_2$][$BF_4$]) was used as the fluorinating agent, which due to its high stability and non-toxicity offered advantages over traditional routes.[119] The crystal structure of a Ru(II) arene complex of the novel hybrid fluorophosphine ligand, $Ph_2PFBF_3$, has been reported; the ligand was coordinated to the metal *via* the P centre of the $Ph_2P$ moiety and the F atom of the $BF_4$.[120] The only other example of a Ru complex of a difluorophosphine was reported by Cavell *et al.*[121] In conjunction with the coordination of the difluoro-diazophosphole **1.11** discussed above, the synthesis of [CpRuCl(**1.11**)($PPh_3$)] was described; analysis of the complicated $^{31}P$ and $^{19}F$ NMR spectra was reported and showed agreement with calculated spectra.[121]

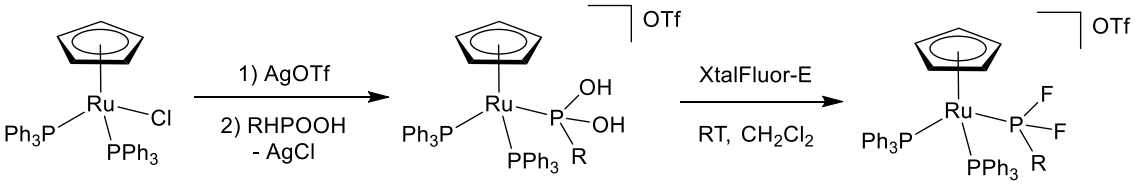


**Scheme 1.9** Synthesis of Ru-fluorophosphine complexes, where R = H, F, Ph.[119]

To the best of our knowledge, Schromburg *et al.* have reported the only examples of osmium coordination of a fluorophosphine; the syntheses of osmium clusters of $t$Bu$_2$PF were described and the complexes characterised by X-ray crystallography.[122]

### 1.3.7 Group 9 coordination chemistry

There are few examples of cobalt complexes of fluorophosphines. In 1973, [CoX$_2$($t$Bu$_2$PF)$_2$] complexes, where X = Cl, Br or I, were synthesised.[89] Spectroscopic data for the complexes were collected and showed a tetrahedral geometry about the Co centre.[89] The reaction of the fluorophosphines, $(CF_3)_{3-x}PF_x$, with [Co(CO)$_3$(NO)] gave [Co(CO)$_2$(NO)L], where L = $(CF_3)_{3-x}PF_x$.[123] Displacement reactions between a range of free phosphines (L') and the coordinated ligand (L) in [Co(CO)$_2$(NO)L] were carried out; relative to other halophosphines the fluorophosphines had the strongest tendency to displace the coordinated ligand.[123] Stelzer *et al.* have prepared the Co(I) complexes [CoXL$_4$] (where X = Br or I and L = $t$Bu$_2$PF or PhPF$_2$), from the Co(II) precursors [COX$_2$L$_3$].[78] The [CoX$_2$(PhPF$_2$)$_3$] complex was reduced using Zn/Hg and gave the unexpected complex, Hg[Co(PhPF$_2$)$_4$]$_2$.[78]

Traditionally the reaction of phosphine ligands with [Rh$_2$Cl$_2$(CO)$_4$] give the *trans*-[RhCl(CO)L$_2$] complexes. Schmutzler *et al.* showed that the reaction of 2 equiv. of the aryl-fluorophosphine **1.13** (Section 1.3.6) with [Rh$_2$Cl$_2$(CO)$_4$] gave [Rh$_2$Cl$_2$(CO)$_2$(**1.13**)$_2$]; the addition of a further 2 equiv. of **1.13** led to the expected *trans*-[RhCl(CO)(**1.13**)$_2$] complex (Scheme 1.10).[103] By contrast, PF$_3$ displaces either the CO or π-alkene from a variety of Rh(I) precursors to give the binuclear species [Rh$_2$Cl$_2$(PF$_3$)$_4$].[121] Nixon *et al.* synthesised [Rh$_2$Cl$_2$(PF$_3$)$_4$] from the reaction of [Rh$_2$Cl$_2$(C$_2$H$_4$)$_4$] with PF$_3$ under mild conditions; analogous behaviour was observed when using the difluorophosphine $(CF_3)PF_2$.[124,125] Nixon also showed that upon the addition of $(CF_3)PF_2$ to [Rh$_2$Cl$_2$(PF$_3$)$_4$], PF$_3$ was displaced by $(CF_3)PF_2$.[124] The mixed phosphine Rh complex, [RhCl(PPh$_3$)$_2${$(CF_3)PF_2$}], was also synthesised by Nixon *et al.*[124]

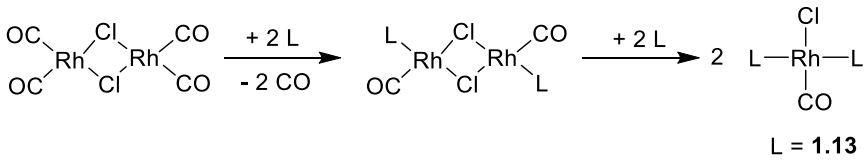


**Scheme 1.10** Synthesis of *trans*-[RhCl(CO)(**1.13**)$_2$].[103]

Decomposition of the difluoro-diazophosphole **1.11** (Section 1.3.5) was observed upon reaction with the Rh(I) binuclear precursors [$Rh_2Cl_2(CO)_4$] and [$Rh_2Cl_2(cod)_2$].[121] It was suggested that the Rh-Cl bonds were not cleaved due to the poor σ-donor capacity of **1.11**, but as discussed above $PF_3$ can react readily with these precursors.[121] Furthermore, ligand **1.11** reacts readily with the binuclear [$Cp^*_2Rh_2Cl_4$] precursor to give [Cp*$RhCl_2$(**1.11**)$_2$].[121] Similar to $PF_3$, ligand **1.11** displaced both CO ligands from [$CpRh(CO)_2$] to give [CpRh(**1.11**)$_2$]; typically phosphines only displace one of the CO ligands.[121]

### 1.3.8 Group 11 coordination chemistry

To the best of our knowledge, Kruck *et al.* have been the only research group to report group 11 complexes of fluorophosphines. In 1996, they reported the synthesis of the difluorophosphine Au(I) complexes, [$Au(CF_3)(RPF_2)$] and [$AuCl(RPF_2)$], where R = *t*Bu, Ph or Cp.[48]

## 1.4 Coordination chemistry of fluorophosphites

Compared to fluorophosphines and difluorophosphines, there are fewer reports of metal complexes of fluorophosphites or difluorophosphinites; this section summarises those complexes which have been reported to date.

### 1.4.1 Ni coordination chemistry

As with fluorophosphines, there have been several reports of zerovalent [$NiL_4$] complexes of fluorophosphites. In 1963, Schmutzler *et al.* described the synthesis of [$NiL_4$] complexes from the reaction of [$Ni(CO)_4$] with ligands such as the 5-membered cyclic fluorophosphite **1.16** (Scheme 1.11) and the difluorophosphinites, *n*$PrOPF_2$ and $PhOPF_2$.[59,126] In 1967, Schmutzler interpreted the $^{31}P$ and $^{19}F$ NMR spectra obtained for such complexes.[82] One of the conclusions made for these $NiL_4$ complexes was that the M-P bond has a significant amount of π-bonding.[82] Detailed analysis of the $^{31}P$ and $^{19}F$ NMR spectra of [Ni(**1.16**)$_4$] was also carried out by Lynden-Bell; group theory methods

were used to construct the $[AX]_4$ nuclear spin Hamiltonian for the tetrahedral system.[127] The synthesis of $[NiL_4]$, where L = $MeOPF_2$, was described by Kruck *et al.* from the methanolysis of $[Ni(ClPF_2)_4]$; the high reactivity of the P-Cl bond ensures rapid reaction at ambient temperature and in the absence of solvent.[128]

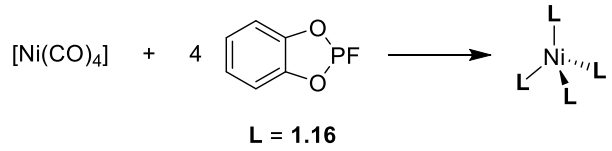


**L = 1.16**

**Scheme 1.11** Synthesis of $[Ni(\mathbf{1.16})_4]$.[59,126]

Cassoux *et al.* have also studied the magneto-optical effects of $[NiL_4]$ complexes.[83,129] In 1969, they reported the synthesis and characterisation of a range of fluorophosphite $[Ni\{(RO)_2PF\}_4]$ and difluorophosphinite $[Ni(ROPF_2)_4]$ complexes, where R = Et, Pr, Bu or Pn.[130] Detailed analysis of the $^{31}P$ and $^{19}F$ NMR spectra has also been described and the coordination chemical shifts calculated.[131] A decrease in the $^1J_{P,F}$ values was observed upon coordination.[131] The effect of the substituent was also discussed and the fluorophosphite complexes were compared to the chlorophosphite analogues.[131] Goodfellow *et al.* reported the heteronuclear INDOR spectra of the $[NiL_4]$ complexes, where L = **1.16** or $(PhO)_2PF$, and calculated the magnitudes and relative signs of the coupling constants.[132] There are only two reports of nickel-carbonyl complexes of fluorophosphites, which include a mixture of bidentate and monodentate ligands.[59,126] There are no reports of Ni(II) complexes of fluorophosphite ligands.

### 1.4.2 Pt and Pd coordination chemistry

There are a few reports of zerovalent platinum complexes of fluorophosphites. In conjunction with the $[NiL_4]$ complexes discussed above, Goodfellow *et al.* also presented the heteronuclear INDOR spectra of the $[PtL_4]$ complexes, where L = **1.16** or $(PhO)_2PF$; the complexes have a $[AX]_4$ ($T_d$) spin system.[132] The complexes were synthesised from the reaction of $[Pt(cod)_2]$ and a 10% excess of ligand (Scheme 1.12).[132] The magnitudes of the coupling constants were calculated and it was shown that the $^2J_{P,P}$ values for the Pt(0) complexes were significantly larger than the analogous Ni(0) complexes (*ca.* 100 vs. 20 Hz).[132] Matos *et al.* reported the synthesis of the Pt(0) complex $[Pt(PPh_3)_2L]$, where L is the 6-membered fluorophosphite **1.17**, from the reaction of $[Pt(PPh_3)_2(C_2H_4)]$ with **1.17**.[133] Relative to the chlorophosphite analogue, the $^1J_{P,Pt}$ value was significantly higher (6603 vs.

4856 Hz), as expected from the presence of the more electronegative fluorine atom which increases the s-character in the Pt-P bond.[133]

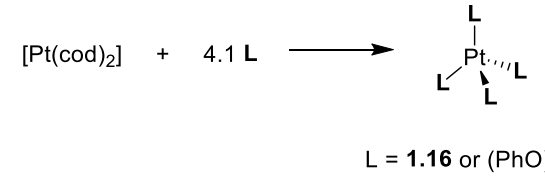


**Scheme 1.12** Synthesis of $[PtL_4]$ complexes, where L = **1.16** or $(PhO)_2PF$.[132]

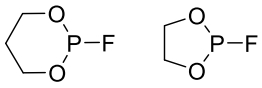


**1.17** **1.18**

The only reported example of a fluorophosphite complex of the type $[PtCl_2L_2]$ is the *cis*-$[PtCl_2(PhOPF_2)_2]$ complex.[134] There have been a few reports of mixed phosphine Pt(II) complexes. In 1976, Schmutzler *et al.* prepared the *cis*-$[PtCl_2(PEt_3)(ROPF_2)]$ complexes, where R = *n*Bu or Ph, from the reaction of $ROPF_2$ and $[PtCl_2(PEt_3)_2]$; this was the first example of a Pt(II) difluorophosphinite complex.[135] The analogous Pd(II) complex was also reported.[135]

In 2000, Matos *et al.* also reported the synthesis of the *cis*-$[PtCl_2(PEt_3)L]$ complexes, where L are the 5-membered cyclic fluorophosphites **1.16** and **1.18**.[133] Unlike the Pt(0) complexes discussed above, the $^1J_{P,Pt}$ values decreased upon changing the ligand from a chlorophosphite to a fluorophosphite.[133] This was attributed to the lower stability of the fluorophosphite complexes, since they can be regarded as a combination of a hard acid-soft base; the Pt-P bond should be longer in the fluorophosphite complexes than in the chlorophosphite analogues and hence result in a lower $^1J_{P,Pt}$.[133] The analogous Pd(II) complexes have also been prepared.[133]

A range of difluorophosphinites $ROPF_2$ have been synthesised from the silicon-phosphorus exchange reaction of the silyl ethers $ROSiMe_3$ and $ClPF_2$ (where R = *p*-substituted benzyl group, neopentyl, 1-adamantyl); high yields were achieved under mild conditions.[136] The difluorophosphinites (L') were reacted with $[PtCl_2L_2]$ (L = $PPh_3$ or $PEt_3$) to give the $[PtClL_2(L')][Cl]$ complexes, which in some cases continued to react in an Arbuzov-Michaelis type fashion and produce $[PtClL_2(PF_2O)]$ and RCl.[136]

The binuclear species, $[Pt_2I_4\{(PhO)_2PF\}_2]$, was synthesised by Goggin *et al.*[137] Detailed analysis of the $^{31}P$ and $^{19}F$ NMR spectra showed that the complex existed as both the *trans*

and *cis* isomers in a $CDCl_3$ solution; the major component was identified as the *trans*-isomer.[137] The analogous Pd(II) dimer existed as two isomers in solution, but NMR could not be used to elucidate their structures due to the absence of a suitable spin-active Pd nucleus.[137]

### 1.4.3 Mo(0) coordination chemistry

There are a few examples of $[Mo(CO)_3L_3]$ complexes with fluorophosphite ligands. In 1963, Schmutzler *et al.* reported the first synthesis of $[Mo(CO)_3L_3]$ complexes using the cyclic fluorophosphite **1.16** (Section 1.4.1) and difluorophosphinites, $PrOPF_2$ and $PhOPF_2$.[59,82,126] The complexes were characterised and analysis of their $^{31}P$ and $^{19}F$ NMR spectra was carried out.[59,82,126] In 1971, Schmutzler *et al.* also presented a theoretical analysis of the $^{19}F$ NMR spectrum of a general $[AX_n]_3$ spin system, which was then applied to the *mer*-$[Mo(CO)_3L_3]$ complexes, where L = **1.16** or $PhOPF_2$, to yield the various coupling constants.[138] They showed that the magnitude of $^2J_{P,P}$ increased with the electronegativity of the group attached to the P atom.[138] In 1997, the lab of Schmutzler reported the synthesis of the allyldifluorophosphinite **1.19** and explored its coordination chemistry.[139] Included in this study was the synthesis of *fac*-$[Mo(CO)_3(\mathbf{1.19})_3]$, which was characterised from its IR, NMR and mass spectra.[139]

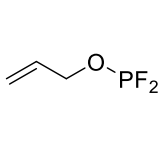


**1.19**

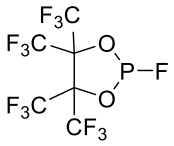


**1.20**

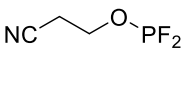


**1.21**

In 1977, Schmutzler *et al.* reported the first example of a fluorophosphite *cis*-$[Mo(CO)_4L_2]$ complex.[140] The cyclic fluorophosphite, **1.20**, was synthesised from the reduction of a fluorophosphazophosphorane by $Ph_2PSiMe_3$ (Scheme 1.13); the fluorophosphite **1.20** displaced the coordinated alkene from $[Mo(CO)_4(nbd)]$ to give *cis*-$[Mo(CO)_4(\mathbf{1.20})_2]$.[140] The IR and NMR data for the complex were reported.[140] The *cis*-$[Mo(CO)_4L_2]$ complex of the difluorophosphinite **1.21** has also been prepared from $[Mo(CO)_4(nbd)]$ by Rankin *et al.*, but due to its instability to air and moisture it was not isolated.[56] The hexa-substituted $[MoL_6]$ complexes have been reported for the fluorophosphites, $(n\text{PrO})_2PF$ and $(MeO)_2PF$, and the difluorophosphinites, $n\text{PrOPF}_2$ and $MeOPF_2$.[141]

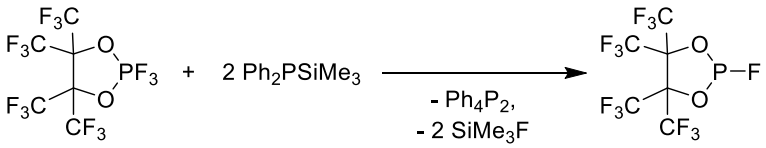


**1.20**

**Scheme 1.13** Synthesis of cyclic fluorophosphite **1.20**.

### 1.4.4 Other Group 6 metal coordination chemistry

There are a limited number of examples of other Group 6 metal complexes of fluorophosphites. Krivykh *et al.* have presented new chromium arene complexes containing either mono-, bi- or tridentate difluorophosphinites.[142] They demonstrated that under UV irradiation, the difluorophosphinites can replace CO ligands from arene-tricarbonylchromium complexes (Scheme 1.14).[143,144] All three CO ligands can be displaced by the fluorophosphite to form a novel chelated chromium derivative.[143,144] The complexes were characterised by NMR and IR spectroscopy[143] and detailed analysis of the mass spectra of the complexes was also reported.[145] Krivykh *et al.* also showed that such polydentate complexes can be prepared from electrochemical oxidation of the arene-tricarbonylchromium complex; this route offers a novel method of CO substitution by other ligands in transition metal complexes.[146,147]

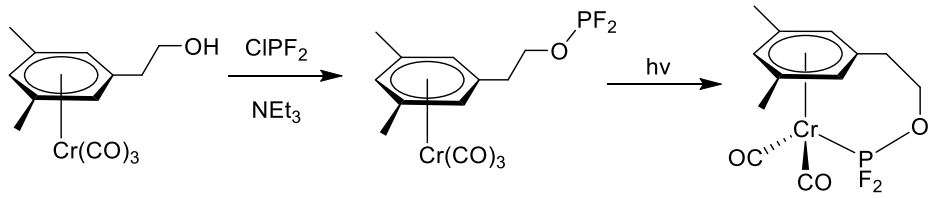


**Scheme 1.14** Synthesis of a mono-chelate chromium arene-difluorophosphinite complex.[143]

Schmutzler *et al.* have synthesised *fac*- and *mer*-isomers of $[Cr(CO)_3(L)_3]$ (where L = **1.19**) from $[Cr(CO)_3(C_7H_8)]$.[139] They also prepared $[W(CO)_5L]$ (where L = **1.19**) from $[W(CO)_5(THF)]$.[139] Both complexes were characterised by IR and NMR spectroscopy and mass spectrometry.[139] It was shown that the allylic difluorophosphinite was coordinated *via* the phosphorus only; the allylic π-system was not involved in the metal-ligand bonding.[139] The Cr and W analogues of the hexa-substituted $[MoL_6]$ complexes described in Section 1.4.3 were also synthesised; the ease with which the complexes could be prepared was in the order Mo > W > Cr.[141] There are no reported examples of Group 7 metal complexes of fluorophosphites to the best of our knowledge.

### 1.4.5 Group 8 metal coordination chemistry

Iron carbonyl complexes have attracted interest due to their fluxionality resulting from either the ligand adopting an axial or equatorial position.[148] In 1969, the fluorophosphite complexes $[Fe(CO)_4\{(MeO)_{3-x}PF_x\}]$ were prepared from methanolysis of the trifluorophosphine analogue.[116] Rapid isomerisation was observed upon replacement of the fluorine group by OMe since the fluorophosphite complexes displayed a preference for axial positions (in contrast to the fluorophosphines in Section 1.3.6).[116] It was suggested that electronic effects determine which isomer is formed. Consequently, Ruff *et al.* prepared the $[Fe(CO)_4L]$ complexes, where L is both the bulky and highly electronegative difluorophosphinite, $(CF_3)_2CNCOPF_2$.[148] The analogous fluorophosphite $(RO)_2PF$ and phosphite $(RO)_3P$ complexes were also synthesised (where R = $(CF_3)_2CNC$).[148] A mixture of both the axial and equatorial isomers were observed for the fluorophosphite complexes, in contrast to the phosphite analogue where only the equatorial isomer was present.[148]

Schmutzler *et al.* synthesised the $[Fe(CO)_4L]$ complex, where L = **1.19** (Section 1.4.3), from $[Fe(CO)_5]$ and showed that the allylic difluorophosphinite occupied an axial position.[139] Similar to its Group 6 coordination described above, the difluorophosphinite coordinated *via* only the phosphorus atom.[139] The 7-membered cyclic fluorophosphite **1.22** was prepared from the reaction of 2,2-biphenol and $Cl_2PF$ by Schmutzler *et al.*[149] Attempts to synthesise the ligand from the corresponding chlorophosphite were unsuccessful since the reaction of $PCl_3$ and 2,2-biphenol gave the undesired 7-membered cyclic diphosphite.[149] The reaction of $[Fe_2(CO)_9]$ and **1.22** gave the $[Fe(CO)_4$(**1.22**)$]$ complex (Scheme 1.15).[149]

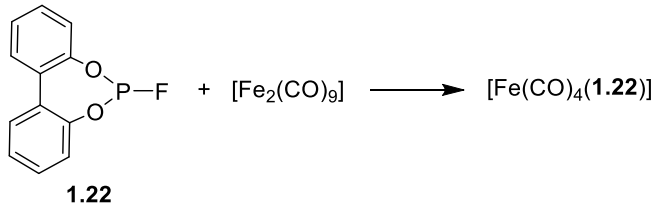


**1.22**

**Scheme 1.15** Synthesis of $[Fe(CO)_4$(**1.22**)$]$.[149]

Schmutzler *et al.* reported the synthesis of several ruthenium complexes of $n$PrOPF$_2$, including $[RuCl(CO)H(PPh_3)_2(n\text{PrOPF}_2)]$ which was characterised by X-ray crystallography.[150] In 2000, the fluorophosphite complexes, *trans*-$[(dppe)_2RuH(L')]$, where L' = $(RO)_2PF$ and R = Me, Et, $i$Pr, were prepared from the reaction of the hydride complexes, *trans*-$[(dppe)_2RuH(L)]$ (where L = $P(OR)_3$) and $HBF_4.Et_2O$.[151] The stability of

the resulting complex appeared to be dependent on the cone angle of the *trans* phosphine ligand; increasing the steric hindrance of the *trans* phosphine decreased the strength of the metal-phosphine bonding.[151]

### 1.4.6 Group 9 metal coordination chemistry

Group 9 metal complexes of fluorophosphites are rare. The only examples of cobalt complexes of fluorophosphites were reported by Clark *et al.* in 1968.[152] Methanolysis of the $[Co(NO)(CO)_x(PF_3)_{3-x}]$ complexes was carried out to yield the fluorophosphite complexes $[Co(NO)(CO)_x(L)_{3-x}]$, where L = $MeOPF_2$ or $(MeO)_2PF$.[152] As the degree of solvolysis was increased, the stretching frequencies of the CO and NO bands in the IR spectra of the complexes decreased.[152]

The $[Rh_2Cl_2(CO)_2L_2]$ complex, where L = *n*$PrOPF_2$, was synthesised from the reaction of ligand with $[Rh_2Cl_2(CO)_2(C_2H_4)_2]$; unlike $PF_3$ (see Section 1.3.7), the difluorophosphinite did not displace the CO ligands from the rhodium centre.[153] In 1985, Nixon *et al.* reported the synthesis of the binuclear fluorophosphite species, $[Rh_2Cl_2(\mathbf{1.16})_4]$, from the reaction of the cyclic fluorophosphite **1.16** and $[Rh_2Cl_2(C_6H_{10})_2]$ (Scheme 1.16).[154] The $^{31}P$ and $^{19}F$ NMR spectra of the complex were obtained and the coupling constants calculated.[154] Treatment of the binuclear complex $[Rh_2Cl_2(\mathbf{1.16})_4]$ with $NMe_4Cl$ gave $[NMe_4][RhCl_2(\mathbf{1.16})_2]$.[154]

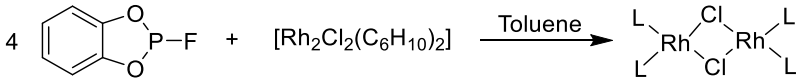


**1.16** L = **1.16**

**Scheme 1.16** Synthesis of the binuclear complex, $[Rh_2Cl_2(\mathbf{1.16})_4]$.[154]

## 1.5 Catalytic applications of fluorophos complexes

### 1.5.1 Fluorophosphites in hydroformylation catalysis

The most notable example of the application of fluorophos ligands in homogeneous catalysis is the use of cyclic fluorophosphites, such as Ethanox 398™ (**1.23**), in Rh-catalysed hydroformylation by Eastman.[155,156] Fluorophosphites were initially approached with scepticism because it was assumed that the P-F bond of Ethanox 398™ would be highly reactive to hydrolysis or disproportionation, leading to the generation of free fluoride ions.[156,157] This would be detrimental to the activity of the hydroformylation

catalyst since the damaging effects of halogens on hydroformylation had been well documented.[158–160]

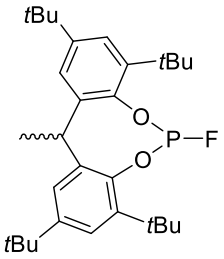


**1.23**

However, Klender *et al.* demonstrated the unexpected high stability of **1.23** and other fluorophosphites to hydrolysis.[161,162] Even at elevated temperatures (up to 350 °C) or under reflux in aqueous isopropanol, no free fluoride ions were generated.[161,162] The stability and hence the success of **1.23** was attributed to the 8-membered phosphacycle which entropically stabilises the ligand, and the bulky *t*Bu substituents which sterically protect the P-centre. Other ways of hampering the degradation of fluorophosphite-containing catalysts was using another Group 8 metal in addition to the catalyst or by adding an epoxide to the reaction mixture.[163,164] A suitable concentration of either stabiliser was required to react with the strongly acidic by-products generated throughout catalysis; these acidic conditions are known to catalyse the degradation of the fluorophosphite ligand.[164]

In 1998, Eastman first reported the use of fluorophosphites as ligands for hydroformylation catalysis, where a range of alkenes were tested such as propylene and octene.[165] Before this, there had been no reports of Ethanox 398™ as a ligand for transition metals despite its numerous applications as an antioxidant and a flame retardant.[166] Subsequently, Eastman have described the use of fluorophosphites in Rh-catalysed hydroformylation of sterically hindered olefins,[155] the preparation of glycoaldehyde from formaldehyde (Scheme 1.17)[167] and low pressure hydroformylation of terminal and internal olefins.[157] Catalysts from a range of fluorophosphites were shown by Eastman to display unusual "ligand acceleration effects" for the hydroformylation of simple alkenes, where increasing the concentration of ligand increased the hydroformylation activity.[168,169]

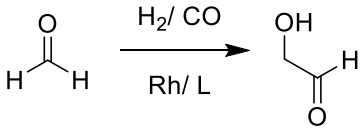


**Scheme 1.17** Catalytic hydroformylation of formaldehyde to produce glycolaldehyde.[167]

The production of propionaldehyde from the hydroformylation of ethylene is an important industrial reaction. Typically, ethylene from commercial sources contains variable amounts of acetylene impurities which can be detrimental to the catalyst depending on the phosphorus ligand used.[170,171] Eastman have reported that hydroformylation catalysts using fluorophosphites can tolerate high levels of alkyne impurities in an alkene feed stream; remarkably no loss of hydroformylation catalytic activity was observed when using an ethylene feed stream containing 1,000 ppm of acetylene.[170,171]

Since the phosphorus atom in Ethanox 398™ is part of a ring, *cis* and *trans* stereoisomers of the ligand are possible (Figure 1.4). In the *cis* isomer (*cis*-**1.23**), the lone pair on the P-atom is in a pseudo-axial orientation whereas, in the *trans* isomer (*trans*-**1.23**) it is in a pseudo-equatorial orientation.[172,173] A detailed coordination study of the isomers of Ethanox 398™ has shown the preferential coordination of *trans*-**1.23** to metals such as Pt and Rh.[174] Eastman have developed a method of separating the isomers of Ethanox 398™ and have also shown that *trans*-**1.23** binds preferentially to Rh, even at low concentrations of *trans*-**1.23**.[172,173] The effect of isomer ratio on hydroformylation catalysis was also explored; studies showed that increasing the amount of *trans*-**1.23** increased the *n*-selectivity and catalytic activity observed.[172,173]

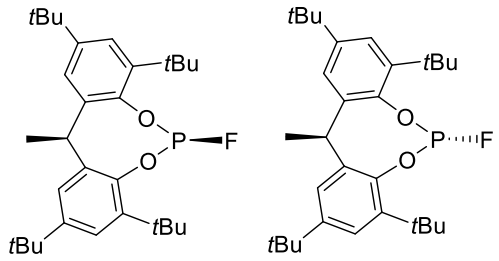


*cis*-**1.23** *trans*-**1.23**

**Figure 1.4** Geometric isomers of Ethanox 398™ (**1.23**).

In 2013, the synthesis of stable amido-fluorophosphite ligands (*e.g.* **1.24**) were reported by Eastman.[175,176] The ligands were readily prepared from the reaction of the corresponding amido-chlorophosphites and ammonium fluoride.[175,176] The Rh catalysts of these ligands gave high catalytic activity in the hydroformylation of various alkenes.[175,176] A wide range of selectivities was accessed through varying the reaction conditions.[175,176]

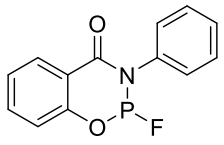

**1.24**

### 1.5.2 Other catalytic applications

In 2012, Pringle *et al.* prepared remarkably stable fluorophosphines based on a phospha-adamantane cage (CgPF, **1.25**) or a phosphabicycle (*s*-PhobPF, **1.26**).[177] The thermal stability of ligands **1.25** and **1.26** was partly attributed to their constrained C-P-C angles, which inhibited disproportionation.[177] Rhodium catalysts of **1.25** and **1.26** displayed comparable activity to $PPh_3$ in the catalytic hydroformylation of 1-heptene (Scheme 1.18) and increased *n*-selectivity was achieved using the Rh-catalyst derived from CgPF (**1.25**).[177] Catalysts derived from **1.25** and **1.26** were tested in the Ni-catalysed hydrocyanation of 3-pentenenitrile to yield adiponitrile (ADN); the Ni-catalyst derived from **1.25** showed excellent catalytic activity, comparable to commercial catalysts.[177–180] This was the first example of the successful application of fluorophosphines in homogeneous catalysis.

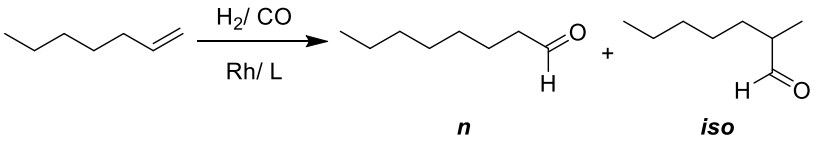


**Scheme 1.18** Catalytic hydroformylation of 1-heptene using catalysts derived from ligands **1.25** – **1.26**.[177]

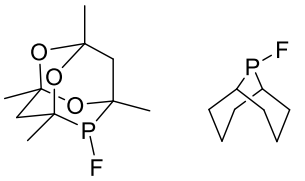

**1.25** CgPF **1.26** *s*-PhobPF

A range of 3,3'-substituted BINOL-based fluorophosphites (**1.27a**-**d**) were synthesised from their corresponding chlorophosphites and tested in the Rh-catalysed asymmetric hydrogenation of benchmark substrates (Scheme 1.19).[181] High catalytic activities and enantioselectivities were achieved, particularly when using MAA (methyl-2-acetamidoacrylate) as the substrate (*ee* = 95% (*S*) for Rh-**1.27b**).[181] The enantioselectivity was dependent on the 3,3-substituent, increasing in the order H < Ph < *p*-tolyl, and when using the very bulky mesityl ligand a drop in *ee* was observed.[181]

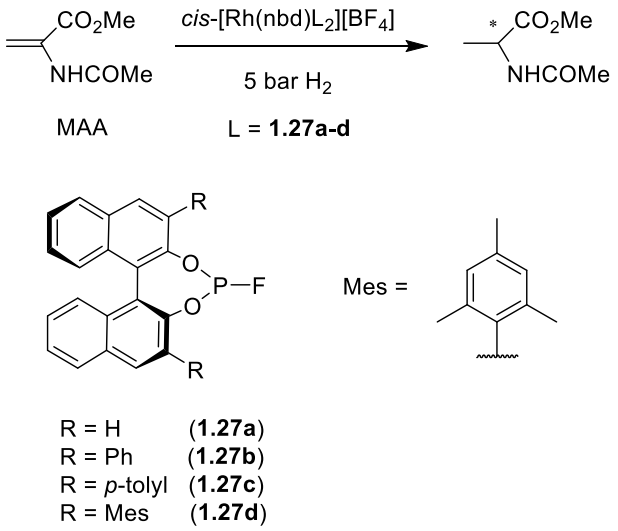


**Scheme 1.19** Catalytic asymmetric hydrogenation of MAA using catalysts derived from ligands **1.27a**-**d**.[181]

The fluorophosphite, BIFOP-F (**1.28**), was employed as a ligand in an enantioselective intramolecular Pd-catalysed alkyl-aryl cross-coupling reaction by Goldfuss *et al.*[182] Moderate enantioselectivity (*ee* = 64%) and good yields were achieved relative to when using catalysts derived from BIFOP-Cl and BIFOP-Br; this was attributed to the high electronegativity of the fluorine atom.[182] In 2019, Goldfuss *et al.* also tested ligand **1.28** in the enantioselective Cu-catalysed 1,4-addition of organozinc and Grignard reagents to enones.[183] However, no conversion was observed due to decomposition of the ligand under the reaction conditions.[183]

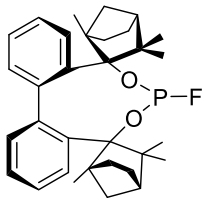


**1.28**
BIFOP-F

## 1.6 Conclusions

From the late 1960s research into the synthesis and metal coordination chemistry of fluorophos ligands has flourished. These developments have culminated in the Eastman hydroformylation process, which was established in the late 1990s. Subsequently, Eastman have applied fluorophosphites to a range of hydroformylation processes with great success. Presently, there are sporadic reports of fluorophos coordination chemistry, however, future developments might be anticipated leading on from this breakthrough by Eastman.

## 1.7 References


1 J. A. Gillespie, E. Zuidema, P. W. N. M. van Leeuwen and P. C. J. Kamer, in *Phosphorus (III) Ligands in Homogeneous Catalysis*, eds. P. C. J. Kamer and P. W. N. M. van Leeuwen, Wiley-VCH, 2012, pp. 1–26.

2 P. W. N. M. van Leeuwen, in *Homogeneous Catalysis, Understanding the Art*, Kluwer Academic Publishers, Dordrecht, 2004, pp. 139–174.

3 A. G. Orpen and N. G. Connelly, *Organometallics*, 1990, **9**, 1206–1210.

4 A. G. Orpen and N. G. Connelly, *J. Chem. Soc. Chem. Commun.*, 1985, 1310–1311.

5 C. A. Tolman, *J. Am. Chem. Soc.*, 1970, **92**, 2953–2956.

6 A. Roodt, S. Otto and G. Steyl, *Coord. Chem. Rev.*, 2003, **245**, 121–137.

7 C. A. Tolman, *Chem. Rev.*, 1977, **77**, 313–348.

8 D. R. Anton and R. H. Crabtree, *Organometallics*, 1983, **2**, 621–627.

9 S. C. van der Slot, J. Duran, J. Luten, P. C. J. Kamer and P. W. N. M. van Leeuwen, *Organometallics*, 2002, **21**, 3873–3883.

10 D. White, B. C. Taverner, N. J. Coville and P. W. Wade, *J. Organomet. Chem.*, 1995, **495**, 41–51.

11 J. F. Nixon and J. R. Swain, *Platinum Met. Rev.*, 1975, **19**, 22–29.

12 T. Kruck, *Angew. Chemie Int. Ed.*, 1967, **6**, 53–67.

13 J. F. Nixon, *Adv. Inorg. Chem. Radiochem.*, 1985, **29**, 41–141.

14 B. J. Chatt and A. A. Williams, *J. Chem. Soc.*, 1951, **0**, 3061–3067.

15 J. Chatt, *Nature*, 1950, **165**, 637–638.

16 L. Heuer, *Platinum Met. Rev.*, 1991, **35**, 86–93.

17 J. F. Nixon, *Endeavour*, 1973, **32**, 19–24.

18 K. Zou, Q. S. Li, Y. Xie, R. B. King and H. F. Schaefer, *Chem. A Eur. J.*, 2008, **14**, 11149–11157.

19 T. Drews, D. Rusch, S. Seidel, S. Willemsen and K. Seppelt, *Chem. A Eur. J.*, 2008, **14**, 4280–4286.

20 H. Stammreich, K. Kawai and O. Sala, *J. Chem. Phys.*, 1961, **35**, 2168–2174.

21 F. D. Calvo, V. Mirabello, M. Caporali, W. Oberhauser, K. Raltchev, K. Karaghiosoff and M. Peruzzini, *Dalton Trans.*, 2016, **45**, 2284–2293.

22 P. Kundig, M. Moskovits and G. A. Ozin, *J. Mol. Struct.*, 1972, **14**, 137–144.

23 P. Doz, T. Kruck and K. Baur, *Angew. Chemie Int. Ed.*, 1965, **4**, 521.

24 P. Doz, T. Kruck and K. Baur, *Angew. Chemie*, 1965, **77**, 505–506.

25 H. Huber, P. Kundig, M. Moskovits and G. A. Ozin, *Nat. Phys. Sci.*, 1972, **235**, 98–100.

26 G. Wilkinson, *J. Am. Chem. Soc.*, 1951, **73**, 5501–5502.

27 M. Akbulut, T. E. Madey, L. Parenteau and L. Sanche, *J. Chem. Phys*, 1996, **105**, 6043–6051.

28 C. Elbadawi, M. Toth and C. J. Lobo, *ACS Appl. Mater. Interfaces*, 2013, **5**, 9372–9376.

29 K. Landheer, S. G. Rosenberg, L. Bernau, P. Swiderek, I. Utke, C. W. Hagen and D. H. Fairbrother, *J. Phys. Chem. C*, 2011, **115**, 17452–17463.

30 M. Ishikawa, I. Muramoto, H. Machida, S. Imai, A. Ogura and Y. Ohshita, *Thin Solid Films*, 2007, **515**, 8246–8249.

31 C. L. Hammill, R. J. Clark, C. W. Ross, A. G. Marshall and J. Schmutz, *Inorg. Chem.*, 1997, **36**, 5973–5977.

32 R. Friedemann and K. Seppelt, *Eur. J. Inorg. Chem.*, 2013, 1197–1206.

33 N. Arnold, R. Bertermann, F. M. Bickelhaupt, H. Braunschweig, M. Drisch, M. Finze, F. Hupp, J. Poater and J. A. P. Sprenger, *Chem. A Eur. J.*, 2017, **23**, 5948–5952.

34 L. K. Peterson and S. Huang, *Inorganica Chim. Acta*, 1993, **203**, 87–91.

35 G. Frenking, K. Wichmann, N. Fröhlich, J. Grobe, W. Golla, D. Le Van, B. Krebs and M. Lä, *Organometallics*, 2002, **21**, 2921–2930.

36 C. G. Barlow, D. L. Miller and R. A. Newmark, *Magn. Reson. Chem.*, 2000, **38**, 38–42.

37 C. C. Grimm, P. E. Brotman and R. J. Clark, *Organometallics*, 1990, **9**, 1119–1123.

38 C. C. Grimm and R. J. Clark, *Organometallics*, 1990, **9**, 1123–1127.

39 A. L. Balch, B. J. Davis and M. M. Olmstead, *Inorg. Chem.*, 1993, **32**, 3937–3942.

40 A. L. Balch, B. J. Davis and M. M. Olmstead, *J. Am. Chem. Soc.*, 1990, **112**, 8593–8595.

41 H.-Q. Yang, Q.-S. Li, Y. Xie, B. R. King and H. F. Schaefer, *Mol. Phys.*, **108**, 2477–2489.

42 S. Gong, C. Wang, Q.-S. Li, Y. Xie and R. B. King, *J. Coord. Chem.*, 2012, **65**, 2459–2477.

43 S. Gong, Q. Luo, Q.-S. Li, Y. Xie, R. B. King and H. F. Schaefer, *New J. Chem.*, 2015, **39**, 3708–3718.

44 R. B. King, *Stud. Chem.*, 2016, **3**, 29–38.

45 M. Bodenbinder, G. Balzer, H. Willner, G. Hagele, F. Mistry and F. Aubke, *Can. J. Chem.*, 1996, **74**, 2392–2394.

46 W. Fuß and M. Ruhe, *Zeitschrift für Naturforsch.*, 1992, **47b**, 591–593.

47 F. Schödel, M. Bolte, M. Wagner and H. W. Lerner, *Zeitschrift fur Anorg. und Allg. Chemie*, 2006, **632**, 652–654.

48 A. Grafe and T. Kruck, *J. Organomet. Chem.*, 1996, **506**, 31–35.

49 H. V. Nanishankar, M. Nethaji and B. R. Jagirdar, *Eur. J. Inorg. Chem.*, 2004, 3048–3056.

50 R. M. Chin, J. Barrera, R. H. Dubois, L. E. Helberg, M. Sabat, T. Y. Bartucz, A. J. Lough, R. H. Morris and W. D. Harman, *Inorg. Chem.*, 1997, **36**, 3553–3558.

51 J. A. Howard, R. Jones, M. Tomietto and A. Joly, *Inorg. Chem.*, 1995, **34**, 3097–3098.

52 R. L. Cook and J. G. Morse, *Inorg. Chem.*, 1984, **23**, 2332–2336.

53 D. L. Gallup and J. G. Morse, *J. Organomet. Chem.*, 1978, **159**, 477–482.

54 W. E. Hill, B. G. Rackley and L. M. Silva-Trivino, *Inorganica Chim. Acta*, 1983, **75**, 51–56.

55 E. P. Kundig, C. Dupre, B. Bourdin, A. Cunningham and D. Pons, *Helevetica Chim. Acta*, 1994, **77**, 421–428.

56 J. Davis and D. W. H. Rankin, *J. Chem. Soc. Dalon Trans. Inorg. Chem.*, 1990, **3**, 881–

885.

57 G. A. Bell, D. W. H. Rankin and P. F. Reinisch, *J. Chem. Soc. Dalton Trans.*, 1987, **12**, 3023–3027.

58 G. A. Bell and D. W. H. Rankin, *J. Chem. Soc. Dalt. Trans. Inorg. Chem.* , 1986, **8**, 1689–1692.

59 R. Schmutzler, *US Patent*, 1966, US 3242171.

60 R. B. King, *Acc. Chem. Res.*, 1980, **13**, 243–248.

61 A. B. Burg and G. Brendel, *J. Am. Chem. Soc.*, 1958, **80**, 3198–3202.

62 D. J. Grant, M. H. Matus, J. R. Switzer, D. A. Dixon, J. S. Francisco and K. O. Christe, *J. Phys. Chem. A*, 2008, **112**, 3145–3156.

63 F. Seel, K. Rudolph and W. Gombler, *Angew. Chemie Int. Ed.*, 1967, **6**, 7708.

64 V. F. Seel and K. Rudolph, *Zeitschrift fur Anorg. und Allg. Chemie*, 1968, **359**, 233–244.

65 C. Brown, M. Murray and R. Schmutzler, *J. Chem. Soc. C*, 1970, 878–881.

66 L. Riesel, J. Haenel and G. Ohms, *J. Fluor. Chem.*, 1988, **38**, 335–340.

67 R. Schmutzler, O. Stelzer and J. F. Liebman, *J. Fluor. Chem.*, 1984, **25**, 289–299.

68 M. Fild and R. Schmutzler, *J. Chem. Soc. A*, 1970, 2359–2364.

69 M. Fild and R. Schmutzler, *J. Chem. Soc. A*, 1969, 840–848.

70 H. G. Ang and R. Schmutzler, *J. Chem. Soc. A*, 1969, 702–703.

71 J. F. Nixon and M. D. Sexton, *Inorg. Nucl. Chem. Lett.*, 1968, **4**, 275–278.

72 J. F. Nixon and M. D. Sexton, *J. Chem. Soc. A*, 1969, 1089–1091.

73 A. B. Burg and G. B. Street, *Inorg. Chem.*, 1966, **5**, 1532–1537.

74 J. F. Nixon, *J. Chem. Soc. A*, 1967, 1136–1139.

75 R. Schmutzler, *Chem. Ber.*, 1965, **98**, 552–556.

76 V. F. Seel, K. Rudolph and R. Budenz, *Zeitschrift fur Anorg. und Allg. Chemie*, 1965, **341**, 196–202.

77 R. Schmutzler, in *Advances in Chemistry*, ed. D. H. Busch, 1962, pp. 150–160.

78 R. Bartsch, M. Hausard and O. Stelzer, *Chem. Ber.*, 1978, **111**, 1420–1433.

79 F. Seel, K. Ballreich and R. Schmutzler, *Chem. Ber.*, 1961, **94**, 1173–1184.

80 R. M. Lynden-Bell, J. F. Nixon and R. Schmutzler, *J. Chem. Soc. A*, 1970, 565–567.

81 C. G. Barlow and J. F. Nixon, *Inorg. Nucl. Chem. Lett.*, 1966, **2**, 323–328.

82 G. S. Reddy and R. Schmutzler, *Inorg. Chem.*, 1967, **6**, 823–830.

83 M. H. Micoud, J. M. Savariault and P. Cassoux, *Bull. Soc. Chim. Fr.*, 1972, 3774–3782.

84 O. Stelzer and R. Schmutzler, *J. Chem. Soc. A Inorganic, Phys. Theor.*, 1971, 2867–2873.

85 G. V Roschenthaler and R. Schmutzler, *J. Inorg. Nucl. Chem.*, 1976, 17–21.

86 W. S. Sheldrick and O. Stelzer, *J. Chem. Soc. Dalton Trans.*, 1973, 926–929.

87 M. Corosine and F. Crasnier, *J. Mol. Struct.*, 1975, **27**, 105–111.

88 O. Stelzer and R. Schmutzler, *Inorg. Synth.*, 1978, **18**, 173–179.

89 O. Stelzer and E. Unger, *J. Chem. Soc. Dalton Trans.*, 1973, 1783–1788.

90 J. F. Nixon and M. D. Sexton, *J. Chem. Soc. A*, 1970, 321–323.

91 L. Heuer, P. G. Jones and R. Schmutzler, *New J. Chem.*, 1990, **14**, 891.

92 J. Chatt, R. Mason and D. W. Meek, *J. Am. Chem. Soc.*, 1975, **97**, 3826–3827.

93 A. Al-ohaly and J. F. Nixon, *Inorganica Chim. Acta*, 1980, **41**, 105–109.

94 N. A. Jasim, R. N. Perutz, A. C. Whitwood, T. Braun, J. Izundu, B. Neumann, S. Rothfeld and H.-G. Stammler, *Organometallics*, 2004, **23**, 6140–6149.

95 L. Heuer and R. Schmutzler, *J. Fluor. Chem.*, 1988, **39**, 197–216.

96 L. Heuer, U. K. Bode, P. G. Jones and R. Schmutzler, *Zeitschrift fuer Naturforschung, B Chem. Sci.* , 1989, **44**, 1082–1092.

97 J. R. Goerlich, J.-V. Weiss, P. G. Jones and R. Schmutzler, *Phosphorus, Sulfur and Silicon*, 1992, **66**, 223–243.

98 V. Plack, J. R. Goerlich, A. Fischer, H. Thonnessen, P. G. Jones and R. Schmutzler, *Zeitschrift fur Anorg. und Allg. Chemie*, 1995, **621**, 1080–1092.

99 J. Wesemann, P. G. Jones, D. Schomburg, L. Huer and R. Schmutzler, *Chem. Ber.*, 1992, **125**, 2187–2197.

100 L. Heuer, D. Schomburg and R. Schmutzler, *Chem. Ber.*, 1989, **122**, 1473–1476.

101 R. Schmutzler and L. Heuer, *Polyhedron*, 1991, **10**, 2737–2742.

102 L. Heuer, P. C. Jones and R. Schmutzler, *J. Fluor. Chem.*, 1990, **46**, 243–254.

103 T. G. Meyer, P. G. Jones and R. Schmutzler, *Zeitschrift fuer Naturforschung, B Chem. Sci.*, 1993, **48**, 875–885.

104 L. Heuer, M. Sell and R. Schmutzler, *Polyhedron*, 1987, **6**, 1295–1307.

105 M. D. Mikoluk and R. G. Cavell, *Inorg. Chem.*, 1999, **38**, 1971–1981.

106 M. D. Mikoluk, R. Mcdonald and R. G. Cavell, *Inorg. Chem.*, 1999, **38**, 4056–4063.

107 V. L. Capel, K. B. Dillon, A. E. Goeta, J. A. K. Howard, P. K. Monks, M. R. Probert, H. J. Shepherd and N. V Zorina, *Dalton Trans.*, 2011, **40**, 1808–1816.

108 M. Pabel, A. C. Willis and S. B. Wild, *Angew. Chemie*, 1994, **106**, 1971–1973.

109 M. Pabel, A. C. Willis and S. B. Wild, *Inorg. Chem.*, 1996, **35**, 1244–1249.

110 O. Stelzer and E. Unger, *Chem. Ber.*, 1975, 1246–58.

111 C. G. Barlow, J. F. Nixon, J. R. Swain, P. Xi, R. Jefferson, J. F. Nixon and J. R. Swain, *J. Chem. Soc. A*, 1969, 1082–1087.

112 C. G. Barlow, J. F. Nixon and M. Webster, *J. Chem. Soc. A*, 1968, 2216–2223.

113 F. T. Delbeke, E. G. Claeys and G. P. van der Kelen, *J. Organomet. Chem.*, 1970, **25**, 219–222.

114 J. Grobe, D. Le Van and W. Meyring, *Zeitschrift für Anorg. und Allg. Chemie*, 1990, **586**, 149–158.

115 R. C. Dobbie, *J. Chem. Soc. A*, 1971, 230–233.

116 C. A. Udovich, R. J. Clark and H. Haas, *Inorg. Chem.*, 1969, **8**, 1066–1072.

117 C. M. Hoidn, J. Leitl, C. G. P. Ziegler, I. G. Shenderovich and R. Wolf, *Eur. J. Inorg. Chem.*, 2019, **2019**, 1434.

118 W. S. Sheldrick and O. Stelzer, *Chem. Ber.*, 1977, **110**, 3421–3429.

119 F. Delgado Calvo, V. Mirabello, M. Caporali, W. Oberhauser, K. Raltchev, K. Karaghiosoff and M. Peruzzini, *Dalton Trans.*, 2016, **45**, 2284–2293.

120 W.-R. Yao, Z.-H. Liu and Q.-F. Zhang, *Acta Crystallogr. Sect. C*, 2003, **C59**, 156–

158.

121 M. D. Mikoluk, R. Mcdonald and R. G. Cavell, *Organometallics*, 1999, **18**, 3306–3315.

122 L. Heuer and D. Schomburg, *J. Organomet. Chem.*, 1995, **495**, 53–59.

123 R. C. Dobbie and S. Morton, *J. Chem. Soc. Dalton Trans.*, 1976, 1421–1423.

124 D. A. Clement and J. F. Nixon, *J. Chem. Soc. Dalon Trans. Inorg. Chem.*, 1972, **22**, 2553–2557.

125 D. A. Clement, J. F. Nixon and M. D. Sexton, *J. Chem. Soc. Chem. Commun.*, 1969, **24**, 1509–1510.

126 R. Schmutzler, *Chem. Ber.*, 1963, **96**, 2435–2450.

127 R. M. Lynden-Bell, *Mol. Phys.*, 1968, **15**, 523–531.

128 T. Kruck, M. Hofler, H. Jung and H. Blume, *Angew. Chemie Int. Ed.*, 1969, **8**, 522–523.

129 J.-M. Savariault, P. Cassoux and J.-F. Labarre, *J. Chim. Phys. Physico-Chimie Biol.*, 1970, 235–239.

130 J. M. Savariault, P. Cassoux and J. F. Labarre, *Comptes Rendus L'académie des Sci.*, 1969, **269**, 496–498.

131 P. Cassoux, J.-M. Savariault and J.-P. Laurent, *J. Chim. Phys. Physico-Chimie Biol.*, 1970, **67**, 258–261.

132 C. Crocker and R. J. Goodfellow, *J. Chem. Soc. Dalton Trans.*, 1977, 1687–1689.

133 R. M. Matos, R. F. F. Da Costa, V. F. Knupp, J. André, D. Silva and B. F. T. Passos, *J. Braz. Chem. Soc*, 2000, **11**, 311–316.

134 J. Grosse and R. Schmutzler, *J. Chem. Soc. Dalon Trans. Inorg. Chem.*, 1976, **5**, 412–417.

135 J. Grosse and R. Schmutzler, *J. Chem. Soc. Dalon Trans. Inorg. Chem.*, 1976, **5**, 405–412.

136 W. Krüger, M. Sell and R. Schmutzler, *Z. Naturforsch*, 1983, **38**, 1074–1080.

137 C. Crocker and P. L. Goggin, *J. Chem. Res. Synopses*, 1978, 93.

138 R. K. Harris, J. R. Woplin and R. Schmutzler, *Berichte der Bunsengesellschaft für Phys. Chemie*, 1971, **75**, 134–140.

139 A. Blauwitz, R. Gereke, H.-J. Plinta and R. Schmutzler, *Zeitschrift fur Anorg. und Allg. Chemie*, 1997, **623**, 1317–1324.

140 G.-V. Roschenthaler, A. J. Gibson and R. Schmutzler, *Chem. Ber.*, 1977, **110**, 611–618.

141 R. Mathieu and R. Poilblanc, *Inorg. Chem.*, 1972, **11**, 1858–1861.

142 A. N. Nesmeyanov, V. V Krivykh and M. I. Rybinskaya, *Bull. Acad. Sci. USSR*, 1978, 975.

143 A.-N. Nesmeyanox, V. V Krivykh, G. A. Panosyan, P. V Petrovskii and M. I. Rybinskaya, *J. Organomet. Chem.*, 1979, **164**, 167–175.

144 V. V Krivykh, M. V Tolstaya and M. I. Rybinskaya, *Bull. Acad. Sci. USSR*, 1986, 2155–2157.

145 N. I. Vasyukova, Y. S. Nekrasov, V. V Krivykh and M. I. Rybinskaya, *J. Organomet. Chem.*, 1980, **201**, 283–291.

146 M. G. Peterleitner, M. V Tolstaya, V. V Krivykh, L. I. Denisovitch and M. I. Rybinskaya, *J. Organomet. Chem.*, 1983, **254**, 313–315.

147 M. G. Peterleitner, M. V Tolstaya, V. V Krivikh, L. I. Denisovich, M. I. Ribinskaya and D. N. Kravtsov, *Bull. Acad. Sci. USSR*, 1986, 605–610.

148 D. P. Bauer and J. K. Ruff, *Inorg. Chem.*, 1983, **22**, 1686–1689.

149 T. G. Meyer, A. Fischer, P. G. Jones and R. Schmutzler, *Zeitschrift fur Naturforschung, B*, 1993, **48**, 659–71.

150 J. W. Gilje, R. Schmutzler, W. S. Sheldrick and V. Wray, *Polyhedron*, 1983, **2**, 603–606.

151 N. Mathew, B. R. Jagirdar, R. S. Gopalan and G. U. Kulkarni, *Organometallics*, 2000, **19**, 4506–4517.

152 R. J. Clark and K. A. Morgan, *Inorganica Chim. Acta*, 1968, **2**, 93–96.

153 A. Maisonnat, P. Kalck and R. Poilblanc, *Inorg. Chem.*, 1974, **13**, 661–667.

154 P. B. Hitchcock, S. Morton and J. F. Nixon, *J. Chem. Soc. Dalton Trans.*, 1985, 1295–1301.

155 W. A. Slegeir, *World Patent*, 2001, WO 01/51441 A1.

156 T. A. Puckette, *Top. Catal.*, 2012, **55**, 421–425.

157 T. A. Puckette, *Chem. Ind.*, 2007, **115**, 31–38.

158 A. A. Oswald, N. J. Torris, G. Jermasen, A. A. Westner and W. I-der Huang, *US Patent*, 1983, US 4595753.

159 K. Tau, *US Patent*, 1985, US 4605781.

160 A. G. Abatjoglou and D. R. Bryant, *US Patent*, 1988, US 5059710.

161 G. J. Klender, V. J. Gatto, K. R. Jones and C. W. Calhoun, *Polym. Prepr.*, 1993, **24**, 156.

162 G. J. Klender, in *Advances in Chemistry*, ed. R. L. Clough, American Chemical Society, Washington D.C., 1996, pp. 396–423.

163 T. A. Puckette and G. S. Tolleson, *World Patent*, 2003, WO 03/061822 A2.

164 T. A. Puckette, G. S. Tolleson, T. J. Devon and J. Stavinoha, *World Patent*, 2002, WO 02/098825 A2.

165 T. A. Puckette and G. E. Struck, *US Patent*, 1998, US 5840647 A.

166 N. Kaprinidis, G. Chandrika and J. Zingg, *World Patent*, 2004, WO 2004/031286 A1.

167 T. A. Puckette, *US Patent*, 2007, US 7301054 B1.

168 Y.-S. Liu and J. L. Rodgers, *World Patent*, 2009, WO 2009/085160 A1.

169 Y.-S. Liu and J. L. Rodgers, *US Patent*, 2009, US 2009/0171121 A1.

170 T. A. Puckette, *World Patent*, 2010, WO 2010/030339 A1.

171 T. A. Puckette, *US Patent*, 2010, US 2010/0069679 A1.

172 T. A. Puckette, X. Shan, J. Lee Rodgers and B. E. Green, *US Patent*, 2017, US 9550179 B1.

173 T. A. Puckette, S. Xiaopeng, J. L. Rodgers and B. E. Green, *World Patent*, 2017, WO 2017/044277 A1.

174 S.-W. Lo, *Masters Thesis*, 2013, Univeristy of Bristol.

175 T. A. Puckette, *US Patent*, 2013, US 2013/0046112 A1.

176 T. A. Puckette, *World Patent*, 2013, WO 2013/025363 A1.

177 N. Fey, M. Garland, J. P. Hopewell, C. L. McMullin, S. Mastroianni, A. G. Orpen and P. G. Pringle, *Angew. Chemie Int. Ed.*, 2012, **51**, 118–122.

178 S. Mastroianni, P. Pringle, J. Hopewell and M. Garland, *World Patent*, 2013, WO 2013/045524 A1.

179 S. Mastroianni, P. Pringle, J. Hopewell and M. Garland, *French Patent*, 2013, FR 2980792 A1.

180 S. Mastroianni, P. Pringle, M. Garland and J. Hopewell, *World Patent*, 2010, WO 2010/145960 A1.

181 S. Papadouli, *PhD Thesis*, 2015, Univeristy of Bristol.

182 R. B. Trillo, M. Leven, J. M. Neudörfl and B. Goldfuss, *Adv. Synth. Catal.*, 2012, **354**, 1451–1465.

183 E. Brü, J. R.-M. Neudö and B. Goldfuss, *New J. Chem.*, 2019, **43**, 4787–4799.

# Chapter 2

# Synthesis and coordination chemistry of cyclic fluorophosphites

## 2.1 Introduction

Dioxaphosphacyclic ligands are ubiquitous in homogeneous catalysis.[1] Such ligands are entropically stabilised relative to their acyclic analogues containing a $P(OAr)_2$ moiety.[1] Additionally, they are less susceptible to hydrolytic P-O cleavage (Scheme 2.1), which is a valuable property for their application in industrial catalysis.

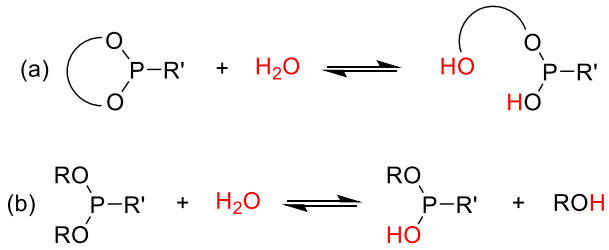


**Scheme 2.1** Hydrolysis of (a) cyclic phosphorus ligands and (b) acyclic $R'P(OAr)_2$ analogues.

In the 1980s and 1990s, cyclic aryl phosphites, such as **2.1**, emerged as important ligands for hydroformylation[2–7] and hydrocyanation.[8–13] Inspired by these discoveries there have been numerous subsequent applications of cyclic aryl phosphites,[14–18] phosphoramidites (R' = N, *e.g.* **2.2**)[19,20] and phosphonites (R' = C, *e.g.* **2.3**)[21–23] in a range of catalyses. With the exception of Ethanox 398™ (**2.4**),[24] there are very few examples of cyclic fluorophosphites (R' = F) as ligands for transition metals (see Section 1.5). Cyclic fluorophosphites can be readily prepared from cyclic chlorophosphites. In general, the cyclic ligands of most interest in the literature contain 7- or 8-membered phosphacycles derived from 2,2'-biphenols.

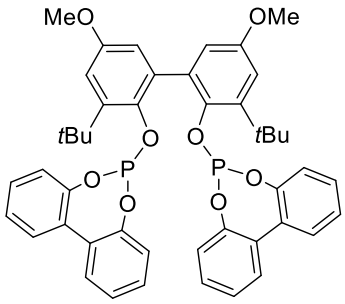


**2.1**

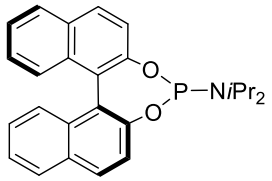


**2.2**

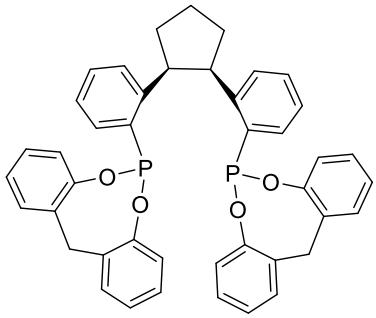


**2.3**

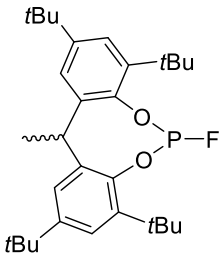


**2.4**
Ethanox 398™

Discovered over 40 years ago, the Tolman electronic parameter (TEP), the ν(CO) for $[Ni(CO)_3(PX_3)]$, remains one of the most commonly used measures of the σ/π -bonding of a phosphorus ligand to a transition metal.[25,26] There is a near-continuum of TEP values between $tBu_3P$ and $P(OPh)_3$, but a near-void between $P(OPh)_3$ and $PF_3$. Consequently, the coordination chemistry of the strong π-acceptors, cyclic fluorophosphites, is of intrinsic interest since their bonding properties should populate this gap. Furthermore, unlike $PF_3$, cyclic fluorophosphites are amenable to modification. As shown for Ethanox 398™ (**2.4**), decoration of the aryl rings with substituents is possible. In addition, the fluorophosphite phosphacycle ring size can be varied. Both of these modifications provide ample opportunity for the stereoelectonics of these ligands to be fine-tuned.

Accordingly, we aimed to synthesise the cyclic fluorophosphites **L**$_{2.1\text{-}2.4}$ containing 5- to 8-membered phosphacycles and probe the effect of ring size on their coordination properties. To gauge the effect of the fluoro substituent, the coordination chemistry of the 6-membered comparator phosphite, **L**$_{2.5}$, was also to be investigated. The limited coordination chemistry of the 5- and 7-membered fluorophosphites, **L**$_{2.1}$ and **L**$_{2.3}$, has been discussed in Section 1.4. The effect of substitution on the aryl rings of the 5- and 6-membered ligands, **L**$_{2.1}$ and **L**$_{2.2}$, was also to be probed.

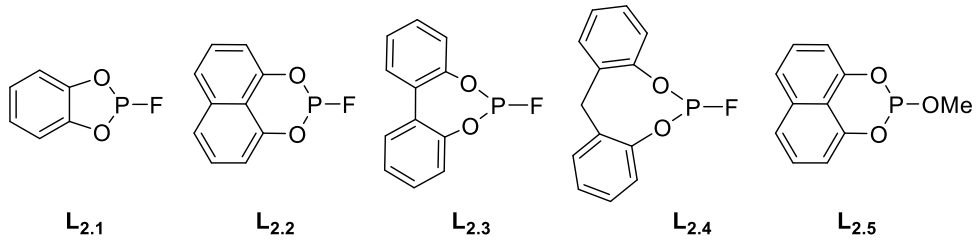


**L**$_{2.1}$ **L**$_{2.2}$ **L**$_{2.3}$ **L**$_{2.4}$ **L**$_{2.5}$

The prediction that there is a correlation between the phosphacycle ring size and the electronics of the ligand can be attributed to the energies of the frontier orbitals.[27–29] The Walsh diagram, shown in Figure 2.1, shows how the energies of the molecular orbitals of a $PX_3$ molecule depend on its geometry.[27,28,30] As the symmetry is lowered from planar ($D_{3h}$) towards trigonal pyramidal ($C_{3v}$), the HOMO (σ) and LUMO (π) orbitals become more bonding and so are lowered in energy ($2a_1$ and $2e$ respectively).[30] Consequently, a more pyramidalised $PX_3$ molecule should be a poorer σ-donor but a stronger π-acceptor. As the phosphacycle ring size of the cyclic fluorophosphites **L**$_{2.1\text{-}2.4}$ decreases (from 8- to 5-membered), the P-centre becomes progressively more pyramidalised and hence the energies of the frontier orbitals will decrease. Therefore, it is predicted that the σ-donor capacity will decrease and the π-acceptor capacity will increase.[30] Pringle *et al.* have previously shown a clear correlation between the phosphacycle ring size (C-P-C angle) and donor properties of a series of cyclic mono- and diphosphines.[29,31]

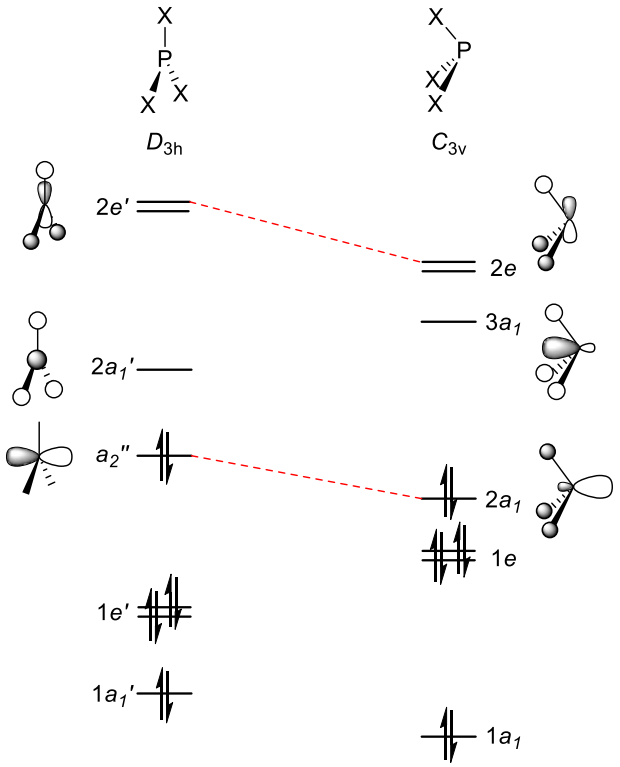


**Figure 2.1** Walsh diagram of a $PX_3$ molecule.[30]

One of the central aims of this part of the project was to determine the veracity of these predicted trends in the metal-binding properties of the cyclic fluorophosphites **L**$_{2.1\text{-}2.4}$. This was to be attempted by preparing a range of coordination complexes of the cyclic fluorophosphites and exploring correlations between ring size and the spectroscopic (IR and NMR) properties or structural features (from X-ray crystallography) of the complexes.

All of the work within this Chapter was performed by the author, with the exception of the initial synthesis of ligand **L**$_{2.3}$ and complexes **2.7c** and **2.8c**, which was carried out by Eliza G. Hunt, a PhD student who worked under the supervision of the author.

## 2.2 Synthesis of cyclic fluorophosphites

### 2.2.1 Synthesis of chlorophosphite intermediates

Cyclic fluorophosphites **L**$_{2.1\text{-}2.4}$ and the comparator phosphite ligand **L**$_{2.5}$ have been prepared from the corresponding cyclic chlorophosphites, **2.5a**-**d**. The chlorophosphite precursors were prepared by the modified literature method (see Chapter 7 for experimental details) of the reaction of the dihydroxyarene with $PCl_3$ in the presence of $NEt_3$ (Scheme 2.2).[1,32–35]

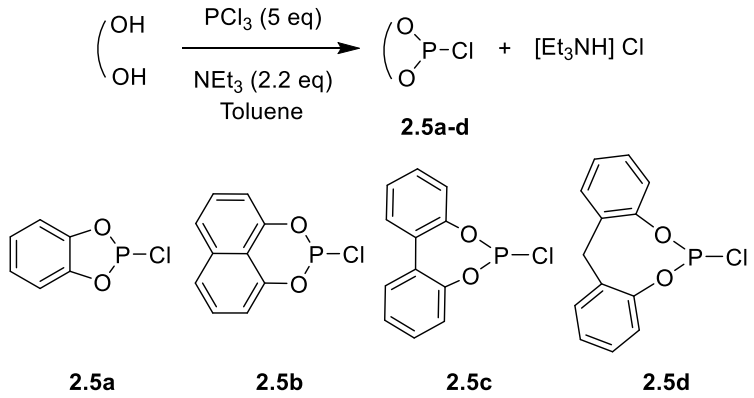


**Scheme 2.2** Modified literature syntheses of chlorophosphites **2.5a**-**d**.

Avoiding the formation of spirophosphorane P(V) by-products (such as **x**) was often challenging using the above method, particularly in the synthesis of the 5-membered **2.5a** (see Chapter 4 for more details). In addition, only 60% conversion of the dichlorophosphorus intermediate, **y**, formed in the synthesis of the 8-membered **2.5d**, was achieved using the above procedure.

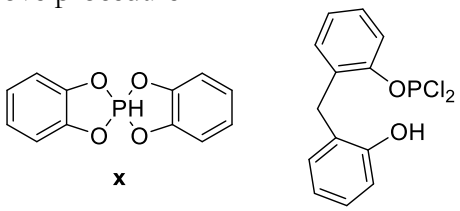


**x** **y**

A novel route to **2.5a**-**d** from the silyl ethers **2.6a**-**d**, which involved a silicon-phosphorus exchange reaction, has been developed (Scheme 2.3). The silyl ethers **2.6a**-**d** were readily prepared from the dihydroxyarene and purified by distillation. All chlorophosphites were obtained in good yields and high purity. This route to chlorophosphites **2.5a**-**d** required 2 steps, but this disadvantage is balanced by the simplicity of the work-up since the $ClSiMe_3$ by-product is volatile. Furthermore, this route overcomes the issues of the formation of spirophosphorane side-products (for **2.5a**) and incomplete conversion (for **2.5d**) encountered in the method described above (Scheme 2.2).

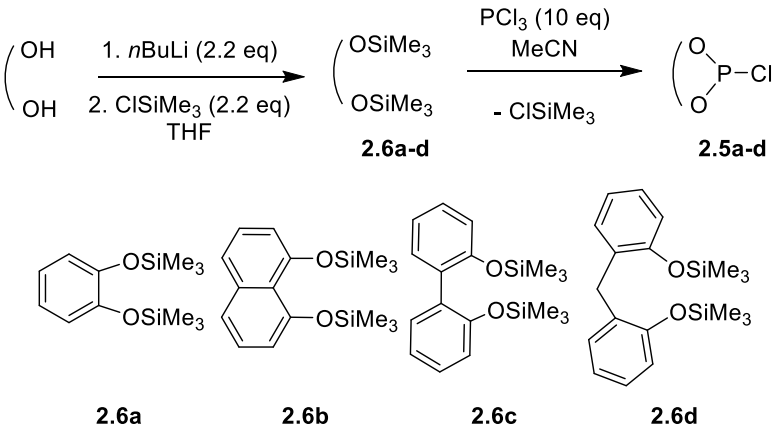


**Scheme 2.3** Route to chlorophosphites **2.5a**-**d** *via* the silyl ethers **2.6a**-**d**. Compounds **2.6a** and **2.6c** have been previously reported.[36,37]

### 2.2.2 Synthesis of fluorophosphites and comparator phosphite

Treatment of chlorophosphites **2.5a**-**d** with 2 equiv. $SbF_3$ (Scheme 2.4) gave the fluorophosphites $\mathbf{L_{2.1\text{-}2.4}}$ in moderate yields (55-73%). All ligands were fully characterised and data for fluorophosphites $\mathbf{L_{2.1}}$[38–40] and $\mathbf{L_{2.3}}$[41] compared to the literature. The $^{31}P\{^1H\}$ and $^{19}F\{^1H\}$ NMR spectra for $\mathbf{L_{2.1\text{-}2.4}}$ each showed a characteristic doublet with large $^1J_{P,F}$ values (1241-1309 Hz). No correlations are apparent between the phosphacycle ring size and the values of $^1J_{P,F}$, $\delta_P$ or $\delta_F$ (Table 2.1).

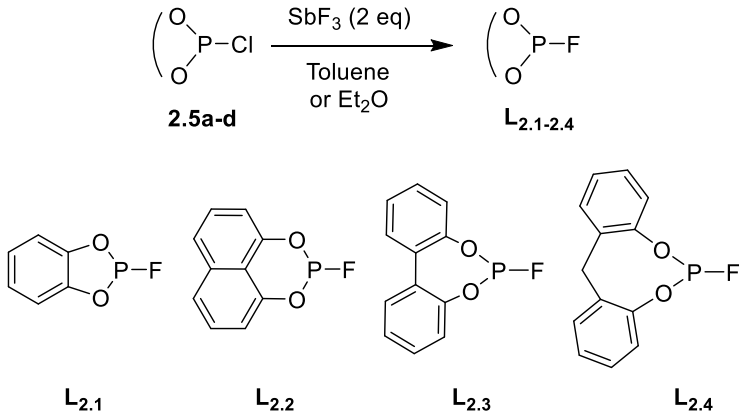


**Scheme 2.4** Synthesis of $\mathbf{L_{2.1\text{-}2.4}}$.

**Table 2.1.** NMR data for fluorophosphites $\mathbf{L_{2.1\text{-}2.4}}$.[a]

| Ligand | $\delta_P$ / ppm | $\delta_F$ / ppm | $^1J_{P,F}$ / Hz |
|---|---|---|---|
| $\mathbf{L_{2.1}}$ | 124.3 | -37.2 | 1306 |
| $\mathbf{L_{2.2}}$ | 100.6 | -52.7 | 1241 |
| $\mathbf{L_{2.3}}$ | 135.8 | -52.4 | 1309 |
| $\mathbf{L_{2.4}}$ | 107.8 | -62.2 | 1254 |

[a] Measured in $C_6D_6$.

Despite using a short silica column to purify ligands $\mathbf{L_{2.2\text{-}2.4}}$, the presence of $SbCl_3$ contaminent was identified based upon the following observations: (a) the reaction of 2 equiv. of $\mathbf{L_{2.2\text{-}2.4}}$ with $[Pt(nbe)_3]$ gave significant amounts (5-25%) of *cis*-$[PtCl_2L_2]$ complexes in addition to the expected Pt(0) species (see Section 2.5); (b) upon the addition of $SbCl_3$ to this reaction mixture an increase in *cis*-$[PtCl_2L_2]$ was observed; (c) the assignment of *cis*-$[PtCl_2L_2]$ complexes was based on the products obtained from the reaction of 2 equiv. of $\mathbf{L_{2.2\text{-}2.4}}$ with $[PtCl_2(cod)]$ (see Section 2.3). The amount of the $SbCl_3$ impurity present was capricious and batch dependent. Passing the ligands through a short florisil column and stirring the ligands with florisil over 2 h usually removed all of the $SbCl_3$. The presence of minor amounts of $SbCl_3$ had no apparent effect on the ligands' coordination chemistry but did affect the ligands' performance in hydroformylation catalysis (see Chapter 3).

Treatment of the chlorophosphite **2.5b** with MeOH in the presence of $NEt_3$ gave the phosphite ligand $\mathbf{L_{2.5}}$ (Scheme 2.5) in a good yield (82%). The $^{31}P$ NMR spectrum was a quartet ($\delta_P$ = 113.9 ppm, $^3J_{P,H}$ = 12 Hz).[42]

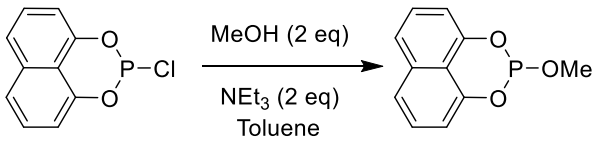


**2.5b** $\mathbf{L_{2.5}}$

**Scheme 2.5** Synthesis of $\mathbf{L_{2.5}}$.

The 5-membered cyclic fluorophosphite $\mathbf{L_{2.1}}$ is highly moisture sensitive, but the P-F bonds in the other fluorophosphacycles $\mathbf{L_{2.2\text{-}2.4}}$ are considerably more resistant to hydrolysis than the P-Cl bond in the corresponding chlorophosphites **2.5a**-**d**. In the

presence of water (0.55 M in MeOH), the approximate times for samples to be 50% hydrolysed were: $\mathbf{L}_{2.1}$ < 2 min; $\mathbf{L}_{2.2}$ 24 h; $\mathbf{L}_{2.3}$ 40 h; $\mathbf{L}_{2.4}$ 2 h.

### 2.3 Synthesis of *cis*-[Mo(CO)$_4$L$_2$] complexes of fluorophosphites

Complexes of the type *cis*-[Mo(CO)$_4$L$_2$] were targeted as a way to compare the stereoelectronic properties of $\mathbf{L}_{2.1\text{-}2.5}$ from their IR spectra and X-ray crystal structures. Ligands $\mathbf{L}_{2.1\text{-}2.5}$ react smoothly with [Mo(CO)$_4$(nbd)] (nbd = norbornadiene) in $CH_2Cl_2$ to give the *cis*-[Mo(CO)$_4$L$_2$] complexes **2.7a**-**e**, where L = $\mathbf{L}_{2.1\text{-}2.5}$ (Scheme 2.6).

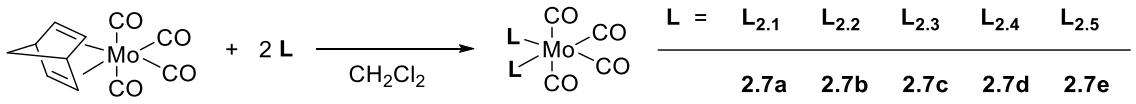


**Scheme 2.6** Synthesis of the *cis*-[Mo(CO)$_4$L$_2$] complexes **2.7a**-**e**.

**Table 2.2** NMR data for complexes **2.7a**-**e**.[a]

| Ligand | Complex | $\delta_P$ / ppm | $^1J_{P,F}$ / Hz[b] | $\Delta\delta$ / ppm |
|---|---|---|---|---|
| $\mathbf{L}_{2.1}$ | **2.7a** | 170.2 | 1318 | 46 |
| $\mathbf{L}_{2.2}$ | **2.7b** | 144.3 | 1248 | 44 |
| $\mathbf{L}_{2.3}$ | **2.7c** | 174.0 | 1229 | 38 |
| $\mathbf{L}_{2.4}$ | **2.7d** | 148.2 | 1204 | 41 |
| $\mathbf{L}_{2.5}$ | **2.7e** | 151.1 | - | 37 |

[a] Measured in $CD_2Cl_2$. [b] Calculated from $N = |^1J_{P,F} + {}^3J_{P,F}|$.

The $^{31}P\{^1H\}$ and $^{19}F\{^1H\}$ NMR spectra for complexes **2.7a**-**d** showed a doublet of triplets which is a deceptively simple pattern for the AA'XX' spin system; the separation of the doublet (corresponding to $N = |^1J_{P,F} + {}^3J_{P,F}|$) is of the order of 1200 Hz in each case. The NMR spectra were simulated using the calculated coupling constants given in Chapter 7. Figure 2.2 shows an example of the excellent agreement between the (a) observed and (b) simulated $^{31}P\{^1H\}$ NMR spectra (complex **2.7a**). Values computed for $^2J_{P,P}$ are of the order of 50 Hz; consistent with a *cis*-geometry.[43] The coordination chemical shift $\Delta\delta$ for $\mathbf{L}_{2.1\text{-}2.4}$ in **2.7a**-**d** is *ca.* +40 ppm which is similar to that for $\mathbf{L}_{2.5}$ in **2.7e**. There do not appear to be consistent correlations between the NMR data for **2.7a**-**d** and the ring size of the fluorophosphites $\mathbf{L}_{2.1\text{-}2.4}$ (Table 2.2).

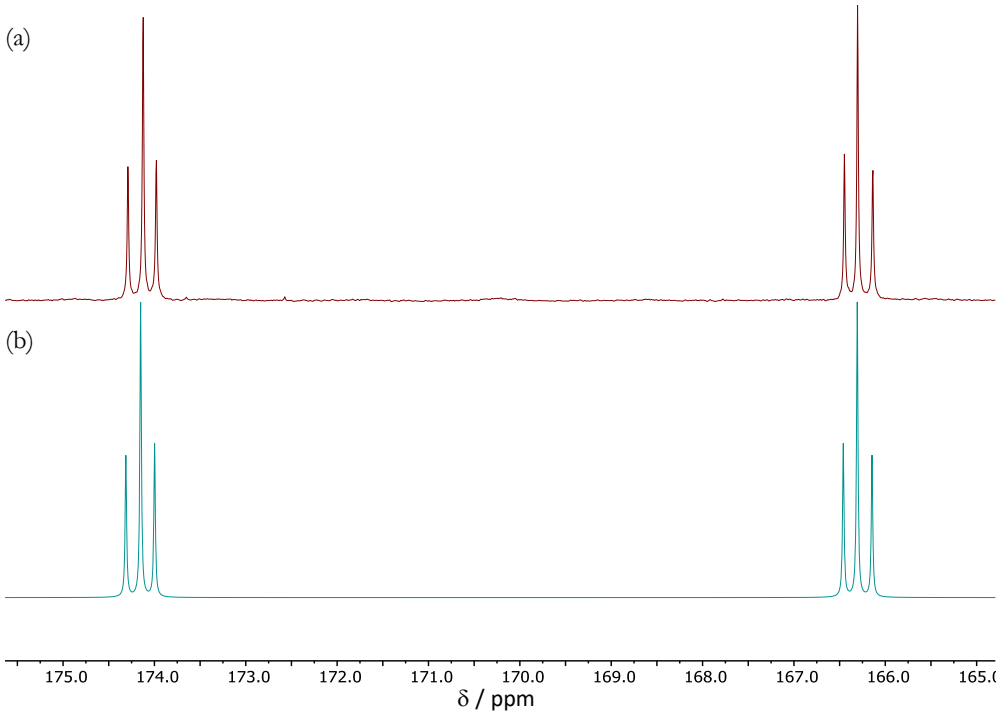


**Figure 2.2** (a) Observed $^{31}P\{^{1}H\}$ NMR spectrum of complex **2.7a**; (b) simulated $^{31}P\{^{1}H\}$ NMR spectrum of complex **2.7a** using calculated coupling constants given in Chapter 7.

The IR spectra for complexes **2.7a**-**e** are consistent with a *cis*-geometry of ligands. The ν(CO) ($A_1$) values for $[Mo(CO)_4L_2]$ can be used as a proxy for the TEP since they are linearly related.[44] From the values illustrated in Figure 2.3 and IR data given in Chapter 7, the fluorophosphites $\mathbf{L_{2.1\text{-}2.4}}$ sit between $PF_3$ and $P(OPh)_3$ in terms of their TEP, with the smallest phosphacycle $\mathbf{L_{2.1}}$ being closest to $PF_3$. This is consistent with the reported correlation between the ligand ring size and energies of the frontier orbitals: the smaller the O–P–O angle, the lower lying the HOMO and LUMO energies (see Section 2.1).[27–29] The ν(CO) values for the complexes **2.7b** and **2.7e** featuring the six-membered phosphacycles $\mathbf{L_{2.2}}$ and $\mathbf{L_{2.5}}$ (2066 and 2051 $cm^{-1}$ respectively) reflect the significant difference between the ligands having P– F and P–OMe fragments.

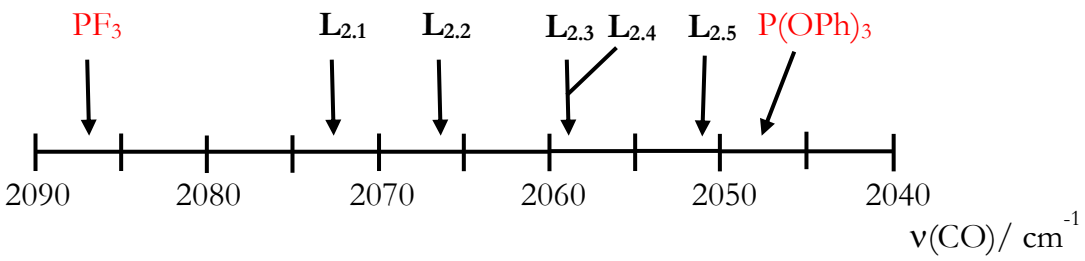


**Figure 2.3** ν(CO) bands for **2.7a**-**e** (see Chapter 7 for values).[45,46]

Crystals suitable for X-ray crystallography of each of complexes **2.7a**-**e** were grown by slow diffusion of hexane into a saturated $CH_2Cl_2$ solution of the complex or by storing a saturated hexane solution of the complex at -20 °C; selected metrical data are given in Table 2.3. In each case, the crystal structures confirmed the *cis*-geometry of the complexes (Figure 2.4). The Mo-P bond lengths decrease in the order **2.7d** > **2.7c** > **2.7b** > **2.7a**, consistent with increasing Mo–P bond strength as the phosphacycle ring size decreases as a result of the π-acceptor capacity increasing in the order $\mathbf{L_{2.1}} > \mathbf{L_{2.2}} > \mathbf{L_{2.3}} > \mathbf{L_{2.4}}$. The Mo-P π-bonding should perturb the bond lengths and angles around the P atom[27–29] but these effects may be very subtle since no trends in P-O/P-F bond lengths or O-P-F angles are evident in the crystallographic data. The Mo-P bond length in complex **2.7b** is considerably shorter than in **2.7e**, consistent with the fluorophosphite $\mathbf{L_{2.2}}$ having a greater π-acceptor capacity than its phosphite analogue, $\mathbf{L_{2.5}}$. The fluorophosphite ligands adopt a *syn*-conformation in complexes **2.7a** and **2.7c** and an *anti*-conformation in complexes **2.7b** and **2.7d** (Figure 2.4), which may be indicative of *syn*- and *anti*-conformers being close in energy.

The steric properties of the P-ligands in **2.7a**-**e** were assessed using the solid angles approach[47] for the ligands calculated from the crystal structures, with the G parameter ($G^x$) representing the area of the metal centre shielded by the ligand. Interpretation of the $G^x$ values given in Table 2.3 is complicated by there being two values for $\mathbf{L_{2.3}}$ in **2.7c** and for $\mathbf{L_{2.4}}$ in **2.7d.** This arises because the coordinated ligands adopt different geometries, and hence there are two unique P environments in the crystallographic asymmetric unit. Nevertheless, the data suggest that in the Mo structures of **2.7a**-**e**, $\mathbf{L_{2.1}}/\mathbf{L_{2.2}}$ have similar bulk, as do $\mathbf{L_{2.3}}/\mathbf{L_{2.4}}$ and that $\mathbf{L_{2.1}}/\mathbf{L_{2.2}}$ are smaller than $\mathbf{L_{2.3}}/\mathbf{L_{2.4}}$; the phosphite $\mathbf{L_{2.5}}$ is larger than its fluorophosphite analogue $\mathbf{L_{2.2}}$.

**Table 2.3** Selected bond lengths (Å) from the molecular structures of complexes **2.7a-e**.

| Ligand | Complex | Mo-P / Å | P-F / Å | Mo-C / Å[a] | G[x] [b] (%) |
|---|---|---|---|---|---|
| $L_{2.1}$ | **2.7a** | 2.3794(4) | 1.5735(10) | 2.0330(17) | 17.5 |
| $L_{2.2}$ | **2.7b** | 2.3846(6) | 1.5832(13) | 2.042(2) | 17.3 |
| $L_{2.3}$ | **2.7c** | 2.3891(4) | 1.5744(10) | 2.0532(16) | 20.3 |
| | | | | 2.0466(16) | 21.0 |
| $L_{2.4}$ | **2.7d** | 2.4037(6) | 1.5758(14) | 2.015(3) | 17.8 |
| | | | | 2.032(2) | 23.4 |
| $L_{2.5}$ | **2.7e** | 2.4270(4) | - | 2.0165(18) | 18.5 |
| | | 2.4163(4) | | 2.0258(17) | 20.0 |

[a] Mo-C bond length *trans* to P. [b] The G[x] areas were calculated using the following van der Waals radii (Å): C 1.7, H 1.09, F 1.47, Mo 2, O 1.52 and P 1.8.

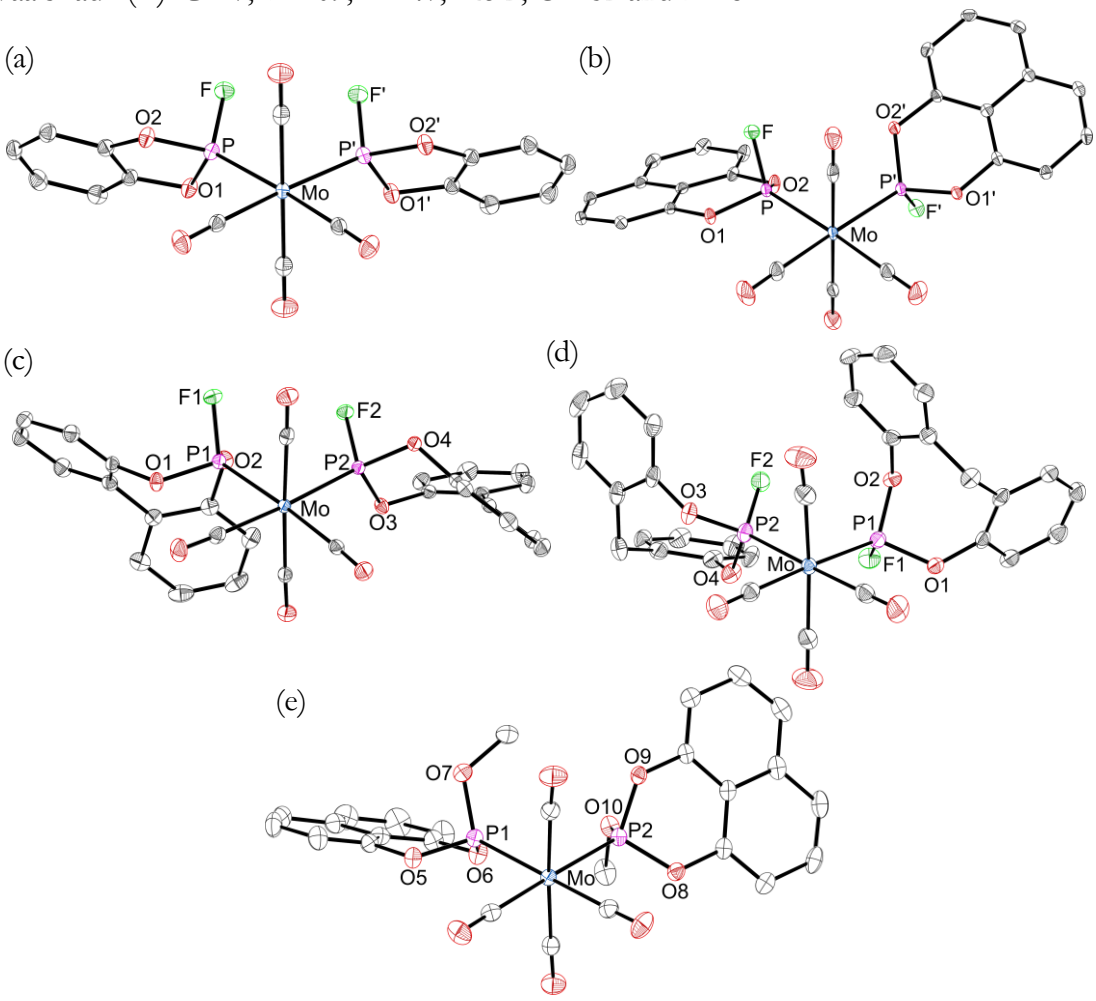


**Figure 2.4** Crystal structures of *cis*-[Mo(CO)$_4$L$_2$] complexes: (a) L = $L_{2.1}$ (**2.7a**); (b) L = $L_{2.2}$ (**2.7b**); (c) L = $L_{2.3}$ (**2.7c**); (d) L = $L_{2.4}$ (**2.7d**); (e) L = $L_{2.5}$ (**2.7e**). The hydrogen atoms are omitted for clarity. Thermal ellipsoids at 50% probability. See Table 2.3 for selected bond lengths. See Appendix for experimental details.

## 2.4 Platinum(II) coordination of cyclic fluorophosphites

The reaction of 2 equiv. of ligands $\mathbf{L_{2.2\text{-}2.5}}$ with $[PtCl_2(cod)]$ (cod = 1,5-cyclooctadiene) in $CH_2Cl_2$ gave the *cis*-$[PtCl_2L_2]$ complexes **2.8b-e**, where L = $\mathbf{L_{2.2\text{-}2.5}}$ (Scheme 2.7). The $^{31}P\{^1H\}$ and $^{19}F\{^1H\}$ NMR spectra for each fluorophosphite complex (**2.8b-d**) showed a characteristic AA'XX' pattern.

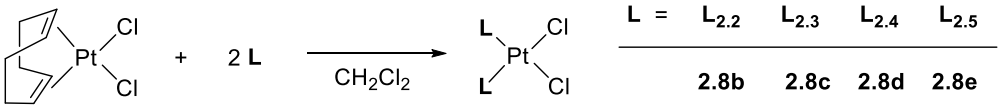


**Scheme 2.7** Synthesis of the *cis*-$[PtCl_2L_2]$ complexes **2.8b-e**.

**Table 2.4** NMR data for complexes **2.8b-e**.[a]

| Ligand | Complex | $\delta_P$ / ppm | $^1J_{P,Pt}$ / Hz | $^1J_{P,F}$ / Hz[b] |
|---|---|---|---|---|
| **$PF_3$** | *cis*-$[PtCl_2(PF_3)_2]$[48] | 65.6 | 6479 | 1318 |
| **$L_{2.2}$** | **2.8b** | 63.6 | 6172 | 1248 |
| **$L_{2.3}$** | **2.8c** | 80.8 | 6056 | 1229 |
| **$L_{2.4}$** | **2.8d** | 58.2 | 6209 | 1204 |
| **$L_{2.5}$** | **2.8e** | 62.7 | 5869 | - |

[a] Measured in $CD_2Cl_2$. [b] Calculated from $N = |^1J_{P,F} + {}^3J_{P,F}|$.

The $^{31}P\{^1H\}$ and $^{19}F\{^1H\}$ NMR spectra of complexes **2.8b-d** were simulated using the calculated coupling constants given in Chapter 7. Figure 2.5 shows an example of the excellent agreement between the (a) observed and (b) simulated $^{31}P\{^1H\}$ NMR spectra (complex **2.8b**). Values calculated for $^2J_{P,P}$ are of the order of 25 Hz consistent with a *cis*-geometry.[49] The large $^1J_{P,Pt}$ values are also indicative of a *cis*-geometry. There is no consistent correlation between the $^1J_{P,Pt}$ values for **2.8b-d** and the ring size of $\mathbf{L_{2.2\text{-}2.4}}$. However, the $^1J_{P,Pt}$ values for fluorophosphites $\mathbf{L_{2.2\text{-}2.4}}$ in **2.8b-d** sit between $PF_3$ in *cis*-$[PtCl_2(PF_3)_2]$[48] and phosphite $\mathbf{L_{2.5}}$ in **2.8e** (Table 2.4). This is consistent with the relationship between π-acceptor capacity and Pt-P bond strength: the stronger the π-acceptor capacity of the ligand, the stronger the Pt-P bond leading to a higher $^1J_{P,Pt}$ value. The trend in $^1J_{P,F}$ values or $\Delta J_{P,F(complex-ligand)}$ for $PF_3$ and fluorophosphites $\mathbf{L_{2.2\text{-}2.4}}$ in *cis*-$[PtCl_2(PF_3)_2]$ and **2.8b-d** respectively do not reflect this. The coordination chemical shift Δδ for $\mathbf{L_{2.2\text{-}2.4}}$ in **2.8b-d** ranges from -37 to -55 ppm similar to that for $\mathbf{L_{2.5}}$ in **2.8e**.

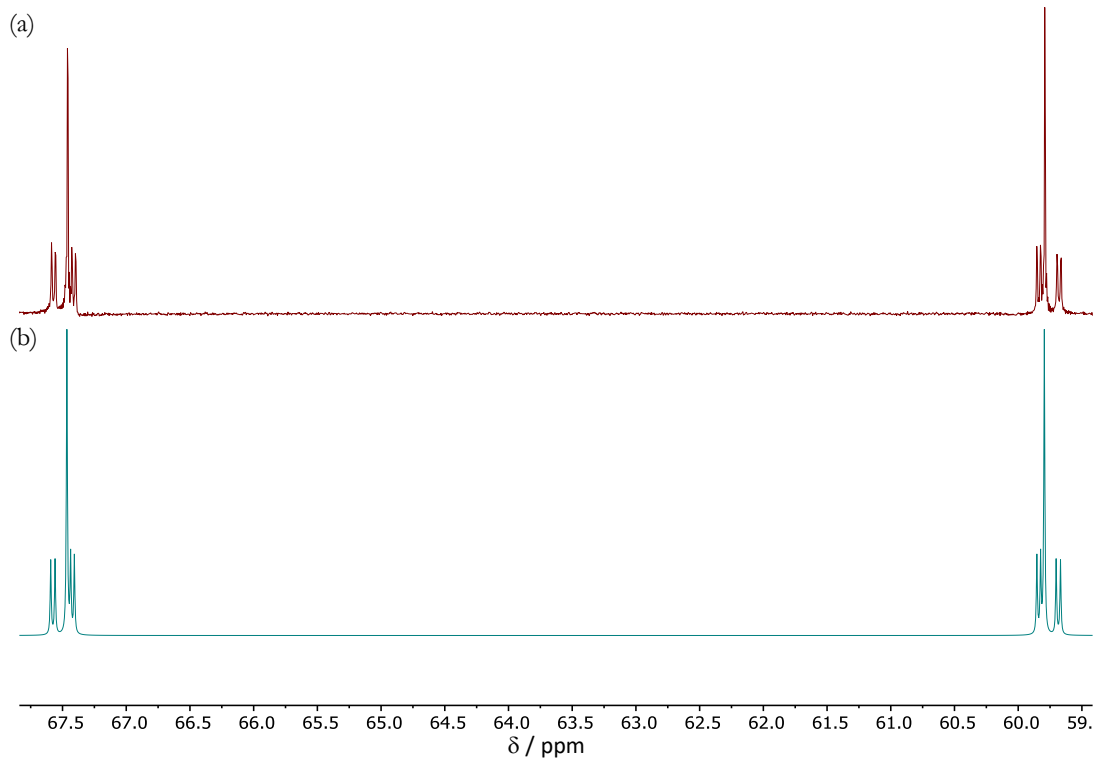


**Figure 2.5** (a) Observed $^{31}P\{^{1}H\}$ NMR spectrum of complex **2.8b**; (b) simulated $^{31}P\{^{1}H\}$ NMR spectrum of complex **2.8b** using calculated coupling constants given in Chapter 7. $^{195}Pt$ satellite signals have been omitted for clarity.

Crystals suitable for X-ray crystallography of complexes **2.8c** and **2.8e** were grown by slow diffusion of hexane or pentane respectively into a saturated $CH_2Cl_2$ solution of the complex. In both cases, the crystal structures confirmed the *cis*-geometry of the complexes and showed the ligands are arranged in a square planar geometry about the Pt centre (Figures 2.6 – 2.7). The fluorophosphite ligands adopt an *anti*-conformation in complex **2.8c**. Whereas, the phosphite ligands adopt a *syn*-conformation in complex **2.8e**. There is no consistent correlation between the Pt-P bond lengths and electronic properties of ligands $\mathbf{L}_{2.3}$ and $\mathbf{L}_{2.5}$.

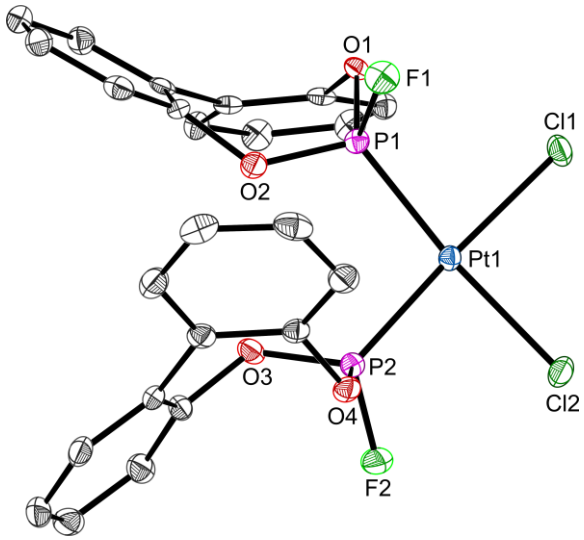


**Figure 2.6** Crystal structure of **2.8c**. The hydrogen atoms are omitted for clarity. Thermal ellipsoids at 50% probability. Selected bond lengths (Å) and angles (°): P1-F1 1.540(2), P2-F2 1.545(2), Pt1-P1 2.1938(9), Pt1-P2 2.1889(9), P1-Pt1-P2 98.14(3), Cl1-Pt1-Cl2 90.16(3), O1-P1-O2 105.17(13), O4-P2-O5 105.70(14). See Appendix for experimental details.

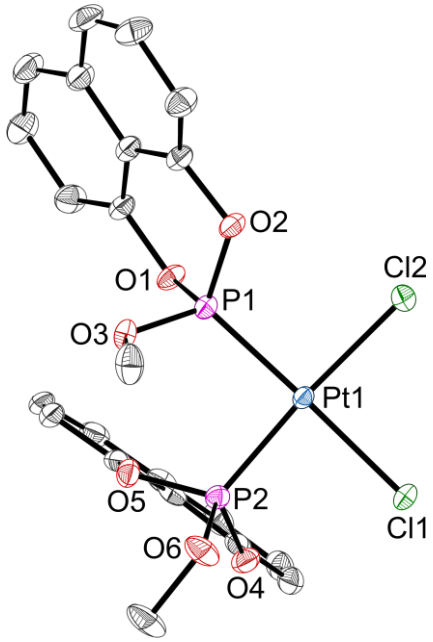


**Figure 2.7** Crystal structure of **2.8e**. The hydrogen atoms are omitted for clarity. Thermal ellipsoids at 50% probability. Selected bond lengths (Å) and angles (°): P1-O3 1.5754(18), P2-O6 1.5562(18), Pt1-P1 2.1949(6), Pt1-P2 2.1993(6), P1-Pt1-P2 93.24(2), Cl1-Pt1-Cl2 89.69(2), O1-P1-O2 104.53(9), O4-P2-O5 101.95(9). See Appendix for experimental details.

Relative to ligands **L2.2-2.4**, the P-F bond of the 5-membered fluorophosphite **L2.1** was kinetically labile upon reaction with [$PtCl_2$(cod)]. However, the reaction of 2 equiv. of **L2.1** with [$PtMe_2$(cod)] in $d_8$-toluene gave *cis*-[$PtMe_2$(**L2.1**)$_2$] (**2.9a**) (Scheme 2.8). A characteristic AA'XX' pattern was observed in the $^{31}P\{^1H\}$ and $^{19}F\{^1H\}$ NMR spectra; the calculated NMR data is given in Chapter 7.

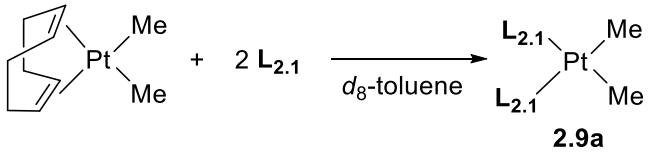


**2.9a**

**Scheme 2.8** Synthesis of *cis*-[$PtMe_2$(**L2.1**)$_2$] complex **2.9a**.

The $^1J_{P,Pt}$ value of 3070 Hz for complex **2.9a**, indicative of a *cis*-geometry, is considerably smaller than that of the *cis*-[$PtCl_2L_2$] complexes (**2.8b**-**e**); this can be attributed to the high *trans*-influence of $Me^-$ ligands relative to $Cl^-$.[50] The $^1J_{P,Pt}$ value of 3070 Hz for complex **2.9a** is smaller than that of the strongly electron withdrawing $PF_3$ in *cis*-[$PtMe_2(PF_3)_2$] ($^1J_{P,Pt}$ = 3300 Hz).[50,51] This is as expected since $PF_3$ is a stronger π-acceptor than **L2.1**, resulting in a stronger Pt-P bond and a higher $^1J_{P,Pt}$ value. The coordination chemical shift Δδ for **L2.1** in **2.9a** and $PF_3$ in *cis*-[$PtMe_2(PF_3)_2$] is *ca.* +20 ppm.[51]

## 2.5 Platinum(0) coordination of cyclic fluorophosphites

The reaction of 4 equiv. of ligands **L2.1-2.5** with [$Pt(nbe)_3$] (nbe = norbornene) in THF gave the 4-coordinate, 18-electron complexes, [$PtL_4$] (**2.10a**-**e**), where L = **L2.1-2.5** (Scheme 2.9). The $^{195}Pt\{^1H\}$ NMR spectra for each fluorophosphite complex showed a binomial quintet of quintets. Goodfellow *et al.* have previously synthesised complex **2.10a** from [$Pt(cod)_2$] and **L2.1**.[52] Complicated AA'$_3$XX'$_3$ patterns for the $^{31}P\{^1H\}$ and $^{19}F\{^1H\}$ NMR spectra were obtained for each of the [$PtL_4$] complexes **2.10a,c,d** (see Figure 2.8 for the NMR spectra of **2.10c**). The $^1J_{P,Pt}$ values increase in the order **2.10a** > **2.10c** > **2.10d** > **2.10e** (Table 2.5), consistent with increasing Pt-P bond strength as a result of the π-acceptor capacity increasing in the order **L2.1** > **L2.3** > **L2.4** > **L2.5**, as shown from the *cis*-[$Mo(CO)_4L_2$] complexes (Section 2.3).

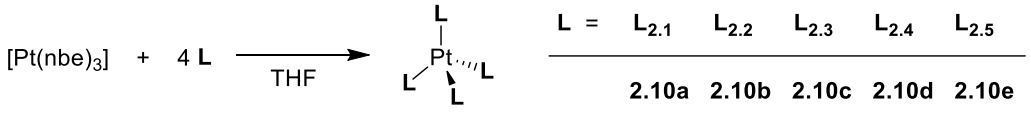


**Scheme 2.9** Synthesis of the [$PtL_4$] complexes **2.10a**-**e**.

**Table 2.5** NMR data for complexes **2.10a**,**c**-**e**.[a]

| Ligand | Complex | $\delta_P$ / ppm | $^1J_{P,Pt}$ / Hz |
|---|---|---|---|
| $\mathbf{L_{2.1}}$ | **2.10a** | 118.0 | 6102 |
| $\mathbf{L_{2.3}}$ | **2.10c** | 127.1 | 6000 |
| $\mathbf{L_{2.4}}$ | **2.10d** | 155.6 | 5981 |
| $\mathbf{L_{2.5}}$ | **2.10e** | 110.1 | 5745 |

[a] Measured in $d_8$-THF.

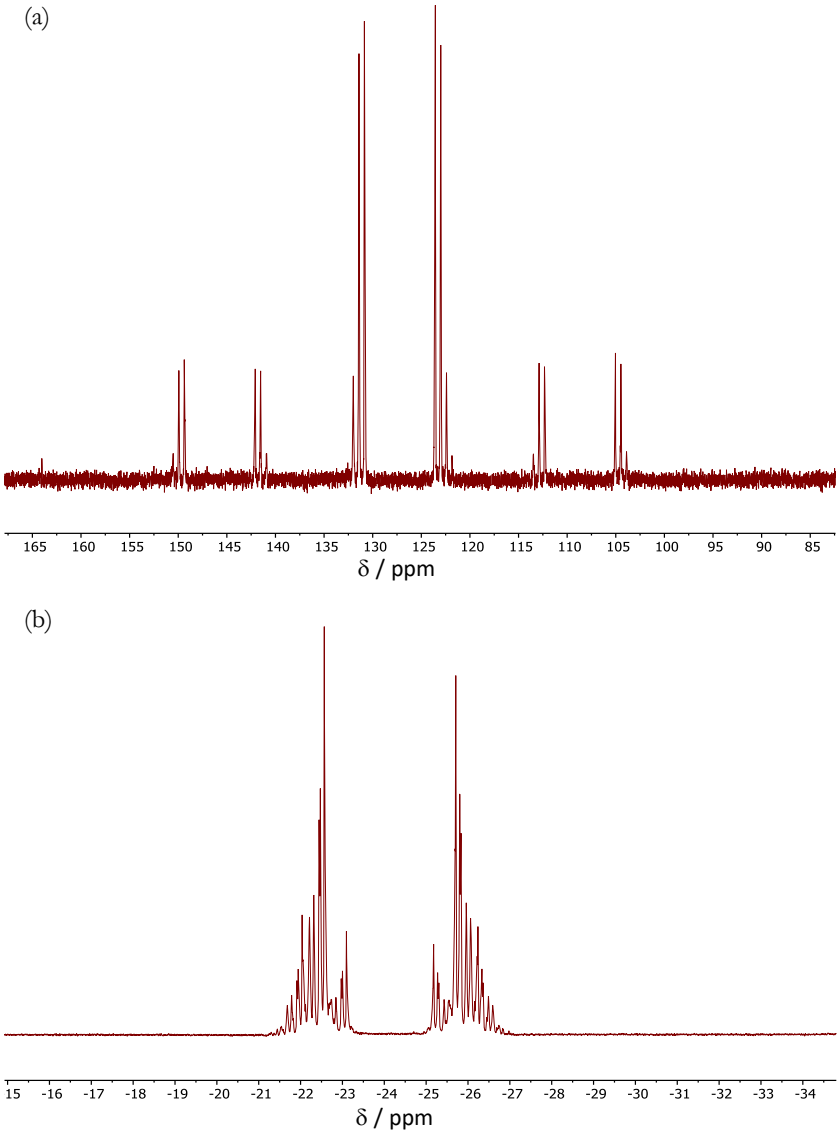

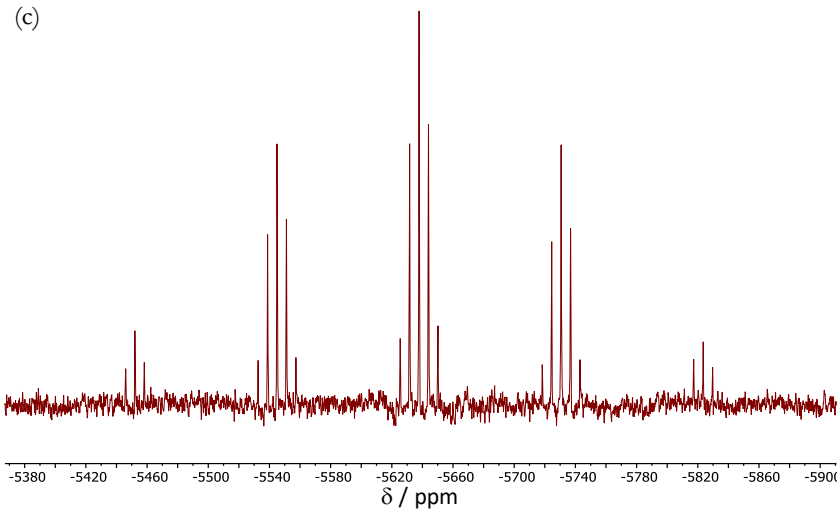


**Figure 2.8** NMR spectra of [Pt($\mathbf{L}_{2.3}$)$_4$] (**2.10c**) in *d*$_8$-THF. (a) $^{31}$P{$^1$H}; (b) $^{19}$F{$^1$H}; (c) $^{195}$Pt{$^1$H}.

The complex [Pt($\mathbf{L}_{2.2}$)$_4$] (**2.10b**) is insoluble in all common organic solvents and so we were unable to characterise it by NMR spectroscopy. However, crystals of **2.10b** suitable for X-ray crystallography were obtained by the slow diffusion of layered chlorobenzene solutions of [Pt(nbe)$_3$] and $\mathbf{L}_{2.2}$ into each other. The crystal structure (Figure 2.9) confirmed the coordination of four ligands to the Pt(0) in an approximately tetrahedral arrangement. There are multiple, intermolecular π...π and C-H....π interactions between the aryl rings of the ligands detected in the solid state producing an extended structure (Figure 2.9b); these intermolecular interactions may explain the lack of solubility of **2.10b**. Crystals of the analogous phosphite complex, [Pt($\mathbf{L}_{2.5}$)$_4$] (**2.10e**), suitable for X-ray crystallography were obtained by slow diffusion of hexane into a saturated THF solution of the complex (Figure 2.10). In contrast to its fluorophosphite analogue, complex **2.10e** is soluble in all common organic solvents, in accord its crystal structure shows no intermolecular π...π and C-H....π interactions. The Pt-P bond length in complex **2.10b** is only slightly shorter (*ca.* 0.08Å) than in its phosphite analogue **2.10e**, despite $\mathbf{L}_{2.2}$ having a significantly greater π-acceptor capacity than $\mathbf{L}_{2.5}$.

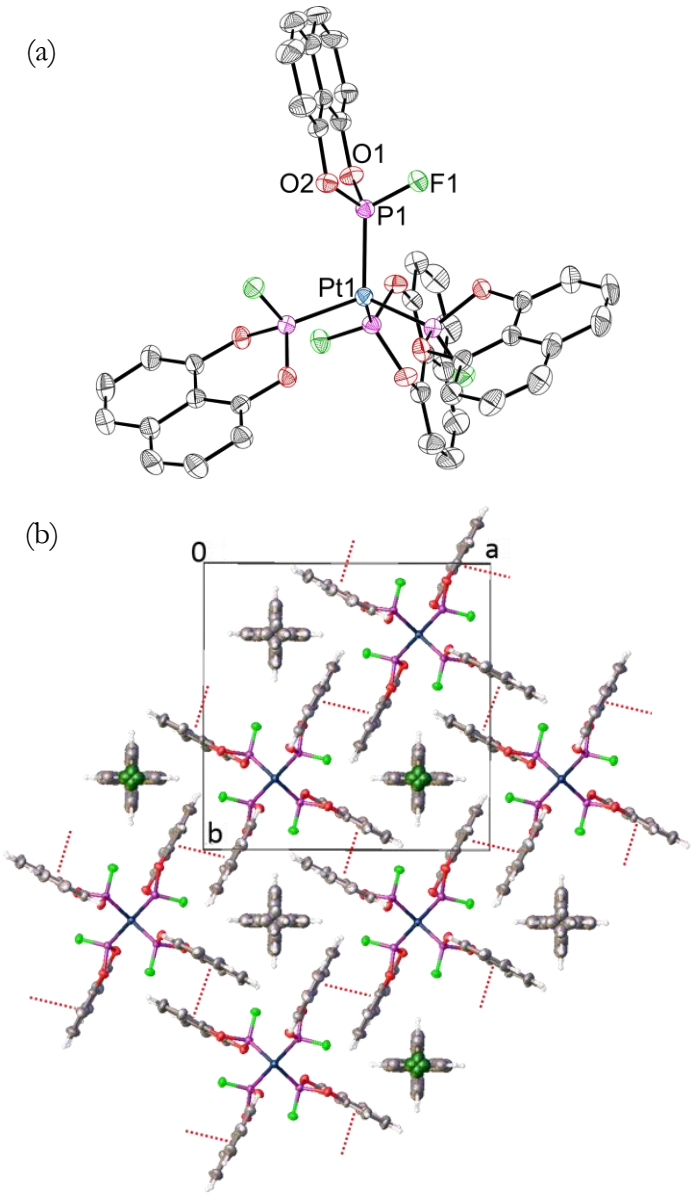


**Figure 2.9** Crystal structure of [Pt(**L**$_{2.2}$)$_4$].$C_6H_5Cl$. Thermal ellipsoids at 50% probability. (a) Molecular structure of **2.10b** ($C_6H_5Cl$ solvate molecules and hydrogens are omitted for clarity). Selected bond lengths (Å) and angles (°): P1-F1 1.575(3), Pt1-P1 2.2303(12), P1-Pt1-P1(-0.5+*y*, 1-*x*, -*z*) 107.61(3), O1-P1-O2 102.61(18). (b) Extended structure highlighting the intermolecular π...π interactions indicated by red dashed lines. The π...π interaction distances are 3.964 Å with a shift of 2.07 Å. Weak C-H-π interactions with C-H-plane ~2.87 Å (or H-centroid distance of 3.03 Å), plane centroid-H-C angle 157° are also present but these are not highlighted. See Appendix for experimental details.

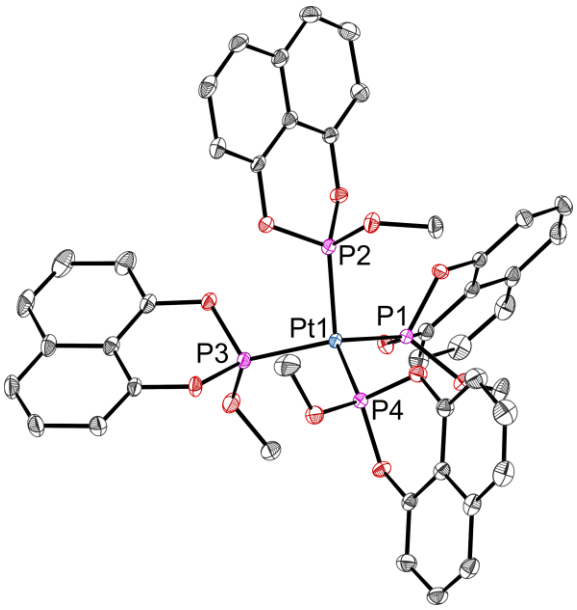


**Figure 2.10** Crystal structure of **2.10e**. The hydrogen atoms are omitted for clarity. Thermal ellipsoids at 50% probability. Selected bond lengths (Å) and angles (°): P1-O3 1.6089(13), Pt1-P1 2.2284(5), P1-Pt1-P2 104.822(17), O1-P1-O2 10.86(7). See Appendix for experimental details.

The formation of the 18-electron [PtL$_4$] complex is common to L = PF$_3$, the fluorophosphites **L**$_{2.1\text{-}2.4}$, phosphite **L**$_{2.5}$ and P(OPh)$_3$.[53] In contrast, upon the reaction of 4 equiv. of Ethanox 398$^{TM}$ (**2.4**, Section 2.1) with [Pt(nbe)$_3$] no [PtL$_4$] complex was observed. The reaction mixture contained [Pt(**2.4**)$_3$] (**2.11f**) (60%, identified by the quartet of quartets for its $^{195}$Pt{$^1$H} NMR signal), [Pt(**2.4**)$_2$(nbe)] (**2.12f**) (10%, identified by the triplet of triplets for its $^{195}$Pt{$^1$H} NMR signal) and the two isomers of free ligand **2.4** in a 2:1 ratio (30%) (Scheme 2.10). The difference in reactivity between **L**$_{2.4}$ and **2.4** with [Pt(nbe)$_3$] can be attributed to the greater steric bulk of Ethanox 398$^{TM}$ (**2.4**).

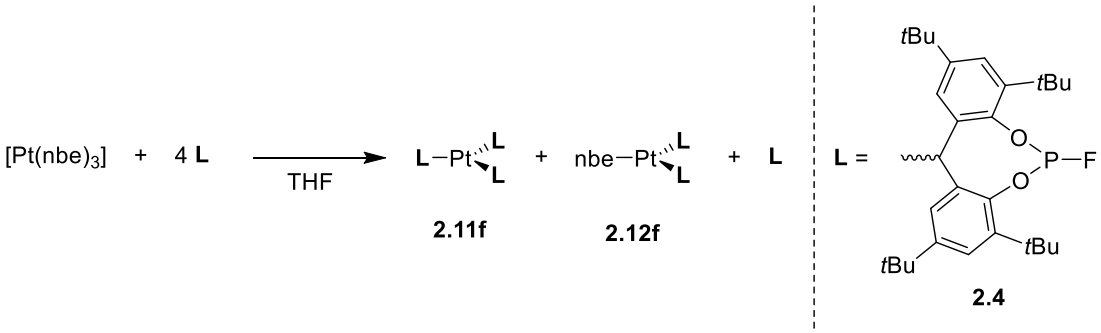


**Scheme 2.10** Reaction of 4 equiv. **2.4** with [Pt(nbe)$_3$].

Differences emerged between the fluorophosphites **L**$_{2.1\text{-}2.4}$ in the reaction of [Pt(nbe)$_3$] with 2 equiv. of **L**$_{2.1\text{-}2.4}$. The expectation was that [PtL$_2$(nbe)] (L = **L**$_{2.1\text{-}2.4}$) would be the products but instead, the equilibria shown in Scheme 2.11 involving Pt(0) species **2.10**-

**2.13** were observed. Structures **2.10**-**2.13** have been assigned on the basis of the characteristic splitting patterns present in the $^{31}P\{^{1}H\}$ NMR spectra and the multiplicity of the $^{195}Pt\{^{1}H\}$ NMR signals (see Chapter 7 for the data). Despite the stability of the three-coordinate [Pt(**2.4**)$_3$] complex (**2.11f**) above, the [PtL$_3$] species **2.11a**-**d** were not detected but are presumably intermediates that are unstable with respect to **2.10a**-**d** and **2.12a**-**d**. Addition of 2 equiv. of **L**$_{2.1}$ to [Pt(nbe)$_3$] gave a mixture of **2.10a** (identified as above), **2.12a** (identified by the AA'XX' pattern for its $^{31}P\{^{1}H\}$ NMR signal and the triplet of triplets for its $^{195}Pt\{^{1}H\}$ NMR signal), **2.13a** (identified by the doublet for its $^{31}P\{^{1}H\}$ NMR signal and doublet of doublets for its $^{195}Pt\{^{1}H\}$ NMR signal). Addition of 2 equiv. of **L**$_{2.2}$ to [Pt(nbe)$_3$] gave an insoluble white precipitate assumed to be **2.10b** (see above) and in the filtrate **2.12b** and **2.13b** were both identified by $^{31}P\{^{1}H\}$ and $^{195}Pt\{^{1}H\}$ NMR spectroscopy. Addition of 2 equiv. of **L**$_{2.3}$ to [Pt(nbe)$_3$] initially gave [PtL$_4$] (**2.10c**) which, over the next 2 h, equilibrated to a mixture of **2.10c**, **2.12c** and **2.13c**. Addition of 2 equiv. of **L**$_{2.4}$ to [Pt(nbe)$_3$] initially gave [PtL$_4$] (**2.10d**) which then converted to predominantly **2.12d** (see Figure 2.11). Addition of 2 equiv. of **2.4** to [Pt(nbe)$_3$] gave three isomers of [PtL$_2$(nbe)] (**2.12f**) in approximately a 1:12:2 ratio. The proportions of the species obtained at equilibrium are given in Scheme 2.11.

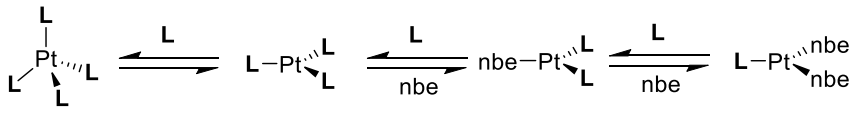


**2.10a-f** **2.11a-f** **2.12a-f** **2.13a-f**

| | | | | |
|---|---|---|---|---|
| L = **L**$_{2.1}$ | 77% | - | 16% | 7% |
| L = **L**$_{2.3}$ | 40% | - | 44% | 16% |
| L = **L**$_{2.4}$ | 6% | - | 91% | 3% |
| L = **2.4** | - | - | 100% | - |

**Scheme 2.11** Proportions of the species observed at equilibrium upon reaction of 2 equiv. L with [Pt(nbe)$_3$].

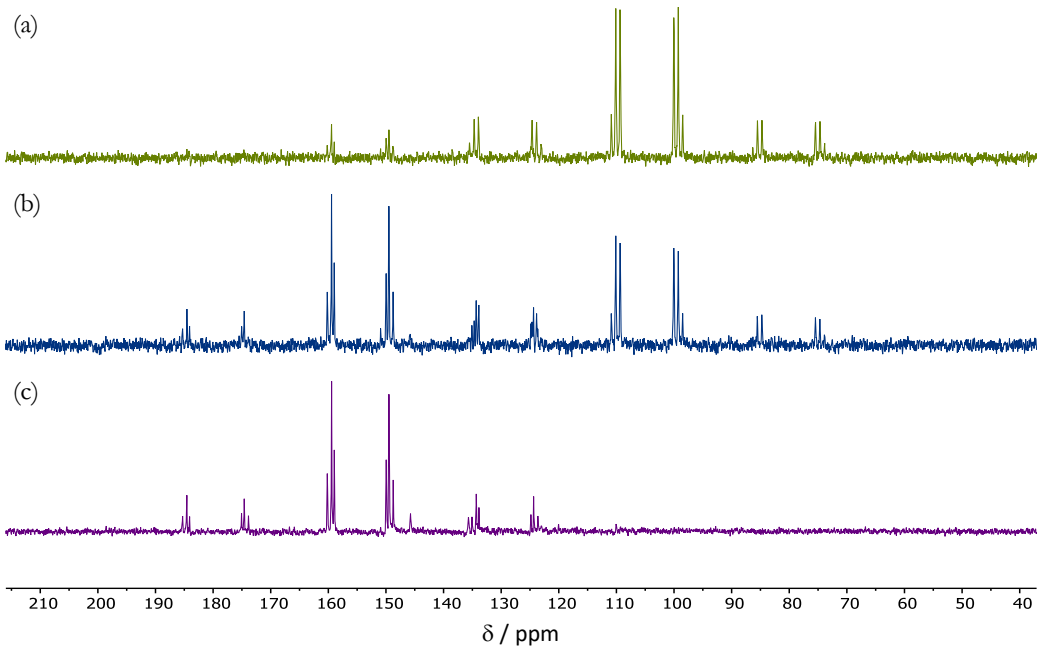


**Figure 2.11** *In situ* $^{31}P\{^{1}H\}$ NMR spectra observed upon reaction of 2 equiv. **L**$_{2.4}$ with [Pt(nbe)$_3$] at (a) 5 min (**2.10d** observed only); (b) 30 min (**2.10d** and **2.12d** observed); (c) 1 h (**2.12d** observed only).

Interpretation of the data is complicated by the accuracy of integrating the $^{31}P\{^{1}H\}$ or $^{19}F\{^{1}H\}$ NMR signals, the presence of small amounts (<5%) of [Pt(nbe)$_3$] which are impractical to detect in the $^{195}Pt\{^{1}H\}$ NMR spectra; moreover for the **L**$_{2.2}$ system, precipitation of **2.10b** makes the mixture inhomogeneous and therefore is not included. Despite these provisos, it appears that there is a trend in the amount of [PtL$_2$(nbe)] formed with increasing size and decreasing π-acceptor capacity of the phosphacycle and vice versa for the trend in the amount of [PtL$_4$] formed. Furthermore, [PtL$_2$(nbe)] is the sole product when using the bulkiest ligand, Ethanox 398$^{TM}$ **2.4**. Similar trends were observed upon the reaction of 3 equiv. of **L**$_{2.1\text{-}2.4}$ and **2.4** with [Pt(nbe)$_3$].

When 2 equiv. of **L**$_{2.5}$ was added to [Pt(nbe)$_3$], the product was initially **2.10e** which equilibrated over 1 h to give **2.10e** (35%), **2.12e** (53%) and **2.13e** (12%) identified from the quintet, triplet and doublet respectively in the $^{195}Pt\{^{1}H\}$ NMR spectrum. The Pt(0) chemistry of the phosphite **L**$_{2.5}$ therefore resembles that of **L**$_{2.3}$.

## 2.6 Rhodium(I) coordination of cyclic fluorophosphites

Nixon *et al.* showed that $[Rh_2Cl_2(\mathbf{L_{2.1}})_4]$ (**2.14a**) is the product of the addition of $\mathbf{L_{2.1}}$ to $[Rh_2Cl_2(C_6H_{10})_2]$.[54] Complex **2.14a** is also the sole product of the reaction of $[Rh_2Cl_2(CO)_4]$ with 4 equiv. of $\mathbf{L_{2.1}}$ (Scheme 2.12) as shown by the absence of CO bands in the IR spectrum and the $^{19}F\{^1H\}$ and $^{31}P\{^1H\}$ NMR spectra. This is an indication of the high π-acidity of $\mathbf{L_{2.1}}$ since displacing CO from $[Rh_2Cl_2(CO)_4]$ is a reaction observed with $PF_3$[55] and a few chelating fluoroaryl diphosphines.[56–58]

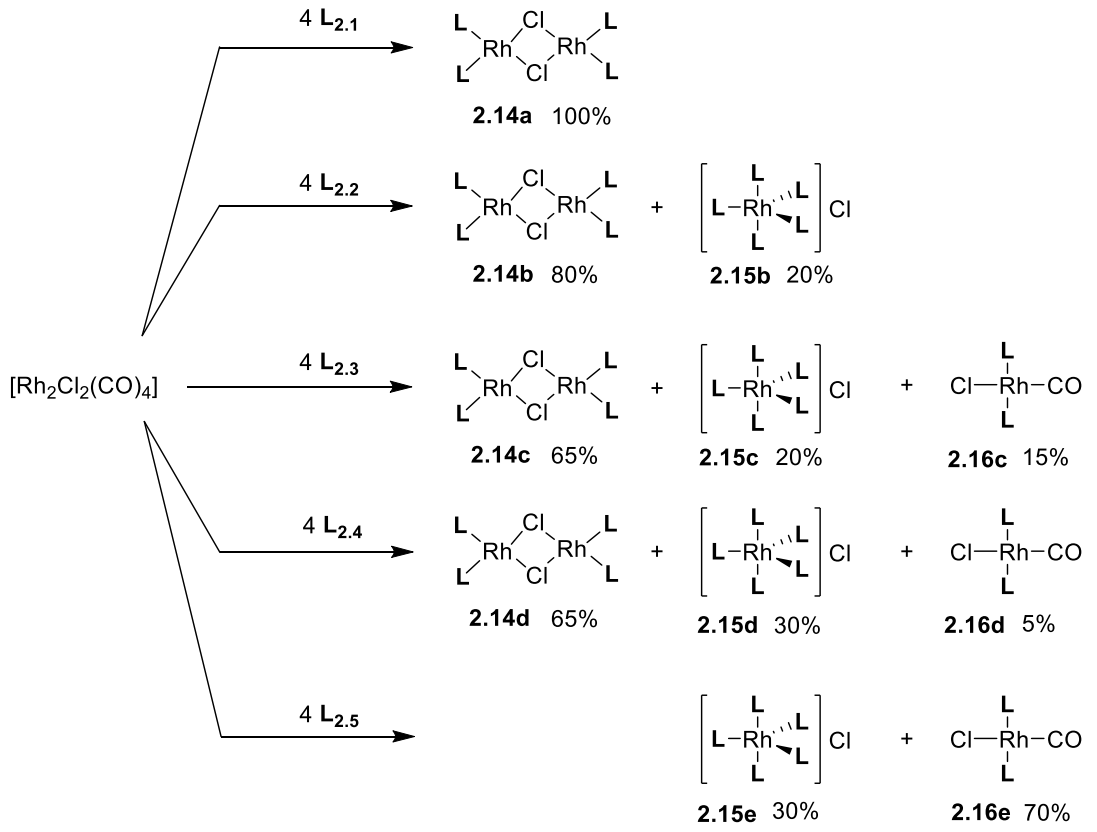


**Scheme 2.12** Proportions of the Rh(I) complexes **2.14**-**2.16** observed upon reaction of 4 equiv. $\mathbf{L_{2.1\text{-}2.5}}$ with $[Rh_2Cl_2(CO)_4]$.

When $[Rh_2Cl_2(CO)_4]$ was treated with 4 equiv. of $\mathbf{L_{2.2}}$, two P-containing products formed that have been identified from their $^{31}P\{^1H\}$ and $^{19}F\{^1H\}$ NMR spectra; the broad spectra obtained at ambient temperature were resolved at -40 °C indicating that the species were exchanging on the NMR timescale (Figure 2.12). The binuclear complex **2.14b** formed by displacement of CO by $\mathbf{L_{2.2}}$ was assigned to the major component (*ca.* 80%) of the product mixture on the basis of the observation that the same species was formed exclusively upon addition of 4 equiv. of $\mathbf{L_{2.2}}$ to $[Rh_2Cl_2(cod)_2]$ (see Chapter 7). The minor component of the product from $[Rh_2Cl_2(CO)_4]$ was assigned to the salt $[Rh(\mathbf{L_{2.2}})_5]Cl$ (**2.15b**) featuring

the five-coordinate Rh cation on the basis of: (a) the complicated $^{31}P\{^{1}H\}$ and $^{19}F\{^{1}H\}$ spectra, as expected for a $AA'_4XX'_4M$ spin system; (b) the reaction of 5 equiv. of $\mathbf{L_{2.2}}$ to $[Rh(cod)_2][BF_4]$ (Scheme 2.14) gave a single product which had the same $^{31}P\{^{1}H\}$ NMR spectrum as **2.15b** and in the $^{19}F\{^{1}H\}$ NMR spectrum, two signals in the ratio 5:4 were observed, consistent with the structure $[Rh(\mathbf{L_{2.2}})_5][BF_4]$ (**2.15b'**). The IR spectrum of the product mixture showed bands for $[Rh_2Cl_2(CO)_4]$, as would be expected to balance the stoichiometry (Scheme 2.12) but no other Rh–CO bands.

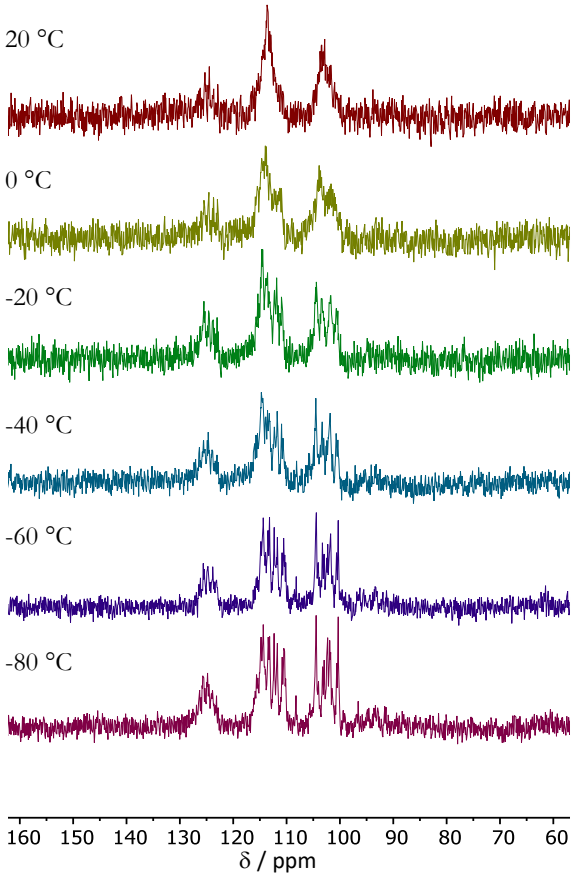


**Figure 2.12** Low temperature $^{31}P\{^{1}H\}$ NMR spectra of complex **2.14b** and **2.15b** in $CD_2Cl_2$.

According to $^{31}P\{^{1}H\}$ and $^{19}F\{^{1}H\}$ NMR spectroscopy, the mixtures of products formed from the addition of fluorophosphites $\mathbf{L_{2.3}}$ or $\mathbf{L_{2.4}}$ to $[Rh_2Cl_2(CO)_4]$ contained binuclear **2.14c** or **2.14d**, and the salts **2.15c** or **2.15d** (Scheme 2.12). In addition, minor products (<15%) were observed which were tentatively assigned to the structures *trans*-$[RhCl(CO)L_2]$ (**2.16c** or **2.16d**) on the basis of the IR spectrum of the mixtures which showed ν(CO) bands at 2032 $cm^{-1}$ (for **2.16c**) and 2028 $cm^{-1}$ (for **2.16d**). It was found that the reaction of $[Rh_2Cl_2(CO)_4]$ with phosphite $\mathbf{L_{2.5}}$ gave **2.16e** as the major product (70%)

with a ν(CO) band at 2023 $cm^{-1}$. There is a trend in the reactions of $[Rh_2Cl_2(CO)_4]$ with the fluorophosphites on increasing the ring size from $\mathbf{L_{2.1}}$ to $\mathbf{L_{2.4}}$: the chemistry with $\mathbf{L_{2.1}}$ resembles $PF_3$ and as the ring size expands the chemistry progressively moves towards resembling that of phosphite $\mathbf{L_{2.5}}$.

In addition, differences emerged between ligands $\mathbf{L_{2.2}}$ and $\mathbf{L_{2.3}}$ upon the reaction of 10 equiv. of ligand with $[Rh_2Cl_2(CO)_4]$ (Scheme 2.13). Ligand $\mathbf{L_{2.3}}$ gave a single product which had the same $^{31}P\{^1H\}$ and $^{19}F\{^1H\}$ NMR spectra as **2.15c** above. In contrast, the $^{31}P\{^1H\}$ NMR spectrum for the reaction with $\mathbf{L_{2.2}}$ gave predominantly a doublet which was resolved at -40 °C (Figure 2.13) to give an equilibrium mixture of **2.14b**, **2.15b** and free ligand $\mathbf{L_{2.2}}$ (Scheme 2.13).

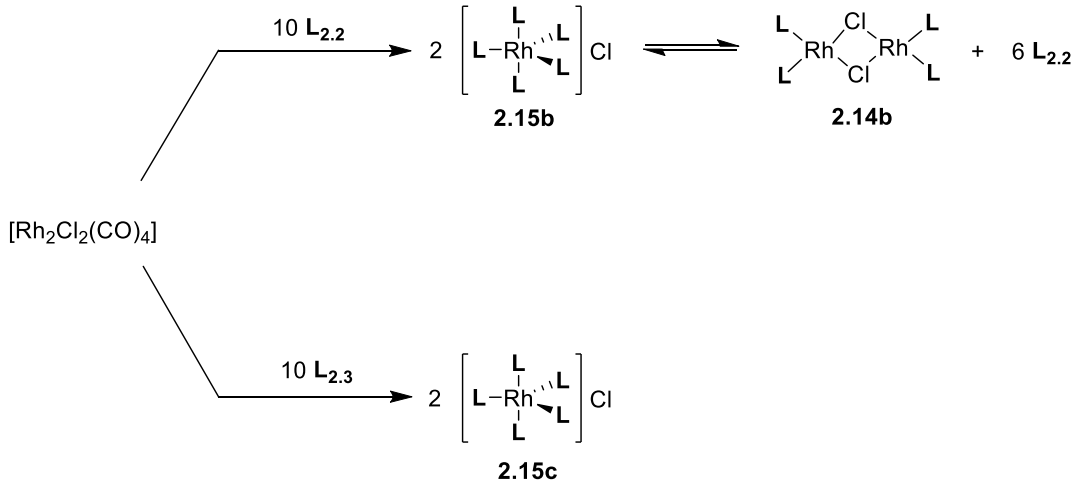


**Scheme 2.13** Reaction of 10 equiv. $\mathbf{L_{2.2\text{-}2.3}}$ with $[Rh_2Cl_2(CO)_4]$.

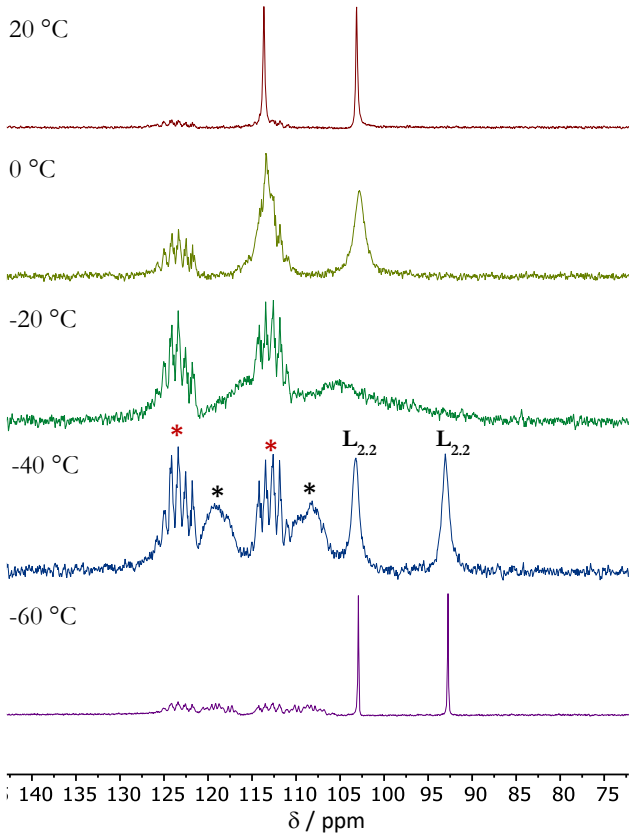


**Figure 2.13** Low temperature $^{31}P\{^{1}H\}$ NMR spectra of the reaction of 10 equiv. **L**$_{2.2}$ with $[Rh_2Cl_2(CO)_4]$: **2.14b** (*), **2.15b** (*) and **L**$_{2.2}$ in $CD_2Cl_2$.

The reaction of 5 equiv. of **L**$_{2.2\text{-}2.3}$ and **L**$_{2.5}$ with $[Rh(cod)_2][BF_4]$ in $CH_2Cl_2$ gave the $[RhL_5][BF_4]$ complexes (**2.15b'-c'**, **2.15e'**), where L = **L**$_{2.2\text{-}2.3}$, **L**$_{2.5}$ (Scheme 2.14). Each complex gave the same $^{31}P\{^{1}H\}$ NMR spectrum as the analogous $[RhL_5][Cl]$ salts (**2.15b-c**, **2.15e**) (see above). Crystals of complex **2.15e'** were obtained by slow diffusion of pentane into a saturated $CH_2Cl_2$ solution of the complex. The crystal structure showed whole molecule disorder (relative occupancies 0.824: 0.176) (Figure 2.14), with multiple restraints and constraints required to maintain sensible geometric and thermal parameters. Accordingly, no reliable geometric parameters could be provided; despite this the crystal structure of **2.15e'** was able to confirm the coordination of five ligands around the Rh centre.

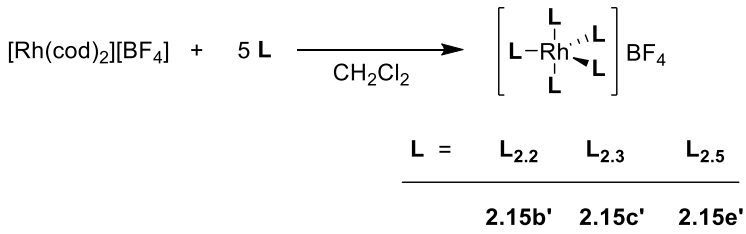


**Scheme 2.14** Synthesis of the $[RhL_5][BF_4]$ complexes **2.15b'-c'** and **2.15e'**.

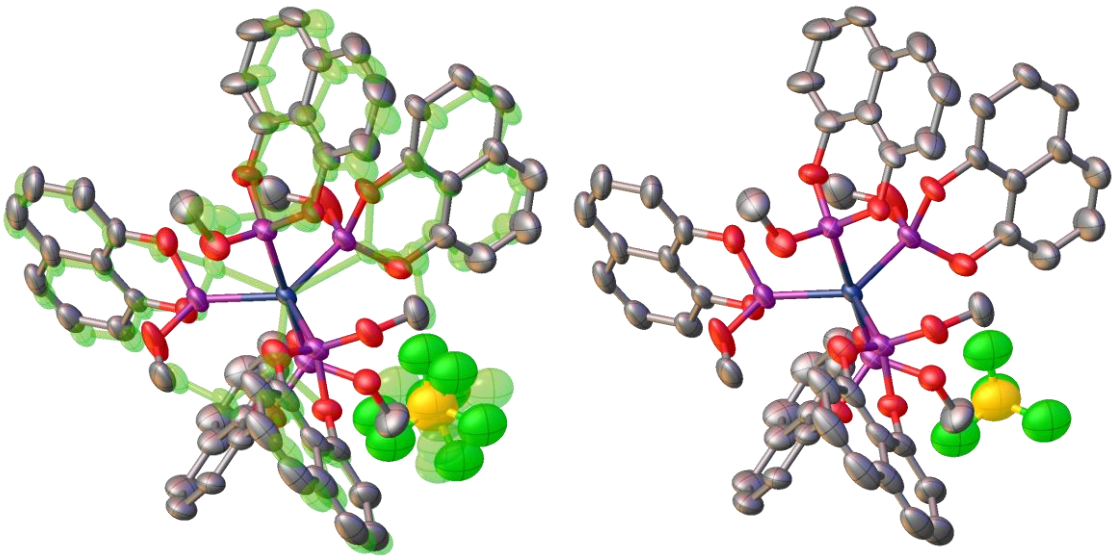

**Figure 2.14** Crystal structure of **2.15e'** (a) shows the molecular disorder (b) molecular disorder has been omitted for clarity. The hydrogen atoms are omitted for clarity. Thermal ellipsoids at 50% probability. The disorder is so extensive that no reliable metrical data could be extracted from the X-ray structure.

## 2.7 Substituted aryl fluorophosphites

### 2.7.1 Synthesis of substituted aryl fluorophosphites

Novel aryl substituted cyclic fluorophosphites $\mathbf{L_{2.6\text{-}2.8}}$ have been prepared from the corresponding cyclic chlorophosphites, **2.5e-g**. The chlorophosphite **2.5e** has been previously reported but was often contaminated with spirophosphorane P(V) by-products.[59] Chlorophosphite **2.5f** has been previously reported from the reaction of diol with excess $PCl_3$.[60] Chlorophosphites **2.5e-f** were prepared herein from the silyl ethers **2.6e-f** (Scheme 2.15); this route was required to minimise the formation of spirophosphorane P(V) by-products. Despite forcing conditions and long reaction times

the formation of **2.5f** only went to 85% completion and the isolated product was contaminated with *ca.* 15% of the mono-silylated diol, **2.6f'**.

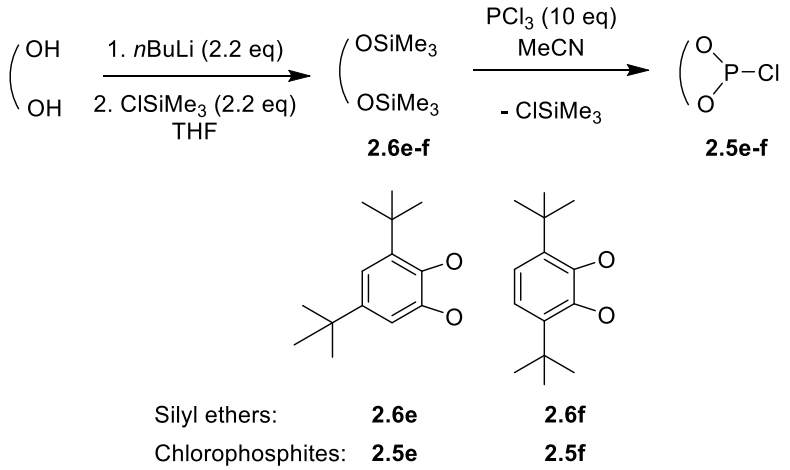


**Scheme 2.15** Route to chlorophosphites **2.5e**-**f** *via* the silyl ethers **2.6e**-**f**. Compound **2.6e** has been previously reported.[61]

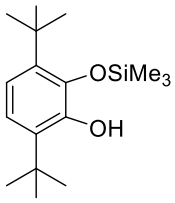


**2.6f'**

The novel chlorophosphite **2.5g** was prepared from the reaction of 2,7-dimethyl-1,8-naphthalenediol[62] with $PCl_3$ in the presence of $NEt_3$ (Scheme 2.16, see Chapter 7 for experimental details). The product was contaminated with *ca.* 7% of an impurity which was tentatively assigned to the mono-methylsubstituted chlorophosphite.

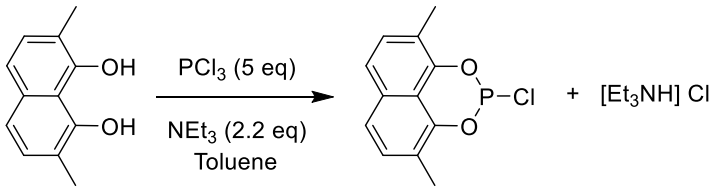


**2.5g**

**Scheme 2.16** Synthesis of chlorophosphite **2.5g**.

Treatment of chlorophosphites **2.5e**-**g** with $SbF_3$ gave the fluorophosphites $\mathbf{L}_{2.6\text{-}2.8}$ (Scheme 2.17) in good yields (*ca.* 75%). Fluorophosphite $\mathbf{L}_{2.8}$ was contaminated with 7% of an impurity, which was tentatively assigned to the mono-methylsubstituted fluorophosphite. All ligands were fully characterised and the $^{31}P\{^1H\}$ and $^{19}F\{^1H\}$ NMR spectra each showed a characteristic doublet with large $^1J_{P,F}$ values of 1235-1292 Hz (see

Chapter 7 for data). The unsymmetrical fluorophoshite $\mathbf{L}_{2.7}$ is unsymmetrical and thus assumed to exist as a racemic mixture. In the presence of water (0.55 M in MeOH) the *t*Bu substituted ligand $\mathbf{L}_{2.7}$ was much less susceptible to hydrolysis than its unsubstituted analogue $\mathbf{L}_{2.1}$; the sample was only 25% hydrolysed after 5 h.

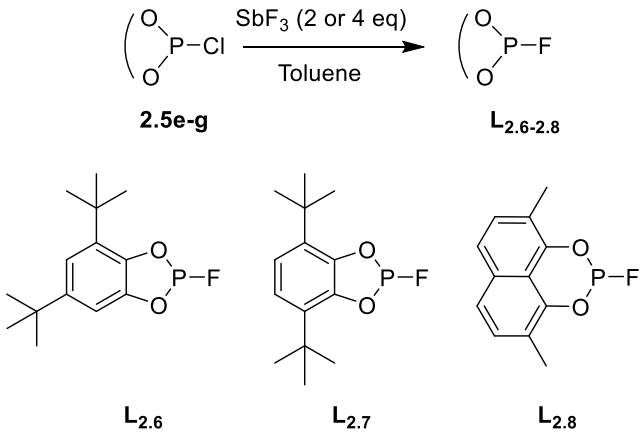


**Scheme 2.17** Synthesis of $\mathbf{L}_{2.6\text{-}2.8}$.

Crystals of $\mathbf{L}_{2.8}$ suitable for X-ray crystallography were obtained by slow evaporation of a saturated toluene solution of the ligand (Figure 2.15). The crystal structure showed that the naphthalene ring lies in the same plane as the two methyl substituents. The P atom is pyramidalised (Σ(angles at P) = 297°) which is consistent with $sp^3$ hybridisation, whereas the other angles within the 6-membered phosphacycle are *ca.* 120°, in line with $sp^2$ hybridisation.

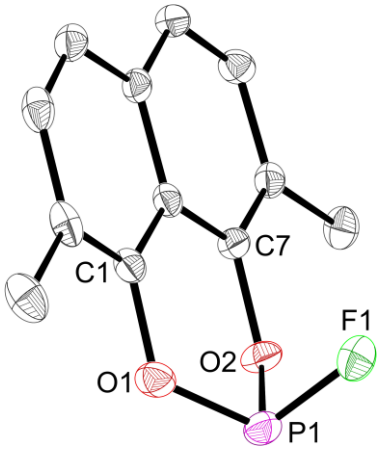


**Figure 2.15** Crystal structure of $\mathbf{L}_{2.8}$. The hydrogen atoms are omitted for clarity. Thermal ellipsoids at 50% probability. Selected bond lengths (Å) and angles (°): P1-F1 1.6062(12), P1-O1 1.6101(13), P1-O2 1.6096(13), O1-P1-O2 102.10(7), O1-P1-F1 97.64(6), O2-P1-F1 98.24(7). See Appendix for experimental details.

### 2.7.2 Synthesis of *cis*-[Mo(CO)$_4$L$_2$] complexes of aryl substituted fluorophosphites

Complexes of the type *cis*-[Mo(CO)$_4$L$_2$] were targeted as a way to compare the electronic properties of fluorophosphites **L$_{2.6\text{-}2.8}$** to their unsubstituted analogues **L$_{2.1\text{-}2.2}$**. The reaction of 2 equiv. of ligands **L$_{2.6\text{-}2.8}$** with [Mo(CO)$_4$(nbd)] (nbd = norbornadiene) in $CH_2Cl_2$ gave the *cis*-[Mo(CO)$_4$L$_2$] complexes **2.7f-h**, where L = **L$_{2.6\text{-}2.8}$** (Scheme 2.18).

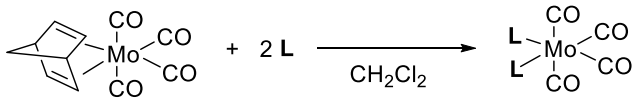


| L = | $L_{2.6}$ | $L_{2.7}$ | $L_{2.8}$ |
|---|---|---|---|
| | **2.7f** | **2.7g** | **2.7h** |

**Scheme 2.18** Synthesis of *cis*-[Mo(CO)$_4$L$_2$] complexes **2.7f-h**.

**Table 2.6** NMR data for complexes **2.7f-h**.[a]

| Ligand | Complex | $\delta_P$ / ppm | $^1J_{P,F}$ / Hz[b] | $\Delta\delta$ / ppm |
|---|---|---|---|---|
| **L$_{2.6}$** | **2.7f** | 168.0 | 1267 | 45 |
| **L$_{2.7}$** | **2.7g** | 165.9 | 1263 | 47 |
| **L$_{2.8}$** | **2.7h** | 144.1 | 1200 | 43 |

[a] Measured in $CD_2Cl_2$. [b] Calculated from $N = |^1J_{P,F} + {}^3J_{P,F}|$.

Similar to complexes **2.7a-d**, the $^{31}P\{^1H\}$ and $^{19}F\{^1H\}$ NMR spectra for complexes **2.7g-h** showed a doublet of triplets, a deceptively simple pattern for the AA'XX' spin system. *Rac* and *meso* diastereomeric complexes of **2.7f** were observed in the $^{31}P\{^1H\}$ NMR spectrum; shown by two overlapping doublet of triplets which appeared as a doublet of quartets. There is excellent agreement between the observed and simulated NMR spectra of complexes **2.7f-h**, using the calculated coupling constants given in Chapter 7. Values of *ca.* 50 Hz for $^2J_{P,P}$ are similar to that of *cis*-[Mo(CO)$_4$(PF$_3$)$_2$] and are indicative of a *cis*-geometry.[63] Substitution on either the phenyl or naphthalene ring of **L$_{2.1}$** or **L$_{2.2}$** appears to have little effect on the NMR data for complexes **2.7f-h** (relative to complexes **2.7a-b**).

The IR spectra for complexes **2.7f-h** are consistent with a *cis*-geometry of ligands. The ν(CO) values shown in Figure 2.16 for complexes **2.7f-h** and **2.7a**, featuring the five-membered phosphacycles **L$_{2.6\text{-}2.7}$** and **L$_{2.1}$**, reflect the small effect substitution with

electron-donating *t*Bu substituents has on the electronic properties of $\mathbf{L_{2.1}}$. Similarly, minimal effect of substitution was observed in complexes **2.7h** and **2.7b**, featuring 6-membered phosphacycles $\mathbf{L_{2.8}}$ and $\mathbf{L_{2.2}}$ respectively. Despite this, when taking electronegativity of substituents and phosphacycle ring size into consideration, the trend in ν(CO) correlates as expected, with π-acceptor capacity increasing in the order $\mathbf{L_{2.1}} > \mathbf{L_{2.6}} \approx \mathbf{L_{2.7}} > \mathbf{L_{2.2}} > \mathbf{L_{2.8}}$.[64]

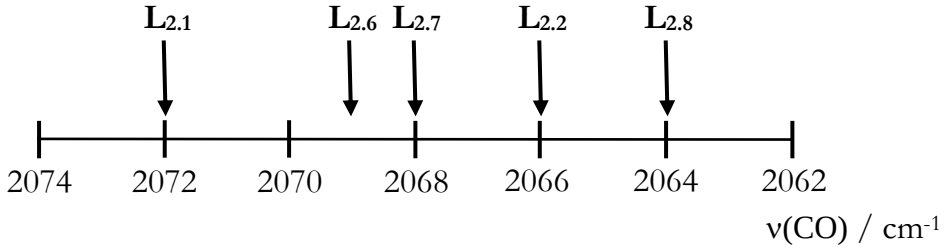


**Figure 2.16** ν(CO) bands for **2.7f**-**h** vs. **2.7a**-**b** (see Chapter 7 for values).

Crystals of **2.7h** suitable for X-ray crystallography were obtained by slow diffusion of hexane into a saturated $CH_2Cl_2$ solution of the complex (Figure 2.17). The crystal structure confirmed the *cis*-geometry of the complex and shows that the fluorophosphite ligands adopt a *syn*-conformation. The Mo-P π-bonding should perturb the bond lengths and angles around the P centre relative to the free ligand ($\mathbf{L_{2.8}}$);[27–29] no trend was observed in the P-F bond length, but a small increase in the F-P-O (by *ca.* 1.6°) and O-P-O (by *ca.* 1.3°) angles was observed in complex **2.7h** (Table 2.7). The Mo-P bond length in complex **2.7h** is slightly longer than in **2.7b** (by *ca.* 0.008 Å), consistent with the substituted fluorophosphite $\mathbf{L_{2.8}}$ being a poorer π-acceptor than its unsubstituted analogue $\mathbf{L_{2.2}}$.[27,28]

**Table 2.7** Selected bond lengths[a] (Å) and angles[a] (°) from the molecular structures of $\mathbf{L_{2.8}}$ and complexes **2.7b**,**h**.

| Ligand | Complex | Mo-P / Å | P-F / Å | F-P-O / ° | O-P-O / ° |
|---|---|---|---|---|---|
| $\mathbf{L_{2.8}}$ | - | - | 1.6062(12) | 97.94(7) | 102.10(7) |
| $\mathbf{L_{2.2}}$ | **2.7b** | 2.3846(6) | 1.5832(13) | 99.50(8) | 103.52(8) |
| $\mathbf{L_{2.8}}$ | **2.7h** | 2.3924(5) | 1.5845(12) | 99.51(7) | 103.35(7) |

[a]Average values have been calculated for simplicity.

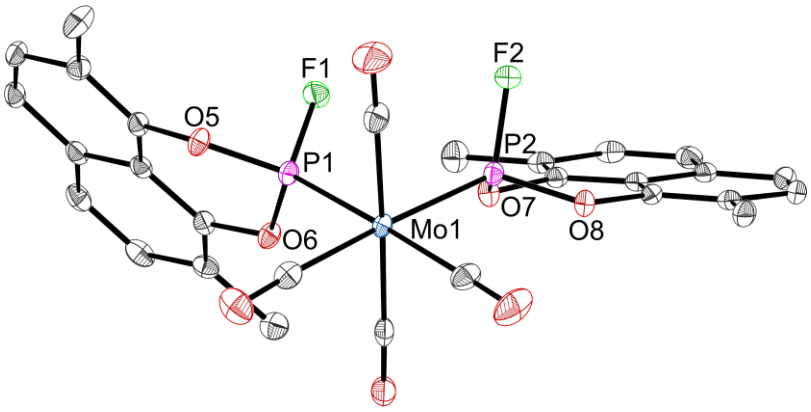


**Figure 2.17** Crystal structure of **2.7h**. The hydrogen atoms are omitted for clarity. Thermal ellipsoids at 50% probability. See Table 2.7 for selected bond lengths (Å) and angles (°). See Appendix for experimental details.

### 2.7.3 Platinum(II) coordination of substituted aryl fluorophosphites

The reaction of 2 equiv. of ligands $\mathbf{L}_{2.6\text{-}2.8}$ with [$PtCl_2$(cod)] (cod = 1,5-cyclooctadiene) in $CH_2Cl_2$ gave the *cis*-[$PtCl_2L_2$] complexes **2.8f-h**, where L = $\mathbf{L}_{2.6\text{-}2.8}$ (Scheme 2.19). Characteristic AA'XX' patterns for the $^{31}P\{^1H\}$ and $^{19}F\{^1H\}$ NMR spectra were obtained for each complex **2.8f-h**. The large $^1J_{P,Pt}$ values are consistent with a *cis*-geometry (Table 2.8). Similar to the *cis*-[$Mo(CO)_4$($\mathbf{L}_{2.6}$)$_2$] complex (**2.7f**), *rac* and *meso* diastereomeric complexes of *cis*-[$PtCl_2$($\mathbf{L}_{2.6}$)$_2$] (**2.8f**) were observed in the $^{31}P\{^1H\}$ NMR spectrum.

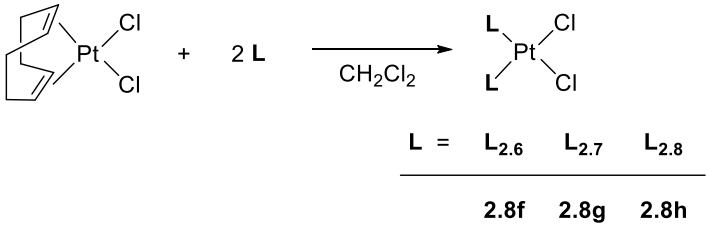


**Scheme 2.19** Synthesis of the *cis*-[$PtCl_2L_2$] complexes **2.8f-h**.

**Table 2.8** NMR data for complexes **2.8f-h**.[a]

| Ligand | Complex | $\delta_P$ / ppm | $^1J_{P,Pt}$ / Hz | $^1J_{P,F}$ / Hz[b] |
|---|---|---|---|---|
| $\mathbf{L}_{2.6}$ | **2.8f** | 89.9, 89.0 | 6032, 6038 | - |
| $\mathbf{L}_{2.7}$ | **2.8g** | 90.0 | 5947 | - |
| $\mathbf{L}_{2.8}$ | **2.8h** | 63.8 | 6159 | 1242 |

[a] Measured in $CD_2Cl_2$. [b] Calculated from $N = |^1J_{P,F} + {}^3J_{P,F}|$.

The $^{31}P\{^{1}H\}$ and $^{19}F\{^{1}H\}$ NMR spectra of complex **2.8h** was simulated using the calculated coupling constants given in Chapter 7. There is excellent agreement between the observed and simulated spectra. The coupling constants for complexes **2.8f**-**g** could not be calculated due to poor signal resolution. The $^{1}J_{P,F}$ and $^{1}J_{P,Pt}$ values of complex **2.8h** are similar to that of the unsubstituted analogue, $\mathbf{L}_{2.2}$ in **2.8b** (see Section 2.4).

### 2.7.4 Rhodium(I) coordination of aryl substituted fluorophosphites

When $[Rh_2Cl_2(CO)_4]$ was treated with 4 equiv. of ligands $\mathbf{L}_{2.6\text{-}2.8}$ (Scheme 2.20), two P-containing species formed and have been identified as $[Rh_2Cl_2L_4]$ complexes (**2.14f**-**h**) and $[RhL_5][Cl]$ salts (**2.15f**-**h**) on the basis of their characteristic NMR spectra and the evidence discussed in Section 2.6 for the unsubtituted analogues. The IR spectra of the reaction mixtures showed bands for $[Rh_2Cl_2(CO)_4]$, but no other Rh-CO bands.

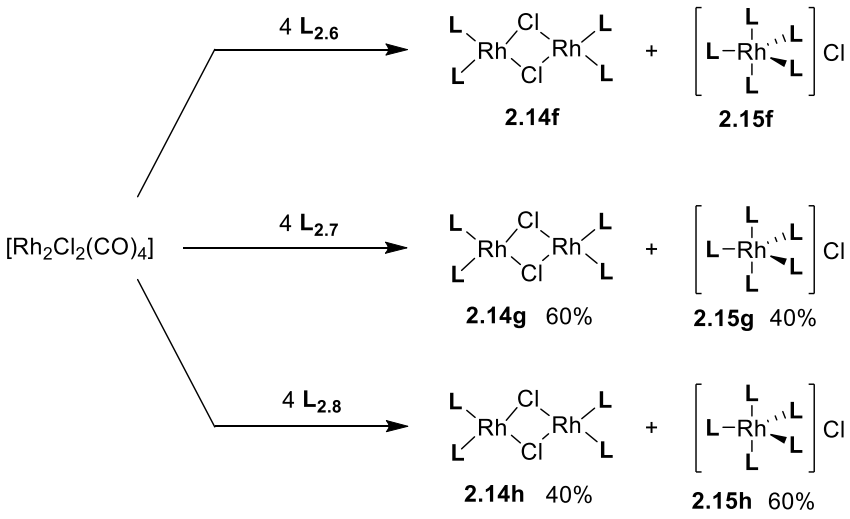


**Scheme 2.20** Proportions of the Rh(I) complexes **2.14**-**2.15** observed upon reaction of 4 equiv. $\mathbf{L}_{2.6\text{-}2.8}$ with $[Rh_2Cl_2(CO)_4]$.

The broad $^{31}P\{^{1}H\}$ NMR spectrum obtained at ambient temperature for the reaction with $\mathbf{L}_{2.6}$ was partially resolved at -80 °C, but due to the presence of *rac* and *meso* complexes for both **2.14f** and **2.15f**, the complicated $^{31}P\{^{1}H\}$ NMR signals were unsuitable for accurate integration. Unlike the reaction with the unsubstituted 5-membered fluorophosphite $\mathbf{L}_{2.1}$, where the binuclear complex **2.14a** was the sole product (see Section 2.6), upon reaction with the *t*Bu-substituted $\mathbf{L}_{2.6}$ and $\mathbf{L}_{2.7}$ the salts **2.15f**-**g** were also observed (Scheme 2.20). Substitution on the phenyl ring moves the chemistry away from that of $PF_3$. A similar trend was observed for the fluorophosphites featuring the six-membered phosphacycles, $\mathbf{L}_{2.2}$ and $\mathbf{L}_{2.8}$; upon reaction with the substituted analogue $\mathbf{L}_{2.8}$, an increase in the amount

of the salt $[RhL_5][Cl]$ (**2.15h**) to 60% was observed (*cf.* 20% when using $\mathbf{L_{2.2}}$). In both cases, the trend is likely a consequence of the balance of electronic factors (stronger π-acceptor ligands stabilise $[Rh_2Cl_2L_4]$) outweighing steric factors (pentacoordinate $[RhL_5][Cl]$ is more crowded than $[Rh_2Cl_2L_4]$).

## 2.8 Conclusions

A series of fluorophosphites **L**$_{2.1\text{-}2.4}$, with varying phosphacycle ring size, has been successfully synthesised. The IR spectra and crystal structures of the *cis*-[Mo(CO)$_4$L$_2$] complexes (**2.7a**-**d**), where L = **L**$_{2.1\text{-}2.4}$, confirmed the expectation that the fluorophosphites would populate the space between P(OAr)$_3$ and PF$_3$, in terms of their σ/ π-bonding to transition metals. Pronounced effects of phosphacycle ring size on the stereoelectronic properties of the ligands were observed, and can be summarised in terms of the following trends for **L**$_{2.1\text{-}2.4}$: (1) the smaller the phosphacycle, the closer the fluorophosphite properties are to PF$_3$, so **L**$_{2.1}$ is the most PF$_3$-like of the series; (2) the steric bulk of the ligands is in the order: **L**$_{2.1}$/**L**$_{2.2}$ < **L**$_{2.3}$/**L**$_{2.4}$. The IR spectra of the *cis*-[Mo(CO)$_4$L$_2$] complexes featuring the six-membered fluorophosphite **L**$_{2.2}$ and phosphite **L**$_{2.5}$ demonstrate the significant effect the P-F fragment has on increasing the π-accepting capacity of the ligand, relative to the P-OMe fragment.

Using these generalisations, the Pt(II), Pt(0) and Rh(I) coordination chemistry of ligands **L**$_{2.1\text{-}2.4}$ could be understood. The $^1J_{P,Pt}$ values of the *cis*-[PtCl$_2$L$_2$] complexes, where L = **L**$_{2.2\text{-}2.4}$, sit between the analogous PF$_3$ and phosphite **L**$_{2.5}$ complexes. The 18-electron [PtL$_4$] complexes are common to the whole series from PF$_3$, through **L**$_{2.1\text{-}2.4}$, to phosphite **L**$_{2.5}$. A trend emerged in the proportions of [PtL$_2$(nbe)] and [PtL$_4$] species observed upon the addition of 2 equiv. of ligand to [Pt(nbe)$_3$]. Using the 5-membered **L**$_{2.1}$, [PtL$_4$] was the major species (77%), whereas with the 8-membered **L**$_{2.4}$ [PtL$_2$(nbe)] predominated (91%). This trend is likely a consequence of the balance of steric factors ([PtL$_4$] is more crowded than [PtL$_2$(nbe)]) and electronic characteristics (fluorophosphites stabilise Pt(0) better than nbe).

The reaction of [Rh$_2$Cl$_2$(CO)$_4$] with P(OAr)$_3$ to give *trans*-[RhCl(CO){P(OAr)$_3$}$_2$] is general. However, the fluorophosphites **L**$_{2.1\text{-}2.4}$ displace CO from [Rh$_2$Cl$_2$(CO)$_4$] to give the binuclear [Rh$_2$Cl$_2$L$_4$] species; this is an excellent demonstration of their PF$_3$-like properties. Furthermore, the observed trend in the extent to which the ligand displaces CO reflects the closeness in its properties to PF$_3$: [Rh$_2$Cl$_2$L$_4$] is the sole product when using the 5-membered **L**$_{2.1}$ but constitutes only 65% of the product when using the 8-membered **L**$_{2.4}$.

Novel aryl-substituted analogues of fluorophosphites **L**$_{2.1}$ and **L**$_{2.2}$ have been synthesised (**L**$_{2.6\text{-}2.8}$). Most likely due to the high steric bulk of the 3,6-*t*Bu substitution in **L**$_{2.7}$, the synthesis of the chlorophosphite precursor did not reach completion and so pure **L**$_{2.7}$ was

not obtained. The synthesis of this ligand should be optimised in the future. The IR spectra of the *cis*-[$Mo(CO)_4L_2$] complexes (**2.7f-h**), where L = $\mathbf{L_{2.6\text{-}2.8}}$, showed that substitution on the aryl ring had a small effect on the electronic properties of the fluorophosphites. Despite this, the trend was as expected whereby substitution on the aryl ring with electron-donating groups (such as *t*Bu or Me) decreases the π-accepting properties of the ligand.

The aryl substituted fluorophosphites $\mathbf{L_{2.6\text{-}2.8}}$ displayed similar Rh(I) coordination behaviour to $\mathbf{L_{2.1\text{-}2.2}}$; the substitution of CO in [$Rh_2Cl_2(CO)_4$] by fluorophosphites $\mathbf{L_{2.6\text{-}2.8}}$ readily occurs. However, increased amounts of [$RhL_5$][Cl] species were observed when using the substituted fluorophosphites, demonstrating how the coordination properties of the substituted ligands move away from that of $PF_3$. The Pt(0) coordination chemistry of the substituted fluorophosphites should be explored to further investigate these differences in behaviour. Decoration of the aryl rings with other substituents should also be considered in order to further tune the stereoelectronic properties of the cyclic fluorophosphites.

## 2.9 References


1 A. Gual, C. Godard, V. de la Fuente and S. Castillon, in *Phosphorus (III) Ligands in Homogeneous Catalysis*, eds. P. C. J. Kamer and P. W. N. M. van Leeuwen, John Wiley & Sons, Ltd., 2012, pp. 81–131.

2 E. Billig, A. G. Abatjoglou and D. R. Bryant, *US Patent*, 1987, US 4668651.

3 E. Billig, A. G. Abatjoglou and D. R. Bryant, *US Patent*, 1988, US 4748261.

4 E. Billig, A. G. Abatjoglou and D. R. Bryant, *US Patent*, 1989, US 4885401.

5 P. W. N. M. van Leeuwen and C. Claver, *Rhodium Catalyzed Hydroformylation*, Kluwer Academic Publishers, 2006.

6 P. W. N. M. van Leeuwen, in *Homogeneous Catalysis, Understanding the Art*, Kluwer Academic Publishers, Dordrecht, 2004, pp. 139–174.

7 R. Franke, D. Selent and A. Borner, *Chem. Rev.*, 2012, **112**, 5675–5732.

8 M. J. Baker, K. N. Harrison, A. G. Orpen, P. G. Pringle and G. Shaw, *J. Chem. Soc. Chem. Commun.*, 1991, **94**, 803–804.

9 M. J. Baker and P. G. Pringle, *J. Chem. Soc. Chem. Commun.*, 1991, **18**, 1292–1293.

10 L. Bini, C. Müller and D. Vogt, *Chem. Commun.*, 2010, **46**, 8325–8334.

11 T. Foo, J. M. Garner, R. Shapiro and W. Tam, *World Patent*, 1996, WO 9622968.

12 L. Bini, C. Müller and D. Vogt, *ChemCatChem*, 2010, **2**, 590–608.

13 K. A. Kreutzer and W. Tam, *World Patent*, 1995, WO 9528228.

14 M. T. Reetz, *Angew. Chemie Int. Ed.*, 2008, **47**, 2556–2588.

15 P. W. N. M. van Leeuwen, P. C. J. Kamer, C. Claver, O. P. Amies and M. Dieguez, *Chem. Rev.*, 2011, **111**, 2077–2118.

16 H. Fernandez-Perez, P. Etayo, A. Panossian and A. Vidal-Ferran, *Chem. Rev.*, 2011, **111**, 2119–2176.

17 K. Takahashi, M. Yamashita, Y. Tanaka and K. Nozaki, *Angew. Chemie Int. Ed.*, 2012, **51**, 4383–4387.

18 L. Iu, J. A. Fuentes, M. E. Janka, K. J. Fontenot and M. L. Clarke, *Angew. Chemie Int. Ed.*, 2019, **58**, 2120–2124.

19 M. van den Berg, A. J. Minnaard, R. M. Haak, M. Leeman, E. P. Schudde, A.

Meetsma, B. L. Feringa, A. H. M. de Vries, C. E. P. Maljaars, C. E. Willans, D. Hyett, J. A. F. Boogers, H. J. W. Henderickx and J. G. de Vries, *Adv. Synth. Catal.*, 2003, **345**, 308–323.

20 J. F. Teichert and B. L. Feringa, *Angew. Chemie Int. Ed.*, 2010, **49**, 2486–2528.

21 A. P. V Göthlich, M. Tensfeldt, H. Rothfuss, M. E. Tauchert, D. Haap, F. Rominger and P. Hofmann, *Organometallics*, 2008, **27**, 2189–2200.

22 A. Gillon, K. Heslop, D. J. Hyett, A. Martorell, A. G. Orpen, P. G. Pringle, C. Claver and E. Fernandez, *Chem. Commun.*, 2000, **2**, 961–962.

23 M. M. Pereira, M. J. F. Calvete, R. M. B. Carrilho and A. R. Abreu, *Chem. Soc. Rev.*, 2013, 6990–7027.

24 Y.-S. Liu and J. L. Rodgers, *US Patent*, 2009, US 2009/0171121 A1.

25 C. A. Tolman, *Chem. Rev.*, 1977, **77**, 313–348.

26 D. Setiawan, R. Kalescky, E. Kraka and D. Cremer, *Inorg. Chem.*, 2016, **55**, 2332–2344.

27 A. G. Orpen and N. G. Connelly, *J. Chem. Soc. Chem. Commun.*, 1985, 1310–1311.

28 A. G. Orpen and N. G. Connelly, *Organometallics*, 1990, **9**, 1206–1210.

29 M. F. Haddow, A. J. Middleton, A. G. Orpen, P. G. Pringle and R. Papp, *Dalton Trans.*, 2009, 202–209.

30 N. C. Norman, *Periodicity and the s- and p-Block Elements*, Oxford University Press, Oxford, 1997.

31 R. A. Baber, M. F. Haddow, A. J. Middleton, A. G. Orpen, P. G. Pringle, A. Haynes, G. L. Williams and R. Papp, *Organometallics*, 2007, **26**, 713–725.

32 J. J. C. van Lier, R. J. M. Hermans and H. M. Buck, *Phosphorus Sulfur Relat. Elem.*, 1984, **19**, 173–188.

33 S. Wagner, M. Rakotomalala, Y. Bykov, O. Walter and M. Doring, *Heteroat. Chem.*, 2012, **25**, 216–222.

34 J. Coetzee, G. R. Eastham, A. M. Z. Slawin and D. J. Cole-Hamilton, *Org. Biomol. Chem.*, 2012, **10**, 3677–3688.

35 J. Gloede, U. Pieper and W. D. Habicher, *Zeitschrift für Anorg. und Allg. Chemie*, 2002, **628**, 877.

36 M. Moghadam, S. Tangestaninejad, V. Mirkhani, I. Mohammadpoor-Baltork and S. Gharaati, *Appl. Organomet. Chem.*, 2009, **23**, 446–454.

37 I. Neda, A. Fischer, T. Kaukorat, P. G. Jones and R. Schmutzler, *Chem. Ber.*, 1994, **127**, 1579–1586.

38 P. P. Onys'ko, T. V Kolodka and A. D. Sinitsa, *Russ. J. Gen. Chem.*, 1993, **63**, 1556–1559.

39 O. Farooq, *New J. Chem.* , 2000, **24**, 81–84.

40 D. J. St-Cyr, M. S. Morin, F. B. Belanger-Gariepy, B. A. Arndtsen, E. H. Krenske and K. N. Houk, *J. Org. Chem.*, 2010, **75**, 4261–4273.

41 T. G. Meyer, A. Fischer, P. G. Jones and R. Schmutzler, *Zeitschrift fur Naturforschung, B*, 1993, **48**, 659–71.

42 L. M. Voropai, N. G. Ruchkina, E. E. Milliaresi and E. E. Nifant'ev, *J. Gen. Chem. os USSR*, 1985, **55**, 55–62.

43 P. S. Pregosin and R. W. Kunz, *NMR Basic Principles and Progress, 16, 31P and 13C NMR of Transition Metal Phosphine Complexes*, Springer-Verlag, 1979.

44 D. R. Anton and R. H. Crabtree, *Organometallics*, 1983, **2**, 621–627.

45 E. C. Alyea and S. Song, *Comments Inorg. Chem.*, 1996, **18**, 189–221.

46 R. J. Clark and P. I. Hoberman, *Inorg. Chem.*, 1965, **4**, 1771–1774.

47 I. A. Guzei and M. Wendt, *Dalton Trans.*, 2006, 3991–3999.

48 D. S. Rycroft, D. W. A. Sharp and J. G. Wright, *Inorg. Nucl. Chem. Lett.* , 1978, **14**, 451–455.

49 R. J. Goodfellow and B. F. Taylor, *J. Chem. Soc. Dalton Trans.*, 1974, 1676–1684.

50 J. A. Iggo, *NMR Spectroscopy in Inorganic Chemistry*, Oxford University Press, 1999.

51 R. Friedemann and K. Seppelt, *Eur. J. Inorg. Chem.*, 2013, 1197–1206.

52 C. Crocker and R. J. Goodfellow, *J. Chem. Soc. Dalton Trans.*, 1977, 1687–1689.

53 C. J. Cobley and P. G. Pringle, *Inorg. Chim. Acta*, 1997, **265**, 107–115.

54 P. B. Hitchcock, S. Morton and J. F. Nixon, *J. Chem. Soc. Dalton Trans.*, 1985, 1295–1301.

55 J. F. Nixon and J. R. Swain, *J. Chem. Soc. Dalton Trans.*, 1972, 1044–1048.

56 T. Korenaga, K. Osaki, R. Maenishi and T. Sakai, *Org. Lett.*, 2009, **11**, 2325–2328.

57 T. Korenaga, A. Ko, K. Uotani, Y. Tanaka and T. Sakai, *Angew. Chemie Int. Ed.*, 2011, **50**, 10703–10707.

58 M. J. Atherton, K. S. Coleman, J. Fawcett, J. H. Holloway, A. Karagar, L. A. Peckb, G. C. Saunders, L. Lei and E. G. Hope, *J. Chem. Soc. Dalton Trans.*, 1995, 4029–4037.

59 E. E. Nifant'ev, T. S. Kukhareva, I. A. Soldatova and T. G. Chukbar, *Zhurnal Obs. Khimii*, 1986, **56**, 2487–2491.

60 W. M. Abdou and M. R. Mahran, *Phosphorus and Sulfur*, 1986, **26**, 119–127.

61 M. Al-Masri, D. Fritsch and H. R. Kricheldorf, *Macromolecules*, 2000, **33**, 7127–7135.

62 M. Poirier, M. Simard and J. D. Wuest, *Organometallics*, 1996, **15**, 1296–1300.

63 F. Ogilvie, R. J. Clark and J. G. Verkade, *Inorg. Chem.*, 1969, **8**, 1904–1907.

64 C. A. Tolman, *J. Am. Chem. Soc.*, 1970, **92**, 2953–2956.

# Chapter 3

# Fluorophosphites for alkene hydroformylation

## 3.1 Introduction

### 3.1.1 Rh-catalysed hydroformylation

Hydroformylation is the addition of "syngas" ($H_2$/CO) to an alkene in the presence of a catalyst to form a mixture of linear (*n*) and branched (*iso*) isomeric aldehydes (Scheme 3.1). Since its fortuitous discovery by Otto Roelen in 1938,[1,2] hydroformylation has developed into one of the most valuable industrial processes.[3] Aldehydes are important intermediates in the synthesis of fine and bulk chemicals. Initially, exclusively cobalt catalysts were applied to hydroformylation until the discovery of the first ligand modified rhodium catalyst, [$RhH(CO)(PPh_3)_3$], by Wilkinson in 1968.[4,5] Rh-catalysts are generally more expensive than Co-catalysts, but due to their extremely high catalytic activities at low temperatures and pressures, they have continued to be the focus of hydroformylation research.

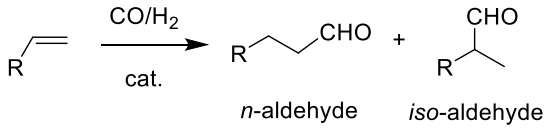


**Scheme 3.1** Catalytic hydroformylation of an alkene.

The use of phosphorus ligands in Rh-catalysed hydroformylation is extensive and has been thoroughly reviewed in many textbook chapters[6–11] and journals.[12–15] Figure 3.1 shows examples of key monophos ligands which have been applied in the Rh-catalysed hydroformylation of alkenes: water-soluble tris(3-sulfophenyl)phosphine trisodium salt (TPPTS, **3.1**),[16] bulky phosphites (*e.g.* **3.2**)[17–20] and cyclic phosphites (*e.g.* **3.3**),[19,21,22]

tris(pyrrolyl)phosphine ($PPyr_3$, **3.4**),[23–25] phosphinines (*e.g.* **3.5**)[26,27] and the cyclic fluorophosphite Ethanox 398™ (**3.6**).[28,29] The use of the fluorophosphite **3.6** for Rh-catalysed hydroformylation has been discussed in Section 1.5 and summarised by Puckette.[30,31]

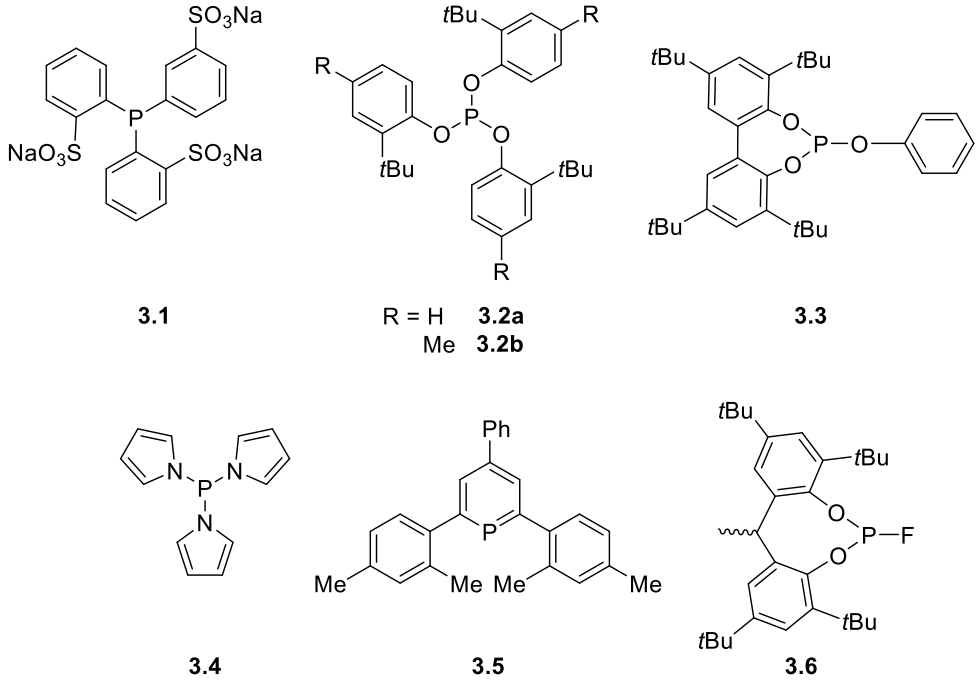


**Figure 3.1** Key examples of monophos ligands used in Rh-catalysed hydroformylation since the discovery of $[RhH(CO)(PPh_3)_3]$.

### 3.1.2 Recent developments in Rh-catalysed hydroformylation

Rh-catalysed hydroformylation was most recently reviewed in 2012.[12] Here the highlights of Rh-catalysed hydroformylation research since 2012 will be presented.

#### *3.1.2.1 Monophos ligands*

Recently, in 2019 a facile synthesis of the azaphosphatriptycene ligand **3.7** was reported; the difficulty of the syntheses of such ligands has limited their use in catalysis previously.[32] The IR spectrum of the corresponding [Rh(acac)(CO)(**3.7**)] complex showed the strong π-acceptor/weak σ-donor character of the ligand.[32] The catalyst derived from **3.7** displayed high activity in the Rh-catalysed hydroformylation of cyclohexene.[32] Borner *et al.* have recently reported the use of bulky *t*Bu phosphinites (*e.g.* **3.8a**) and phosphonites (*e.g.* **3.8b**) in the Rh-catalysed hydroformylation of 1-ocetene.[33,34]

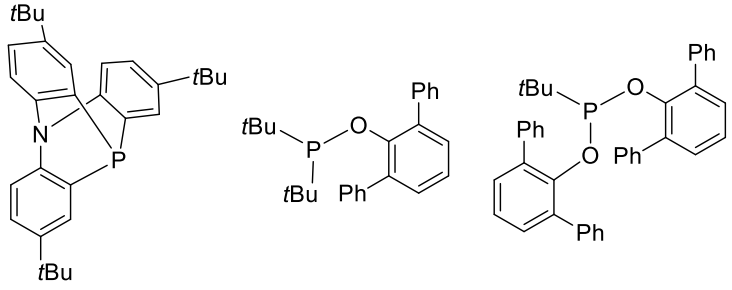


**3.7** **3.8a** **3.8b**

### *3.1.2.2 Diphos ligands*

In 2012, a new class of bidentate phosphoramidite ligands based on a spiroketal backbone (*e.g.* **3.9a**) was reported for the Rh-catalysed hydroformylation of a range of alkenes.[35] Using the catalyst derived from ligand **3.9a**, an excellent linear to branched ratio (*n*:*iso*) of 174 was achieved for the hydroformylation of 1-hexene.[35] Analogous spiroketal-based diphosphite ligands (such as **3.9b**) were also reported for the hydroformylation of terminal and internal alkenes; an *n*:*iso* ratio of up to 93 was obtained.[36] The pyrrolyl and 7-membered phosphacycle substituents have also been employed in the novel diphosphoramidite and diphosphite tridentate ligands, **3.10a** and **3.10b** respectively, by Zheng *et al.*[37] They were tested in the hydroformylation of a range of cyclic olefins.[37] When using cyclohexene as the substrate a high aldehyde yield (92.0%) was obtained using the catalyst derived from ligand **3.10b**; a similar yield was achieved using the catalyst derived from **3.10a** but a higher L/Rh ratio of 20 was required (vs. 5).[37]

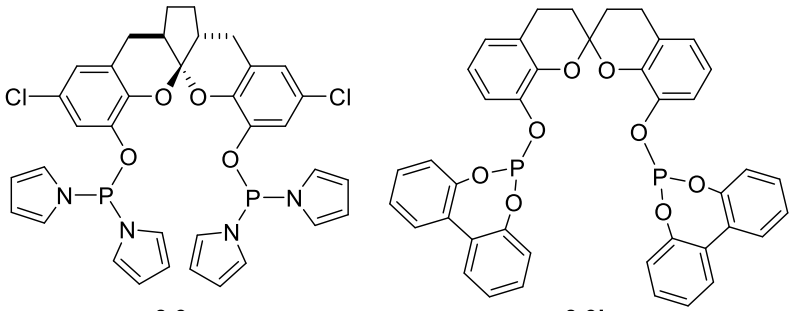


**3.9a** **3.9b**

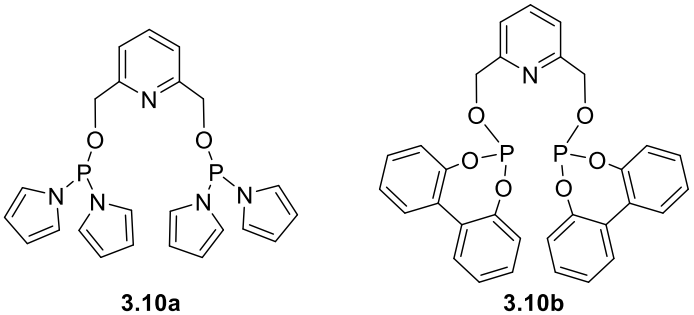


**3.10a** **3.10b**

### *3.1.2.3 Tri- and tetraphos ligands*

Since 2006, Zhang *et al.* have focussed their research efforts into tetraphos ligands for Rh-catalysed hydroformylation. More recently, in 2016 they developed a range of novel tetraphosphite ligands (**3.11**) and applied them to Rh-catalysed hydroformylation of 1-octene.[38] Linear selectivities of up to 98.9% were obtained with **3.11**, when R = Me.[38] In 2014, Zheng *et al.* applied the bi- and tetradentate pyrrolyl phosphanes, **3.12a** and **3.13a**, in the Rh-catalysed hydroformylation of 1-octene, but only moderate regioselectivities were observed.[39] Later in 2019, Zheng *et al.* employed the air-stable phenyl analogues **3.12b** and **3.13b** in the Rh-catalysed hydroformylation of 1-octene and 1-hexene; high yields of aldehyde were obtained even at 40 °C.[40] Additionally, the catalyst derived from **3.13b** could be recycled seven times with retention of catalytic activity and selectivity.[40]

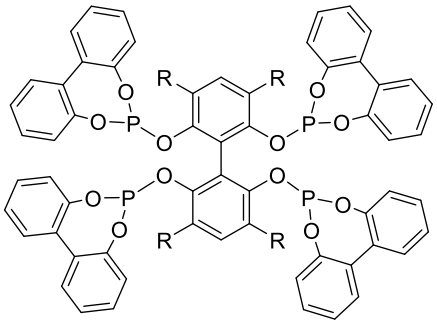

**3.11**

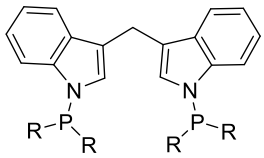

R = pyrrolyl **3.12a**
Ph **3.12b**

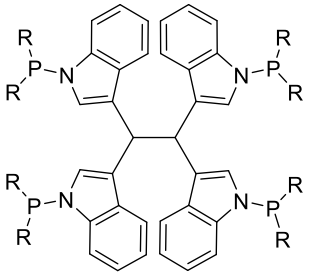

R = pyrrolyl **3.13a**
Ph **3.13b**

In 2019, Borner *et al.* employed tetradentate tripodal phosphinophosphite ligands (*e.g.* **3.14**) in the hydroformylation of 1-octene; preliminary studies gave high yields of aldehyde (up to 92%) but no additional information was disclosed in the patent.[41]

Triphosphorus ligands have rarely been explored as ligands for hydroformylation despite many examples of both bi- and tetradentate phosphorus ligands. The first triphosphorus ligand for regioselective linear hydroformylation was reported in 2013.[42] The novel triphosphoramidite **3.15** was employed in the hydroformylation of a range of terminal and internal alkenes; remarkable *n*-selectivities were observed with a *n*:*iso* ratio of up to 471 achieved.[42]

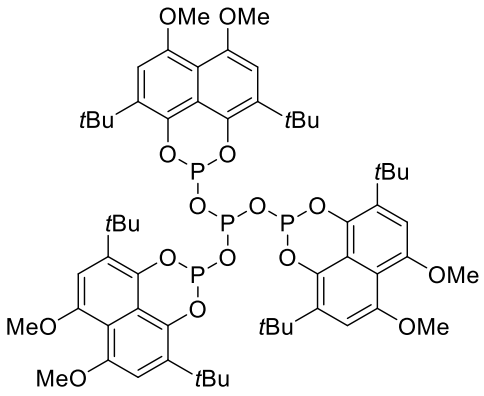


**3.14**

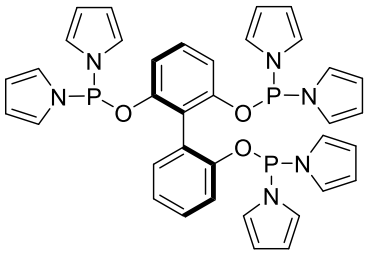

**3.15**

### *3.1.2.4 Branched selective hydroformylation*

To date, there are only a few examples of catalysts that show a preference for branched aldehyde formation in hydroformylation. Branched aldehyde products are increasingly desired due to their use in the fragrance, flavour and life-sciences industries.[43] To achieve branched selective hydroformylation at temperatures used in industry is challenging; originally the best selectivities could only be obtained at low temperatures (*e.g.* 19 °C).[44] Reek *et al.* employed the rhodium encapsulation complex **3.16** in the hydroformylation of propene and a good *iso* selectivity of *ca.* 50% was achieved at 70 °C.[44,45]

Since 2012, Clark *et al.* have demonstrated excellent branched selectivity in the hydroformylation of a range of substrates using a catalyst derived from the phosphite-phospholane bidentate ligand, BOBPHOS (**3.17**).[46] This pioneering work was the first example of an enantioselective hydroformylation to give the branched aldehyde product; an *ee* of up to 93% was achieved.[46] In addition, Clarke *et al.* have applied this system in the hydroformylation of allylglycine derivatives which give chiral intermediates of industrial importance for new antibiotics.[47] The origin of the branched selectivity produced from the Rh/BOBPHOS system has since been investigated in detail.[48,49] In 2019, unprecedentedly high branched-selectivity (82.0%) in the hydroformylation of propene was obtained using the Rh/BOBPHOS system; unusual solvents, such as octafluorotoluene, were crucial to the selectivity observed and high enough temperatures were used to achieve fast conversion.[50–52] Other ligands recently employed in branched selective hydroformylation include nitrogen-centred triphosphines (**3.18**) and phosphine-phosphoramidites (*e.g.* **3.19**); branched selectivities of up to 56% using the catalyst derived from **3.19** were observed in the hydroformylation of propene.[43,53]

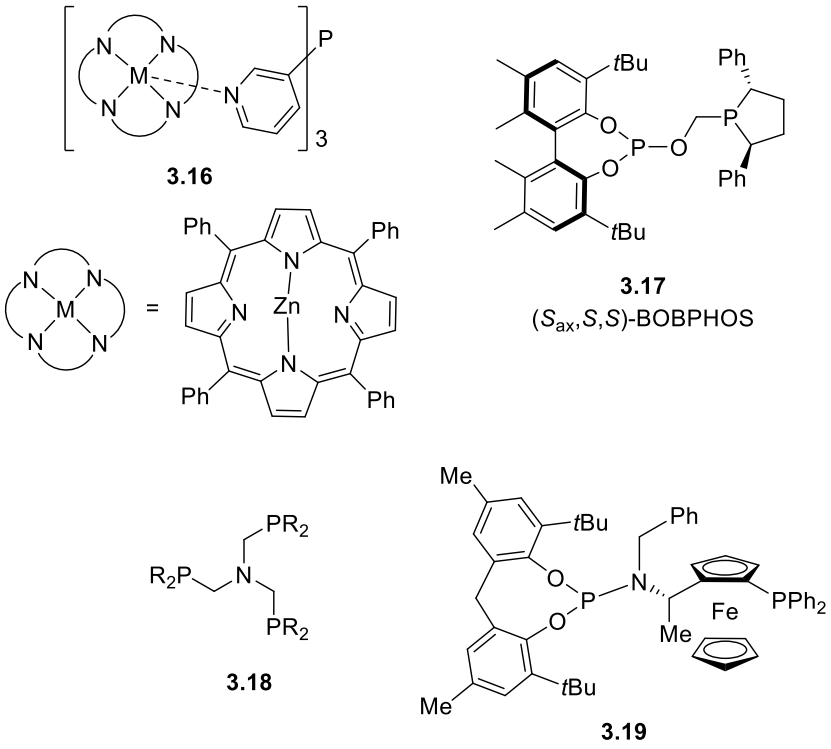


*3.1.2.5 Other active areas of research*

Supramolecular strategies have been used extensively to control both the activity and selectivity of hydroformylation reactions,[54–57] and have recently been reviewed by Reek *et al.*[58] Other current active areas of research in hydroformylation include asymmetric hydroformylation (recently reviewed by Landis *et al.*),[59] biphasic hydroformylation and the use of water-soluble ligands[60–62] and ionic liquid phase hydroformylation (recently reviewed by Haumann *et al.*).[63] Tandem hydroformylation reactions are also increasingly being explored, for example isomerisation-hydroformylation reactions, which are important for the production of linear aldehydes from internal alkenes.[64,65]

### 3.1.3 Mechanism of Rh-catalysed hydroformylation

The mechanism of hydroformylation has been well studied.[6,9,13,66–68] The generally accepted mechanism for Rh-catalysed hydroformylation is the dissociative mechanism shown in Scheme 3.2 (pathway **I**),[6] which was proposed by Wilkinson in the 1960s for the $[RhH(CO)(PPh_3)_3]$ catalyst.[4] The mechanism is based on Heck's original mechanism for Co-catalysed hydroformylation.[69] It proceeds *via* initial CO or ligand dissociation to form the *cis* and *trans* unsaturated species **a** and **b** (Scheme 3.2). Coordination of the alkene (**c** and **d**) is then followed by regioselectivity determining hydride migration to give alkyl complexes **e** and **f**. β-hydride elimination of the alkyl complexes can occur at this point leading to the formation of isomerisation products. Coordination of CO (**g** and **h**) is then

followed by alkyl migration to the CO ligand to form the acyl complexes **i** and **j**. The final irreversible hydrogenolysis step yields the aldehyde product and regenerates complexes **a** and **b**.

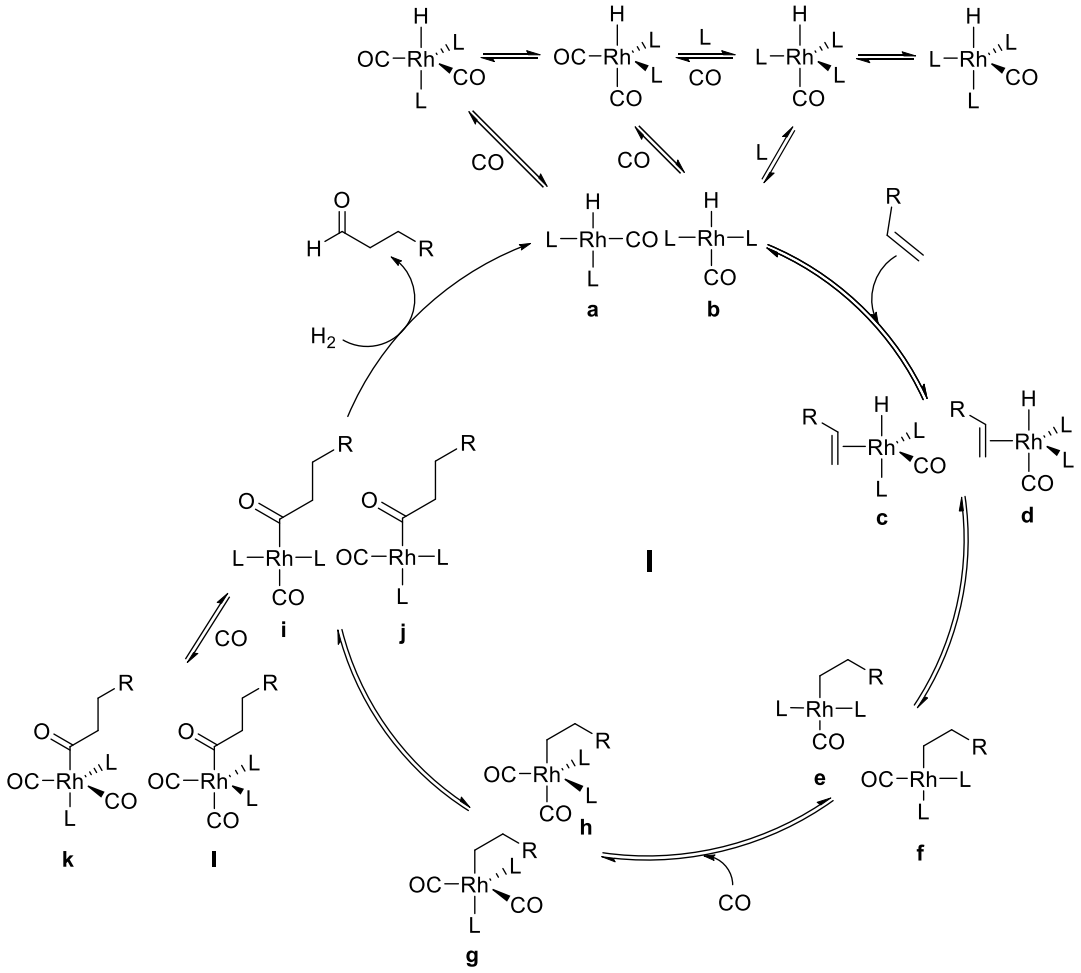

**Scheme 3.2** Simplified mechanism for the Rh-catalysed hydroformylation of an alkene, where L = $PPh_3$. Only the pathway to the linear aldehyde is shown.

Generally, strong π-acceptor ligands (*e.g.* phosphites) facilitate CO dissociation from the $RhH(CO)_2L_2$ complexes and alkene association to form complexes **c** and **d**, resulting in a highly active catalyst.[6] The Rh-L species present in hydroformylation depends on the pressure of CO and the concentration and nature of the ligand. In pathway **I** (Scheme 3.2) the bulky *trans*-$Rh(CO)L_2$ fragment promotes *n*-regioselectivity, since the *n*-alkyl intermediate is favoured over the *iso* isomer.[6] Decreasing the ligand concentration or increasing the CO concentration is known to decrease the *n*-selectivity due to the potential formation of highly active but less selective $Rh(CO)_2L$ species (or even $Rh(CO)_3$ species).

### 3.1.4 Recently proposed "$RhL_3$" mechanism

Recently, Pringle *et al.* have proposed the "$RhL_3$" mechanism (pathway **II**, Scheme 3.3) for Rh-catalysed hydroformylation using a Rh-tris(pyrrolyl)phosphine ($PPyr_3$, **3.4**) catalyst.[70] They observed that upon increasing the $PPyr_3$ concentration from a L/Rh ratio of 4.5 to 40 dramatically increased the *n*-selectivity from a *n*:*iso* ratio of 2 to 48.[70] Whereas, when using the catalyst derived from $PPh_3$ only a small increase from 3 to 6 was observed.[70] It was suggested that the excellent *n*-regioselectivity observed when using high concentrations of $PPyr_3$ was due to the presence of highly selective $RhL_3$ species. Such $RhL_3$ intermediates have previously only been suggested in hydroformylation catalysis as out-of-cycle resting states, as seen in pathway **I** (Scheme 3.2). The $RhL_3$ intermediates in pathway **II**, **B** and **C**, have a high steric bulk which promote the formation of *n*-alkyl Rh complexes and result in increased *n*-selectivity.

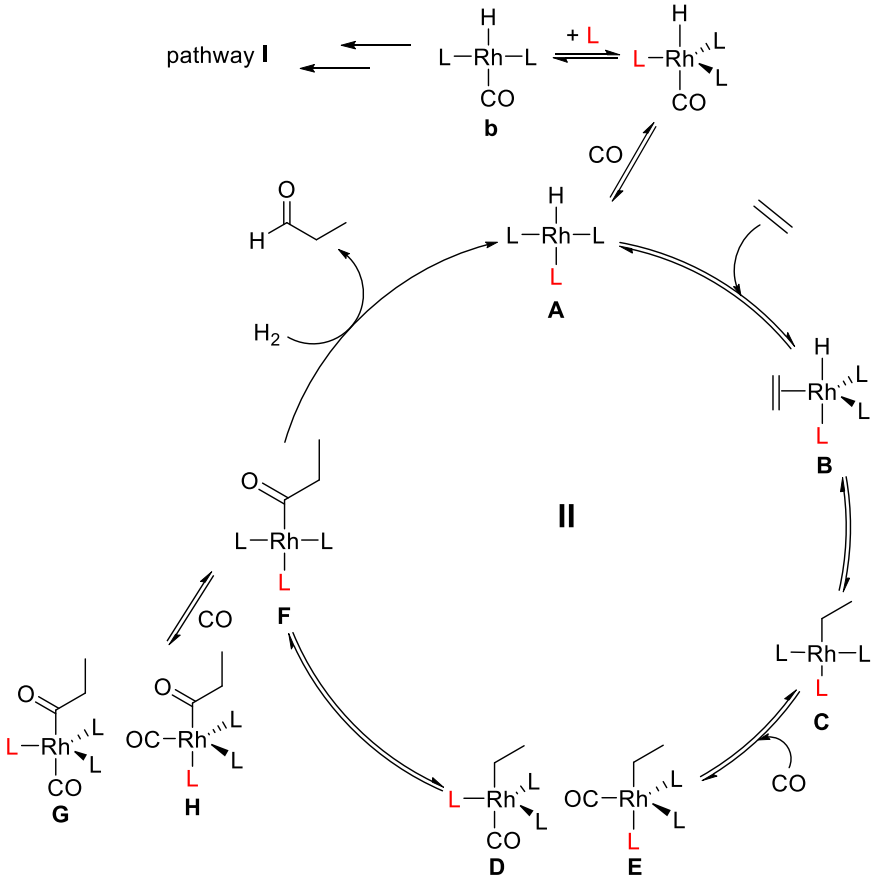


**Scheme 3.3** Simplified "$RhL_3$" mechanism for the Rh-catalysed hydroformylation of ethene, where L = $PPyr_3$.

To explore the viability of the $Rh(CO)L_2$ mechanism (pathway **I**) relative to the $RhL_3$ mechanism (pathway **II**), DFT calculations were carried out for both mechanistic pathways using catalysts derived from $PPh_3$ and $PPyr_3$.[70] It was argued that pathway **II** was accessible for the Rh-$PPyr_3$ catalyst, but less likely to occur for the Rh-$PPh_3$ catalyst.[70] The potential involvement of the highly selective $RhL_3$ species when using high concentrations of $PPyr_3$ explains the remarkable increase in *n*-selectivity described above.

### 3.1.5 Aims of the project

Following the success of Ethanox 398™ (**3.6**, Section 3.1.1) in hydroformylation, the aim of this project was to test the fluorophosphites $\mathbf{L_{2.1\text{-}2.4}}$ and $\mathbf{L_{2.6\text{-}2.8}}$ (Chapter 2) in the Rh-catalysed hydroformylation of 1-hexene. As shown in Chapter 2, the fluorophosphites are strong π-acceptors and so it was anticipated that they would give active hydroformylation catalysts. It was of interest to gauge the effect of phosphacycle ring size on hydroformylation by comparing the 5- to 8-membered fluorophosphites $\mathbf{L_{2.1\text{-}2.4}}$. In addition, the effect of substitution on the aryl rings of the 5- and 6-membered ligands was to be investigated by testing ligands $\mathbf{L_{2.6\text{-}2.8}}$. Following the excellent *n*-selectivity previously obtained when using high concentrations of $PPyr_3$ (Section 3.1.4), it was of interest to probe the effect of fluorophosphite concentration on Rh-catalysed hydroformylation of 1-hexene.

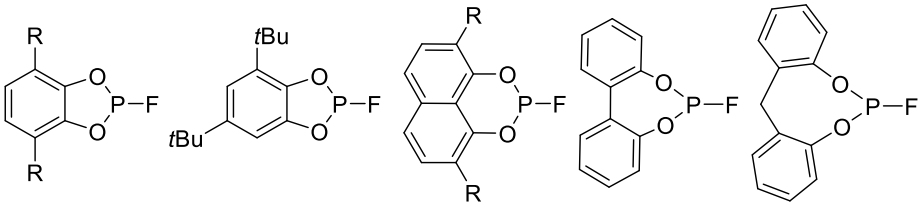


R = H $\mathbf{L_{2.1}}$ R = *t*Bu $\mathbf{L_{2.7}}$ | $\mathbf{L_{2.6}}$ | R = H $\mathbf{L_{2.2}}$ R = Me $\mathbf{L_{2.8}}$ | $\mathbf{L_{2.3}}$ | $\mathbf{L_{2.4}}$

## 3.2 Catalytic hydroformylation of 1-hexene under "concentrated-catalyst" conditions

The fluorophosphites $\mathbf{L_{2.1\text{-}2.4}}$ and $\mathbf{L_{2.6\text{-}2.8}}$ described in Chapter 2 were tested in the Rh-catalysed hydroformylation of 1-hexene. The catalysis performed at the University of Bristol was carried out at a Rh concentration of 3.9 mmol $L^{-1}$ (conditions A) and the results are presented below (see Chapter 7 for experimental details). The selectivity is given as a % rather than as a *n*:*iso* ratio.

### 3.2.1 Effect of fluorophosphite ring size

To probe the effect of fluorophosphite ring size on hydroformylation, the 5- to 8-membered fluorophosphites $\mathbf{L_{2.1\text{-}2.4}}$ were tested in the hydroformylation of 1-hexene (Scheme 3.4). For consistency the catalysis was stopped at *ca.* 30% conversion by quenching the reaction mixture with an excess of tributylphosphite. The selectivity, conversion and turnover frequency to aldehyde products ($TOF_{aldehyde}$) were determined by $^1$H NMR spectroscopy (see Chapter 7 for details) and the results are shown in Table 3.1. A L/Rh ratio of 5 was employed for these initial catalytic runs.

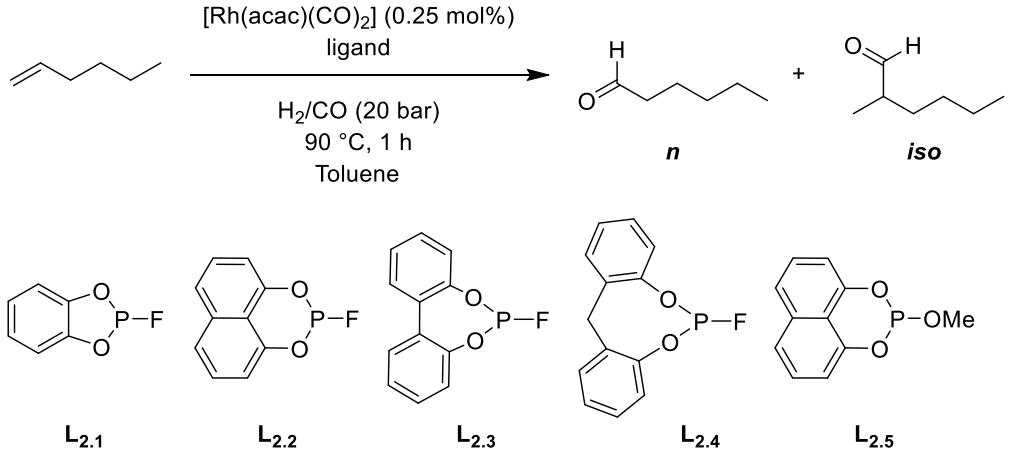


**Scheme 3.4** Catalytic hydroformylation of 1-hexene using ligands $\mathbf{L_{2.1\text{-}2.5}}$.

**Table 3.1** Catalytic hydroformylation of 1-hexene using L/Rh = 5 under conditions A.[a]

| Entry | Ligand | % *n* selectivity | Conversion / %[b] | $TOF_{aldehyde}$ / $h^{-1}$ [c] | Isomerisation / %[d] |
|---|---|---|---|---|---|
| 1* | $\mathbf{L_{2.1}}$ | 0 | 0 | - | 0 |
| 2* | $\mathbf{L_{2.2}}$ | 91.3 | 36 | 669 | 18 |
| 3* | $\mathbf{L_{2.3}}$ | 90.2 | 37 | 112 | 5 |
| 4 | $\mathbf{L_{2.4}}$ | 90.1 | 24 | 32 | 1 |
| 5 | $\mathbf{L_{2.5}}$ | 88.2 | 20 | 36 | 3 |

[a] Method: 4.83 mmol 1-hexene, 0.012 mmol $[Rh(acac)(CO)_2]$, 0.060 mmol ligand (L/Rh = 5), 2.5 $cm^3$ toluene, 20 bar of $H_2$/CO (1/1), 90 °C. [b] Conversion = conversion to aldehydes, *i.e.* 100% - (1-hexene and isomerisation). [c] TOF at the given conversion. [d] Isomerisation to 2- and 3-hexene. Conversion and selectivity were determined by $^1$H NMR spectroscopy. *Result is an average of at least two runs.

The catalyst derived from the 5-membered fluorophosphite **L2.1** showed no hydroformylation activity (Entry 1, Table 3.1); this experiment was repeated. The $^{31}P\{^{1}H\}$ NMR spectrum of the reaction mixture after catalysis showed degradation of **L2.1** had occurred. The signals observed were singlets ($\delta_P \approx$ 8.1, -1.9, -13.7 ppm) and so the P–F bond was no longer intact, suggesting hydrolysis of the ligand had occurred. The 5-membered **L2.1** is extremely sensitive to water (see Chapter 2), which may have been present adventitiously or due to some aldol condensation of a small amount of aldehyde formed. The generation of free fluoride ions from the hydrolysis of fluorophosphite **L2.1** would be detrimental to catalyst activity, according to Puckette *et al.*[71,72]

The catalysts derived from the larger ring fluorophosphites, **L2.2-2.4**, were stable to hydrolysis under catalytic conditions and displayed good hydroformylation activity. The 6-membered ligand **L2.2** gave the most active and *n*-selective catalyst (Entry 2, Table 3.1). The TOF was significantly higher for the catalyst derived from **L2.2** than that of the 7-membered **L2.3**: 669 vs. 112 $h^{-1}$ (Entry 2 vs. 3). However, ligand **L2.2** also gave a highly active isomerisation catalyst, relative to ligands **L2.3-2.4**. The catalysts derived from **L2.3** and **L2.4**, containing 7- and 8-membered rings, gave similar *n*-selectivities (Entries 3 and 4, *ca.* 90%).

Both catalysts derived from **L2.3** and **L2.4** were considerably less active than the 6-membered fluorophosphite **L2.2**. The catalyst derived from the 8-membered **L2.4** gave a particularly low TOF of 32 $h^{-1}$ (Entry 4, Table 3.1). Problems were encountered during the purification of the 8-membered ligand **L2.4**: considerable amounts (*ca.* 25%) of $SbCl_3$ were detected in the ligand (see Chapter 2) but attempts to purify the ligand through silica or florisil often led to the telomerisation of **L2.4**, making complete removal of $SbCl_3$ problematic. The low activity of the catalyst derived from **L2.4** may be attributed to the hydrolysis of $SbCl_3$ under catalytic conditions; the generation of free chloride ions is known to be detrimental to the activity of a hydroformylation catalyst.[21,71,73] The capriciousness of the results obtained when using the other fluorophosphites may also be due to the presence of $SbCl_3$; purification of the ligands through florisil before use was essential to maintaining the catalytic activity.

To explore the effect of the fluoro-substituent on hydroformylation catalysis, the analogous 6-membered phosphite **L2.5** (Scheme 3.4) was also tested in the hydroformylation of 1-hexene (Entry 5, Table 3.1). The TOF when using the 6-membered phosphite ligand **L2.5** was significantly lower than the analogous 6-membered

fluorophosphite **L**$_{2.2}$ (36 vs. 669 h$^{-1}$). The catalyst derived from the phosphite **L**$_{2.5}$ was also less selective towards the *n*-aldehyde *cf.* **L**$_{2.2}$ (88.2 vs. 91.3%, Entry 5 vs. 2). The difference in activity may be attributed to their different donor properties (as seen in Chapter 2); the fluorophosphite **L**$_{2.2}$ is a significantly stronger π-acceptor than the phosphite **L**$_{2.5}$. Increasing the π-accepting properties of the ligand increases the rate of reaction, since CO dissociation and alkene association is facilitated.[9] Stronger π-acceptors also have a higher preference for equatorial sites on the Rh centre, which promotes the formation of the *n*-aldehyde.[9]

### 3.2.2 Effect of ligand concentration

It is well-known that ligand concentration can greatly affect the catalyst selectivity and activity of Rh-catalysed hydroformylation.[71,74] The effect of concentration of ligands **L**$_{2.2}$ and **L**$_{2.3}$ on catalysis was investigated. A range of L/Rh ratios (5-15) were tested in the same volume of solvent and the results are shown in Table 3.2. As above, all reactions were quenched at *ca.* 30% conversion for consistency.

**Table 3.2** Effect of ligand concentration on the catalytic hydroformylation of 1-hexene using **L**$_{2.2\text{-}2.3}$.[a]

| Entry | Ligand | L/Rh ratio | % *n* selectivity | Conversion / %[b] | TOF$_{aldehyde}$ / h$^{-1}$ [c] | Isom. / %[d] |
|---|---|---|---|---|---|---|
| 1* | **L**$_{2.2}$ | 5 | 91.3 | 36 | 669 | 18 |
| 2* | **L**$_{2.2}$ | 10 | 96.6 | 28 | 48 | 15 |
| 3 | **L**$_{2.2}$ | 15 | 99.5 | 26 | 42 | 7 |
| 4* | **L**$_{2.3}$ | 5 | 90.2 | 37 | 112 | 5 |
| 5 | **L**$_{2.3}$ | 10 | 95.1 | 32 | 55 | 1 |

[a] Method: 4.83 mmol 1-hexene, 0.012 mmol [Rh(acac)(CO)$_2$], ligand (L/Rh = 5, 10 or 15), 2.5 cm$^3$ toluene, 20 bar of H$_2$/CO (1/1), 90 °C. [b] Conversion = conversion to aldehydes, *i.e.* 100% - (1-hexene and isomerisation). [c] TOF at the given conversion. [d] Isomerisation to 2- and 3-hexene. Conversion and selectivity were determined by $^1$H NMR spectroscopy. *Results are an average of at least two runs.

For the catalysts derived from both the 6- and 7-membered ligands **L**$_{2.2}$ and **L**$_{2.3}$, increasing the ligand concentration considerably decreased the catalytic activity. For example, the TOF dropped by an order of magnitude for **L**$_{2.2}$ when the L/Rh ratio was increased from

5 to 10 (669 vs. 48 $h^{-1}$, Entry 1 vs. 2, Table 3.2). At a higher ligand concentration the formation of the unsaturated catalytically active species (such as complex **A** in Scheme 3.3, Section 3.1.4) is inhibited, resulting in a decrease in activity.[6]

On the other hand, when using the catalysts derived from $\mathbf{L_{2.2}}$ and $\mathbf{L_{2.3}}$ increasing the ligand concentration significantly increased the *n*-selectivity. Ligand concentration appeared to have a greater influence on selectivity for the 6-membered ligand $\mathbf{L_{2.2}}$, relative to $\mathbf{L_{2.3}}$. Increasing the L/Rh ratio from 5 to 15 for $\mathbf{L_{2.2}}$ greatly increased the *n*-selectivity from 91.3% to a remarkable 99.5% (Entry 1 vs. 3, Table 3.2). At higher ligand concentrations, the coordination equilibria lie towards the more sterically hindered fluorophosphite-rich intermediates, which favour the formation of the *n*-aldehyde.[75] In addition, decreased amounts of isomerisation were observed at higher ligand concentrations for both $\mathbf{L_{2.2}}$ and $\mathbf{L_{2.3}}$ (Entry 1 vs. 3).

As discussed, fluorophosphites $\mathbf{L_{2.2}}$ and $\mathbf{L_{2.3}}$ are very strong π-acceptors (Chapter 2). The combination of their high π-acceptor capacity, relatively small size and significant influence of ligand concentration on *n*-selectivity may suggest the formation of reactive and selective $RhL_3$ species throughout the catalysis.[70] Such ligand-rich catalytic intermediates have been suggested when using $PPyr_3$ (Section 3.1.4).[70] Relative to $RhL_2$, these $RhL_3$ species promote the formation of the *n*-alkyl Rh complex **C** (Scheme 3.3, Section 3.1.4).[70] Since the 6-membered fluorophosphite $\mathbf{L_{2.2}}$ is smaller and a stronger π-acceptor than the 7-membered $\mathbf{L_{2.3}}$ (Chapter 2), the formation of $RhL_3$ species would be more favoured, which may explain why ligand concentration has a greater influence on selectivity for $\mathbf{L_{2.2}}$ relative to $\mathbf{L_{2.3}}$.

### 3.2.3 Effect of fluorophosphite aryl substitution

To probe the effect of substitution on the aryl rings of the 5- and 6-membered fluorophosphites, ligands $\mathbf{L_{2.6\text{-}2.8}}$ were tested in the hydroformylation of 1-hexene (Scheme 3.4). The same conditions as described in Section 3.2.1 (L/Rh = 5) were used and the results are shown in Table 3.3.

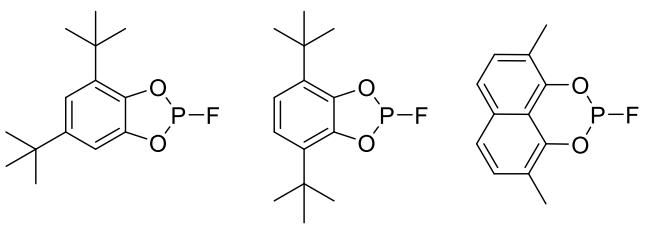


$\mathbf{L_{2.6}}$ $\mathbf{L_{2.7}}$ $\mathbf{L_{2.8}}$

**Table 3.3** Catalytic hydroformylation of 1-hexene using the aryl substituted fluorophosphites $\mathbf{L_{2.6\text{-}2.8}}$.[a]

| Entry | Ligand | L/Rh ratio | % *n* selectivity | Conversion / %[b] | $TOF_{aldehyde}$ / $h^{-1}$ [c] | Isom. / %[d] |
|---|---|---|---|---|---|---|
| 1 | $\mathbf{L_{2.6}}$ | 5 | 0 | 0 | - | 0 |
| 2 | $\mathbf{L_{2.7}}$ | 5 | 0 | 0 | - | 0 |
| 3 | $\mathbf{L_{2.8}}$ | 5 | 92.0 | 48 | 1 656 | 16 |
| 4 | $\mathbf{L_{2.8}}$ | 10 | 99.0 | 33 | 72 | 10 |

[a] Method: 4.83 mmol 1-hexene, 0.012 mmol $[Rh(acac)(CO)_2]$, ligand (L/Rh = 5 or 10), 2.5 $cm^3$ toluene, 20 bar of $H_2$/CO (1/1), 90 °C. [b] Conversion = conversion to aldehydes, *i.e.* 100% - (1-hexene and isomerisation). [c] TOF at the given conversion. [d] Isomerisation to 2- and 3-hexene. Conversion and selectivity were determined by $^1$H NMR spectroscopy.

The catalysts derived from the substituted 5-membered fluorophosphites $\mathbf{L_{2.6\text{-}2.7}}$ displayed zero catalytic activity (Entries 1-2, Table 3.3), similar to the unsubstituted analogue $\mathbf{L_{2.1}}$. The $^{31}P\{^1H\}$ NMR spectrum of the reaction mixture after catalysis when using the 3,5-*t*Bu substituted $\mathbf{L_{2.6}}$ showed complete degradation of the ligand to a P(V) spirophosphorane species, such as species **3.20**. Despite the lack of catalytic activity observed when using the 3,6-*t*Bu substituted fluorophosphite $\mathbf{L_{2.7}}$, the $^{31}P\{^1H\}$ NMR spectrum of the reaction mixture at the end of the catalysis showed the ligand remained intact. The 5-membered fluorophosphites are stronger π-acceptors than the larger ring analogues (Chapter 2). The high π-accepting properties of the 5-membered fluorophosphites may lead to the displacement of CO from $[HRhL_3(CO)]$ to form the inactive $[RhHL_4]$ species.[12] Similar coordination behaviour was shown in Chapter 2, where upon the reaction of ligand $\mathbf{L_{2.7}}$ with $[Rh_2Cl_2(CO)_4]$ displacement of CO occurred. The formation of the $[RhHL_4]$ species may explain the lack of activity observed when using $\mathbf{L_{2.7}}$. Paired with their acute susceptibility to hydrolysis, it would appear that 5-membered fluorophosphites are not suitable ligands for hydroformylation catalysis.

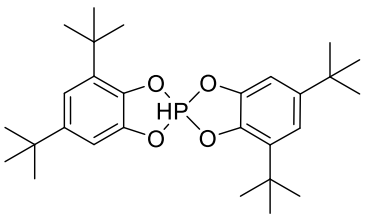


**3.20**

By contrast, the 6-membered aryl substituted fluorophosphite **L2.8** gave a highly active catalyst (Entry 3, Table 3.3), achieving a high TOF of 1 656 $h^{-1}$ when using a L/Rh ratio of 5. The catalyst derived from **L2.8** also displayed good selectivity towards the *n*-aldehyde (92.0%), slighter higher than that of the unsubstituted **L2.2** (91.3%) (L/Rh = 5).

Upon increasing the L/Rh ratio from 5 to 10 for **L2.8** the catalytic activity dramatically decreased from a TOF of 1 656 to 72 $h^{-1}$ (Entry 3 vs. 4, Table 3.3); the activity is highly sensitive to ligand concentration under these "concentrated-catalyst" conditions - at high concentrations the fluorophosphites inhibit catalysis. On the other hand, the *n*-selectivity significantly increased from 92.0 to 99.0% (Entry 3 vs. 4), for reasons explained above (Section 3.2.2). The amount of isomerisation was decreased upon increasing the ligand concentration of **L2.8**.

The *n*-selectivity obtained when using a L/Rh ratio of 10 was also significantly higher than that of the catalyst derived from the unsubstituted analogue **L2.2**, under the same conditions (99.0 vs. 96.6%). This difference in reactivity may be explained by the increased steric bulk of the $RhL_3$ catalytic intermediates when using **L2.8**, which would further promote the formation of the *n*-alkyl Rh complex. Nevertheless, there is a fine balance to be struck regarding steric hindrance: if the ligand is too bulky the dissociation of the $RhL_3$ intermediates to form less selective $RhL_2$ species may be promoted.

### 3.3 Catalytic hydroformylation of 1-hexene under "dilute-catalyst" conditions

Catalytic hydroformylation was also performed at the Leibniz Institute for Catalysis (Rostock, Germany) by the author and Dr. Christoph Kubis, but at a lower Rh concentration of 1.14 mmol $L^{-1}$ and a lower substrate concentration of 1 154 mmol $L^{-1}$ (conditions B). An aliquot of the reaction mixture was collected periodically and GC used to determine the ratio of products (see Chapter 7 for experimental details). Dr. Christoph Kubis (LIKAT, Rostock) performed kinetic modelling to calculate the turnover frequency (TOF). The results are presented and discussed below.

#### 3.3.1 Effect of fluorophosphite ligand

The 6- and 7-membered fluorophosphites **L2.2-2.3** were tested in the hydroformylation of 1-hexene under conditions B using a L/Rh ratio of 5. The kinetic data is presented in Table 3.4 and the product distribution over time is shown in Figures 3.2 and 3.3.

**Table 3.4** Catalytic hydroformylation of 1-hexene using ligands $\mathbf{L_{2.2\text{-}2.3}}$ under conditions B.

| Entry | Ligand | *n* selectivity / % | TOF at 20% conversion / $h^{-1}$ [b] | Yield of aldehyde / % [c] |
|---|---|---|---|---|
| 1 | $\mathbf{L_{2.2}}$ | 85.4 | 1 438 | 72.4 |
| 2 | $\mathbf{L_{2.3}}$ | 86.9 | 2 970 | 88.1 |

[a] Method: 40.3 mmol 1-hexene, 0.04 mmol $[Rh(acac)(CO)_2]$, ligand (L/Rh = 5), 35 $cm^3$ toluene, 20 bar of $H_2$/CO (1/1), 90 °C. [b] TOF at 0.8 mol $L^{-1}$ 1-hexene. [c] Remainder of products are alkenes (1-hexene or isomerisation). Conversion and selectivity were determined by GC.

In general, compared to the "concentrated-catalyst" conditions above (conditions A), the TOFs obtained under these "dilute-catalyst" conditions (conditions B) were significantly higher (*e.g.* 2 438 vs. 669 $h^{-1}$ for $\mathbf{L_{2.2}}$). The TOF is very sensitive to catalyst-concentration: at high concentrations the fluorophosphite ligands appear to inhibit catalysis.

In contrast to the "concentrated-catalyst" conditions above, the 7-membered fluorophosphite $\mathbf{L_{2.3}}$ gave a significantly more active catalyst than the 6-membered analogue $\mathbf{L_{2.2}}$, with a slightly higher *n*-selectivity (Entry 1 vs. 2, Table 3.4). The catalyst derived from the 6-membered fluorophosphite $\mathbf{L_{2.2}}$ appeared to deactivate slightly over time, as seen in Figure 3.2. The dark orange/ brown colour of the reaction mixture after catalysis also suggested degradation of the catalyst. Deactivation of the catalyst under these "dilute-catalyst" conditions may have occurred because the ligand concentration is too low to stabilise the Rh catalytic intermediates. Contrary to this, IR and $^{31}P\{^1H\}$ / $^{19}F\{^1H\}$ NMR spectroscopy of the reaction mixture after catalysis showed no signs of catalyst degradation; at present these observations cannot be reconciled.

Compared to the results carried out under conditions A (Section 3.2), both ligands $\mathbf{L_{2.2\text{-}2.3}}$ gave significantly less *n*-selective catalysts under conditions B. Under "dilute-catalyst" conditions (conditions B), the reaction equilibria (Scheme 3.3, Section 3.1.4) will lie towards the less sterically hindered intermediates (such as RhL and $RhL_2$), which will favour the *iso* aldehyde relative to $RhL_3$. Similar to the results given in Section 3.2, the 6-

membered fluorophosphite $\mathbf{L}_{2.2}$ gave a more active isomerisation catalyst than the 7-membered $\mathbf{L}_{2.3}$ (Figures 3.2 vs. 3.3).

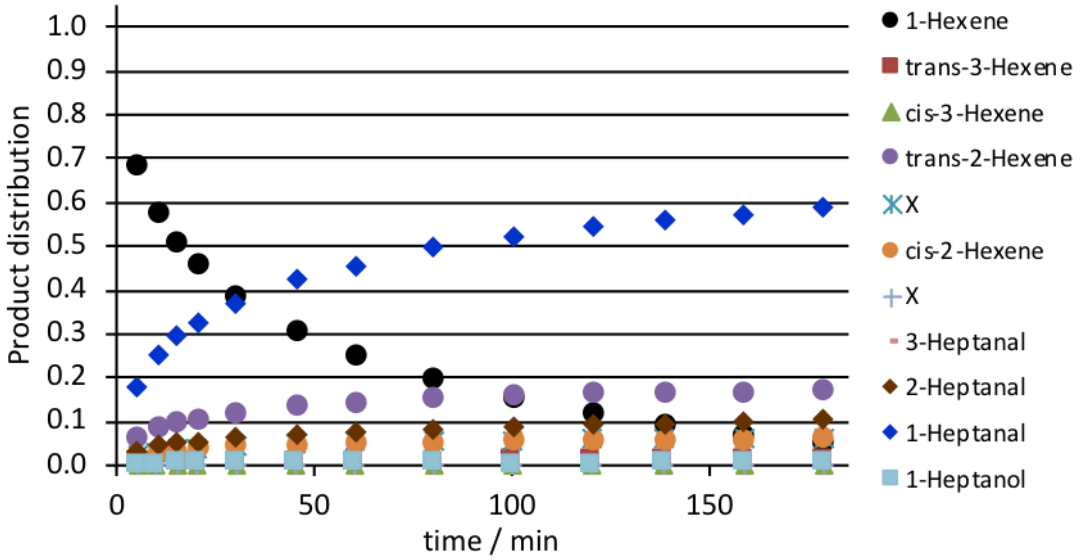


**Figure 3.2** Product distribution over time using ligand $\mathbf{L}_{2.2}$, L/Rh = 5. X = unidentified products.

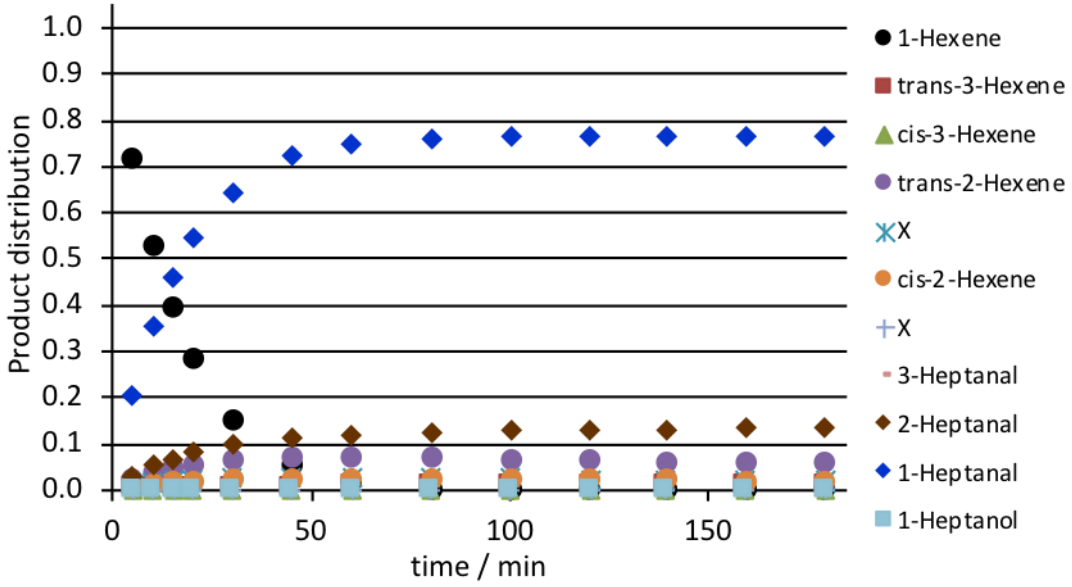


**Figure 3.3** Product distribution over time using ligand $\mathbf{L}_{2.3}$, L/Rh = 5. X = unidentified products.

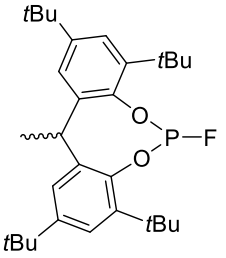


Ethanox 398™
(**3.6**)

The commercially valuable ligand, Ethanox 398™ (**3.6**), was also tested in the catalytic hydroformylation of 1-hexene under conditions B. Results cannot be directly compared with the results above in Table 3.4, since a L/Rh ratio of 20 was used (instead of 5). Nonetheless, ligand **3.6** gave an extremely active catalyst, achieving *ca.* 100% conversion within 15 min. Even using a much higher ligand concentration, the catalyst derived from **3.6** gave a TOF of 14 390 $h^{-1}$, considerably higher than that of $\mathbf{L_{2.2}}$ and $\mathbf{L_{2.3}}$ (see Table 3.4). A good *n*-selectivity of 89.5% was observed. The reaction mixture after catalysis was analysed by $^1$H NMR spectroscopy which showed a broad signal at -9.66 ppm which was assigned to a Rh-hydride species. All reaction mixtures were analysed by IR spectroscopy at the end of the catalysis. For the unsubstituted ligands $\mathbf{L_{2.2\text{-}2.3}}$ no ν(CO) bands were observed in the IR spectra suggesting only [$RhHL_4$] was present after catalysis. Whereas, when using **3.6** one ν(CO) band was observed, which was tentatively assigned to the [$RhHL_3(CO)$] species. This difference in chemistry may be attributed to the higher steric bulk of **3.6**, which would promote the formation of the less sterically hindered $RhL_2$ intermediates *in situ*.

### 3.3.2 Effect of ligand concentration

The effect of ligand concentration for ligands $\mathbf{L_{2.2\text{-}2.3}}$ was investigated under conditions B and the results are presented in Table 3.5 and examples of the kinetic data are shown in Figures 3.4 and 3.5.

**Table 3.5** Effect of ligand concentration for the catalytic hydroformylation of 1-hexene using ligands $\mathbf{L_{2.2\text{-}2.3}}$ under conditions B.

| Entry | L/Rh | Ligand | *n* selectivity / % | TOF at 20% conversion / $h^{-1}$ [b] | Yield of aldehyde / % [c] |
|---|---|---|---|---|---|
| 1 | 5 | $\mathbf{L_{2.2}}$ | 85.4 | 1 438 | 72.4 |
| 2 | 10 | $\mathbf{L_{2.2}}$ | 89.3 | 805 | 75.0 |
| 3 | 15 | $\mathbf{L_{2.2}}$ | 91.2 | 645 | 75.4 |
| 4 | 5 | $\mathbf{L_{2.3}}$ | 86.9 | 2 970 | 88.1 |
| 5 | 10 | $\mathbf{L_{2.3}}$ | 92.7 | 570 | 90.4 |

[a] Method: 40.3 mmol 1-hexene, 0.04 mmol $[Rh(acac)(CO)_2]$, ligand (L/Rh = 5 or 10), 35 $cm^3$ toluene, 20 bar of $H_2/CO$ (1/1), 90 °C. [b] TOF at 0.8 mol $L^{-1}$ 1-hexene. [c] Remainder of products are alkenes (1-hexene or isomerisation). Conversion and selectivity were determined by GC.

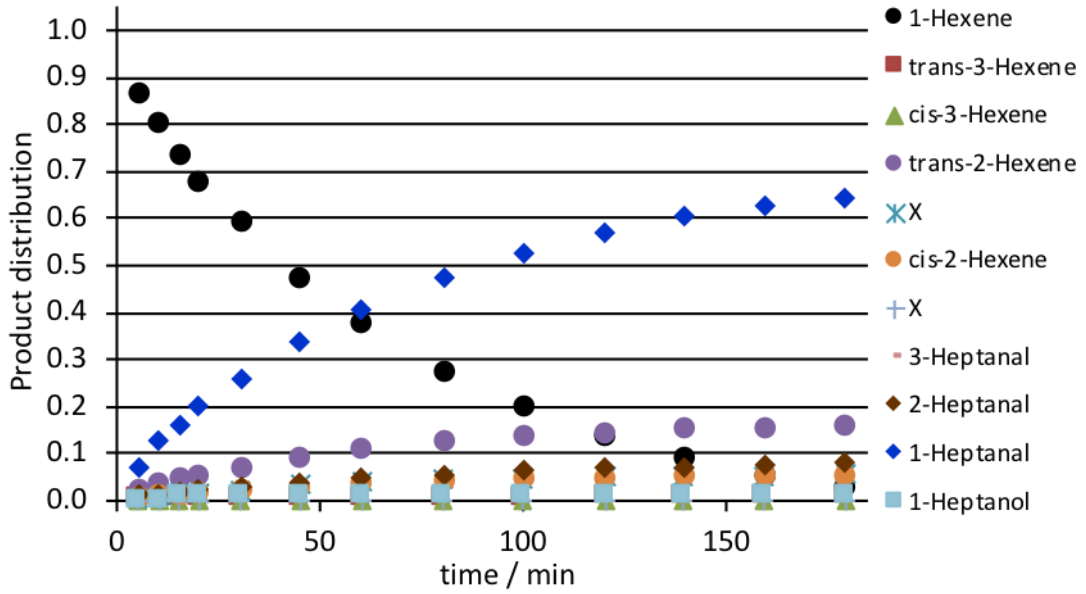


**Figure 3.4** Product distribution over time using ligand $\mathbf{L_{2.2}}$, L/Rh = 10. X = unidentified products.

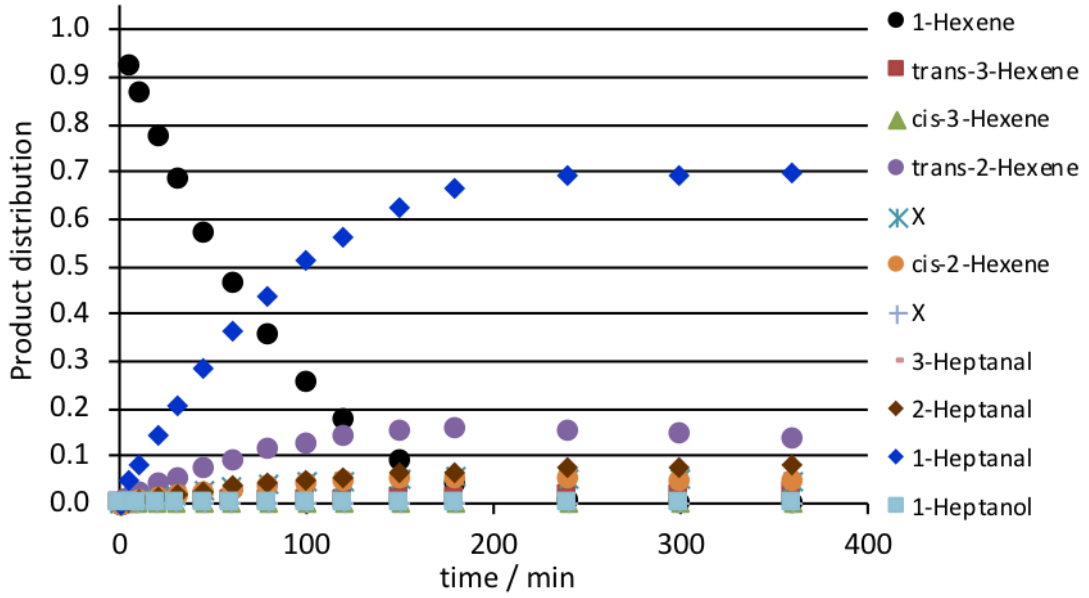


**Figure 3.5** Product distribution over time using ligand **L**$_{2.2}$, L/Rh = 15. X = unidentified products.

An increase in *n*-selectivity and a decrease in activity were observed upon increasing the ligand concentration of both ligands **L**$_{2.2}$ and **L**$_{2.3}$. Using the 6-membered **L**$_{2.2}$ the *n*-selectivity was increased from 85.4 to 91.2% upon increasing the L/Rh ratio from 5 to 15 (Entry 1 vs. 3, Table 3.5). In contrast to conditions A, a greater effect of ligand concentration was observed using the 7-membered fluorophosphite **L**$_{2.3}$. Upon increasing the L/Rh ratio from 5 to only 10 the selectivity increased from 86.9 to 92.7% and the TOF was decreased from 2 970 to 570 $h^{-1}$ (Entry 4 vs. 5).

### 3.3.3 Effect of temperature and pressure

Preliminary studies to probe the effect of temperature on catalysis were carried out for ligands **L**$_{2.2}$ and **3.6** under conditions B and the results are given in Table 3.6.

**Table 3.6** Effect of temperature for the catalytic hydroformylation of 1-hexene using ligands $\mathbf{L_{2.2}}$ and **3.6** under conditions B.

| Entry | Ligand | Temp. / °C | *n* selectivity / % | TOF at 20% conversion / $h^{-1}$ [b] | Yield of aldehyde / % [c] |
|---|---|---|---|---|---|
| 1 | $\mathbf{L_{2.2}}$ | 90 | 89.3 | 805 | 75.0 |
| 2 | $\mathbf{L_{2.2}}$ | 80 | 90.7 | 742 | 80.3 |
| 3 | **3.6** | 90 | 89.5 | 14,390 | 80.5 |
| 4 | **3.6** | 80 | 87.0 | 6,538 | 89.9 |

[a] Method: 40.3 mmol 1-hexene, 0.04 mmol $[Rh(acac)(CO)_2]$, ligand (L/Rh = 10 for $\mathbf{L_{2.2}}$ and 20 for **3.6**), 35 $cm^3$ toluene, 20 bar of $H_2$/CO (1/1), 90 °C or 80 °C. [b] TOF at 0.8 mol $L^{-1}$ 1-hexene. [c] Remainder of products are alkenes (1-hexene or isomerisation). Conversion and selectivity were determined by GC.

To control the catalyst activity for Ethanox 398™ (**3.6**) a L/Rh ratio of 20 was used, compared to 10 when using $\mathbf{L_{2.2}}$. Decreasing the temperature from 90 °C to 80 °C, the activity of the catalyst derived from **3.6** dropped dramatically (Entry 3 vs. 4, Table 3.6), but still surpassed those obtained for $\mathbf{L_{2.2\text{-}2.3}}$ (Table 3.5). However, little difference in *n*-selectivity was observed. In contrast to **3.6**, decreasing the temperature appeared to have minimal effect on the activity and selectivity of the catalyst derived from the 6-membered fluorophosphite $\mathbf{L_{2.2}}$; an explanation for this observation has eluded us. It would be of interest to perform the catalysis using $\mathbf{L_{2.2}}$ at a much lower temperature of 40 °C to confirm this result.

Preliminary studies to probe the effect of CO pressure on catalysis were carried out for ligand $\mathbf{L_{2.2}}$ under conditions B (L/Rh = 10) and the results are given in Table 3.7. The $H_2$ pressure was kept constant, while the CO pressure was increased from 10 to 20 bar ($H_2$/CO = 10/20).

**Table 3.7** Effect of CO pressure for the catalytic hydroformylation of 1-hexene using ligand **L**$_{2.2}$ under conditions B.

| Entry | Ligand | $H_2$:CO / bar | *n* selectivity / % | TOF at 20% conversion / $h^{-1}$ [b] | Yield of aldehyde / % [c] |
|---|---|---|---|---|---|
| 1 | **L**$_{2.2}$ | 10:10 | 89.3 | 805 | 75.0 |
| 2 | **L**$_{2.2}$ | 10:20 | 85.2 | 776 | 81.4 |

[a] Method: 40.3 mmol 1-hexene, 0.04 mmol [Rh(acac)(CO)$_2$], ligand (L/Rh = 10), 35 $cm^3$ toluene, 20 bar of $H_2$/CO (1/1) or 30 bar of $H_2$/CO (1/2), 90 °C. [b] TOF at 0.8 mol $L^{-1}$ 1-hexene. [c] Remainder of products are alkenes (1-hexene or isomerisation). Conversion and selectivity were determined by GC.

Increasing the partial pressure of CO from 10 to 20 bar had a minimal effect on the activity of the catalyst derived from **L**$_{2.2}$, but the *n*-selectivity of the catalyst was significantly decreased (Entry 1 vs. 2, Table 3.7). At a higher CO pressure there would be a decrease in the sterically hindered $RhL_3$ intermediates due to ligand dissociation, which would lead to decreased amounts of *n*-aldehyde, as shown in Scheme 3.5.[8,9,70] This is further supported by the sensitivity of the system to ligand concentration.

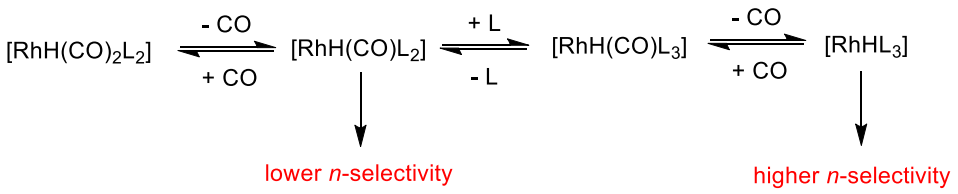


**Scheme 3.5** Initial equilibria forming the active catalyst species.[70]

Due to high amounts of isomerisation observed when using the 6-membered **L**$_{2.2}$, the catalytic hydroformylation of 2-hexene was investigated. A **L**$_{2.2}$/Rh ratio of 10 was used under conditions B. Figure 3.6 shows the product distribution over time. A significant amount of the *iso*-aldehyde (2-heptanal) was observed, suggesting that the 2-hexene formed in the catalysis above contributes to the amount of *iso*-aldehyde formed. An insignificant amount of 1-hexene was observed (Figure 3.6); it is assumed that any 1-hexene present immediately converts to the *n*-aldehyde due to the high reactivity of the *n*-alkyl Rh species. The majority of the 2-hexene consumed was isomerised to *trans*-2-hexene, which increased steadily over time.

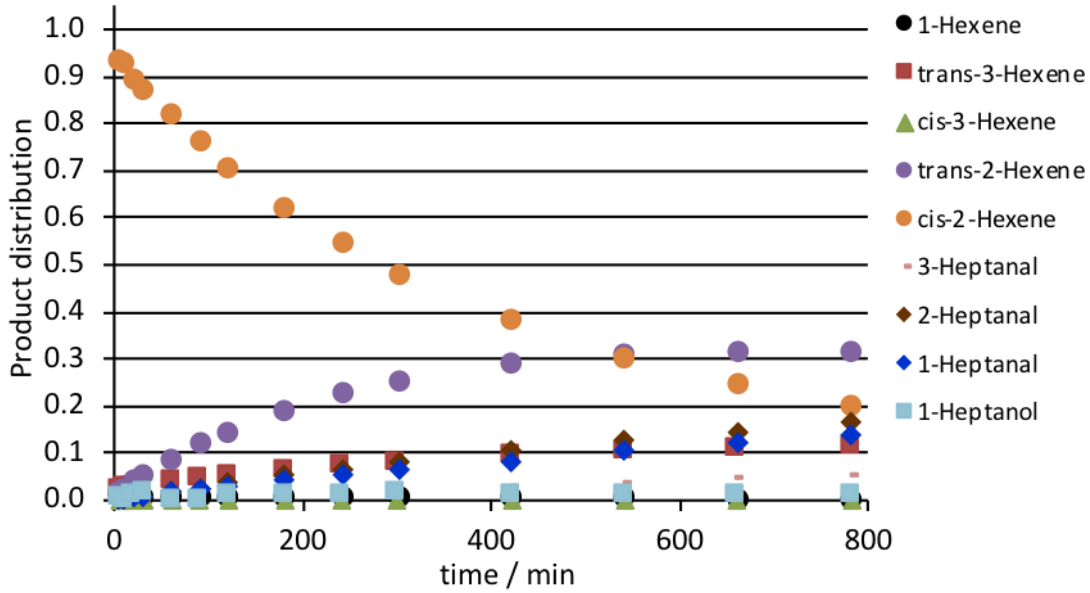


**Figure 3.6** Catalytic hydroformylation of 2-hexene using ligand $\mathbf{L}_{2.2}$, L/Rh = 10.

## 3.4 Conclusions and future work

The 6- to 8-membered ring fluorophosphites **L**$_{2.2\text{-}2.4}$ have been tested in the hydroformylation of 1-hexene and their Rh-catalysts have displayed high activities and *n*-selectivities. In contrast, the catalysts derived from the 5-membered ring fluorophosphites **L**$_{2.1}$ and **L**$_{2.6\text{-}2.7}$ displayed zero hydroformylation activity. To probe the effect of the fluoro-substituent on hydroformylation, the monophosphite **L**$_{2.5}$ has also been tested, which gave a considerably less active and less *n*-selective catalyst than its fluorophosphite analogue **L**$_{2.2}$. The effect of aryl fluorophosphite substitution has also been investigated: the *n*-selectivity of the Rh-catalyst was increased upon Me-substitution at the *ortho* position of the 6-membered fluorophosphite **L**$_{2.2}$ (using a L/Rh ratio of 10, an excellent *n*-selectivity of 99.0% was achieved using substituted **L**$_{2.8}$).

It has been shown that the product distribution was sensitive to the catalysis conditions: at a lower Rh concentration (conditions B) a lower *n*-selectivity was observed. Generally, it has been demonstrated that under both catalytic conditions tested, the ligand concentration has a large effect on the activity and *n*-selectivity of the Rh-catalyst. In general, increasing the L/Rh ratio led to a significant increase in the *n*-selectivity and decrease in activity. This may be associated with the involvement of the sterically hindered $RhL_3$ species, a hypothesis which has previously only been suggested to explain similar observations with Rh-$Pyr_3$ catalysts.[70] A remarkable *n*-selectivity of 99.5% was achieved using a L/Rh ratio of 15 for **L**$_{2.2}$ (under conditions A); to verify this result the experiment should be repeated. Increasing the ligand concentration further to improve the *n*-selectivity should also be considered in the future. However, there is a fine balance to be struck between the higher selectivity of the active $RhL_3$ species and the formation of inactive $RhL_4$ species.

It would be of interest to further explore the involvement of reactive and selective $RhL_3$ species in the catalysis. Preliminary *in situ* high pressure IR studies have been performed by Dr. Christoph Kubis (LIKAT, Rostock) on the hydroformylation catalysis using **L**$_{2.2}$. However, the Rh catalysts appeared to be insoluble in the solvent used (cyclohexane) and hence were undetectable by IR. Future work would focus on resolving this issue using alternative solvents. The application of *in situ* high pressure NMR spectroscopy should also be considered in the future to elucidate the mechanism. Finally, DFT calculations should also be carried out to investigate this hypothesis.

## 3.5 References


1 O. Roelen, *German Patent*, DE 849548.

2 O. Roelen, *US Patent*, 1943, US 2327066.

3 J. G. de Vries, in *C-1 Building Blocks in Organic Synthesis*, ed. P. W. N. M. van Leeuwen, Thieme Medical Publishers, 2014, pp. 193–227.

4 D. Evans, J. A. Osborn and G. Wilkinson, *J. Chem. Soc. A*, 1968, 3133–3142.

5 G. Yagupsky, C. K. Brown and G. Wilkinson, *J. Chem. Soc. A*, 1970, 1392–1401.

6 P. W. N. M. van Leeuwen, in *Homogeneous Catalysis, Understanding the Art*, Kluwer Academic Publishers, Dordrecht, 2004, pp. 139–174.

7 M. Yamashita and K. Nozaki, in *Comprehensive Organometallic Chemistry III*, eds. R. H. Crabtree and D. M. P. Mingos, Elsevier, 2007, pp. 435–464.

8 C. D. Frohning, C. W. Kohlpaintner and H. W. Bohnen, in *Applied Homogeneous Catalysis with Organometallics Compounds*, eds. B. Cornils and W. A. Herrmann, Wiley-VCH, 2002, pp. 31–103.

9 P. W. N. M. van Leeuwen and C. Claver, *Rhodium Catalyzed Hydroformylation*, Kluwer Academic Publishers, 2006.

10 M. Beller, in *Topics in Organometallic Chemistry*, Springer, 2006, pp. 97–165.

11 R. P. Bringer, P. C. J. Kamer and D. Vogt, in *C-1 Building Blocks in Organic Synthesis*, ed. P. W. N. M. van Leeuwen, Thieme Medical Publishers, 2014, pp. 23–62.

12 R. Franke, D. Selent and A. Borner, *Chem. Rev.*, 2012, **112**, 5675–5732.

13 J. A. Gillespie, D. L. Dodds and P. C. J. Kamer, *Dalton Trans.* , 2010, **39**, 2751–2764.

14 S. H. Chikkali, J. I. van der Vlugt and J. N. H. Reek, *Coord. Chem. Rev.*, 2014, **262**, 1–15.

15 A. Gual, C. Godard, S. Castillón and C. Claver, *Tetrahedron: Asymmetry*, 2010, **21**, 1135–1146.

16 L. Gartner, B. Cornils and P. Lappe, *European Patent*, 1983, EP 0107006.

17 P. W. N. M. van Leeuwen and C. F. Roobeek, *J. Organomet. Chem.*, 1983, **258**, 343–350.

18 P. W. N. M. van Leeuwen and C. Roobeek, *European Patent*, 1981, EP 0054986.

19 A. G. Abatjoglou, D. R. Bryant and J. M. Maher, *European Patent*, 1995, EP 0697391.

20 A. van Rooy, E. N. Orij, P. C. J. Kamer, F. van den Aardweg and P. W. N. M. van Leeuwen, *J. Chem. Soc. Chem. Commun.*, 1991, 1096–1097.

21 E. Billig, A. G. Abatjoglou, D. R. Bryant, R. E. Murray and J. M. Mather, *US Patent*, 1986, US 4599206.

22 H. Tricas, O. Diebolt and P. W. N. M. van Leeuwen, *J. Catal.*, 2013, **298**, 198–205.

23 B. Breit, *Chem. Commun.*, 1996, 2071–2072.

24 A. M. Trzeciak, T. Głowiak, R. Grzybek and J. J. Ziółkowski, *J. Chem. Soc. Dalton Trans*, 1997, 1831–1838.

25 R. Jackstell, H. Klein, M. Beller, K. D. Wiese and D. Röttger, *European J. Org. Chem.*, 2001, 3871–3877.

26 B. Breit, R. Winde, T. Mackewitz, R. Paciello and K. Harms, *Chem. Eur. J. A*, 2001, **7**, 3106–3121.

27 R. Paciello, T. Mackewitz, M. Roper and B. Breit, *World Patent*, 2000, WO 00/55164.

28 T. A. Puckette, *US Patent*, 2007, US 7301054 B1.

29 T. A. Puckette, X. Shan, J. Lee Rodgers and B. E. Green, *US Patent*, 2017, US 9,550,179 B1.

30 T. A. Puckette, *Top. Catal.*, 2012, **55**, 421–425.

31 T. A. Puckette, in *Catalysis of Organic Reactions*, ed. S. R. Schmidt, CRC Press, 2007, pp. 31–39.

32 Y. Cao, J. W. Napoline, J. Bacsa, P. Pollet, J. D. Soper and J. P. Sadighi, *Organometallics*, 2019, **38**, 1868–1871.

33 A. Boerner, R. Franke and D. Selent, *European Patent*, 2019, EP 3438110 A1.

34 R. Franke, D. Selent and A. Börner, *European Patent*, 2019, EP 3438111 A1.

35 X. Jia, Z. Wang, C. Xia and K. Ding, *Chem. Eur. J. A*, 2012, **18**, 15288–15295.

36 X. Jia, Z. Wang, C. Xia and K. Ding, *Catal. Sci. Technol.*, 2013, **3**, 1901–1904.

37 Q. Wu, F. Zhou, X. Shu, L. Jian, B. Xu, X. Zheng, M. Yuan, H. Fu, R. Li and H. Chen, *RSC Adv.*, 2016, **6**, 107305–107309.

38 Z. Zhang, C. Chen, Q. Wang, Z. Han, X.-Q. Dong and X. Zhang, *RSC Adv.*, 2016, **6**, 14559–14562.

39 L. Zhang, C. Li, X. Zheng, H. Fu, H. Chen and R. Li, *Catal. Letters*, 2014, **144**, 1074–1079.

40 F. Zhou, L. Zhang, Q. Wu, F. Guo, S. Tang, B. Xu, M. Yuan, H. Fu, R. Li, X. Zheng and H. Chen, *Appl. Organomet. Chem.*, 2019, **33**, 1–10.

41 A. Boerner, R. Franke and D. Selent, *European Patent*, 2019, EP 3459961 A1.

42 W. A. Herrmann, R. Schmid, C. W. Kohlpaintner, T. Priermeier, R. Paciello and L. Siggel, *Org. Lett.*, 2013, **15**, 1048–1051.

43 A. Phanopoulos and K. Nozaki, *ACS Catal.* , 2018, **8**, 5799–5809.

44 D. W. Norman, J. N. H. Reek, T. Renee and M.-L. Besset, *US Patent*, 2014, US 8710275 B2.

45 X. Wang, S. S. Nurttila, W. I. Dzik, R. Becker, J. Rodgers and J. N. H. Reek, *Chem. Eur. J. A*, 2017, **23**, 14769–14777.

46 G. M. Noonan, J. A. Fuentes, C. J. Cobley and M. L. Clarke, *Angew. Chemie Int. Ed.*, 2012, **51**, 2477–2480.

47 R. Pittaway, J. A. Fuentes and M. L. Clarke, *Org. Lett.*, 2017, **19**, 2845–2848.

48 R. C. How, P. Dingwall, R. T. Hembre, J. A. Ponasik, G. S. Tolleson and M. L. Clarke, *Mol. Catal.*, 2017, **434**, 116–122.

49 P. Dingwall, J. Fuentes, L. Crawford, A. M. Z. Slawin, M. Buhl and M. L. Clarke, *J. Am. Chem. Soc.*, 2017, **139**, 15921–15932.

50 L. Iu, J. A. Fuentes, M. E. Janka, K. J. Fontenot and M. L. Clarke, *Angew. Chemie Int. Ed.*, 2019, **58**, 2120–2124.

51 L. Iu, M. Clarke, K. J. Fontenot and M. E. Janka, *World Patent*, 2019, WO 2019108502 A1.

52 L. Iu, M. Clarke and M. E. Janka, *US Patent*, 2019, US 10183961 B1.

53 R. C. How, R. Hembre, J. A. Ponasik, G. S. Tolleson and M. L. Clarke, *Catal. Sci. Technol.*, 2016, **6**, 118–124.

54 V. Agabekov, W. Seiche and B. Breit, *Chem. Sci.*, 2013, **4**, 2418–2422.

55 A. Köpfer and B. Breit, *Angew. Chemie Int. Ed.*, 2015, **54**, 6913–6917.

56 S. S. Nurttila, W. Brenner, J. Mosquera, K. M. van Vliet, J. R. Nitschke and J. N. H. Reek, *Chem. Eur. J. A*, 2019, **25**, 609–620.

57 L. J. Jongkind, J. A. A. W. Elemans and J. N. H. Reek, *Angew. Chemie Int. Ed.*, 2019, **58**, 2696–2699.

58 S. S. Nurttila, P. R. Linnebank, T. Krachko and J. N. H. Reek, *ACS Catal.*, 2018, **8**, 3469–3488.

59 A. C. Brezny and C. R. Landis, *Acc. Chem. Res.*, 2018, **51**, 2344–2354.

60 S. K. Sharma and R. V. Jasra, *Catal. Today*, 2015, **247**, 70–81.

61 M. Zabransky, I. Cisarova, A. M. Trzeciak, W. Alsalahi and P. Stepnicka, *Organometallics*, 2019, **38**, 479–488.

62 N. N. Omosun and G. S. Smith, *Eur. J. Inorg. Chem.*, 2019, 2558–2564.

63 J. Maximilian Marinkovic, A. Riisager, R. Franke, P. Wasserscheid and M. Haumann, *Ind. Eng. Chem. Res.*, 2019, **58**, 2409–2420.

64 M. Vilches-Herrera, L. Domke and A. Borner, *ACS Catal.*, 2014, **4**, 1706–1724.

65 A. Jörke, T. Gaide, A. Behr, A. Vorholt, A. Seidel-Morgenstern and C. Hamel, *Chem. Eng. J.*, 2017, **313**, 382–397.

66 P. C. J. Kamer, A. van Rooy, G. C. Schoemaker and P. W. N. M. van Leeuwen, *Coord. Chem. Rev.*, 2004, **248**, 2409–2424.

67 T. Jongsma, G. Challa and P. W. N. M. van Leeuwen, *J. Organomet. Chem.*, 1991, **421**, 121–128.

68 M. Caporali, P. Frediani, A. Salvini and G. Laurenczy, *Inorganica Chim. Acta*, 2004, **357**, 4537–4543.

69 R. F. Heck, *Acc. Chem. Res.*, 1969, **2**, 10–16.

70 S. Papadouli, *PhD Thesis*, 2015, Univeristy of Bristol.

71 T. A. Puckette, *Chem. Ind.*, 2007, **115**, 31–38.

72 T. A. Puckette, G. S. Tolleson, T. J. Devon and J. Stavinoha, *World Patent*, 2002, WO 02/098825 A2.

73 A. G. Abatjoglou and D. R. Bryant, *US Patent*, 1988, US 5059710.

74 A. Bernas, P. Mäki-Arvela, J. Lehtonen, T. Salmi and D. Y. Murzin, *Ind. Eng. Chem. Res.*, 2008, **47**, 4317–4324.

75 R. L. Pruett and J. A. Smith, *J. Org. Chem.*, 1969, **327**, 327–330.

# Chapter 4

# Five and six membered dioxaphosphacyclic diphosphites for alkene hydroformylation

## 4.1 Introduction

In this section, some highlights of the many applications of diphosphite ligands in Rh-catalysed hydroformylation of alkenes will be discussed. The use of other phosphorus ligands in Rh-catalysed hydroformylation has been the subject of several reviews.[1–8] The mechanism of hydroformylation has also been well documented and so will not be discussed here (see Chapter 3 also).[1,3,7–11]

### 4.1.1 Diphosphites for Rh-catalysed hydroformylation

Dioxaphosphacyclic diphosphites are the most extensively studied diphosphites.[12] In the 1980s, cyclic diphosphites emerged as excellent ligands for Rh-catalysed hydroformylation of alkenes, following the discovery of ligands such as **4.1a**-**c** by Union Carbide Company (UCC) (Figure 4.1).[13–15] Following this pioneering work by Bryant *et al.*, cyclic diphosphites have received abundant attention as ligands for hydroformylation, as summarised in several reviews.[1–3,12] In general, a dramatic increase in selectivity for the *n*-aldehyde was observed upon replacement of bulky monophosphite ligands with bulky diphosphites.[13–16]

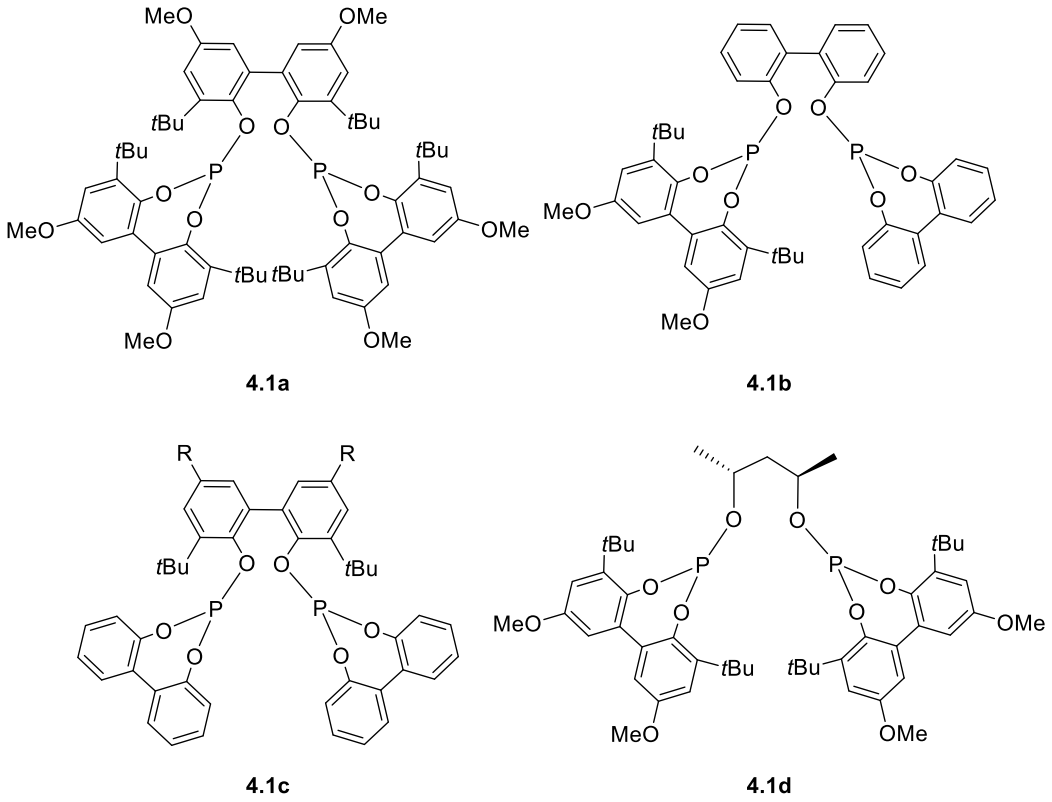


**Figure 4.1** Bulky diphosphites developed by Bryant at UCC for hydroformylation.

Many cyclic diphosphites contain a chiral element, either in the diol backbone or the phosphacycle, and optically pure ligands such as **4.1d** have been applied in asymmetric hydroformylation, but this topic will also not be discussed herein.[1,6,12,17,18]

To date, the most studied cyclic diphosphites contain 7- or 8-membered phosphacycles. There are only a few examples of diphosphites based on 6-membered phosphacycles derived from 1,8-dihydroxynaphthalenes. To the best of our knowledge, the only examples have been reported by Borner *et al.* (*e.g.* ligands **4.2a**-**b**).[19,20] The catalyst derived from the symmetrical diphosphite **4.2a** displayed good *n*-selectivities in the hydroformylation of 1-octene (82-85%).[19,20] Although not formally diphosphites, 6-membered phosphacycles derived from hydroxybenzoates (*e.g.* **4.3**) have been reported.[12,21–24]

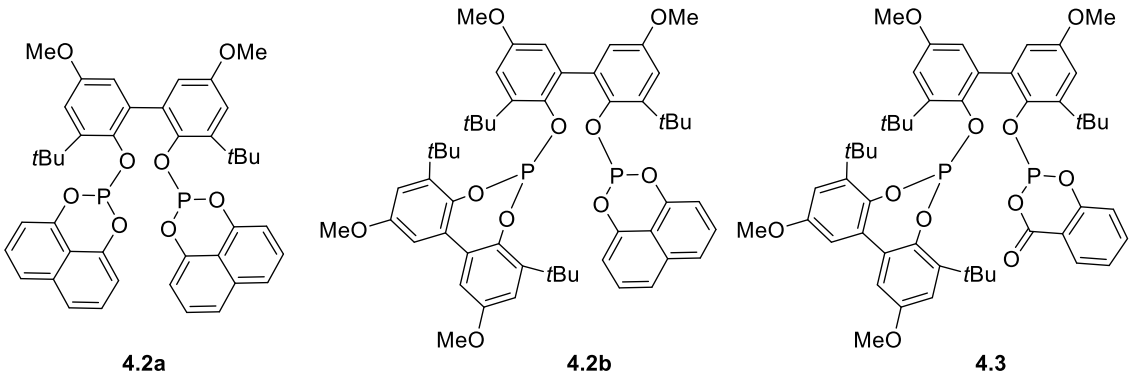


There are reports in patents of the use of 5-membered aromatic diphosphites derived from 1,2-dihydroxybenzene (catechols) with a biphenyl linker, such as **4.4a**-**c**, for the hydroformylation of alkenes and hydroxy-alkenes.[12,25–31] In general, the cyclic diphosphites reported for hydroformylation contain bulky ring substituents (*e.g. t*Bu); not only are these bulky substituents apparently essential to catalyst performance, they have also been shown to increase the ligand's hydrolytic stability.[32,33]

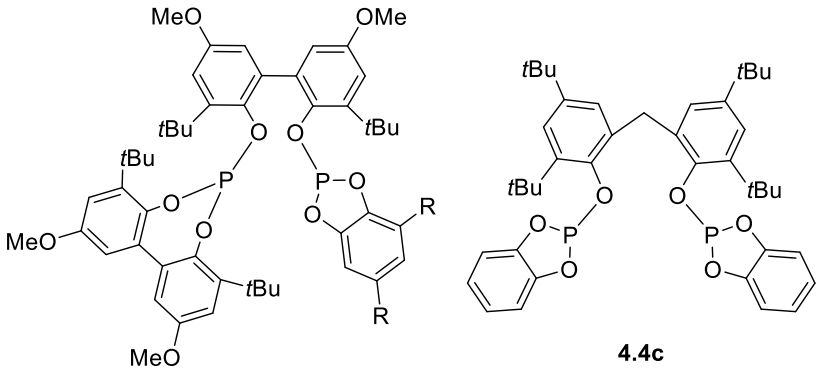


R = H **4.4a**
R = *t*Bu **4.4b**

### 4.1.2 Synthesis of cyclic diphosphites

Cyclic diphosphites are generally synthesised from one of the two-step procedures shown in Scheme 4.1.[12,34] They are mainly derived from cheap and readily available diols and hence their highly modular synthesis makes them amenable to modification through substitution or ring size effects. In Scheme 4.1a, a cyclic chlorophosphite is formed upon the reaction of the corresponding dihydroxyarene and $PCl_3$ in the presence of a base (*e.g.* $NEt_3$). The reaction of the cyclic chlorophosphite with the diol linker affords the desired diphosphite.[12] Cyclic chlorophosphites are versatile intermediates in the synthesis of numerous dioxaphosphacyclic ligands (see Chapter 2). Alternatively, in Scheme 4.1b a bis(dichlorophosphite) is formed upon the reaction of the appropriate diol and $PCl_3$; this

intermediate is then reacted with the corresponding dihydroxyarene to give the expected diphosphite.[12]

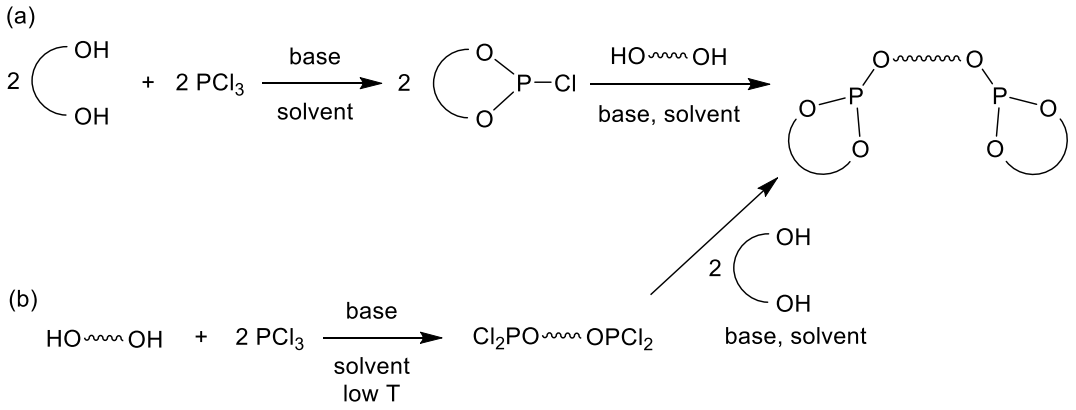


**Scheme 4.1** Conventional methods for the synthesis of cyclic diphosphites.[12]

Symmetrical cyclic diphosphites, comprised of three identical dihydroxyarenes, can be synthesised in one-step from the dihydroxyarene and $PCl_3$ in the presence of a base (Scheme 4.2). All the routes described so far result in salt formation (*e.g.* $[Et_3NH]Cl$) and so an additional purification step is required in the work-up of a potentially hydrolytically sensitive compound.

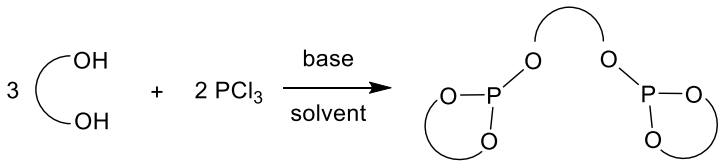


**Scheme 4.2** General synthesis of a symmetrical cyclic diphosphite.

An alternative method to P-O bond formation is the silicon-phosphorus exchange reaction shown in Scheme 4.3. This route was first developed in 1957 when the stepwise replacement of the halogen in $PCl_3$ by $R'OSiMe_3$ gave the corresponding dichlorophosphinites $\{Cl_2P(OR')\}$, chlorophosphites $\{ClP(OR')_2\}$ and phosphites $\{P(OR')_3\}$.[35]

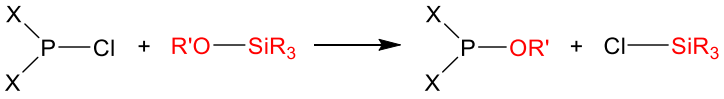


**Scheme 4.3** Generalised Si-P exchange reaction between a chlorophosphine (where X = Cl, OR', R) and silyl ether.

In 2009, Majewski also reported the synthesis of such ligands in addition to mixed trialkylphosphites, $P(OR_1)(OR_2)(OR_3)$, from the HCl-catalysed reaction of the corresponding chlorophosphine and alkoxytrimethylsilane (Scheme 4.4).[36]

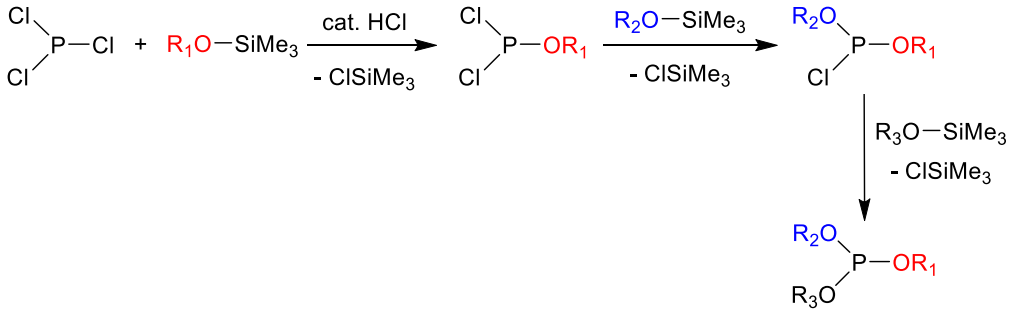


**Scheme 4.4** Synthesis of mixed trialkylphosphites *via* Si-P exchange reaction.

In 2007, Musin *et al.* reported the synthesis of the unusual terephthalate derivative **4.5**, where silylation of terephthalic acid was followed by the silicon-phosphorus exchange reaction shown in Scheme 4.5.[37] To the best of our knowledge there are no other reports of silicon-phosphorus exchange reactions for the synthesis of P-O bonds. Silicon-phosphorus exchange reactions have previously been used to access other P-Y bonds, such as in aminophosphines,[38] C1-diphosphines,[39] optically active C1-phosphine-phosphonites[40] and phosphophosphidites[41] (where Y = N, C or P). In addition, borylphosphines can be prepared from the reaction of a silylphosphine ($R_2PSiMe_3$) with a chloroborane ($R_2BCl$).[42–44]

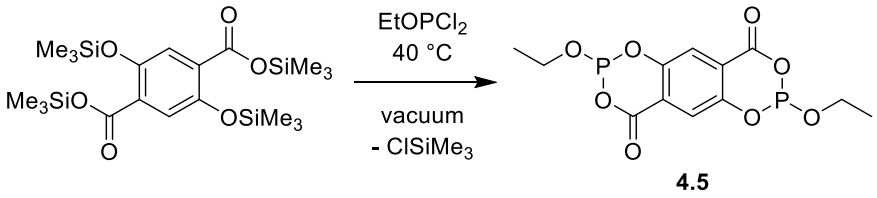


**Scheme 4.5** Example of a Si-P exchange reaction in the synthesis of P-O bonds.

The silicon-phosphorus exchange reaction is an attractive alternative to traditional routes to cyclic chlorophosphites for the following reasons: (a) a simple purification is required due to the volatile by-products; (b) no acidic by-products are generated, which may catalyse the hydrolysis of the P-Cl bond; (c) the method is tolerant of acid-sensitive groups. To the best of our knowledge, this reaction has not yet been applied to the synthesis of cyclic chlorophosphites.

Accordingly, in this project the aim was to investigate the potential of the silicon-phosphorus exchange reaction as a general route to a range of cyclic chlorophosphites. We also aimed to synthesise the symmetrical 6-membered diphosphite, $\mathbf{L_{4.2}}$, and its stereoelectronic properties were to be investigated by preparing a range of its coordination complexes; ligand $\mathbf{L_{4.2}}$ has been claimed previously in patents by Borner *et al.* but was not synthesised.[19,20] It was of interest to gauge the effect of ring size on Rh-catalysed hydroformylation of 1-hexene by comparing ligands $\mathbf{L_{4.1\text{-}4.3}}$, containing 5- to 7-membered phosphacycles.

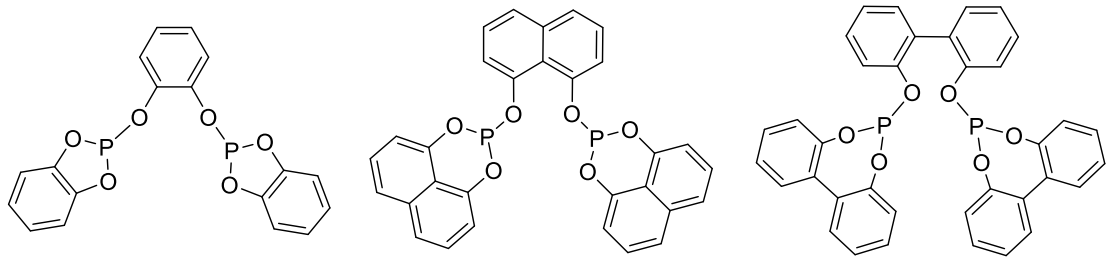

$\mathbf{L_{4.1}}$ $\mathbf{L_{4.2}}$ $\mathbf{L_{4.3}}$

## 4.2 Silicon-phosphorus exchange reaction to chlorophosphites

### 4.2.1 Factors affecting spirophosphorane formation

Cyclic chlorophosphites (**4.6**) are useful intermediates to diphosphites and have been traditionally synthesised from the reaction of the appropriate dihydroxyarene and $PCl_3$ (Scheme 4.6).[12] However, the formation of hydroxyphosphites (**4.7**) can lead to spirophosphorane side-products (**4.8**) during attempted syntheses of 5-membered chlorophosphites and diphosphites.[45–48] Hydroxyphosphites **4.7** are known to be in equilibrium with their spirophosphorane tautomer **4.8** (Scheme 4.6).[49–51]

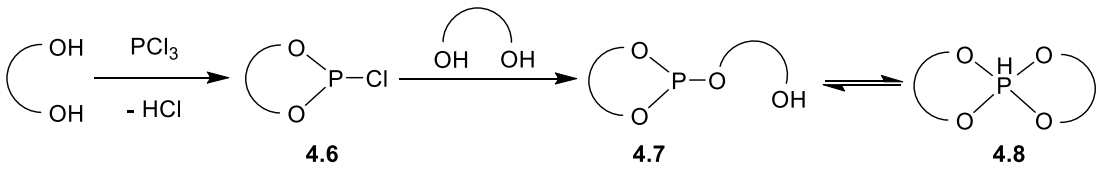


**4.6** **4.7** **4.8**

**Scheme 4.6** General formation of spirophosphorane (**4.8**) side-products during the synthesis of chlorophosphites **4.6**.

The formation of spirophosphorane side-products appeared to be more favoured with 5-membered phosphacycles than with larger ring systems. The equilibria between the hydroxyphosphites **4.7a**-**c** and spirophosphoranes **4.8a**-**c**, have been evaluated computationally for a range of ring sizes (Table 4.1).[52] Relative electronic and Gibbs free

energies for **4.7a**-**c** and **4.8a**-**c**, containing 5- to 7-membered phosphacycles, have been calculated using the M1 method (by Tom Young at the University of Bristol). To be able to detect the equilibrium by $^{31}$P NMR spectroscopy, the minor species should be at least *ca.* 1% of the total concentration, *i.e.* the $|\Delta G_{expt}| < 3$ kcal mol$^{-1}$.

**Table 4.1** Calculated energy differences between **4.7a**-**c** and **4.8a**-**c**.[a]

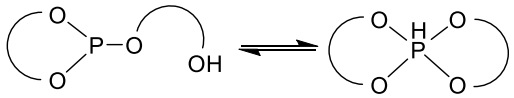


**4.7a-c** **4.8a-c**

| Linker | Compound no. | Ring size | ΔE / kcal mol$^{-1}$ | ΔG / kcal mol$^{-1}$ |
|---|---|---|---|---|
| 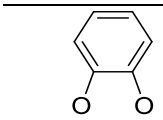 | **a** | 5 | 2.3 | 5.7 |
| 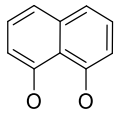 | **b** | 6 | 6.8 | 12.2 |
| 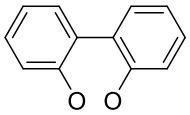 | **c** | 7 | 8.6 | 8.2 |

[a] Computed at PBE0-D3BJ/6 311+G(d,p).

The calculations agree with experimental observation: within error the 5-membered spirophosphorane **4.8a** is sufficiently stable to be in an observable equilibrium with **4.7a**. Whereas, no such observable equilibrium between the 6- or 7-membered analogues, **4.7b**-**c** and **4.8b**-**c**, was predicted ($K < 1 \times 10^{-7}$, 298 K).

To explain the favourable cyclisation for the 5-membered rings, DFT-optimised ground state geometries of **4.7a**-**c** and **4.8a**-**c** were evaluated (Figure 4.2). The high stability of the 5-membered spirophosphorane **4.8a** can be explained on the basis of the following observations. Firstly, the intramolecular hydrogen bond in the hydroxyphosphite **4.7a** deviates the most from linearity (110.8°) and hence is weaker than those in the larger ring systems, **4.7b**-**c**.[53] This is also reflected in the OH…H distance (2.42 Å) which only just falls within the distance required for a strong hydrogen bond (X…H < 2.5 Å).[54] Secondly, deviation from the ideal O-P-O angle of 90° in the spirophosphorane **4.8a** is minimal, relative to those in the larger ring systems, **4.8b**-**c** (Figure 4.2). Finally, upon tautomerisation of the hydroxyphosphite **4.7a** to spirophosphorane **4.8a**, only a small

change in the O-P-O angle of 2.0° is required. Whereas, for the larger ring systems a greater change is necessary: 3.4° for **4.7b**/**4.8b** and 5.9° for **4.7c**/**4.8c**.

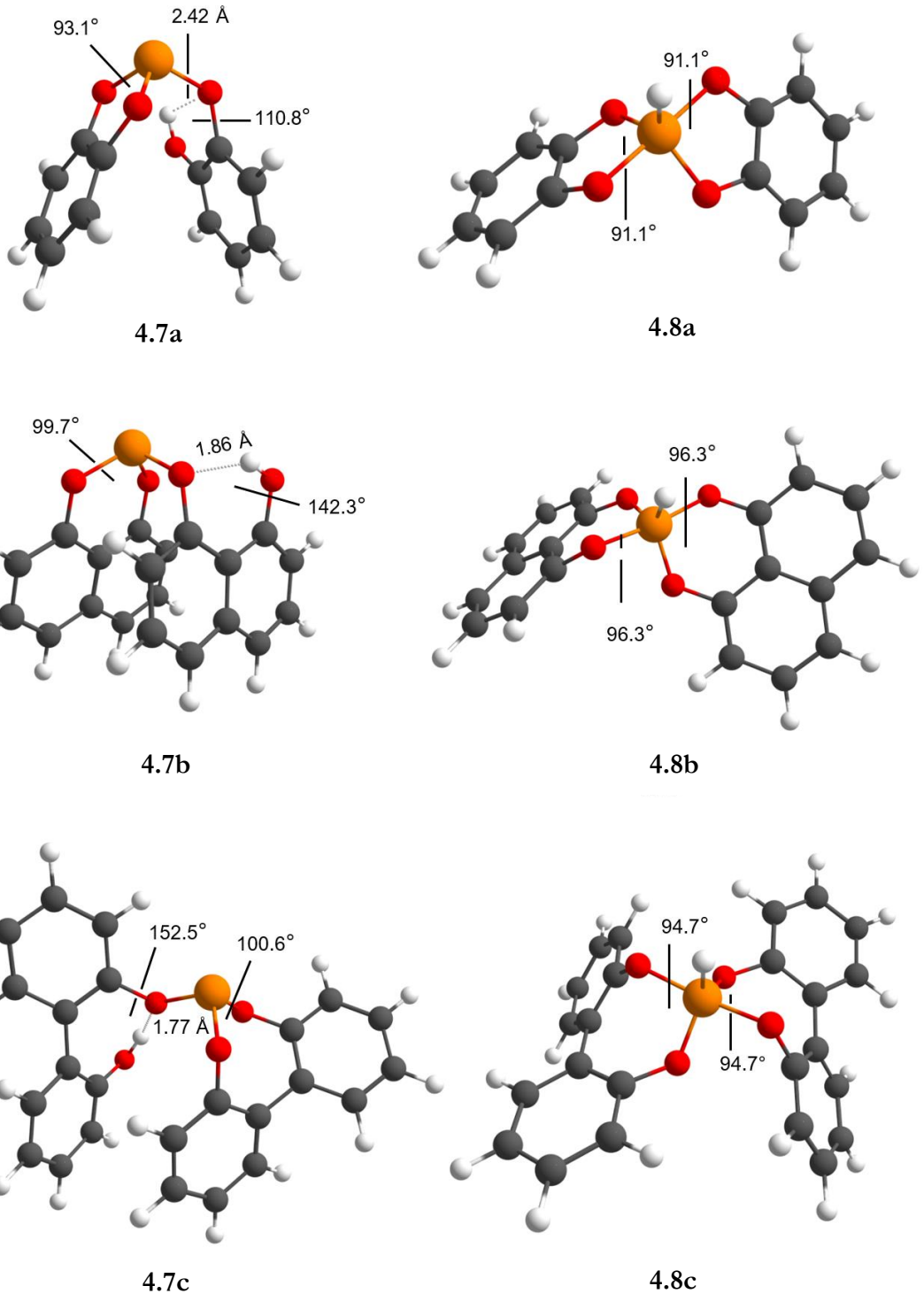


**Figure 4.2** DFT-optimised geometries of hydroxyphosphites **4.7a-c** and spirophosphoranes **4.8a-c**. Significant bond angles (°) and bond lengths (Å) are highlighted. Calculated by Tom Young at the University of Bristol.

To probe the effect of ring-substitution, the relative free energies for the equilibrium have been calculated (by Tom Young at the University of Bristol) for a range of 5-membered substituted analogues of **4.7a**/**4.8a** (Table 4.2). As the steric bulk of the substituents increase, the stability of the spirophosphorane tautomer increases: $\Delta E$ = -5.4 kcal mol$^{-1}$ for when R = *t*Bu (**4.7f**/**4.8f**), *cf.* $\Delta E$ = 2.3 kcal mol$^{-1}$ for when R = H (**4.7a**/**4.8a**).

**Table 4.2** Calculated energy differences between **4.7a**,**d**-**f** and **4.8a,d**-**f**.[a]

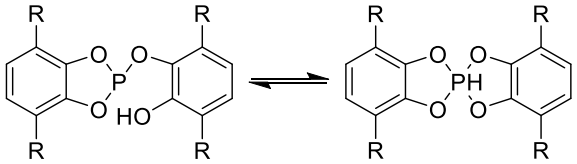


**4.7a,d-f** **4.8a,d-f**

| R = | Compound no. | $\Delta E$ / kcal mol$^{-1}$ |
|---|---|---|
| H | **a** | 2.3 |
| Me | **d** | 1.3 |
| *i*Pr | **e** | -3.3 |
| *t*Bu | **f** | -5.4 |

[a] Computed at PBE0-D3BJ/6 311+G(d,p).

To rationalise this, the geometry-optimised isomers of the *t*Bu substituted **4.7f** and **4.8f** were evaluated using a space filling model (M1 method, Figure 4.3). The steric crowding imposed by the di-*ortho* substitution in hydroxyphosphite **4.7f** is evident (Figure 4.3a). In the corresponding spirophosphorane **4.8f**, a large degree of steric strain is relieved as shown by the 0.42 Å increase in the smallest (*t*Bu)C-C(*t*Bu) distance (Figure 4.3b). Adding to the stability of the spirophosphorane **4.8f** is its close to ideal O-P-O angle of 90.6°.

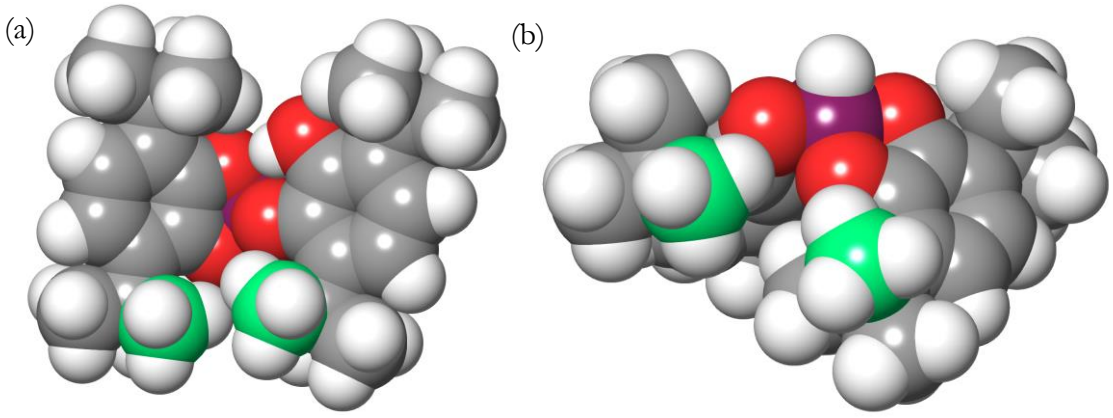


**4.7f** **4.8f**

**Figure 4.3** Space filling models of (a) the hydroxyphosphite **4.7f** and (b) spirophosphorane **4.8f**. Non-bonded carbon atoms encountering the most severe steric clashes are highlighted in green.

### 4.2.2 Effect of solvent

A novel silicon-phosphorus exchange route to chlorophosphites *via* silyl ether intermediates has been developed. As seen in Chapter 2, the 5-membered chlorophosphite **4.6a** was synthesised successfully without the formation of spirophosphorane impurities *via* this route (Scheme 4.7). A range of solvents were tested for the silicon-phosphorus exchange reaction (Table 4.3) between the silyl ether **4.9a** and an excess of $PCl_3$ (2 equiv.) to give **4.6a**. There is a correlation between the polarity of the solvent and rate of reaction: the rate of reaction is amplified when the polarity of the solvent is increased. Hence, acetonitrile was used as the solvent of choice for further studies.

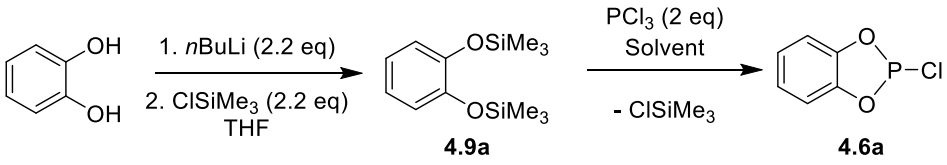


**Scheme 4.7** Route to chlorophosphite **4.6a** *via* the silyl ether **4.9a**.

**Table 4.3** Range of solvents tested for the conversion of **4.9a** to **4.6a** (Scheme 4.7).

| Solvent | $\varepsilon_r$ [a] | Temp. / °C | Conversion[b] / % | Time / h |
|---|---|---|---|---|
| Acetonitrile | 35.94 | 20 | 100 | 1 |
| Propionitrile | 28.26 | 60 | 100 | < 1 |
| Tetrahydrofuran | 7.58 | 60 | 80 | 168 |
| 1,1,2,2-tetrachloroethane | 7.10 | 100 | 100 | 144 |
| Toluene | 2.38 | 100 | 50 | 144 |
| 1,4-dioxane | 2.21 | 60 | 10 | 48 |

[a] Dielectric constants from the literature.[55,56] [b] Determined by integration of $^{31}P\{^1H\}$ NMR signals.

### 4.2.3 Reaction scope

The silicon-phosphorus exchange reaction has been applied to a range of chlorophosphites in Chapter 2, including the 6-membered chlorophosphite **4.6b** (Scheme 4.8). The chiral chlorophosphite **4.6c** was synthesised from the silyl ether **4.9c** in excellent yield and purity (Scheme 4.8). In contrast, the reaction of the corresponding diol with $PCl_3$ gave large amounts (*ca.* 40%) of hydrolysis ($\delta_P$ = 20.8 ppm) in our hands.[57]

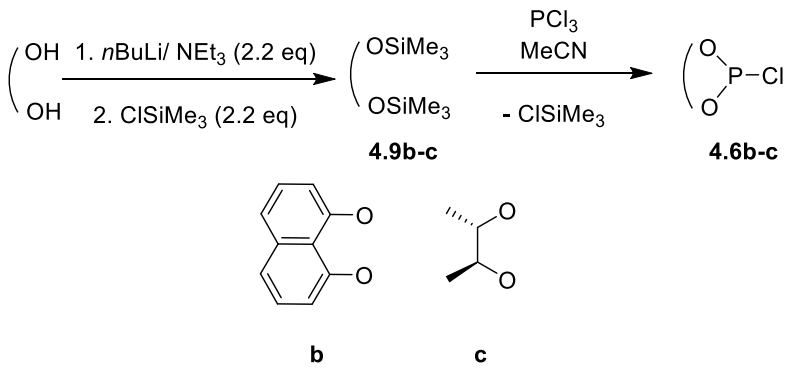


**Scheme 4.8** Route to chlorophosphites **4.6b**-**c** *via* the silyl ethers **4.9b**-**c**. Compound **4.9c** has been previously reported.[58]

Majewski reported the synthesis of several alkyl-dichlorophosphites from their corresponding silyl ethers, but few aryl-dichlorophosphites.[36] Attempts to synthesise dichlorophosphite **4.6d** from the silyl ether **4.9d** were unsuccessful, even in the presence of HCl (10 mol%) or at 60 °C. In contrast, the substituted dichlorophosphites **4.6e**-**g** were successfully synthesised from the silyl ethers **4.9e**-**g** (Scheme 4.9) in near quantitative yields and high purities. There is no consistent correlation between the electronic properties of the aryl substituents and conversion, since the reaction proceeded with silyl ethers containing electron-donating (X = OMe, **4.9e**) or electron-withdrawing (X = $CF_3$, **4.9f**) *ortho*-substituents, but does not proceed when using the unsubstituted analogue (X = H, **4.9d**); an explanation for these observations has eluded us.

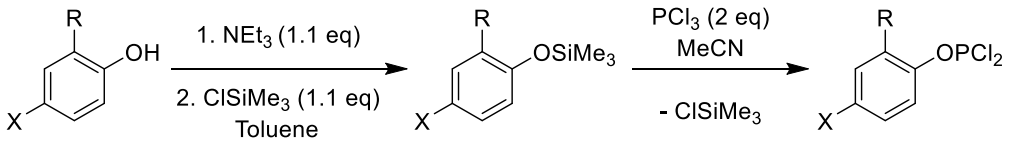


R = H; X = H **4.9d**, OMe **4.9e**, $CF_3$ **4.9f**
R = OMe; X = H **4.9g**

R = H; X = H **4.6d**, OMe **4.6e**, $CF_3$ **4.6f**
R = OMe; X = H **4.6g**

**Scheme 4.9** Route to dichlorophosphites **4.6d**-**g** *via* the silyl ethers **4.9d**-**g**.

The simple work-up, the avoidance of spirophosphorane by-products, and the high yields and purities achieved using this silicon-phosphorus exchange route make it an attractive alternative to traditional routes to chlorophosphites and dichlorophosphites.

## 4.3 Synthesis and coordination of 5- and 6-membered diphosphites

### 4.3.1 Synthesis of diphosphite ligands

The previously reported 5-membered diphosphite $\mathbf{L_{4.1}}$ has been prepared from the reaction of chlorophosphite **4.6a** and silyl ether **4.9a** (Scheme 4.10), involving the silicon-phosphorus exchange reaction described in Section 4.2. Attempts to synthesise *t*Bu substituted analogues of $\mathbf{L_{4.1}}$ *via* this method were unsuccessful; the presence of spirophosphorane by-products were persistent as predicted by calculations in Section 4.2.1.

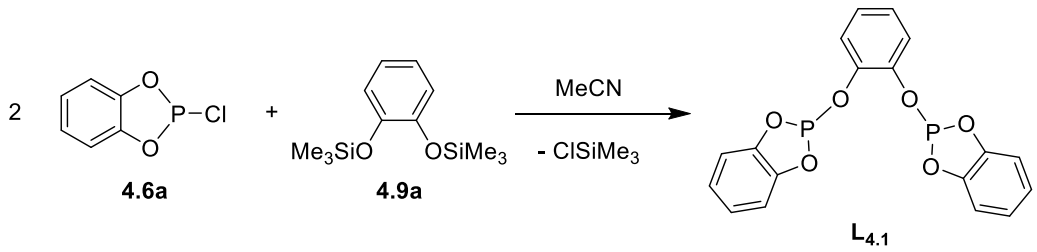


**Scheme 4.10** Synthesis of $\mathbf{L_{4.1}}$.

From the computational studies above (Section 4.2.1), it can be suggested that the synthesis of the 6-membered diphosphite $\mathbf{L_{4.2}}$ should not be so blighted by spirophosphorane formation. Indeed, treatment of the dihydroxyarene with $PCl_3$ in the presence of $NEt_3$ gave the novel diphosphite $\mathbf{L_{4.2}}$ in a good yield (73%) (Scheme 4.11).

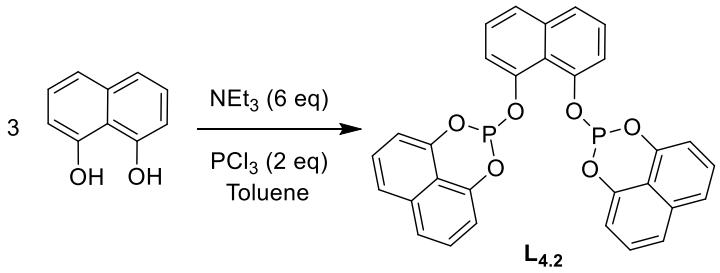


**Scheme 4.11** Synthesis of $\mathbf{L_{4.2}}$.

Crystals suitable for X-ray crystallography of $\mathbf{L_{4.2}}$ were grown by slow diffusion of hexane into a saturated $CH_2Cl_2$ solution of the ligand (Figure 4.4). The P atoms are pyramidalised ($\Sigma$(angles at P) = 297°), consistent with $sp^3$ hybridisation. Whereas, the angles within the 6-membered phosphacycle are *ca.* 120°, in line with $sp^2$ hybridisation. The P centre is out of the plane of the naphthalene ring (P1-O1-C1 121.05(12)°). Figure 4.4b shows the two phosphacycles adopt an *anti*-conformation in the solid state. The sum of the angles at P in the analogous 7-membered diphosphite[59] is *ca.* 3° smaller than in $\mathbf{L_{4.2}}$; the more obtuse O-P-O angles in $\mathbf{L_{4.2}}$ may be as a result of the rigidity of the naphthalene ring. Generally, the more acute the O-P-O angle is, the lower the HOMO and LUMO energies of the ligand.[60–62]

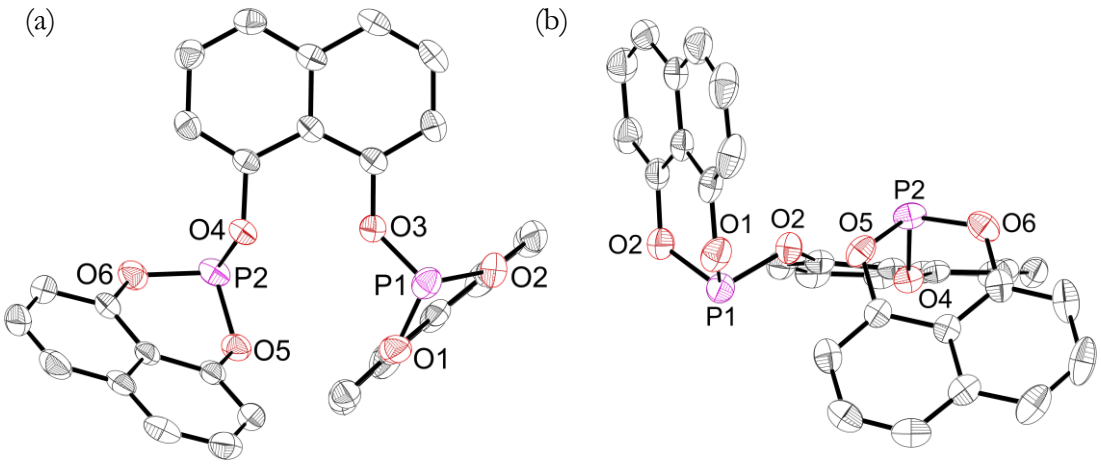


**Figure 4.4** Crystal structure of $\mathbf{L_{4.2}}$. The hydrogen atoms are omitted for clarity. Thermal ellipsoids at 50% probability. Selected bond lengths (Å) and angles (°): P1-O1 1.6297(16), P1-O2 1.6450(15), P1-O3 1.6310(4), P2-O4 1.6292(13), P2-O5 1.6251(14), P2-O6 1.6420(15), O1-P1-O2 99.20(8), O1-P1-O3 96.12(8), O2-P1-O3 101.82(7), O5-P2-O6 99.59(7), O4-P2-O5 95.67(7), O4-P2-O6 101.67(7). See Appendix for experimental details.

### 4.3.2 Synthesis of *cis*-[$PtMe_2$L] complex

The reaction of 1 equiv. of $\mathbf{L_{4.2}}$ with [$PtMe_2$(cod)] (cod = 1,5-cyclooctadiene) in toluene gave the air-stable *cis*-[$PtMe_2$($\mathbf{L_{4.2}}$)] complex, **4.10** (Scheme 4.12). The $^{31}P\{^1H\}$ NMR spectrum of **4.10** gave a singlet with a $^1J_{P,Pt}$ value of 2964 Hz, consistent with a *cis*-geometry of P-atoms. The coordination chemical shift Δδ for $\mathbf{L_{4.2}}$ in **4.10** is +12 ppm.

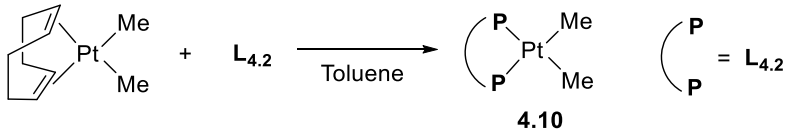


**Scheme 4.12** Synthesis of the *cis*-[$PtMe_2$($\mathbf{L_{4.2}}$)] complex **4.10**.

Crystals suitable for X-ray crystallography of **4.10** were grown by slow diffusion of hexane into a saturated $CH_2Cl_2$ solution of the complex (Figure 4.5). The crystal structure confirmed the *cis* geometry of the complex and showed the ligands are arranged in a slightly distorted square planar geometry around the Pt centre. Relative to the free ligand $\mathbf{L_{4.2}}$, a considerable increase in the sum of the angles at P (by *ca.* 6.8°) was observed.

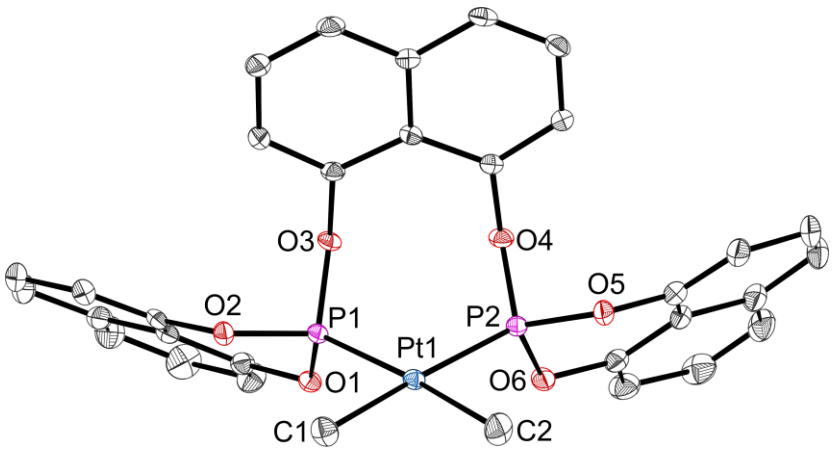


**Figure 4.5** Crystal structure of **4.10**. The hydrogen atoms are omitted for clarity. Thermal ellipsoids at 50% probability. Selected bond lengths (Å) and angles (°): P1-Pt1 2.2201(5), P2-Pt1 2.2219(6), P1-O1 1.6040(15), P1-O2 1.6057(15), P1-O3 1.6199(15), P2-O4 1.6220(15), P2-O5 1.6081(16), P2-O6 1.6043(15), P1-Pt1-P2 92.451(19), C1-P1-C2 83.53(9), O1-P1-O3 103.03(8), O1-P1-O3 96.58(8), O2-P1-O3 103.90(8), O5-P2-O6 102.88(8), O4-P2-O5 103.67(8), O4-P2-O6 97.52(8). See Appendix for experimental details.

### 4.3.3 Synthesis of *cis*-[Mo(CO)$_4$L] complex

The *cis*-[Mo(CO)$_4$L] complex was targeted as a way to assess the electronic properties of the 6-membered diphosphite **L$_{4.2}$**. The reaction of 1 equiv. of **L$_{4.2}$** with [Mo(CO)$_4$(nbd)] (nbd = norbornadiene) in $CH_2Cl_2$ gave the partly insoluble *cis*-[Mo(CO)$_4$(**L$_{4.2}$**)] complex, **4.11** (Scheme 4.13). The $^{31}P\{^1H\}$ NMR signal of complex **4.11** showed a singlet ($\delta_P$ = 147.8 ppm) with a coordination chemical shift $\Delta\delta$ of +47 ppm relative to free **L$_{4.2}$**; the analogous 7-membered diphosphite[59,63] complex, *cis*-[Mo(CO)$_4$(**L$_{4.3}$**)], has a $\Delta\delta$ of +36 ppm.[64]

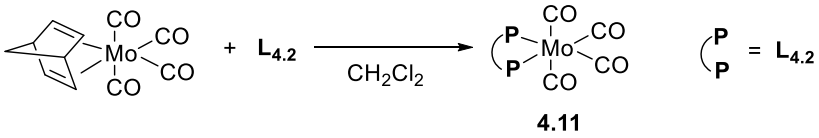


**Scheme 4.13** Synthesis of *cis*-[Mo(CO)$_4$(**L$_{4.2}$**)], **4.11**.

The IR spectrum of complex **4.11** is consistent with a *cis*-geometry of the ligand. The $\nu$(CO) ($A_1$) value for **4.11** is 2057 cm$^{-1}$, showing that **L$_{4.2}$** is a stronger $\pi$-acceptor than the

analogous 6-membered monophosphite **4.12**, where the ν(CO) of *cis*-[Mo(CO)$_4$(**4.12**)$_2$] is 2051 cm$^{-1}$ (Chapter 2).

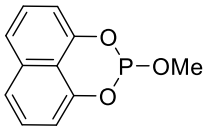


**4.12**

### 4.3.4 Rhodium(I) coordination chemistry

The reaction of 2 equiv. of **L$_{4.2}$** with [Rh$_2$Cl$_2$(CO)$_4$] in $CH_2Cl_2$ gave a single species which was tentatively assigned to the binuclear complex, *trans*-[Rh$_2$Cl$_2$(CO)$_2$(μ-**L$_{4.2}$**)$_2$] **4.13** (Scheme 4.14). Arbitrarily the *syn* isomer is depicted but it is not known whether the *syn* or *anti* isomer is formed.

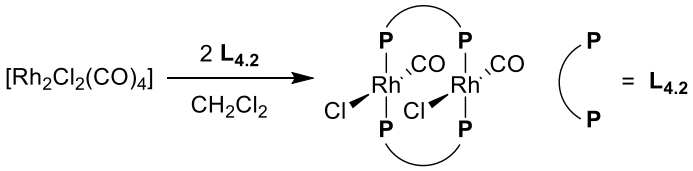


**4.13**

**Scheme 4.14** Synthesis of *trans*-[Rh$_2$Cl$_2$(CO)$_2$(**L$_{4.2}$**)$_2$], **4.13**.

The $^{31}P\{^1H\}$ NMR spectrum of complex **4.13** showed a doublet with $^1J_{P,Rh}$ = 180 Hz, typical of a *trans*-[RhCl(CO)(PR$_3$)$_2$] complex.[65] The chemical equivalence of the phosphorus nuclei excludes the assignment of the product to the mononuclear *cis*-[RhCl(CO)(**L$_{4.2}$**)] complex. Similar ligand-bridged binuclear structures of the type *trans*-[RhCl$_2$(CO)$_2${μ-R$_2$P(CH$_2$)$_3$PR$_2$}$_2$] have been previously reported for several diphosphine ligands,[62,66–68] but for only one diphosphite to the best of our knowledge.[69]

## 4.4 Diphosphite ligands in alkene hydroformylation

The 5- to 7-membered diphosphites, **L$_{4.1\text{-}4.3}$**, were tested in the Rh-catalysed hydroformylation of 1-hexene (Scheme 4.15). The 7-membered diphosphite **L$_{4.3}$** was prepared according to the literature.[59] The selectivity and conversion were determined by $^1H$ NMR spectroscopy (see Chapter 7 for experimental details). The reactions were run for 1 h and the results are shown in Table 4.4 and Figure 4.6.

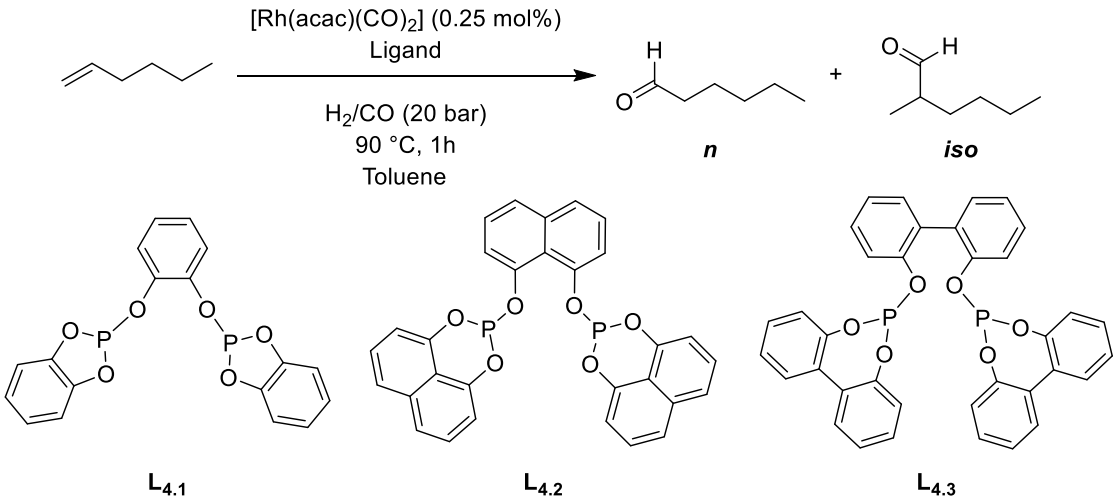


**Scheme 4.15** Catalytic hydroformylation of 1-hexene using **L**$_{4.1\text{-}4.3}$.

**Table 4.4** Catalytic hydroformylation of 1-hexene using **L**$_{4.1\text{-}4.3}$ (see Chapter 7 for experimental details).[a]

| Entry | Ligand | L/ Rh | % *n* selectivity | Conversion[b] /% | Isomerisation[c] / % |
|---|---|---|---|---|---|
| 1 | **L**$_{4.1}$ | 1 | - | - | 11 |
| 2 | **L**$_{4.1}$ | 1.5 | - | - | 11 |
| 3 | **L**$_{4.2}$ | 1 | 77.2 | 39 | 49 |
| 4 | **L**$_{4.2}$ | 1.5 | 82.5 | 32 | 46 |
| 5 | **L**$_{4.2}$ | 2.5 | - | <1 | <1 |
| 6 | **L**$_{4.3}$ | 2.5 | 91.0 | 12 | 2 |

[a] Reaction conditions: 4.83 mmol 1-hexene, 0.012 mmol [Rh(acac)(CO)$_2$], ligand, 1.5 cm$^3$ toluene, 20 bar of CO/ $H_2$ (1/1), 90 °C, 1 h. [b] Conversion = conversion to aldehydes, *i.e.* 100% - (1-hexene and isomerisation). [c] Isomerisation to 2- and 3-hexene. Conversion and selectivity were determined by $^1$H NMR. Each run is an average of two runs.

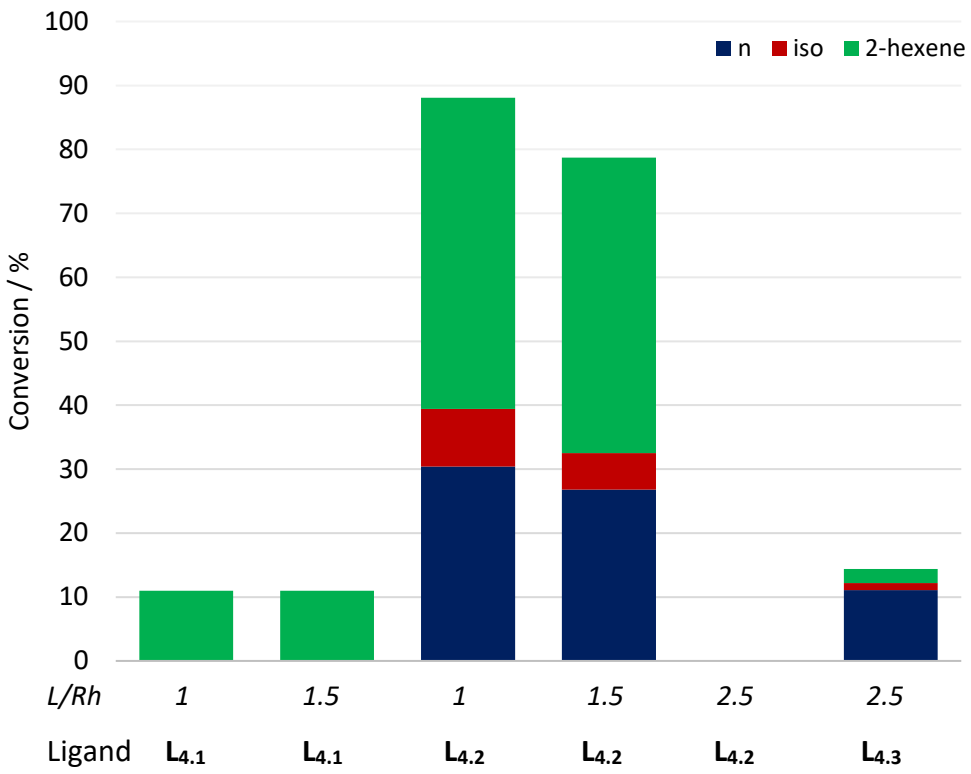


**Figure 4.6** Catalytic hydroformylation of 1-hexene using $\mathbf{L}_{4.1\text{-}4.3}$ at different L/Rh ratios.

The lack of hydroformylation activity when using the catalyst derived from the 5-membered $\mathbf{L}_{4.1}$ (Entries 1 and 2, Table 4.4) can be explained by the observation of complete degradation of the supporting ligand under catalytic conditions. The $^{31}P\{^{1}H\}$ NMR spectrum of the reaction mixture after catalysis showed two signals corresponding to spirophosphorane (**4.8a**) and hydrolysis (**4.14**) degradation products (Scheme 4.16).[70] Isomerisation to 2-hexene was observed in equal amounts when using a L/Rh ratio of 1 and 1.5 (Entry 1 vs. 2), suggesting the same catalytic species may be responsible. Others have previously reported the use of ligand $\mathbf{L}_{4.1}$ in the hydroformylation of propene, but a disappointingly low *n*-selectivity of 60% was observed.[31]

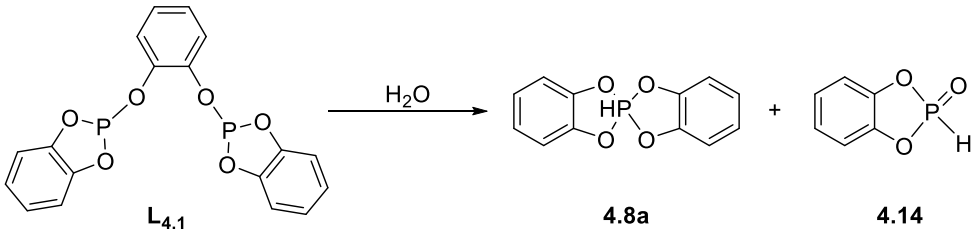


**Scheme 4.16** Degradation of $\mathbf{L}_{4.1}$ under catalytic conditions.

Relative to **L**$_{4.1}$, the 6-membered **L**$_{4.2}$ affords an active catalyst (Entry 1 vs. 3, Table 4.4). A moderate selectivity towards the *n*-aldehyde was observed when using a **L**$_{4.2}$/Rh ratio of 1 (77.2%, Entry 3). Increasing the ligand concentration to a L/Rh ratio of 1.5 considerably increased the *n*-selectivity to 82.5% (Entry 4). In both cases (Entries 3 and 4), isomerisation to 2-hexene was significant; this might be reduced by modifying the catalysis procedure so that the addition of 1-hexene was made under a $CO/H_2$ atmosphere (see experimental details used for Chapter 3).[71] When using higher concentrations of **L**$_{4.2}$ (L/Rh = 2.5, Entry 5) catalytic activity was inhibited. The formation of inactive bis(chelate) species, such as $[RhH(L)_2]$, may be the reason for this. Furthermore, an insoluble yellow precipitate was observed at the end of the catalytic runs, indicating the choice of solvent may be a problem. The 7-membered **L**$_{4.3}$ affords a relatively inactive catalyst when using a L/Rh ratio of 2.5, but a high *n*-selectivity was observed (91.0%, Entry 6). In general, the *n*-selectivities observed do not compete with those obtained when using industrially important diphosphites (Section 4.1.1); it is known that the large steric bulk incorporated in the backbone of these ligands is a crucial feature to obtaining high *n*-selectivity.[3,16,72,73] The lack of steric bulk in the backbone of ligands **L**$_{4.2\text{-}4.3}$ may explain the moderate *n*-selectivities observed.

## 4.5 Conclusions and future work

The formation of spirophosphorane side-products is a persistent issue in the synthesis of P-O bonds in 5-membered aryl dioxaphosphacycles. The equilibria between the spirophosphorane side-products (**4.8a**-**c**) and hydroxyphosphite tautomers (**4.7a**-**c**) have been evaluated computationally for a range of ring sizes and it has been shown that the 5-membered systems are more susceptible to spirophosphorane formation than the larger ring systems, in agreement with the experimental observations. The stability of the 5-membered spirophosphorane (**4.8a**) has been attributed to a combination of its strong intramolecular hydrogen bonds and ideal O-P-O angles.

A silicon-phosphorus exchange reaction has been developed as a novel route to cyclic chlorophosphites **4.6a**-**c** with varying phosphacycle ring sizes (see Chapter 2 also), and a range of aryl dichlorophosphites **4.6e**-**g**. The desired product was obtained in high yield and purity under mild conditions; minimal work-up and purification are required because the only by-product is the volatile $ClSiMe_3$.

The novel 6-membered diphosphite $\mathbf{L_{4.2}}$ has been successfully synthesised and characterised by X-ray crystallography. The IR spectrum of the *cis*-$[Mo(CO)_4(\mathbf{L_{4.2}})]$ complex (**4.11**) revealed the diphosphite $\mathbf{L_{4.2}}$ is a stronger π-acceptor than the 6-membered monophosphite analogue, **4.12**. The ligand-bridged binuclear species, *trans*-$[Rh_2Cl_2(CO)_2(\mu\text{-}\mathbf{L_{4.2}})_2]$ (**4.13**), was prepared upon the addition of the diphosphite to $[Rh_2Cl_2(CO)_4]$. A comparative study of the coordination chemistry of diphosphites $\mathbf{L_{4.1\text{-}4.3}}$, containing the 5- to 7-membered phosphacycles, should be carried out in the future to probe the effect of ring size on their coordination properties.

Diphosphites $\mathbf{L_{4.1\text{-}4.3}}$ with varying phosphacycle ring size have been tested in the Rh-catalysed hydroformylation of 1-hexene. The catalyst derived from the 5-membered diphosphite $\mathbf{L_{4.1}}$ displayed no hydroformylation activity due to complete degradation under reaction conditions. By contrast, the catalyst derived from the 6-membered $\mathbf{L_{4.2}}$ displayed good catalyst performance but increasing the ligand concentration to a L/Rh ratio of 2.5 inhibited the catalysis. Substitution of the aryl rings of $\mathbf{L_{4.2}}$ should be considered in the future to further increase the *n*-selectivity achieved during catalysis and hinder the formation of inactive $[RhH(L)_2]$ species at higher ligand concentrations. For example, the aryl substituted ligands **4.15a**-**b** should be explored since the syntheses of the corresponding dihydroxyarene precursors have been previously reported.[74] Diphosphites containing 6-membered phosphacycles should be the focus of future

studies due to their stability to the catalysis conditions (relative to their 5-membered analogues), their promising catalyst performance and the limited reports of such ligands in the literature.

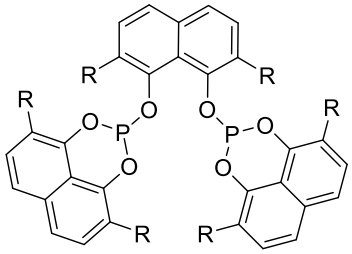

R = Me (**4.15a**)
R = Ph (**4.15b**)

## 4.6 References


1 P. W. N. M. van Leeuwen, in *Homogeneous Catalysis, Understanding the Art*, Kluwer Academic Publishers, Dordrecht, 2004, pp. 139–174.

2 R. Franke, D. Selent and A. Borner, *Chem. Rev.*, 2012, **112**, 5675–5732.

3 P. W. N. M. van Leeuwen and C. Claver, *Rhodium Catalyzed Hydroformylation*, Kluwer Academic Publishers, 2006.

4 J. A. Gillespie, D. L. Dodds and P. C. J. Kamer, *Dalton Trans.*, 2010, **39**, 2751–2764.

5 S. M. Chikkali, J. I. van der Vlugt and J. N. H. Reek, *Coord. Chem. Rev.*, 2014, **262**, 1–15.

6 A. Gual, C. Godard, S. Castillón and C. Claver, *Tetrahedron: Asymmetry*, 2010, **21**, 1135–1146.

7 M. Yamashita and K. Nozaki, in *Comprehensive Organometallic Chemistry III*, eds. R. H. Crabtree and D. M. P. Mingos, Elsevier, 2007, pp. 435–464.

8 M. Beller, in *Topics in Organometallic Chemistry*, Springer, 2006, pp. 1–65.

9 O. Diebolt, P. W. N. M. van Leeuwen and P. C. J. Kamer, *ACS Catal.*, 2012, **2**, 2357–2370.

10 P. C. J. Kamer, A. van Rooy, G. C. Schoemaker and P. W. N. M. van Leeuwen, *Coord. Chem. Rev.*, 2004, **248**, 2409–2424.

11 C. D. Frohning, C. W. Kohlpaintner and H. W. Bohnen, in *Applied Homogeneous Catalysis with Organometallics Compounds*, eds. B. Cornils and W. A. Herrmann, Wiley-VCH, 2002, pp. 31–103.

12 A. Gual, C. Godard, V. de la Fuente and S. Catsillón, in *Phosphorus (III) Ligands in Homogeneous Catalysis*, John Wiley & Sons, Ltd., 2012, pp. 81–131.

13 E. Billig, A. G. Abatjoglou and D. R. Bryant, *US Patent*, 1987, US 4668651.

14 E. Billig, A. G. Abatjoglou and D. R. Bryant, *US Patent*, 1988, US 4748261.

15 E. Billig, A. G. Abatjoglou and D. R. Bryant, *US Patent*, 1989, US 4885401.

16 E. Billig, A. G. Abatjoglou, D. R. Bryant, R. E. Murray and J. M. Mather, *US Patent*, 1986, US 4599206.

17 M. Diéguez, O. Pàmies and C. Claver, *Tetrahedron Asymmetry*, 2004, **15**, 2113–2122.

18 J. E. Babin and G. T. Whiteker, *World Patent*, 1993, WO 93/03839.

19 D. Rottger, R. Kadyrov, A. Borner, D. Selent and D. Hess, *US Patent*, 2003, US 20030195368 A1.

20 D. Rottger, R. Kadyrov, A. Borner, D. Selent and D. Hess, *World Patent*, 2002, WO 02/00670 A1.

21 D. Selent, D. Hess, K. Wiese, D. Röttger, C. Kunze and A. Börner, *Angew. Chemie Int. Ed. English*, 2001, **40**, 1696–1698.

22 D. Selent, R. Franke, C. Kubis, A. Spannenberg, W. Baumann, B. Kreidler and A. Borner, *Organometallics*, 2011, **30**, 4509–4514.

23 M. Alhaffar, R. Suleiman, H. Shakil and B. El Ali, *React. Kinet. Mech. Catal.*, 2011, **104**, 323–336.

24 J. Tijani and B. El Ali, *J. Organomet. Chem.*, 2007, **682**, 3492–3497.

25 J. R. Briggs, D. L. Packett, D. R. Bryant, G. Phillips, D. J. Schreck, K. D. Olson, T. C. Eisenschmid and E. S. Brigham, *US Patent*, 1998, US 5821389.

26 T. Sugioka, J. Tokuyasu, T. Tsuruta and H. Iwasaki, *World Patent*, 2007, WO 2007/114445 A1.

27 T. C. Eisenschmid, R. R. Peterson, G. A. Miller and A. G. Abatjoglou, *World Patent*, 2008, WO 2008115740 A1.

28 J. R. Briggs, D. L. Packette, D. R. Bryant, A. G. Phillips, D. J. Schreck, K. D. Olson, E. B. Tjaden and A. S. Guram, *World Patent*, 1997, WO 97/40001.

29 G. Haoran, L. Zhu, H. Wang, T. Bao and Y. Wang, *Chinese Patent*, 2009, CN 101565353 A.

30 Y. Sedo, H. Itagaki, I. Nakajima and T. Sato, *Japanese Patent*, 1998, JP 10130190 A.

31 P. M. Lorz, B. Werner, M. Roeper and D. Koeffer, *European Patent* , 1992, EP 472071 A1.

32 P. W. N. M. van Leeuwen, *Appl. Catal. A Gen.*, 2001, **212**, 61–81.

33 B. Zhang, H. Jiao, D. Michalik, S. Klob, L. M. Deter, D. Selent, A. Spannenberg, R. Franke and A. Borner, *ACS Catal.*, 2016, **6**, 7554–7565.

34 M. M. Pereira, M. J. F. Calvete, R. M. B. Carrilho and A. R. Abreu, *Chem. Soc. Rev.*, 2013, 6990–7027.

35 B. J. Fertig, W. Gerrard and H. Herbst, *J. Chem. Soc.*, 1957, 1488–1492.

36 P. Majewski, *Phosphorus, Sulfur and Silicon*, 2009, **184**, 942–955.

37 L. M. Abdrakhmanova, V. F. Mironov, T. A. Baronova and R. Z. Musin, *Russ. J. Org. Chem.*, 2007, **43**, 1090–1091.

38 R. Keat, *J. Chem. Soc. Dalton Trans.*, 1974, 876–880.

39 J. Cámpora, C. M. Maya, I. Matas, B. Claasen, P. Palma and E. Lvarez, *Inorg. Chim. Acta*, 2006, **359**, 3191–3196.

40 E. L. Hazeland, A. M. Chapman, P. G. Pringle and H. A. Sparkes, *Chem. Commun.*, 2015, **51**, 10206–10209.

41 A. D. Gorman, J. A. Cross, R. A. Doyle, T. R. Leonard, P. G. Pringle and H. A. Sparkes, *Eur. J. Inorg. Chem.*, 2019, 1633–1639.

42 J. A. Bailey, M. Ploeger and P. G. Pringle, *Inorg. Chem.*, 2014, **53**, 7763–7769.

43 J. A. Bailey, H. A. Sparkes and P. G. Pringle, *Chem. Eur. J. A*, 2015, **21**, 5360–5363.

44 A. D. Gorman, J. A. Bailey, N. Fey, T. A. Young, H. A. Sparkes and P. G. Pringle, *Angew. Chemie Int. Ed.*, 2018, **57**, 15802–15806.

45 E. E. Nifant'ev, T. S. Kukhareva, I. A. Soldatova, S. Belostotskaya, V. V Ershov and L. K. Vasyanina, *Zhurnal Obs. Khimii*, 1988, **58**, 2242–2246.

46 E. E. Nifant'ev, T. S. Kukhareva, I. A. Soldatova and T. G. Chukbar, *Zhurnal Obs. Khimii*, 1986, **56**, 2487–2491.

47 K. N. Harrison, *PhD Thesis*, 1990, University of Bristol.

48 S. Belostotskaya, N. L. Komissarova, T. I. Prokof'eva, V. B. Vol'eva and V. V Ershov, *Izv. Akad. Nauk SSSR*, 1979, 2385–2388.

49 S. B. Tzokov, R. T. Momtcheva and D. D. Petkov, *Phosphorus, Sulfur and Silicon*, 2004, **179**, 1095–1111.

50 E. E. Nifant'ev, T. S. Kukhareva and I. A. Soldatova, *Zhurnal Obs. Khimii*, 1989, **59**, 2504–2507.

51 E. V Popova, V. F. Mironov, E. A. Ishmaeva, N. M. Azancheev, Y. M. Volodina and I. I. Patsanovskii, *Russ. J. Gen. Chem.*, 1999, **69**, 43–47.

52 T. Young, *Masters Thesis*, 2017, University of Bristol.

53 W. G. Schneider, *J. Chem. Phys.*, 1955, **23**, 26–30.

54 L. C. Remer and J. H. Jensen, *J. Phys. Chem. A*, 2000, **104**, 9266–9275.

55 C. Reichardt and T. Welton, *Solvents and Solvent Effects in Organic Chemistry*, Wiley-VCH: Weinheim, 2011.

56 J. Nath and A. D. Tripathi, *J. Chem. Soc. Faraday Trans.*, 1984, **80**, 1517–1524.

57 S. Zbaida and E. Bruer, *J. Org. Chem.*, 1982, **47**, 1073–1077.

58 J. C. Shattuck, C. M. Shreve and S. E. Solomon, *Org. Lett.*, 2001, **3**, 3021–3023.

59 M. J. Baker, K. N. Harrison, A. G. Orpen, P. G. Pringle and G. Shaw, *J. Chem. Soc. Chem. Commun.*, 1991, **94**, 803–804.

60 A. G. Orpen and N. G. Connelly, *J. Chem. Soc. Chem. Commun.*, 1985, 1310–1311.

61 A. G. Orpen and N. G. Connelly, *Organometallics*, 1990, **9**, 1206–1210.

62 M. F. Haddow, A. J. Middleton, A. G. Orpen, P. G. Pringle and R. Papp, *Dalton Trans.*, 2009, 202–209.

63 M. Vijjulatha, S. Kumaraswamy, K. C. Kumara Swamy and U. Engelhardt, *Polyhedron*, 1999, **18**, 2557–2562.

64 M. Hariharasarma, C. H. Lake, C. L. Watkins and G. M. Gray, *Organometallics*, 1999, **18**, 2593–2600.

65 B. E. Mann, C. Masters and B. L. Shaw, *J. Chem. Soc.* , 1971, 1104–1106.

66 A. Sanger, *J. Chem. Soc. Chem. Commun.*, 1975, 893–984.

67 A. L. Balch and B. Tulyathan, *Inorg. Chem.*, 1977, **16**, 2840–2845.

68 G. A. Orpen, *Organometallics*, 1990, **9**, 1222–1227.

69 E. E. Nifant'ev, E. N. Rasadkina, E. V Ronkova, A. R. Bekker, N. S. Magomedova and V. K. Bel'skii, *Zhurnal Obs. Khimii*, 1994, **64**, 1448–1454.

70 J. J. C. van Lier, R. J. M. Hermans and H. M. Buck, *Phosphorus Sulfur Relat. Elem.*, 1984, **19**, 173–188.

71 E. Zuidema, P. E. Goudriaan, B. H. G. Swennenhuis, P. C. J. Kamer, P. W. N. M. van Leeuwen, M. Lutz and A. L. Spek, *Organometallics*, 2010, **29**, 1210–1221.

72 A. van Rooy, P. C. J. Kamer, P. W. N. M. van Leeuwen, K. Goubitz, J. Fraanje, N. Veldman and A. L. Spek, *Organometallics*, 1996, **15**, 835–847.

73 E. Billig, A. G. Abatjoglou and D. R. Bryant, *European Patent* , 1987, EP 1987213639.

74 M. Poirier, M. Simard and J. D. Wuest, *Organometallics*, 1996, **15**, 1296–1300.

# Chapter 5

# Pyridyl monophosphines for methoxycarbonylation

## 5.1 Introduction

### 5.1.1 Catalytic methoxycarbonylation of alkynes

Alkynes are readily available building blocks, which can be used to produce both fine and bulk chemicals in large quantities and at low cost. Since the pioneering work of Reppe in the late 1930s,[1] the one step, atom efficient Pd-catalysed alkoxycarbonylation of alkynes to produce either the branched or linear α,β-unsaturated ester has been extensively studied (Scheme 5.1). The chemo- and regioselectivity of the reaction can be varied by tuning the reaction conditions and catalytic system used. Reppe reported the hydroxycarbonylation of acetylene (Scheme 5.1, R = R' = H), which became an extremely important industrial process for the production of acetic acid, employed at BASF.[1] Recent developments in Pd-catalysed carbonylation of alkynes using a range of nucleophiles have been well-reviewed.[2–9] The methoxycarbonylation of propyne (Scheme 5.1, R = R' = Me) and phenylacetylene (Scheme 5.1, R = Ph, R' = Me) will be considered in detail herein. Although palladium catalysts dominate carbonylation research, other transition metal catalysts, such as Rh, Ni and Fe, have been successfully used and recently reviewed.[10,11]

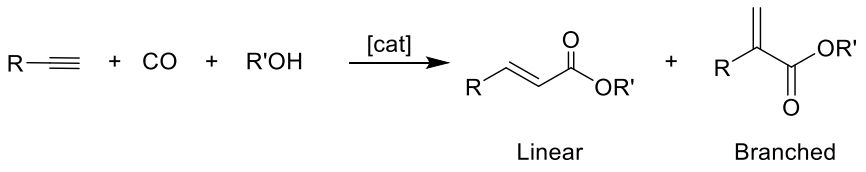


**Scheme 5.1** Catalytic alkoxycarbonylation of alkynes.

#### *5.1.1.1 Propyne methoxycarbonylation*

The Pd-catalysed methoxycarbonylation of propyne has been extensively studied because the branched product is the commercially valuable methyl methacrylate (MMA); this process was first developed by Shell (Scheme 5.2).[12–15] MMA is an important precursor to the polymer, poly(methyl methacrylate) (PMMA), also known as Perspex, Plexiglass or Acrylic.[16,17] PMMA has a wide range of applications including in the photonics, semiconductor and paint industries due to its desirable properties (*e.g.* it is shatterproof, transparent and easily mouldable).[17]

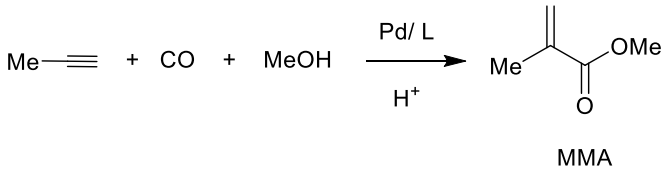


**Scheme 5.2** Catalytic methoxycarbonylation of propyne to produce MMA.

MMA can be accessed *via* many different synthetic routes using a range of $C_2$-$C_4$ hydrocarbon feedstocks, which have been summarised and compared by Nagai.[16] One of these routes is Lucite's "Alpha" Process, which is a two-step, high-yielding process that involves the Pd-catalysed methoxycarbonylation of ethene.[18,19] The success of this process has resulted in its commercialisation on a multi-tonne scale. However, the synthesis of MMA *via* the Pd-catalysed methoxycarbonylation of propyne is an attractive alternative to the "Alpha" Process since only one step is required and it is 100% atom efficient.[20] Moreover, propyne is a readily available feedstock obtainable from naphtha crackers.[20] Despite attraction commercially, efforts to commercialise this route have failed partly due to catalyst poisoning by the propadiene (allene) impurities that contaminate the propyne feedstream.[2,21] Propadiene is known to react with the catalyst to form inactive π-allyl complexes.[2,21]

#### *5.1.1.2 Phenylacetylene methoxycarbonylation*

The Pd-catalysed methoxycarbonylation of other alkyl and aryl alkynes has been well studied.[3,20] The methoxycarbonylation of phenylacetylene (Scheme 5.3) is of particular interest since the branched product, methyl atropate, is a valuable precursor for an important class of nonsteroidal anti-inflammatory agents, including the well-known compounds such as naproxen, ibuprofen and fenoprofen (Figure 5.1).[3] Relative to the branched isomer, reports of the synthesis of linear esters from alkynes are limited to only a few catalyst systems.[3,22,23] The linear product from the methoxycarbonylation of phenylacetylene, methyl cinnamate, is used in the perfume industry.[24,25]

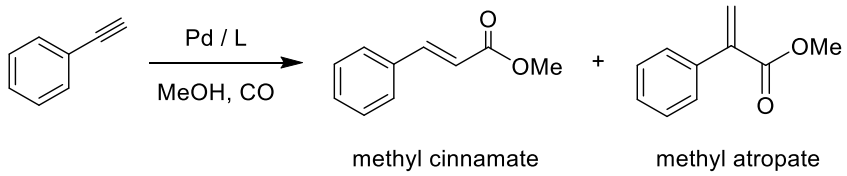


**Scheme 5.3** Catalytic methoxycarbonylation of phenylacetylene.

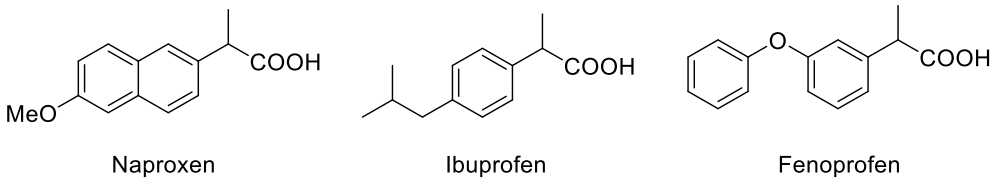


**Figure 5.1** Anti-inflammatory agents which can be synthesised from methyl atropate.[3]

### 5.1.2 Pyridyl phosphines in alkyne methoxycarbonylation

Pyridyl phosphines display hemilabile coordination behaviour to transition metals since P-monodentate, N-monodentate and P,N-bidentate coordination modes are possible.[26] This hemilability can be exploited during catalysis (see Section 5.1.3). The coordination chemistry of pyridyl phosphine ligands and their application in homogeneous catalysis has been well documented.[26,27]

#### *5.1.2.1 $Ph_2P(2\text{-}Py)$ ligands in alkyne methoxycarbonylation*

The use of catalysts derived from pyridyl phosphine ligands, first reported by Drent *et al.* in the late 1980s, is still the benchmark for alkyne methoxycarbonylation (Scheme 5.4).[12–15,28,29] Upon replacement of one of the phenyl rings in ligand $PPh_3$ with a 2-pyridyl (2-Py) ring ($Ph_2P(2\text{-}Py)$, $\mathbf{L_{5.1}}$), Drent observed a dramatic increase in catalyst performance in the methoxycarbonylation of propyne.[12,13] Despite the use of mild conditions (45 °C and 0.006 mol% catalyst loading), unprecedented activities and selectivities were achieved: > 40,000 turnovers per hour and 98.9% branched selectivity (*cf.* 89% selectivity when using $PPh_3$).[12,13] This rate enhancement was significantly diminished when using the 3-pyridyl (**5.1a**) and 4-pyridyl (**5.1b**) analogues, leading Drent to speculate that the spatial orientation of the 2-pyridyl N-atom was key to this ligand's exceptional performance.[12,13]

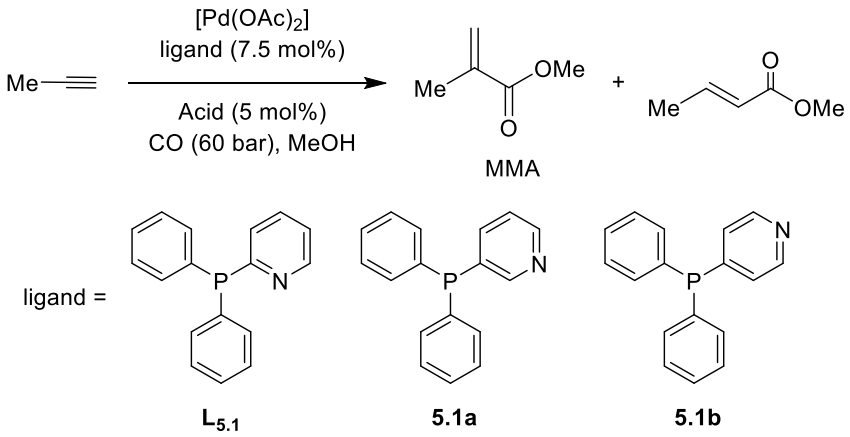


**Scheme 5.4** Pd-catalysed methoxycarbonylation of propyne using pyridyl phosphines.[12,13]

In addition, the catalyst activity was highly dependent on the type and amount of acid promoter used.[12,13] By changing the acid from TsOH (*p*-toluenesulfonic acid) to MsOH (methanesulfonic acid), the rate doubled.[12,13] In contrast, in the presence of strongly coordinating acids, HCl and acetic acid, the rate decreased dramatically to 10-100 turnovers per hour.[12,13] The high reactivity observed with TsOH and MsOH was attributed to the weakly coordinating nature of their conjugate base anions, resulting in increased availability of the coordination sites around the metal centre to the substrate molecules and/or phosphine ligand.[12,13]

Drent observed that upon substitution of more than one phenyl group with a 2-pyridyl on the ligand, the catalytic activity decreased, but minimal effect on the selectivity was seen.[12,13] The effect of substitution on the 2-pyridyl ring itself was also investigated. Me-substitution at the 6-position of the 2-pyridyl ring (**5.1c**) gave a more active and selective catalyst than the unsubstituted analogue; the branched selectivity was increased from 98.9% to 99.95%.[12,13] However, when the Me-substituent was in the 4-position, no impact on the selectivity was observed.[12,13] The electronic effect of the ligand on selectivity appeared to be minimal, which was confirmed as the catalysts derived from the 6-OMe ligand (**5.1d**) and 6-Br ligand (**5.1e**) gave essentially the same branched selectivity (99.65%).[12,13] Importantly, both catalysts (**5.1d**-**e**) were considerably less active than the 6-Me analogue (**5.1c**).[12,13] Drent *et al.* observed similar effects when using other alkynes (*e.g.* acetylene and phenylacetylene) and using a variety of nucleophilic sources (*e.g.* water, alcohols, thiols, carboxylic acids and amines).[12,13]

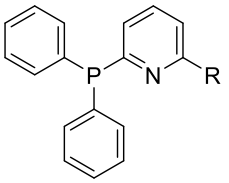

R = Me (**5.1c**)
OMe (**5.1d**)
Br (**5.1e**)

*5.1.2.2 Other P, N-ligands in phenylacetylene methoxycarbonylation*

Inspired by the work of Drent, numerous monophosphine ligands which have the ability to form P,N (or other heteroatom) chelates have been designed, synthesised and tested in alkyne methoxycarbonylation. Diphosphines bearing the 2-pyridyl moiety have also been successfully applied to alkene methoxycarbonylation, but will not be discussed herein.[30–33]

Exploratory research has been carried out into the effect of varying substitution of the phenyl rings of $Ph_2P(2\text{-Py})$ (**L**$_{5.1}$). In 2005, van Koten *et al.* reported the use of new $Ar_2P(2\text{-Py})$ ligands, **5.2a**-**b**, in the methoxycarbonylation of phenylacetylene.[34] The highest activity and selectivity towards the branched product was achieved using the catalyst derived from **5.2b**; using $scCO_2$ as the solvent high branched selectivities were observed (>99%).[34] Pringle *et al.* have recently tested a range of CgP(Py) ligands (such as **5.3**), where CgP = 6-phospha-2,4,8-trioxa-1.3.5.7-tetramethyladamant-6-yl, in the methoxycarbonylation of phenylacetylene.[35] The catalyst derived from CgP(2-Py) was not as effective as $Ph_2P(2\text{-Py})$ (**L**$_{5.1}$), but most CgP(Py) ligands showed good activity and selectivity towards the branched product.[35] The catalytic performance was enhanced upon Me-substitution at the 6-position of the 2-pyridyl ring (ligand **5.3**), as observed with the $Ph_2P$ analogue.[35]

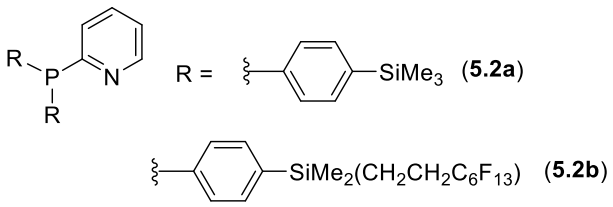

R = (**5.2a**)

(**5.2b**)

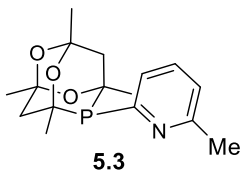

**5.3**

Clarke *et al.* showed the catalyst derived from ligand **5.4** displayed low activity but good branched selectivity (90%) in the methoxycarbonylation of phenylacetylene.[36] The coordination chemistry of the quinoline derived ligand was also investigated and it was shown that the ligand preferred to adopt a monodentate coordination mode but can also act as a bi- or tridentate ligand.[36] Iminophosphine ligands **5.5** were reported by Scrivanti

*et al.* but the derived catalysts for the methoxycarbonylation of phenylacetylene displayed low yields despite employing relatively harsh conditions compared to when using $\mathbf{L_{5.1}}$.[37] This was attributed to the formation of acetophenone side-products resulting from the hydration of the substrate.[37]

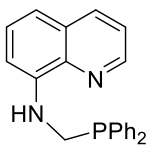


**5.4**

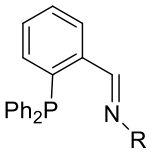


**5.5**

Recently Li *et al.* tested ligands **5.6** in the methoxycarbonylation of a range of alkyl and aryl alkynes, including phenylacetylene.[38] High catalytic activity and branched selectivity were observed and it was shown that P-substitution at the 1-position of the carbazole was critical to catalytic performance.[38] The activity observed using the catalyst derived from **5.6** (when R = Cy) was higher than the benchmark ligand $\mathbf{L_{5.1}}$; this was attributed to a stronger preference for P,N-chelation to Pd for **5.6**.[38] A series of bi-, tri- and tetraphosphines (*e.g.* **5.7a**-**c**) has recently been tested in the methoxycarbonylation of phenylacetylene and shown that using water as an additive promotes catalytic activity.[39] The catalyst derived from the ionic tridentate ligand **5.7b** displayed the highest activity and selectivity (up to 95%), which was attributed to its high π-acceptor capacity.[39] Evidently, the pyrazole-nitrogen is not a determining factor in catalyst performance.

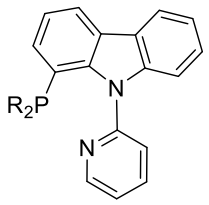


**5.6**

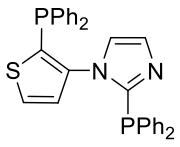


**5.7a**

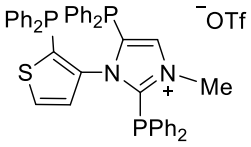


**5.7b**

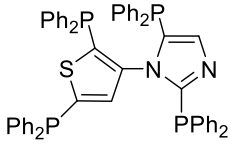


**5.7c**

A series of 2-pyrimidyl phosphines was reported by Reetz *et al.*, and the catalyst derived from ligand **5.8** displayed comparable activity to $Ph_2P$(2-Py) ($\mathbf{L_{5.1}}$) in the methoxycarbonylation of phenylacetylene and 1-hexyne.[40] Evidence of P,N chelation to the Pd centre was observed upon the addition of $AgBF_4$ to $[PdCl_2(\mathbf{5.8})_2]$.[40] It was suggested that this hemilabile behaviour and the ability to protonate the pyrimidyl moieties were key to the catalytic activity,[40] as originally proposed by Drent for $Ph_2P$(2-Py) ligands (Section 5.1.3).[12,13] A decrease in activity was observed upon increasing the number of pyrimidyl substituents on the ligand, analogous to $\mathbf{L_{5.1}}$.[40]

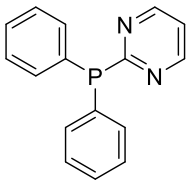

**5.8**

Scrivanti *et al.* tested the (2-furyl)phosphines **5.9a**-**c** in the methoxycarbonylation of phenylacetylene.[41,42] Even when using harsher reaction conditions, ligands **5.9a**-**b** gave very low activity catalysts compared to $Ph_2P(2\text{-}Py)$ (**L**$_{5.1}$), but good branched selectivity was observed (up to 95%).[41] The catalyst derived from the mixed 2-furyl/2-pyridyl ligand (**5.9c**) gave selectivities that rival **L**$_{5.1}$ and higher catalytic activities at low acid concentrations.[42] A Pd-catalyst of another OPN ligand, **5.10**, was shown by Tooze *et al.* to give comparable activity to those of ligands **5.9a**-**b**, but with improved catalyst stability.[43] It can be suggested that the 2-pyridyl's direct link to the P-atom was essential, since when a ligand with a $CH_2$ linker between the P centre and 2-pyridyl moiety was tested no catalytic activity was observed.[43]

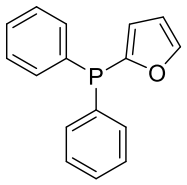

**5.9a**

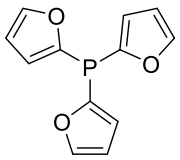

**5.9b**

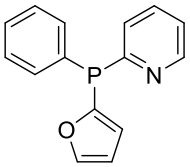

**5.9c**

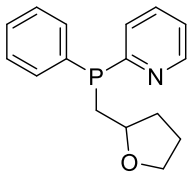

**5.10**

Recently, Beller *et al.* reported a class of new diphosphine ligands bearing 2-pyridyl and *t*Bu substituents (ligands **5.11a**-**b**).[44] The resulting catalysts are highly active and selective for the dialkoxycarbonylation of a range of alkyl and aromatic alkynes.[44] It was demonstrated that the chemo- and regioselectivity of the methoxycarbonylation of phenylacetylene was controlled by varying the ligand.[44] Using the catalyst derived from **5.11a**, the reaction gave the 1,4-dicarboxylic acid product, whereas using the catalyst derived from **5.11b** the selectivity was switched to the branched α,β-unsaturated ester (Scheme 5.5).[44]

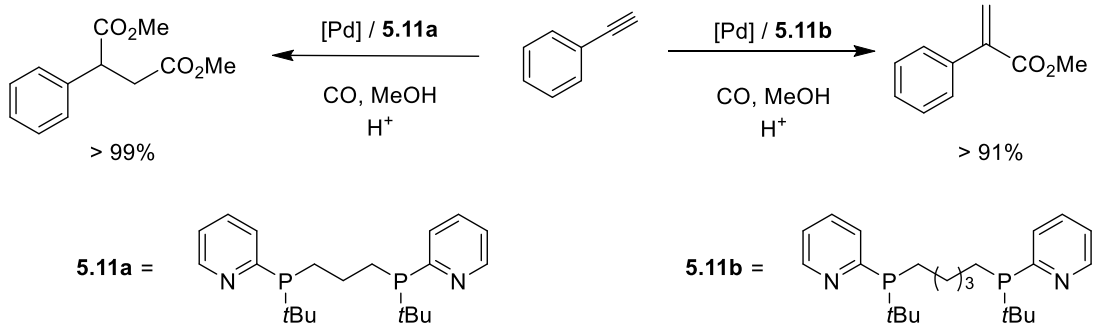


**Scheme 5.5** Ligand controlled chemoselectivity in the methoxycarbonylation of phenylacetylene.[44]

### 5.1.3 Mechanism of alkyne methoxycarbonylation using P,N ligands

The mechanism of alkyne methoxycarbonylation by Pd complexes of 2-pyridyl phosphines has been extensively investigated and the experimental evidence for the proposed mechanisms summarised by Drent and Cole-Hamilton.[45]

#### *5.1.3.1 Original carbomethoxy mechanism*

In 1993, Drent originally proposed a mechanism (cycle **A**, Scheme 5.6) termed the carbomethoxy mechanism, in an attempt to rationalise the remarkable performance of the Pd-$Ph_2P$(2-Py) catalyst.[12,13] It was later termed the "non-classical" carbomethoxy mechanism by Cole-Hamilton *et al.*[46] In 1999, Dervisi *et al.* reported a series of alkoxycarbonyl complexes which supported this mechanism.[21] The dramatic rate enhancement observed when using $\mathbf{L_{5.1}}$ was attributed to its pyridyl-N acting as a "proton-messenger" in the final protonolysis step of the catalytic cycle {step (f), Scheme 5.6}.[12,13] Another key feature to the success of $\mathbf{L_{5.1}}$ was its ability to coordinate to the Pd centre *via* either a $\kappa^1$-(P) or $\kappa^2$-(P,N) coordination mode.[12,13] Acting as a transient P,N-chelate, it was suggested $\mathbf{L_{5.1}}$ can stabilise catalytic intermediates, yet the relative ease of dissociation of the pyridyl-N allowed for substrate binding. For the 3- and 4-pyridyl analogues (**5.1a**-**b**), the complexes are unable to adopt the conformations necessary to enable P,N-chelation, hence they cannot stabilise the catalytic intermediates. This accounts for their relative lack of catalytic activity.

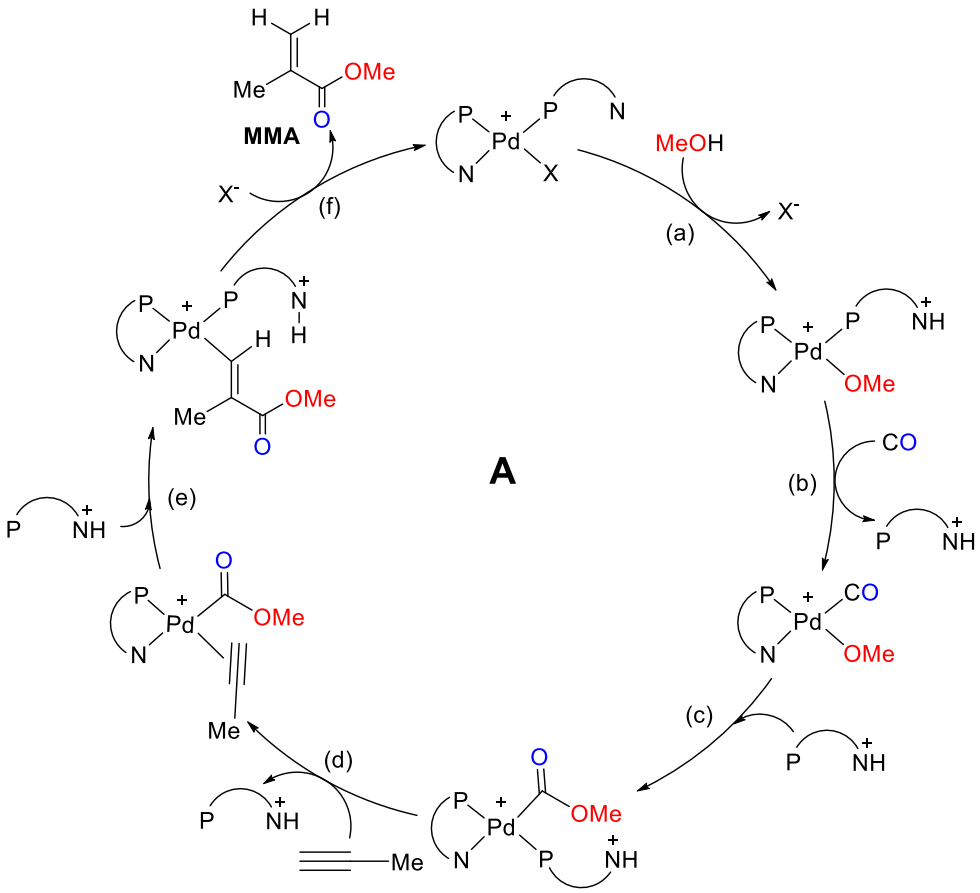


**Scheme 5.6** Carbomethoxy mechanism proposed by Drent for alkyne methoxycarbonylation using ligand $\mathbf{L_{5.1}}$.[12,13]

Drent suggested that the turnover-limiting step of catalytic cycle **A** (Scheme 5.6) was the protonolysis step (step (f)) at low acid concentrations and propyne insertion (step (d)) at higher acid concentrations.[12,13] As discussed in Section 5.1.2.1, steric effects play an important role in determining the selectivity. Drent proposed that the selectivity-determining step was the migratory insertion of the propyne into the Pd-acyl bond (step (e)).[12,13] It was suggested that the carbomethoxy group of this catalytic intermediate would be *cis* to the phosphine donor due to its higher *trans* influence (Figure 5.2).[12,13] As a result, the pyridyl ring would be coordinated *cis* to the propyne. Me-substitution at the 6-position of the 2-pyridyl ring (ligand **5.1c**) would then limit the available space for the coordinated propyne. Therefore, to reduce unfavourable steric interactions, shown in configuration **5.12a**, the methyl group of the propyne must be orientated away from the Pd-centre (configuration **5.12b**); this pathway then leads to the branched product.[12,13]

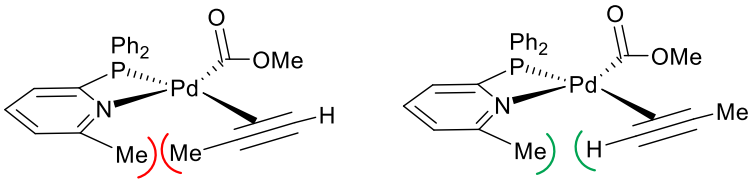


**Figure 5.2** Spatial configurations in the selectivity determining step.[13]

#### *5.1.3.2 In situ base mechanism*

Scrivanti *et al.* proposed the "non-classical" hydride route as an alternative mechanism for alkyne methoxycarbonylation, which occurs *via* a Pd(0) complex.[47,48] Labelling studies were performed which suggested a proton transfer from the 2-pyridyl ligand to the coordinated alkyne initiated the cycle.[47,48]

In 2015, Bühl *et al.* probed four different catalytic pathways for alkyne alkoxycarbonylation using computational methods.[46,49] The most viable pathway calculated was an *in situ* base mechanism (cycle **B**, Scheme 5.7), based on Scrivanti's "non-classical" Pd(0) mechanism.[46] The other pathways were discounted based on either insurmountable calculated energy barriers or incorrect predictions of regioselectivities.[46] It was suggested that the selectivity-determining step in cycle **B** was the protonation of the coordinated propyne (step (a), cycle **B**, Scheme 5.7), which was governed by the steric effects of the ligand (similar to Drent's original mechanism).[46,49] Bühl *et al.* proposed that the turnover-limiting step was the final solvolysis step, which releases MMA and regenerates the catalyst (step (e), cycle **B**).[46,49] Similar to Drent's original mechanism, the dual role of the P,N ligand as a proton messenger (steps (a) and (e), cycle **B**) and a hemilabile ligand (steps (b) and (d), cycle **B**) was proposed as key to its success.[12,13,46,49]

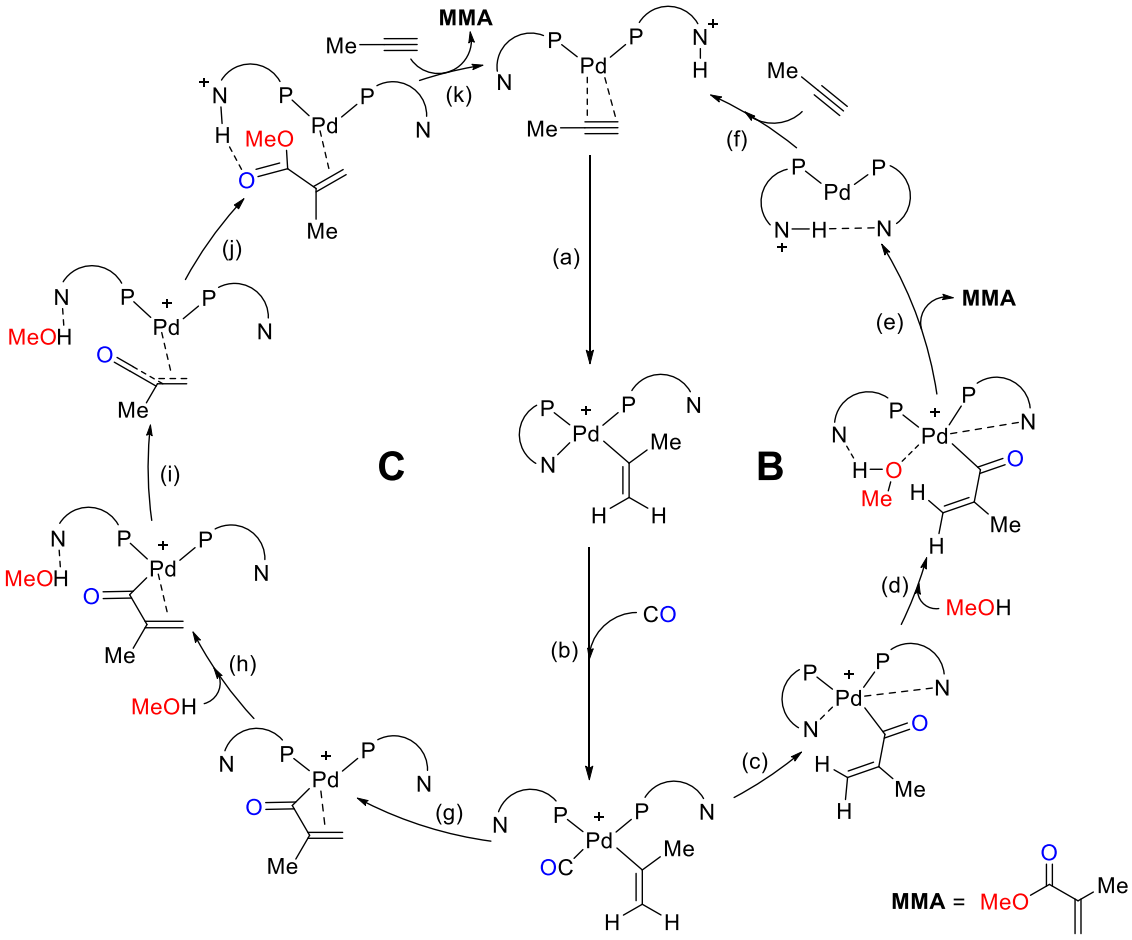


**Scheme 5.7** *In situ* base mechanisms proposed by Bühl *et al.* for alkyne methoxycarbonylation.

Based on pathway **B**, Bühl *et al.* predicted that upon replacement of $Ph_2P(2\text{-Py})$ with the 4-$NMe_2$ substituted ligand **5.13**, an increase in the overall catalytic activity would be observed due to the increase in basicity of the pyridyl-N.[46,49] However, recently Pringle *et al.* have shown that the catalyst derived from **5.13** was considerably less active than its unsubstituted analogue, $\mathbf{L_{5.1}}$, for the methoxycarbonylation of phenylacetylene.[50,51] The choice of substrate (*i.e.* phenylacetylene or propyne) should not affect the computed pathway **B**.[51]

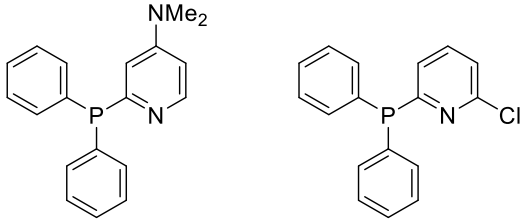

**5.13** $\mathbf{L_{5.2}}$

Given this experimental evidence, Bühl *et al.* proposed a modified *in situ* base mechanism, pathway **C** in Scheme 5.7, which was fully characterised by density functional theory.[51] It was found that upon further examination of the acyl intermediate resulting from step (c) of the original pathway **B**, the isomeric acryloyl intermediate was also energetically accessible (step (g), pathway **C**).[51] Key to this new proposed mechanism were the highly reactive acryloyl and ketene-type intermediates formed in steps (g)-(i) (pathway **C**), which until now had not been suggested as intermediates for alkoxycarbonylation. The proposed selectivity-determining step was the same as in the original pathway (step (a), Scheme 5.7). This re-calculated pathway (**C**) agreed with the experimental results discussed above for ligand **5.13**: the overall energy barrier for ligand **5.13** was now 1.4 kcal $mol^{-1}$ higher than that of $\mathbf{L_{5.1}}$. The reason proposed for this rectification was that the highest energy transition state (HETS) for pathway **C** is the product release rather than methanolysis step, and so the effect of basicity of the ligand is significantly reduced. This led the authors to predict that reducing the basicity of the ligand would have the opposite effect. It was shown that Cl-substitution at the 6-position of the 2-pyridyl ring (ligand $\mathbf{L_{5.2}}$) led to a small decrease in the overall energy barrier: 0.9 kcal $mol^{-1}$ and 0.5 kcal $mol^{-1}$ for the mono- and di-cationic calculated pathways respectively.[51] Indeed, for the methoxycarbonylation of propyne, Drent has previously shown that the catalyst derived from ligand $\mathbf{L_{5.2}}$ was more active than that of $\mathbf{L_{5.1}}$.[14] However, slightly different conditions were used, so there remained a need to test ligands $\mathbf{L_{5.2}}$ and $\mathbf{L_{5.1}}$ under the same conditions.

### 5.1.4 Aims of the project

Inspired by Bühl's prediction, we aimed to synthesise and test ligand $\mathbf{L_{5.2}}$ in the methoxycarbonylation of phenylacetylene under the same conditions to those used for $Ph_2P(2\text{-}Py)$ ($\mathbf{L_{5.1}}$) so their catalytic activity could be directly compared.

As discussed in Section 5.1.2, there have been numerous reports of the application of aryl 2-pyridyl phosphines in alkoxycarbonylation, but there are limited examples of alkyl 2-pyridyl monophosphines. Furthermore, the effect of substitution on the 2-pyridyl ring has been well studied.[12,13,35] Therefore, we aimed to synthesise and test a range of alkyl 2-pyridyl phosphines, $\mathbf{L_{5.3\text{-}5.5}}$, in the Pd-catalysed methoxycarbonylation of various alkynes to probe the effect of the alkyl substituent in $R_2P(2\text{-}Py)$ on catalysis. The ability of the ligands to display P-monodentate ($\kappa^1$) and/or P,N-chelate ($\kappa^2$) coordination to Pd(II) and Pt(II) was also to be investigated and the stereoelectronic properties of the ligands assessed.

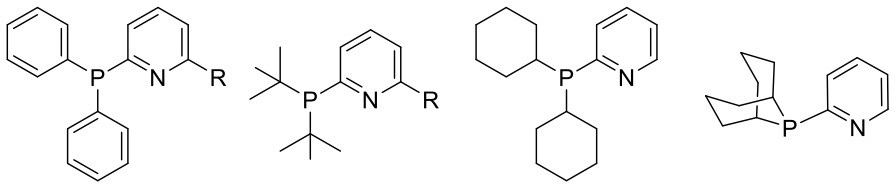


R = H ($L_{5.1}$) = Cl ($L_{5.2}$) | R = H ($L_{5.3a}$) = Me ($L_{5.3b}$) | $L_{5.4}$ | $L_{5.5}$

## 5.2 Predicted pyridylphosphine for methoxycarbonylation

### 5.2.1 Synthesis of 6-chloropyridyl phosphine $L_{5.2}$

Ligand $L_{5.2}$ was synthesised in a good yield (74%) from the following modified literature procedure (see Chapter 7 for details).[52] $HPPh_2$ was treated with *n*BuLi in THF at -78 °C, followed by the reaction with 2,6-dichloropyridine at -78 °C (Scheme 5.8). Low temperatures were necessary to avoid the formation of 2,6-bis(diphenylphosphino)pyridine, **x**.

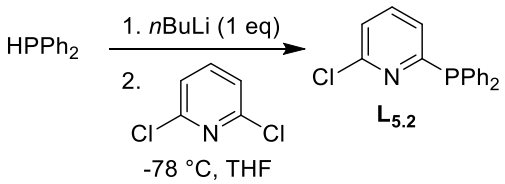


**Scheme 5.8** Synthesis of $L_{5.2}$.

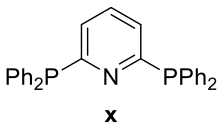


**x**

Crystals of $L_{5.2}$ suitable for X-ray crystallography were grown from a saturated MeOH solution of the ligand (Figure 5.3). The crystal structure of $L_{5.2}$ shows the P atom is pyramidalised; the sum of angles at P is similar to that of $L_{5.1}$ (305° vs. 306°).[53] The P1-C13 bond length in $L_{5.1}$ and $L_{5.2}$ are the same (within 3 esd); the Cl-substituent on the 2-pyridyl ring of $L_{5.2}$ has little effect on its structure in the solid state.

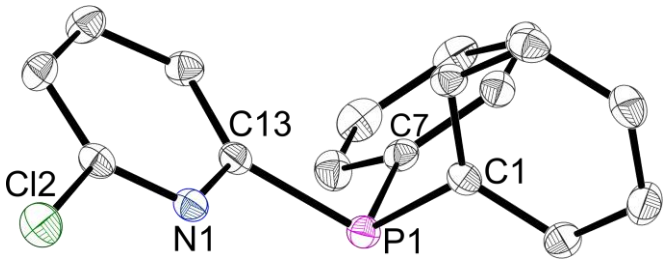


**Figure 5.3** Crystal structure of $\mathbf{L_{5.2}}$. The hydrogen atoms are omitted for clarity. Thermal ellipsoids at 50% probability. Selected bond lengths (Å) and angles (°): P1-C1 1.8294(17), P1-C7 1.8289(17), P1-C13 1.8422(17), C1-P1-C7 102.70(7), C7-P1-C13 101.99(7), C1-P1-C13 100.60(7). See Appendix for experimental details.

### 5.2.2 Catalytic methoxycarbonylation of phenylacetylene

Ligands $\mathbf{L_{5.1}}$ and $\mathbf{L_{5.2}}$ were tested in the Pd-catalysed methoxycarbonylation of phenylacetylene (Scheme 5.9). Under standard conditions modified from the literature[36] (Method A, Chapter 7), catalysts derived from both $\mathbf{L_{5.1}}$ and $\mathbf{L_{5.2}}$ gave 100% conversion. However, in order to directly compare the activity of the catalysts, less than 100% conversion was required. To achieve this, the catalysis was then performed using half the concentration of acid, ligand and Pd (Method B); the reaction was run for 15 min or 1 h. The results are shown in Table 5.1 and Figure 5.4.

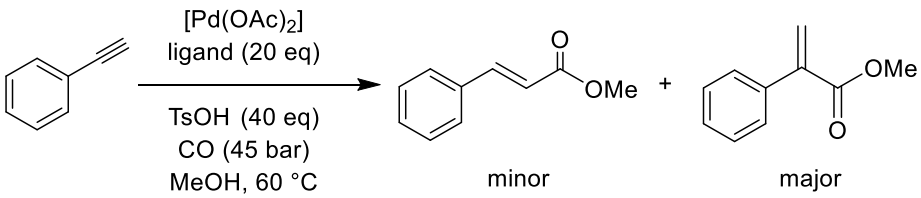


**Scheme 5.9** Catalytic methoxycarbonylation of phenylacetylene.[36]

**Table 5.1** Catalytic methoxycarbonylation of phenylacetylene using either Method A or Method B (Chapter 7).

| Entry | Ligand | Method[a] | Conv. at 15 min[b] / % | Conv. at 1 h[b] / % | Branched selectivity[c] / % |
|---|---|---|---|---|---|
| 1 | **L5.1** | A | - | 100 | > 99 |
| 2 | **L5.2** | A | - | 100 | > 99 |
| 3 | **L5.1** | B | 88 | 100 | > 99 |
| 4 | **L5.2** | B | 99 | 100 | > 99 |

[a] Method A: 5.5 mmol phenylacetylene, 5.5 x $10^{-3}$ mmol $Pd(OAc)_2$, 0.22 mmol $TsOH.H_2O$, 0.11 mmol ligand, 1.5 $cm^3$ MeOH, 45 bar of CO, 60 °C. Method B: 5.5 mmol phenylacetylene, 2.75 x $10^{-3}$ mmol $Pd(OAc)_2$, 0.11 mmol $TsOH.H_2O$, 0.055 mmol ligand, 1.5 $cm^3$ MeOH, 45 bar of CO, 60 °C. [b] Conversion and selectivity were determined by $^1H$ NMR spectroscopy. Each result is an average of two runs. [c] The rest of the product was the linear isomer.

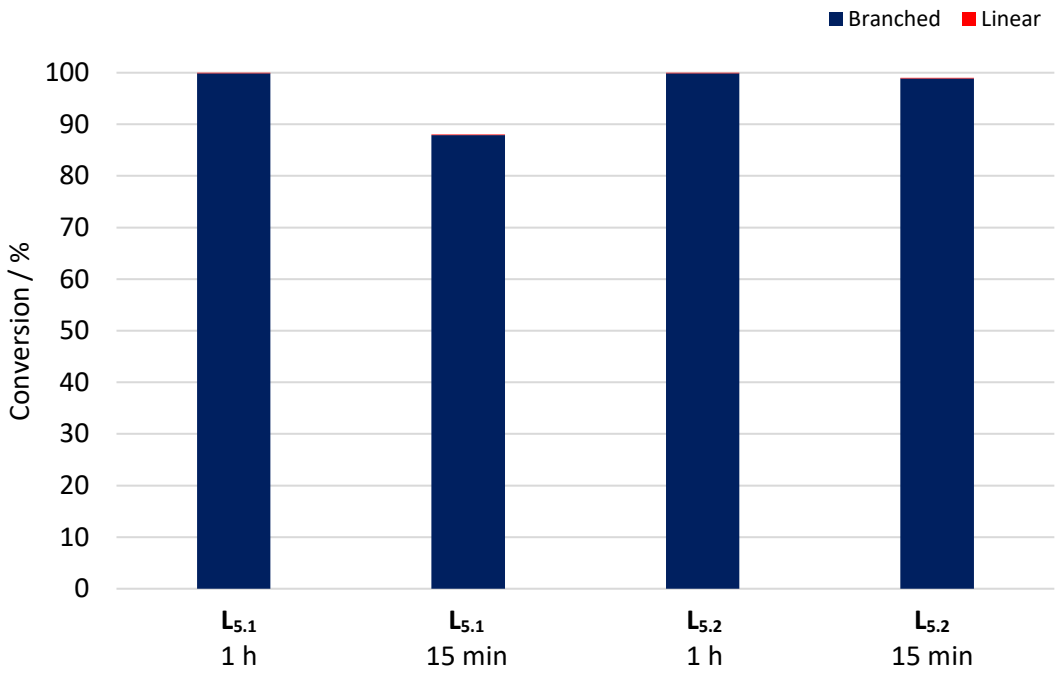


**Figure 5.4** Catalytic methoxycarbonylation of phenylacetylene using Method B. Conversion at 1 h or 15 min.

Both ligands gave highly active and selective catalysts under standard conditions, Method A (Entries 1 and 2, Table 5.1). Under the modified conditions (Method B) and a reaction time of 1 h, the high activity and selectivity of both ligands was maintained (Entries 3 and 4, 1 h). However, at a shorter reaction time of 15 min, the conversion for the catalyst

derived from $\mathbf{L_{5.1}}$ was significantly lower than for the catalyst derived from $\mathbf{L_{5.2}}$: 88% vs. 99% (Entry 3 vs. Entry 4, 15 min). High selectivities for both ligands were retained under these conditions. As explained in Section 5.1.3, a slight decrease in the overall reaction barrier was predicted for the $\mathbf{L_{5.2}}$ system relative to $\mathbf{L_{5.1}}$. These catalytic results show that the $\mathbf{L_{5.2}}$ does indeed produce a more active catalyst.[51]

### 5.2.3 Platinum(II) coordination of $\mathbf{L_{5.2}}$

The reaction of 1 or 2 equiv. of $\mathbf{L_{5.2}}$ with $[PtCl_2(cod)]$ (cod = 1,5-cyclooctadiene) in $CH_2Cl_2$ gave the *cis*-$[PtCl_2(\mathbf{L_{5.2}})_2]$ complex **5.14** (Scheme 5.10). The $^{31}P\{^1H\}$ NMR spectrum of **5.14** gave a singlet with a $^1J_{P,Pt}$ value of 3695 Hz, indicative of a *cis* geometry. The analogous *cis*-$[PtCl_2(\mathbf{L_{5.1}})_2]$ complex has been previously synthesised and shows a $^1J_{P,Pt}$ coupling similar to that of complex **5.14**.[54]

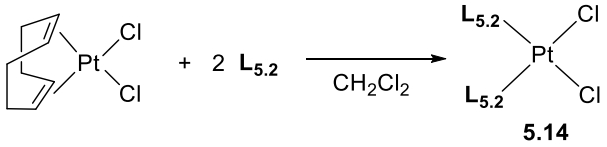


**Scheme 5.10** Synthesis of *cis*-$[PtCl_2(\mathbf{L_{5.2}})_2]$, **5.14**.

Crystals of **5.14** suitable for X-ray crystallography were grown by slow diffusion of hexane into a saturated $CH_2Cl_2$ solution of the complex (Figure 5.5). The crystal structure confirmed the *cis* geometry of phosphine ligands around the Pt centre, in a distorted square planar arrangement. Relative to free ligand, an increase in the sum of angles at P was observed (by *ca.* 7°), as expected from the Pt-P π-bonding.[55,56] The Pt-P bond lengths in **5.14** are similar to those of *cis*-$[PtCl_2(\mathbf{L_{5.1}})_2]$.[57]

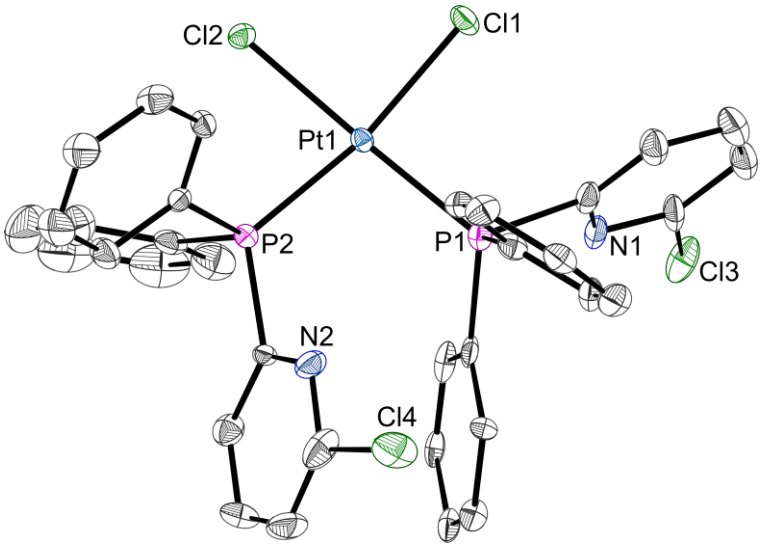


**Figure 5.5** Crystal structure of **5.14**. The hydrogen atoms are omitted for clarity. Disordered atoms in pyridyl and phenyl rings are omitted for clarity. Thermal ellipsoids at 50% probability. Selected bond lengths (Å) and angles (°): Pt1-P1 2.2553(14), Pt1-P2 2.2548(13), Pt1-Cl1 2.3470(13), Pt1-Cl2 2.3674(13), P1-Pt1-P2 99.22(5), P1-Pt1-Cl1 90.01(5), P2-Pt1-Cl2 82.74(5), Cl1-Pt1-Cl2 88.10(5). See Appendix for experimental details.

It is widely reported that the ability of 2-pyridylphosphines to exhibit both P-monodentate and P,N-bidentate behaviour is key to the successful application of such ligands in methoxycarbonylation catalysis.[12,46] To investigate whether **L**$_{5.2}$ would exhibit such hemilabile behaviour, complex **5.14** was treated with 1 equiv. of $AgBF_4$ in $CH_2Cl_2$ to yield *cis*-[PtCl(κ$^2$-**L**$_{5.2}$)(κ$^1$-**L**$_{5.2}$)][$BF_4$] **5.15** (Scheme 5.11).

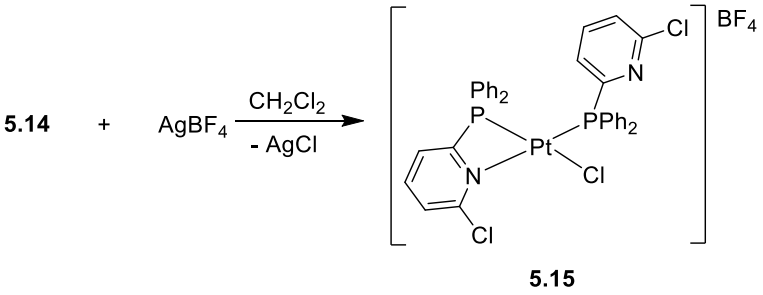


**Scheme 5.11** Synthesis of complex **5.15**.

The $^{31}P\{^1H\}$ NMR spectrum of complex **5.15** gave two doublets at $\delta_P$ = 4.3 ppm ($^2J_{P,P}$ = 6 Hz, $^1J_{P,Pt}$ = 3940 Hz) and -41.9 ppm ($^2J_{P,P}$ = 6 Hz, $^1J_{P,Pt}$ = 3141 Hz). The signal at -41.9 ppm was assigned to the P,N-chelate due to its large upfield shift, which is characteristic of 4-membered Pt chelates.[35,54,58–60] The small $^2J_{P,P}$ and large $^1J_{P,Pt}$ values of **5.15** are

consistent with a *cis* geometry of phosphine ligands.[61] Ligand $\mathbf{L_{5.2}}$ demonstrates both P-monodentate and P,N-bidentate behaviour in complex **5.15**.

### 5.2.4 Palladium(II) coordination of $\mathbf{L_{5.2}}$

The reaction of 1 equiv. of $\mathbf{L_{5.2}}$ with $[PdCl_2(NCPh)_2]$ in $CH_2Cl_2$ gave *cis*-$[PdCl_2(\mathbf{L_{5.2}})_2]$ (*cis*-**5.16**) (Scheme 5.12), resulting in a 1:1 mixture of $[PdCl_2(NCPh)_2]$ and **5.16**. In contrast, Iggo *et al.* have shown the analogous reaction with $\mathbf{L_{5.1}}$ gave the P,N-chelate complex $[PdCl_2(\kappa^2\text{-}\mathbf{L_{5.1}})]$, in addition to the *cis*- and *trans*-$[PdCl_2(\mathbf{L_{5.1}})_2]$ complexes.[59] Reaction of 2 equiv. of $\mathbf{L_{5.2}}$ with $[PdCl_2(NCPh)_2]$ gave a mixture of *cis*- and *trans*-$[PdCl_2(\mathbf{L_{5.2}})_2]$ (**5.16**) in a 7:3 ratio (Scheme 5.12); analogous behaviour has been observed when using 2 equiv. of $\mathbf{L_{5.1}}$.[59]

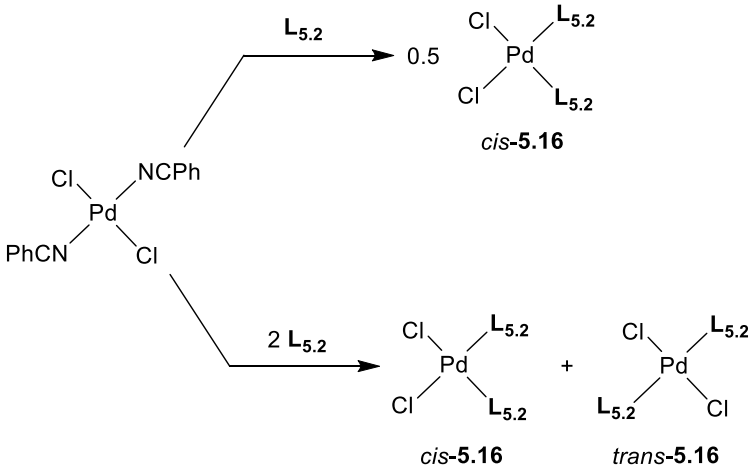


**Scheme 5.12** Reaction of $[PdCl_2(NCPh)_2]$ with 1 or 2 equiv. $\mathbf{L_{5.2}}$.

Crystals suitable for X-ray crystallography of *cis*-**5.16** were grown by slow diffusion of hexane into a saturated $CH_2Cl_2$ solution of *cis*-/*trans*-**5.16** (Figure 5.6). The crystal structure obtained showed a *cis* geometry of phosphine ligands around the Pd centre, in a distorted square planar arrangement. In comparison to free ligand, an increase of *ca.* 9° in the sum of angles at P was observed.

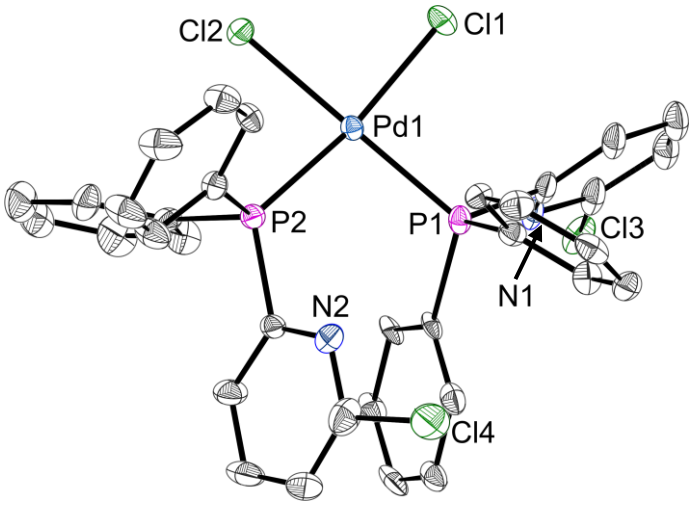


**Figure 5.6** Crystal structure of *cis*-**5.16**. The hydrogen atoms are omitted for clarity. Disordered atoms in pyridyl and phenyl rings are omitted for clarity. Thermal ellipsoids at 50% probability. Selected bond lengths (Å) and angles (°): Pd1-P1 2.2691(16), Pd1-P2 2.2638(16), Pd1-Cl1 2.3302(15), Pd1-Cl2 2.3568(14), P1-Pd1-P2 98.53(6), P1-Pd1-Cl1 89.54(6), P2-Pd1-Cl2 82.30(5), Cl1-Pd1-Cl2 89.73(5). See Appendix for experimental details.

Treatment of *cis*-/*trans*-**5.16** with 1 equiv. of $AgBF_4$ gave species that could not be identified by $^{31}P\{^1H\}$ NMR spectroscopy as a result of signal broadening, which could not be resolved at low temperature. The expected product from the addition of 2 equiv. of $AgBF_4$ to *cis*-/*trans*-**5.16** in $CH_2Cl_2$ was the bis-chelate complex $[Pd(\kappa^2\text{-}\mathbf{L_{5.2}})_2][BF_4]_2$, where chloride abstraction by $Ag^+$ from only the Pd centre has occurred. However, this product was not observed. Instead, the $^{31}P\{^1H\}$ NMR spectrum of the isolated mixture at ambient temperature showed four broadened signals at 34.1, 32.7, -5.3 ($w_{1/2} \approx 30$ Hz) and -31.8 ($w_{1/2} \approx 180$ Hz) ppm. The signal at -5.3 ppm was assigned to free ligand $\mathbf{L_{5.2}}$. Two isomers of complex **5.17** have been tentatively assigned as the other products, where chloride abstraction has occurred both at the Pd centre and on the pyridyl ring of the ligand (Scheme 5.13). The signals are broad at ambient temperature, possibly due to exchange between the P-monodentate and P,N-bidentate coordination modes occurring on the NMR timescale (**5.17a**/**b**, Scheme 5.14). Mass spectrometry showed a signal for the product complex **5.17** ($[M\text{-}BF_4]^+$, see Chapter 7). However, there was also a signal which corresponded to a palladium complex containing three chlorine atoms, with the formula $C_{34}H_{26}Cl_3N_2P_2Pd$.

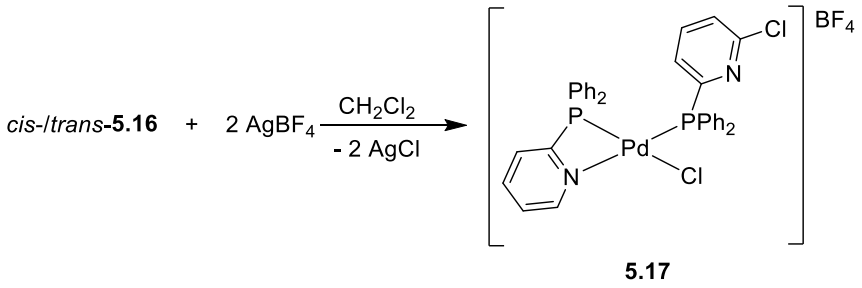


**Scheme 5.13** Synthesis of complex **5.17**.

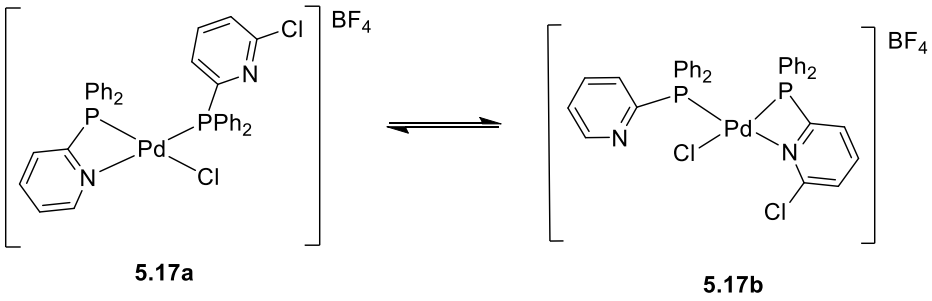


**Scheme 5.14** Exchange occurring between isomers of complex **5.17**.

Upon cooling the solution to -90 °C, the signals at 34.1 and 32.7 ppm in the $^{31}P\{^{1}H\}$ NMR spectrum resolved into a sharp doublet at 37.8 ppm with a $^{2}J_{P,P}$ of 28 Hz and a broad singlet at 40.3 ppm ($w_{1/2} \approx 250$ Hz) (Figure 5.7). The signal at -31.8 ppm resolved into two doublets at -30.1 and -35.5 ppm with $^{2}J_{P,P}$ couplings *ca.* 30 Hz, consistent with a *cis* geometry of P atoms. The four signals were observed in *ca.* a 1:1:1:1 ratio; hence a 1:1 ratio of complexes **5.17a** and **5.17b** has been tentatively assigned (Scheme 5.14).

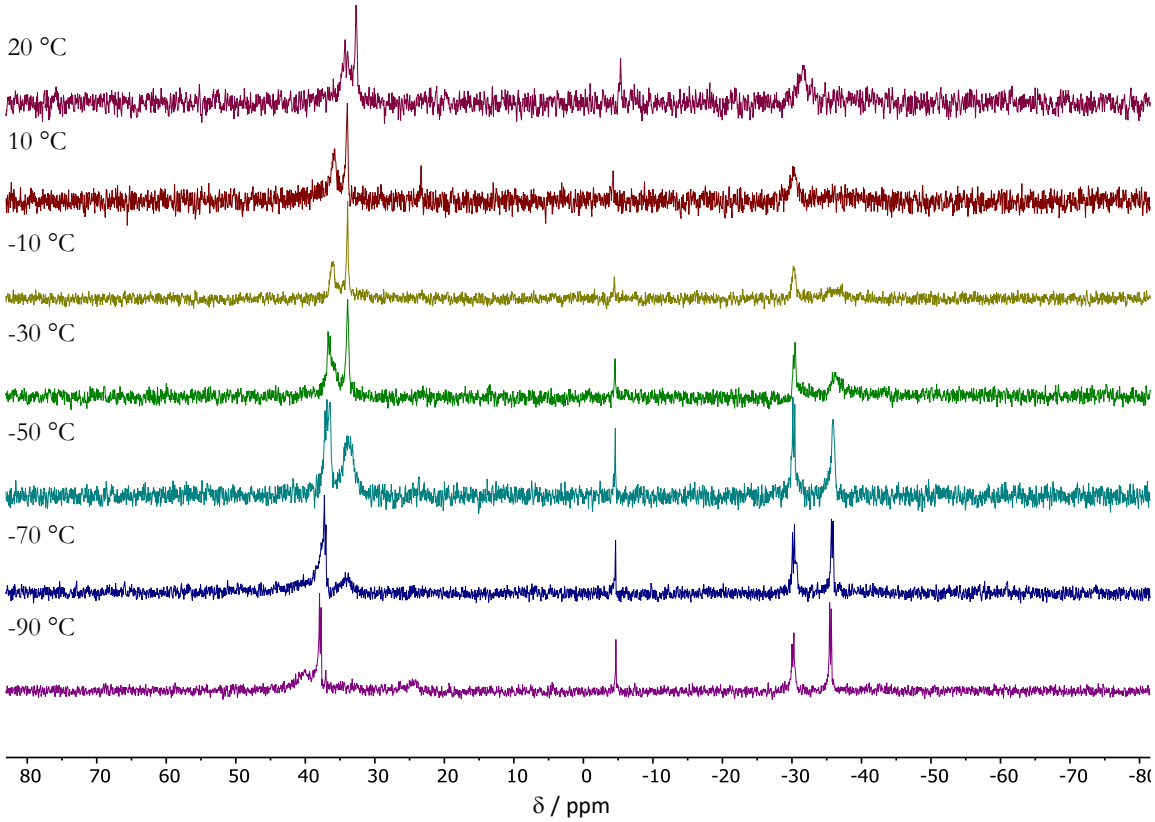


**Figure 5.7** Low temperature $^{31}P\{^{1}H\}$ NMR spectra of **5.17a/b** in $CD_2Cl_2$.

### 5.2.5 Rhodium(I) coordination of $L_{5.2}$

To assess the electronic properties of ligand $\mathbf{L_{5.2}}$, the *trans*-[RhCl(CO)($\mathbf{L_{5.2}}$)$_2$] complex **5.18** was obtained from the reaction of 4 equiv. of $\mathbf{L_{5.2}}$ with $[Rh_2Cl_2(CO)_4]$ in $CH_2Cl_2$ (Scheme 5.15).

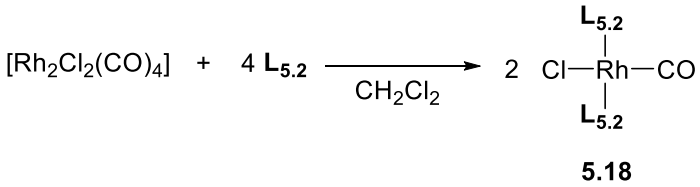


**5.18**

**Scheme 5.15** Synthesis of *trans*-[RhCl(CO)($\mathbf{L_{5.2}}$)$_2$], **5.18**.

At ambient temperature, the $^{31}P\{^{1}H\}$ NMR spectrum of **5.18** gave a broad signal at 30.4 ppm ($w_{1/2} \approx 70$ Hz). The fluxionality of complex **5.18** may be attributed to an equilibrium occurring on the NMR timescale between a mononuclear and binuclear Rh species, as shown in Scheme 5.16. Upon cooling the solution to -90 °C, the signal resolved into a doublet showing a $^{1}J_{P,Rh}$ value of 128 Hz, similar to that of $\mathbf{L_{5.1}}$ in the analogous *trans*-[RhCl(CO)($\mathbf{L_{5.1}}$)$_2$] complex.[62] Cooling the solution shifted the equilibrium towards the mononuclear *trans*-[RhCl(CO)L$_2$] complex, **5.18** (Scheme 5.16).

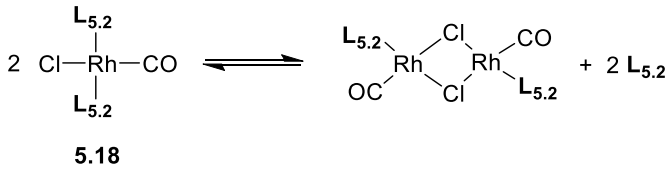


**Scheme 5.16** Equilibrium observed between mononuclear and binuclear Rh species.

The IR spectrum of complex **5.18** showed a broad signal with a ν(CO) ($A_1$) value of 1987 $cm^{-1}$. This value is significantly higher than the analogous *trans*-[RhCl(CO)($\mathbf{L_{5.1}}$)$_2$] complex, which has a ν(CO) ($A_1$) value of 1975 $cm^{-1}$.[63] The unexpectedly high value for complex **5.18** may be attributed to the presence of the binuclear species, [$Rh_2Cl_2(CO)_2$($\mathbf{L_{5.2}}$)$_2$], in solution, shown in the equilibrium above (Scheme 5.16). Subsequently, the electronic properties of $\mathbf{L_{5.2}}$ cannot be directly compared to $\mathbf{L_{5.1}}$.

However, in the crystal structure obtained from the mixture there was no evidence of the binuclear species. Crystals of *trans*-[RhCl(CO)($\mathbf{L_{5.2}}$)$_2$] (**5.18**) suitable for X-ray crystallography were grown by slow diffusion of hexane into a saturated $CH_2Cl_2$ solution of the complex (Figure 5.8). The crystal structure confirmed the *trans* geometry of phosphine ligands. Relative to free ligand $\mathbf{L_{5.2}}$, an increase in the sum of angles at P was observed (by *ca.* 7°). The Rh-P bond length in complex **5.18** is shorter than in the analogous *trans*-[RhCl(CO)($\mathbf{L_{5.1}}$)$_2$] complex (2.3023(7) vs 2.3131(4) Å).[63] This subtle effect is consistent with Rh-P bond strength increasing as the π-acceptor capacity of the ligand increases ($\mathbf{L_{5.2}}$ > $\mathbf{L_{5.1}}$). These effects are not detected in the corresponding Rh-C or C-O bond lengths.

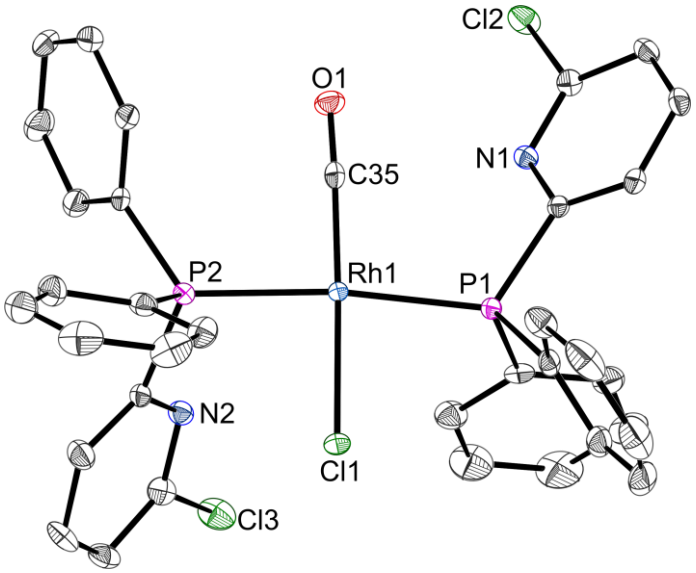


**Figure 5.8** Crystal structure of **5.18**. The hydrogen atoms are omitted for clarity. Thermal ellipsoids at 50% probability. Selected bond lengths (Å) and angles (°): Rh1-C35 1.824(3), O1-C35 1.145(3), Rh1-Cl1 2.3614(6), Rh1-P1 2.3049(7), Rh1-P2 2.2997(7), Cl1-Rh1-C35 177.22(10), P1-Rh1-P2 172.98(3). See Appendix for experimental details.

### 5.3 Synthesis of other $R_2P(2\text{-Py})$ ligands

Although there have been many developments into the effects of modifying the pyridyl substituent of $Ar_2P(2\text{-Py})$ ligands on methoxycarbonylation catalysis, there are limited reports of the use of alkyl pyridyl monophosphines $R_2P(2\text{-Py})$. In particular, bulky alkyl phosphines have not been explored. Herein, a range of alkyl pyridyl phosphines, $R_2P(2\text{-Py})$, will be investigated as ligands, including the bulky pyridyl phosphine, $t\text{Bu}_2P(2\text{-Py})$.

Treatment of 2-bromopyridine with *n*BuLi at -78 °C, followed by the addition of the appropriate chlorophosphine gave the pyridylphosphines **L**$_{5.3a}$ and **L**$_{5.4}$ in good yields (60-75%) (Scheme 5.17). This procedure was modified from a literature method.[64,65]

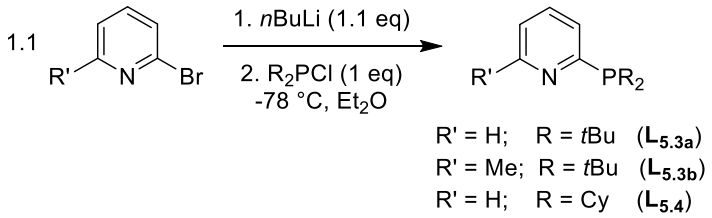


**Scheme 5.17** Synthesis of **L**$_{5.3\text{-}5.4}$.

Substitution at the 6-position of the pyridyl ring of **L**$_{5.1}$ has shown to increase selectivity towards the desired branched product (see Section 5.1.2).[12,13] Therefore, the 6-Me

analogue of the *t*Bu$_2$P derived **L$_{5.3a}$** was synthesised (**L$_{5.3b}$**). This novel ligand **L$_{5.3b}$** was prepared from 2-bromo-6-methylpyridine *via* the lithium-halogen exchange reaction, followed by nucleophilic substitution, described in Scheme 5.17.

The lithium-halogen exchange route was attempted for the PhobP analogue **L$_{5.5}$** (PhobP = 9-phosphabicyclo[3.3.1]nonan-9-yl), but led to dimeric R$_2$P-PR$_2$ side-products. Hence, ligand **L$_{5.5}$** was synthesised *via* the Pd-catalysed P-arylation of *s*-PhobPH, based on a previous literature procedure and the Weferling method (Scheme 5.18).[66,67] Dimeric R$_2$P-PR$_2$ side-products were a persistent issue, thus **L$_{5.5}$** could only be obtained in 90% purity and a low yield (20%).

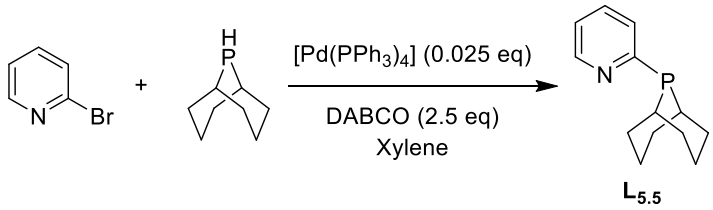


**Scheme 5.18** Synthesis of **L$_{5.5}$**.

## 5.4 Catalytic methoxycarbonylation of phenylacetylene using R$_2$P(2-Py) ligands

### 5.4.1 Catalysis under standard conditions

Ligands **L$_{5.3\text{-}5.5}$** were tested in the Pd-catalysed methoxycarbonylation of phenylacetylene under standard conditions, modified from the literature (Method A, Chapter 7) (Scheme 5.19).[36] The reaction was run for 4.5 h and/or 1 h; the results are shown in Table 5.2 and Figures 5.9 and 5.10.

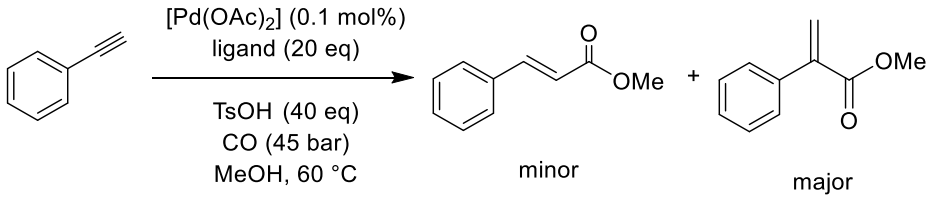


**Scheme 5.19** Catalytic methoxycarbonylation of phenylacetylene.

**Table 5.2** Catalytic methoxycarbonylation of phenylacetylene using Method A (Chapter 7).[a]

| Entry | Ligand | Conversion at 4.5 h[b] / % | Conversion at 1h[b] / % | Branched selectivity[c] / % |
|---|---|---|---|---|
| 1 | **L$_{5.1}$** | 100 | 100 | 99 |
| 2 | **L$_{5.3a}$** | 100 | 99 | 99 |
| 3 | **L$_{5.3b}$** | - | 96 | 99 |
| 4 | **L$_{5.4}$** | 6 | - | 72 |
| 5 | **L$_{5.5}$** | 24 | - | 97 |
| 6 | *t*Bu$_2$PPh | - | 2 | 54 |

[a]Method A: 5.5 mmol phenylacetylene, 5.5 x $10^{-3}$ mmol Pd(OAc)$_2$, 0.22 mmol TsOH.H$_2$O, 0.11 mmol ligand, 1.5 cm$^3$ MeOH, 45 bar of CO, 60 °C. [b]Conversion and selectivity were determined by $^1$H NMR spectroscopy. Each result is an average of two runs. [c]The rest of the product was the linear isomer.

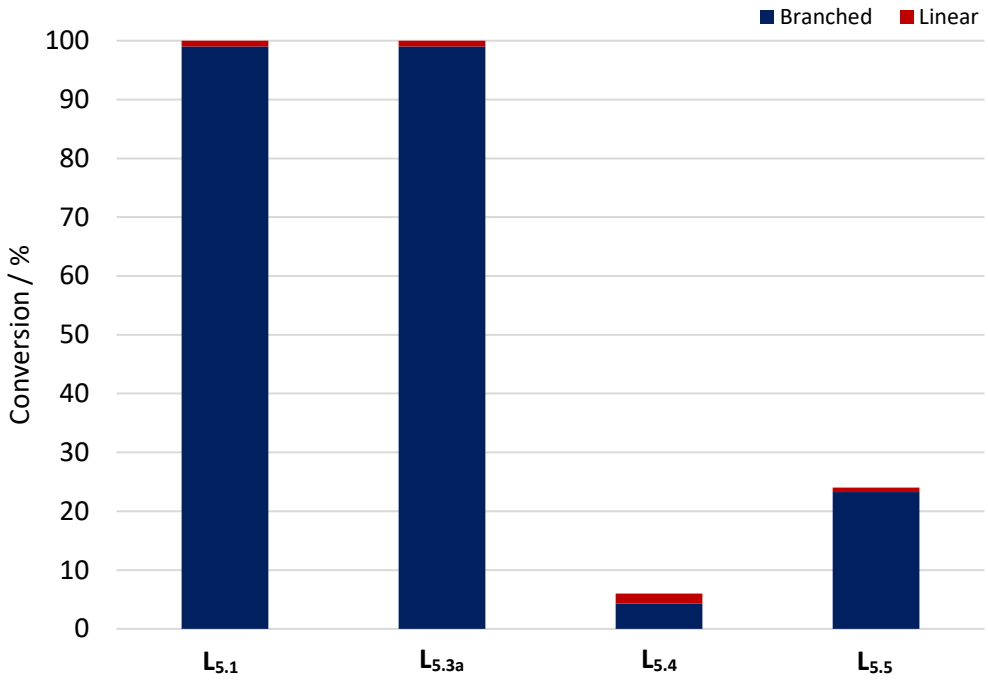


**Figure 5.9** Methoxycarbonylation of phenylacetylene. Conversion at 4.5 h.

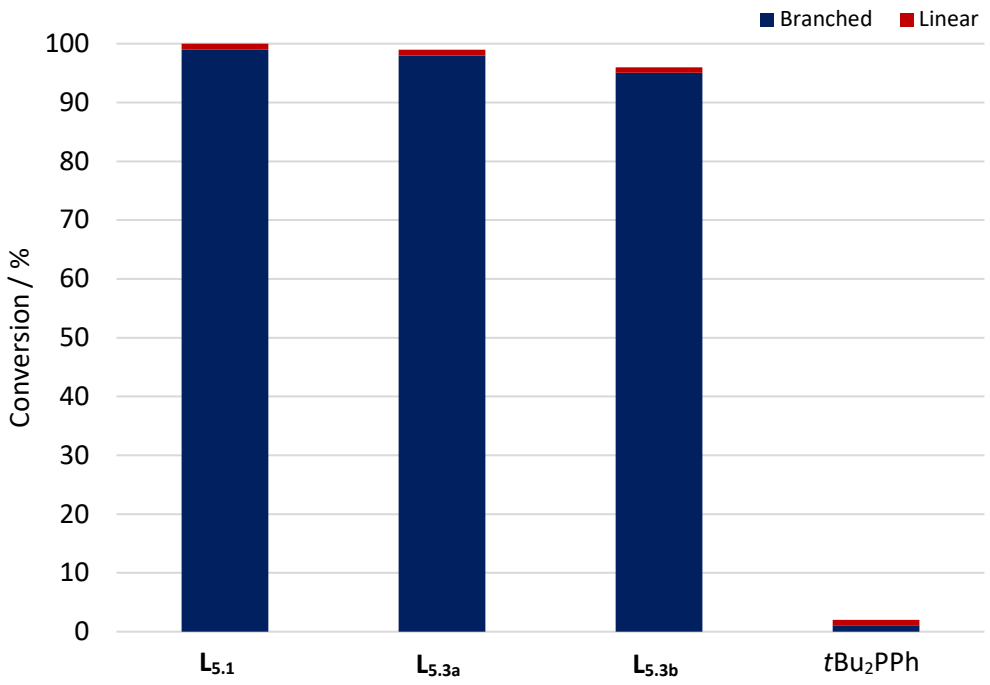


**Figure 5.10** Methoxycarbonylation of phenylacetylene. Conversion at 1 h.

Comparing the pyridyl phosphines, **L**$_{5.1}$, **L**$_{5.3a}$, **L**$_{5.4}$ and **L**$_{5.5}$ (Figure 5.9), the catalyst derived from the $Cy_2P$ ligand **L**$_{5.4}$ was the least active and selective (Entry 4, Table 5.2). The catalyst derived from the *s*-PhobP analogue **L**$_{5.5}$ also displayed low activity, but in this case high branched selectivity was achieved (Entry 5). Pleasingly, the *t*$Bu_2P$ ligand **L**$_{5.3a}$ gave a highly active catalyst, achieving 100% conversion within 4.5 h, while obtaining excellent branched selectivity (Entry 2, 4.5 h). This result rivals those observed when using the $Ph_2P$ analogue **L**$_{5.1}$.

To explore the catalytic activity of the *t*$Bu_2P$ ligand **L**$_{5.3a}$ further, catalytic runs were carried out using analogous ligands (Figure 5.10). At a shorter reaction time of 1 h, using the catalyst derived from **L**$_{5.3a}$, high branched selectivity and activity were retained (Entry 2, 1 h, Table 5.2). To probe the effect of substitution at the 6-position of the 2-pyridyl ring, the Me-substituted ligand **L**$_{5.3b}$ was tested. When using the catalyst derived from **L**$_{5.3b}$, a drop in branched selectivity was observed (to 96%) relative to when using the unsubstituted ligand **L**$_{5.3a}$ (Entry 3 vs. 2, 1 h). This contrasts with the $Ph_2P$ ligand **L**$_{5.1}$, where substitution at the 6-position of the pyridyl ring led to increased branched selectivity.[12,13] Ligand **L**$_{5.3a}$ gave a considerably more active catalyst than *t*$Bu_2PPh$ (Entry 2 vs. 6) and therefore the 2-pyridyl ring appears essential to high catalyst performance (as seen with **L**$_{5.1}$).[12,13]

### 5.4.2 Catalysis on a larger scale

The promising results obtained with the *t*Bu$_2$P based ligand **L$_{5.3a}$** prompted its testing on a much larger scale. This is generally the next stage in commercial development and to achieve this ligand **L$_{5.3a}$** was tested in collaboration with Lucite.[68] They tested ligands **L$_{5.1}$** and **L$_{5.3a}$** for the methoxycarbonylation of phenylacetylene (Scheme 5.20) under standard conditions but using 30 times the amount of substrate (0.1 mol% Pd, Method C). The reactions were also carried out at a lower catalyst loading of 0.01 mol% Pd (Method D) and the results are given in Table 5.3 and Figure 5.11. Due to chemical shift drifting of MeOH and starting material resonances in the $^1$H NMR spectra, a new method of $^1$H NMR spectroscopic analysis was developed to determine the conversion and selectivity (see Chapter 7 for details).[68] A theoretical maximum turnover number (TON) was calculated according to Equation 1, which assumes full conversion of the phenylacetylene.

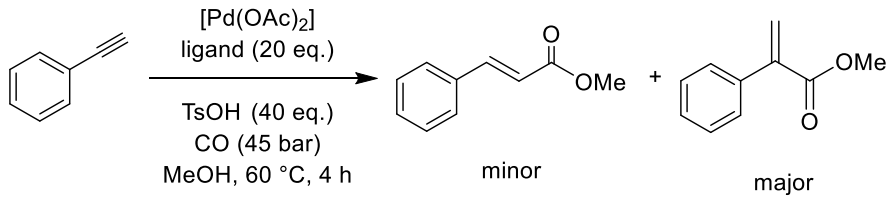


**Scheme 5.20** Scaled up catalytic methoxycarbonylation of phenylacetylene.

$$\text{Max TON} = \frac{\text{mol product}}{\text{mol Pd}}$$

**Equation 1** Calculation of maximum turnover number (TON).

**Table 5.3** Catalytic methoxycarbonylation of phenylacetylene using Method C (0.1 mol% Pd) or D (0.01 mol% Pd).[a]

| Entry | Ligand | Method[a] | Max TON | Conversion[b] / % |
|---|---|---|---|---|
| 1 | **L$_{5.1}$** | C | 990 | 100 |
| 2 | **L$_{5.1}$** | D | 8,890 | 34 |
| 3 | **L$_{5.3a}$** | C | 1,000 | 100 |
| 4 | **L$_{5.3a}$** | D | 9,180 | 37 |

[a] Method C: (0.1 mol% Pd), 165 mmol phenylacetylene, 0.164 mmol Pd(OAc)$_2$, 6.73 mmol TsOH.H$_2$O, 3.35 mmol ligand, 300 cm$^3$ MeOH, 45 bar of CO, 60 °C, 4 h. Method D: (0.01 mol% Pd) 166 mmol phenylacetylene, 0.0209 mmol Pd(OAc)$_2$, 0.736 mmol TsOH.H$_2$O, 0.337 mmol ligand, 300 cm$^3$ MeOH, 45 bar of CO, 60 °C, 4 h. [b] Conversion was determined by $^1$H NMR spectroscopy (see Chapter 7).

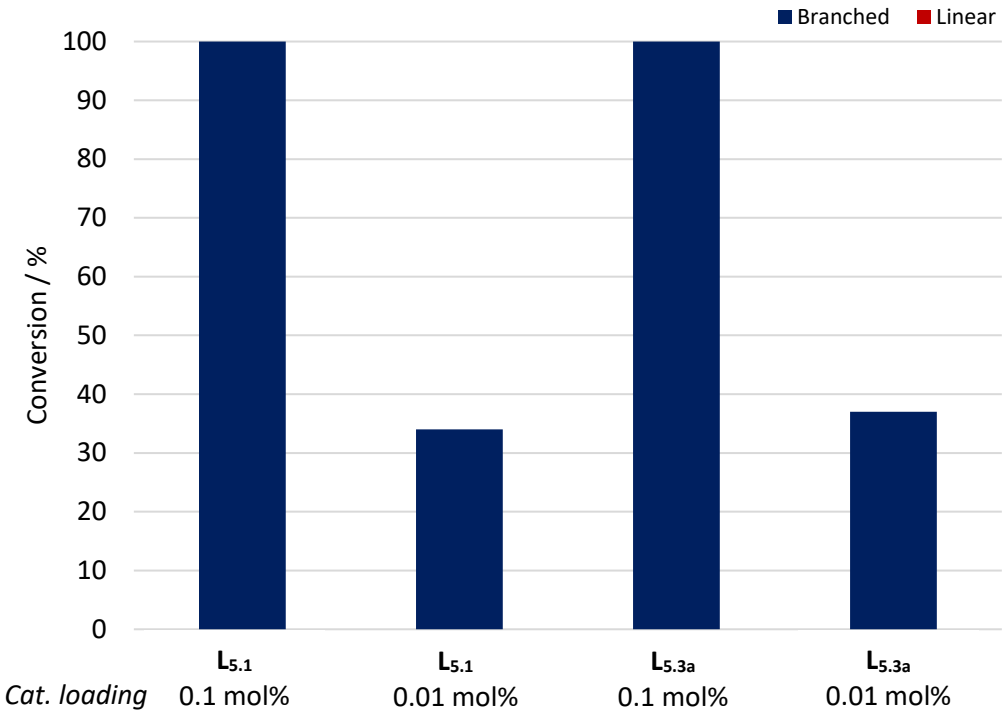


**Figure 5.11** Methoxycarbonylation of phenylacetylene using different catalyst loadings. Conversion at 4 h.

Catalysts derived from both **L**$_{5.1}$ and **L**$_{5.3a}$ displayed 100% selectivity towards the branched product in all catalytic runs. Pleasingly, the results obtained by Lucite show no loss in catalyst activity and selectivity when the reaction is performed on a scale more relevant to industry. 100% conversion was achieved when using both catalysts derived from **L**$_{5.1}$ and **L**$_{5.3a}$ (Entry 1 and 3, Table 5.3) with similar TONs. Decreasing the catalyst loading to 0.01 mol% Pd (Method D) saw a considerable decrease in activity to *ca.* 35% for both **L**$_{5.1}$ and **L**$_{5.3a}$ (Entry 2 and 4). Under these modified conditions, the TON for the *t*Bu$_2$P ligand **L**$_{5.3a}$ was slightly higher than that obtained when using the Ph$_2$P ligand **L**$_{5.1}$.

In an attempt to increase the TON at low catalyst loading (0.01 mol% Pd), the concentration of acid and ligand were increased to give a 1:60:120 ratio of Pd: ligand: acid (Method E). Ligands **L**$_{5.1}$ and **L**$_{5.3a}$ were tested under these optimised conditions and the results are given in Table 5.4.

**Table 5.4** Catalytic methoxycarbonylation of phenylacetylene using a 1:60:120 ratio of Pd: ligand: acid at 0.01 mol% Pd (Method E).[a]

| Entry | Ligand | Max TON | Conversion[b] / % |
|---|---|---|---|
| 1 | **L5.1** | 9,260 | 100 |
| 2 | **L5.3a** | 10,000 | 100 |

[a] Method E: (0.01 mol% Pd), 165 mmol phenylacetylene, 0.0165 mmol $Pd(OAc)_2$, 2.01 mmol $TsOH.H_2O$, 1.00 mmol ligand, 300 $cm^3$ MeOH, 45 bar of CO, 60 °C, 4 h. [b] Conversion was determined by $^1H$ NMR spectroscopy (see Chapter 7).

Indeed, increasing the acid and ligand concentration increased the conversion to 100% for both ligands **L5.1** and **L5.3a**, while retaining 100% branched selectivity (Table 5.4). In addition, high TONs of *ca.* 10,000 were calculated. To further increase the TON for the *t*$Bu_2P$ ligand **L5.3a** at a 1:60:120 ratio of Pd: L: acid, the amount of substrate was increased to 829 mmol (Method F, Table 5.5). A longer reaction time of 22 h was required to achieve 75% conversion. Under these conditions an excellent TON of 48,900 was achieved.

**Table 5.5** Catalytic methoxycarbonylation of phenylacetylene using an increased amount of substrate (Method F).[a]

| Entry | Ligand | Max TON | Conversion[b] / % |
|---|---|---|---|
| 1 | **L5.3a** | 48,900 | 75 |

[a] Method F: 829 mmol phenylacetylene, 0.0169 mmol $Pd(OAc)_2$, 2.00 mmol $TsOH.H_2O$, 0.995 mmol ligand, 300 $cm^3$ MeOH, 45 bar of CO, 60 °C, 22 h. [b] Conversion was determined by $^1H$ NMR spectroscopy (see Chapter 7).

## 5.5 Catalytic methoxycarbonylation of other substrates

### 5.5.1 Catalytic methoxycarbonylation of propyne on a large scale

As previously discussed, the valuable monomer, MMA, can be obtained in one step from the methoxycarbonylation of propyne (see Section 5.1.1). Ligands **L5.1** and **L5.3a** were tested by Lucite on a relatively large scale in the Pd-catalysed methoxycarbonylation of propyne (Scheme 5.21). The reaction was run using 0.02 mol% Pd for 4 or 24 h, and the results are shown in Table 5.6. The reaction product mixture was analysed by gas chromatography (GC). Due to its volatility, the amount of propyne could not be accurately quantified and thus % conversion could not be calculated. Instead, gas uptake, TON and mass of MMA produced were used to indicate conversion (Table 5.6 and Figure

5.12). The TON calculated for these runs is the actual TON since an accurate value of the MMA produced was obtained.

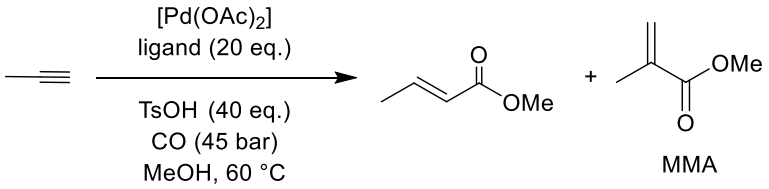


**Scheme 5.21** Catalytic methoxycarbonylation of propyne on a large scale.

**Table 5.6** Catalytic methoxycarbonylation of propyne using 0.02 mol% Pd (Method G).[a]

| Entry | Ligand | Reaction time / h | TON | MMA produced[b] / g | Branched selectivity[c] / % |
|---|---|---|---|---|---|
| 1 | **L**$_{5.1}$ | 4 | 3,373 | 55.8 | 99.7 |
| 2 | **L**$_{5.3a}$ | 4 | 560 | 9.0 | 100 |
| 3 | **L**$_{5.3a}$ | 24 | 2,400 | 39.0 | 99.4 |

[a] Method G: 0.02 mol% Pd, 1:20:40 ratio of Pd: ligand: acid, 45 bar of CO, 60 °C. [b] Conversion and selectivity were determined by GC. Each result is an average of two or more runs. [c] The rest of the product was the linear isomer.

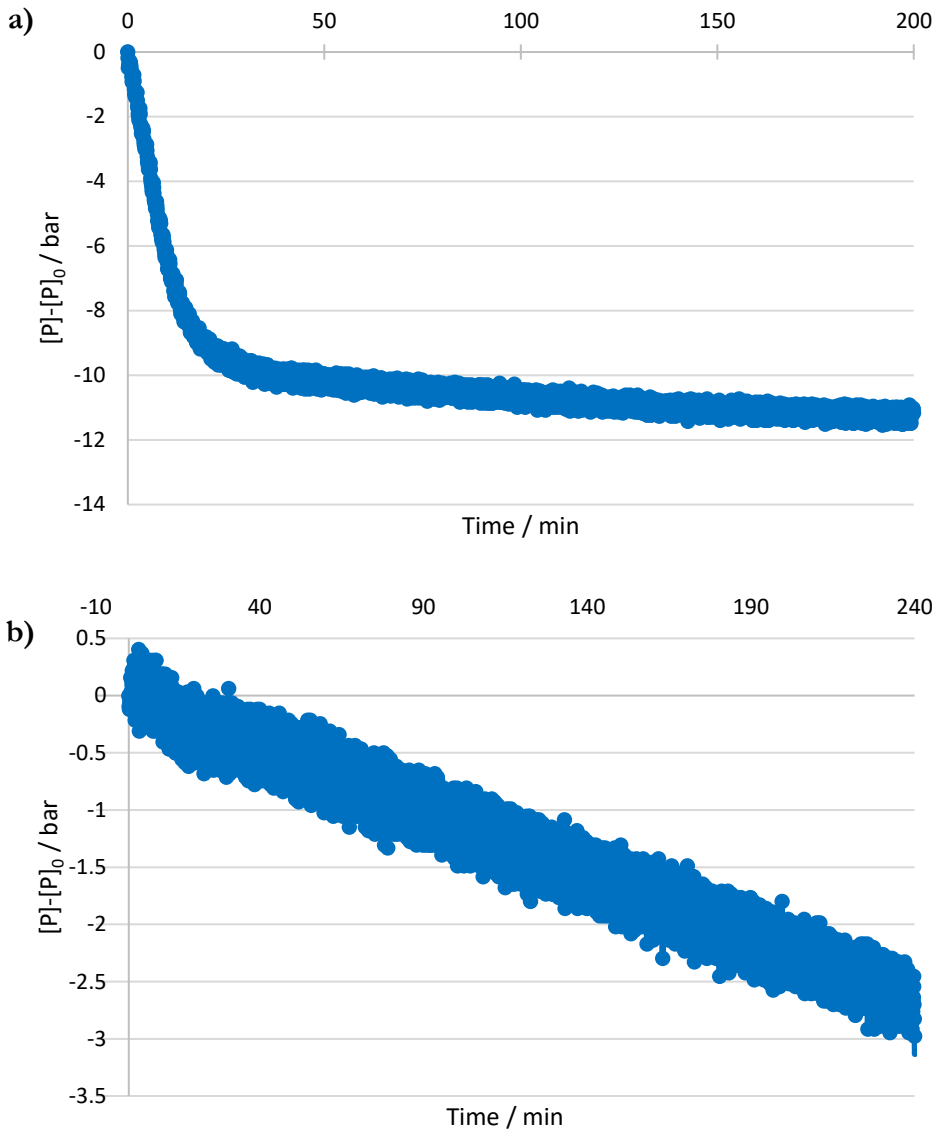


**Figure 5.12** Gas uptake monitored over time for the catalytic methoxycarbonylation of propyne using a) $\mathbf{L}_{5.1}$ and b) $\mathbf{L}_{5.3a}$.

As expected,[12–15] the $Ph_2P$ ligand $\mathbf{L}_{5.1}$ gave a highly active catalyst (Entry 1, Table 5.6). The gas uptake was monitored over time and appeared to plateau within 1 h (Figure 5.12a), suggesting full conversion had been achieved. In contrast, the $t$Bu$_2$P ligand $\mathbf{L}_{5.3a}$ affords a much less active catalyst. Within 4 h, the gas uptake did not plateau (Figure 5.12b), suggesting the reaction did not reach full conversion. Moreover, to support this the TON and amount of MMA produced was significantly higher (*ca.* 6 x) when using the catalyst derived from the $Ph_2P$ ligand $\mathbf{L}_{5.1}$ (Entry 1 vs. 2). Nevertheless, the catalyst derived from $\mathbf{L}_{5.3a}$ remained active over the 4 h and gave 100% branched selectivity under these conditions (Entry 2). To probe whether the $\mathbf{L}_{5.3a}$ catalyst would maintain 100% selectivity

at a higher conversion, the reaction time was extended to 24 h; 100% conversion was achieved under these conditions (Entry 3). However, the selectivity dropped slightly to 99.4%, marginally lower than that of **L**$_{5.1}$. Increasing the catalyst loading from 0.02 to 0.2 mol% Pd, 100% conversion could be achieved in less than 4 h, with retention of high branched selectivity (99.4%). Although the *t*Bu$_2$P ligand **L**$_{5.3a}$ gave a considerably less active catalyst than that of the Ph$_2$P analogue **L**$_{5.1}$, it displayed comparable branched selectivity.

### 5.5.2 Catalytic methoxycarbonylation of 3,3-dimethylbutyne

Ligands **L**$_{5.1}$, **L**$_{5.3a}$ and the analogues of the *t*Bu$_2$P derived ligand **L**$_{5.3a}$ (**L**$_{5.3b}$ and *t*Bu$_2$PPh) were tested in the Pd-catalysed methoxycarbonylation of 3,3-dimethylbutyne under modified literature conditions (Scheme 5.22).[36] 3,3-dimethylbutyne is a more challenging substrate than phenylacetylene and propyne for this reaction; the branched product can also be used in mechanistic studies as a trapping agent.[69] The reaction was run for 1 h and the results are shown in Table 5.7 and Figure 5.13.

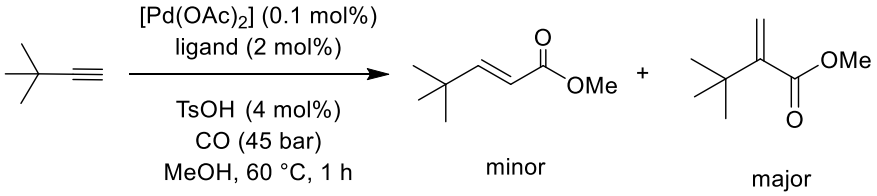


**Scheme 5.22** Catalytic methoxycarbonylation of 3,3-dimethylbutyne.

**Table 5.7** Catalytic methoxycarbonylation of 3,3-dimethylbutyne.[a]

| Entry | Ligand | Conversion[b] / % | Branched selectivity[c] / % |
|---|---|---|---|
| 1 | **L**$_{5.1}$ | 92 | 90 |
| 2 | **L**$_{5.3a}$ | 99 | 99 |
| 3 | **L**$_{5.3b}$ | 99 | 98 |
| 4 | *t*Bu$_2$PPh | 0 | 0 |

[a]Method H: 5.5 mmol 3,3-dimethylbutyne, 5.5 x $10^{-3}$ mmol Pd(OAc)$_2$, 0.22 mmol TsOH.H$_2$O, 0.11 mmol ligand, 1.5 cm$^3$ MeOH, 45 bar of CO, 60 °C, 1 h. [b] Conversion and selectivity were determined by $^1$H NMR spectroscopy. Each result is an average of two runs. [c] The rest of the product was the linear isomer.

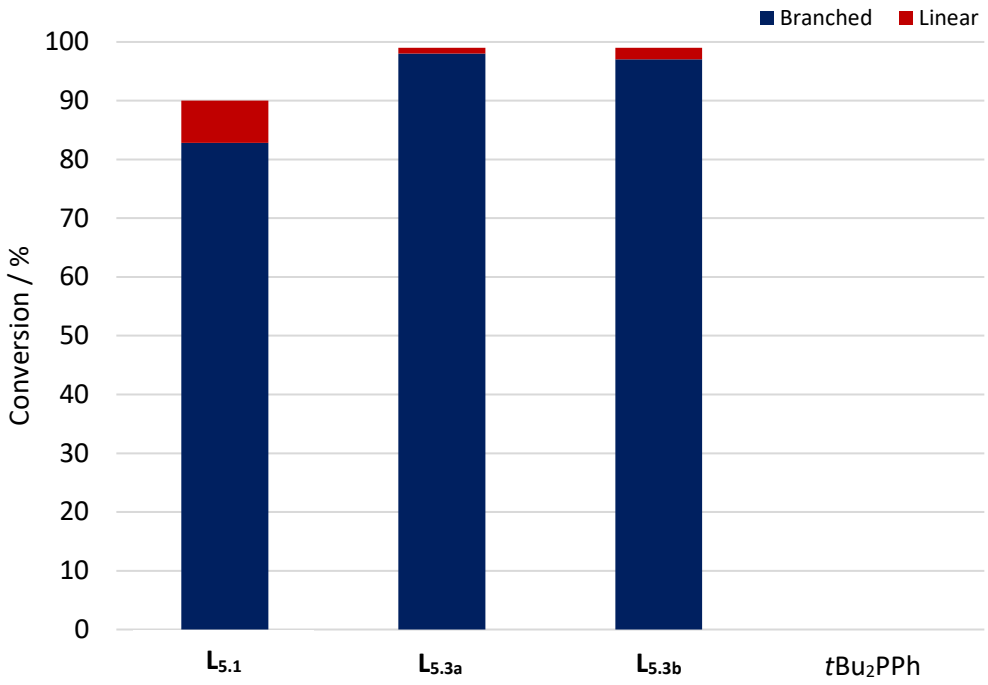


**Figure 5.13** Methoxycarbonylation of 3,3-dimethylbutyne. Conversion at 1 h.

The catalyst derived from the *t*Bu$_2$P ligand **L$_{5.3a}$** displayed excellent conversion and branched selectivity within 1 h (Entry 2, Table 5.7). The substituted analogue **L$_{5.3b}$** displayed similar results to **L$_{5.3a}$**, suggesting Me-substitution of the pyridyl ring has little effect on the catalytic performance. Similar effects were observed when using phenylacetylene as the substrate (Section 5.4.1). Relative to **L$_{5.3a}$**, the Ph$_2$P analogue **L$_{5.1}$** displayed low selectivity towards the branched product (90 vs. 99%, Entry 1 vs. 2). No conversion was observed when using *t*Bu$_2$PPh, suggesting once again that the 2-pyridyl ring in **L$_{5.3a}$** is critical to its excellent catalytic performance.

## 5.6 Platinum(II) coordination of R$_2$P(2-Py) ligands

To investigate the significant difference in catalytic activities observed between the *t*Bu$_2$P derived ligand **L$_{5.3a}$** and the Cy$_2$P analogue **L$_{5.4}$** (Section 5.4), their Pt(II) coordination chemistry was studied. The product of the reaction between [PtCl$_2$(cod)] and ligand was dependent of the amount of ligand used; the reaction using 1 equiv. of ligand will be discussed first. The ability of the ligands to display P-monodentate and P,N-bidentate coordination will be discussed. The reactivity of ligands **L$_{5.3a}$** and **L$_{5.4}$** will be compared to the Ph$_2$P analogue **L$_{5.1}$**.

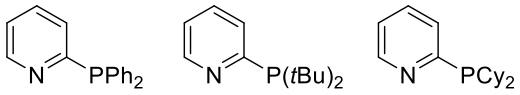


$\mathbf{L_{5.1}}$ $\mathbf{L_{5.3a}}$ $\mathbf{L_{5.4}}$

The reaction of 1 equiv. of the *t*Bu$_2$P ligand $\mathbf{L_{5.3a}}$ with [PtCl$_2$(cod)] (cod = 1,5-cyclooctadiene) in $CH_2Cl_2$ gave a 1:1 mixture of [PtCl$_2$($\kappa_2$-$\mathbf{L_{5.3a}}$)] (**5.19a**) and *trans*-[PtCl($\kappa_2$-$\mathbf{L_{5.3a}}$)($\kappa_1$-$\mathbf{L_{5.3a}}$)][Cl] (*trans*-**5.20a**) (Scheme 5.23). The $^{31}P\{^1H\}$ NMR spectrum of *trans*-**5.20a** gave two doublets at 39.5 ppm ($^2J_{P,P}$ = 363 Hz, $^1J_{P,Pt}$ = 2565 Hz) and -18.1 ppm ($^2J_{P,P}$ = 363 Hz, $^1J_{P,Pt}$ = 1916 Hz). The upfield signal at -18.1 ppm, assigned to the P,N-chelate, is characteristic of a 4-membered chelate.[35,54,58–60] The large $^2J_{P,P}$ and small $^1J_{P,Pt}$ values of *trans*-**5.20a** are consistent with a *trans* phosphine geometry.[61,70] In contrast, the reaction of 1 equiv. of the Cy$_2$P ligand $\mathbf{L_{5.4}}$ with [PtCl$_2$(cod)] in $CH_2Cl_2$ gave a 1:1 mixture of *trans*-[PtCl$_2$($\mathbf{L_{5.4}}$)$_2$] (*trans*-**5.21b**) and the remaining [PtCl$_2$(cod)] (Scheme 5.23). The $^{31}P\{^1H\}$ NMR spectrum of *trans*-**5.21b** gave a singlet with a $^1J_{P,Pt}$ value *ca.* 2500 Hz, indicative of a *trans* geometry.

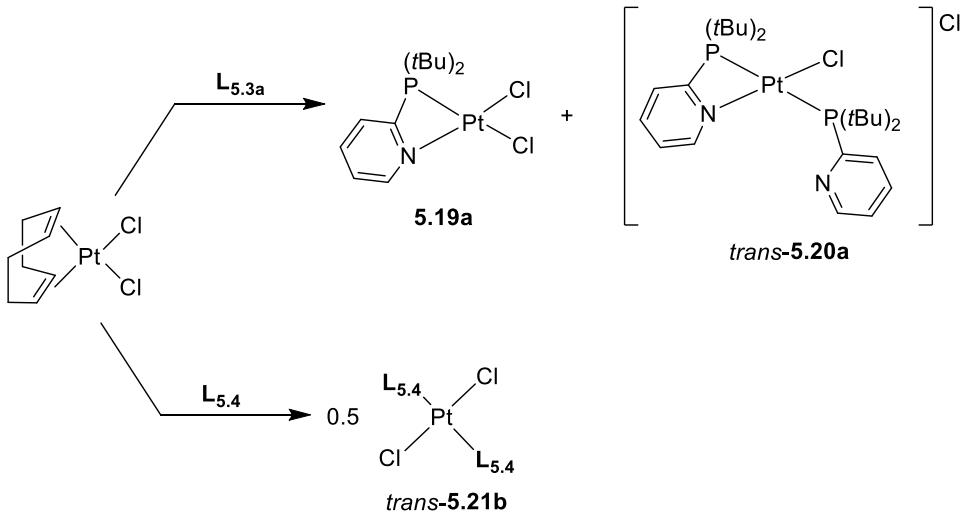


**Scheme 5.23** Reaction of [PtCl$_2$(cod)] with 1 equiv. $\mathbf{L_{5.3a\text{-}5.4}}$.

This difference in coordination behaviour has been attributed to the steric bulk of $\mathbf{L_{5.3a}}$ and $\mathbf{L_{5.4}}$. It has been shown that chelation of phosphines (including cyclometallation) can be promoted and stabilised by increasing the steric hindrance around the P-donor.[71–74] In particular, significant effects were shown when using *t*Bu geminal substituents, also known as the "*gem*-di-*tert*-butyl-effect".[73,74] Accordingly, P,N-chelation is favoured above when using the more sterically encumbered *t*Bu$_2$P ligand $\mathbf{L_{5.3a}}$, relative to when using the

$Cy_2P$ analogue $\mathbf{L_{5.4}}$. This may explain the low catalytic activity observed when using the $Cy_2P$ ligand $\mathbf{L_{5.4}}$ discussed earlier.

Crystals of **5.19a** suitable for X-ray crystallography were grown by slow diffusion of hexane into a saturated $CH_2Cl_2$ solution of **5.19a** and *trans*-**5.20a** (Figure 5.14). The crystal structure of **5.19a** confirmed the formation of the P,N-chelate and showed a distorted square planar geometry around the Pt centre. There is a significant degree of ring strain as shown by the acute P,N-chelate bite angle of 70.88(12)°, similar to that of $\mathbf{L_{5.3a}}$ in the analogous [$PtMe_2(\kappa_2$-$\mathbf{L_{5.3a}}$)] complex (70.0(2)°).[71]

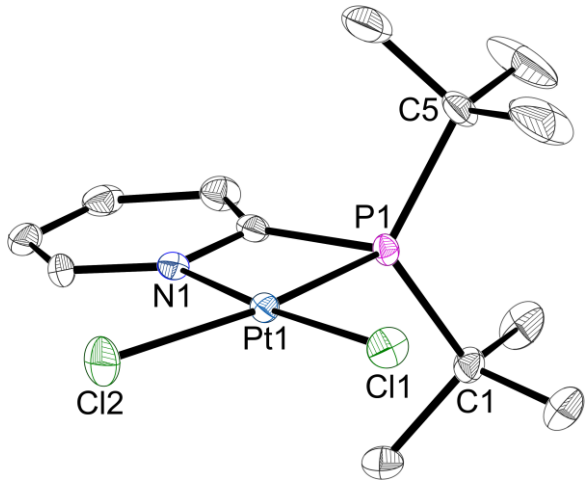


**Figure 5.14** Crystal structure of **5.19a**. The hydrogen atoms are omitted for clarity. Thermal ellipsoids at 50% probability. Selected bond lengths (Å) and angles (°): Pt1-P1 2.2325(13), Pt1-N1 2.019(4), Pt1-Cl1 2.2984(12), Pt1-Cl2 2.3524(12), P1-C1 1.864(5), P1-C5 1.860(5), P1-Pt1-N1 70.88(12), Cl1-Pt1-Cl2 92.05(5). See Appendix for experimental details.

However, when [$PtCl_2$(cod)] was treated with 2 equiv. of ligand, different products were observed. The reaction of 2 equiv. of $\mathbf{L_{5.3a}}$ and $\mathbf{L_{5.4}}$ with [$PtCl_2$(cod)] (cod = 1,5-cyclooctadiene) in $CH_2Cl_2$ gave predominantly complexes **5.20a**-**b** (Scheme 5.24). The $^{31}P\{^1H\}$ NMR spectrum of *trans*-**5.20a** was the same as above; free ligand $\mathbf{L_{5.3a}}$ and *trans*-**5.21a** were also present (*ca.* 25%) (see Chapter 7 for more details). The $^{31}P\{^1H\}$ NMR spectrum of *cis*-**5.20b** gave two doublets at 21.5 ppm ($^2J_{P,P}$ = 7 Hz, $^1J_{P,Pt}$ = 3601 Hz) and -22.8 ppm ($^2J_{P,P}$ = 7 Hz, $^1J_{P,Pt}$ = 3110 Hz). The small $^2J_{P,P}$ and large $^1J_{P,Pt}$ values are consistent with a *cis* geometry.[61,70] The difference in the geometry of the products from the *t*$Bu_2P$ ligand $\mathbf{L_{5.3a}}$ and $Cy_2P$ ligand $\mathbf{L_{5.4}}$ can be associated with the greater steric bulk of the *t*$Bu_2P$ moiety, forcing isomerisation at the Pt centre, favouring a *trans* phosphine geometry. In

contrast to ligands $\mathbf{L_{5.3a}}$ and $\mathbf{L_{5.4}}$, the reaction of 2 equiv. of the $Ph_2P$ ligand $\mathbf{L_{5.1}}$ with $[PtCl_2(cod)]$ gave the *cis*-$[PtCl_2(\mathbf{L_{5.1}})_2]$ complex.[50,54] P,N-chelation of $\mathbf{L_{5.3a}}$ and $\mathbf{L_{5.4}}$ may be promoted by the stronger donor properties of the ligands, relative to $\mathbf{L_{5.1}}$.

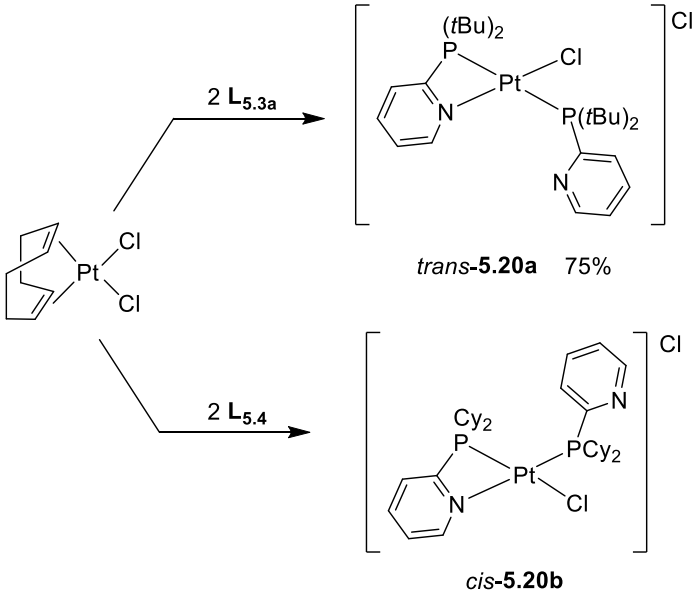


**Scheme 5.24** Reaction of $[PtCl_2(cod)]$ with 2 equiv. $\mathbf{L_{5.3a}}$ and $\mathbf{L_{5.4}}$.

## 5.7 Palladium(II) coordination of $R_2P$(2-Py) ligands

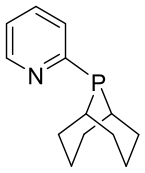


$\mathbf{L_{5.5}}$

To further investigate the reactivity of ligands $\mathbf{L_{5.3\text{-}5.5}}$, their Pd(II) coordination was explored. Similar to their Pt(II) coordination chemistry above, the resulting product mixture was dependent of the amount of ligand used. The reaction of 1 equiv. of the $tBu_2P$ ligand $\mathbf{L_{5.3a}}$ with $[PdCl_2(NCPh)_2]$ in $CH_2Cl_2$ gave $[PdCl_2(\kappa_2\text{-}\mathbf{L_{5.3a}})]$ (**5.22a**) as the sole product (Scheme 5.25). The upfield $^{31}P\{^1H\}$ NMR signal ($\delta_P$ = -11.3 ppm) for **5.22a** is characteristic of a four-membered P,N-chelate ring.[59]

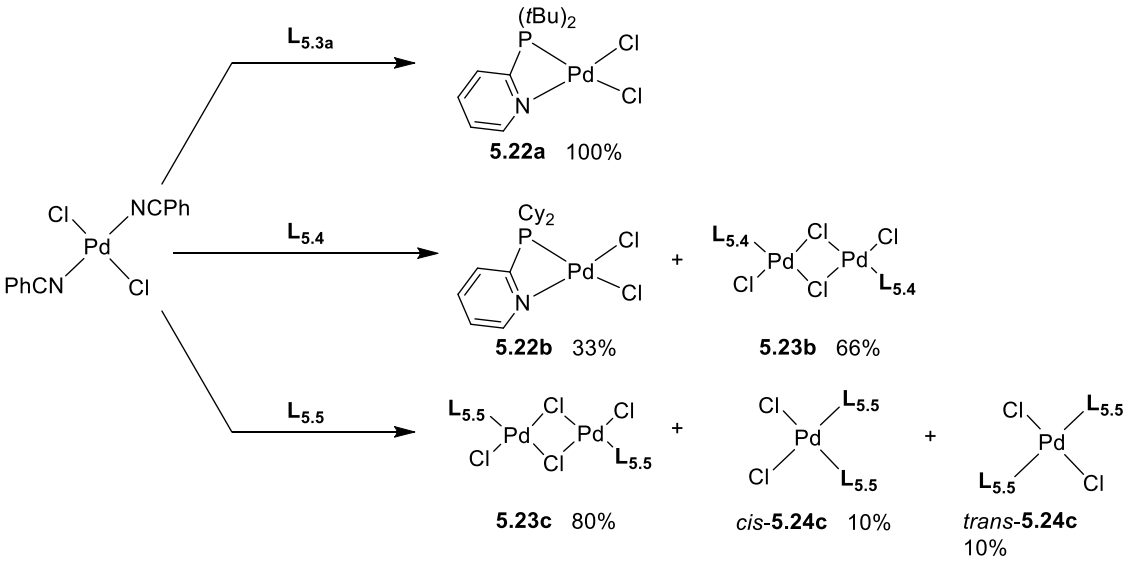


**Scheme 5.25** Reaction of $[PdCl_2(NCPh)_2]$ with 1 equiv. $\mathbf{L_{5.3\text{-}5.5}}$.

The analogous reaction using the $Cy_2P$ ligand $\mathbf{L_{5.4}}$ gave a 1:2 mixture of $[PdCl_2(\kappa_2\text{-}\mathbf{L_{5.4}})]$ (**5.22b**) and $[Pd_2Cl_4(\mathbf{L_{5.4}})_2]$ (**5.23b**) (Scheme 5.25). Mass spectrometry supported the presence of the binuclear species, **5.23b**. As above, the $^{31}P\{^1H\}$ NMR signal of **5.22b** showed a characteristic upfield shift ($\delta_P$ = -30.2 ppm). The reaction of 1 equiv. of the $Ph_2P$ analogue $\mathbf{L_{5.1}}$ with $[PdCl_2(NCPh)_2]$ gave a mixture of $[PdCl_2(\kappa^2\text{-}\mathbf{L_{5.1}})]$, *cis*-$[PdCl_2(\mathbf{L_{5.1}})_2]$ and *trans*-$[PdCl_2(\mathbf{L_{5.1}})_2]$ complexes.[59] Ligands $\mathbf{L_{5.1}}$, $\mathbf{L_{5.3a}}$ and $\mathbf{L_{5.4}}$ all exhibit P,N-chelation in the above reactions. The strongest preference for P,N-chelation occurs upon reaction with the $t$Bu$_2$P ligand $\mathbf{L_{5.3a}}$, which is attributed to the high steric bulk of the $t$Bu$_2$P moiety and "*gem*-di-*tert*-butyl-effects".[71,74] There is no evidence of P,N-chelation upon reaction of $[PdCl_2(NCPh)_2]$ with the *s*-PhobP analogue $\mathbf{L_{5.5}}$; the $^{31}P\{^1H\}$ NMR spectrum showed only the presence of the binuclear species $[Pd_2Cl_4(\mathbf{L_{5.5}})_2]$ (**5.23c**, *ca.* 80%) and *cis*- and *trans*-$[PdCl_2(\mathbf{L_{5.5}})_2]$ (**5.24c**) (Scheme 5.25). Mass spectrometry confirmed the presence of these species (see Chapter 7). The reason for this observed difference in reactivity is unknown.

Crystals of **5.22a** suitable for X-ray crystallography were grown by slow diffusion of hexane into a saturated $CH_2Cl_2$ solution of the complex (Figure 5.15). The crystal structure confirmed the formation of the P,N-chelate. The acute P,N-chelate bite angle of 70.78(3)° indicates a considerable degree of ring strain is present, similar to that of its Pt analogue (Figure 5.14). The $Ph_2P$ ligand $\mathbf{L_{5.1}}$ also shows a similar degree of ring strain in the previously reported *cis*-$[PdCl(\kappa_2\text{-}\mathbf{L_{5.1}})(\kappa_1\text{-}\mathbf{L_{5.1}})][BF_4]$ complex.[59]

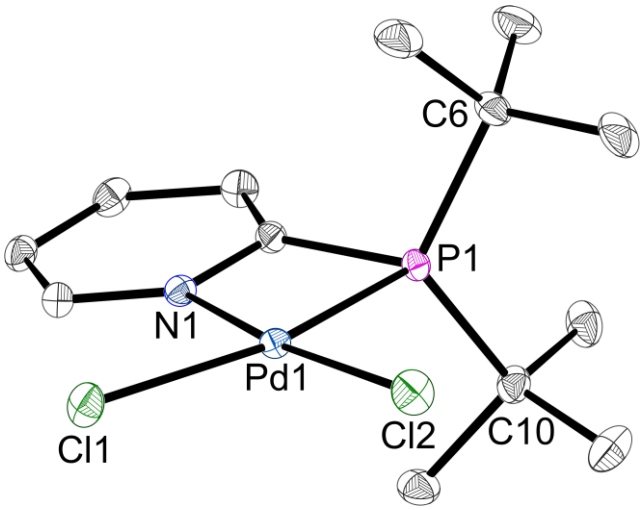


**Figure 5.15** Crystal structure of **5.22a**. The hydrogen atoms are omitted for clarity. Thermal ellipsoids at 50% probability. Selected bond lengths (Å) and angles (°): Pd1-P1 2.2341(4), Pd1-N1 2.0186(12), Pd1-Cl1 2.3548(4), Pd1-Cl2 2.2904(4), P1-C6 1.8556(14), P1-C10 1.8568(15), P1-Pd1-N1 70.78(3), Cl1-Pd1-Cl2 95.847(14). See Appendix for experimental details.

When $[PdCl_2(NCPh)_2]$ was treated with 2 equiv. of ligand, different reactivity was observed. Upon the reaction of 2 equiv. of the *t*Bu$_2$P ligand **L$_{5.3a}$** with $[PdCl_2(NCPh)_2]$ in $CH_2Cl_2$, an equilibrium between *trans*-$[PdCl_2(\mathbf{L_{5.3a}})_2]$ (*trans*-**5.24a**), $[PdCl_2(\kappa^2\text{-}\mathbf{L_{5.3a}})]$ (**5.22a**) and free ligand **L$_{5.3a}$** was observed (Scheme 5.26). This equilibrium was confirmed since the addition of **L$_{5.3a}$** (1 equiv.) to the reaction mixture resulted in an increase of *trans*-**5.24a** as the equilibrium is shifted to the left. The reaction using the Cy$_2$P analogue **L$_{5.4}$** gave a 3:1 mixture of *trans*-$[PdCl_2(\mathbf{L_{5.4}})_2]$ (*trans*-**5.24b**) and $[Pd_2Cl_4(\mathbf{L_{5.4}})_2]$ (**5.23b**) respectively (Scheme 5.26). The presence of the binuclear complex, **5.23b**, was confirmed by mass spectrometry. Whereas, the reaction using the *s*-PhobP ligand **L$_{5.5}$** gave a 9:1 mixture of *cis*- and *trans*-$[PdCl_2(\mathbf{L_{5.5}})_2]$ (**5.24c**) (Scheme 5.26). Even though it has been shown that CgP and PhobP are sterically similar,[75] the analogous reaction using CgP(2-Py) gave only the *trans* isomer, *trans*-$[PdCl_2(CgP(2\text{-}Py))_2]$.[35] Similar behaviour to **L$_{5.5}$** has been reported when using the Ph$_2$P ligand **L$_{5.1}$**; the reaction of 2 equiv. of **L$_{5.1}$** with $[PdCl_2(cod)]$ gave a mixture of the *cis*- and *trans*-$[PdCl_2(\mathbf{L_{5.1}})_2]$ complexes.[59]

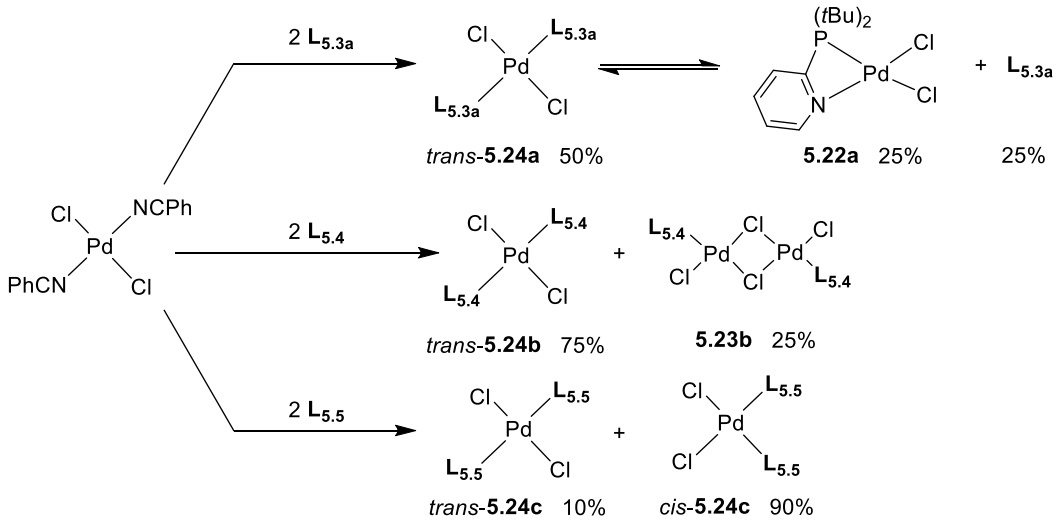


**Scheme 5.26** Reaction of $[PdCl_2(NCPh)_2]$ with 2 equiv. $\mathbf{L_{5.3\text{-}5.5}}$.

In summary, it is clear that the *t*$Bu_2$P ligand $\mathbf{L_{5.3a}}$ displays the strongest preference for P,N-chelation to Pt and Pd compared to the other ligands, and hence may readily form a P,N-chelate during catalysis.

Crystals of *trans*-**5.24a** suitable for X-ray crystallography were grown by slow diffusion of hexane into a saturated $CH_2Cl_2$ solution of *trans*-**5.24a**, **5.22a** and $\mathbf{L_{5.3a}}$ (Figure 5.16). The crystal structure confirmed the *trans* geometry of the ligands around the Pd centre, in a square planar arrangement. The Pd-P bond length in the analogous *trans*-$[PdCl_2(\mathbf{L_{5.1}})_2]$ complex is shorter than that in *trans*-**5.24a** (2.3125(4) vs. 2.3784(4) Å).[59] This may be attributed to the higher steric bulk of the *t*BuP ligand $\mathbf{L_{5.3a}}$ relative to the $Ph_2P$ ligand $\mathbf{L_{5.1}}$.

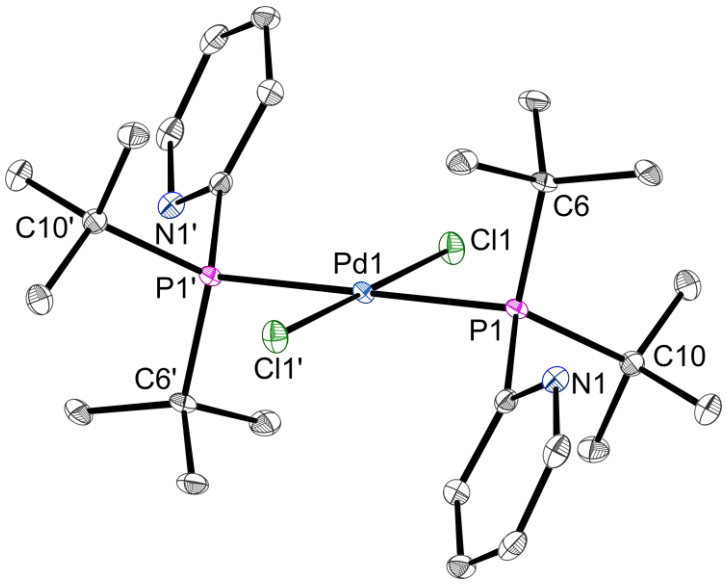


**Figure 5.16** Crystal structure of *trans*-**5.24a**. The hydrogen atoms are omitted for clarity. Thermal ellipsoids at 50% probability. Atoms suffixed with a dash (') are related by symmetry operation (-x, -y, -z). Selected bond lengths (Å) and angles (°): Pd-P1 2.3784(4), Pd1-Cl1 2.3082(4), Pd1-C1 1.9025(17), Pd1-C5 1.8816(16), P1-Pd1-P1 180.000, Cl1-Pd1-Cl1 180.000, P1-Pd1-Cl1 91.194(14). See Appendix for experimental details.

Crystals of *cis*-**5.24c** suitable for X-ray crystallography were grown by slow diffusion of hexane into a saturated $CH_2Cl_2$ solution of *cis*- and *trans*-**5.24c** (Figure 5.17). The crystal structure confirmed the *cis* geometry of ligands around the Pd centre, in a distorted square planar arrangement. Coordinated PhobPR ligands are known to have high rigidity,[76] which may explain the tetrahedral distortion of *cis*-**5.24c** (Cl-Pd-P ≈ 170°) (Figure 5.17). The phobane substituents of $\mathbf{L_{5.5}}$ adopt an *anti*-conformation in *cis*-**5.24c**. The pyridine rings of $\mathbf{L_{5.5}}$ are twisted towards the Pd centre, suggesting there may be some interaction between the pyridyl-N and the Pd; similar effects were observed in the previously reported crystal structure of *trans*-**5.24c** (synthesised by a similar method).[67] The Pd-P bond length is *ca.* 0.04 Å longer in the previously synthesised *trans*-**5.24c**[67] than in *cis*-**5.24c**, which can be attributed to the high *trans*-influence of $PR_3$ ligands relative to $Cl^-$.

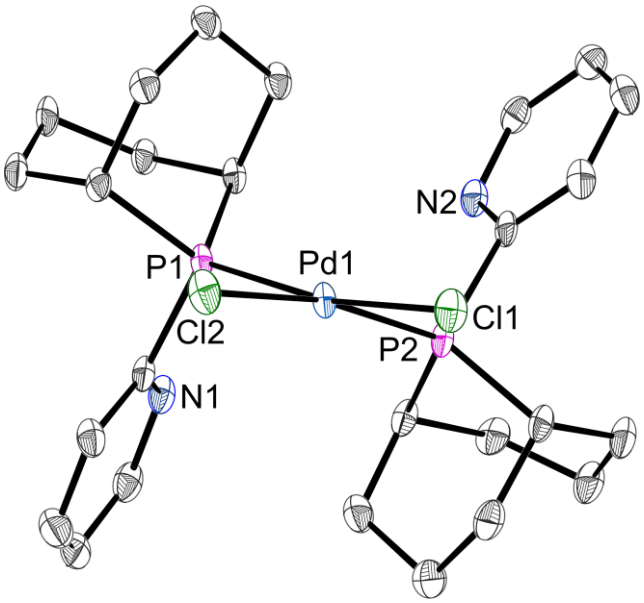


**Figure 5.17** Crystal structure of *cis*-**5.24c**. The hydrogen atoms and disordered solvent molecule are omitted for clarity. Thermal ellipsoids at 50% probability. Selected bond lengths (Å) and angles (°): Pd1-P1 2.2755(10), Pd1-P2 2.2719(9), Pd1-Cl1 2.3631(9), Pd1-Cl2 2.3543(9), Cl1-Pd1-Cl2 88.316(3), P1-Pd1-P2 95.52(3), P1-Pd1-Cl1 169.96(4), P2-Pd1-Cl2 169.15(4). See Appendix for experimental details.

### 5.7.1 Formation of P,N-chelate

In the above Pd(II) coordination studies, the *s*-PhobP derived ligand $\mathbf{L_{5.5}}$ did not display any $\kappa^2$-(P,N) coordination. To probe if such P,N-chelation was possible 1 equiv. of $AgBF_4$ was added to *cis*/*trans*-**5.24c** in $CH_2Cl_2$, and the chloride abstraction from **5.24c** led to a solution of $[PdCl(\kappa^2\text{-}\mathbf{L_{5.5}})(\kappa^1\text{-}\mathbf{L_{5.5}})][BF_4]$ (*cis*-**5.25c**$[BF_4]$) and a white precipitate of AgCl (Scheme 5.27).

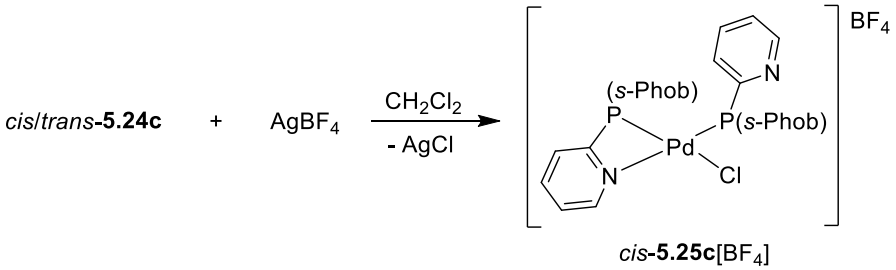


**Scheme 5.27** Synthesis of *cis*-**5.25c**$[BF_4]$.

The *in situ* $^{31}P\{^1H\}$ NMR spectrum of *cis*-**5.25c**$[BF_4]$ gave two doublets at 29.2 ppm ($^2J_{P,P}$ = 9 Hz) and -36.1 ppm ($^2J_{P,P}$ = 9 Hz). The small $^2J_{P,P}$ value is consistent with a *cis* geometry.[61] The characteristic upfield shift at -36.1 ppm was assigned to the P,N-chelate.[35,54,58–60] This coordination behaviour demonstrates the ability of $\mathbf{L_{5.5}}$ to exhibit both P-monodentate and P,N-bidentate behaviour, even though it is not as readily

observed as with ligands $\mathbf{L_{5.3\text{-}5.4}}$. Analogous behaviour to $\mathbf{L_{5.5}}$ has been reported using the $Ph_2P$ analogue $\mathbf{L_{5.1}}$ and CgP(2-Py); however, both of these comparator complexes displayed fluxionality at ambient temperature.[35,59]

## 5.8 Rhodium(I) coordination of $R_2P$(2-Py) ligands

Complexes of the type *trans*-[RhCl(CO)$L_2$] were targeted as a way to compare the electronic properties of $\mathbf{L_{5.3\text{-}5.5}}$ from their IR spectra. Reaction of 4 equiv. of $\mathbf{L_{5.3\text{-}5.5}}$ with [$Rh_2Cl_2(CO)_4$] in $CH_2Cl_2$ gave the *trans*-[RhCl(CO)$L_2$] complexes (**5.26a**-**c**), where L = $\mathbf{L_{5.3\text{-}5.5}}$ (Scheme 5.28).

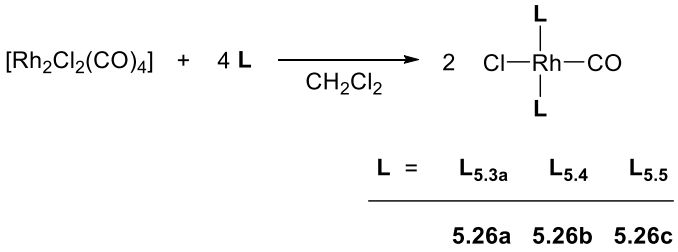


**Scheme 5.28** Synthesis of *trans*-[RhCl(CO)$L_2$] complexes **5.26a**-**c**.

The $^{31}P\{^1H\}$ NMR spectra of the $Cy_2P$ and PhobP complexes **5.26b**-**c** showed a doublet with a $^1J_{P,Rh}$ value of *ca.* 120 Hz, consistent with a *trans* geometry, similar to that of the $Ph_2P$ ligand $\mathbf{L_{5.1}}$ in *trans*-[RhCl(CO)($\mathbf{L_{5.1}}$)$_2$].[62] The $^{31}P\{^1H\}$ NMR spectrum of the reaction with the *t*$Bu_2P$ ligand $\mathbf{L_{5.3a}}$ at ambient temperature showed a sharp signal at 39.5 ppm (assigned to free ligand, $\mathbf{L_{5.3a}}$) and two broad signals at 60.3 ppm ($w_{1/2} \approx 260$ Hz) and 43.3 ppm ($w_{1/2} \approx 310$ Hz) in a 3:1 ratio (Scheme 5.29). Upon cooling the solution to -90 °C, the signal at 43.3 ppm resolved into a broad doublet of doublets at 66.5 ppm ($^2J_{P,P}$ = 242 Hz, $^1J_{P,Rh}$ = 128 Hz) and a broad doublet at 16.7 ppm ($^2J_{P,P}$ = 226 Hz) (Figure 5.18). Based on this, the mixture was tentatively assigned to complexes **5.26a** and **5.26a'** (Scheme 5.29). The upfield signal at 16.7 ppm was assigned to the 4-membered P,N-chelate of **5.26a'** and the signal at 66.5 ppm to the monodentate-P of **5.26a'**. The large $^2J_{P,P}$ values are consistent with a *trans* geometry.[77] Both signals remain broad at low temperature (-90 °C) due to exchange between P-monodentate and P,N-bidentate coordination modes occurring on the NMR timescale. In addition, upon cooling the solution the signal for complex **5.26a** ($\delta_P$ = 60.3 ppm at 25 °C) diminished, as the equilibrium shown in Scheme 5.29 shifted towards complex **5.26a'**. Similar to the Pd(II) and Pt(II) coordination above, the steric bulk of the *t*$Bu_2P$ ligand $\mathbf{L_{5.3a}}$ promotes P,N-chelation.

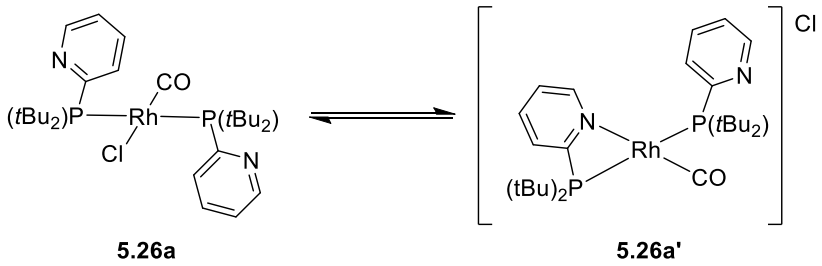


**5.26a** **5.26a'**

**Scheme 5.29** Observed equilibrium between **5.26a** and **5.26a'**.

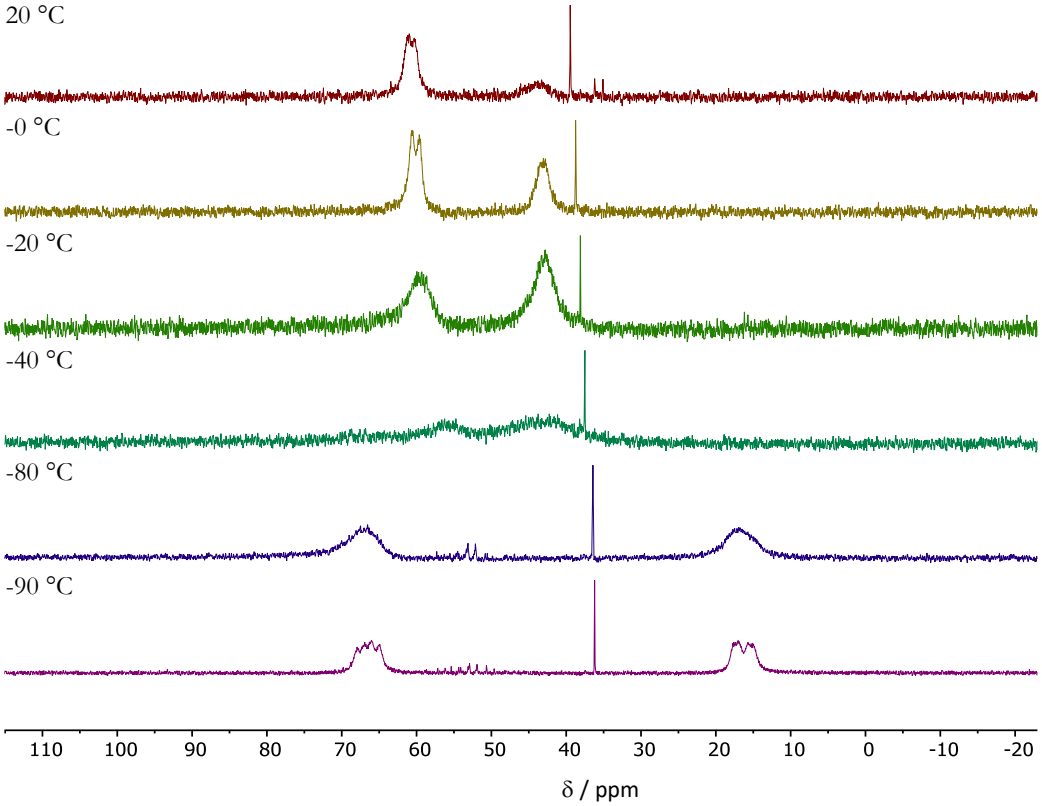


**Figure 5.18** Low temperature $^{31}P\{^{1}H\}$ NMR spectra of the equilibrium between complexes **5.26a** and **5.26a'**.

The IR data for complexes **5.26a**-**c** is given in Table 5.8. The data suggests that ligands $\mathbf{L}_{5.3\text{-}5.5}$ are weaker π-acceptors/ stronger σ-donors than the $Ph_2P$ and CgP analogues.[50,63] The trend in ν(CO) ($A_1$) values suggests the π-acceptor capacity increases in the order CgP(2-Py) > $\mathbf{L}_{5.1}$ > $\mathbf{L}_{5.5}$ > $\mathbf{L}_{5.4}$ > $\mathbf{L}_{5.3a}$, which is consistent with the electronegativity of the $R_2P$ moieties increasing in the order CgP > $Ph_2P$ > PhobP > $Cy_2P$ > $t$Bu$_2$P. The opposite trend in σ-donor ability can also be suggested.

**Table 5.8** IR data for *trans*-[RhCl(CO)$L_2$] complexes **5.26a**-**c**.

| Ligand | Complex | ν(CO) ($A_1$)[a] / cm$^{-1}$ |
|---|---|---|
| $\mathbf{L_{5.3a}}$ | **5.26a** | 1956 |
| $\mathbf{L_{5.4}}$ | **5.26b** | 1961 |
| $\mathbf{L_{5.5}}$ | **5.26c** | 1969 |
| $\mathbf{L_{5.1}}$[63] | - | 1975[b] |
| CgP(2-Py)[50] | - | 1988 |

[a] Measured in $CH_2Cl_2$. [b] As a KBr disc.

## 5.9 Protonation studies of the *t*$Bu_2$P(2-Py) ligand

An important factor contributing to the success of 2-pyridylphosphine ligands in methoxycarbonylation catalysis is their ability to act as a "proton messenger" (Section 5.1.3).[12,13,46,49,51] Since the catalytic performance of the *t*$Bu_2$P ligand $\mathbf{L_{5.3a}}$ rivalled that of the $Ph_2$P analogue $\mathbf{L_{5.1}}$ in the methoxycarbonylation of phenylacetylene (Section 5.4), its ability to be protonated was investigated. Accordingly, 1 equiv. of TsOH.$H_2O$ was added to the equilibrium mixture of *trans*-[$PdCl_2$($\mathbf{L_{5.3a}}$)$_2$] (*trans*-**5.24a**), [$PdCl_2$($\kappa^2$-$\mathbf{L_{5.3a}}$)] (**5.22a**) and free ligand $\mathbf{L_{5.3a}}$ in $CH_2Cl_2$ (Scheme 5.30).

The resulting $^{31}P\{^1H\}$ NMR spectrum gave a broad singlet at 32.0 ppm (40%, $w_{1/2} \approx 70$ Hz) and a relatively sharp singlet at -11.3 ppm (60%, $w_{1/2} \approx 7$ Hz) which were assigned to protonated ligand ($\mathbf{L_{5.3H}}^+$) and [$PdCl_2$($\kappa^2$-$\mathbf{L_{5.3a}}$)] (**5.22a**) respectively (Scheme 5.30). Upon the addition of acid, we postulate ligand $\mathbf{L_{5.3a}}$ in *trans*-**5.24a** becomes protonated at the pyridyl nitrogen and dissociates from the Pd centre, leaving a vacant site available for P,N-chelation, hence giving rise to an increase in **5.22a** and the generation of $\mathbf{L_{5.3H}}^+$ (Scheme 5.30).

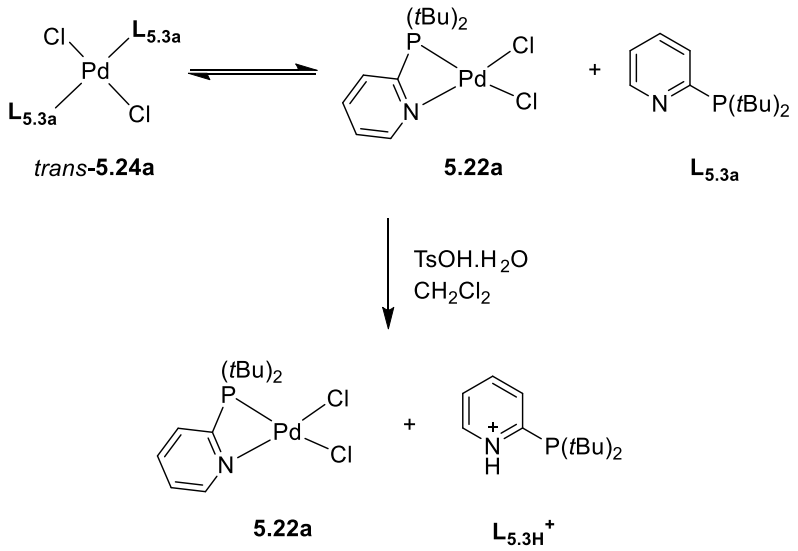


**Scheme 5.30** Protonation studies of $\mathbf{L_{5.3a}}$ in $CH_2Cl_2$.

Upon cooling the solution to -80 °C the signal at 32.0 ppm sharpened slightly ($w_{1/2} \approx 40$ Hz) and a new signal was observed at 54.4 ppm which was assigned to *trans*-**5.24a** (Figure 5.19). The signal for $\mathbf{L_{5.3H}}^+$ remained broad due to the pyridyl N-H exchanging. As the solution is cooled the equilibrium shown in Scheme 5.31, which is assumed to exist at ambient temperature, was shifted to the left. Due to the unreliably of $^{31}$P NMR integration,[78] the shift to the *trans*-**5.24a** complex was not reflected in the corresponding integrals. This experiment shows that the *t*Bu$_2$P ligand $\mathbf{L_{5.3a}}$ can be readily protonated.

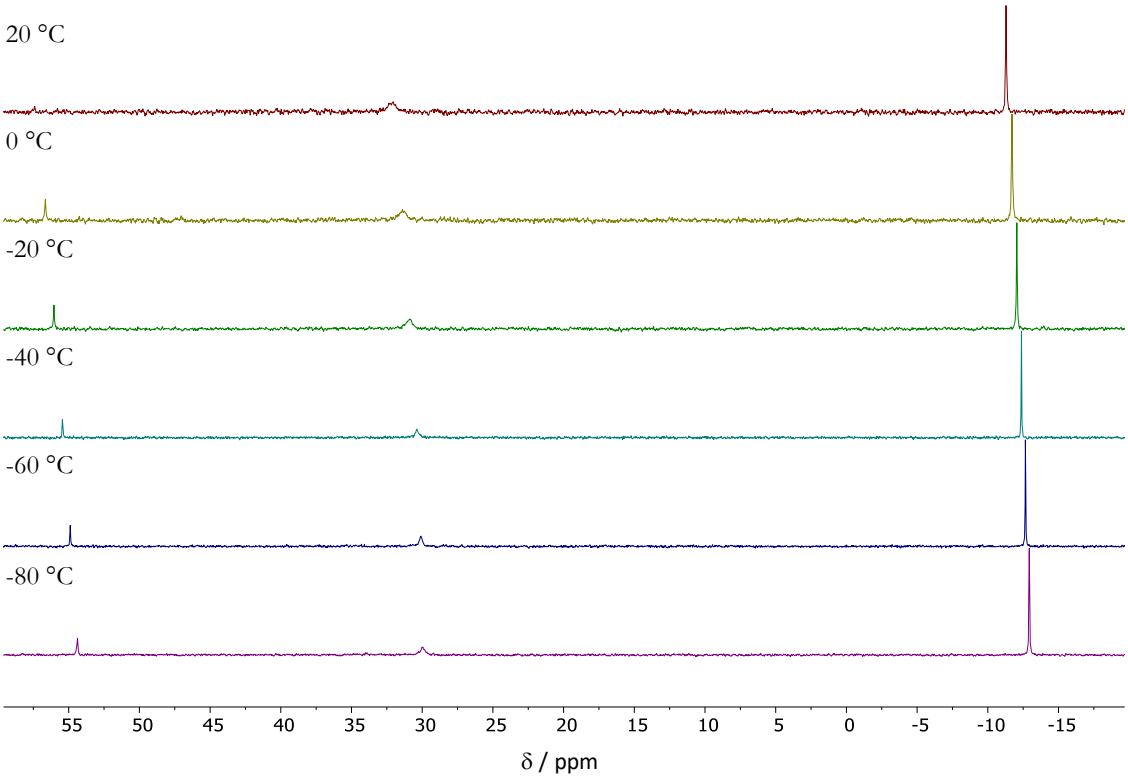


**Figure 5.19** Low temperature $^{31}P\{^{1}H\}$ NMR spectra of the protonation studies of **$L_{5.3a}$** in $CH_2Cl_2$.

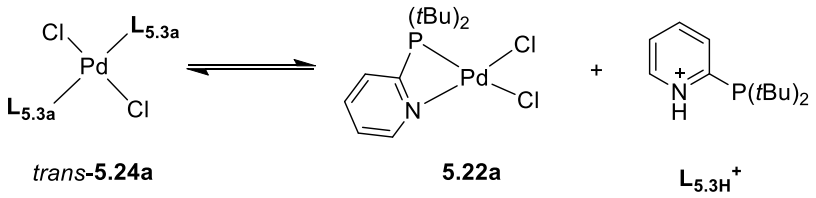


**Scheme 5.31** Equilibrium that exists upon protonation of Pd-**$L_{5.3a}$** species.

## 5.10 Conclusions

Bühl *et al.* recently proposed a revised mechanism for methoxycarbonylation catalysis, which involved highly reactive acryloyl and ketene type intermediates (Section 5.1.3).[51] It was predicted that a rate enhancement would be observed when the 6-chloropyridyl phosphine **L5.2** was used as the supporting ligand (*cf.* $Ph_2P$(2-Py), **L5.1**). Herein, it has been demonstrated that ligand **L5.2** did indeed produce a more active catalyst for the methoxycarbonylation of phenylacetylene, relative to **L5.1**.

The Pt(II) and Pd(II) coordination chemistry of **L5.2** has been investigated. The ability of **L5.2** to form a P,N-chelate was only observed upon the addition of $AgBF_4$ to the $[MCl_2(\mathbf{L5.2})_2]$ complexes (where M = Pt or Pd); analogous behaviour has been observed when using $Ph_2P$(2-Py) (**L5.1**).[59] Both $\kappa^1$- and $\kappa^2$-coordination modes of ligand **L5.2** have been observed, which is widely reported to be key to the success of 2-pyridyl phosphines in methoxycarbonylation catalysis.[12,13]

The effect of the pyridyl group in $Ph_2P$(Py) on catalytic methoxycarbonylation catalysis has been extensively studied,[12,13,35] but there are limited reports using alkyl pyridyl phosphines ($R_2P$(2-Py)).[35,44,79] Consequently, a series of alkyl pyridyl phosphines, **L5.3a**, **L5.4** and **L5.5**, has been synthesised and tested in the catalytic methoxycarbonylation of phenylacetylene. The alkyl substituent had a significant effect on catalysis: the catalysts derived from the $Cy_2P$ and PhobP ligands, **L5.4** and **L5.5** respectively, displayed poor catalyst performance. However, the *t*$Bu_2P$ ligand **L5.3a** gave a highly active and selective catalyst, rivalling the performance of the catalyst derived from the $Ph_2P$ ligand **L5.1**.

To probe the effect of substitution at the 6-position of the *t*$Bu_2P$ ligand **L5.3a**, the 6-Me analogue **L5.3b** has been synthesised and tested in the catalytic methoxycarbonylation of phenylacetylene. Me-substitution at the 6-position of the pyridyl ring had little effect on catalyst performance (unlike the $Ph_2P$ analogue **L5.1**);[12,13] similar results were observed when using 3,3-dimethylbutyne as the substrate. The lack of activity observed when using the catalyst derived from *t*$Bu_2$PPh suggested the 2-pyridyl ring of *t*$Bu_2P$(2-Py) (**L5.3a**) is critical to its excellent catalyst performance. In the catalytic methoxycarbonylation of propyne, the catalyst derived from the *t*$Bu_2P$ ligand **L5.3a**, although less active, displayed comparable selectivity towards MMA as the $Ph_2P$ ligand **L5.1**.

Propadiene impurities in the propyne feed stream have been shown to lead to a loss in methoxycarbonylation activity when using the $Ph_2P$ ligand **L5.1**;[21] catalysts of the *t*$Bu_2P$

ligand **L**$_{5.3a}$ may tolerate higher levels of allene impurities in the propyne stream and this should be investigated in the future.

The Pt(II) and Pd(II) coordination chemistry of ligands **L**$_{5.3a}$, **L**$_{5.4}$ and **L**$_{5.5}$ has been investigated. The ability of the $Cy_2P$ and *t*$Bu_2P$ ligands (**L**$_{5.3a}$ and **L**$_{5.4}$) to demonstrate a $\kappa^2$-(P,N) coordination mode has been demonstrated in solution from the characteristic $^{31}P\{^1H\}$ NMR spectra, and in the solid state for the *t*$Bu_2P$ derived **L**$_{5.3a}$ from the crystal structures of the [$MCl_2(\kappa^2$-**L**$_{5.3a}$)] complexes (where M = Pt or Pd). The PhobP ligand **L**$_{5.5}$ only displayed P,N-chelation upon the addition of $AgBF_4$ to [$PdCl_2$(**L**$_{5.5}$)$_2$] (**5.24c**). The IR spectra for the *trans*-[$RhCl(CO)L_2$] complexes, where L = **L**$_{5.3\text{-}5.5}$, showed that the σ-donor ability of the ligands increased in the order **L**$_{5.3a}$ > **L**$_{5.4}$ > **L**$_{5.5}$, consistent with the electronegativity of the alkyl substituents. The *trans*-[RhCl(CO)(**L**$_{5.3a}$)$_2$] complex (**5.26a**) displayed exchange between $\kappa^1$-(P) and $\kappa^2$-(P,N) coordination modes.

In summary, all ligands **L**$_{5.3\text{-}5.5}$ displayed both P-monodentate and P,N-bidentate coordination modes; the *t*$Bu_2P$ ligand **L**$_{5.3a}$ exhibited the strongest preference for P,N-chelation to Pt, Pd and Rh, which was attributed to its high steric bulk relative to the other ligands. The ability of the *t*$Bu_2P$ ligand **L**$_{5.3a}$ to be protonated and its propensity for P,N-chelation may explain its superior catalyst performance. DFT calculations should be carried out in the future to investigate the mechanism of catalytic methoxycarbonylation using alkyl pyridyl phosphines, such as *t*$Bu_2P$(2-Py).

## 5.11 References


1 R. Stadler and W. Reppe, *US Patent*, 1953, US 3023237.

2 G. Kiss, *Chem. Rev.*, 2001, **101**, 3435–3456.

3 A. Brennführer, H. Neumann and M. Beller, *ChemCatChem*, 2009, **1**, 28–41.

4 P. Kalck and M. Urrutigoïty, *Inorganica Chim. Acta*, 2015, **431**, 110–121.

5 R. Chinchilla and C. Nájera, *Chem. Rev.*, 2014, **114**, 1783–1826.

6 M. Beller, J. Seayad, A. Tillack and H. Jiao, *Angew. Chemie Int. Ed.*, 2004, **43**, 3368–3398.

7 S. Doherty, J. G. Knight and M. Betham, *Chem. Commun.*, 2006, 88–90.

8 M. Beller, in *Topics in Organometallic Chemistry*, Springer, 2006, pp. 97–165.

9 B. Breit and L. Diab, in *Comprehensive Organic Synthesis*, ed. P. Knochel, Elsevier, 2014, pp. 995–1053.

10 J. B. Peng, F. P. Wu and X. F. Wu, *Chem. Rev.*, 2019, **119**, 2090–2127.

11 S. Quintero-Duque, K. M. Dyballa and I. Fleischer, *Tetrahedron Lett.*, 2015, **56**, 2634–2650.

12 E. Drent, P. Arnoldy and P. H. M. Budzelaar, *J. Organomet. Chem.*, 1993, **455**, 247–253.

13 E. Drent, P. Arnoldy and P. H. M. Budzelaar, *J. Organomet. Chem.*, 1994, **475**, 57–63.

14 E. Drent, W. W. Jager and J. J. Suykerbuyk, *World Patent*, 1995, WO 199505357.

15 E. Drent and D. H. L. Pello, *World Patent*, 1995, WO 199503269.

16 K. Nagai, *Appl. Catal. A Gen.*, 2001, **221**, 367–377.

17 B. Harris, *Ingenia*, 2010, 18–23.

18 W. Clegg, G. R. Eastham, M. R. J. Elsegood, R. P. Tooze, X. L. Wang and K. Whiston, *Chem. Commun.*, 1999, 1877–1878.

19 R. P. Tooze, G. R. Eatsham, K. Whiston and X. L. Wang, *World Patent*, 1996, WO 9619434.

20 D. J. Cole-Hamilton and E. Drent, *Applied Homogeneous Catalysis with Organometallic*

*Complexes*, Wiley-VCH: Weinheim, 2016.

21 A. Dervisi, P. G. Edwards, P. D. Newman, R. P. Tooze, S. J. Coles and M. B. Hursthouse, *J. Chem. Soc. Dalton Trans.*, 1999, 1113–1120.

22 M. Akao, S. Sugawara, K. Amino and Y. Inoue, *J. Mol. Catal. A Chem.*, 2000, **157**, 117–122.

23 Y. Sakurai, S. Sakaguchi and Y. Ishii, *Tetrahedron Lett.*, 1999, **40**, 1701–1704.

24 A. Viña and E. Murillo, *J. Braz. Chem. Soc*, 2003, **14**, 744–749.

25 A. Alberto, A. A. Nunez Magro, L.-M. Robb, P. J. Pogorzelec, A. M. Z. Slawin, G. R. Eastham and D. J. Cole-Hamilton, *Chem. Sci.*, 2010, **1**, 723–730.

26 M. K. Rong, F. Holtrop, J. C. Slootweg and K. Lammertsma, *Coord. Chem. Rev.*, 2019, **380**, 1–16.

27 P. Espinet and K. Soulantica, *Coord. Chem. Rev.*, 1999, **193–195**, 499–556.

28 W. Drent and W. W. Jager, *US Patent*, 1998, US 5719313.

29 E. Drent, P. H. M. Budzelaar and W. W. Jager, *US Patent*, 1992, US 509962.

30 K. Dong, R. Sang, X. Fang, R. Franke, A. Spannenberg, H. Neumann, R. Jackstell and M. Beller, *Angew. Chemie Int. Ed.*, 2017, **56**, 5267–5271.

31 K. Dong, X. Fang, S. Gülak, R. Franke, A. Spannenberg, H. Neumann, R. Jackstell and M. Beller, *Nat. Commun.*, 2017, **8**, 14117–14123.

32 K. Dong, R. Sang, Z. Wei, J. Liu, R. D. Uhren, A. Spannenberg, H. Jiao, H. Neumann, R. Jackstell, R. Franke and M. Beller, *Chem. Sci.* , 2018, **9**, 2510–2516.

33 R. Sang, J. Liu, K. Dong, R. Jackstell, M. Beller and R. Franke, *European Patent*, 2019, EP 3441384 A1.

34 J. J. M. de Pater, E. P. Maljaars, E. de Wolf, M. Lutz, A. L. Spek, B.-J. Deelman, C. J. Elsevier and van Koten, *Organometallics*, 2005, **24**, 5299–5310.

35 T. A. Shuttleworth, A. M. Miles-Hobbs, P. G. Pringle and H. A. Sparkes, *Dalton Trans.*, 2016, **46**, 125–137.

36 M. L. Clarke, D. J. Cole-Hamilton, D. F. Foster, A. M. Z. Slawin and J. D. Woollins, *J. Chem. Soc. Dalton Trans.*, 2002, 1618–1624.

37 A. Scrivanti, U. Matteoli, V. Beghetto, S. Antonaroli, R. Scarpelli and B. Crociani,

*J. Mol. Catal. A Chem.*, 2001, **170**, 51–56.

38 H. Qi, Z. Huang, M. Wang, P. Yang, C. Du, S. Chen and Y. Li, *J. Catal.*, 2018, **363**, 63–68.

39 D. Yang, L. Liu, D. L. Wang, Y. Lu, X. L. Zhao and Y. Liu, *J. Catal.*, 2019, **371**, 236–244.

40 M. T. Reetz, R. Demuth and R. Goddard, *Tetrahedron Lett.*, 1998, **39**, 7089–7092.

41 A. Scrivanti, V. Beghetto, M. Zanato and U. Matteoli, *J. Mol. Catal. A Chem.*, 2000, **160**, 331–336.

42 A. Scrivanti, V. Beghetto, E. Campagna and U. Matteoli, *J. Mol. Catal. A Chem.*, 2001, **168**, 75–80.

43 M. J. Green, K. J. Cavell, P. G. Edwards, R. P. Tooze, B. W. Skelton and A. H. White, *Dalton Trans.*, 2004, 3251–3260.

44 J. Liu, K. Dong, R. Franke, H. Neumann, R. Jackstell and M. Beller, *J. Am. Chem. Soc.*, 2018, **140**, 10282–10288.

45 D. J. Cole-Hamilton and E. Drent, in *Applied Homogeneous Catalysis with Organometallics Compounds*, eds. B. Cornils, W. A. Herrmann, M. Beller and R. Paciello, Wiley-VCH, 2017, pp. 118–145.

46 L. Crawford, D. J. Cole-Hamilton and M. Bühl, *Organometallics*, 2015, **34**, 438–449.

47 A. Scrivanti, V. Beghetto, E. Campagna, M. Zanato and U. Matteoli, *Organometallics*, 1998, **17**, 630–635.

48 A. Scrivanti, M. Bertoldini, V. Beghetto, U. Matteoli, A. Venzo, *J Organomet. Chem.*, 2009, **694**, 131-136.

49 L. Crawford, D. J. Cole-Hamilton, E. Drent and M. Bühl, *Chem. Eur. J.* , 2014, **20**, 13923–13926.

50 T. A. Shuttleworth, *PhD Thesis*, 2016, Univeristy of Bristol.

51 S. Ahmad, A. Lockett, T. A. Shuttleworth, A. M. Miles-Hobbs, P. G. Pringle and M. Bühl, *Phys. Chem. Chem. Phys*, 2019, **21**, 8543–8552.

52 T. Zhang, Y. Qin, D. Wu, R. Zhou, X. Yi and C. Liu, *Synth. Commun.*, 2005, **35**, 1889–1895.

53 J.-P. Charland, *Acta Crystallogr.* , 1989, **C45**, 680–681.

54 J. P. Farr, M. M. Olmstead, F. E. Wood and A. L. Balch, *J. Am. Chem. Soc.*, 1983, **105**, 792–798.

55 A. G. Orpen and N. G. Connelly, *J. Chem. Soc. Chem. Commun.*, 1985, 1310–1311.

56 A. G. Orpen and N. G. Connelly, *Organometallics*, 1990, **9**, 1206–1210.

57 N. H. Gama, A. Y. F. Elkhadir, B. G. Gordham, B. D. Kana, J. Darkwa and D. Meyer, *Biometals*, 2016, **29**, 637–650.

58 V. K. Jain, V. S. Jakkal and R. Bohra, *J. Organomet. Chem.*, 1990, **389**, 417–426.

59 J. Liu, C. Jacob, K. J. Sheridan, F. Al-Mosule, B. T. Heaton, J. A. Iggo, M. Matthews, J. Pelletier, R. Whyman, J. F. Bickley and A. Steiner, *Dalton Trans.*, 2010, **39**, 7921–7935.

60 Y. Cabon, H. Kleijn, M. A. Siegler, A. L. Spek, R. J. M. Klein Gebbink and J. Deelman, *Dalton Trans.* , 2010, **39**, 2423.

61 R. J. Goodfellow and B. F. Taylor, *J. Chem. Soc. Dalton Trans.*, 1974, 1676–1684.

62 J. P. Farr, M. M. Olmstead and A. L. Balch, *J. Am. Chem. Soc.*, 1980, **102**, 6654–6656.

63 P. Steinhoff, R. Steinbock, A. Friedrich, B. G. Schieweck, C. Cremer, K.-N. Truong and M. E. Tauchert, *Dalton Trans.*, 2018, **47**, 10439–10442.

64 D. Pingen, C. Müller and D. Vogt, *Angew. Chemie Int. Ed.*, 2010, **49**, 8130–8133.

65 P. G. Edwards, I. A. Fallis and B. S. Young, *GB Patent*, 2001, GB 2378182 A.

66 N. Weferling, *Zeitschrift für Anorg. und Allg. Chemie*, 1987, **548**, 55–62.

67 P. S. Marsh, *PhD Thesis*, 2003, University of Bristol.

68 M. Nixon, M. Waugh and G. R. Eastham, *Unpublished Work*, 2019, Lucite.

69 L.-H. Xu and E. P. Kundig, *Helevetica Chim. Acta*, 1994, **77**, 1480–1484.

70 S. O. Grim, R. L. Keiter and W. Mcfarlane, *Inorg. Chem.*, 1967, **6**, 1133–1137.

71 E. G. Bowes, D. D. Beattie and J. A. Love, *Inorg. Chem.*, 2019, **58**, 2925–2929.

72 A. R. H. Bottomley, C. Crocker and B. L. Shaw, *J. Organomet. Chem.*, 1983, **250**, 617–626.

73 B. L. Shaw, *J. Organomet. Chem.*, 1980, **200**, 307–318.

74 B. L. Shaw, *J. Am. Chem. Soc.*, 1975, **97**, 3856–3857.

75 D. L. Dodds, J. Floure, M. Garland, M. F. Haddow, T. R. Leonard, C. L. McMullin, A. G. Orpen and P. G. Pringle, *Dalton Trans.*, 2011, **40**, 7137–7146.

76 J. M. Lister, M. Carreira, M. F. Haddow, A. Hamilton, C. L. McMullin, A. G. Orpen, P. G. Pringle and T. E. Stennett, *Organometallics*, 2014, **33**, 702–714.

77 J. A. Iggo, *NMR Spectroscopy in Inorganic Chemistry*, Oxford University Press, 1999.

78 A. E. Derome, *Modern NMR Techniques for Chemistry Research*, 1987.

79 Ei. Drent and W. W. Jager, *World Patent*, 1995, WO 95/14001.

# Chapter 6

# Achiral monophosphines for enantioselective hydrogenation

## 6.1 Introduction

### 6.1.1 Rh-catalysed asymmetric hydrogenation

The demand for a single enantiomer of a chiral compound is essential in the pharmaceutical industry, and increasingly important in the fragrance, agrochemical, flavour and food industries. Asymmetric catalysis can be used to access a single enantiomer. Asymmetric hydrogenation is the reduction of a prochiral olefin, ketone or imine using molecular hydrogen. In 1968, following the discovery of Wilkinson's hydrogenation catalyst [$RhCl(PPh_3)_3$],[1] Knowles and Horner independently reported the first example of asymmetric hydrogenation.[2,3] The use of optically active phosphorus ligands in asymmetric hydrogenation is ubiquitous and has been extensively reviewed.[4–10] Figure 6.1 displays the different elements of chirality in such ligands, for example P-chirality (*e.g.* **6.1**),[11] backbone chirality (*e.g.* **6.2**),[12,13] axial chirality (*e.g.* **6.3**)[14–16] and substituent chirality (*e.g.* **6.4**).[17,18]

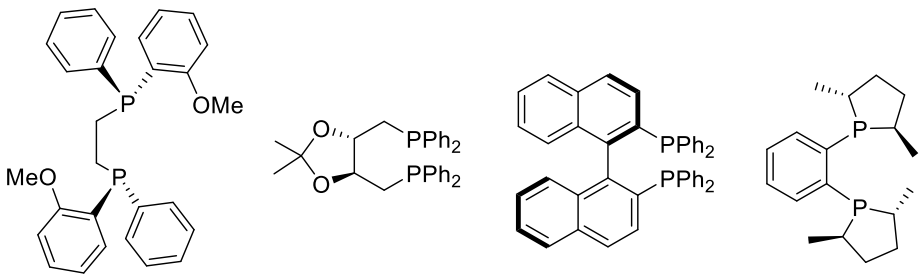


**Figure 6.1** Examples of phosphorus ligands used in asymmetric hydrogenation.

For many years, research into asymmetric hydrogenation has focussed on the use of chiral bidentate phosphorus ligands due to their inherent conformational rigidity resulting from their chelation to a metal centre. However, since the pioneering work of Pringle *et al.*, DeVries *et al.* and Reetz *et al.* in 2000, monodentate phosphorus ligands (such as **6.5**) have received increasing attention.[7,19–23] The biaryl backbone in **6.5** leads to restricted rotation about the M-P bond favouring one rotamer, which in some cases increases the chiral induction relative to when using the bidentate analogues.[19]

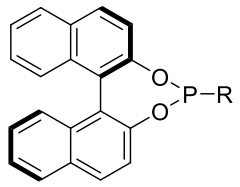


**6.5**
R = $CR'_3$, OR' or $NR'_2$

The mechanism of asymmetric hydrogenation has been previously well documented, and so will not be considered in detail.[4,24–26] As discussed, bidentate phosphorus ligands have inherent conformational rigidity leading to a highly defined chiral environment around the metal centre of the catalyst. It is well known that upon coordination of the classical bidentate ligand, dppe (1,2-bis(diphenylphosphino)ethane), a 5-membered chelate ring forms which will adopt two enantiomeric conformations, $\delta$ and $\lambda$ (Scheme 6.1).[27–29] In 1983, Knowles developed a model called the "quadrant rule" to describe the chiral environment around the metal centre (Scheme 6.1), which was used to determine the configuration of the product.[30] The quasi-axial P-substituents that are edge-on with respect to the $MP_2$ plane have a greater steric hindrance (highlighted quadrants) relative to the quasi-equatorial P-substituents that are face on.[31] Subsequently, the enantiofacial binding of the prochiral substrate and thus the absolute stereochemistry of the product will be influenced by the ligand conformation. Diphosphines which induce a $\delta$-chirality of the chelate ring consistently give *R*-hydrogenation products.[31,32] Hindering interconversion between the two conformers ($\delta$ and $\lambda$) may lead to chiral amplification, which can be achieved through the incorporation of a bulky substituent on the ligand backbone.[31,33]

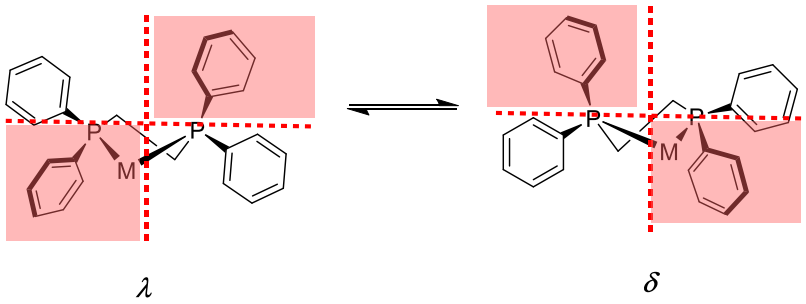


**Scheme 6.1** Quadrant rule of metal complexes of diphosphines.

### 6.1.2 *Tropos* ligands

Many asymmetric catalysts are metal complexes of chiral and atropisomeric (*atropos*) ligands, such as BINAP (2,2'-bis(diphenylphosphino)-1,1'-binaphthyl, **6.3**, Section 6.1.1). *Atropos* ligands are rigid molecules because rotation about their chiral axis is inhibited, whereas *tropos* ligands are flexible.[34] Scheme 6.2 shows the atropisomerism of biphenyl compounds: rotation about the C-C single bond is inhibited when steric hindrance between the R/R' substituents is large enough (*e.g.* when R = $NO_2$ and R' = $CO_2H$).[35] Racemic catalysts bearing *tropos* ligands have been broadly employed in asymmetric catalysis and well documented.[34,36–39] *Tropos* ligands are versatile, highly modular and easy to synthesise since no enantiomeric resolution is required.[38]

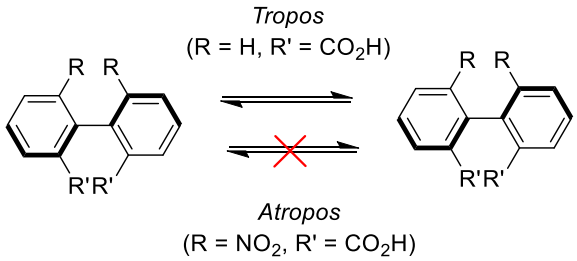


**Scheme 6.2** Atropisomerism of biphenyl compounds.

Racemic catalysts derived from *tropos* ligands can be resolved using either a "chiral controller" (Strategy A) or a "chiral activator" (Strategy B), as explained in Scheme 6.3.[38] In Strategy A, one enantiomer of the racemic catalyst is activated by a chiral activator (A*). Whereas, in Strategy B, a chiral controller (C*) is used to control the chirality of the racemic catalyst, which means it can be easily recovered and reused.[38] Both strategies have been developed in asymmetric catalysis and reviewed by Mikami *et al.*[38,40,41]

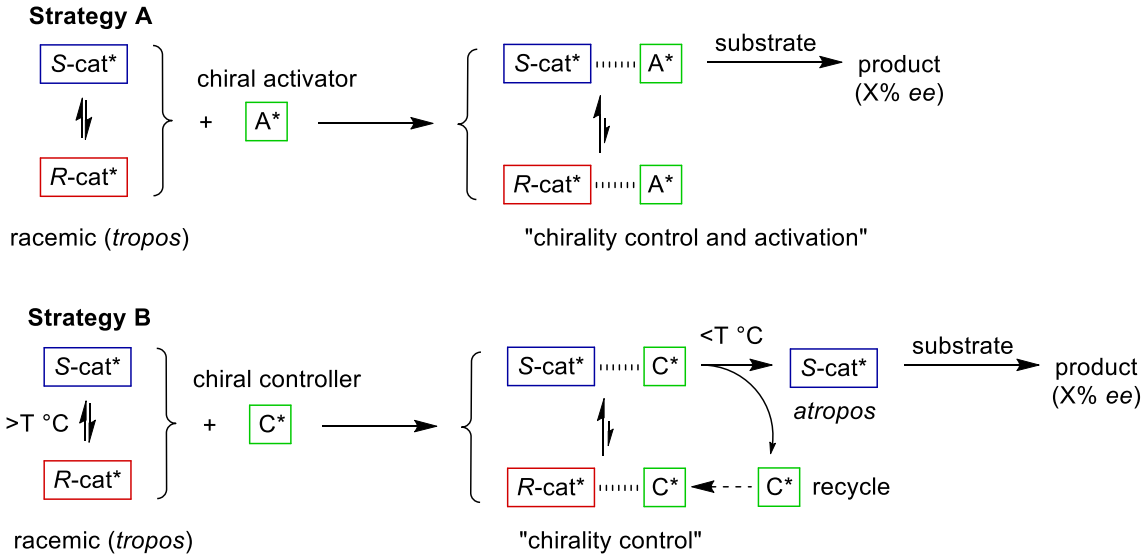


**Scheme 6.3** Control of a racemic *tropos* catalyst using a chiral controller or activator.[38]

Enantiomerically pure chiral dienes have been extensively applied as ligands in asymmetric catalysis,[42] but their application as chiral activators in the resolution of *tropos* ligands is rare. In 2008, Brown *et al.* employed the enantiomerically pure diene, (*S*,*S*)-cod* ((*S*,*S*)-bicyclo[3.3.1]nona-2,6-diene), to resolve BIPHEP and its derivatives (Scheme 6.4).[43] Upon the addition of [Rh(acac)((*S*,*S*)-cod*)] to BIPHEP, the two diastereomeric products resolved over time into a single diastereomer (an *atropos* precatalyst), as shown in the equilibrium in Scheme 6.4.[43] When R = OR' (R' = Me, *i*Pr or Bn) both diastereomeric products were observed at ambient temperature in a 1:1 ratio; resolution to the preferred diastereomer required gentle heating (50 °C).[43] The resolved complexes were tested in asymmetric hydrogenation and moderate enantioselectivities were observed (up to 85% *ee* for the O*i*Pr-BIPHEP derivative).[43] The enantioselectivity was further increased to 95% using an excess of (*S*,*S*)-cod*; it was suggested that the catalyst configuration was further controlled by preventing free ligand racemisation.[43] As anticipated, when using the non-equilibrated diastereomeric mixture of complexes in catalysis no enantioselectivity was observed.[43]

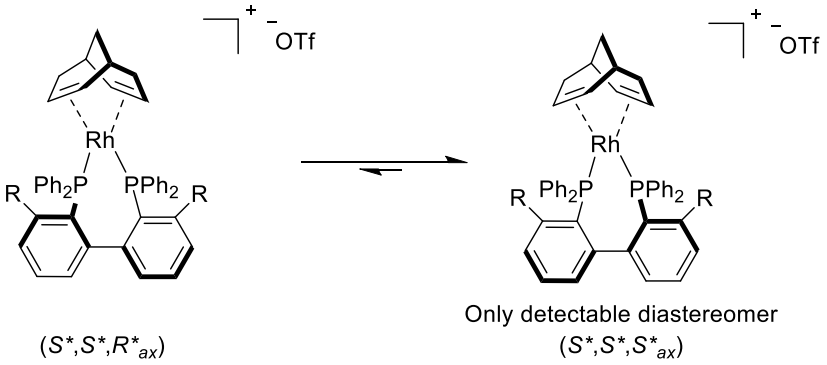


**Scheme 6.4** *In situ* resolution of Rh-BIPHEP diastereomers using (*S*,*S*)-cod*.

### 6.1.3 Restricted M-P rotation in tertiary phobane complexes

Complexes of bidentate phosphorus ligands are generally more stable than their monodentate analogues owing to the chelate effect. However, monodentate phosphorus ligands are easier to synthesise due to their readily accessible and inexpensive precursors. Furthermore, they are suitable candidates for high throughput experiments and so it is easier to introduce structural diversity.[44] Pseudo-chelates combine these advantages of mono- and bidentate ligands. Pseudo-chelates are the combination of two monodentate ligands that are functionalised with complementary binding motifs, which form a pseudo-backbone *via* self-assembly.[44]

Recently, Pringle *et al.* showed that the restricted M-P rotation in tertiary phobane metal complexes can be exploited to produce complexes with pseudo-chelate properties based on steric effects.[45,46] Bicyclic tertiary PhobPR ligands (PhobP = 9-phospha[3.3.1]bicyclononane) have been extensively applied in homogeneous catalysis[47–50] and exist in three isomeric forms, *s*-, $a_5$- and $a_7$-PhobPR (Figure 6.2). Despite the apparent low bulkiness of PhobPR ligands, unexpectedly high barriers to M-P rotation were observed for *trans*-[$MCl_2$(PhobPBu)$_2$] complexes (where M = Pt or Pd), which gave rise to *anti* and *syn* conformations (Scheme 6.5).[45,46] Computational studies suggested that the restricted M-P rotation was attributed to the rigidity of the bicycle of PhobP.[45] A combination of NMR spectroscopy and computational studies also demonstrated that the barrier to M-P rotation was dependent on the steric bulk of the R substituent of PhobPR: as the size of R increases the barrier increases.[45] Restricted M-P rotation has been previously observed when using the inherently bulky *t*Bu$_2$PR ligands; the barriers to M-P rotation calculated by Shaw *et al.* for such complexes were of a similar magnitude to the "non-bulky" PhobPR complexes reported by Pringle *et al.*[45,51,52]

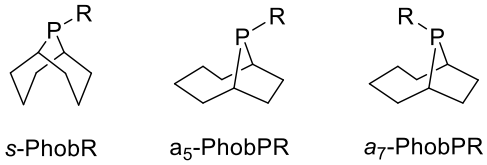


**Figure 6.2** *Sym* (*s*) and *asym* (*a*) isomeric forms of PhobPR.

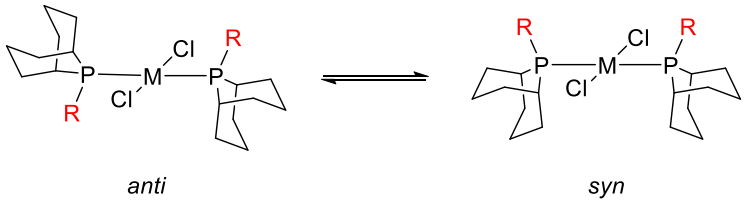


**Scheme 6.5** Fluxionality displayed by *trans*-[$MCl_2(PhobPR)_2$] complexes.

Similarly, structural rigidity was observed for the analogous *cis*-[$PtX_2(PhobPR)_2$] complexes (where X = Cl or Me).[46] However, three conformations were anticipated (Scheme 6.6) since the *anti*-form is a pair of enantiomers, $\delta$ and $\lambda$, labelled by analogy to the conformations of dppe chelates (Scheme 6.1). For all the *cis* complexes considered, there was a thermodynamic preference for the *anti*-conformation over the *syn*-conformation, and the epimerisation appeared to have an exceptionally high kinetic barrier.[46] Using optically pure PhobPR ligands (when R = *(R)-iso*-pentyl or *(R)-sec*-pentyl) the two diastereomeric *anti*-conformers ($\delta$ and $\lambda$) were identifiable by $^{31}P\{^1H\}$ NMR spectroscopy.[46]

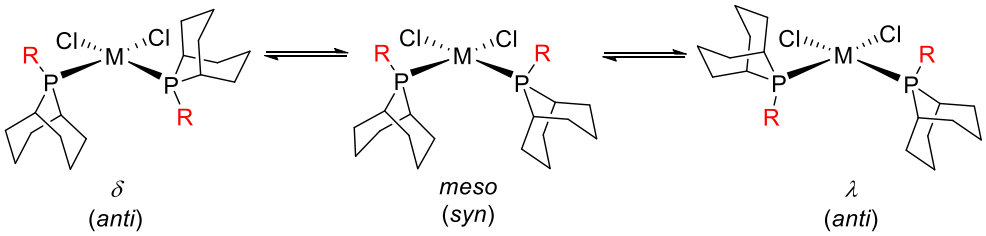


**Scheme 6.6** Fluxionality displayed by *cis*-[$MCl_2(PhobPR)_2$] complexes.

The high rigidity of coordinated PhobPR ligands was exploited in asymmetric catalysis.[46] The *cis*-[Rh(nbd)(PhobPR*)$_2$][$BF_4$] complex (where R = (*R*)-*i*Pn and nbd = norbornadiene) was synthesised and, as expected from the above discussion, two diastereomeric *anti*-conformers were observed ($\delta$ and $\lambda$).[46] Resolution of the *anti*-conformers was achieved through selective crystallisation, and the optically pure $\lambda$-[Rh(nbd)(*s*-PhobP-(*R*)-*i*Pn)$_2$][$BF_4$] complex was tested in the Rh-catalysed asymmetric hydrogenation of methyl-2-acetamidoacrylate (MAA).[46] However, extremely low

temperatures of -50 °C were required to preserve the chirality of the catalyst, so conversion was low.[46] Nonetheless, enantioselectivity was achieved (*ee* = 40%) using the single diastereomer.[46] The enantioselectivity was attributed to the chirality of the *anti*-conformer rather than the chirality of the R* substituent of PhobPR* since the diastereomeric mixture of complexes ($\delta$-/ $\lambda$-[Rh]) gave essentially zero *ee*.[46]

### 6.1.4 Aims of the project

To advance these recent developments by Pringle *et al.*, we aimed to design an optically active catalyst with achiral PhobPR ligands. Rather than using the chirality of the R* substituent in PhobPR*, resolution of the diastereomeric conformers of *cis*-[Rh((*S*,*S*)-cod*)(PhobPR)$_2$][OTf] complexes (where PhobPR = **L$_{6.1\text{-}6.5}$**, Figure 6.3) was to be attempted by using the enantiomerically pure diene, (*S*,*S*)-cod*. We aimed to synthesise the chiral diene according to Scheme 6.7, as previously reported by Brown *et al.*[53,54] The PhobPR ligands were synthesised by J. Lister (University of Bristol) according to literature methods.[46]

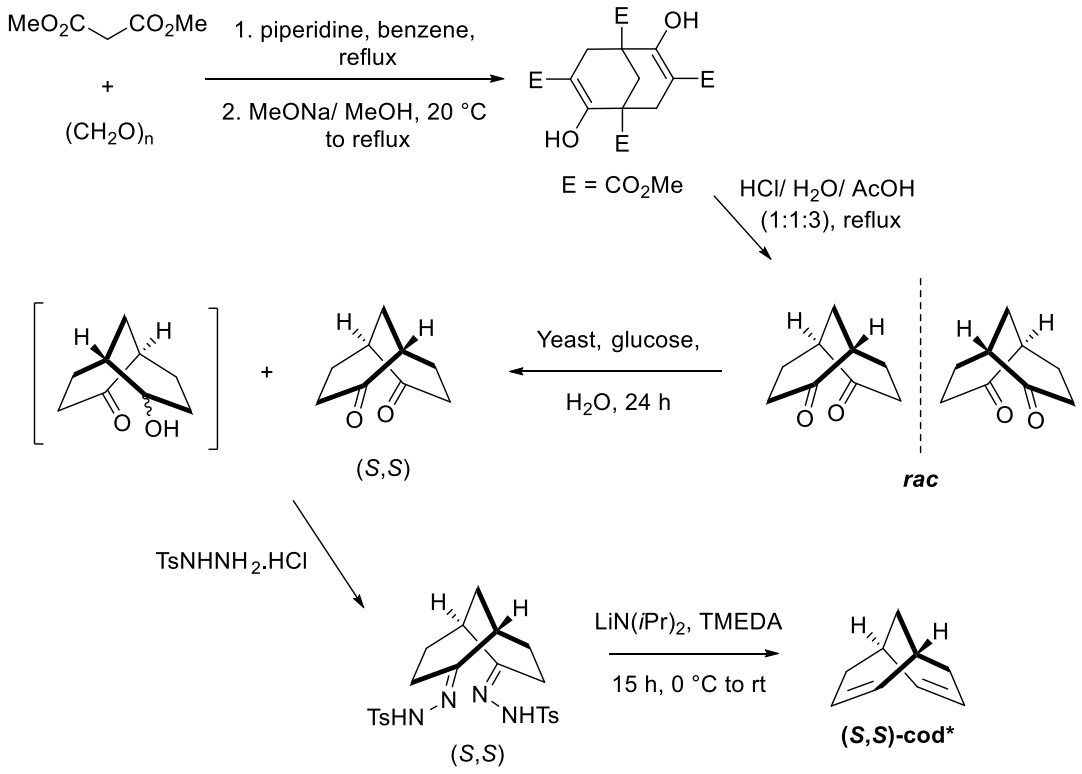


**Scheme 6.7** Synthesis of enantiomerically pure (*S*,*S*)-cod*, TMEDA = tetramethylethylenediamine.

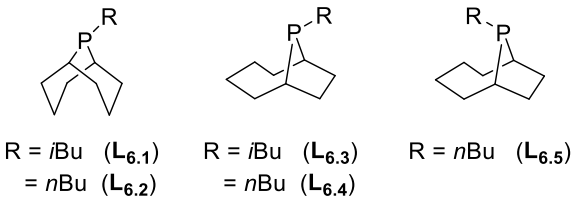


**Figure 6.3** PhobPR ligands studied in this project.

The fluxionality of the conformers of *cis*-[Rh((*S*,*S*)-cod*)(PhobPR)$_2$][OTf] was also to be investigated. We attempted to demonstrate that rotamer-derived chirality alone can produce asymmetric induction by testing the resolved complex in Rh-catalysed asymmetric hydrogenation.

## 6.2 *cis*-[Rh(cod*)(PhobPR)$_2$][OTf] complexes

In this section, the fluxionality of the *cis*-[Rh(cod*)(PhobPR)$_2$][OTf] complexes was investigated; the chiral diene, cod*, was used either as a single enantiomer, (*S*,*S*)-cod*, or as a racemic mixture, *rac*-cod*. The racemic mixture, *rac*-cod*, was predominantly used for the following studies since its resolution required an additional two steps to its synthesis (Scheme 6.7, Section 6.1.4).

### 6.2.1 Synthesis and resolution of the chiral rotamers

The reaction of [Rh($C_2H_4$)$_2$(acac)] with 1.2 equiv. of *rac*-cod* or (*S*,*S*)-cod* in $CDCl_3$ gave the starting complexes [Rh(acac)(*rac*-cod*)] (*rac*-**6.6**) and [Rh(acac)((*S*,*S*)-cod*)] {(*S*,*S*)-**6.6**} respectively (Scheme 6.8).[54] Moderate yields of *ca.* 65% were achieved.

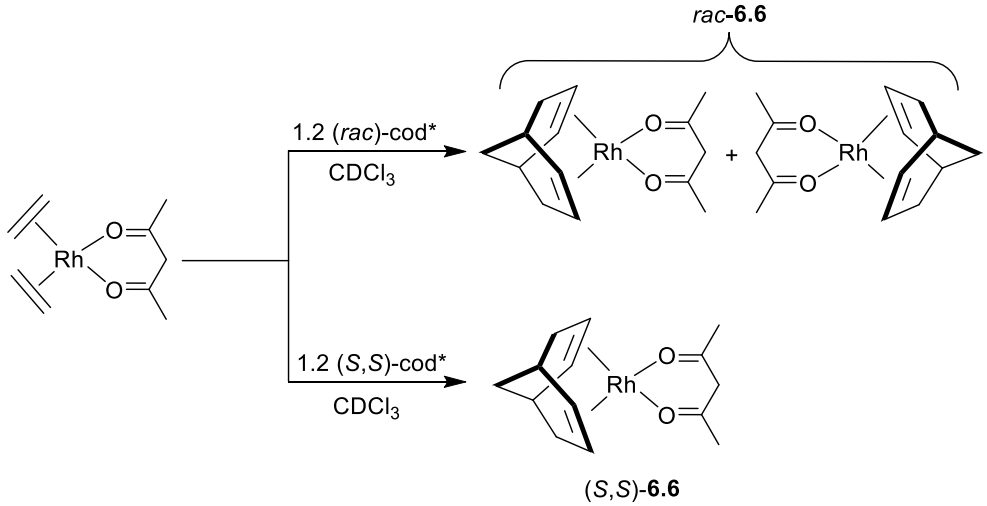


**Scheme 6.8** Synthesis of the [Rh(acac)(cod*)] complexes (*S*,*S*)-**6.6** and *rac*-**6.6**.

The reaction of 2 equiv. of ligands $\mathbf{L_{6.1\text{-}6.5}}$ with [Rh(acac)(*rac*-cod*)] (*rac*-**6.6**) in $CH_2Cl_2$ in the presence of $Me_3SiOTf$ gave the *cis*-[Rh(*rac*-cod*)$L_2$][OTf] complexes **6.7a**-**e**, where L = $\mathbf{L_{6.1\text{-}6.5}}$ (Scheme 6.9). The enantiomerically pure *cis*-[Rh((*S*,*S*)-cod*)$L_2$][OTf] complexes **6.7a**-**b***, where L = $\mathbf{L_{6.1\text{-}6.2}}$, were obtained from a similar procedure but using, [Rh(acac)((*S*,*S*)-cod*)] ((*S*,*S*)-**6.6**), as the starting precursor.

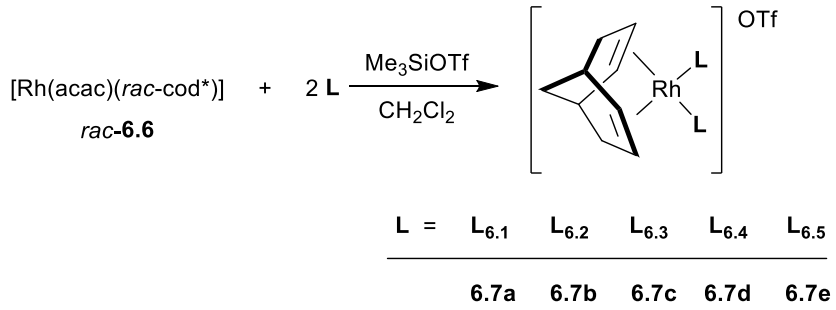


**Scheme 6.9** Synthesis of *cis*-[Rh(*rac*-cod*)$L_2$][OTf] complexes **6.7a**-**e**.

The $^{31}P\{^1H\}$ NMR spectra for complexes **6.7a**-**e** showed two doublets with $^1J_{P,Rh}$ values of *ca.* 140 Hz (Figure 6.4, Table 6.1). The signals correspond to the two diastereomeric *anti*-conformations of the complexes, $\delta$ and $\lambda$ (Scheme 6.10). When using *rac*-cod* each doublet corresponds to a pair of enantiomers, $\delta$-(*S*,*S*)/ $\lambda$-(*R*,*R*) (conformer **A**) and $\delta$-(*R*,*R*)/ $\lambda$-(*S*,*S*) (conformer **B**), as shown in Scheme 6.10. It has been previously reported for the *cis*-[$PtX_2$(PhobPR)$_2$] complexes, where X = Cl or Me, that an *anti*-conformation is preferred over a *syn*-conformation;[46] a similar thermodynamic has been identified here.

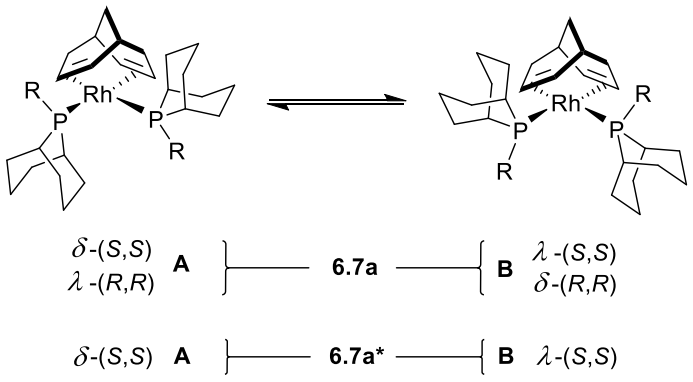


**Scheme 6.10** Fluxionality displayed by the *anti*-conformers of complex **6.7a**, R = *i*Bu.

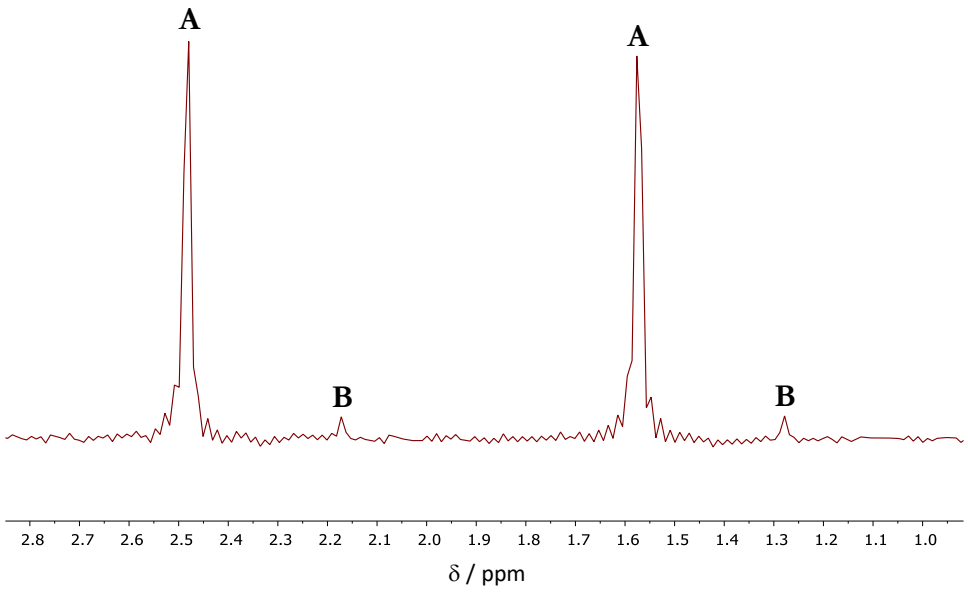


**Figure 6.4** $^{31}P\{^{1}H\}$ NMR spectrum of complex **6.7a**, showing a thermodynamic preference for one *anti*-conformer (**A**).

**Table 6.1** $^{31}P\{^{1}H\}$ NMR data for complexes **6.7a**-**e**.[a]

| Ligand | Complex | $\delta_P$/ppm | $^{1}J_{P,Rh}$ / Hz | % major conformer[b] |
|---|---|---|---|---|
| $\mathbf{L}_{6.1}$ | **6.7a** | 2.0, 1.7 | 147, 145 | 95 |
| $\mathbf{L}_{6.2}$ | **6.7b** | 4.2, 0.4 | 145, 146 | 96 |
| $\mathbf{L}_{6.3}$ | **6.7c** | 41.8, 40.3 | 142, 140 | 90 |
| $\mathbf{L}_{6.4}$ | **6.7d** | 40.7, 40.5 | 142, 141 | 93 |
| $\mathbf{L}_{6.5}$ | **6.7e** | 40.7, 38.8 | 142, 140 | 65 |

[a] Measured in $CD_2Cl_2$. [b] Determined by integration of $^{31}P\{^{1}H\}$ NMR signals.

All complexes **6.7a**-**e** were successfully resolved using the chiral diene cod*; there was a significant thermodynamic preference for one of the *anti*-conformers (*ca.* 90% major isomer), except for complex **6.7e** where a 65:35 ratio of the *anti*-conformers was observed (Table 6.1). The ratio of the conformers was dependent on the ligand employed.

Crystallisation of the racemic mixture of the four enantiomers of complex **6.7a** was set up by slow diffusion of hexane into a saturated chlorobenzene solution of the complex. Fortuitously, crystals suitable for X-ray crystallography of a single enantiomer of the complex were grown, the $\delta$-(*S*,*S*) conformer, $\delta$-[Rh((*S*,*S*)-cod*)($\mathbf{L}_{6.1}$)$_2$][OTf] (Figure 6.5). The crystals were redissolved and the resulting $^{31}P\{^{1}H\}$ NMR spectrum confirmed they

were of the major conformer. Crystallisation of the racemic complex **6.7b** was set up from slow diffusion of hexane into a saturated chlorobenzene solution of the complex. Crystals suitable for X-ray crystallography of two enantiomers of complex **6.7b**, $\delta$-(*S*,*S*) (Figure 6.6) and $\lambda$-(*R*,*R*) (Figure 6.7), were grown. The two structures have been separated into two Figures for clarity (Figures 6.6 and 6.7).

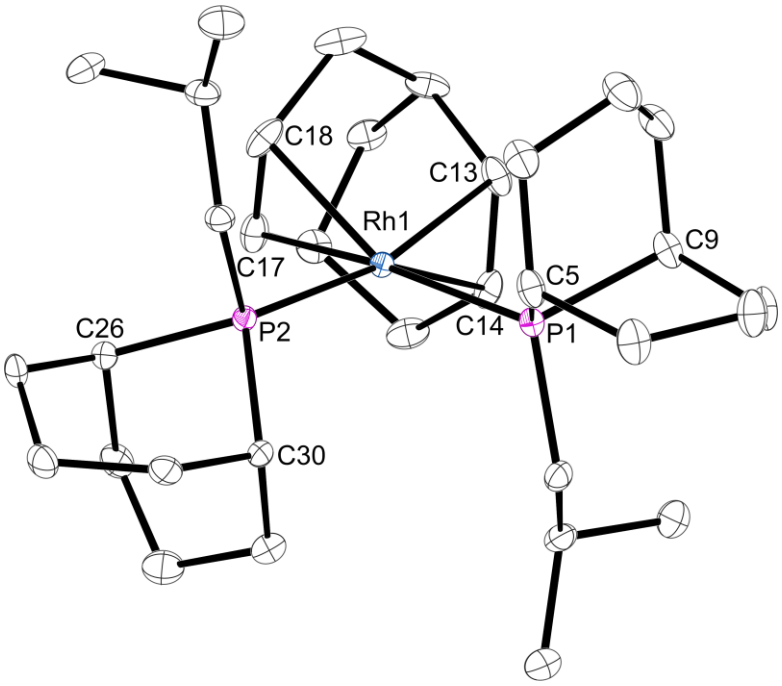


**Figure 6.5** Crystal structure of $\delta$-[Rh((*S*,*S*)-cod*)(**L**$_{6.1}$)$_2$][OTf] (**6.7a**). The hydrogen atoms and [OTf]$^-$ have been omitted for clarity. Thermal ellipsoids at 50% probability. Selected bond lengths (Å) and angles (°): Rh1-P1 2.3390(7), Rh1-P2 2.3462(7), Rh1-C13 2.301(2), Rh1-C14 2.230(2), Rh1-C17 2.287(3), Rh1-C18 2.226(3), P1-Rh1-P2 93.66(2), C14-Rh1-C17 78.52(9), C13-Rh1-C18 78.47(10), C5-P1-C9 93.92(11), C26-P2-C30 94.19(11). See Appendix for details.

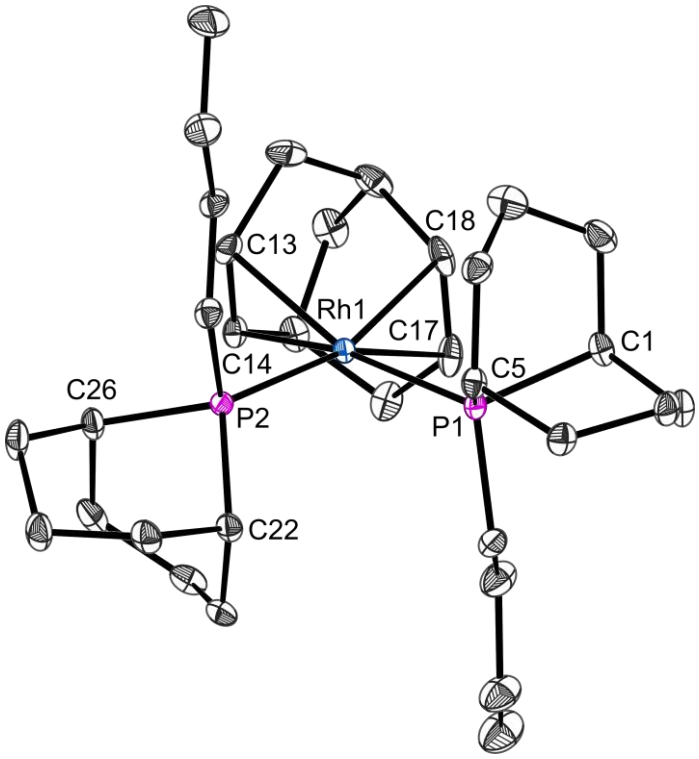


**Figure 6.6** Crystal structure of $\delta$-[Rh((*S*,*S*)-cod*)(**L**$_{6.2}$)$_2$][OTf] (**6.7b**). The hydrogen atoms, [OTf]$^-$ counterions and $\lambda$-(*R*,*R*) conformer have been omitted for clarity. Thermal ellipsoids at 50% probability. Disorder from the *n*Bu chain has been omitted for clarity. Selected bond lengths (Å) and angles (°): Rh1-P1 2.3225(7), Rh1-P2 2.3252(6), Rh1-C13 2.236(2), Rh1-C14 2.256(2), Rh1-C17 2.239(3), Rh1-C18 2.269(3), P1-Rh1-P2 92.80(2), C14-Rh1-C17 79.37(9), C13-Rh1-C18 79.3(1), C1-P1-C5 94.75(12), C22-P2-C26 94.87(12). See Appendix for details.

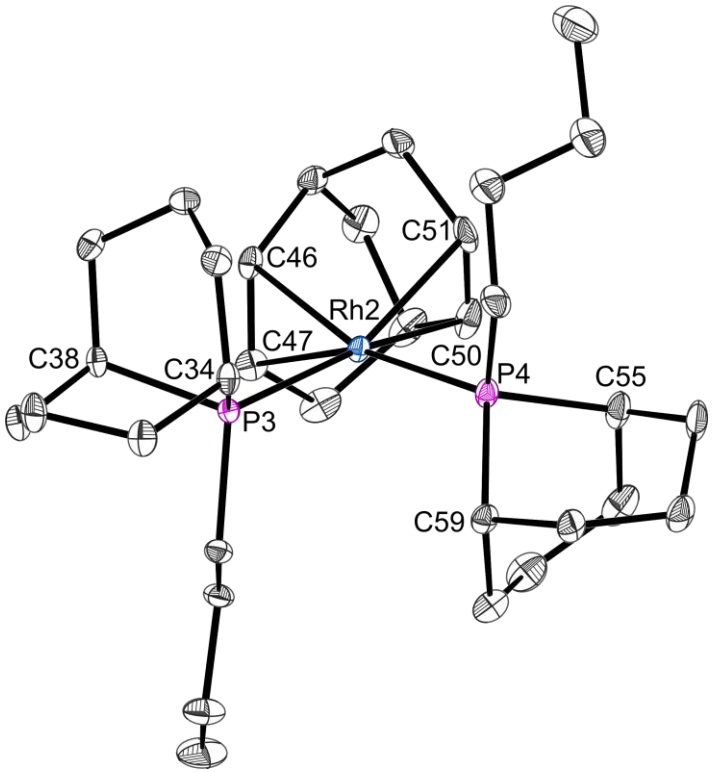


**Figure 6.7** Crystal structure of $\lambda$-[Rh(*R*,*R*-cod*)(**L**$_{6.2}$)$_2$][OTf] (**6.7b**). The hydrogen atoms, [OTf]$^-$ counterions and $\delta$-(*S*,*S*) conformer have been omitted for clarity. Thermal ellipsoids at 50% probability. Disorder from the phobane substituent has been omitted for clarity. Selected bond lengths (Å) and angles (°): Rh2-P3 2.3216(6), Rh2-P4 2.3193(7), Rh2-C46 2.275(2), Rh2-C47 2.241(3), Rh2-C50 2.260(3), Rh2-C51 2.222(3), P3-Rh1-P4 93.24(2), C47-Rh2-C50 79.77(10), C46-Rh2-C51 79.39(10), C55-Rh2-C59 94.64(12), C34-Rh2-C38 94.92(11). See Appendix for details.

In each case, the crystal structures confirmed a *cis* geometry of the complex and showed a square planar geometry about the Rh(I) centre. The crystal structures of the $\delta$-conformers of complexes **6.7a** (containing the *s*-PhobP*i*Bu ligand) and **6.7b** (containing the *s*-PhobP*n*Bu ligand) are similar (Figures 6.5 and 6.6). The P1-Rh1-P2 angle of complex **6.7a** is slightly larger than that of **6.7b** (by 0.86(2)°); although this effect is very subtle, it may reflect the greater steric bulk of the *i*BuP ligand **L**$_{6.1}$, relative to the *n*BuP analogue **L**$_{6.2}$. In accordance with this, the C-Rh-C diene bite angle of the *i*Bu complex **6.7a** is 0.85(9)° smaller than that of the *n*Bu analogue **6.7b**. The bond lengths and angles of the two enantiomers ($\delta/\lambda$) of complex **6.7b** are very similar (Figures 6.6 and 6.7).

The C-Rh-C diene bite angle in complex **6.7a** (Figure 6.5) is *ca.* 12.5° larger than that of nbd in the analogous $\lambda$-[Rh(nbd)(**L**$_{6.1}$)$_2$][BF$_4$] complex (nbd = norbornadiene).[46] Accordingly, the P-Rh-P angle in **6.7a** is *ca.* 11.5° smaller than that of $\lambda$-[Rh(nbd)(**L**$_{6.1}$)$_2$][BF$_4$].[46] These observations are consistent with the higher steric bulk of cod* relative to nbd. The P-Rh-P angle of complex **6.7b** (average = 93.02(2)°, Figures 6.6 and 6.7) is strikingly small compared to that of the achiral analogue $\delta$-[Rh(cod)(**L**$_{6.2}$)$_2$][BF$_4$] (by *ca.* 9°).[46] This implies that cod* is more sterically encumbered than its achiral analogue, cod. The previously reported [Rh((*S*,*S*)-cod*)(BIPHEP)][OTf] complex also has a small P-Rh-P angle of 90.20(3)°.[43] Since the diene bite angles (C-Rh-C) of **6.7b** and $\delta$-[Rh(cod)(**L**$_{6.2}$)$_2$][BF$_4$] are very similar, it is suggested that it is the rigidity of the cod* that induces the reduction in the P-Rh-P angle.[46] As a result of this rigidity, cod* may be preorganised to be more strongly bound to the metal centre; this effect is not reflected in the corresponding C-Rh bond lengths.

### 6.2.2 Kinetic study of the epimerisation of the Rh-complexes

A kinetic study of the epimerisation of complexes **6.7a**-**e** was carried out. The synthesis of complexes **6.7a**-**e** (see Section 6.2.1) was monitored over time and the relative concentrations of each conformer were determined through integration of their $^{31}$P{$^1$H} NMR signals. Since the *rac*-cod* was used for the purpose of these studies, each doublet in the $^{31}$P{$^1$H} NMR spectrum corresponds to a pair of enantiomers (**A** and **B**, Section 6.2.1).

Figure 6.8 shows the series of $^{31}$P{$^1$H} NMR spectra collected for the *s*-PhobP*i*Bu complex **6.2a** at ambient temperature. Initially, conformer **A** was the minor product, where a 1:8 ratio of **A**: **B** was detected. However, over time the amount of **A** increased relative to **B** and within 100 min the 20:1 thermodynamic ratio of **A**: **B** was established. When diastereomerically pure crystals of **A** were dissolved in $CH_2Cl_2$ at -80 °C, a similar equilibrium was established immediately, showing that the major diastereomer was the $\delta$-(*S*,*S*) conformer.

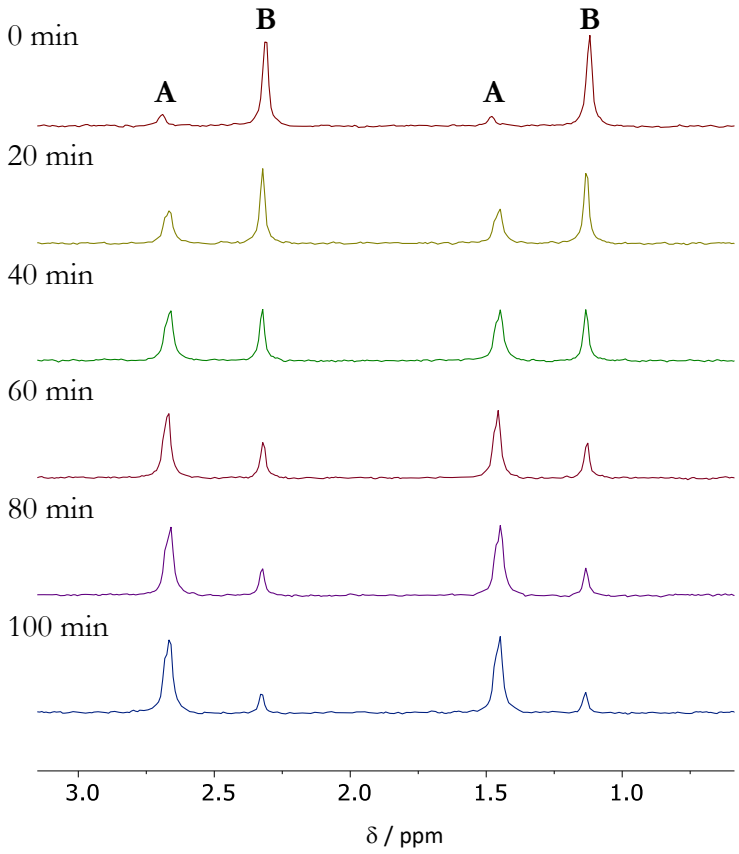


**Figure 6.8** $^{31}P\{^{1}H\}$ NMR spectra of the epimerisation between conformers A and B (for complex **6.7a**).

A plot of the relative concentrations of **A** and **B** against time is shown in Figure 6.9. The integrated first order rate law was then applied to the kinetic data to give the straight-line plot of $\ln[\mathbf{A}]/[\mathbf{A}]_0$ against time (Figure 6.10). The straight line indicates that the epimerisation of complex **6.7a** is a first order process. The rate constant k was calculated from the gradient of the graph as 3.4 $x10^{-4}$ $s^{-1}$ and the half-life ($t_{1/2}$) = 34 min. The racemisation of the previously reported *cis*-[Rh(nbd)(*s*-PhobP*i*Pn)$_2$][$BF_4$] is also a first order process and the rate constants (k) at a range of temperatures (-15 to -35 °C) were of the same order of magnitude as that calculated for complex **6.7a**.[46]

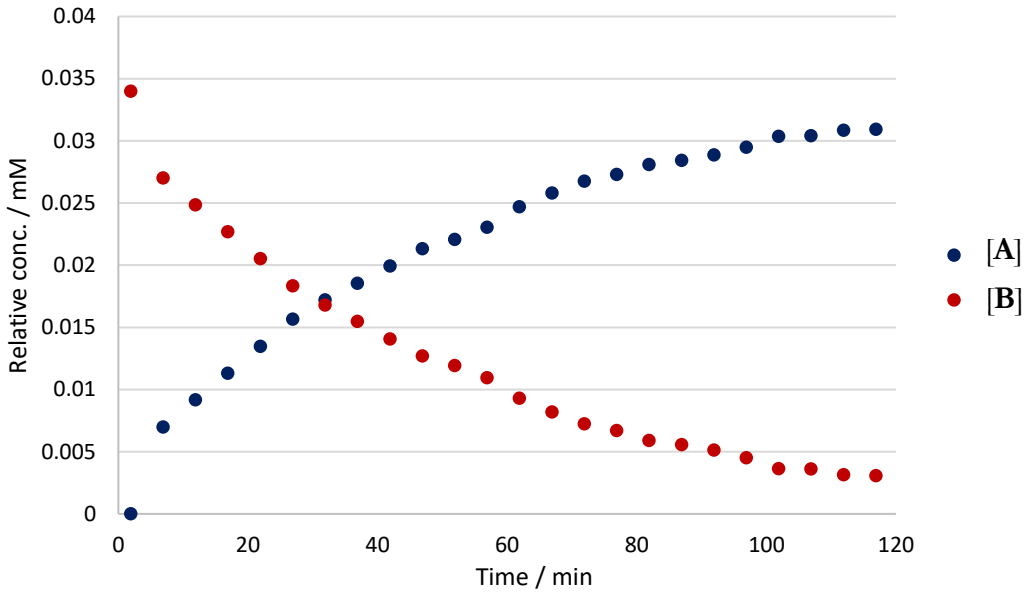


**Figure 6.9** Plot of the relative concentrations of conformers **A** and **B** (complex **6.7a**) against time.

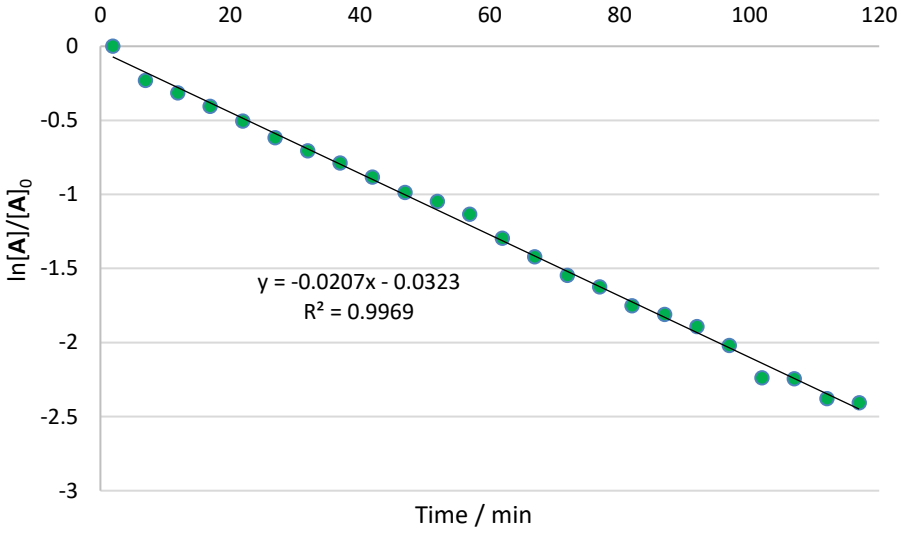


**Figure 6.10** First order kinetic plot of the epimerisation of complex **6.7a**.

Analogous kinetic data was collected for complexes **6.2b**-**e**, but the ratio of conformers that was initially observed did not change over time. The thermodynamic ratio of conformers was immediately established for these complexes.

## 6.3 Catalytic asymmetric hydrogenation

Since high resolution of the *anti*-conformers of the *s*-PhobP*i*Bu complex **6.7a** was achieved, complex **6.7a** was tested in the Rh-catalysed asymmetric hydrogenation of standard substrates, methyl-2-acetamidoacrylate (MAA) and methyl-2-acetamidocinnamate (MAC) under various conditions (Scheme 6.11). In the following studies the pre-prepared racemic complex *cis*-[Rh(*rac*-cod*)(**L**$_{6.1}$)$_2$][OTf] (**6.7a**) was used initially to optimise conversion. Once the conditions had been optimised, the catalysis was carried out using the enantiopure pre-prepared complex, *cis*-[Rh((*S*,*S*)-cod*)(**L**$_{6.1}$)$_2$][OTf] (**6.7a***), in an attempt to achieve enantioselective induction.

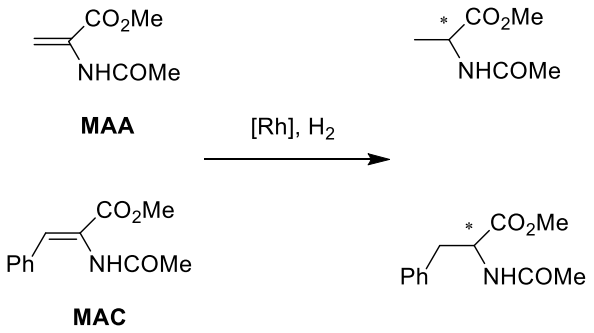


**Scheme 6.11** Catalytic asymmetric hydrogenation of MAA and MAC.

Initial catalytic runs were carried out using MAA at 25 °C and 5 bar of $H_2$ in $CH_2Cl_2$. Within 1 h, using a catalyst loading of 1 mol%, 100% conversion of the substrate was achieved using complex **6.7a**. As previously demonstrated by Pringle *et al.*, low temperatures are required to preserve the optical activity of the separate diastereomers.[46] The catalysis was thus carried out at 12 °C, but to offset the lower temperature an increased pressure of 10 bar of $H_2$ was required. The reaction was run for 1 h using both MAA and MAC and the results are shown in Table 6.2.

**Table 6.2** Catalytic asymmetric hydrogenation at 12 °C.[a]

| Entry | Catalyst | Substrate | Conversion[b] / % | *ee* / % |
|---|---|---|---|---|
| 1 | **6.7a** | MAA | 100 | 1 (*R*) |
| 2 | **6.7a** | MAC | 65 | 2 (*S*) |
| 3 | **6.7a*** | MAA | 100 | 2 (*S*) |

[a] Method: 0.200 mmol substrate, 0.002 mmol **6.7a** or **6.7a***, 5 cm$^3$ $CH_2Cl_2$, 10 bar of $H_2$, 12 °C, 1 h. [b] Conversion and *ee* were determined by GC. Each result is an average of two runs.

A higher conversion was achieved when using MAA relative to MAC (Entry 1 vs. 2, Table 6.2) and so MAA was used as the substrate for the subsequent studies. Using the enantiopure catalyst (**6.7a***) no enantioselectivity was observed under these conditions (Entry 3). In an attempt to slow epimerisation of the catalyst and encourage enantioselectivity, the temperature was further decreased to 0 °C. A higher catalyst loading (10 mol% Rh), higher pressure of $H_2$ (20 bar) and more concentrated solutions (3 $cm^3$ of $CH_2Cl_2$) were used to compensate for the lower temperature (Table 6.3).

**Table 6.3** Catalytic asymmetric hydrogenation at 0 °C.[a]

| Entry | Catalyst | Conversion[b] / % | *ee* / % |
|---|---|---|---|
| 1 | **6.7a** | 100 | 2 (*R*) |
| 2 | **6.7a*** | 100 | 2 (R) |

[a] Method: 0.200 mmol MAA, 0.020 mmol **6.7a** or **6.7a***, 3 $cm^3$ $CH_2Cl_2$, 20 bar of $H_2$, 0 °C, 1 h. [b] Conversion and *ee* were determined by GC. Each result is an average of two runs.

Using both complexes **6.7a** and **6.7a*** 100% conversion was observed. Unfortunately, essentially zero enantioselectivity was found using the enantiopure catalyst, **6.7a*** (Entry 2, Table 6.3). The temperature was further decreased to -50 °C and despite forcing conditions of a very high catalyst loading (50 mol%) and a high $H_2$ pressure (20 bar), no conversion was observed.

A preliminary experiment was carried out to determine the lowest temperature conversion could be observed (using 10 mol% Rh and 20 bar of $H_2$). The temperature of the reaction mixture was gradually increased from -40 °C to -10 °C and after a reaction time of 1 h at a specific temperature a sample of the reaction mixture was analysed. This experiment was repeated for a range of solvents and the results are shown in Table 6.4.

**Table 6.4** Catalytic asymmetric hydrogenation at a range of temperatures and using a range of solvents.[a]

| Entry | Catalyst | Temperature / °C | Solvent | Conversion / % | *ee* / % |
|---|---|---|---|---|---|
| 1 | **6.7a** | -40 | $CH_2Cl_2$ | 0 | - |
| 2 | **6.7a** | -40 | THF | 0 | - |
| 3 | **6.7a** | -40 | Acetone | 0 | - |
| 4 | **6.7a** | -40 | MeOH | 0 | - |
| 5 | **6.7a** | -20 | $CH_2Cl_2$ | 2 | 0 |
| 6 | **6.7a** | -20 | THF | 4 | 2 (*S*) |
| 7 | **6.7a** | -20 | Acetone | 0 | - |
| 8 | **6.7a** | -20 | MeOH | 1 | - |
| 9 | **6.7a** | -10 | $CH_2Cl_2$ | 100 | 2 (*R*) |
| 10 | **6.7a** | -10 | THF | 100 | 2 (*S*) |
| 11 | **6.7a** | -10 | Acetone | 99 | 4 (*S*) |
| 12 | **6.7a** | -10 | MeOH | 100 | 2 (*S*) |

[a] Method: 0.200 mmol MAA, 0.020 mmol **6.7a**, 3 $cm^3$ solvent, 20 bar of $H_2$, 1 h. [b] Conversion and *ee* were determined by GC. Each result is an average of two runs.

As expected, zero enantioselectivity was produced since the racemic catalyst **6.7a** was used; this shows that an *ee* of up to 4% should be considered as within experimental error (Table 6.4). The lowest temperature at which any conversion was observed was -20 °C, and the highest conversions were attained when using $CH_2Cl_2$ and THF (Entries 5 and 6). A high catalyst loading (50 mol%) and a high pressure of $H_2$ (45 bar) were required to increase the conversion at -20 °C, THF was used as the solvent and the results are shown in Table 6.5. To aid solubility of the catalyst at this temperature less substrate was used (see Method, Table 6.5).

**Table 6.5** Catalytic asymmetric hydrogenation at -20 °C.[a]

| Entry | Catalyst | Conversion[b] / % | *ee* / % |
|---|---|---|---|
| 1 | **6.7a** | 60 | 2 (*R*) |
| 2 | **6.7a*** | 66 | 2 (R) |

[a] Method: 0.052 mmol MAA, 0.026 mmol **6.7a** or **6.7a***, 3 $cm^3$ THF, 45 bar of $H_2$, -20 °C, 1 h. [b] Conversion and *ee* were determined by GC. Each result is an average of two runs.

Under these forcing conditions good conversions were achieved at -20 °C (*ca.* 60%, Table 6.5). However, using the enantiopure catalyst **6.7a*** enantioselective induction was not observed. A temperature of -50 °C was required for the previously reported *λ*-[Rh(nbd)(*a*$_5$-PhobP*i*Pn)$_2$][BF$_4$] complex to preserve its chirality and allow for enantioselective induction.[46] Unfortunately, the catalysis using **6.7a*** at -50 °C was too slow to achieve any conversion, but the chirality of **6.7a*** could not be preserved at -20 °C.

## 6.4 NMR studies of the hydrogenation catalysts

### 6.4.1 Hydrogenation of cod*

To gain further insight into the hydrogenation of the catalyst, the reaction mixtures were analysed by $^{31}$P{$^1$H} NMR spectroscopy after catalysis and *in situ*. The reaction mixture at the end of the catalytic run at -20 °C was analysed (Entry 2, Table 6.5). Surprisingly, the resulting $^{31}$P{$^1$H} NMR spectrum showed that the original complex (**6.7a***) remained intact, despite conversion being observed. Brown *et al.* observed a similarly puzzling result when using the analogous [Rh((*S*,*S*)-cod*)(*S*-BIPHEP)]$^+$ complex.[43] Subsequently, they then showed that using an excess of diene (10 mol%) increased the enantioselectivity of the product.[43] No increase in *ee* was observed when using an excess of (*S*,*S*)-cod* with our system. To encourage the hydrogenation of cod*, complex **6.7a** was pressurised with 45 bar of H$_2$ at ambient temperature, in *d*$_8$-THF for 1 h (Scheme 6.12).

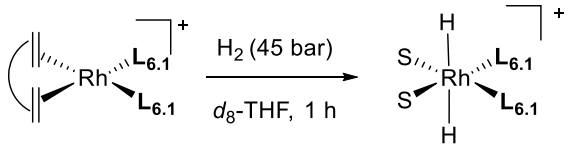


**6.7a** **6.8**, 60%
S = solvent molecule

**Scheme 6.12** Hydrogenation of complex **6.7a** with no substrate present.

The resulting $^{31}$P{$^1$H} NMR spectrum gave two doublets at 21.6 ppm (60%, $^1J_{P,Rh}$ = 115 Hz) and 2.4 ppm (40%, $^1J_{P,Rh}$ = 147 Hz), which were assigned to complexes **6.8** and **6.7a** respectively (Scheme 6.12). The *cis*-[RhH$_2$S$_2$(**L$_{6.1}$**)$_2$][OTf] complex (**6.8**) was assigned based on the following observations: (a) the small $^1J_{P,Rh}$ value of 115 Hz is indicative of a Rh(III) species; (b) a hydride signal was observed in the $^1$H NMR spectrum ($\delta_H$ = -23.85 ppm, dt, $^1J_{H,Rh}$ = 37 Hz, $^2J_{H,P}$ = 15 Hz) consistent with the presence of equivalent P atoms such as in complex **6.8**; (c) analogous species are common in previous NMR studies of Rh-diphos

hydrogenation catalysts.[24,55] To observe near complete conversion to complex **6.8** (*ca.* 90%), the reaction time had to be extended to 4 h. These studies show that cod* is considerably more stable to hydrogenation that its achiral analogue, cod. This can be attributed to the rigidity and pre-organisation of cod*, which leads to the cod* being bound more strongly to the metal centre (see Section 6.2.1).

Upon addition of 1 equiv. of cod* to complex **6.8** (generated as above), 50% of **6.8** was converted to *cis*-[RhS$_2$(**L$_{6.1}$**)$_2$][OTf] (**6.9**, Scheme 6.13). The $^{31}$P{$^1$H} NMR spectrum of complex **6.9** showed a broad doublet ($w_{1/2} \approx 40$ Hz) at 31.4 ppm with a large $^1J_{P,Rh}$ value of 206 Hz. This is consistent with a Rh(I) species containing ligands with a low *trans* influence (*e.g.* solvent molecules) *trans* to the P-donor.[56] The reason for the broadness of the signal is unknown. The presence of only 50% of this complex also supported this assignment since only 1 equiv. of cod* was added.

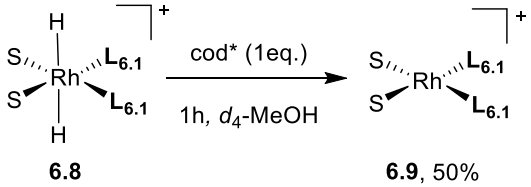


**6.8** **6.9**, 50%

**Scheme 6.13** Synthesis of *cis*-[RhS$_2$(**L$_{6.1}$**)$_2$][OTf] (**6.9**).

Complex **6.9** readily formed (Scheme 6.13), suggesting that cod* can be easily hydrogenated under these conditions; this seems to be at odds with the studies described above. Due to the sterically demanding coordinated cod*, it is possible that the conversion of complex **6.7a** to **6.8** is very slow, but once complex **6.8** forms the cod* readily displaces the labile solvent molecules and hydrogenation of the diene ensues rapidly.

### 6.4.2 Addition of substrate

To investigate the species formed *in situ* upon the addition of substrate, 6 equiv. of MAA was added to complex **6.8** in MeOH and left to react for 1 h (Scheme 6.14). Complex **6.8** was synthesised as above (Scheme 6.12), but the reaction was left for 6 h to allow for complete conversion.

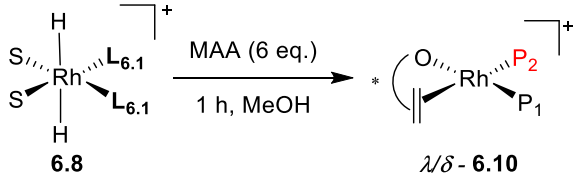


**6.8** $\lambda/\delta$ - **6.10**

**Scheme 6.14** Synthesis of complex **6.10**.

The resulting $^{31}P\{^{1}H\}$ NMR spectrum gave predominantly (*ca.* 70%) two sets of doublets of doublets in a 2:1 ratio, consistent with the presence of two closely related products (Figure 6.11). The two *anti*-conformers of the *cis*-[Rh($\kappa_2$-MAA)($\mathbf{L_{6.1}}$)$_2$][OTf] complex (**6.10**) were assigned as the products based on the following observations: (a) the small $^{2}J_{P,P}$ values of *ca.* 40 Hz are consistent with a *cis* geometry; (b) the large $^{1}J_{P,Rh}$ values of *ca.* 155 Hz are typical of Rh(I) species; (c) two diastereomers of complex **6.10** would be expected since MAA is pro-chiral, $\delta$-(*R*)/ $\lambda$-(*S*) and $\delta$-(*S*)/ $\lambda$-(*R*) (**C** and **D** in Scheme 6.15).

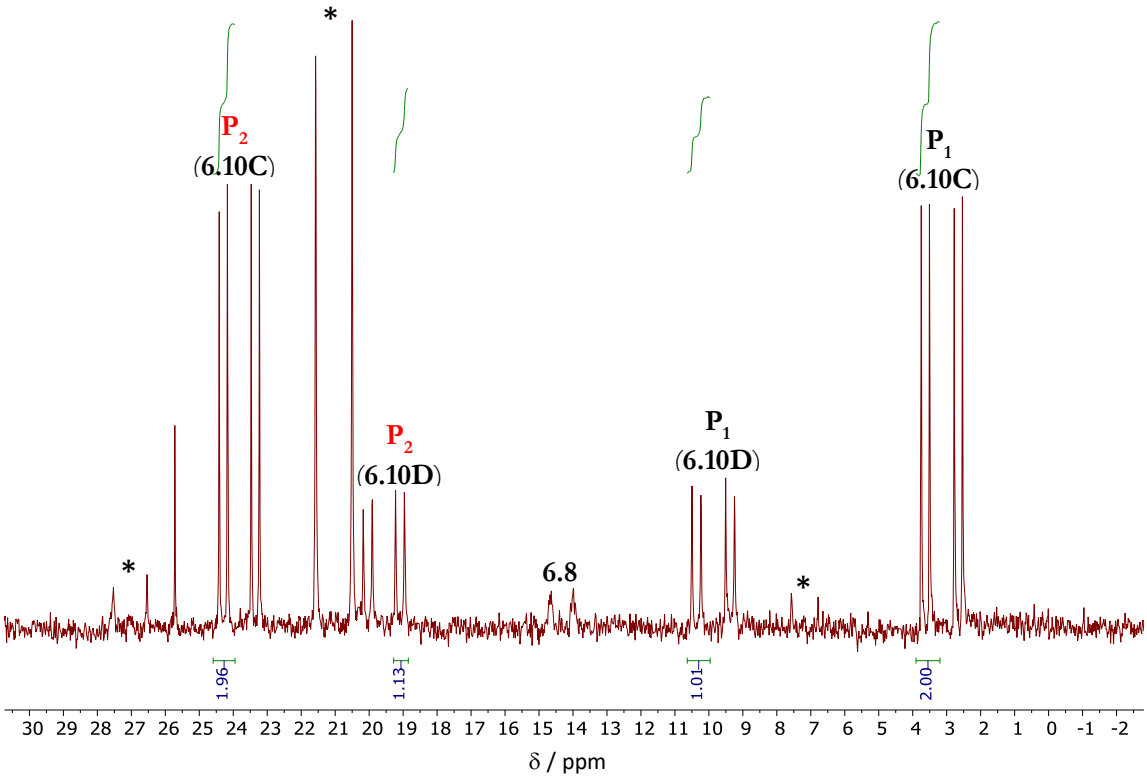


**Figure 6.11** $^{31}P\{^{1}H\}$ NMR of the reaction of MAA and complex **6.8** in MeOH. ***** = unidentified Rh complexes.

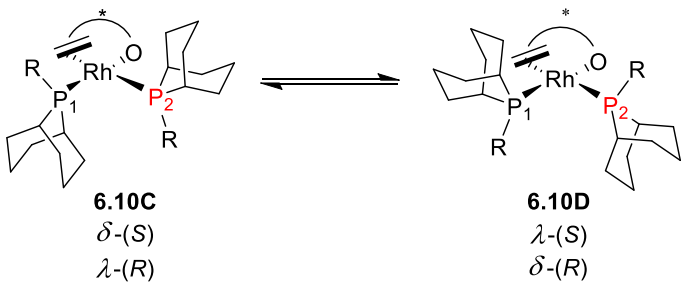


**Scheme 6.15** Fluxionality displayed by the *anti*-conformers of complex **6.10**.

### 6.4.3 Conclusions of NMR studies and relation to catalysis

The following conclusions can be drawn from the NMR studies above. As discussed in Section 6.4.1, the hydrogenation of the catalyst precursor *cis*-[Rh(cod*)($\mathbf{L_{6.1}}$)$_2$]$^+$ (**6.7a**) to generate the catalytically active species, *cis*-[RhH$_2$S$_2$($\mathbf{L_{6.1}}$)$_2$]$^+$ (**6.8**) and *cis*-[RhS$_2$($\mathbf{L_{6.1}}$)$_2$]$^+$ (**6.9**), is very slow; the conversion of **6.7a** to **6.8** reached only 90% completion within 4 h, even under forcing conditions (45 bar of $H_2$, 298 K). Hence, when catalysis was carried out at -20 °C full recovery of precursor **6.7a** was observed (> 99% by $^{31}$P{$^1$H} NMR spectroscopy). Coordinated cod* appears to be significantly more resistant to hydrogenation than its achiral analogue, cod. This may be as a consequence of the increased strength of the Rh-cod* binding resulting from the preorganised rigid structure of cod* and/or the effective large steric bulk of cod* inhibiting the approach of $H_2$ for oxidative addition.

Despite this, 66% conversion using complex **6.7a*** was observed at -20 °C after 1 h. The question then arises of what the catalyst is in this instance, the following hypotheses have been suggested:

a) Complex *cis*-[Rh((*S*,*S*)-cod*)($\mathbf{L_{6.1}}$)$_2$]$^+$ (**6.7a***) itself may be the catalyst, undergoing oxidative addition to give [RhH$_2$((*S*,*S*)-cod*)($\mathbf{L_{6.1}}$)$_2$]$^+$. The cod* is then substituted by MAA and complex **6.7a*** is reformed at the end of the catalysis by recoordination of the non-hydrogenated cod*. This is considered unlikely since it has been shown that cod* is rapidly hydrogenated by *cis*-[RhH$_2$S$_2$($\mathbf{L_{6.1}}$)$_2$]$^+$ (**6.8**) and an *ee* of greater than zero would be expected.
b) A small amount of *cis*-[Rh((*S*,*S*)-cod*)($\mathbf{L_{6.1}}$)$_2$]$^+$ (**6.7a***) is hydrogenated to give *cis*-[RhH$_2$S$_2$($\mathbf{L_{6.1}}$)$_2$]$^+$ (**6.8**) which is extremely active, so even at low levels the observed conversion is achieved. The amount of **6.8** present would have to be undetectable by $^{31}$P NMR spectroscopy (< 1%) and (as above) an *ee* of greater than zero would be expected.
c) Another species 'X' is responsible for the catalysis, where 'X' does not have any coordinated P-ligands (*e.g.* colloidal Rh), gives a very broad $^{31}$P{$^1$H} signal (*e.g.* a fluxional or paramagnetic complex) or is extremely active at low concentrations (*e.g.* a monophos complex, such as [RhH$_2$S$_3$($\mathbf{L_{6.1}}$)]$^+$).

The monophos complex is considered to be the most plausible hypothesis since it easily accounts for the zero *ee* observed, and further experimental studies also support this. The

formation of a monophos complex may be promoted by the increased steric hindrance of cod* relative to cod.

At higher temperatures, conversion of *cis*-[Rh(cod*)($\mathbf{L_{6.1}}$)$_2$]$^+$ (**6.7a**) to catalytically active species **6.8** was observed. Scheme 6.16 shows the suggested pathway for the hydrogenation of *cis*-[Rh(cod*)(PhobPR)$_2$]$^+$ complexes. Zero *ee* was observed at higher temperatures because of the lack of optical stability of either or both *cis*-[RhH$_2$S$_2$($\mathbf{L_{6.1}}$)$_2$]$^+$ (**6.8**) and *cis*-[RhS$_2$($\mathbf{L_{6.1}}$)$_2$]$^+$ (**6.9**) intermediates (Scheme 6.16). If this epimerisation were slow relative to MAA hydrogenation, which should be possible at low temperatures, an *ee* would be expected. For the reasons above, this seems a forlorn hope for the cod* complexes discussed herein due to their resistance to hydrogenation at low temperatures.

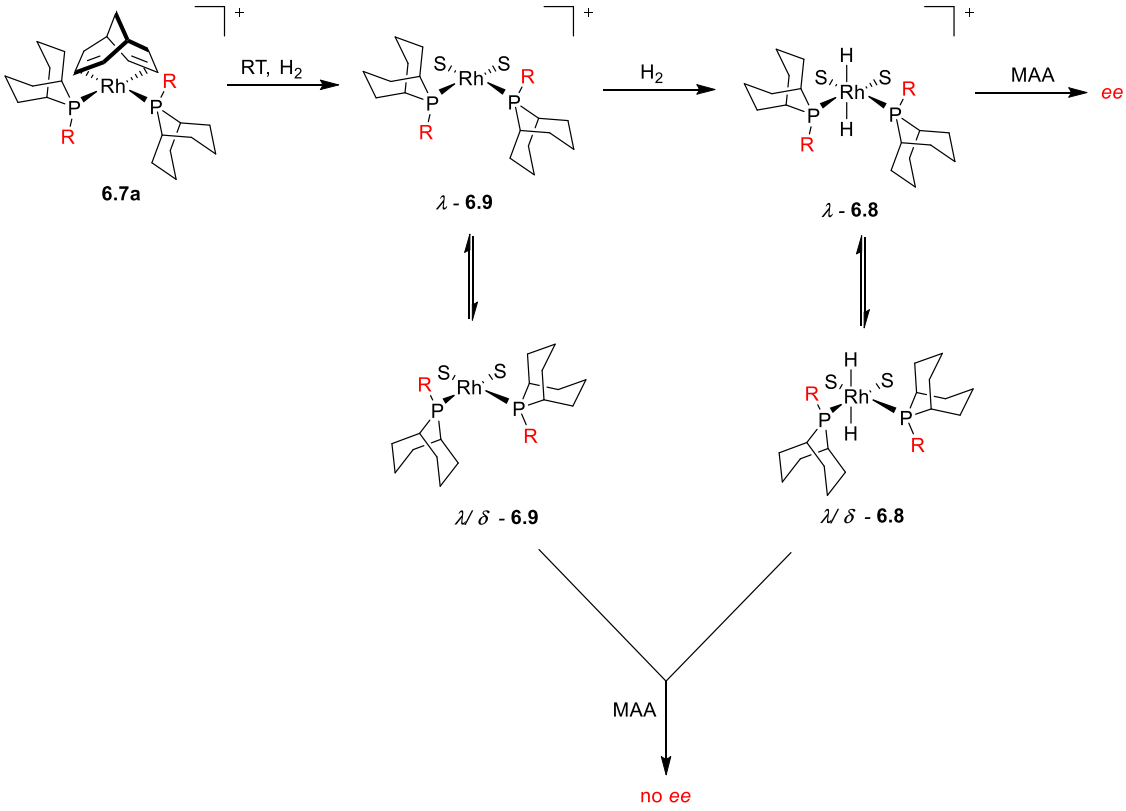


**Scheme 6.16** Suggested pathway for the hydrogenation of complex **6.7a** and the epimerisation of intermediates **6.8** and **6.9**, R = *i*Bu.

## 6.5 Conclusions and future work

A series of complexes of the type [Rh(cod*)$L_2$][OTf] (**6.7a**-**e**), where L = $\mathbf{L_{6.1\text{-}6.5}}$, has been successfully synthesised. The $^{31}P\{^1H\}$ NMR spectra of the complexes confirmed the expectation that two diastereomeric *anti*-conformations ($\delta$ and $\lambda$) would exist and showed that a resolution of up to 96% was achieved using the chiral diene, cod*. The crystal structures of complexes **6.7a**-**b** showed a surprisingly small P-Rh-P angle, relative to the values in the achiral cod analogues; this was attributed to the higher steric bulk of cod* resulting from its preorganised rigid structure. Kinetic data for the epimerisation of complex **6.7a** showed the process was first order.

The enantiopure complex, *cis*-[Rh((*S*,*S*)-cod*)($\mathbf{L_{6.1}}$)$_2$][OTf] (**6.7a***), was tested in the asymmetric hydrogenation of MAA and MAC. Despite the use of low temperatures (-20 °C) no enantioselectivity was observed. To prevent complex epimerisation the temperature was further decreased to -40 °C, but no conversion was detected. NMR studies of the hydrogenation catalysis showed that hydrogenation of the catalyst precursor *cis*-[Rh(cod*)($\mathbf{L_{6.1}}$)$_2$]$^+$ (**6.7a**) was sluggish, despite forcing conditions (45 bar $H_2$, 4 h, 298 K). This was attributed to the increased strength of the Rh-cod* binding. No enantioselectivity was observed at ambient temperature due to the lack of optical stability of either or both of the catalytically active intermediates, *cis*-[$RhH_2S_2$($\mathbf{L_{6.1}}$)$_2$]$^+$ (**6.8**) and *cis*-[$RhS_2$($\mathbf{L_{6.1}}$)$_2$]$^+$ (**6.9**) (Section 6.4.3), under the reaction conditions.

In order to induce enantioselectivity, complex **6.7a*** should be a more active hydrogenation catalyst. The catalysis should then proceed at low enough temperatures to prevent epimerisation of the *anti*-conformers and preserve optical activity. Therefore, the replacement of cod* with a less bulky chiral diene should be considered in the future, for example, chiral norbornadiene ((*S*,*S*)-nbd*, **6.11**) reported by van der Eycken or (*R*,*R*)-bod* (**6.12**) reported by Hayashi.[57,58]

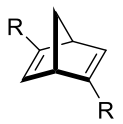


**6.11**


**6.12**

## 6.6 References


1 J. A. Osborn, F. H. Jardine, J. F. Young and G. Wilkinson, *J. Chem. Soc. A*, 1966, 1711–1732.

2 W. S. Knowles and M. J. Sabacky, *Chem. Commun.*, 1968, 1445–1446.

3 H. Buthe, H. Siegel and L. Horner, *Angew. Chem., Int. Ed.*, 1968, **7**, 942.

4 P. Etayo and A. Vidal-Ferran, *Chem. Soc. Rev*, 2013, **42**, 728–754.

5 W. Tang and X. Zhang, *Chem. Rev.*, 2003, **103**, 3029–3069.

6 W. Zhang, Y. Chi and X. Zhang, *Acc. Chem. Res.*, 2007, **40**, 1278–1290.

7 G. Erre, S. Enthaler, K. Junge, S. Gladiali and M. Beller, *Coord. Chem. Rev.*, 2008, **252**, 471–491.

8 H. Fernandez-Perez, P. Etayo, A. Panossian and A. Vidal-Ferran, *Chem. Rev.*, 2011, **111**, 2119–2176.

9 J. M. Brown, *Organometallics*, 2014, **33**, 5912–5923.

10 O. I. Kolodiazhnyi, *Phosphorus, Sulfur and Silicon*, 2014, **189**, 1102–1131.

11 B. D. Vineyard, W. S. Knowles, M. J. Sabacky, G. L. Bachman and D. J. Weinkauff, *J. Am. Chem. Soc.*, 1977, **99**, 5946–5952.

12 H. B. Kagan and T. Dang, *J. Am. Chem. Soc.*, 1972, **672**, 6429–6433.

13 H. B. Kagan, N. Langlois, E. Tuan and P. Dang, *J. Organomet. Chem.*, 1975, **90**, 353–365.

14 A. Miyashita, A. Yasuda, H. Takaya, K. Toriumi, T. Ito, T. Souchi and R. Noyori, *J. Am. Chem. Soc.*, 1980, **102**, 7932–7934.

15 A. Miyashita and H. Takaya, *Tetrahedron*, 1984, **40**, 1245–1253.

16 R. Noyori, M. Ohta, M. Kitamura, T. Ohta and H. Takaya, *J. Am. Chem. Soc.*, 1986, **108**, 7117–7119.

17 M. J. Burk, *J. Am. Chem. Soc.*, 1991, **113**, 8518–8519.

18 M. J. Burk, *Acc. Chem. Res.*, 2000, **33**, 363–372.

19 A. Gillon, K. Heslop, D. J. Hyett, A. Martorell, A. G. Orpen, P. G. Pringle, C. Claver and E. Fernandez, *Chem. Commun.*, 2000, **2**, 961–962.

20 M. T. Reetz and G. Mehler, *Angew. Chem., Int. Ed.*, 2000, **39**, 3889–3890.

21 M. van den Berg, A. J. Minnaard, E. P. Schudde, J. van Esch, H. M. de Vries, J. de Vries and B. L. Feringa, *Tetrahedron*, 2000, 11539–11540.

22 M. T. Reetz and T. Sell, *Tetrahedron Lett.*, 2000, **41**, 6333–6336.

23 M. T. Reetz, G. Mehler, A. Meiswinkel and T. Sell, *Tetrahedron Lett.*, 2002, **43**, 7941–7943.

24 I. D. Gridnev and T. Imamoto, *Acc. Chem. Res.*, 2004, **37**, 633–644.

25 T. Imamoto, in *Hydrogenation*, IntechOpen., 2012, pp. 3–30.

26 J. G. de Vries and C. J. Elsevier, in *The Handbook of Homogeneous Hydrogenation*, Wiley-VCH, 2007, pp. 3–27.

27 M. D. Fryzuk and B. Bosnich, *J. Am. Chem. Soc.*, 1977, **99**, 6262–6267.

28 R. G. Ball and N. C. Payne, *Inorg. Chem.*, 1977, **16**, 1187–1191.

29 H. Brunner, A. Winter and J. Breu, *J. Organomet. Chem.*, 1998, **553**, 285–306.

30 W. S. Knowles, *Acc. Chem. Res.*, 1983, **16**, 106–112.

31 A. Borner, in *Phosphorus Ligands in Asymmetric Catalysis*, Wiley-VCH, 2008, pp. 99–113.

32 I. D. Gridnev, N. Higashi, K. Asakura and T. Imamoto, *J. Am. Chem. Soc.* , 2000, **122**, 7183–7194.

33 M. D. Fryzuk and B. Bosnich, *J. Am. Chem. Soc.* , 1978, **100**, 5491–5494.

34 K. Mikami, K. Aikawa, Y. Yusa, J. J. Jodry and M. Yamanaka, *Synlett*, 2002, 1561–1578.

35 G. H. Christie and J. J. Kenner, *J. Chem. Soc.*, 1922, **121**, 614.

36 P. J. Walsh, A. E. Lurain and J. Balsells, *Chem. Rev.*, 2003, **103**, 3297–3344.

37 I. Otero and A. Borner, in *Phosphorus Ligands in Asymmetric Catalysis*, 2008, pp. 307–329.

38 K. Aikawa and K. Mikami, *Chem. Commun.*, 2012, **48**, 11050–11069.

39 J. M. Crawford and M. S. Sigman, *Synth.*, 2019, **51**, 1021–136.

40 M. Ueki, *Angew. Chem. Int. Ed. Engl.*, 2000, **112**, 3532–3556.

41 K. Mikami and M. Yamanaka, *Chem. Rev.*, 2003, **103**, 3369–3400.

42 C. Defieber, H. Grützmacher and E. M. Carreira, *Angew. Chem., Int. Ed.*, 2008, **47**, 4482–4502.

43 T. Punniyamurthy, M. Mayr, A. S. Dorofeev, C. J. R. Bataille, S. Gosiewska, B. Nguyen, A. R. Cowley and J. M. Brown, *Chem. Commun.*, 2008, 5092–5094.

44 J. I. van der Vlugt and J. N. H. Reek, in *Phosphorus (III) Ligands in Homogeneous Catalysis*, eds. P. C. J. Kamer and P. W. N. M. van Leeuwen, Wiley-VCH, 2012, pp. 427–447.

45 J. M. Lister, M. Carreira, M. F. Haddow, A. Hamilton, C. L. McMullin, A. G. Orpen, P. G. Pringle and T. E. Stennett, *Organometallics*, 2014, **33**, 702–714.

46 J. M. Lister, *PhD Thesis*, 2013, University of Bristol.

47 J. L. van Winkle, S. Lorenzo, R. C. Morris and R. F. Mason, *US Patent*, 1969, US 3420898.

48 P. N. Bungu and S. Otto, *Dalton Trans.*, 2007, 2876–2884.

49 H. C. L. Abbenhuis, U. Burckhardt, V. Gramlich, C. Kollner, P. Pregosin, R. Salzmann and A. Togni, *Oragnometallics*, 1995, **14**, 759–766.

50 J. H. Downing, V. Gee and P. G. Pringle, *Chem. Commun.*, 1997, 1527–1528.

51 A. Bright, B. E. Mann, C. Masters, B. L. Shaw, R. M. Slade and R. E. Stainbank, *J. Am. Chem. Soc. A*, 1971, 1826.

52 B. L. Shaw, *J. Organomet. Chem.*, 1980, **200**, 307–318.

53 G. Mislin and M. Miesch, *Eur. J. Org. Chem.*, 2001, 1753–1759.

54 M. Mayr, C. J. R. Bataille, S. Gosiewska, J. A. Raskatov and J. M. Brown, *Tetrahedron Asymmetry*, 2008, **19**, 1328–1332.

55 I. D. Gridnev and T. Imamoto, *Chem. Commun.*, 2009, 7447–7464.

56 J. A. Iggo, *NMR Spectroscopy in Inorganic Chemistry*, Oxford University Press, 1999.

57 T. Noel, K. Vandyck and J. van der Eycken, *Tetrahedron*, 2007, **63**, 12961–12967.

58 N. Tokunaga, Y. Otomaru, K. Okamoto, K. Ueyama, R. Shintani and T. Hayashi, *J. Am. Chem. Soc.*, 2004, **126**, 13584–13585.

# Chapter 7

# Experimental

## 7.1 General considerations

Unless otherwise stated, all reactions were carried out using standard Schlenk line techniques or glove-box techniques under an atmosphere of dry $N_2$ or Ar using oven-dried glassware (200 °C). Toluene, THF, $CH_2Cl_2$, $Et_2O$, hexane and MeCN were collected from a Grubbs type solvent system and deoxygenated by three successive freeze-pump-thaw cycles and stored over 3 Å or 4 Å molecular sieves, which had been previously activated under reduced pressure ($10^{-2}$ Torr) at 200 °C for 18 h. Chlorobenzene was dried over $CaH_2$, distilled and deoxygenated by three successive freeze-pump-thaw cycles and stored over 4 Å molecular sieves. MeOH and pentane were purchased as anhydrous and degassed by bubbling with $N_2$ for 30 min and stored over 3 Å and 4 Å molecular sieves respectively. Xylene, $CD_2Cl_2$, $CDCl_3$, $C_6D_6$ and *d*$_8$-THF were dried over activated 4 Å molecular sieves and deoxygenated by three successive freeze-pump-thaw cycles.

The following reagents were distilled prior to use: $SiMe_3Cl$, $PCl_3$, *o*-phenylene chlorophosphite, *t*$Bu_2PCl$ and $Cy_2PCl$. $NEt_3$ was dried over $CaH_2$, distilled and deoxygenated by three successive freeze-pump-thaw cycles and stored over 4 Å molecular sieves. All dihydroxyarenes and diols were dissolved in toluene before use and the volatiles were then removed under reduced pressure; this was repeated twice to remove $H_2O$. $[Mo(CO)_4(nbd)]$ was dissolved in $CH_2Cl_2$ and filtered through florisil. 1-hexene was purified by passing it through a short alumina column. The following reagents were prepared by the author according to literature methods: 3,6-di-*tert*-butylcatechol,[1] 2,7-di-*methyl*-1,8-naphthalenediol[2] and *rac*-/(*S*,*S*)-cod*.[3] The following reagents were prepared according to the literature: $[PtCl_2(cod)]$,[4] $[PtMe_2(cod)]$,[5] $[Pt(nbe)_3]$,[6] $[PdCl_2(NCPh)_2]$,[7] *s*-PhobPH[8] and ligands $\mathbf{L}_{6.1\text{-}6.5}$.[9] All other reagents were purchased from commercial sources and used without further purification.

All NMR spectra were recorded on a Jeol ECP (Eclipse) 300, Jeol ECS 300, Varian 400-MR, or Jeol ECS 400 spectrometer at ambient temperature unless otherwise stated. Chemical shifts were referenced to residual solvent ($^{1}$H and $^{13}$C), 85% $H_3PO_4$ ($^{31}$P) and $CFCl_3$ ($^{19}$F). The external reference used for $^{195}$Pt was the absolute frequency 21.4 MHz (for TMS 1H = 100MHz). Mass spectra were carried out by the University of Bristol Spectrometry Service on a VG Analytical Autospec (EI) or VG Analytical Quattro (ESI) spectrometer. Crystal structures were determined by the University of Bristol Crystallography Service, using a Bruker APEX II or Bruker AXS Microstar diffractometer (see Appendix for more details). Infra-red spectroscopy was carried out on a Perkin Elmer Spectrum One FT-IR Spectrometer.

## 7.2 Chapter 2

### 7.2.1 Synthesis of 2.6a

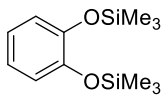


A solution of catechol (0.400 g, 3.63 mmol) in THF (20 mL) was cooled to -78 °C and *n*BuLi (5.00 mL, 7.99 mmol, 1.6 M in hexanes) was added dropwise over 10 min. The reaction mixture was then allowed to warm to ambient temperature and stirred for a further 2 h. $SiMe_3Cl$ (1.01 mL, 7.99 mmol) was then added dropwise over 10 min and the reaction mixture stirred for 20 h. The volatiles were removed under reduced pressure and the residue was dissolved in toluene (20 mL). The suspension was filtered, and the solid washed with toluene (3 x 10 mL). The volatiles were removed under reduced pressure to yield the crude product. Purification by distillation (70 °C, 0.5 Torr) gave the product as a colourless oil (0.786 g, 85%). $^{1}$H NMR (400 MHz, $CDCl_3$): $\delta_H$ (ppm) 6.86 (m, 4H, ArC*H*), 0.28 (s, $^{1}J_{H,C}$ = 119 Hz, 18H, Si(C$H_3$)$_3$). $^{13}$C{$^{1}$H} NMR (101 MHz, $CDCl_3$): $\delta_C$ (ppm) 124.8 (s, Ar*C*O), 122.0 (s, Ar*C*H), 121.3 (s, Ar*C*H), 0.5 (s, $^{1}J_{C,Si}$ = 60 Hz, Si(*C*$H_3$)$_3$). $^{1}$H and $^{13}$C{$^{1}$H} NMR data agreed with the literature data.[10]

### 7.2.2 Synthesis of 2.6b

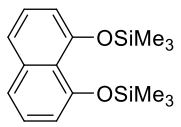


A solution of 1,8-dihydroxynaphthalene (2.00 g, 12.5 mmol) in THF (35 mL) was cooled to -78 °C and *n*BuLi (17.2 mL, 27.5 mmol, 1.6 M in hexanes) was added dropwise over 10 min. The reaction mixture was then allowed to warm to ambient temperature and stirred for a further 2 h. $SiMe_3Cl$ (3.49 mL, 27.5 mmol) was then added dropwise over 10 min and the reaction mixture stirred for 20 h. The volatiles were removed under reduced pressure and the residue was dissolved in toluene (30 mL). The suspension was filtered, and the solid washed with toluene (3 x 15

mL). The volatiles were removed under reduced pressure to yield the crude product. Purification by Kugelruhr distillation (110 °C, 1 x$10^{-6}$ Torr) gave the product as a colourless oil (2.72 g, 72%). $^{1}$H NMR (400 MHz, $CDCl_3$): $\delta_H$ (ppm) 7.41 (d, $J_{H,H}$ = 8.1 Hz, 2H, ArC*H*), 7.27 (t, $J_{H,H}$ = 7.8 Hz, 2H, ArC*H*), 6.80 (d, $J_{H,H}$ = 7.4 Hz, 2H, ArC*H*), 0.27 (s, $^{1}J_{H,C}$ = 118.9 Hz, 18H, Si(C$H_3$)$_3$). $^{13}$C{$^{1}$H} NMR (101 MHz, $CDCl_3$): $\delta_C$ (ppm) 152.0 (s, Ar*C*O), 138.0 (s, Ar*C*), 126.0 (s, Ar*C*H), 122.6 (s, Ar*C*), 121.9 (s, Ar*C*H), 116.2 (s, Ar*C*H), 0.7 (s, $^{1}J_{C,Si}$ = 60 Hz, Si(*C*H$_3$)$_3$). HR-MS (EI): m/z calcd. for $C_{16}H_{24}O_2Si_2$ $[M]^+$ = 304.1315; obs. = 304.1309.

### 7.2.3 Synthesis of 2.6c

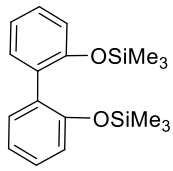


A solution of 2,2'-dihydroxybiphenyl (0.100 g, 0.536 mmol) in THF (10 mL) was cooled to -78 °C and *n*BuLi (0.737 mL, 1.18 mmol, 1.6 M in hexanes) was added dropwise over 10 min. The reaction mixture was then allowed to warm to ambient temperature and stirred for a further 2 h. $SiMe_3Cl$ (1.50 mL, 1.18 mmol) was then added dropwise over 10 min and the reaction mixture stirred for 20 h. The volatiles were removed under reduced pressure and the residue was dissolved in toluene (10 mL). The suspension was filtered, and the solid washed with toluene (3 x 5 mL). The volatiles were removed under reduced pressure to yield the crude product. Purification by distillation (110 °C, 0.5 Torr) gave the product as a yellow oil (0.101 g, 57%). $^{1}$H NMR (400 MHz, $CDCl_3$): $\delta_H$ (ppm) 7.31-7.18 (m, 4H, ArC*H*), 7.00 (m, 2H, ArC*H*), 6.88 (dd, $J_{H,H}$ = 8.1, 1.2 Hz, 2H, ArC*H*), 0.08 (s, 18H, Si(C$H_3$)$_3$). $^{13}$C{$^{1}$H} NMR (101 MHz, $CDCl_3$): $\delta_C$ (ppm) 153.2 (s, Ar*C*O), 132.0 (s, Ar*C*H), 131.0 (s, Ar*C*), 128.3 (s, Ar*C*H), 120.8 (s, Ar*C*H), 119.7 (s, Ar*C*H), 0.4 (s, Si(*C*H$_3$)$_3$). $^{1}$H and $^{13}$C{$^{1}$H} NMR data agreed with the literature data.[11]

### 7.2.4 Synthesis of 2.6d

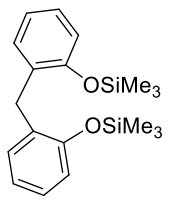


A solution of bis(2-hydroxyphenyl)methane (1.50 g, 7.49 mmol) in THF (30 mL) was cooled to -78 °C and *n*BuLi (10.3 mL, 16.5 mmol, 1.6 M in hexanes) was added dropwise over 10 min. The reaction mixture was then allowed to warm to ambient temperature and stirred for a further 2 h. $SiMe_3Cl$ (2.09 mL, 16.5 mmol) was then added dropwise over 10 min and the reaction mixture stirred for 20 h. The volatiles were removed under reduced pressure and the residue was dissolved in toluene (25 mL). The suspension was filtered, and the solid washed with toluene (3 x 15 mL). The volatiles were removed under reduced

pressure to yield the crude product. Purification by Kugelruhr distillation (170 °C, 0.1 Torr) gave the product as a colourless oil (1.82 g, 71%). $^{1}$H NMR (400 MHz, $CDCl_3$): $\delta_H$ (ppm) 7.10 (td, $J_{H,H}$ = 7.7, 1.9 Hz, 2H, ArC*H*), 7.01 (dd, $J_{H,H}$ = 7.6, 1.9 Hz, 2H, ArC*H*), 6.88 (td, $J_{H,H}$ = 6.9, 1.3 Hz, 2H, ArC*H*), 6.82 (dd, $J_{H,H}$ = 8.0, 1.3 Hz, 2H, ArC*H*), 3.91 (s, 2H, C$H_2$), 0.25 (s, 18H, Si(C$H_3$)$_3$). $^{13}$C{$^{1}$H} NMR (101 MHz, $CDCl_3$): $\delta_C$ 153.7 (s, Ar*C*O), 131.7 (s, Ar*C*), 130.9 (s, Ar*C*H), 127.0 (s, Ar*C*H), 121.3 (s, Ar*C*H), 118.8 (s, Ar*C*H), 30.7 (s, *C*H$_2$), 0.6 (s, $^{1}J_{C,Si}$ = 60 Hz, Si(*C*H$_3$)$_3$). HR-MS (ESI): m/z calcd. for $C_{19}H_{28}NaO_2Si_2$ $[M+Na]^+$ = 367.1520; obs. = 367.1527.

**General procedure for the synthesis of the *t*Bu substituted silyl ethers (2.6e-f)**

A solution of the dihydroxyarene (0.200 g, 0.900 mmol) in THF (8 mL) was cooled to -78 °C and *n*BuLi (1.24 mL, 1.98 mmol, 1.6 M in hexanes) was added dropwise over 10 min. The reaction mixture was then allowed to warm to ambient temperature and stirred for a further 2 h. $SiMe_3Cl$ (0.251 mL, 1.98 mmol) was then added dropwise over 10 min and the reaction mixture stirred for 20 h. The volatiles were removed under reduced pressure and the residue was dissolved in toluene (10 mL). The suspension was filtered, and the solid washed with toluene (3 x 10 mL). The volatiles were removed under reduced pressure to yield the crude product. For the synthesis of **2.6f**, the 3,6-di-*tert*-butylcatechol was synthesised according to a modified literature.[1]

### 7.2.5 Synthesis of 2.6e

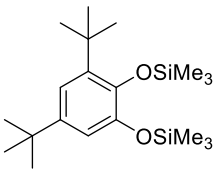


Purification by Kugelruhr distillation (100 °C, 0.1 Torr) gave the product as a white solid (0.249 g, 82%). $^{1}$H NMR (400 MHz, $CDCl_3$): $\delta_H$ (ppm) 6.93 (s, 1H, ArC*H*), 6.82 (s, 1H, ArC*H*), 1.39 (s, 9H, C(C$H_3$)$_3$) 1.30 (s, 9H, C(C$H_3$)$_3$), 0.38 (s, 9H, OSi(C$H_3$)$_3$), 0.32 (s, 9H, OSi(C$H_3$)$_3$). $^{13}$C{$^{1}$H} NMR (101 MHz, $CDCl_3$): $\delta_C$ (ppm) 145.1 (s, Ar*C*), 142.5 (s, Ar*C*), 142.1 (s, Ar*C*), 140.2 (s, Ar*C*), 116.1 (s, Ar*C*H), 114.2 (s, Ar*C*H), 35.3 (s, *C*(CH$_3$)$_3$), 34.4 (s, *C*(CH$_3$)$_3$), 31.7 (s, C(*C*H$_3$)$_3$), 30.2 (s, C(*C*H$_3$)$_3$), 2.4 (s, $^{1}J_{C,Si}$ = 61 Hz, Si(*C*H$_3$)$_3$), 1.2 (s, $^{1}J_{C,Si}$ = 60 Hz, Si(*C*H$_3$)$_3$). HR-MS (EI): m/z calcd. for $C_{20}H_{38}O_2Si_2$ $[M+H]^+$ = 367.2410; obs. = 367.2434. $^{1}$H NMR data agreed with the literature data.[12]

### 7.2.6 Synthesis of 2.6f

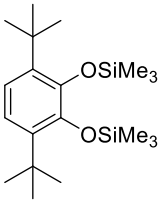


Purification by Kugelruhr distillation (100 °C, 0.1 Torr) gave the product as a pale green oil (0.221 g, 83%). $^{1}$H NMR (400 MHz, $CDCl_3$): $\delta_H$ (ppm) 6.80 (s, 2H, ArC*H*), 1.36 (s, 18H, C(C*H*$_3$)$_3$), 0.18 (s, 18H, Si(C*H*$_3$)$_3$). $^{13}$C{$^{1}$H} NMR (101 MHz, $CDCl_3$): $\delta_C$ (ppm) 146.6 (s, Ar*C*O), 138.8 (s, Ar*C*), 118.9 (s, Ar*C*H), 34.7 (s, *C*(CH$_3$)$_3$), 31.1 (s, C(*C*H$_3$)$_3$), 1.6 (s, $^{1}J_{C,Si}$ = 60 Hz, Si(*C*H$_3$)$_3$). HR-MS (EI): m/z calcd. for $C_{20}H_{38}O_2Si_2$ $[M+H]^+$ = 367.2410; obs. = 367.2427.

### 7.2.7 Synthesis of 2.5b (from dihydroxyarene)

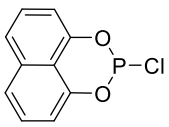


A solution of 1,8-dihydroxynaphthalene (1.47 g, 9.20 mmol) in toluene (50 mL) was added dropwise to a mixture of $PCl_3$ (4.01 mL, 46.0 mmol) and $NEt_3$ (2.82 mL, 20.2 mmol) in toluene (15 mL) at -78 °C. The reaction mixture was gradually warmed to ambient temperature and stirred for 20 h. The reaction mixture was filtered, and the solid washed with toluene (3 x 15 mL). The volatiles were removed under reduced pressure to yield the product as a pale yellow solid (1.71 g, 83%). $^{31}$P{$^{1}$H} NMR (162 MHz, $C_6D_6$): $\delta_P$ (ppm) 132.9 (s). $^{1}$H NMR (400 MHz, $C_6D_6$): $\delta_H$ (ppm) 7.13 (d, $J_{H,H}$ = 8.2 Hz, 2H, ArC*H*), 6.91 (t, $J_{H,H}$ = 8.0 Hz, 2H, ArC*H*), 6.71 (d, $J_{H,H}$ = 7.6 Hz, 2H, ArC*H*). $^{31}$P{$^{1}$H} and $^{1}$H NMR data agreed with the literature data.[13]

### 7.2.8 Synthesis of 2.5c (from dihydroxyarene)

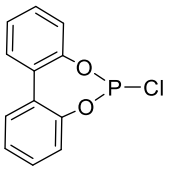


A solution of 2,2'-dihydroxybiphenyl (2.00 g, 10.7 mmol) in toluene (60 mL) was added dropwise to a mixture of $PCl_3$ (4.69 mL, 53.7 mmol) and $NEt_3$ (3.29 mL, 23.6 mmol) in toluene (15 mL) at -78 °C. The reaction mixture was gradually warmed to ambient temperature and stirred for 20 h. The reaction mixture was filtered, and the solid washed with toluene (3 x 15 mL). The volatiles were removed under reduced pressure to yield the product as a pale yellow oil (2.36 g, 87%). $^{31}$P{$^{1}$H} NMR (162 MHz, $C_6D_6$): $\delta_P$ (ppm) 179.7 (s). $^{1}$H NMR (400 MHz, $C_6D_6$): $\delta_H$ (ppm) 7.07 (dd, $J_{H,H}$ = 7.2, 1.8 Hz, 2H, ArC*H*), 6.94 (m, 4H, ArC*H*), 6.89 (m, 2H, ArC*H*). $^{31}$P{$^{1}$H} and $^{1}$H NMR data agreed with the literature data.[14]

### 7.2.9 Synthesis of 2.5a (from silyl ether 2.6a)

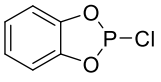


To a solution of **2.6a** (0.125 g, 0.491 mmol) in MeCN (2 mL) was added $PCl_3$ (0.428 mL, 4.91 mmol). The reaction mixture was stirred until completion (2 h), as identified by $^{31}$P{$^{1}$H} NMR spectroscopy. The volatiles were

removed under reduced pressure to yield the product as a pale yellow solid (0.0860 g, 99%). $^{31}P\{^{1}H\}$ NMR (162 MHz, $C_6D_6$): $\delta_P$ (ppm) 174.4 (s). $^{1}H$ NMR (400 MHz, $C_6D_6$): $\delta_H$ (ppm) 6.73 (m, 2H, ArC*H*), 6.55 (m, 2H, ArC*H*). $^{31}P\{^{1}H\}$ and $^{1}H$ NMR data agreed with the literature data.[15]

### 7.2.10 Synthesis of 2.5b (from silyl ether 2.6b)

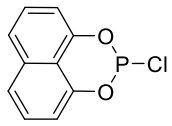

To a solution of **2.6b** (2.38 g, 7.80 mmol) in MeCN (40 mL) was added $PCl_3$ (6.81 mL, 78.0 mmol). The reaction mixture was heated at 60 °C until completion (20 h), as identified by $^{31}P\{^{1}H\}$ NMR spectroscopy. The volatiles were removed under reduced pressure to yield the product as a white solid (1.68 g, 96%). $^{31}P\{^{1}H\}$ NMR (162 MHz, $C_6D_6$): $\delta_P$ (ppm) 133.0 (s). $^{1}H$ NMR (400 MHz, $C_6D_6$): $\delta_H$ (ppm) 7.14 (d, $J_{H,H}$ = 8.3 Hz, 2H, ArC*H*), 6.92 (t, $J_{H,H}$ = 8.0 Hz, 2H, ArC*H*), 6.71 (d, $J_{H,H}$ = 7.6 Hz, 2H, ArC*H*). $^{31}P\{^{1}H\}$ and $^{1}H$ NMR data agreed with the literature data.[13]

### 7.2.11 Synthesis of 2.5c (from silyl ether 2.6c)

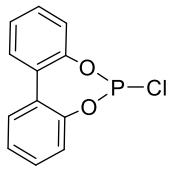

To a solution of **2.6c** (0.100 g, 0.303 mmol) in MeCN (2 mL) was added $PCl_3$ (0.264 mL, 3.03 mmol). The reaction mixture was stirred until completion (3 h), as identified by $^{31}P\{^{1}H\}$ NMR spectroscopy. The volatiles were removed under reduced pressure to yield the product as a pale-yellow oil (0.0770 g, 99%). $^{31}P\{^{1}H\}$ NMR (162 MHz, $C_6D_6$): $\delta_P$ (ppm) 179.5 (s). $^{1}H$ NMR (400 MHz, $C_6D_6$): $\delta_H$ (ppm) 7.48 (dd, $J_{H,H}$ = 7.6, 1.6 Hz, 2H, ArC*H*), 7.37 (m, 4H, ArC*H*), 7.38 (dd, $J_{H,H}$ = 8.0, 0.8 Hz, 2H, ArC*H*). $^{31}P\{^{1}H\}$ and $^{1}H$ NMR data agreed with the literature data.[14]

### 7.2.12 Synthesis of 2.5d (from silyl ether 2.6d)

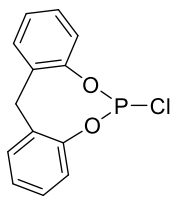

To a solution of **2.6d** (1.82 g, 5.28 mmol) in MeCN (25 mL) was added $PCl_3$ (4.61 mL, 52.8 mmol). The reaction mixture was heated at 50 °C for 48 h. The volatiles were then removed under reduced pressure. To ensure complete conversion of the dichlorophosphorus intermediate, the isolated crude product was redissolved in MeCN (20 mL) and heated at 60 °C for 20 h. Upon completion of the reaction as identified by $^{31}P\{^{1}H\}$ NMR spectroscopy, the volatiles were removed under reduced pressure to yield the product as a white solid (1.35 g, 95%). $^{31}P\{^{1}H\}$ NMR (162 MHz, $C_6D_6$): $\delta_P$ (ppm) 125.7 (s), -0.7 (s, 7% hydrolysis). $^{31}P\{^{1}H\}$ NMR data agreed with the literature data.[16] $^{1}H$ NMR (400 MHz, $C_6D_6$): $\delta_H$ (ppm)

6.88 (d, $J_{H,H}$ = 7.4 Hz, 2H, ArC*H*), 6.75 (m, 6H, ArC*H*), 4.24 (d, $^2J_{H,H}$ = 13.2 Hz, 1H, C$H_2$), 3.01 (d, $^2J_{H,H}$ = 13.0 Hz, 1H, C$H_2$), contained signals for 7% hydrolysis product. $^{13}C\{^1H\}$ NMR (101 MHz, $C_6D_6$): $\delta_C$ (ppm) 150.3 (d, $^2J_{C,P}$ = 15 Hz, Ar*C*O), 134.5 (s, Ar*C*), 130.1 (s, Ar*C*H), 127.8 (s, Ar*C*H), 125.9 (s, Ar*C*H), 123.7 (s, Ar*C*H), 33.8 (s, *C*$H_2$).

### 7.2.13 Synthesis of 2.5e (from silyl ether 2.6e)

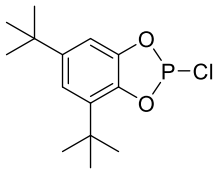


To a solution of **2.6e** (1.30 g, 3.54 mmol) in MeCN (30 mL) was added $PCl_3$ (1.55 mL, 17.7 mmol). The reaction mixture was stirred at 40 °C for 24 h. Upon completion, as identified by $^{31}P\{^1H\}$ NMR spectroscopy, the volatiles were removed under reduced pressure to yield the product as a clear oil (0.742 g, 75%). $^{31}P\{^1H\}$ NMR (162 MHz, $C_6D_6$): $\delta_P$ (ppm) 172.1 (s, >97%). $^{31}P\{^1H\}$ NMR data fitted with the literature data.[17] $^1H$ NMR (400 MHz, $C_6D_6$): $\delta_H$ (ppm) 7.08 (s, 1H, ArC*H*), 7.00 (s, 1H, ArC*H*), 1.31 (s, 9H, C(C$H_3$)$_3$), 1.07 (s, 9H, C(C$H_3$)$_3$). $^{13}C\{^1H\}$ NMR (101 MHz, $C_6D_6$): $\delta_C$ (ppm) 147.8 (s, Ar*C*), 145.0 (d, $^2J_{C,P}$ = 7 Hz, Ar*C*O), 144.9 (d, $^2J_{C,P}$ = 7 Hz, Ar*C*O), 140.5 (s, Ar*C*), 118.4 (s, Ar*C*H), 109.7 (s, Ar*C*H), 35.0 (s, *C*(CH$_3$)$_3$), 34.7 (s, *C*(CH$_3$)$_3$), 31.6 (s, C(*C*H$_3$)$_3$), 29.7 (s, C(*C*H$_3$)$_3$). HR-MS (EI): m/z calcd. for $C_{14}H_{20}ClO_2P$ $[M]^+$ = 286.0889; obs. = 286.0889.

### 7.2.14 Synthesis of 2.5f (from silyl ether 2.6f)

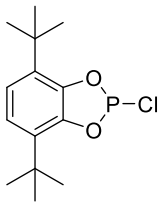


To a solution of **2.6f** (0.927 g, 2.53 mmol) in MeCN (20 mL) was added $PCl_3$ (1.10 mL, 12.6 mmol). The reaction mixture was stirred at 40 °C for 24 h, which was gradually increased to 70 °C after 2 days. After 6 days, volatiles were removed under reduced pressure; MeCN (15 mL) and $PCl_3$ (1.10 mL, 12.6 mmol) were then added to the residue. 24 h later, the volatiles were removed under reduced pressure to yield the product as a yellow oil (contained 15% of **2.6f'**). $^{31}P\{^1H\}$ NMR (162 MHz, $C_6D_6$): $\delta_P$ (ppm) 167.3 (s, 92%), 166.0 (s, 1%), -25.3 (s, 7%, P(V) hydrolysis). $^{31}P\{^1H\}$ NMR data fitted with the literature data.[1,18] $^1H$ NMR (400 MHz, $C_6D_6$): $\delta_H$ (ppm) 7.03 (s, 2H, ArC*H*), 1.41 (s, 18H, C(C$H_3$)$_3$). $^{13}C\{^1H\}$ NMR (101 MHz, $C_6D_6$): $\delta_C$ (ppm) 142.5 (d, $^2J_{C,P}$ = 8 Hz, Ar*C*O), 135.5 (s, Ar*C*), 120.9 (s, Ar*C*H), 118.5 (s), 29.7 (s, C(*C*H$_3$)$_3$), 29.5 (s, *C*(CH$_3$)$_3$). $^1H$ and $^{13}C\{^1H\}$ NMR spectra contained signals for **2.6f'**.

### 7.2.15 Synthesis of 2.5g (from dihydroxyarene)

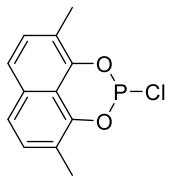

A solution of 2,7-dimethylnapthalene-1,8-diol[2] (0.388 g, 2.06 mmol) in toluene (15 mL) was added dropwise to a mixture of $PCl_3$ (1.80 mL, 20.6 mmol) and $NEt_3$ (0.632 mL, 4.53 mmol) in toluene (10 mL) at -78 °C. The reaction mixture was gradually warmed to ambient temperature and stirred for 20 h. The reaction mixture was filtered, and the solid washed with toluene (3 x 10 mL). The volatiles were removed under reduced pressure to yield the product as a pale yellow solid (0.420 g, 81%). $^{31}P\{^1H\}$ NMR (162 MHz, $C_6D_6$): $\delta_P$ (ppm) 132.7 (s, 7%, mono-Me product), 132.3 (s, 93%). $^1H$ NMR (400 MHz, $C_6D_6$): $\delta_H$ (ppm) 7.09 (d, $J_{H,H}$ = 8.3 Hz, 2H, ArC*H*), 6.81 (d, $J_{H,H}$ = 8.4 Hz, 2H, ArC*H*), 2.05 (s, 6H, C$H_3$). $^{13}C\{^1H\}$ NMR (101 MHz, $C_6D_6$): $\delta_C$ (ppm) 140.2 (d, $^2J_{C,P}$ = 5 Hz, Ar*C*O), 132.6 (d, $^3J_{C,P}$ = 2 Hz, Ar*C*), 129.5 (s, Ar*C*H), 123.0 (s, Ar*C*H), 122.5 (d, $J_{C,P}$ = 2 Hz, Ar*C*), 116.9 (d, $J$ = 15 Hz, Ar*C*), 15.0 (s, *C*$H_3$).

### 7.2.16 Synthesis of $L_{2.1}$

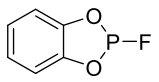

A solution of **2.5a** (4.50 g, 25.2 mmol) in $Et_2O$ (10 mL) was added to a suspension of $SbF_3$ (9.01 g, 50.4 mmol) in $Et_2O$ (10 mL). The reaction mixture was stirred at ambient temperature for 20 h. The resultant mixture was fractionated by vacuum distillation (0.1 Torr) using cooling baths at -20 °C, -40 °C and -78 °C. The traps at -20 °C and -40 °C contained clear oils, which upon NMR analysis were found to be pure $\mathbf{L_{2.1}}$ (1.45 g, 73%). $^{31}P\{^1H\}$ NMR (162 MHz, $C_6D_6$): $\delta_P$ (ppm) 124.3 (d, $^1J_{P,F}$ = 1306 Hz). $^{19}F\{^1H\}$ NMR (377 MHz, $C_6D_6$): $\delta_F$ (ppm) -37.2 (d, $^1J_{F,P}$ = 1306 Hz). $^1H$ NMR (400 Hz, $C_6D_6$): $\delta_H$ (ppm) 7.21 (dd, $J_{H,H}$ = 6.0, 3.4 Hz, 2H, ArC*H*), 7.09 (dd, $J_{H,H}$ = 6.0, 3.4 Hz, 2H, ArC*H*). $^{31}P\{^1H\}$, $^{19}F\{^1H\}$ and $^1H$ NMR data agreed with the literature data.[19]

### 7.2.17 Synthesis of $L_{2.2}$

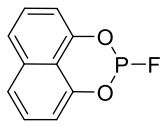

A solution of **2.5b** (1.10 g, 4.90 mmol) in toluene (15 mL) was added to a suspension of $SbF_3$ (1.75 g, 9.80 mmol) in toluene (15 mL). The reaction mixture was stirred at ambient temperature until completion and then passed through a short silica column which was washed with toluene (3 x 10 mL). The solvent was removed under reduced pressure to yield the product as a colourless oil (0.560 g, 55%). $^{31}P\{^1H\}$ NMR (162 MHz, $C_6D_6$): $\delta_P$ (ppm) 100.6 (d, $^1J_{P,F}$ = 1241 Hz). $^{19}F\{^1H\}$

NMR (377 MHz, $C_6D_6$): $\delta_F$ (ppm) -52.7 (d, $^1J_{F,P}$ = 1241 Hz). $^1$H NMR (400 MHz, $C_6D_6$): $\delta_H$ (ppm) 7.11 (d, $J_{H,H}$ = 8.4 Hz, 2H, ArC*H*), 6.91 (t, $J_{H,H}$ = 7.9 Hz, 2H, ArC*H*), 6.69 (d, $J_{H,H}$ = 7.6 Hz, 2H, ArC*H*). $^{13}$C{$^1$H} NMR (101 MHz, $C_6D_6$): $\delta_C$ (ppm) 142.6 (s, Ar*C*O), 134.9 (s, Ar*C*), 127.3 (s, Ar*C*H), 122.9 (s, Ar*C*H), 116.3 (d, $^2J_{C,P}$ = 16 Hz, Ar*C*), 112.2 (s, Ar*C*H). HR-MS (EI): m/z calcd. for $C_{10}H_6FO_2P$ $[M]^+$ = 208.0089; obs. = 208.0087.

### 7.2.18 Synthesis of $L_{2.3}$

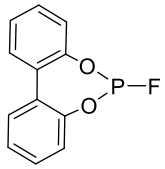

A solution of **2.5c** (2.36 g, 10.0 mmol) in toluene (30 mL) was added to a suspension of $SbF_3$ (3.58 g, 20.0 mmol) in toluene (20 mL). The reaction mixture was stirred at ambient temperature until completion and then passed through a short silica column which was washed with toluene (3 x 15 mL). The solvent was removed under reduced pressure to yield the product as a white solid (1.54 g, 66%). $^{31}$P{$^1$H} NMR (162 MHz, $C_6D_6$): $\delta_P$ (ppm) 135.8 (d, $^1J_{P,F}$ = 1309 Hz). $^{31}$P{$^1$H} data agreed with the literature data.[20] $^{19}$F{$^1$H} NMR (377 MHz, $C_6D_6$): $\delta_F$ (ppm) -52.4 (d, $^1J_{F,P}$ = 1309 Hz). $^1$H NMR (400 MHz, $C_6D_6$): $\delta_H$ (ppm) 7.39 (dd, $J_{H,H}$ = 7.6, 1.8 Hz, 2H, ArC*H*), 7.30 (td, $J_{H,H}$ = 7.7, 1.8 Hz, 2H, ArC*H*), 7.27-7.22 (m, 2H, ArC*H*), 7.13 (dt, $J_{H,H}$ = 7.9, 1.2 Hz, 2H, ArC*H*). $^{13}$C{$^1$H} NMR (101 MHz, $C_6D_6$): $\delta_C$ (ppm) 148.5 (m, Ar*C*O), 131.2 (d, $^3J_{C,P}$ = 3 Hz, Ar*C*), 130.4 (s, Ar*C*H), 129.6 (s, Ar*C*H), 126.0 (s, Ar*C*H), 122.3 (s, Ar*C*H).

### 7.2.19 Synthesis of $L_{2.4}$

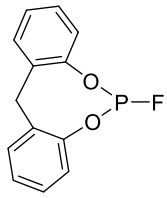

A solution of **2.5d** (1.75 g, 6.61 mmol) in toluene (25 mL) was added to a suspension of $SbF_3$ (2.36 g, 13.2 mmol) in toluene (15 mL). The reaction mixture was stirred at ambient temperature until completion and then passed through a short silica column which was washed with toluene (3 x 15 mL). The solvent was removed under reduced pressure to yield the product as a colourless oil (1.20 g, 73%). $^{31}$P{$^1$H} NMR (162 MHz, $C_6D_6$): $\delta_P$ (ppm) 107.8 (d, $^1J_{P,F}$ = 1254 Hz). $^{19}$F{$^1$H} NMR (377 MHz, $C_6D_6$): $\delta_F$ (ppm) -62.2 (d, $^1J_{F,P}$ = 1254 Hz, >96%). $^1$H NMR (400 MHz, $C_6D_6$): $\delta_H$ (ppm) 6.88 (d, $J_{H,H}$ = 7.3 Hz, 2H, ArC*H*), 6.77 (m, 6H, ArC*H*), 4.02 (d, $^2J_{H,H}$ = 13.6 Hz, 1H, C$H_2$), 3.31 (d, $^2J_{H,H}$ = 13.7 Hz, 1H, C$H_2$). $^{13}$C{$^1$H} NMR (101 MHz, $C_6D_6$): $\delta_C$ (ppm) 148.5 (t, $J$ = 7 Hz, Ar*C*O), 133.7 (d, $^3J_{C,P}$ = 2 Hz, Ar*C*), 130.2 (s, Ar*C*H), 128.4 (s, Ar*C*H), 125.7 (s, Ar*C*H), 122.9 (d, $J_{C,P}$ = 2 Hz, Ar*C*H), 34.4 (s, *C*$H_2$). HR-MS (MALDI): m/z calcd. for $C_{13}H_{10}FO_2P$ $[M+H]^+$ = 249.0475; obs. = 249.0481.

### 7.2.20 Synthesis of $L_{2.5}$

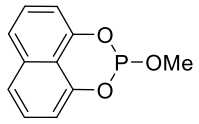

$NEt_3$ (0.31 mL, 2.2 mmol) was added to a solution of MeOH (90 μL, 2.2 mmol) in toluene (8 mL). This reaction mixture was then added dropwise over 10 min to a solution of **2.5b** (0.250 g, 1.11 mmol) in toluene (10 mL) at -78 °C. After 30 min at -78 °C, the reaction mixture was passed through a short silica column and the silica was then washed with toluene (3 x 10 mL). The volatiles were removed under reduced pressure to yield the product as a white solid (0.201 g, 82%). $^{31}P\{^1H\}$ NMR (162 MHz, $C_6D_6$): $\delta_P$ (ppm) 113.9 (s). $^{31}P\{^1H\}$ data agreed with the literature data.[21] $^{31}P$ NMR (162 MHz, $C_6D_6$): $\delta_P$ (ppm) 113.9 (q, $^3J_{P,H}$ = 12 Hz). $^1H$ NMR (400 MHz, $C_6D_6$): $\delta_H$ (ppm) 7.13 (d, $J_{H,H}$ = 7.7 Hz, 2H, ArC*H*), 6.99 (t, $J_{H,H}$ = 8.0 Hz, 2H, ArC*H*), 6.79 (d, $J_{H,H}$ = 7.5 Hz, 2H, ArC*H*), 3.16 (d, $^3J_{H,P}$ = 11.5 Hz, 3H, O(C$H_3$)). $^{13}C\{^1H\}$ NMR (101 MHz, $C_6D_6$): $\delta_C$ (ppm) 145.2 (d, $^2J_{C,P}$ = 4 Hz, Ar*C*O), 135.5 (d, $^3J_{C,P}$ = 2 Hz, Ar*C*), 127.5 (s, Ar*C*H), 122.3 (s, Ar*C*H), 117.3 (m, Ar*C*), 112.1 (s, Ar*C*H), 50.1 (d, $^2J_{C,P}$ = 13 Hz, $^2J_{H,C}$ = 146.1 Hz, O(*C*$H_3$)). HR-MS (ESI): m/z calcd. for $C_{11}H_{10}O_3P$ $[M+H]^+$ = 221.0368; obs. = 221.0360.

### 7.2.21 Synthesis of $L_{2.6}$

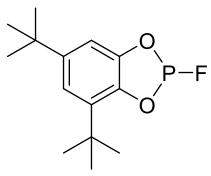

A solution of **2.5e** (0.742 g, 2.59 mmol) in toluene (20 mL) was added to a suspension of $SbF_3$ (1.85 g, 10.4 mmol) in toluene (10 mL). The reaction mixture was stirred at ambient temperature until completion and then passed through a short silica column which was washed with toluene (3 x 10 mL). The solvent was removed under reduced pressure to yield the product as a cloudy white oil (0.559 g, 80%). $^{31}P\{^1H\}$ NMR (162 MHz, $C_6D_6$): $\delta_P$ (ppm) 123.4 (d, $^1J_{P,F}$ = 1292 Hz, >97%). $^{19}F\{^1H\}$ NMR (377 MHz, $C_6D_6$): $\delta_F$ (ppm) -36.5 (d, $^1J_{F,P}$ = 1292 Hz). $^1H$ NMR (400 Hz, $C_6D_6$): $\delta_H$ (ppm) 7.11 (s, 1H, ArC*H*), 7.05 (s, 1H, ArC*H*), 1.38 (s, 9H, C(C$H_3$)$_3$), 1.17 (s, 9H, C(C$H_3$)$_3$). $^{13}C\{^1H\}$ NMR (101 MHz, $C_6D_6$): $\delta_C$ (ppm) 147.2 (s, Ar*C*), 144.4 (d, $^2J_{C,P}$ = 7 Hz, Ar*C*O), 139.9 (d, $^2J_{C,P}$ = 7 Hz, Ar*C*O), 136.0 (s, Ar*C*), 117.9 (s, Ar*C*H), 109.0 (s, Ar*C*H), 35.0 (s, *C*(CH$_3$)$_3$), 34.7 (s, *C*(CH$_3$)$_3$), 31.7 (s, C(*C*H$_3$)$_3$), 29.7 (s, C(*C*H$_3$)$_3$). HR-MS (MALDI): m/z calcd. for $C_{14}H_{20}O_2P$ $[M-F]^+$ = 251.1195; obs. = 251.1199.

### 7.2.22 Synthesis of $L_{2.7}$

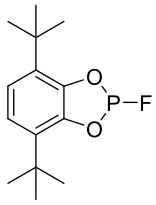

A solution of **2.5f** (0.725 g, 2.53 mmol) in toluene (20 mL) was added to a suspension of $SbF_3$ (1.81 g, 10.1 mmol) in toluene (10 mL). The reaction mixture was stirred at ambient temperature until completion and then passed through a short silica column which was washed with toluene (3 x 10 mL). The solvent was removed under reduced pressure to yield the product as a colourless oil (0.512 g, 75%); the product contained 15% **2.6f'**. $^{31}P\{^1H\}$ NMR (162 MHz, $C_6D_6$): $\delta_P$ (ppm) 119.3 (d, $^1J_{P,F}$ = 1286 Hz, 93%), -24.9 (s, 7%, P(V) hydrolysis). $^{19}F\{^1H\}$ NMR (377 MHz, $C_6D_6$): $\delta_F$ (ppm) -37.0 (d, $^1J_{F,P}$ = 1286 Hz, 97%). $^1H$ NMR (400 MHz, $C_6D_6$): $\delta_H$ (ppm) 6.86 (s, 2H, ArC*H*), 1.35 (s, 18H, C(C*H*$_3$)$_3$). HR-MS (MALDI): m/z calcd. for $C_{14}H_{20}O_2P$ $[M-F]^+$ = 251.1195; obs. = 251.1201.

### 7.2.23 Synthesis of $L_{2.8}$

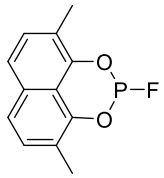

A solution of **2.5g** (0.420 g, 1.66 mmol) in toluene (10 mL) was added to a suspension of $SbF_3$ (0.594 g, 3.33 mmol) in toluene (10 mL). The reaction mixture was stirred at ambient temperature until completion and then passed through a short silica column which was washed with toluene (3 x 10 mL). Volatiles were removed under reduced pressure to yield the product as a white semi-solid (0.294 g, 75%). Crystals suitable for analysis by single crystal X-ray diffraction were grown by slow evaporation of a saturated toluene solution of $\mathbf{L_{2.8}}$. Contained 7% of the mono-Me product. $^{31}P\{^1H\}$ NMR (162 MHz, $C_6D_6$): $\delta_P$ (ppm) 100.9 (d, $^1J_{P,F}$ = 1235 Hz), 100.8 (d, $^1J_{P,F}$ = 1237 Hz, 7%, mono-Me product). $^{19}F\{^1H\}$ NMR (376 MHz, $C_6D_6$): $\delta_F$ (ppm) -51.8 (d, $^1J_{F,P}$ = 1235 Hz), -52.5 (d, $^1J_{F,P}$ = 1237 Hz, 7%). $^1H$ NMR (400 MHz, $C_6D_6$): $\delta_H$ (ppm) 7.14 (d, $J_{H,H}$ = 8.5 Hz, 2H, ArC*H*), 6.88 (d, $J_{H,H}$ = 8.4 Hz, 2H, ArC*H*), 2.12 (s, $^1J_{H,C}$ = 12.8 Hz, 6H, C*H*$_3$). $^{13}C\{^1H\}$ NMR (101 MHz, $C_6D_6$): $\delta_C$ (ppm) 139.7 (t, $^2J_{C,P}$ = 4 Hz, Ar*C*O), 132.6 (d, $^3J_{C,P}$ = 2 Hz, Ar*C*), 129.6 (s, Ar*C*H), 122.5 (s, Ar*C*H), 121.5 (s, Ar*C*), 117.0 (s, Ar*C*), 15.1 (s, *C*H$_3$). HR-MS (MALDI): m/z calcd. for $C_{12}H_{10}FO_2P$ $[M+H]^+$ = 237.0475; obs. = 237.0469.

**Simulated NMR spectra of the fluorophosphite complexes**

For complexes **2.7**, **2.8** and **2.12**, all *J* values were calculated from |K|, |L|, |M| and |N| (determined from Equations 1-4) and the corresponding $^{31}P\{^1H\}$ NMR spectrum (see Figure 7.1 for example of the labelled $^{31}P\{^1H\}$ NMR spectrum of complex **2.8b**).

Using these values, the $^{31}P\{^{1}H\}$ and $^{19}F\{^{1}H\}$ NMR spectra were simulated in Mestrenova. The calculated *J* values are given in the experimental data below.

$$|K| = |J_{AA'} + J_{XX'}| \quad (1)$$

$$|L| = |J_{AX} - J_{AX'}| \quad (2)$$

$$|M| = |J_{AA'} - J_{XX'}| \quad (3)$$

$$|N| = |J_{AX} + J_{AX'}| \quad (4)$$

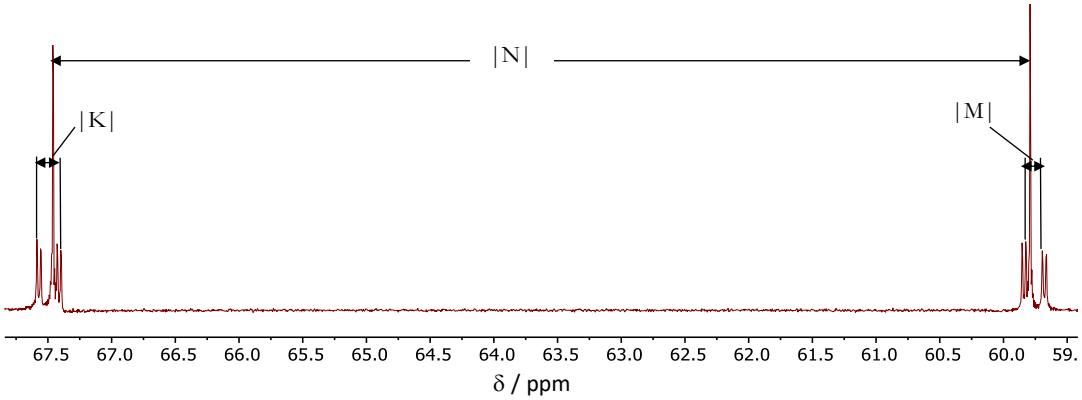


**Figure 7.1** Labelled $^{31}P\{^{1}H\}$ NMR spectrum of $[PtCl_2(\mathbf{L_{2.2}})_2]$ (**2.8b**).

**General procedure for the synthesis of *cis*-[Mo(CO)$_4$L$_2$] complexes (2.7a-h)**

To a solution of $[Mo(CO)_4(nbd)]$ (0.0200 g, 0.0670 mmol) in $CH_2Cl_2$ (0.5 mL) was added a solution of the ligand (0.133 mmol) in $CH_2Cl_2$ (0.5 mL) and stirred for 4 h.

### 7.2.24 Synthesis of *cis*-[Mo(CO)$_4$(L$_{2.1}$)$_2$] (2.7a)

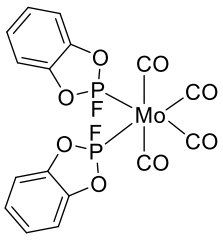


Upon completion of the reaction, the volatiles were removed under reduced pressure and the crude product was dissolved in toluene (2 mL). The volatiles were then removed under reduced pressure to yield the product as a pale-yellow solid (0.0300 g, 86%). Crystals suitable for analysis by single crystal X-ray diffraction were grown by storing a saturated hexane solution of **2.7a** at -20 °C for 48 h. $^{31}P\{^{1}H\}$ NMR (162 MHz, $CD_2Cl_2$): $\delta_P$ (ppm) 170.2 (app. dt, *N* = 1270 Hz, $^{1}J_{P,F}$ = 1271 Hz, $^{2}J_{P,P'}$ = 51 Hz, $^{4}J_{F,F'}$ = 0 Hz, $^{3}J_{P,F'}$ = -1 Hz). $^{19}F\{^{1}H\}$ NMR (377 MHz, $CD_2Cl_2$): $\delta_F$ (ppm) -0.9 (app. dt, *N* = 1270 Hz, $^{1}J_{F,P}$ = 1271 Hz, $^{2}J_{P,P'}$ = 51 Hz, $^{4}J_{F,F'}$ = 0 Hz, $^{3}J_{F',P}$ = -1 Hz). $^{1}H$ NMR (400 MHz, $CD_2Cl_2$): $\delta_H$ (ppm) 7.17 (m, 2H, ArC*H*), 7.12 (m, 2H, ArC*H*). $^{13}C\{^{1}H\}$ NMR (101 MHz, $CD_2Cl_2$): $\delta_C$ (ppm) 205.9 (m, Mo-*C*O), 202.9 (t, $^{2}J_{C,P}$ = 14 Hz, Mo-*C*O), 145.4 (d, $^{2}J_{C,P}$ = 6

Hz, Ar*C*O), 124.6 (s, Ar*C*H), 113.3 (m, Ar*C*H). HR-MS (ESI): m/z calcd. for $C_{16}H_8FMoO_8P_2$ $[M\text{-}F]^+$ = 506.8731; obs. = 506.8749. IR ($CH_2Cl_2$): ν(CO) = 2072 $cm^{-1}$.

### 7.2.25 Synthesis of *cis*-[Mo(CO)$_4$(L$_{2.2}$)$_2$] (2.7b)

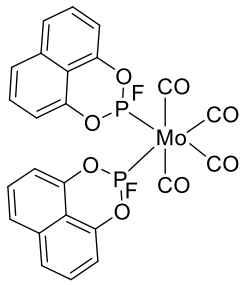

Upon completion of the reaction, the volatiles were removed under reduced pressure. The product was precipitated with hexane (2 mL). The solid was allowed to settle, and supernatant was removed; residual solvent was then removed from the solid under reduced pressure to yield the product as a pale-yellow solid (0.0270 g, 65%). Crystals suitable for analysis by single crystal X-ray diffraction were grown by slow diffusion of hexane into a saturated $CH_2Cl_2$ solution of **2.7b**. $^{31}P\{^1H\}$ NMR (162 MHz, $CD_2Cl_2$): $\delta_P$ (ppm) 144.3 (app. dt, *N* = 1194 Hz, $^1J_{P,F}$ = 1199 Hz, $^2J_{P,P'}$ = 51 Hz, $^4J_{F,F'}$ = 0 Hz, $^3J_{P,F'}$ = -5 Hz). $^{19}F\{^1H\}$ NMR (377 MHz, $CD_2Cl_2$): $\delta_F$ (ppm) -23.2 (app. dt, *N* = 1194 Hz, $^1J_{F,P}$ = 1199 Hz, $^2J_{P,P'}$ = 51 Hz, $^4J_{F,F'}$ = 0 Hz, $^3J_{F',P}$ = -5 Hz). $^1H$ NMR (400 MHz, $CD_2Cl_2$): $\delta_H$ (ppm) 7.62 (d, $J_{H,H}$ = 8.4 Hz, 2H, ArC*H*), 7.45 (m, 2H, ArC*H*), 7.06 (d, $J_{H,H}$ = 7.6 Hz, 2H, ArC*H*). $^{13}C\{^1H\}$ NMR (101 MHz, $CD_2Cl_2$): $\delta_C$ (ppm) 207.5 (m, Mo-*C*O), 204.0 (t, $^2J_{C,P}$ = 15 Hz, Mo-*C*O), 144.8 (m, Ar*C*), 135.5 (s, Ar*C*), 128.1 (s, Ar*C*H), 123.9 (s, Ar*C*H), 115.7 (d, $^2J_{C,P}$ = 16 Hz, Ar*C*O), 112.8 (s, Ar*C*H). HR-MS (ESI): m/z calcd. for $C_{24}H_{12}F_2MoO_8P_2$ $[M]^+$ = 625.9030; obs. = 625.9006. IR ($CH_2Cl_2$): ν(CO) = 2066 $cm^{-1}$.

### 7.2.26 Synthesis of *cis*-[Mo(CO)$_4$(L$_{2.3}$)$_2$] (2.7c)

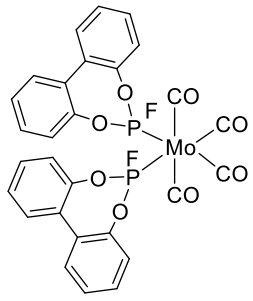

Upon completion of the reaction, the volatiles were removed under reduced pressure. Hexane (5 mL) was added, and the mixture was kept at -20 °C for 20 h. Once the product had precipitated, the solid was allowed to settle, and the supernatant was removed; residual solvent was then removed under reduced pressure from the solid to yield the product as a pale-yellow solid (0.0320 g, 71%). Crystals suitable for analysis by single crystal X-ray diffraction were grown by slow diffusion of hexane into a saturated $CH_2Cl_2$ solution of **2.7c**. $^{31}P\{^1H\}$ NMR (162 MHz, $CD_2Cl_2$): $\delta_P$ (ppm) 174.0 (app. dt, *N* = 1225 Hz, $^1J_{P,F}$ = 1227 Hz, $^2J_{P,P'}$ = 49 Hz, $^4J_{F,F'}$ = 0 Hz, $^3J_{P,F'}$ = -2 Hz). $^{19}F\{^1H\}$ NMR (377 MHz, $CD_2Cl_2$): $\delta_F$ (ppm) -21.4 (app. dt, *N* = 1225 Hz, $^1J_{F,P}$ = 1227 Hz, $^2J_{P,P'}$ = 49 Hz, $^4J_{F,F'}$ = 0 Hz, $^3J_{F',P}$ = -2 Hz). $^1H$ NMR (400 MHz, $CD_2Cl_2$): $\delta_H$ (ppm) 7.54 (d, $J_{H,H}$ = 7.6 Hz, 2H, ArC*H*), 7.41 (m, 4H, ArC*H*), 7.26 (d, $J_{H,H}$ = 7.9 Hz, 2H,

ArC*H*). $^{13}C\{^{1}H\}$ NMR (101 MHz, $CD_2Cl_2$): $\delta_C$ (ppm) 208.4 (m, Mo-*C*O), 204.9 (t, $^{2}J_{C,P}$ = 14 Hz, Mo-*C*O), 148.7 (m, Ar*C*O), 130.9 (s, Ar*C*H), 130.4 (s, Ar*C*H), 130.0 (s, Ar*C*), 127.0 (s, Ar*C*H), 122.5 (s, Ar*C*H). HR-MS (ESI): m/z calcd. for $C_{28}H_{16}F_2MoNaO_8P_2$ $[M+Na]^+$ = 700.9241; obs. = 700.9240. IR ($CH_2Cl_2$): ν(CO) = 2059 $cm^{-1}$.

### 7.2.27 Synthesis of *cis*-[Mo(CO)$_4$(L$_{2.4}$)$_2$] (2.7d)

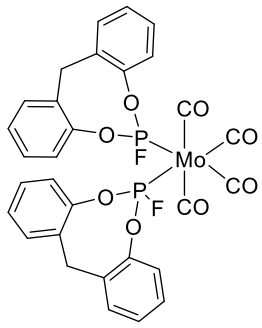


Upon completion of the reaction, the volatiles were removed under reduced pressure. The product was precipitated with hexane (2 mL). The solid was allowed to settle, and the supernatant was removed; residual solvent was then removed from the solid under reduced pressure to yield the product as a pale-yellow solid (0.0270 g, 48%). Crystals suitable for analysis by single crystal X-ray diffraction were grown by slow diffusion of hexane into a saturated $CH_2Cl_2$ solution of **2.7d**. $^{31}P\{^{1}H\}$ NMR (162 MHz, $CD_2Cl_2$): $\delta_P$ (ppm) 148.2 (app. dt, *N* = 1188 Hz, $^{1}J_{P,F}$ = 1189 Hz, $^{2}J_{P,P'}$ = 49 Hz, $^{4}J_{F,F'}$ = 0 Hz, $^{3}J_{P,F'}$ = -2 Hz). $^{19}F\{^{1}H\}$ NMR (377 MHz, $CD_2Cl_2$): $\delta_F$ (ppm) -29.3 (app. dt, *N* = 1188 Hz, $^{1}J_{F,P}$ = 1189 Hz, $^{2}J_{P,P'}$ = 49 Hz, $^{4}J_{F,F'}$ = 0 Hz, $^{3}J_{F',P}$ = -2 Hz). $^{1}H$ NMR (400 MHz, $CD_2Cl_2$): $\delta_H$ (ppm) 7.37 (d, $J_{H,H}$ = 7.3 Hz, 2H, ArC*H*), 7.22 (m, 4H, ArC*H*), 7.11 (d, $J_{H,H}$ = 7.9 Hz, 2H, ArC*H*), 4.46 (d, $^{2}J_{H,H}$ = 14.4 Hz, 1H, C$H_2$), 3.70 (d, $^{2}J_{H,H}$ = 14.5 Hz, 1H, C$H_2$). $^{13}C\{^{1}H\}$ NMR (101 MHz, $CD_2Cl_2$): $\delta_C$ (ppm) 208.3 (m, Mo-*C*O), 204.8 (m, Mo-*C*O), 149.4 (m, Ar*C*O), 132.4 (d, $^{3}J_{C,P}$ = 3 Hz, Ar*C*), 131.2 (s, Ar*C*H), 129.1 (s, Ar*C*H), 126.9 (s, Ar*C*H), 122.9 (d, $J_{C,P}$ = 3 Hz, Ar*C*H), 35.0 (s, *C*$H_2$). HR-MS (ESI): m/z calcd. for $C_{30}H_{20}F_2MoNaO_8P_2$ $[M+Na]^+$ = 728.9555; obs. = 728.9550. IR ($CH_2Cl_2$): ν(CO) = 2058 $cm^{-1}$.

### 7.2.28 Synthesis of *cis*-[Mo(CO)$_4$(L$_{2.5}$)$_2$] (2.7e)

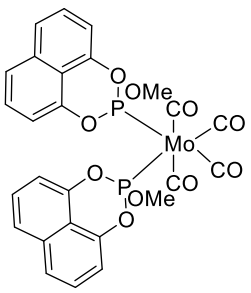


Upon completion of the reaction, the volatiles were removed under reduced pressure. The product was precipitated with hexane (2 mL). The solid was allowed to settle, and the supernatant was removed; residual solvent was then removed from the solid under reduced pressure to yield the product as a white solid (0.0290 g, 67%). Crystals suitable for analysis by single crystal X-ray diffraction were grown by storing a saturated pentane solution of **2.7e**. $^{31}P\{^{1}H\}$ NMR (162 MHz, $CD_2Cl_2$): $\delta_P$ (ppm) 151.1 (s). $^{31}P$ NMR (162 MHz, $CD_2Cl_2$): $\delta_P$ (ppm) 151.1 (m). $^{1}H$ NMR (400 MHz, $CD_2Cl_2$): $\delta_H$ (ppm) 7.55 (d, $J_{H,H}$ = 8.3 Hz, 2H, ArC*H*), 7.39 (t, $J_{H,H}$ =

8.0 Hz, 2H, ArC*H*), 6.92 (d, $J_{H,H}$ = 7.5 Hz, 2H, ArC*H*), 3.68 (m, 3H, O(C$H_3$)). $^{13}C\{^1H\}$ NMR (101 MHz, $CD_2Cl_2$): $\delta_C$ (ppm) 210.2 (m, Mo-*C*O), 206.1 (t, $^2J_{C,P}$ = 14 Hz, Mo-*C*O), 146.0 (s, Ar*C*), 135.5 (s, Ar*C*), 128.0 (s, Ar*C*H), 123.1 (s, Ar*C*H), 116.0 (s, Ar*C*), 112.5 (s, Ar*C*H), 52.7 (s, O(*C*$H_3$)). HR-MS (ESI): m/z calcd. for $C_{24}H_{19}MoO_8P_2$ $[M\text{-}2(CO)+H]^+$ = 594.9615; obs. = 594.9614. IR ($CH_2Cl_2$): ν(CO) = 2051 $cm^{-1}$.

### 7.2.29 Synthesis of *cis*-[Mo(CO)$_4$(L$_{2.6}$)$_2$] (2.7f)

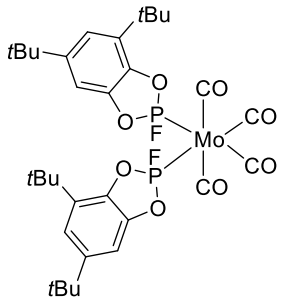


Upon completion of the reaction, the volatiles were removed under reduced pressure and the crude product was dissolved in toluene (2 mL). The volatiles were then removed under reduced pressure (8 x$10^{-6}$ Torr) to yield the product as an off-white solid. $^{31}P\{^1H\}$ NMR (162 MHz, $CD_2Cl_2$): $\delta_P$ (ppm) 168.0 (vir. dq, *N* = 1266 Hz, ≈90%), 22.5 (s, 3%, hydrolysis), -21.7 (s, 3%, P(V) hydrolysis), -22.3 (s, 5%, P(V) hydrolysis). $^{19}F\{^1H\}$ NMR (377 MHz, $CD_2Cl_2$): $\delta_F$ (ppm) -1.8 (*rac*/*meso*, app. dt, *N* = 1267 Hz, $^1J_{F,P}$ = 1267 Hz, $^2J_{P,P'}$ = 51 Hz, $^4J_{F,F'}$ = 0 Hz, $^3J_{F',P}$ = -0.4 Hz), -2.2 (*rac*/ *meso*, app. dt, *N* = 1263 Hz, $^1J_{F,P}$ = 1263 Hz, $^2J_{P,P'}$ = 51 Hz, $^4J_{F,F'}$ = 0 Hz, $^3J_{F',P}$ = -0.4 Hz). $^1H$ NMR (400 MHz, $CD_2Cl_2$): $\delta_H$ (ppm) 7.11 (m, 1H, ArC*H*, *rac*/*meso*), 7.07 (t, $J_{H,H}$ = 1.7 Hz, 1H, ArC*H*, *rac*/*meso*), 7.06 (t, $J_{H,H}$ = 1.7 Hz, 1H, ArC*H*, *rac*/*meso*), 7.03 (d, $J_{H,H}$ = 1.7 Hz, 1H, ArC*H*, *rac*/*meso*), 1.37 (br. s, 9H, C(C$H_3$)$_3$, *rac*/*meso*), 1.32 (br. s, 9H, C(C$H_3$)$_3$, *rac*/*meso*), 1.31 (m, 18H, C(C$H_3$)$_3$, *rac* and *meso*). $^{13}C\{^1H\}$ NMR (101 MHz, $CD_2Cl_2$): $\delta_C$ (ppm) 203.2 (m, Mo-*C*O *rac* and *meso*), 147.8 (d, $^2J_{C,P}$ = 8 Hz, Ar*C*O *rac* and *meso*), 145.4 (d, *J* = 4 Hz, Ar*C rac* and *meso*), 141.1 (d, $^2J_{C,P}$ = 6 Hz, Ar*C*O *rac* and *meso*), 136.0 (m, Ar*C rac* and *meso*), 118.7 (s, Ar*C*H *rac*/*meso*) 118.6 (s, Ar*C*H, *rac*/*meso*), 108.4 (m, Ar*C*H *rac* and *meso*), 35.5 (s, *C*(CH$_3$)$_3$, *rac* and *meso*), 35.0 (d, *J* = 3 Hz, *C*(CH$_3$)$_3$, *rac* and *meso*), 31.9 (d, *J* = 2 Hz C(*C*H$_3$)$_3$, *rac* and *meso*), 29.8 (s, C(*C*H$_3$)$_3$, *rac*/*meso*), 29.7 (s, C(*C*H$_3$)$_3$, *rac*/*meso*). HR-MS (ESI): m/z calcd. for $C_{32}H_{40}F_2MoO_8P_2$ $[M]^+$ = 750.1223; obs. = 750.1232. IR ($CH_2Cl_2$): ν(CO) = 2069 $cm^{-1}$.

### 7.2.30 Synthesis of *cis*-[Mo(CO)$_4$(L$_{2.7}$)$_2$] (2.7g)

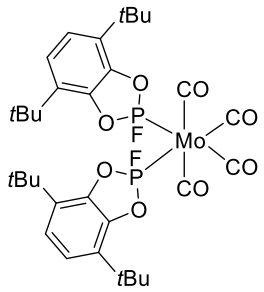

Upon completion of the reaction, the volatiles were removed under reduced pressure and the crude product was dissolved in toluene (2 mL). The volatiles were then removed under reduced pressure (8 x$10^{-6}$ Torr) to yield the product as a light brown semi-solid. Contained 15% **2.6f'** and 10% [Mo(CO)$_4$(nbd)]. $^{31}$P{$^1$H} NMR (162 MHz, $CD_2Cl_2$): $\delta_P$ (ppm) 165.9 (app. dt, *N* = 1262 Hz, $^1J_{P,F}$ = 1263 Hz, $^2J_{P,P'}$ = 51 Hz, $^4J_{F,F'}$ = 0 Hz, $^3J_{P,F'}$ = -0.4 Hz, ≈90%), -25.1 (s, 10%, P(V) hydrolysis). $^{19}$F{$^1$H} NMR (377 MHz, $CD_2Cl_2$): $\delta_F$ (ppm) -1.9 (app. dt, *N* = 1263 Hz, $^1J_{F,P}$ = 1263 Hz, $^2J_{P,P'}$ = 51 Hz, $^4J_{F,F'}$ = 0 Hz, $^3J_{F',P}$ = -0.4 Hz, 96%). $^1$H NMR (400 MHz, $CD_2Cl_2$): $\delta_H$ (ppm) 7.01 (s, 2H, ArC*H*), 1.38 (br. s, 18H, C(C*H*$_3$)$_3$). $^{13}$C{$^1$H} NMR (101 MHz, $CD_2Cl_2$): $\delta_C$ (ppm) 203.3 (t, $^2J_{C,P}$ = 15 Hz, Mo-*C*O), 143.6 (d, $^2J_{C,P}$ = 7 Hz, Ar*C*O), 134.6 (d, *J* = 5 Hz, Ar*C*), 121.3 (s, Ar*C*H), 31.5 (s, *C*(CH$_3$)$_3$), 29.8 (s, C(*C*H$_3$)$_3$). NMR spectra contain signals for **2.6f'**. HR-MS (ESI): m/z calcd. for $C_{32}H_{40}FMoO_8P_2$ $[M-F]^+$ = 731.1237; obs. = 731.1. IR ($CH_2Cl_2$): ν(CO) = 2068 cm$^{-1}$.

### 7.2.31 Synthesis of *cis*-[Mo(CO)$_4$(L$_{2.8}$)$_2$] (2.7h)

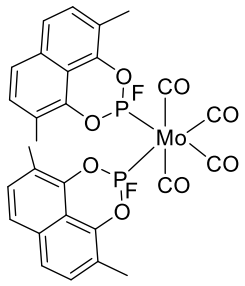

Upon completion of the reaction, the volatiles were removed under reduced pressure. The product was precipitated with hexane (2 mL). The solid was allowed to settle, and the supernatant was removed; residual solvent was then removed from the solid under reduced pressure to yield the product as a white solid (0.0328 g, 72%). Crystals suitable for analysis by single crystal X-ray diffraction were grown by slow diffusion of hexane into a saturated $CH_2Cl_2$ solution of **2.7h**. $^{31}$P{$^1$H} NMR (162 MHz, $CD_2Cl_2$): $\delta_P$ (ppm) 144.1 (app. dt, *N* = 1197 Hz, $^1J_{P,F}$ = 1200 Hz, $^2J_{P,P'}$ = 53 Hz, $^4J_{F,F'}$ = 0 Hz, $^3J_{P,F'}$ = -1 Hz). $^{19}$F{$^1$H} NMR (377 MHz, $CD_2Cl_2$): $\delta_F$ (ppm) -23.1 (app. dt, N = 1199 Hz, $^1J_{F,P}$ = 1200 Hz, $^2J_{P,P'}$ = 53 Hz, $^4J_{F,F'}$ = 0 Hz, $^3J_{F',P}$ = -1 Hz). $^1$H NMR (400 MHz, $CD_2Cl_2$): $\delta_H$ (ppm) 7.46 (d, $J_{H,H}$ = 8.4 Hz, 2H, ArC*H*), 7.25 (d, $J_{H,H}$ = 8.4 Hz, 2H, ArC*H*), 2.32 (s, 6H, C*H*$_3$). $^{13}$C{$^1$H} NMR (101 MHz, $CD_2Cl_2$): $\delta_C$ (ppm) 204.4 (m, Mo-*C*O), 141.5 (s, Ar*C*), 132.7 (s, Ar*C*), 130.0 (s, Ar*C*H), 123.2 (s, Ar*C*H), 122.2 (s, Ar*C*), 115.6 (s, Ar*C*), 15.1 (s, *C*H$_3$). HR-MS (MALDI): m/z calcd. for $C_{28}H_{20}F_2MoNaO_8P_2$ $[M+Na]^+$ = 704.9554; obs. = 704.9548. IR ($CH_2Cl_2$): ν(CO) = 2064 cm$^{-1}$.

**General procedure for the synthesis of *cis*-[$PtCl_2L_2$] complexes 2.8b-e**

To a solution of [$PtCl_2$(cod)] (0.0200 g, 0.0535 mmol) in $CH_2Cl_2$ (0.5 mL) was added a solution of the ligand (0.112 mmol) in $CH_2Cl_2$ (0.5 mL) and stirred for 4 h. Upon completion of the reaction, the volatiles were removed under reduced pressure. The product was precipitated with hexane (2 mL). The solid was allowed to settle and the supernatant removed; the remaining residue was then washed with hexane (3 x 1 mL). Residual solvent was then removed from the solid under reduced pressure to yield the product.

### 7.2.32 Synthesis of *cis*-[$PtCl_2(L_{2.2})_2$] (2.8b)

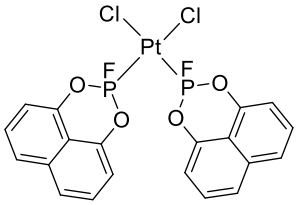


White solid (0.0220 g, 61%). $^{31}P\{^1H\}$ NMR (162 MHz, $CD_2Cl_2$): $\delta_P$ (ppm) 63.6 (AA'XX', $N$ = 1243 Hz, $^1J_{P,Pt}$ = 6172 Hz, $^1J_{P,F}$ = 1248 Hz, $^2J_{P,P'}$ = 25 Hz, $^4J_{F,F'}$ = 5 Hz, $^3J_{P,F'}$ = -5 Hz). $^{19}F\{^1H\}$ NMR (377 MHz, $CD_2Cl_2$): $\delta_F$ (ppm) -39.6 (AA'XX', $N$ = 1242 Hz, $^2J_{F,Pt}$ = 632 Hz, $^1J_{F,P}$ = 1248 Hz, $^2J_{P,P'}$ = 25 Hz, $^4J_{F,F'}$ = 5 Hz, $^3J_{F',P}$ = -5 Hz). $^1H$ NMR (400 MHz, $CD_2Cl_2$): $\delta_H$ (ppm) 7.74 (d, $J_{H,H}$ = 8.4 Hz, 2H, ArC*H*), 7.51 (t, $J_{H,H}$ = 8.1 Hz, 2H, ArC*H*), 7.13 (d, $J_{H,H}$ = 7.7 Hz, 2H, ArC*H*). $^{13}C\{^1H\}$ NMR (101 MHz, $CD_2Cl_2$): $\delta_C$ (ppm) 143.8 (m, Ar*C*O), 135.6 (s, Ar*C*), 128.4 (s, Ar*C*H), 125.4 (s, Ar*C*H), 114.4 (d, $J_{C,P}$ = 14 Hz, Ar*C*), 113.7 (m, Ar*C*H). HR-MS (ESI): m/z calcd. for $C_{20}H_{12}F_2O_4P_2ClPt$ $[M\text{-}Cl]^+$ = 646.9505; obs. = 646.9492.

### 7.2.33 Synthesis of *cis*-[$PtCl_2(L_{2.3})_2$] (2.8c)

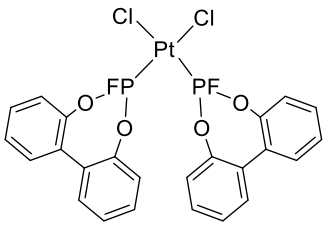


White solid. Crystals suitable for analysis by single crystal X-ray diffraction were grown by slow diffusion of hexane into a saturated $CH_2Cl_2$ solution of **2.8c**. $^{31}P\{^1H\}$ NMR (162 MHz, $CD_2Cl_2$): $\delta_P$ (ppm) 80.8 (AA'XX', $N$ = 1226 Hz, $^1J_{P,Pt}$ = 6056 Hz, $^1J_{P,F}$ = 1229 Hz, $^2J_{P,P'}$ = 22 Hz, $^4J_{F,F'}$ = 2 Hz, $^3J_{P,F'}$ = -3 Hz). $^{19}F\{^1H\}$ NMR (377 MHz, $CD_2Cl_2$): $\delta_F$ (ppm) -44.6 (AA'XX', $N$ = 1227 Hz, $^1J_{F,Pt}$ = 649 Hz, $^1J_{F,P}$ = 1229 Hz, $^2J_{P,P'}$ = 22 Hz, $^4J_{F,F'}$ = 2 Hz, $^3J_{F',P}$ = -3 Hz). $^1H$ NMR (400 MHz, $CD_2Cl_2$): $\delta_H$ (ppm) 7.50 (dd, $J_{H,H}$ = 6.8, 2.6 Hz, 2H, ArC*H*), 7.43 (m, 4H, ArC*H*), 7.64 (d, $J_{H,H}$ = 7.5 Hz, 2H, ArC*H*). $^{13}C\{^1H\}$ NMR (101 MHz, $CD_2Cl_2$): $\delta_C$ (ppm) 147.5 (d, $^2J_{C,P}$ = 148 Hz, Ar*C*O), 131.1 (s, 2 x Ar*C*H), 128.8 (s, Ar*C*), 128.2 (s, Ar*C*H), 122.3 (s, Ar*C*H). HR-MS (ESI): m/z calcd. for $C_{24}H_{16}Cl_2F_2NaO_4P_2Pt$ $[M\text{-}Na]^+$ = 755.9412; obs. = 755.9439.

### 7.2.34 Synthesis of *cis*-[$PtCl_2(L_{2.4})_2$] (2.8d)

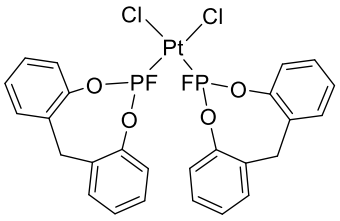

White solid (0.0340 g, 83%). $^{31}P\{^1H\}$ NMR (162 MHz, $CD_2Cl_2$): $\delta_P$ (ppm) 58.2 (AA'XX', $N$ = 1200 Hz, $^1J_{P,Pt}$ = 6209 Hz, $^1J_{P,F}$ = 1204 Hz, $^2J_{P,P'}$ = 24 Hz, $^4J_{F,F'}$ = 2 Hz, $^3J_{P,F'}$ = -4 Hz). $^{19}F\{^1H\}$ NMR (377 MHz, $CD_2Cl_2$): $\delta_F$ (ppm) -52.1 (AA'XX', N = 1197 Hz, $^2J_{F,Pt}$ = 574 Hz, $^1J_{F,P}$ = 1204 Hz, $^2J_{P,P'}$ = 24 Hz, $^4J_{F,F'}$ = 2 Hz, $^3J_{F',P}$ = -4 Hz). $^1H$ NMR (400 MHz, $CD_2Cl_2$): $\delta_H$ (ppm) 7.40 (d, $J_{H,H}$ = 6.9 Hz, 2H, ArC*H*), 7.25 (m, 6H, ArC*H*), 4.52 (d, $^2J_{H,H}$ = 14.3 Hz, 1H, C$H_2$), 3.71 (d, $^2J_{H,H}$ = 14.7 Hz, 1H, C$H_2$). $^{13}C\{^1H\}$ NMR (101 MHz, $CD_2Cl_2$): $\delta_C$ (ppm) 148.6 (d, $^2J_{C,P}$ = 13 Hz, Ar*C*O), 132.0 (s, Ar*C*), 131.4 (s, Ar*C*H), 129.7 (s, Ar*C*H), 129.1 (s, Ar*C*H), 122.4 (s, Ar*C*H), 34.1 (s, *C*$H_2$). HR-MS (ESI): m/z calcd. for $C_{26}H_{16}Cl_2FO_4P_2Pt$ [M-F-$2H_2$]$^+$ = 737.9533; obs. = 738.0.

### 7.2.35 Synthesis of *cis*-[$PtCl_2(L_{2.5})_2$] (2.8e)

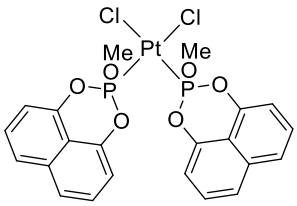

White solid (0.0260 g, 69%). Crystals suitable for analysis by single crystal X-ray diffraction were grown by slow diffusion of pentane into a saturated $CH_2Cl_2$ solution of **2.8e**. $^{31}P\{^1H\}$ NMR (162 MHz, $CD_2Cl_2$): $\delta_P$ (ppm) 62.7 (s, $^1J_{P,Pt}$ = 5869 Hz). $^{31}P$ NMR (162 MHz, $CD_2Cl_2$): $\delta_P$ (ppm) 62.7 (m, $^1J_{P,Pt}$ = 5869 Hz). $^1H$ NMR (400 MHz, $CD_2Cl_2$): $\delta_H$ (ppm) 7.66 (d, $J_{H,H}$ = 8.4 Hz, 2H, ArC*H*), 7.43 (t, $J_{H,H}$ = 8.0 Hz, 2H, ArC*H*), 6.95 (d, $J_{H,H}$ = 7.7 Hz, 2H, ArC*H*), 3.99 (m, 3H, O(C$H_3$)). $^{13}C\{^1H\}$ NMR (101 MHz, $CD_2Cl_2$): $\delta_C$ (ppm) 144.9 (vir. t, $^2J_{C,P}$ = 4Hz, Ar*C*O), 135.6 (s, Ar*C*), 128.2 (s, Ar*C*H), 124.4 (s, Ar*C*H), 114.9 (vir. t, $J$ = 7 Hz, Ar*C*), 113.3 (vir. t, $J$ = 3 Hz, Ar*C*H), 56.3 (vir. t, $^3J_{C,P}$ = 2 Hz, O(*C*$H_3$)). HR-MS (ESI): m/z calcd. for $C_{22}H_{18}Cl_2NaO_6P_2Pt$ [M+Na]$^+$ = 727.9498; obs. = 727.9496.

### General procedure for the synthesis of *cis*-[$PtCl_2L_2$] complexes 2.8f-g

To a solution of [$PtCl_2$(cod)] (0.0150 g, 0.0400 mmol) in $CH_2Cl_2$ (0.5 mL) was added a solution of the ligand (0.0220 g, 0.112 mmol) in $CH_2Cl_2$ (0.5 mL) and stirred for 4 h. Upon completion of the reaction, the volatiles were removed under reduced pressure and the crude product was dissolved in toluene (2 mL). The volatiles were then removed under reduced pressure (8 x$10^{-6}$ Torr) to yield the product.

### 7.2.36 Synthesis of *cis*-[$PtCl_2(L_{2.6})_2$] (2.8f)

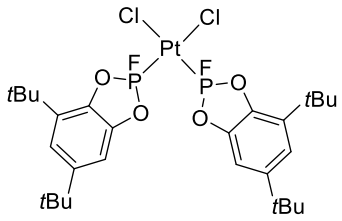

Off-white solid (0.0120 g, 37%). $^{31}P\{^1H\}$ NMR (162 MHz, $CD_2Cl_2$): $\delta_P$ (ppm) 89.9 (AA'XX', $N$ = 1306 Hz, $^1J_{P,Pt}$ = 6032 Hz, *rac/meso*), 89.0 (AA'XX', $N$ = 1310 Hz, $^1J_{P,Pt}$ = 6038 Hz, *rac/meso*). $^{19}F\{^1H\}$ NMR (377 MHz, $CD_2Cl_2$): $\delta_F$ (ppm) -21.3 (AA'XX').

### 7.2.37 Synthesis of *cis*-[$PtCl_2(L_{2.7})_2$] (2.8g)

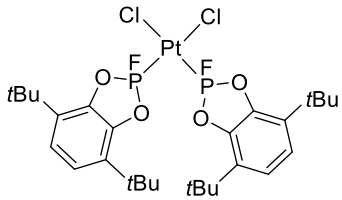

White solid. Contaminated with *ca.* 10% **2.6f'**. $^{31}P\{^1H\}$ NMR (162 MHz, $C_6D_6$): $\delta_P$ (ppm) 90.0 (AA'XX', $N$ = 1296 Hz, $^1J_{P,Pt}$ = 5947 Hz, $^1J_{P,F}$ = 1296 Hz), -24.5 (s, 5%, hydrolysis P(V)). $^{19}F\{^1H\}$ NMR (377 MHz, $C_6D_6$): $\delta_F$ (ppm) -18.3 (AA'XX', $N$ = 1296 Hz, $^2J_{F,Pt}$ = 777 Hz). $^1H$ NMR (400 MHz, $C_6D_6$): $\delta_H$ (ppm) 6.77 (s, 2H, ArC*H*), 1.25 (s, 18H, C($CH_3$)$_3$), contains signals for 10% **2.6f'**.

### 7.2.38 Synthesis of *cis*-[$PtCl_2(L_{2.8})_2$] (2.8h)

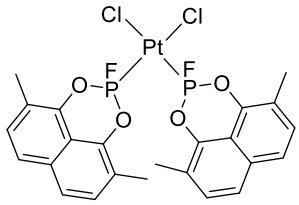

To a solution of [$PtCl_2$(cod)] (0.0200 g, 0.0535 mmol) in $CH_2Cl_2$ (0.5 mL) was added a solution of $\mathbf{L_{2.8}}$ (0.0260 g, 0.112 mmol) in $CH_2Cl_2$ (0.5 mL) and stirred for 4 h. Upon completion of the reaction, the volatiles were removed under reduced pressure. The product was precipitated with hexane (2 mL). The solid was allowed to settle and the supernatant removed; the remaining residue was then washed with hexane (3 x 1 mL). Residual solvent was then removed from the solid under reduced pressure to yield the product as a pale red solid. $^{31}P\{^1H\}$ NMR (162 MHz, $CD_2Cl_2$): $\delta_P$ (ppm) 63.8 (AA'XX', $N$ = 1238 Hz, $^1J_{P,Pt}$ = 6159 Hz, $^1J_{P,F}$ = 1242 Hz, $^2J_{P,P'}$ = 28 Hz, $^4J_{F,F'}$ = 3 Hz, $^3J_{P,F'}$ = -5 Hz, >93%), 54.9 (br. s). $^{19}F\{^1H\}$ NMR (377 MHz, $CD_2Cl_2$): $\delta_F$ (ppm) -39.5 (AA'XX', $N$ = 1237 Hz, $^2J_{F,Pt}$ = 633 Hz, $^1J_{F,P}$ = 1242 Hz, $^2J_{P,P'}$ = 28 Hz, $^4J_{F,F'}$ = 3Hz, $^3J_{F',P}$ = -5 Hz). $^1H$ NMR (400 MHz, $CD_2Cl_2$): $\delta_H$ (ppm) 7.57 (d, $J_{H,H}$ = 8.5 Hz, 2H, ArC*H*), 7.29 (d, $J_{H,H}$ = 8.4 Hz, 2H, ArC*H*), 2.30 (s, 6H, $CH_3$), contained signals for 10% [$PtCl_2$(cod)].

### 7.2.39 Synthesis of *cis*-[PtMe$_2$(L$_{2.1}$)$_2$] (2.9a)

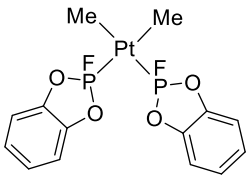

To a solution of [PtMe$_2$(cod)] (0.0200 g, 0.0600 mmol) in $d_8$-toluene (0.5 mL) was added a solution of **L$_{2.1}$** (0.0190 g, 0.120 mmol) in $d_8$-toluene (0.5 mL). Due to the high hydrolytic sensitivity of product, the by-product cod was not removed. $^{31}P\{^1H\}$ NMR (162 MHz, $d_8$-toluene): $\delta_P$ (ppm) 143.4 (AA'XX', $N$ = 1341 Hz, $^1J_{P,Pt}$ = 3070 Hz, $^1J_{P,F}$ = 1347 Hz, $^2J_{P,P'}$ = 19 Hz, $^4J_{F,F'}$ = 2 Hz, $^3J_{P,F'}$ = -6 Hz, 96%). $^{19}F\{^1H\}$ NMR (377 MHz, $d_8$-toluene): $\delta_F$ (ppm) -27.9 (AA'XX', $N$ = 1341 Hz, $^2J_{F,Pt}$ = 344 Hz, $^1J_{F,P}$ = 1347 Hz, $^2J_{P,P'}$ = 19 Hz, $^4J_{F,F'}$ = 2 Hz, $^3J_{F',P}$ = -6 Hz >92%). HR-MS (EI): m/z calcd. for $C_{14}H_{14}F_2O_4P_2Pt$ $[M\text{-}H]^-$ = 540.9990; obs. = 540.9973.

**General procedure for the synthesis of [PtL$_4$] complexes (2.10a,c-d)**

To a solution of [Pt(nbe)$_3$] (0.0200 g, 0.0419 mmol) in THF (0.5 mL) was added a solution of the ligand (0.168 mmol) in THF (0.5 mL). Upon completion of the reaction, the volatiles were removed under reduced pressure. The product was precipitated with hexane (2 mL). The solid was allowed to settle, and the supernatant was removed and remaining solid washed with hexane (3 x 1 mL). Residual solvent was then removed from the solid under reduced pressure to yield the product.

### 7.2.40 Synthesis of [Pt(L$_{2.1}$)$_4$] (2.10a)

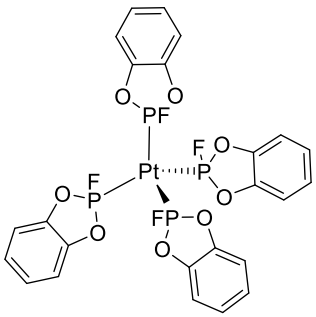

White solid (0.0290 g, 84%). $^{31}P\{^1H\}$ NMR (162 MHz, $d_8$-THF): $\delta_P$ (ppm) 118.0 (>99%, AA'$_3$XX'$_3$, $N$ = 1256 Hz, $^1J_{P,Pt}$ = 6102 Hz). $^{19}F\{^1H\}$ NMR (377 MHz, $d_8$-THF): $\delta_F$ (ppm) -7.2 (AA'$_3$XX'$_3$). $^{31}P\{^1H\}$ and $^{19}F\{^1H\}$ NMR data agreed with the literature data.[22]

### 7.2.41 Synthesis of $[Pt(L_{2.3})_4]$ (2.10c)

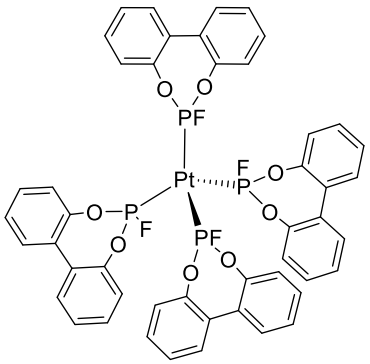

Off-white solid (0.0420 g, 88%). $^{31}P\{^1H\}$ NMR (162 MHz, $d_8$-THF): $\delta_P$ (ppm) 127.1 (AA'$_3$XX'$_3$, $N$ = 1181 Hz, $^1J_{P,Pt}$ = 6000 Hz). $^{19}F\{^1H\}$ NMR (377 MHz, $d_8$-THF): $\delta_F$ (ppm) -23.9 (AA'$_3$XX'$_3$). $^{195}Pt\{^1H\}$ NMR (65 MHz, $d_8$-THF): $\delta_{Pt}$ (ppm) -5638 (qq, $^1J_{Pt,P}$ = 5999 Hz, $^2J_{Pt,F}$ = 399 Hz). $^1H$ NMR (400 MHz, $d_8$-THF): $\delta_H$ (ppm) 7.47 (dd, $J_{H,H}$ = 7.1, 2.3 Hz, 2H, ArC*H*), 7.24 (tt, $J_{H,H}$ = 7.4, 5.4 Hz, 4H, ArC*H*), 7.06 (m, 2H, ArC*H*). $^{13}C\{^1H\}$ NMR (101 MHz, $d_8$-THF): $\delta_C$ (ppm) 149.9 (s, Ar*C*O), 131.5 (s, Ar*C*), 130.7 (s, Ar*C*H), 130.3 (s, Ar*C*H), 126.7 (s, Ar*C*H), 123.4 (s, Ar*C*H). HR-MS (ESI): m/z calcd. for $C_{48}H_{32}F_4NaO_8P_4Pt$ $[M+Na]^+$ = 1154.0528; obs. = 1154.0539.

### 7.2.42 Synthesis of $[Pt(L_{2.4})_4]$ (2.10d)

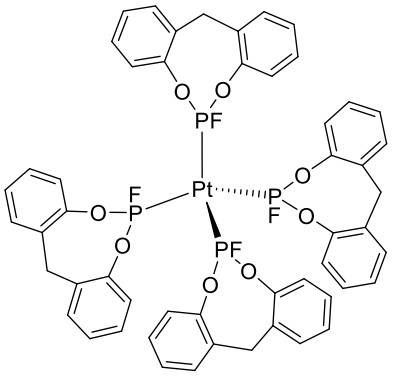

Off-white solid (0.0380 g, 85%). $^{31}P\{^1H\}$ NMR (162 MHz, $d_8$-THF): $\delta_P$ (ppm) 155.6 (AA'XX', **2.12d**), 105.7 (AA'$_3$XX'$_3$, $N$ = 1132 Hz, $^1J_{P,Pt}$ = 5981 Hz, **2.10d**, >93%). $^{19}F\{^1H\}$ NMR (377 MHz, $d_8$-THF): $\delta_F$ (ppm) -27.8 (AA'$_3$XX'$_3$, **2.10d**, >93%) -43.9 (AA'XX', **2.12d**). $^{195}Pt\{^1H\}$ NMR (65 MHz, $d_8$-THF): $\delta_{Pt}$ (ppm) -5282 (tt, $^1J_{Pt,P}$ = 6107 Hz, $^2J_{Pt,F}$ = 454 Hz, **2.12d**), -5640 (qq, $^1J_{Pt,P}$ = 5983 Hz, $^2J_{Pt,F}$ = 354, **2.10d**). $^1H$ NMR (400 MHz, $d_8$-THF): $\delta_H$ (ppm) 7.29 (d, $J_{H,H}$ = 7.3 Hz, 2H, ArC*H*), 7.15 (t, $J_{H,H}$ = 7.3 Hz, 2H, ArC*H*), 7.05 (t, $J_{H,H}$ = 7.3 Hz, 2H, ArC*H*), 6.91 (d, $J_{H,H}$ = 7.9 Hz, 2H, ArC*H*), 4.27 (d, $^2J_{H,H}$ = 14.2 Hz, 1H, C$H_2$), 3.63 (d, $^2J_{H,H}$ = 13.9 Hz, 1H, C$H_2$). $^{13}C\{^1H\}$ NMR (101 MHz, $d_8$-THF): $\delta_C$ (ppm) 150.5 (s, Ar*C*O), 133.4 (s, Ar*C*), 131.3 (s, Ar*C*H), 128.8 (s, Ar*C*H), 126.3 (s, Ar*C*H), 123.8 (s, Ar*C*H), 35.7 (s, *C*$H_2$). HR-MS (ESI): m/z calcd. for $C_{52}H_{40}F_4NaO_8P_4Pt$ $[M+Na]^+$ = 1210.1154; obs. = 1210.1160.

### 7.2.43 Synthesis of [Pt($L_{2.2}$)$_4$] (2.10b)

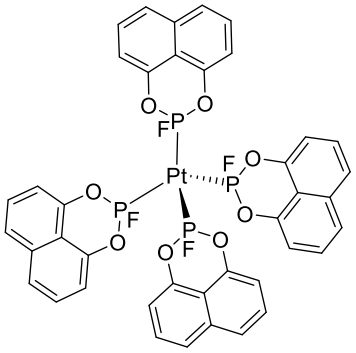

A chlorobenzene solution (1.5 mL) of [Pt(nbe)$_3$] (0.0150 g, 0.0314 mmol) was layered with a chlorobenzene solution (1.5 mL) of **$L_{2.2}$** (0.0226 g, 0.126 mmol). The mixture was left to stand and within 24 h crystals of **2.10b** suitable for X-ray crystallography were obtained. The product was insoluble in all common organic solvents.

### 7.2.44 Synthesis of [Pt($L_{2.5}$)$_4$] (2.10e)

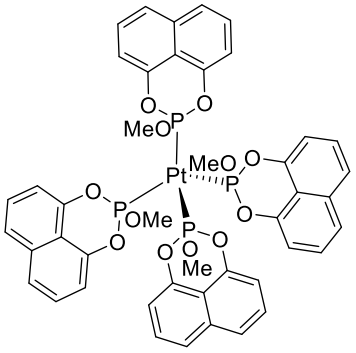

To a solution of [Pt(nbe)$_3$] (0.0200 g, 0.0419 mmol) in THF (0.5 mL) was added a solution of **$L_{2.5}$** (0.0369 g, 0.168 mmol) in THF (0.5 mL). Upon completion of the reaction, the volatiles were removed under reduced pressure and the crude product was dissolved in toluene (1 mL). The volatiles were then removed under reduced pressure to yield the product as a white solid (0.0430 g, 96%). Crystals suitable for analysis by single crystal X-ray diffraction were grown by slow diffusion of hexane into a saturated THF solution of **2.10e**. $^{31}P\{^1H\}$ NMR (162 MHz, *d*$_8$-THF): $\delta_P$ (ppm) 110.1 (s, $^1J_{P,Pt}$ = 5745 Hz). $^{31}P$ NMR (162 MHz, d$_8$-THF): $\delta_P$ (ppm) 110.1 (m, $^1J_{P,Pt}$ = 5745 Hz). $^{195}Pt\{^1H\}$ NMR (65 MHz, *d*$_8$-THF): $\delta_{Pt}$ (ppm) -5678.5 (q, $^1J_{Pt,P}$ = 5746 Hz). $^1H$ NMR (400 MHz, *d*$_8$-THF): $\delta_H$ (ppm) 7.48 (d, $J_{H,H}$ = 8.3 Hz, 2H, ArC*H*), 7.35 (t, $J_{H,H}$ = 7.9 Hz, 2H, ArC*H*), 6.93 (d, $J_{H,H}$ = 7.5 Hz, 2H, ArC*H*), 3.65 (m, 3H, O(C*H*$_3$)). $^{13}C\{^1H\}$ NMR (101 MHz, *d*$_8$-THF): $\delta_C$ (ppm) 147.6 (s, Ar*C*O), 136.2 (s, Ar*C*), 128.1 (s, Ar*C*H), 122.6 (s, Ar*C*H), 177.4 (s, Ar*C*), 112.6 (s, Ar*C*H), 52.9 (s, O(*C*H$_3$)). HR-MS (ESI): m/z calcd. for $C_{44}H_{36}NaO_{12}P_4Pt$ $[M+Na]^+$ = 1098.0701; obs. = 1098.0690.

### 7.2.45 Reaction between Ethanox 398$^{TM}$ (2.4) and [Pt(nbe)$_3$] in a 4:1 stoichiometry

**2.11f**

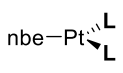

**2.12f**

To a solution of [Pt(nbe)$_3$] (0.0100 g, 0.0209 mmol) in THF (0.5 mL) was added a solution of **2.4** (0.0369 g, 0.168 mmol) in THF (0.5 mL). Upon completion of the reaction, a mixture of products was observed by *in situ* $^{31}P\{^1H\}$, $^{19}F\{^1H\}$ and $^{195}Pt\{^1H\}$ NMR spectroscopy. $^{31}P\{^1H\}$ NMR (162 MHz, THF): $\delta_P$ (ppm) 163.5 (AA'$_2$XX'$_2$, *N* = 1137 Hz, $^1J_{P,Pt}$ = 7600 Hz, **2.11f**), 146.0 (AA'XX', *N* = 1246 Hz, **2.12f**), 132.3 (d, $^1J_{P,F}$ = 1254 Hz, **2.4**), 107.1 (br. d, $^1J_{P,F}$ =

1238 Hz, **2.4**). $^{19}F\{^{1}H\}$ NMR (377 MHz, THF): $\delta_F$ (ppm) -21.7 (br. AA'XX', *N* = 1286 Hz, 1%, **2.12f**), -33.4 (AA'XX', *N* = 1247 Hz, 9%, **2.12f**), -41.6 (AA'$_2$XX'$_2$, *N* = 1138 Hz, 59%, **2.11f**), -49.4 (AA'XX, *N* = 1161 Hz, 1%, **2.12f**), -62.3 (d, $^{1}J_{F,P}$ = 1248 Hz, 23%, **2.4**), -74.2 (d, $^{1}J_{F,P}$ = 1255 Hz, 7%, **2.4**). $^{195}Pt\{^{1}H\}$ NMR (65 MHz, THF): $\delta_{Pt}$ (ppm) -5085.5 (qq, $^{1}J_{Pt,P}$ = 7607 Hz, $^{2}J_{Pt,F}$ = 591 Hz, **2.11f**), 5317.8 (tt, $^{1}J_{Pt,P}$ = 6088 Hz, $^{2}J_{Pt,F}$ = 537 Hz, **2.12f**).

**General procedure for the NMR study of the reaction between ligand and [Pt(nbe)$_3$] in a 2:1 stoichiometry**

To a solution of [Pt(nbe)$_3$] (0.0200 g, 0.0419 mmol) in THF (0.5 mL) was added a solution of the ligand (0.0838 mmol) in THF (0.5 mL). The reaction mixture was analysed by *in situ* $^{31}P\{^{1}H\}$, $^{19}F\{^{1}H\}$ and $^{195}Pt\{^{1}H\}$ NMR spectroscopy.

### 7.2.46 Reaction with $L_{2.1}$

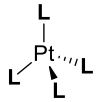


**2.10a**

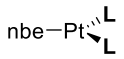


**2.12a**

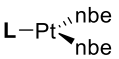


**2.13a**

$^{31}P\{^{1}H\}$ NMR (162 MHz, $d_8$-THF): $\delta_P$ (ppm) 167.2 (br. AA'XX', *N* = 1281 Hz, 16%, **2.12a**), 157.6 (d, $^{1}J_{P,F}$ = 1337 Hz, $^{1}J_{P,Pt}$ = 6314 Hz, 7%, **2.13a**), 118.0 (AA'$_3$XX'$_3$, *N* = 1256 Hz, $^{1}J_{P,Pt}$ = 6102 Hz, 77%, **2.10a**). $^{19}F\{^{1}H\}$ NMR (377 MHz, $d_8$-THF): $\delta_F$ (ppm) -7.3 (AA'$_3$XX'$_3$, **2.10a**), -22.8 (br. AA'XX', **2.12a**), -23.2 (d, $^{1}J_{F,P}$ = 1337 Hz, $^{2}J_{F,Pt}$ = 714 Hz, **2.13a**). $^{195}Pt\{^{1}H\}$ NMR (65 MHz, $d_8$-THF): $\delta_{Pt}$ (ppm) -5571.9 (qq, $^{1}J_{Pt,P}$ = 6098 Hz, $^{2}J_{Pt,F}$ = 445 Hz, **2.10a**), -5688.8 (dd, $^{1}J_{Pt,P}$ = 6314 Hz, $^{2}J_{Pt,F}$ = 716 Hz, **2.13a**).

### 7.2.47 Reaction with $L_{2.2}$

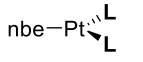


**2.12b**

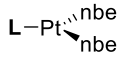


**2.13b**

Immediately an insoluble precipitate formed (assumed to be **2.10b**), the following species were observed in the filtrate: $^{31}P\{^{1}H\}$ NMR (162 MHz, $d_8$-THF): $\delta_P$ (ppm) 140.0 (AA'XX', *N* = 1238 Hz, $^{1}J_{P,Pt}$ = 6525 Hz, $^{1}J_{P,F}$ = 1271 Hz, $^{2}J_{P,P'}$ = 182 Hz, $^{4}J_{F,F'}$ = 0 Hz, $^{3}J_{P,F'}$ = -34 Hz, 23%, **2.12b**), 129.2 (d, $^{1}J_{P,F}$ = 1268 Hz, $^{1}J_{P,Pt}$ = 6423 Hz, 77%, **2.13b**). $^{19}F\{^{1}H\}$ NMR (377 MHz, $d_8$-THF): $\delta_F$ (ppm) -37.6 (AA'XX', $^{1}J_{F,P}$ = 1271 Hz, $^{2}J_{P,P'}$ = 182 Hz, $^{4}J_{F,F'}$ = 0 Hz, $^{3}J_{F',P}$ = -34 Hz, $^{2}J_{F,Pt}$ = 593 Hz, **2.12b**), -39.3 (d, $^{1}J_{F,P}$ = 1268 Hz, $^{2}J_{F,Pt}$ = 611 Hz, **2.13b**). $^{195}Pt\{^{1}H\}$ NMR (65 MHz, $d_8$-THF): $\delta_{Pt}$ (ppm) -5224.3 (tt, $^{1}J_{Pt,P}$ = 6521 Hz, $^{1}J_{Pt,F}$ = 597 Hz, **2.12b**), -5687.2 (dd, $^{1}J_{Pt,P}$ = 6424 Hz, $^{2}J_{Pt,F}$ = 613 Hz, **2.13b**).

### 7.2.48 Reaction with $L_{2.3}$

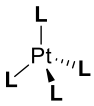
**2.10c**

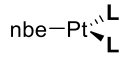
**2.12c**

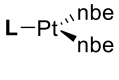
**2.13c**

$^{31}P\{^{1}H\}$ NMR (162 MHz, THF): $\delta_P$ (ppm) 167.8 (AA'XX', $N$ = 1267 Hz, $^{1}J_{P,Pt}$ = 6275 Hz, $^{1}J_{P,F}$ = 1293 Hz, $^{2}J_{P,P'}$ = 167 Hz, $^{4}J_{F,F'}$ = 5 Hz, $^{3}J_{P,F'}$ = -26 Hz, 44%, **2.12c**), 156.4 (d, $^{1}J_{P,F}$ = 1291 Hz, $^{1}J_{P,Pt}$ = 6215 Hz, 16%, **2.13c**), 127.1 (AA'$_3$XX'$_3$, $N$ = 1181 Hz, $^{1}J_{P,Pt}$ = 6000 Hz, 40%, **2.10c**). $^{19}F\{^{1}H\}$ NMR (377 MHz, THF): $\delta_F$ (ppm) -23.9 (AA'$_3$XX'$_3$, **2.10c**), -37.5 (AA'XX', $^{2}J_{F,Pt}$ = 596 Hz, $^{1}J_{F,P}$ = 1293 Hz, $^{2}J_{P,P'}$ = 167 Hz, $^{4}J_{F,F'}$ = 5 Hz, $^{3}J_{F',P}$ = -26 Hz, **2.12c**), -39.1 (d, $^{1}J_{F,P}$ = 1291 Hz, $^{2}J_{F,Pt}$ = 642 Hz, **2.13c**).

### 7.2.49 Reaction with $L_{2.4}$

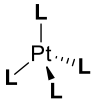
**2.10d**

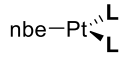
**2.12d**

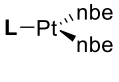
**2.13d**

$^{31}P\{^{1}H\}$ NMR (162 MHz, $d_8$-THF): $\delta_P$ (ppm) 155.4 (AA'XX', $N$ = 1212 Hz, $^{1}J_{P,Pt}$ = 6115 Hz, $^{1}J_{P,F}$ = 1224 Hz, $^{2}J_{P,P'}$ = 147 Hz, $^{4}J_{F,F'}$ = 0 Hz, $^{3}J_{P,F'}$ = -12 Hz, **2.12d**), 141.6 (d, $^{1}J_{P,F}$ = 1224 Hz, $^{1}J_{P,Pt}$ = 6253 Hz, **2.13d**). $^{19}F\{^{1}H\}$ NMR (377 MHz, $d_8$-THF): $\delta_F$ (ppm) -27.8 (AA'$_3$XX'$_3$, 6%, **2.10d**), -43.8 (AA'XX', $^{2}J_{F,Pt}$ = 454 Hz, $^{1}J_{F,P}$ = 1224 Hz, $^{2}J_{P,P'}$ = 147 Hz, $^{4}J_{F,F'}$ = 0 Hz, $^{3}J_{F',P}$ = -12 Hz, 91%, **2.12d**), -45.2 (d, $^{1}J_{F,P}$ = 1223 Hz, 3%, **2.13d**). $^{195}Pt\{^{1}H\}$ NMR (65 MHz, $d_8$-THF): $\delta_{Pt}$ (ppm) -5282.0 (tt, $^{1}J_{Pt,P}$ = 6110 Hz, $^{2}J_{Pt,F}$ = 454 Hz, **2.12d**), -5751.2 (dd, $^{1}J_{Pt,P}$ = 6252 Hz, $^{2}J_{Pt,F}$ = 567 Hz, **2.13d**). HR-MS (ESI): m/z calcd. for $C_{33}H_{31}O_4PtF_2P_2$ (**2.12d**) $[M+H]^+$ = 786.1320; obs. = 786.1313.

### 7.2.50 Reaction with $L_{2.5}$

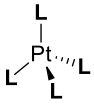
**2.10e**

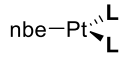
**2.12e**

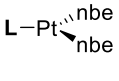
**2.13e**

$^{31}P\{^{1}H\}$ NMR (162 MHz, $d_8$-THF): $\delta_P$ (ppm) 147.5 (s, $^{1}J_{P,Pt}$ = 5941 Hz, 53%, **2.12e**), 136.0 (s, $^{1}J_{P,Pt}$ = 5895 Hz, 12%, **2.13e**), 108.2 (s, $^{1}J_{P,Pt}$ = 5744 Hz, 35%, **2.10e**). $^{195}Pt\{^{1}H\}$ NMR (65 MHz, $d_8$-THF): $\delta_{Pt}$ (ppm) -5255.0 (t, $^{1}J_{Pt,P}$ = 5942 Hz, **2.12e**), -5685.7 (q, $^{1}J_{Pt,P}$ = 5744 Hz, **2.10e**), -5707.5 (d, $^{1}J_{Pt,P}$ = 5902 Hz, **2.13e**).

### 7.2.51 Reaction with Ethanox 398™ (2.4)

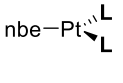
**2.12f**

Three unassigned isomers of complex **2.12f** were observed. $^{31}P\{^{1}H\}$ NMR (162 MHz, THF): $\delta_P$ (ppm) 148.2 (AA'XX', **2.12f**), 147.5 (AA'XX', **2.12f**), 146.1 (br. AA'XX', $N$ = 1252 Hz, $^{1}J_{P,Pt}$ = 6117 Hz, **2.12f**). $^{19}F\{^{1}H\}$ NMR (377 MHz, THF): $\delta_F$ (ppm) -21.7 (AA'XX', $N$ = 1275 Hz, $^{2}J_{F,Pt}$ = 493 Hz, 7%, **2.12f**), -33.4 (br. AA'XX', $N$ = 1246 Hz, $^{2}J_{F,Pt}$ = 537 Hz, 82%, **2.12f**), -49.4 (AA'XX', $N$ = 1161 Hz, $^{2}J_{F,Pt}$

= 318 Hz, 11%, **2.12f**). $^{195}Pt\{^1H\}$ NMR (65 MHz, THF): $\delta_{Pt}$ (ppm) -5303.8 (tt, $^1J_{Pt,P}$ = 6033 Hz, $^2J_{Pt,F}$ = 492 Hz, **2.12f**), -5313.7 (tt, $^1J_{Pt,P}$ = 6093 Hz, $^2J_{Pt,F}$ = 542 Hz, **2.12f**), 5304.6 (tt, $^1J_{Pt,P}$ = 6032 Hz, $^2J_{Pt,F}$ = 495 Hz, **2.12f**).

### 7.2.52 Synthesis of $[Rh_2Cl_2(L_{2.1})_4]$ (2.14a) from $[Rh_2Cl_2(CO)_4]$

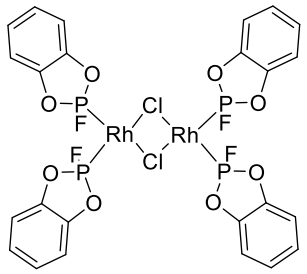

To a solution of $[Rh_2Cl_2(CO)_4]$ (0.0200 g, 0.0514 mmol) in $C_6D_6$ (0.5 mL) was added a solution of $\mathbf{L_{2.1}}$ (0.0160 g, 0.103 mmol) in $C_6D_6$ (0.5 mL). After 2 h, the reaction mixture was saturated with $N_2$ by three successive freeze-pump-thaw cycles to give an orange solution. $^{31}P\{^1H\}$ NMR (162 MHz, $C_6D_6$): $\delta_P$ (ppm) 134.8 (br. d, $^1J_{P,F}$ = 1323 Hz). $^{19}F\{^1H\}$ NMR (377 MHz, $C_6D_6$): $\delta_F$ (ppm) -9.5 (br. d, $^1J_{F,P}$ = 1314 Hz). $^{31}P\{^1H\}$ and $^{19}F\{^1H\}$ NMR data fitted with literature data.[23]

**General procedure for the NMR study of the reaction between ligand and $[Rh_2Cl_2(CO)_4]$ in a 4:1 stoichiometry**

To a solution of $[Rh_2Cl_2(CO)_4]$ (0.0150 g, 0.0386 mmol) in $CH_2Cl_2$ (0.5 mL) was added a solution of the ligand (0.154 mmol) in $CH_2Cl_2$ (0.5 mL). After 2 h, the reaction mixture was saturated with $N_2$ by three successive freeze-pump-thaw cycles.

### 7.2.53 Synthesis of $[Rh_2Cl_2(L_{2.2})_4]$ (2.14b)/ $[Rh(L_{2.2})_5][Cl]$ (2.15b)

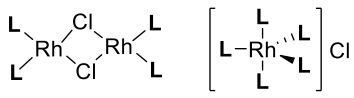

**2.14b** **2.15b**

$^{31}P\{^1H\}$ NMR (162 MHz, $CD_2Cl_2$): $\delta_P$ (ppm) 113.0 ($AA'_4MM'_4X$, ≈ 20%, **2.15b**), 112.6 (br. d, $^1J_{P,F}$ = 1354 Hz, ≈ 80%, **2.14b**). $^{19}F\{^1H\}$ NMR (377 MHz, $CD_2Cl_2$): $\delta_F$ (ppm) -19.5 ($AA'_4MM'_4X$, **2.15b**), -30.1 (br. d, **2.14b**). HR-MS (nanospray): m/z calcd. for $C_{50}H_{30}F_5O_{10}P_5Rh$ [**2.15b**-Cl]$^+$ = 1142.95; obs. =1143.03.

### 7.2.54 Synthesis of $[Rh_2Cl_2(L_{2.3})_4]$ (2.14c)/ $[Rh(L_{2.3})_5][Cl]$ (2.15c)/ *trans*-$[RhCl(CO)(L_{2.3})_2]$ (2.16c)

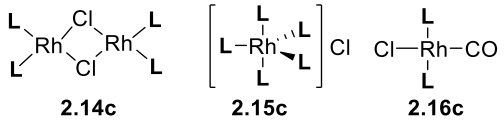

**2.14c** **2.15c** **2.16c**

$^{31}P\{^1H\}$ NMR (162 MHz, $CD_2Cl_2$): $\delta_P$ (ppm) 144.4 ($AA'_4MM'_4X$, **2.15c**), 129.1 (br. d, $^1J_{P,F}$ = 1260 Hz, **2.14c**). $^{19}F\{^1H\}$ NMR (377 MHz, $CD_2Cl_2$): $\delta_F$ (ppm) -19.1 ($AA'_4MM'_4X$, ≈ 18%, **2.15c**), -31.1 (br. d, ≈ 15%, $^1J_{F,P}$ = 1152 Hz, **2.16c**), -44.1 (br. d, $^1J_{F,P}$ = 1152 Hz, ≈ 67%, **2.14c**). HR-MS (ESI): m/z calcd. for

$C_{60}H_{40}F_5O_{10}P_5Rh$ [**2.15c**-Cl]$^+$ = 1273.0279; obs. = 1273.0287. IR ($CH_2Cl_2$): ν(CO) of **2.16c** = 2032 $cm^{-1}$.

### 7.2.55 Synthesis of $[Rh_2Cl_2(L_{2.4})_4]$ (2.14d)/ $[Rh(L_{2.4})_5][Cl]$ (2.15d)/ *trans*-$[RhCl(CO)(L_{2.4})_2]$ (2.16d)

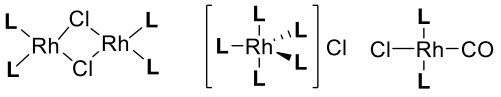


**2.14d** **2.15d** **2.16d**

$^{31}P\{^1H\}$ NMR (162 MHz, $CD_2Cl_2$): $\delta_P$ (ppm) 115.6 ($AA'_4MM'_4X$, ≈ 30%, **2.15d**) 108.8 (br. d, $^1J_{P,F}$ = 1211 Hz, ≈ 70%, **2.14d**). $^{19}F\{^1H\}$ NMR (377 MHz, $CD_2Cl_2$): $\delta_F$ (ppm) -36.5 ($AA'_4MM'_4X$, ≈ 23%, **2.15d**), -38.3 (d, $^1J_{F,P}$ = 1223 Hz, ≈ 4%, **2.16d**), -52.3 (br. d, $^1J_{F,P}$ = 1205 Hz, ≈ 73%, **2.14d**). HR-MS (ESI): m/z calcd. for $C_{65}H_{50}F_5O_{10}P_5Rh$ [**2.15d**-Cl]$^+$ = 1343.1062; obs. = 1343.1135. IR ($CH_2Cl_2$): ν(CO) of **2.16d** = 2028 $cm^{-1}$.

### 7.2.56 Synthesis of $[Rh(L_{2.5})_5][Cl]$ (2.15e)/ *trans*-$[RhCl(CO)(L_{2.5})_2]$ (2.16e)

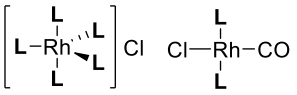


**2.15e** **2.16e**

$^{31}P\{^1H\}$ NMR (122 MHz, $CH_2Cl_2$): $\delta_P$ (ppm) 122.6 (d, $^1J_{P,Rh}$ = 127 Hz, 28%, **2.15e**), 119.8 (d, $^1J_{P,Rh}$ = 181 Hz, 2%), 113.1 (d, $^1J_{P,Rh}$ = 210 Hz, 70%, **2.16e**). IR ($CH_2Cl_2$): ν(CO) of **2.16e** = 2023 $cm^{-1}$.

### 7.2.57 Synthesis of $[Rh_2Cl_2(L_{2.6})_4]$ (2.14f)/ $[Rh(L_{2.6})_5][Cl]$ (2.15f)

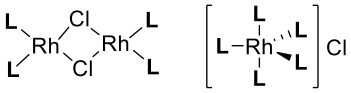


**2.14f** **2.15f**

$^{31}P\{^1H\}$ NMR (162 MHz, $CD_2Cl_2$, -80 °C): $\delta_P$ (ppm) 143.1 (br. s, **2.15f**), 130.4 (dd, $^1J_{P,F}$ = 1314 Hz, $^2J_{P,Rh}$ = 321 Hz, **2.14f**), 130.0 (dd, $^1J_{P,F}$ = 1317 Hz, $^2J_{P,Rh}$ = 320 Hz, **2.14f**), 116.8 (br. s, **2.15f**). $^{19}F\{^1H\}$ NMR (377 MHz, $CD_2Cl_2$): $\delta_F$ (ppm) -1.9 ($AA'_4MM'_4X$, **2.15f**), -11.8 (br. d, $^1J_{F,P}$ = 1285 Hz, **2.14f**).

### 7.2.58 Synthesis of $[Rh_2Cl_2(L_{2.7})_4]$ (2.14g)/ $[Rh(L_{2.7})_5][Cl]$ (2.15g)

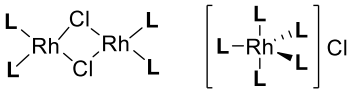


**2.14g** **2.15g**

$^{31}P\{^1H\}$ NMR (162 MHz, $CD_2Cl_2$): $\delta_P$ (ppm) 134.8 ($AA'_4MM'_4X$, ≈ 38%, **2.15g**), 128.2 (br. d, $^1J_{P,F}$ = 1308 Hz, ≈ 55%, **2.14g**), -25.6 (s, 8%, hydrolysis P(V)).

### 7.2.59 Synthesis of $[Rh_2Cl_2(L_{2.8})_4]$ (2.14h)/ $[Rh(L_{2.8})_5][Cl]$ (2.15h)

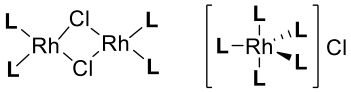


**2.14h** **2.15h**

$^{31}P\{^1H\}$ NMR (162 MHz, $CD_2Cl_2$): $\delta_P$ (ppm) 120.1 ($AA'_4MM'_4X$, ≈ 60%, **2.15h**), 107.3 (br. d, $^1J_{P,F}$ = 1268 Hz, ≈ 40%, **2.14h**). $^{19}F\{^1H\}$ NMR (377 MHz, $CD_2Cl_2$): $\delta_F$

(ppm) -20.5 (AA'$_4$MM'$_4$X, **2.15h**), -39.2 (br. d, **2.14h**). HR-MS (ESI): m/z calcd. for $C_{60}H_{50}F_5O_{10}P_5Rh$ [**2.15h**-Cl]$^+$ = 1283.1; obs. = 1283.1.

### 7.2.60 Synthesis of [$Rh_2Cl_2(L_{2.2})_4$] (2.14b) from [$Rh_2Cl_2(cod)_2$]

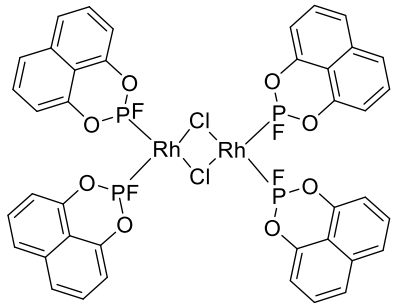

To a solution of [$Rh_2Cl_2(cod)_2$] (0.0200 g, 0.0406 mmol) in $CH_2Cl_2$ (0.5 mL) was added a solution of $\mathbf{L_{2.2}}$ (0.0337 g, 0.162 mmol) in $CH_2Cl_2$ (0.5 mL). Upon completion of the reaction, the volatiles were removed under reduced pressure. The product was precipitated with hexane (*ca.* 2 mL). The solid was allowed to settle, and the supernatant was removed and remaining solid washed with hexane (3 x 1 mL). Residual solvent was then removed from the solid under reduced pressure to yield the product as an orange solid. $^{31}P\{^1H\}$ NMR (162 MHz, $CD_2Cl_2$): $\delta_P$ (ppm) 108.2 (dd, $^1J_{P,F}$ = 1222 Hz, $^1J_{P,Rh}$ = 328 Hz). $^{19}F\{^1H\}$ NMR (377 MHz, $CD_2Cl_2$): $\delta_F$ (ppm) -30.8 (d, $^1J_{F,P}$ = 1232 Hz). HR-MS (nanospray): m/z calcd. for $C_{40}H_{23}ClF_4O_8P_4Rh_2$ [M-Cl]$^+$ =1072.8157; obs. =1072.8163.

### 7.2.61 NMR study of the reaction between $L_{2.2}$ and [$Rh_2Cl_2(CO)_4$] in a 10:1 stoichiometry

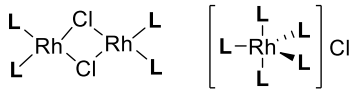

**2.14b** **2.15b**

To a solution of [$Rh_2Cl_2(CO)_4$] (0.0150 g, 0.0386 mmol) in $CH_2Cl_2$ (0.5 mL) was added a solution of $\mathbf{L_{2.2}}$ (0.0803 g, 0.386 mmol) in $CH_2Cl_2$ (0.5 mL). After 2 h, the reaction mixture was saturated with $N_2$ by three successive freeze-pump-thaw cycles. $^{31}P\{^1H\}$ NMR (122 MHz, -50 °C, $CH_2Cl_2$): $\delta_P$ (ppm) 118.8 (AA'$_4$MM'$_4$X, ≈ 36%, **2.15b**), 112.6 (br. dm, ≈ 38%, **2.14b**), 98.0 (d, $^1J_{P,F}$ = 1239 Hz, ≈ 26%, $\mathbf{L_{2.2}}$). $^{19}F\{^1H\}$ NMR (377 MHz, $CH_2Cl_2$): $\delta_F$ (ppm) -19.5 (AA'$_4$MM'$_4$X, **2.15b**), -38.3 (br. d, **2.14b** and $\mathbf{L_{2.2}}$). HR-MS (ESI): m/z calcd. for $C_{50}H_{30}F_5O_{10}P_5Rh$ [**2.15b**-Cl]$^+$ = 1142.9; obs. =1142.9.

### 7.2.62 Synthesis of $[Rh(L_{2.3})_5][Cl]$ (2.15c)

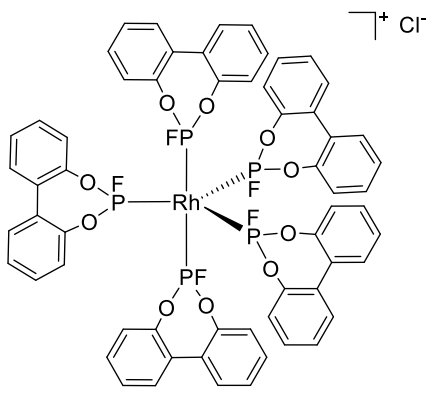

To a solution of $[Rh_2Cl_2(CO)_4]$ (0.0150 g, 0.0386 mmol) in $CH_2Cl_2$ (0.5 mL) was added a solution of **$L_{2.3}$** (0.0900 g, 0.386 mmol) in $CH_2Cl_2$ (0.5 mL). After 2 h, the volatiles were removed under reduced pressure to yield the product as a yellow/ green solid. $^{31}P\{^1H\}$ NMR (162 MHz, $CD_2Cl_2$): $\delta_P$ (ppm) 143.8 (AA'$_4$MM'$_4$X), 121.7 (dd, $^1J_{P,F}$ = 1243 Hz, $^1J_{P,Rh}$ = 240 Hz, ≈ 3%, **2.16c**). $^{19}F\{^1H\}$ NMR (377 MHz, $CD_2Cl_2$): $\delta_F$ (ppm) -18.9 (AA'$_4$MM'$_4$X, > 93%), -23.5 (br. s, 3%), -34.0 (d, $^1J_{F,P}$ = 1245 Hz, 5%). $^1H$ NMR (400 MHz, $CD_2Cl_2$): $\delta_H$ (ppm) 7.40 (m, 4H, ArC*H*), 7.30 (m, 2H, ArC*H*), 7.06 (d, $J_{H,H}$ = 8.1 Hz, 2H, ArC*H*). $^{13}C\{^1H\}$ NMR (101 MHz, $CD_2Cl_2$): $\delta_C$ (ppm) 148.4 (s, Ar*C*O), 131.2 (s, Ar*C*H), 130.7 (s, Ar*C*H), 128.9 (s, Ar*C*), 128.0 (s, Ar*C*H), 121.8 (s, Ar*C*H). HR-MS (ESI): m/z calcd. for $C_{60}H_{40}F_5O_{10}P_5Rh$ $[M\text{-}Cl]^+$ = 1273.0279; obs. = 1273.0276.

**General procedure for the synthesis of $[RhL_5][BF_4]$ complexes 2.15b', 2.15c', 2.15e'**

To a solution of $[Rh(cod)_2][BF_4]$ (0.0150 g, 0.0369 mmol) in $CH_2Cl_2$ (0.5 mL) was added a solution of ligand (0.185 mmol) in $CH_2Cl_2$ (0.5 mL). Upon completion of the reaction, the volatiles were removed under reduced pressure. The product was precipitated with hexane (*ca.* 2 mL). The solid was allowed to settle, and the supernatant was removed; the remaining solid was then washed with hexane (3 x 1 mL). Residual solvent was removed from the solid under reduced pressure to yield the product.

### 7.2.63 Synthesis of $[Rh(L_{2.2})_5][BF_4]$ (2.15b')

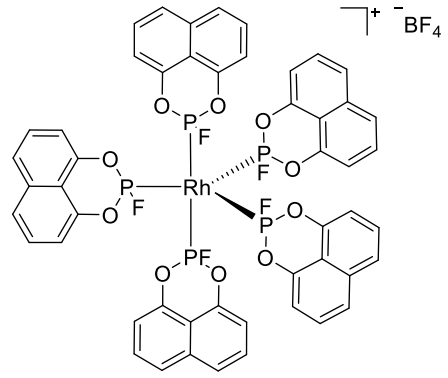

Pale green solid (0.0390 g, 65%). $^{31}P\{^1H\}$ NMR (162 MHz, $CD_2Cl_2$): $\delta_P$ (ppm) 118.5 (AA'$_4$MM'$_4$X, $^1J_{P,F}$ = 1286 Hz). $^{19}F\{^1H\}$ NMR (377 MHz, $CD_2Cl_2$): $\delta_F$ (ppm) -19.4 (AA'$_4$MM'$_4$X, $^1J_{F,P}$ = 1290 Hz, 5F, $[Rh(PF)_5][BF_4]$), -153.2 (2 s, 4F, 4:1 [$^{11}BF_4$]: [$^{10}BF_4$]). $^1H$ NMR (400 MHz, $CD_2Cl_2$): $\delta_H$ (ppm) 7.74 (d, $J_{H,H}$ = 8.3 Hz, 2H, ArC*H*), 7.50 (t, $J_{H,H}$ = 8.1 Hz, 2H, ArC*H*), 7.03 (d, $J_{H,H}$ = 7.7 Hz, 2H, ArC*H*). $^{13}C\{^1H\}$ NMR (101 MHz, $CD_2Cl_2$):

$\delta_C$ (ppm) 143.9 (s, Ar*C*O), 135.6 (s, Ar*C*), 128.4 (s, Ar*C*H), 125.3 (s, Ar*C*H), 114.8 (m, Ar*C*), 113.4 (s, Ar*C*H). HR-MS (ESI): m/z calcd. for $C_{50}H_{30}F_5O_{10}P_5Rh$ $[M\text{-}BF_4]^+$ = 1142.9497; obs. = 1142.9483.

### 7.2.64 Synthesis of $[Rh(L_{2.3})_5][BF_4]$ (2.15c')

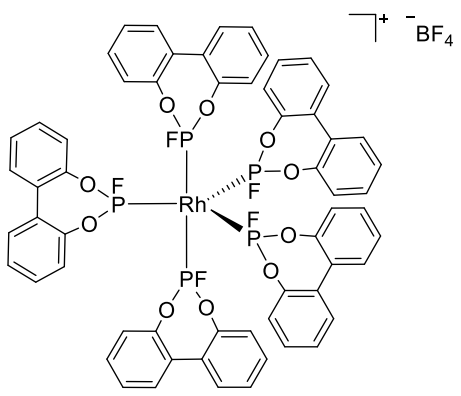

Yellow/ green solid (0.0351 g, 70%) $^{31}P\{^1H\}$ NMR (162 MHz, $CD_2Cl_2$): $\delta_P$ (ppm) 144.6 (AA'$_4$MM'$_4$X, $^1J_{P,F}$ = 1294 Hz). $^{19}F\{^1H\}$ NMR (377 MHz, $CD_2Cl_2$): $\delta_F$ (ppm) -18.9 (AA'$_4$MM'$_4$X, $^1J_{F,P}$ = 1192 Hz, 5F, $[Rh(PF)_5][BF_4]$), -149.5 (s, 4F, $[BF_4]$). $^1H$ NMR (400 MHz, $CD_2Cl_2$): $\delta_H$ (ppm) 7.38 (t, $J_{H,H}$ = 7.5 Hz, 4H, ArC*H*), 7.29 (t, $J_{H,H}$ = 8.2 Hz, 2H, ArC*H*), 7.05 (d, $J_{H,H}$ = 8.2 Hz, 2H, ArC*H*), contains signals for residual cod. $^{13}C\{^1H\}$ NMR (101 MHz, $CD_2Cl_2$): $\delta_C$ (ppm) 148.5 (s, Ar*C*O), 131.3 (s, Ar*C*), 130.7 (s, Ar*C*H), 129.0 (s, Ar*C*H), 128.0 (s, Ar*C*H), 121.9 (s, Ar*C*H). HR-MS (ESI): m/z calcd. for $C_{60}H_{40}F_5O_{10}P_5Rh$ $[M\text{-}BF_4]^+$ = 1273.0279; obs. = 1273.0276.

### 7.2.65 Synthesis of $[Rh(L_{2.5})_5][BF_4]$ (2.15e')

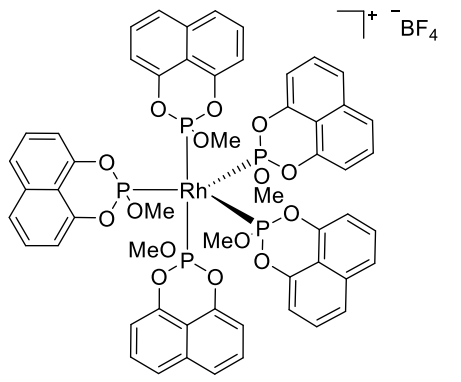

Orange solid. Crystals suitable for analysis by single crystal X-ray diffraction were grown by slow diffusion of hexane into a saturated pentane solution of **2.15e'**; the molecular structure obtained was heavily disordered (see Section 2.6). $^{31}P\{^1H\}$ NMR (162 MHz, $CD_2Cl_2$): $\delta_P$ (ppm) 112.8 (d, $^1J_{P,Rh}$ = 187 Hz). $^1H$ NMR (400 MHz, $CD_2Cl_2$): $\delta_H$ (ppm) 7.57 (d, $J_{H,H}$ = 8.4 Hz, 2H, ArC*H*), 7.36 (t, $J_{H,H}$ = 8.0 Hz, 2H, ArC*H*), 6.67 (d, $J_{H,H}$ = 7.6 Hz, 2H, ArC*H*), 3.72 (m, 3H, OC$H_3$), contains signals for *ca.* 10% residual cod. HR-MS (ESI): m/z calcd. for $C_{55}H_{45}O_{15}P_5Rh$ $[M\text{-}BF_4]^+$ = 1203.0496; obs. = 1203.0455.

## 7.3 Chapter 3

**General procedure for catalytic hydroformylation of 1-hexene (conditions A)**

Before use in catalysis the fluorophosphite ligands ($L_{2.2\text{-}2.4}$) were passed through a florisil column with toluene and/ or stirred in suspension of florisil/ toluene. Solutions of

[Rh(acac)(CO)$_2$] (0.012 mmol) in toluene (0.5 mL) and the ligand in toluene (1.0 mL) were added to a single cell autoclave (SS 316) under a nitrogen atmosphere. The autoclave was fitted with a pressure transducer and a separate reservoir. The autoclave was flushed with three cycles of CO/H$_2$ (*ca.* 10 bar) and subsequently pressurised to 15 bar and heated at 90 °C. After 1.5 h, a solution of 1-hexene (0.6 mL, 4.83 mmol) in toluene (1 mL) was added to the separate reservoir, which was flushed with three cycles of CO/H$_2$ (*ca.* 20 bar). Using overpressure, the substrate was injected into the autoclave and a total pressure of 20 bar CO/H$_2$ was established. The reaction mixture was heated at 90 °C for the appropriate time (for active runs a pressure drop of ≈ 0.5 bar was observed before quenching with a solution of *t*Bu$_3$P (1 mL) in toluene (1 mL)). The autoclave was then transferred to an ice bath, and once cooled the system was vented. A small sample of the reaction mixture was dissolved in CDCl$_3$ and analysed by $^1$H NMR spectroscopy. Conversion and selectivity were determined by integration of the 2,3-hexene alkene proton ($\delta_H$ = 5.48 ppm), 1-hexene alkene proton ($\delta_H$ = 5.88 ppm), the 2-methyl-hexanal aldehyde proton (*iso* aldehyde, $\delta_H$ = 9.65 ppm) and the heptanal aldehyde proton (*n* aldehyde, $\delta_H$ = 9.79 ppm).

The following equation was used to calculate the turnover frequency (TOF).

$$\text{TOF} = \left(\frac{\text{mol aldehyde product}}{\text{mol Rh}}\right) / \text{time}$$

**General procedure for catalytic hydroformylation of 1-hexene (conditions B)**

The following procedure was carried out by the author and Dr. C Kubis at the LIKAT (Rostock, Germany). Solutions of [Rh(acac)(CO)$_2$] (0.04 mmol) in toluene (5 mL) and the ligand in toluene (10 mL) were added to a 200 mL stainless steel autoclave (premex reactor AG, Leimen, Germany) under an Ar atmosphere. This was then washed in with toluene (20 mL) and the autoclave was flushed with three cycles of CO/H$_2$ (*ca.* 20 bar) and subsequently pressurised to 20 bar. The autoclave was then heated to 90 °C using an oil bath thermostat. After 1 h, 1-hexene (5 mL, 40.3 mmol) was added to the autoclave with an 8 mL stainless steel syringe using a syringe pump (PHD Ultra 4400, Harvard Apparatus GmbH, March-Hugstetten, Germany). An aliquot of the reaction mixture was collected periodically throughout the reaction by a connected automated sampling device (ASD) into GC vials under an Ar atmosphere. A pressure controller (Brooks Instrument, Hatfield, PA, USA) was used to maintain the pressure at 20 bar of CO/H$_2$ during the reaction. The reaction mixture was heated at 90 °C for the appropriate time. After, the

system was cooled to ambient temperature and the system was vented. A small sample of the reaction mixture was analysed by $^{31}P\{^{1}H\}$ NMR and IR spectroscopy (keeping the sample under an atmosphere of Ar).

The samples collected throughout the reaction were analysed by GC and the conversion and selectivity were determined.

## 7.4 Chapter 4

**General procedure for the synthesis of silyl ethers 4.9c,e-g**

To a solution of the diol (0.100 g) in toluene (2 mL) $NEt_3$ (2.2 eq.) was added. $SiMe_3Cl$ (2.2 or 1.1 eq.) was then added dropwise over 10 min and the reaction mixture stirred for 20 h. The suspension was filtered, and the solid washed with toluene (3 x 5 mL). The volatiles were removed under reduced pressure to yield the product.

### 7.4.1 Synthesis of 4.9c

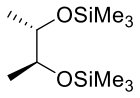


Colourless oil (0.168 g, 65%). $^{1}H$ NMR (400 MHz, $CDCl_3$): $\delta_H$ (ppm) 3.61 (m, 2H, C*H*), 1.05 (m, 6H, C$H_3$), 0.09 (s, 18H, OSi(C$H_3$)$_3$). $^{13}C\{^{1}H\}$ NMR (101 MHz, $CDCl_3$): $\delta_C$ (ppm) 77.1 (s, *C*H), 18.2 (s, *C*$H_3$), 0.3 (s, OSi(*C*$H_3$)$_3$). $^{1}H$ and $^{13}C\{^{1}H\}$ NMR data agreed with the literature data.[24]

### 7.4.2 Synthesis of 4.9e

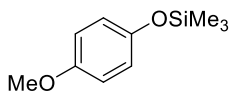


Yellow oil (0.0900 g, 57%). $^{1}H$ NMR (400 MHz, $CDCl_3$): $\delta_H$ (ppm) 6.73 (d, $J$ = 0.7 Hz 4H, ArC*H*), 3.71 (s, 3H, OC$H_3$), 0.20 (s, 9H, OSi(C$H_3$)$_3$). $^{13}C\{^{1}H\}$ NMR (101 MHz, $CDCl_3$): $\delta_C$ (ppm) 154.4 (s, Ar*C*). 149.0 (s, Ar*C*), 120.8 (s, Ar*C*H), 114.6 (s, Ar*C*H), 55.7 (s, O*C*$H_3$), 0.2 (s, OSi(*C*$H_3$)$_3$). $^{1}H$ and $^{13}C\{^{1}H\}$ NMR data agreed with the literature data.[25]

### 7.4.3 Synthesis of 4.9f

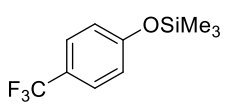


Colourless oil (0.0400 g, 28%). $^{1}H$ NMR: (400 MHz, $CDCl_3$): $\delta_H$ (ppm) 7.51 (d, $J$ = 8.4 Hz, 2H, ArC*H*), 6.91 (d, $J$ = 8.4 Hz, 2H, ArC*H*), 0.30 (s, 9H, OSi(C$H_3$)$_3$). $^{13}C\{^{1}H\}$ NMR (101 MHz, $CDCl_3$): $\delta_C$ (ppm) 158.3 (s, Ar*C*$F_3$), 127.1 (q, $^{3}J_{C,F}$ = 4 Hz, Ar*C*H), 123.8 (q, $^{2}J_{C,F}$ = 34 Hz, Ar*C*), 120.3 (s, Ar*C*H), 0.3 (s, OSi(*C*$H_3$)$_3$), quat. C undetectable. $^{1}H$ NMR data agreed with the literature data.[26]

### 7.4.4 Synthesis of 4.9g

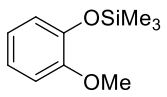


Colourless oil (0.0840 g, 53%). $^{1}$H NMR (400 MHz, $CDCl_3$): $\delta_H$ (ppm) 6.82-6.97 (m, 4H, ArC*H*), 3.83 (s, 3H, OC$H_3$), 0.27 (s, 9H, OSi(C$H_3$)$_3$). $^{13}$C{$^{1}$H} NMR (101 MHz, $CDCl_3$): $\delta_C$ (ppm) 151.1 (s, Ar*C*), 144.7 (s, Ar*C*), 122.0 (s, Ar*C*H), 121.1 (s, Ar*C*H), 121.0 (s, Ar*C*H), 112.2 (s, Ar*C*H), 55.5 (s, O*C*H$_3$), 0.4 (s, OSi(*C*H$_3$)$_3$). $^{1}$H and $^{13}$C{$^{1}$H} NMR data agreed with the literature data.[27]

**General procedure for the synthesis of chlorophosphites 4.6c,e-f**

To a solution of the appropriate silyl ether in MeCN (0.6 M) was added $PCl_3$ (2 eq.). Upon completion, as identified by $^{31}$P{$^{1}$H} NMR spectroscopy, the volatiles were removed under reduced pressure to yield the product.

### 7.4.5 Synthesis of 4.6c

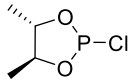


Yellow oil (0.0520 g, 95%). $^{31}$P{$^{1}$H} NMR (162 MHz, $CDCl_3$): $\delta_P$ (ppm) 171.3 (s). $^{31}$P{$^{1}$H} NMR data fitted with literature.[28] $^{1}$H NMR (400 MHz, $CDCl_3$): $\delta_H$ (ppm) 4.43 (m, 1H, C*H*), 3.39 (m, 1H, C*H*), 1.53 (d, $J_{H,H}$ = 6.2 Hz, 3H, C$H_3$), 1.52 (d, $J_{H,H}$ = 6.2 Hz, 3H, C$H_3$). $^{13}$C{$^{1}$H} NMR (101 MHz, $CDCl_3$): $\delta_C$ (ppm) 82.0 (s, 2x *C*H), 19.2 (s, *C*H$_3$), 17.5 (s, *C*H$_3$).

### 7.4.6 Synthesis of 4.6e

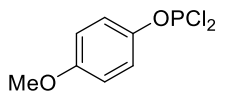


Yellow oil (0.0820 g, 90%). $^{31}$P{$^{1}$H} NMR (162 MHz, $CDCl_3$): $\delta_P$ (ppm) 178.6 (s). $^{31}$P{$^{1}$H} NMR data fitted with the literature data.[29] $^{1}$H NMR (400 MHz, $CDCl_3$): $\delta_H$ (ppm) 7.11 (d, $J_{H,H}$ = 9.2 Hz, 2H, ArC*H*), 6.91 (d, $J_{H,H}$ = 9.2 Hz, 2H, ArC*H*), 3.81 (s, 3H, OC$H_3$). $^{13}$C{$^{1}$H} NMR (101 MHz, $CDCl_3$): $\delta_C$ (ppm) 157.6 (s, Ar*C*), 144.2 (d, $^{2}J_{C,P}$ = 12 Hz, Ar*C*), 122.7 (d, $J$ = 5 Hz, Ar*C*H), 114.6 (s, Ar*C*H), 55.7 (s, O*C*H$_3$).

### 7.4.7 Synthesis of 4.6f

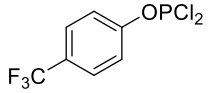


Yellow oil (0.0370 g, 94%). $^{31}$P{$^{1}$H} NMR (162 MHz, $CDCl_3$): $\delta_P$ (ppm) 178.1 (s). $^{1}$H NMR (400 MHz, $CDCl_3$): $\delta_H$ (ppm) 7.68 (d, $J$ = 8.7 Hz, 2H, ArC*H*), 7.31 (d, $J$ = 8.7 Hz, 2H, ArC*H*). $^{13}$C{$^{1}$H} NMR (101 MHz, $CDCl_3$): $\delta_C$ (ppm) 152.8 (d, $J$ = 12 Hz, Ar*C*), 127.1 (q, $^{3}J_{C,F}$ = 4 Hz, Ar*C*H), 122.4 (q, $J$ = 5 Hz, Ar*C*H), two quat. C's undetectable.

### 7.4.8 Synthesis of $L_{4.1}$

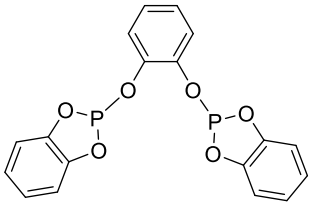

Silyl ether **4.9a** (0.329 g, 1.29 mmol) was added to the chlorophosphite **4.6a** (0.452 g, 2.56 mmol) in MeCN (3 mL). The reaction mixture was stirred at ambient temperature for 4 h. The volatiles were removed under reduced pressure to yield to crude product, which was redissolved in toluene (5 mL). The solution was then passed through a short silica column, which was then washed with toluene (3 x 2 mL). The solvent was removed under reduced pressure to yield the product as a white semi-solid (0.400 g, 80%). $^{31}P\{^{1}H\}$ NMR (162 MHz, $CDCl_3$): $\delta_P$ (ppm) 129.9 (s). $^{1}H$ NMR (400 MHz, $CDCl_3$): $\delta_H$ (ppm) 7.10 (m, 4H, ArC*H*), 6.99 (m, 6H, ArC*H*), 6.90 (m, 2H, ArC*H*). $^{31}P\{^{1}H\}$ NMR data agreed with the literature.[15]

### 7.4.9 Synthesis of $L_{4.2}$

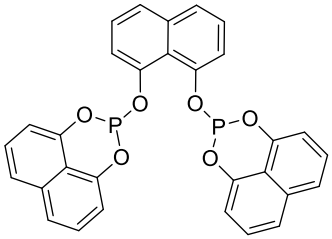

1,8-dihydroxynapthalene (1.00 g, 6.24 mmol) in toluene (15 mL) was cooled to 0 °C and $NEt_3$ (1.74 mL, 12.5 mmol) and $PCl_3$ (0.36 mL, 4.2 mmol) were then added dropwise. The reaction mixture was allowed to warm to ambient temperature and stirred for 2 h. The reaction mixture was filtered, and the solid washed with toluene (3 x 10 mL). Volatiles were removed under reduced pressure to yield the crude product as a light yellow solid. A toluene (20 mL) solution of the crude product was then passed through a short silica column, which was washed with toluene (3 x 10 mL). Volatiles were removed under reduced pressure to yield the product as an off-white solid (0.810 g, 73%). Crystals suitable for analysis by single crystal X-ray diffraction were grown by slow diffusion of hexane into a saturated $CH_2Cl_2$ solution of $L_{4.2}$. $^{31}P\{^{1}H\}$ NMR (162 MHz, $CDCl_3$): $\delta_P$ (ppm) 100.9 (s). $^{1}H$ NMR (400 MHz, $CDCl_3$): $\delta_H$ (ppm) 7.49 (d, $J_{H,H}$ = 8.3 Hz, 4H, ArC*H*), 7.41 (m, 6H, ArC*H*), 7.18 (t, $J_{H,H}$ = 7.9 Hz, 2H, ArC*H*), 7.06 (d, $J_{H,H}$ = 7.5 Hz, 4H, ArC*H*), 6.93 (d, $J_{H,H}$ = 7.5 Hz, 2H, ArC*H*). $^{13}C\{^{1}H\}$ NMR (101 MHz, $CDCl_3$): $\delta_C$ (ppm) 146.3 (s, Ar*C*O), 144.4 (m, Ar*C*O), 137.1 (s, Ar*C*), 135.1 (s, Ar*C*), 127.3 (s, Ar*C*H), 126.1 (s, Ar*C*H), 125.1 (s, Ar*C*H), 122.3 (s, Ar*C*H), 121.3 (t, $J$ = 2 Hz, Ar*C*), 119.3 (t, $J$ = 4 Hz, Ar*C*H), 117.1 (m, Ar*C*), 112.1 (s, Ar*C*H). HR-MS (MALDI): m/z calcd. $C_{30}H_{18}O_6P_2$ $[M+Na]^+$ = 559.0471; obs. = 559.471.

### 7.4.10 Synthesis of *cis*-[$PtMe_2(L_{4.2})$] (4.10)

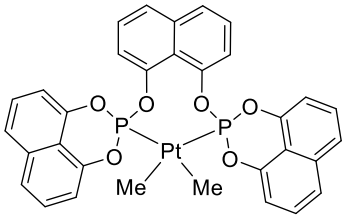


To a solution of [$PtMe_2$(cod)] (0.0150 g, 0.0450 mmol) in toluene (0.5 mL) was added a solution of **$L_{4.2}$** (0.0480 g, 0.0450 mmol) in toluene (0.5 mL). Precipitation of the product immediately occurred. The solid was allowed to settle and the supernatant removed. In air, the remaining residue was washed with toluene (3 x 1 mL). Residual solvent was then removed from the solid under reduced pressure to yield the product as a pale yellow solid (0.0240 g, 70%). Crystals suitable for analysis by single crystal X-ray diffraction were grown by slow diffusion of hexane into a saturated $CH_2Cl_2$ solution of **4.10**. $^{31}P\{^1H\}$ NMR (162 MHz, $CD_2Cl_2$): $\delta_P$ (ppm) 112.6 (s, $^1J_{P,Pt}$ = 2964 Hz). $^1H$ NMR (400 MHz, $CD_2Cl_2$): $\delta_H$ (ppm) 7.74 (d, $J_{H,H}$ = 8.3 Hz, 6H, ArC*H*), 7.62 (t, $J$ = 8.0 Hz, 4H, ArC*H*), 7.35 (m, 6H, ArC*H*), 6.84 (d, $J_{H,H}$ = 7.6 Hz, 2H, ArC*H*), 0.82 (s, $^2J_{H,Pt}$ = 73.0 Hz, 6H, Pt-C$H_3$). $^{13}C\{^1H\}$ NMR (101 MHz, $CD_2Cl_2$): $\delta_C$ (ppm) 145.6 (s, Ar*C*O), 144.3 (s, Ar*C*O), 135.9 (s, Ar*C*), 129.5 (s, Ar*C*), 128.7 (s, Ar*C*), 128.3 (s, Ar*C*H), 127.3 (s, Ar*C*H), 126.9 (s, Ar*C*H), 125.8 (s, Ar*C*), 124.0 (s, Ar*C*H), 122.2 (s, Ar*C*H), 113.2 (s, Ar*C*H), 21.7 (s, Pt-*C*$H_3$).

### 7.4.11 Synthesis of *cis*-[$Mo(CO)_4(L_{4.2})$] (4.11)

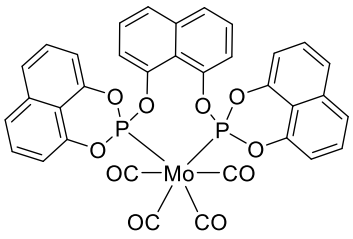


To a solution of [$Mo(CO)_4$(nbd)] (0.0150 g, 0.0499 mmol) in $CH_2Cl_2$ (0.5 mL) was added a solution of **$L_{4.2}$** (0.0300 g, 0.0550 mmol) in $CH_2Cl_2$ (0.5 mL). Precipitation of the product occurred within 10 min. Upon completion, the volatiles were removed under reduced pressure. The product was precipitated with hexane (2 mL). The solid was allowed to settle, and the supernatant removed; the remaining residue was then washed with hexane (3 x 1 mL). Residual solvent was removed from the solid under reduced pressure to yield the product as a yellow solid. The product was partially soluble in all common organic solvents. $^{31}P\{^1H\}$ NMR (162 MHz $CD_2Cl_2$): $\delta_P$ (ppm) 147.8 (s). $^1H$ NMR (400 MHz, $CD_2Cl_2$): $\delta_H$ (ppm) 7.71 (d, $J_{H,H}$ = 8.4 Hz, 6H, ArC*H*), 7.60 (t, $J$ = 8.0 Hz, 4H, ArC*H*), 7.38 (t, $J$ = 8.0 Hz, 2H, ArC*H*), 7.30 (d, $J_{H,H}$ = 7.5 Hz, 4H, ArC*H*), 6.84 (d, $J_{H,H}$ = 7.7 Hz, 2H, ArC*H*) HR-MS (EI): m/z calcd. for $C_{34}H_{18}MoO_{10}P_2$ $[M+H]^+$ = 746.9473; obs. = 746.9510; $[M+Na]^+$ = 768.9320; obs. = 768.9330. IR ($CH_2Cl_2$): ν(CO) = 2057 $cm^{-1}$.

### 7.4.12 Synthesis of *trans*-[$Rh_2Cl_2(CO)_2(\mu\text{-}L_{4.2})_2$] (4.13)

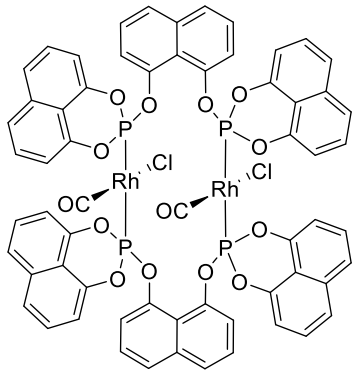

To a solution of [$Rh_2Cl_2(CO)_4$] (0.0200 g, 0.0514 mmol) in $CH_2Cl_2$ (1 mL) was added a solution of **L**$_{4.2}$ (0.0550 g, 0.103 mmol) in $CH_2Cl_2$ (1 mL). After 2 h, upon completion of the reaction, the volatiles were removed under reduced pressure. The product was precipitated with hexane (5 mL). The solid was allowed to settle and the supernatant removed; the remaining residue was then washed with hexane (3 x 1 mL). Residual solvent was then removed from the solid under reduced pressure to yield the product as a yellow solid (0.0410 g, 57%). The product was partially soluble in all common organic solvents. $^{31}P\{^1H\}$ NMR (162 MHz, $CD_2Cl_2$): $\delta_P$ (ppm) 122.1 (d, $^1J_{P,Rh}$ = 180 Hz). $^1H$ NMR (400 MHz, $CD_2Cl_2$): $\delta_H$ (ppm) 7.78 (d, $J$ = 8.5 Hz, 4H, ArC*H*), 7.59 (t, $J$ = 8.0 Hz, 4H, ArC*H*), 7.48 (m, 2H, ArC*H*), 7.29 (t, $J$ = 8.0 Hz, 2H, ArC*H*), 7.06 (d, $J$ = 7.7 Hz, 4H, ArC*H*), 6.89 (d, $J$ = 7.7 Hz, 2H, ArC*H*). IR (solid phase): $\nu$(CO) = 2059, 1980 $cm^{-1}$.

### 7.4.13 Catalytic hydroformylation of 1-hexene using $L_{4.1\text{-}4.3}$

Catalysis was performed using a Baskerville "Multi-Cell" autoclave. The appropriate ligand was added to the autoclave and the system was put under an atmosphere of $N_2$. A solution of [Rh(acac)$(CO)_2$] (0.012 mmol) in toluene (0.5 mL) was then added. This was then washed in using toluene (1 mL) and the autoclave was flushed with three cycles of $CO/H_2$ (*ca.* 10 bar). The autoclave was then pressurised to 15 bar and heated at 90 °C. After 1 h, the autoclave was vented and 1-hexene (0.6 mL, 4.83 mmol) was added. The autoclave was then pressurised to 20 bar $CO/H_2$ and heated at 90 °C for 1 h, unless otherwise stated. The autoclave was transferred to an ice bath and once cooled the system was vented. The reaction mixture was analysed by $^1H$ and $^{31}P\{^1H\}$ NMR spectroscopy. The selectivity and conversion were determined as above (Section 7.3 – conditions A).

## 7.5 Chapter 5

### 7.5.1 Synthesis of $L_{5.2}$

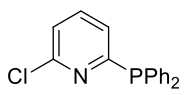

$Ph_2PH$ (2.52 g, 13.5 mmol) in THF (15 mL) was cooled to -78 °C and *n*BuLi (8.45 mL, 13.5 mmol, 1.6 M in hexanes) was added dropwise. After stirring for 30 min at -78 °C the reaction mixture was allowed to warm to ambient

temperature and stirred for 1 h. The reaction mixture was then added dropwise to a solution of 2,6-dichloropyridine (2.00 g, 13.5 mmol) in THF (20 mL) at -78 °C. The reaction mixture was allowed to warm to ambient temperature and stirred for 18 h. Volatiles were removed under reduced pressure and the reaction mixture was dissolved in toluene (20 mL). Deoxygenated $H_2O$ (20 mL) was then added. The toluene layer was extracted, and the aqueous layer washed with toluene (3 x 10 mL). The organic portions were collected, dried over $MgSO_4$, filtered and the volatiles were removed under reduced pressure to yield the crude product as a pale orange solid. Recrystallisation from MeOH gave the product as a white solid (2.44 g). The MeOH supernatant was then placed in a -20 °C freezer where precipitation occurred. The supernatant was removed, and residual solvent removed from the solid under reduced pressure to yield additional product as a white solid (combined yield = 2.97 g, 74%). Crystals suitable for analysis by single crystal X-ray diffraction were grown from a saturated MeOH solution of **$L_{5.2}$**. $^{31}P\{^1H\}$ NMR (162 MHz, $CDCl_3$): $\delta_P$ (ppm) -2.7 (s). $^1H$ NMR (400 MHz, $CDCl_3$): $\delta_H$ (ppm) 7.49 (td, $J_{H,H}$ = 7.8, 1.8 Hz, 1H, Py*H*), 7.38 (m, 10H, Ph*H*), 7.20 (dd, $J_{H,H}$ = 8.0, 0.9 Hz, 1H, Py*H*), 6.95 (dd, 1H, $J_{H,H}$ = 7.5, 0.7 Hz, 1H, Py*H*). $^{31}P\{^1H\}$ and $^1H$ NMR data agreed with the literature.[30]

### 7.5.2 Synthesis of $L_{5.3a}$

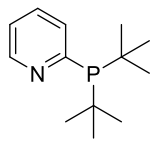


The following procedure was modified from the literature.[31,32] 2-bromopyridine (1.21 ml, 12.7 mmol) in $Et_2O$ (45 mL) was cooled to -78 °C and *n*BuLi (7.96 mL, 12.7 mmol, 1.6 M in hexanes) was added dropwise. After stirring for 1 h at -78 °C, *t*$Bu_2PCl$ (2.20 mL, 11.6 mmol) was added dropwise and the reaction mixture was allowed to warm to ambient temperature. After stirring for 1 h, deoxygenated $H_2O$ (40 mL) was added. The $Et_2O$ layer was extracted, and the aqueous layer washed with $Et_2O$ (3 x 15 mL). The organic portions were combined, dried over $MgSO_4$, filtered and the volatiles were removed under reduced pressure to yield the crude product. The crude product was then passed through silica with $CH_2Cl_2$ and the volatiles were removed. The residue was then purified by distillation (100°C, 0.2 Torr) to yield the product as a pale-yellow oil (1.92 g, 74%). $^{31}P\{^1H\}$ NMR (162 MHz, $CDCl_3$): $\delta_P$ (ppm) 39.9 (s). $^1H$ NMR (400 MHz, $CDCl_3$): $\delta_H$ (ppm) 8.70 (d, $J_{H,H}$ = 4.8 Hz, 1H, Py*H*), 7.57 (m, 2H, Py*H*), 7.16 (m, 1H, Py*H*), 1.21 (d, $^3J_{H,P}$ = 12.0 Hz, 18H, C(C$H_3$)$_3$). $^{31}P\{^1H\}$ and $^1H$ NMR data agreed with the literature.[31]

### 7.5.3 Synthesis of $L_{5.3b}$

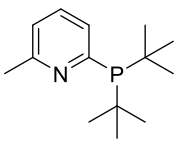

2-bromo-6-methylpyridine (0.30 mL, 2.6 mmol) in $Et_2O$ (10 mL) was cooled to -78 °C and *n*BuLi (1.69 mL, 2.70 mmol, 1.6 M in hexanes) was added dropwise. After stirring for 2 h at -78 °C, *t*$Bu_2PCl$ (0.39 mL, 1.8 mmol) was added and the reaction mixture allowed to warm to ambient temperature. After stirring for 16 h, deoxygenated $H_2O$ (10 mL) was added. The $Et_2O$ layer was extracted and the aqueous layer washed with $Et_2O$ (3 x 10 mL). The organic portions were combined, dried over $MgSO_4$, filtered and the volatiles were removed under reduced pressure to yield the crude product as an orange oil. The crude product was then passed through silica with $CH_2Cl_2$, the volatiles removed under reduced pressure, to yield the product as a colourless oil (0.418 g, 67%). $^{31}P\{^1H\}$ NMR (162 MHz, $CD_2Cl_2$): $\delta_P$ (ppm) 36.8 (s). $^1H$ NMR (400 MHz, $CD_2Cl_2$): $\delta_H$ (ppm) 7.43 (td, $J_{H,H}$ = 7.7, 2.4 Hz, 1H, Py*H*), 7.34 (d, $J_{H,H}$ = 7.7 Hz, 1H, Py*H*), 7.02 (d, $J_{H,H}$ = 7.2 Hz, 1H, Py*H*), 2.51 (s, 3H, C$H_3$), 1.17 (d, $^3J_{H,P}$ = 11.6 Hz, 18H, C(C$H_3$)$_3$). $^{13}C\{^1H\}$ NMR (101 MHz, $CD_2Cl_2$): $\delta_C$ (ppm) 149.2 (s, Py*C*), 134.2 (s, Py*C*), 133.5 (s, Py*C*H), 133.0 (s, Py*C*H), 122.5 (s, Py*C*H), 32.3 (s, *C*(CH$_3$)$_3$), 32.1 (s, *C*(CH$_3$)$_3$), 29.9 (s, C(*C*H$_3$)$_3$), 29.8 (s, C(*C*H$_3$)$_3$), *C*H$_3$ undetectable. HR-MS (EI): calc. for $C_{14}H_{24}NP$ $[M]^+$ = 237.16; obs. = 237.19.

### 7.5.4 Synthesis of $L_{5.4}$

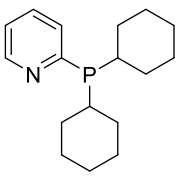

The following procedure was modified from the literature.[33] 2-bromopyridine (0.75 mL, 7.9 mmol) in $Et_2O$ (30 mL) was cooled to -78 °C and *n*BuLi (4.94 mL, 7.91 mmol, 1.6 M in hexanes) was added dropwise. After stirring for 1 h at -78 °C, $Cy_2PCl$ (1.23 mL, 5.54 mmol) was added dropwise and the reaction mixture was allowed to warm to ambient temperature. After stirring for 1 h, deoxygenated $H_2O$ (40 mL) was added. The $Et_2O$ layer was extracted, and the aqueous layer washed with $Et_2O$ (3 x 15 mL). The organic portions were combined, dried over $MgSO_4$, filtered and the volatiles were removed under reduced pressure to yield the crude product. The crude product was then passed through silica with $CH_2Cl_2$, the volatiles removed under reduced pressure, to yield the product as an orange oil (0.894 g, 59%). $^{31}P\{^1H\}$ NMR (162 MHz, $CD_2Cl_2$): $\delta_P$ (ppm) 6.9 (s). $^1H$ NMR (400 MHz, $CD_2Cl_2$): $\delta_H$ (ppm) 8.66 (d, $J_{H,H}$ = 4.9 Hz, 1H, Py*H*), 7.58 (vir. t, $J_{H,H}$ = 7.5 Hz, 1H, Py*H*), 7.47 (m, 1H, Py*H*), 7.17 (m, 1H, Py*H*), 2.08 (vir. td, *J* = 11.7, 3.1 Hz, 2H, Cy*H*), 1.89-1.55 (m, 10H, Cy*H*), 1.40-1.09 (m, 8H, Cy*H*), 0.98 (m, 2H, Cy*H*). $^{31}P\{^1H\}$ and $^1H$ NMR data fitted with literature.[33]

### 7.5.5 Synthesis of $L_{5.5}$

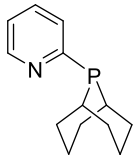

2-bromopyridine (1.10 mL, 11.5 mmol) in xylene (25 mL) was treated with *s*-PhobPH (1.62 g, 11.5 mmol), 1,4-diazabicyclo[2.2.2]octane (DABCO) (3.29 g, 29.5 mmol) and [$Pd(PPh_3)_4$] (0.322 g, 0.295 mmol). The reaction mixture was refluxed at 180 °C for 18 h and then cooled to 100 °C. Xylene (20 mL) was then added to precipitate the product. The solid was allowed to settle and the supernatant removed; the precipitate was then washed with xylene (2 x 10 mL). Volatiles were removed under reduced pressure and the residue triturated with toluene (2 x 10 mL). The volatiles were removed to yield the product as an orange oil (0.420 g, 21%). $^{31}P\{^1H\}$ NMR (162 MHz, $C_6D_6$): $\delta_P$ (ppm) 15.3 (s, P-P species, 9%), -19.6 (s, >85%), contains signals for other unidentified minor impurities. $^1H$ NMR (400 MHz, $C_6D_6$): $\delta_H$ (ppm) 8.54 (d, $J_{H,H}$ = 4.8 Hz, 1H, Py*H*), 7.08 (m, 1H, Py*H*), 6.97 (d, $J_{H,H}$ = 7.6 Hz, 1H, Py*H*), 6.59 (dd, $J_{H,H}$ = 7.5, 4.9 Hz, 1H, Py*H*), 2.46-1.17 (m, 14H, Phob*H*). $^{13}C\{^1H\}$ NMR (101 MHz, $C_6D_6$): $\delta_C$ (ppm) 167.0 (d, $^1J_{C,P}$ = 15 Hz, Py*C*), 150.4 (d, $^3J_{C,P}$ = 5 Hz, Py*C*H), 134.6 (d, $^3J_{C,P}$ = 2 Hz, Py*C*H), 126.1 (d, $^2J_{C,P}$ = 19 Hz, Py*C*H), 120.5 (d, $^4J_{C,P}$ = 2 Hz, Py*C*H), 32.0 (d, $^1J_{C,P}$ = 13 Hz, Phob*C*), 26.2 (d, $J_{C,P}$ = 5 Hz, Phob*C*), 25.4 (d, $J_{C,P}$ = 11 Hz, Phob*C*), 23.5 (d, $J_{C,P}$ = 7 Hz, Phob*C*), 22.4 (d, $J_{C,P}$ = 1 Hz, Phob*C*). HR-MS (ESI): m/z calcd. for $C_{13}H_{18}NP$ $[M]^+$ = 219.1, obs. = 220.1.

### 7.5.6 Synthesis of *cis*-$[PtCl_2(L_{5.2})_2]$ (5.14)

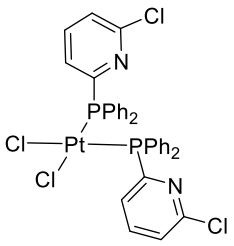

To a solution of $[PtCl_2(cod)]$ (0.0200 g, 0.0535 mmol) in $CH_2Cl_2$ (1 mL) was added a solution of **$L_{5.2}$** (0.0318 g, 0.107 mmol) in $CH_2Cl_2$ (1 mL). Upon completion, the product was precipitated with hexane (5 mL). The solid was allowed to settle, and supernatant was removed; residual solvent was then removed from the solid to yield the product as a white solid (0.0302 g, 70%). Crystals suitable for analysis by single crystal X-ray diffraction were grown by slow diffusion of hexane into a saturated $CH_2Cl_2$ solution of **5.14**. $^{31}P\{^1H\}$ NMR (162 MHz, $CD_2Cl_2$): $\delta_P$ (ppm) 11.0 (s, $^1J_{P,Pt}$ = 3695 Hz). $^1H$ NMR (400 MHz, $CD_2Cl_2$): $\delta_H$ (ppm) 7.92 (dd, $J_{H,H}$ = 7.6, 4.7 Hz, 1H, Py*H*), 7.64 (dd, *J* = 11.0, 8.3 Hz, 4H, Ph*H*), 7.59 (td, $J_{H,H}$ = 7.8, 3.4 Hz, 1 Hz, Py*H*), 7.41 (t, $J_{H,H}$ = 7.5 Hz, 2H, Py*H*), 7.25 (m, 6H, Ph*H*). $^{13}C\{^1H\}$ NMR (126 MHz, $CD_2Cl_2$): $\delta_C$ (ppm) 156.3 (d, *J* = 1 Hz, Ar*C*), 155.6 (d, *J* = 1 Hz, Ar*C*), 151.6 (q, *J* = 9 Hz, Ar*C*), 138.8 (vir. t, *J* = 5 Hz, Py*C*H), 135.9 (vir. t, *J* = 5 Hz, Ph*C*H), 131.8 (s, Py*C*H), 130.1 (m, Py*C*H), 128.5 (vir. t, *J* = 6 Hz, Ph*C*H), 126.1 (s, Ph*C*H). HR-MS (ESI): m/z calcd. for $C_{34}H_{26}Cl_3N_2P_2Pt$ $[M\text{-}Cl]^+$

= 824.0282, obs. = 824.0278.

### 7.5.7 Synthesis of *cis*-[PtCl(κ²-$L_{5.2}$)(κ¹-$L_{5.2}$)][$BF_4$] (5.15)

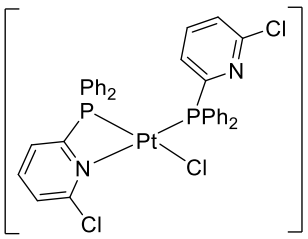

A solution of complex **5.14** (0.0320 g, 0.0368 mmol) in $CH_2Cl_2$ (2 mL) was added to $AgBF_4$ (0.0720 g, 0.0368 mmol). Immediately a white precipitate formed. Upon completion, the supernatant was removed and the precipitate washed with $CH_2Cl_2$ (3 x 1 mL). The washings and supernatant were combined, and the volatiles removed under reduced pressure to yield the product as a white solid (0.0210 g, 63%). $^{31}P\{^1H\}$ NMR (162 MHz, $CD_2Cl_2$): $\delta_P$ (ppm) 4.3 (d, $^2J_{P,P}$ = 6 Hz, $^1J_{P,Pt}$ = 3940 Hz, κ¹-$Ph_2P$), -41.9 (s, $^2J_{P,P}$ = 6 Hz, $^1J_{P,Pt}$ = 3141 Hz, κ²-$Ph_2P$). $^1H$ NMR (400 MHz, $CD_2Cl_2$): $\delta_H$ (ppm) 8.13 (td, $J_{H,H}$ = 8.0, 2.9 Hz, 1H, Py*H*), 7.83-7.78 (m, 4H, ArC*H*), 7.73-7.70 (m, 5H, ArC*H*), 7.62 (td, $J_{H,H}$ = 7.4, 2.0 Hz, 4H, ArC*H*), 7.54 (dd, $J_{H,H}$ = 7.7, 5.2 Hz, 1H, ArC*H*), 7.49-7.45 (m, 9H, ArC*H*), 7.15 (dd, $J_{H,H}$ = 8.1, 2.5 Hz, 1H, Py*H*), 7.05 (dd, $J_{H,H}$ = 7.6, 4.8 Hz, 1H, Py*H*). $^{13}C\{^1H\}$ NMR (101 MHz, $CD_2Cl_2$): $\delta_C$ (ppm) 143.0 (d, $J_{C,P}$ = 5 Hz, Ar*C*), 140.1 (d, $J_{C,P}$ = 9 Hz, Ar*C*), 135.3 (d, $J_{C,P}$ = 11 Hz, Ar*C*), 134.9 (d, $J_{C,P}$ = 13 Hz, Ar*C*), 134.4 (s, Ar*C*H), 133.4 (s, Ar*C*H), 131.8 (s, Ar*C*H), 130.3 (d, $J_{C,P}$ = 13 Hz, Ar*C*H), 129.6 (d, $J_{C,P}$ = 12 Hz, Ar*C*H), 129.4 (m, Ar*C*H), 128.8 (s, Ar*C*H), 128.6 (s, Ar*C*H), 127.8 (s, Ar*C*H), 126.3 (s, Ar*C*H), 125.6 (s, Ar*C*H), 119.0 (s, Ar*C*H), two quat. C's undetectable. HR-MS (ESI): m/z calcd. for $C_{34}H_{26}Cl_3N_2P_2Pt$ $[M\text{-}BF_4]^+$ = 824.0282, obs. = 824.0305.

### 7.5.8 Synthesis of *cis*-[$PdCl_2$($L_{5.2}$)$_2$] (*cis*-5.16)

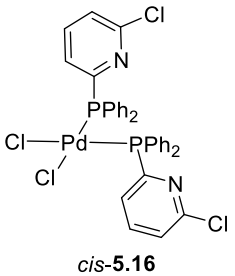

*cis*-**5.16**

To a solution of [$PdCl_2$(NCPh)$_2$] (0.0200 g, 0.0521 mmol) in $CH_2Cl_2$ (1 mL) was added a solution of $\mathbf{L_{5.2}}$ (0.0156 g, 0.0521 mmol) in $CH_2Cl_2$ (1 mL). The product was identified as the *cis* isomer from the subsequent reaction and crystal structure obtained (Section 7.5.9). *In situ* $^{31}P\{^1H\}$ NMR (162 MHz, $CH_2Cl_2$): $\delta_P$ (ppm) 28.5 (s).

### 7.5.9 Synthesis of *cis*- and *trans*-[$PdCl_2(L_{5.2})_2$] (5.16)

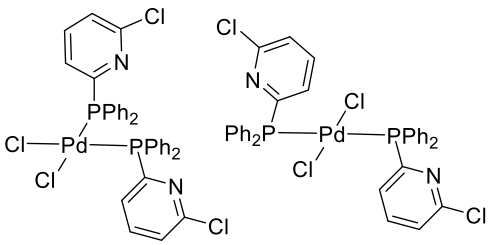


*cis*-**5.16** *trans*-**5.16**

To a solution of [$PdCl_2(NCPh)_2$] (0.0200 g, 0.0521 mmol) in $CH_2Cl_2$ (1 mL) was added a solution of $\mathbf{L_{5.2}}$ (0.0310 g, 0.104 mmol) in $CH_2Cl_2$ (1 mL). Upon completion of the reaction, the volatiles were removed under reduced pressure. The product was precipitated with hexane (*ca.* 5 mL) and the solid was allowed to settle. The supernatant was removed, and remaining residue washed with hexane (3 x 3 mL). Residual solvent was then removed from the solid under reduced pressure to yield the product as a pale-yellow solid (0.0230 g, 58%). Crystals of *cis*-**5.16** suitable for analysis by single crystal X-ray diffraction were grown by slow diffusion of hexane into a saturated $CH_2Cl_2$ solution of the mixture of *cis*- and *trans*-**5.16**. $^{31}P\{^1H\}$ NMR (162 MHz, $CD_2Cl_2$): $\delta_P$ (ppm) 29.2 (s, *cis*-**5.16**, 68%), 23.7 (s, *trans*-**5.16**, 32%). $^1H$ NMR (400 MHz, $CD_2Cl_2$): $\delta_H$ (ppm) 7.86 (m, 1H, Py*H*), 7.69 (dd, $J_{H,H}$ = 11.8, 7.5 Hz, 4H, ArC*H*), 7.57-7.43 (m, 4H, Ph*H*), 7.36-7.26 (m, 4H, Ph*H*). $^{13}C\{^1H\}$ NMR (101 MHz, $CD_2Cl_2$): $\delta_C$ (ppm) 157.6 (d, $J_{C,P}$ = 2 Hz, Ar*C*), 157.0 (d, $J_{C,P}$ = 2 Hz, Ar*C*), 156.7 (s, Ar*C*), 156.4 (s, Ar*C*), 151.9 (m, Ar*C*), 151.7 (m, Ar*C*), 139.0 (m, Py*C*H), 138.6 (vir. t, $J$ = 4 Hz, Py*C*H), 136.1 (vir. t, $J$ = 6 Hz, Ph*C*H), 135.9 (vir. t, $J$ = 5 Hz, Ph*C*H), 131.9 (s, Py*C*H), 131.7 (s, Py*C*H), 130.6 (vir. t, $J$ = 12 Hz, Ar*C*H), 129.0 (m, Ar*C*H), 128.7 (m, Ar*C*H), 128.6 (m, Ar*C*H), 125.9 (s, Ph*C*H), 125.6 (s, Ph*C*H). HR-MS (ESI): m/z calcd. for $C_{34}H_{26}Cl_3N_2P_2Pd$ $[M\text{-}Cl]^+$ = 734.9670, obs. = 734.9663.

### 7.5.10 Synthesis of *cis*-[$PdCl(\kappa^2\text{-}L_{5.1})(\kappa^1\text{-}L_{5.2})][BF_4]$ (5.17)

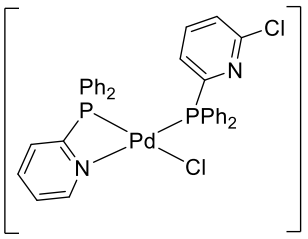


A solution of *cis*- and *trans*-**5.16** (0.0200 g, 0.0259 mmol) in $CH_2Cl_2$ (2 mL) was added to $AgBF_4$ (0.0100 g, 0.0518 mmol). Immediately precipitate formed. Upon completion, the supernatant was removed, and the precipitate washed with $CH_2Cl_2$ (3 x 1 mL). The washings and supernatant were combined, and the volatiles were removed under reduced pressure to yield the product as an orange solid. A 1:1 mixture of complexes **5.17a** and **5.17b** was observed. $^{31}P\{^1H\}$ NMR (122 MHz, $CD_2Cl_2$, -90 °C): $\delta_P$ (ppm) 40.3 (br. s), 37.8 (d, $^2J_{P,P}$ = 28 Hz, $\kappa^1$-$Ph_2P$), 24.3 (br. s, $\kappa^1$-$Ph_2P$), -4.7 (s, $\mathbf{L_{5.2}}$), -30.1 (d, $^2J_{P,P}$ = 33 Hz, $\kappa^2$-$Ph_2P$), -35.5 (d, $^2J_{P,P}$ = 29 Hz, $\kappa^2$-$Ph_2P$). $^1H$ NMR (400 MHz, $CD_2Cl_2$): $\delta_H$ (ppm) 8.03-7.96 (br. m, 2H,

ArC*H*), 7.72 (br. dt, *J* = 9.2, 4.1 Hz, 7H, ArC*H*), 7.59 (br. m, 5H, ArC*H*), 7.49-7.41 (br. m, 12H, ArC*H*).

### 7.5.11 Synthesis of *trans*-[RhCl(CO)($L_{5.2}$)$_2$] (5.18)

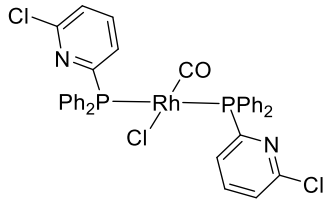

To a solution of [$Rh_2Cl_2(CO)_4$] (0.0200 g, 0.0515 mmol) in $CH_2Cl_2$ (1 mL) was added a solution of **$L_{5.2}$** (0.0613 g, 0.206 mmol) in $CH_2Cl_2$ (1 mL). Upon completion, the volatiles were removed under reduced pressure to yield the product as a yellow solid (0.0640 g, 82%). Crystals suitable for analysis by single crystal X-ray diffraction were grown by slow diffusion of hexane into a saturated $CH_2Cl_2$ solution of **5.18**. $^{31}P\{^1H\}$ NMR (122 MHz, $CD_2Cl_2$, -90°C): $\delta_P$ (ppm) 30.8 (d, $^1J_{P,Rh}$ = 128 Hz). $^1H$ NMR (400 MHz, $CD_2Cl_2$): $\delta_H$ (ppm) 7.86 (d, $J_{H,H}$ = 6.9 Hz, 4H, Ph*H*), 7.69 (d, $J_{H,H}$ = 7.0 Hz, 1H, Py*H*), 7.63 (t, $J_{H,H}$ = 7.7 Hz, 1H, Py*H*), 7.51-7.43 (m, 6H, Ph*H*), 7.31 (dd, $J_{H,H}$ = 7.8, 1.1 Hz, 1H, Py*H*). $^{13}C\{^1H\}$ NMR (101 MHz, $CD_2Cl_2$): $\delta_C$ (ppm) 186.9 (d, $^1J_{C,Rh}$ = 74 Hz, Rh-*C*O), 159.8 (br. s, Ar*C*), 152.0 (s, Ar*C*), 138.9 (s, Py*C*H), 135.7 (s, Ph*C*H), 132.4 (s, Ar*C*), 131.2 (s, Ph*C*H), 129.9 (s, Py*C*H), 128.8 (s, Ph*C*H), 125.4 (s, Py*C*H). HR-MS (ESI): m/z calcd. for $C_{35}H_{26}Cl_2N_2OP_2Rh$ $[M\text{-}Cl]^+$ = 724.9947, obs. = 724.9939. IR ($CH_2Cl_2$): ν(CO) = 1987 $cm^{-1}$.

**General procedure for the reaction between ligand and [$PtCl_2$(cod)] in a 1:1 ratio**

To a solution of [$PtCl_2$(cod)] (0.0200 g, 0.0535 mmol) in $CH_2Cl_2$ (1 mL) was added a solution of ligand (0.0535 mmol) in $CH_2Cl_2$ (1 mL). Upon completion, the product was precipitated with hexane (*ca.* 15 mL). The solid was allowed to settle, and the supernatant was removed; the precipitate was then washed with hexane (3 x 3 mL). Residual solvent was removed from the solid under reduced pressure to yield the product(s).

### 7.5.12 Synthesis of [$PtCl_2$(κ$^2$-$L_{5.3a}$)] (5.19a)/ *trans*-[PtCl(κ$^2$-$L_{5.3a}$)(κ$^1$-$L_{5.3a}$)][Cl] (*trans*-5.20a)

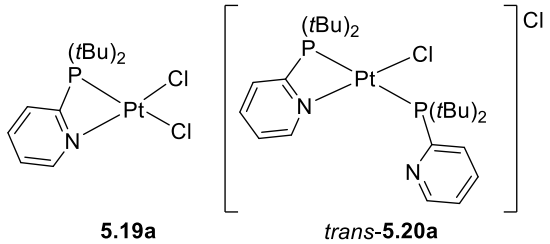

**5.19a** *trans*-**5.20a**

White solid. Crystals of **5.19a** suitable for analysis by single crystal X-ray diffraction were grown by slow diffusion of hexane into a saturated $CH_2Cl_2$ solution of the mixture of **5.19a** and *trans*-**5.20a**.$^{31}P\{^1H\}$ NMR (162 MHz, $CD_2Cl_2$): $\delta_P$ (ppm) 39.5 (d, $^2J_{P,P}$ = 363 Hz, $^1J_{P,Pt}$ = 2565 Hz, 25%, κ$^1$-*Pt*$Bu_2$ *trans*-**5.20a**), -15.1 (s, $^1J_{P,Pt}$ = 3136 Hz, 50%, **5.19a**), -18.1 (d, $^2J_{P,P}$ = 363 Hz, $^1J_{P,Pt}$ =

1916 Hz, 25%, κ²-*Pt*$tBu_2$ *trans*-**5.20a**). HR-MS (ESI): m/z calcd. for *trans*-**5.20a** $C_{26}H_{44}ClN_2P_2Pt$ $[M\text{-}Cl]^+$ = 676.2316; obs = 676.2329.

### 7.5.13 Synthesis of *trans*-[$PtCl_2(L_{5.4})_2$] (*trans*-5.21b)

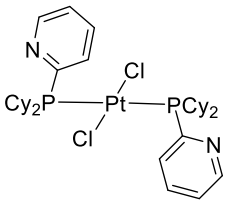

Cream solid. Contains *trans*-**5.21b** and [$PtCl_2$(cod)] in *ca.* a 1:1 ratio (as expected). $^{31}P\{^1H\}$ NMR (162 MHz, $CD_2Cl_2$): $\delta_P$ (ppm) 27.5 (s, $^1J_{P,Pt}$ = 2481 Hz). $^1H$ NMR (400 MHz, $CD_2Cl_2$): $\delta_H$ (ppm) 8.68 (d, $J_{H,H}$ = 4.4 Hz, 1H, Py*H*), 7.90 (d, $J_{H,H}$ = 7.6 Hz, 1H, Py*H*), 7.72 (dt, $J_{H,H}$ = 7.6, 4.0 Hz, 1H, Py*H*), 7.30 (m, 1H, Py*H*), 1.83-1.66 (m, 8H, Cy*H*), 1.48-1.25 (m, 8H, Cy*H*), 1.13 (m, 4H, Cy*H*), 0.86 (m, 2H, Cy*H*), contains signals for [$PtCl_2$(*cod*)]. HR-MS (ESI): m/z calcd. for $C_{34}H_{52}ClN_2P_2Pt$ $[M\text{-}Cl]^+$ = 781.3, obs. = 781.3.

**General procedure for the reaction between ligand and [$PtCl_2$(cod)] in a 2:1 ratio**

To a solution of [$PtCl_2$(cod)] (0.0200 g, 0.0535 mmol) in $CH_2Cl_2$ (1 mL) was added a solution of ligand (0.107 mmol) in $CH_2Cl_2$ (1 mL). Upon completion, the product was precipitated with hexane (*ca.* 15 mL). The solid was allowed to settle and the supernatant removed; the precipitate was then washed with hexane (3 x 3 mL). Residual solvent was then removed from the solid under reduced pressure to yield the product.

### 7.5.14 Synthesis of *trans*-[PtCl(κ²-$L_{5.3a}$)(κ¹-$L_{5.3a}$)][Cl] (*trans*-5.20a)

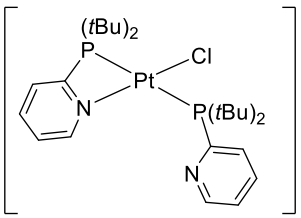

White solid. $^{31}P\{^1H\}$ NMR (162 MHz, $CD_2Cl_2$): $\delta_P$ (ppm) 42.2 (s, $^1J_{P,Pt}$ = 2482 Hz, 10%, *trans*-**5.21a**), 40.0 (d, $^2J_{P,P}$ = 363 Hz, $^1J_{P,Pt}$ = 2571 Hz, κ¹-*t*$Bu_2P$ *trans*-**5.20a**), 39.4 (br. s, 15%, $\mathbf{L_{5.3a}}$), -17.8 (d, $^2J_{P,P}$ = 363 Hz, $^1J_{P,Pt}$ = 1916 Hz, κ²-*t*$Bu_2P$ *trans*-**5.20a**). $^1H$ NMR (400 MHz, $CD_2Cl_2$): $\delta_H$ (ppm) 8.85 (d, $J_{H,H}$ = 4.8 Hz, 1H, Py*H*), 8.70-8.58 (m, 2H, Py*H*), 7.99 (m, 1H, Py*H*), 7.91 (t, $J_{H,H}$ = 6.7 Hz, 1H, Py*H*), 7.69 (m, 1H, Py*H*), 7.47 (m, 1H, Py*H*), 7.40 (t, $J_{H,H}$ = 6.9 Hz, 1H, Py*H*), 1.66-1.24 (m, 74H, *t*Bu-C($CH_3$)$_3$ (all species)), also contained signals for *trans*-**5.21a** and $\mathbf{L_{5.3a}}$. HR-MS (ESI): calc. for *trans*-**5.20a** $C_{26}H_{44}ClN_2P_2Pt$ $[M\text{-}Cl]^+$ = 676.2313; obs = 676.2316.

### 7.5.15 Synthesis of *cis*-[PtCl(κ²-$L_{5.4}$)(κ¹-$L_{5.4}$)][Cl] (*cis*-5.20b)

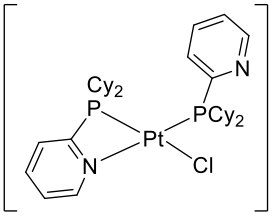

Cream solid. $^{31}P\{^1H\}$ NMR (162 MHz, $CD_2Cl_2$): $\delta_P$ (ppm) 21.5 (d, $^2J_{P,P}$ = 7 Hz, $^1J_{P,Pt}$ = 3601 Hz, κ¹-$Cy_2P$), -22.8 (d, $^2J_{P,P}$ = 7 Hz, $^1J_{P,Pt}$ = 3110 Hz, κ²-$Cy_2P$). $^1H$ NMR (400 MHz, $CD_2Cl_2$): $\delta_H$ (ppm) 9.04 (t, $J_{H,H}$ = 4.2 Hz, 1H, Py*H*), 8.89 (d, $J_{H,H}$ = 4.7 Hz,

1H, Py*H*), 8.49 (m, Py*H*), 8.14 (br. s, 1H, Py*H*), 7.94 (m, 1H, Py*H*), 7.87 (t, $J_{H,H}$ = 6.6 Hz, 1H, Py*H*), 7.74 (d, $J_{H,H}$ = 7.9 Hz, 1H, Py*H*), 7.60 (m, 1H, Py*H*), 1.96-1.67 (m, 22H, Cy*H*), 1.55-1.28 (m, 14H, Cy*H*), 1.22-0.96 (m, 6H, Cy*H*), 0.86 (m, 2H, Cy*H*), 0.59 (m), contains signals for *ca.* 10% [$PtCl_2$(cod)]. HR-MS (ESI): m/z calcd. for $C_{34}H_{52}ClN_2P_2Pt$ $[M\text{-}Cl]^+$ = 781.3, obs. = 781.3.

**General procedure for the reaction between ligand and [$PdCl_2(NCPh)_2$)] in a 1:1 ratio**

To a solution of [$PdCl_2(NCPh)_2$] (0.0200 g, 0.0521 mmol) in $CH_2Cl_2$ (1 mL) was added a solution of ligand (0.0521 mmol) in $CH_2Cl_2$ (1 mL). Upon completion, the solvent was removed under reduced pressure and the crude product was dissolved in toluene (5 mL). Volatiles were then removed under reduced pressure to yield the product(s).

### 7.5.16 Synthesis of [$PdCl_2(\kappa^2\text{-}L_{5.3a})$] (5.22a)

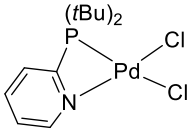


Yellow solid (0.0100 g, 48%). Crystals suitable for analysis by single crystal X-ray diffraction were grown by slow diffusion of hexane into a saturated $CH_2Cl_2$ solution of **5.22a**. $^{31}P\{^1H\}$ NMR (162 MHz, $CD_2Cl_2$): $\delta_P$ (ppm) -11.3 (s). $^1H$ NMR (400 MHz, $CD_2Cl_2$): $\delta_H$ (ppm) 8.88 (m, 1H, Py*H*), 8.08 (tt, $J_{H,H}$ = 7.9, 1.8 Hz, 1H, Py*H*), 7.64 (m, 1H, Py*H*), 7.55 (dd, $J_{H,H}$ = 7.9, 4.1 Hz, 1H, Py*H*), 1.60 (d, $^3J_{H,P}$ = 17.1 Hz, 18H, C($CH_3$)$_3$). $^{13}C\{^1H\}$ NMR (101 MHz, $CD_2Cl_2$): $\delta_C$ (ppm) 149.4 (d, $^1J_{C,P}$ = 9 Hz, Py*C*), 139.9 (d, $^2J_{C,P}$ = 4 Hz, Py*C*H), 130.8 (d, $^3J_{C,P}$ = 3 Hz, Py*C*H), 128.5 (d, $^3J_{C,P}$ = 1 Hz, Py*C*H), 116.9 (s, Py*C*H), 37.8 (d, $^1J_{C,P}$ = 12 Hz, *C*($CH_3$)$_3$), 29.7 (d, $^2J_{C,P}$ = 3 Hz, C(*C*$H_3$)$_3$). HR-MS (ESI): m/z calcd. for $C_{13}H_{22}ClNPPd$ $[M\text{-}Cl]^+$ = 364.02, obs. = 364.02.

### 7.5.17 Synthesis of [$PdCl_2(\kappa^2\text{-}L_{5.4})$] (5.22b) and [$Pd_2Cl_4(L_{5.4})_2$] (5.23b)

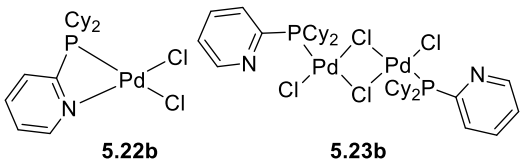


**5.22b** **5.23b**

Yellow solid. $^{31}P\{^1H\}$ NMR (162 MHz, $CD_2Cl_2$): $\delta_P$ (ppm) 42.8 (s, 67%, **5.23b**), -30.2 (s, 33%, **5.22b**). $^1H$ NMR (400 MHz, $CD_2Cl_2$): $\delta_H$ (ppm) 9.12 (s, 1H, Py*H*), 8.30 (m, 1H, Py*H*) 8.06 (m, 1H, Py*H*), 7.94 (m, 1H, Py*H*), 7.78 (s, 1H, Py*H*), 7.69-7.58 (m, 2H, Py*H*), 7.53-7.42 (m, 2H, Py*H*), 3.14 (br. s, 1H, Cy*H*), 2.97 (br. s, 1H, Cy*H*), 2.50-2.30 (m, 5H, Cy*H*), 2.18 (m, 2H, Cy*H*), 2.06 (m, 2H, Cy*H*), 2.00-1.69 (m, 14H, Cy*H*), 1.44-1.20

(m, 12H, Cy*H*), 1.14 (m, 2H, Cy*H*). HR-MS (ESI): m/z calcd. for **5.23b** $C_{34}H_{56}Cl_3N_2P_2Pd_2$ $[M\text{-}Cl+2H_2]^+$ = 871.4, obs. = 871.1.

### 7.5.18 Synthesis of $[Pd_2Cl_4(L_{5.5})_2]$ (5.23c), *cis*- and *trans*-$[PdCl_2(L_{5.4})_2]$ (5.24c)

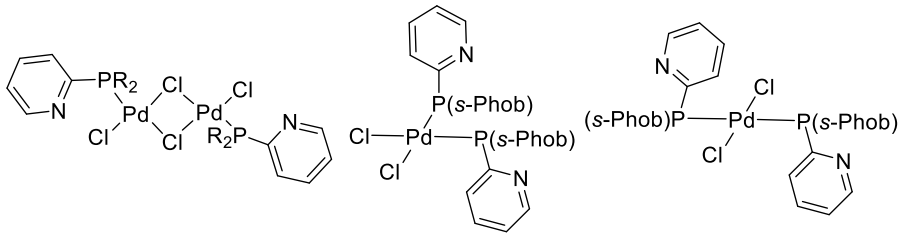


**5.23c** *cis*-**5.24c** *trans*-**5.24c**

Light orange solid. $^{31}P\{^1H\}$ NMR (162 MHz, $CD_2Cl_2$): $\delta_P$ (ppm) 34.2 (br. s, 80%, **5.23c**), 15.8 (s, 10%, *trans*-**5.24c**), 13.7 (s, 10%, *cis*-**5.24c**). HR-MS (ESI): m/z calcd. for **5.24** $C_{26}H_{38}ClN_2P_2Pd$ $[M\text{-}Cl+H_2]^+$ = 581.1, obs. = 581.1; for **5.23c** $C_{26}H_{38}Cl_3N_2P_2Pd_2$ $[M\text{-}Cl+H_2]^+$ = 757.0, obs. = 756.9.

### General procedure for the reaction between ligand and $[PdCl_2(NCPh)_2]$ in a 2:1 ratio

To a solution of $[PdCl_2(NCPh)_2]$ (0.0200 g, 0.0521 mmol) in $CH_2Cl_2$ (1 mL) was added a solution of ligand (0.104 mmol) in $CH_2Cl_2$ (1 mL). Upon completion, the solvent was removed under reduced pressure and the crude product was dissolved in toluene (5 mL). Volatiles were then removed under reduced pressure to yield the product(s).

### 7.5.19 Synthesis of $[PdCl_2(\kappa^2\text{-}L_{5.3a})]$ (5.22a), *trans*-$[PdCl_2(L_{5.3a})_2]$ (*trans*-5.24a) and $L_{5.3a}$

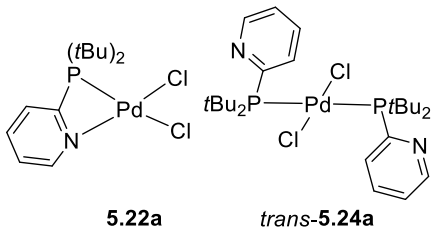


**5.22a** *trans*-**5.24a**

Yellow solid. Crystals of *trans*-**5.24a** suitable for analysis by single crystal X-ray diffraction were grown by slow diffusion of hexane into a saturated $CH_2Cl_2$ solution of the mixture of **5.22a**, *trans*-**5.24a** and $L_{5.3a}$. $^{31}P\{^1H\}$ NMR (162 MHz, $CD_2Cl_2$): $\delta_P$ (ppm) 52.8 (s, 50%, *trans*-**5.24a**), 39.3 (s, 25%, $L_{5.3a}$), -11.7 (s, 25%, **5.22a**). $^1H$ NMR (400 MHz, $CD_2Cl_2$): $\delta_H$ (ppm) 8.89 (br. s, 1H, Py*H*), 8.68 (br s, 1H, Py*H*), 8.60 (d, $J_{H,H}$ = 3.4 Hz, 1H, Py*H*), 8.07 (tt, $J_{H,H}$ = 8.0, 1.9 Hz, 1H, Py*H*), 7.95 (d, $J_{H,H}$ = 8.1 Hz, 1H, Py*H*), 7.69-7.61 (m, 2H, Py*H*), 7.61-7.52 (m, 3H, Py*H*), 7.26-7.10 (m, 4H, Py*H*), 1.60 (d, $^3J_{H,P}$ = 17.1 Hz, 36H, C(C$H_3$)$_3$), 1.20 (d, $^3J_{H,P}$ = 11.6 Hz, 18H, C(C$H_3$)$_3$).

### 7.5.20 Synthesis of $[Pd_2Cl_4(L_{5.4})_2]$ (5.23b) and *trans*-$[PdCl_2(L_{5.4})_2]$ (*trans*-5.24b)

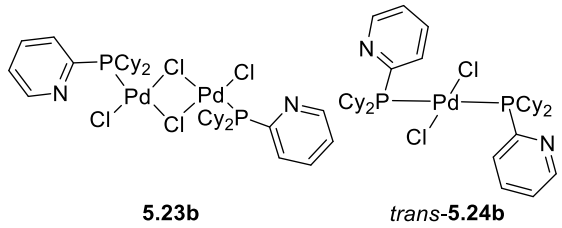


**5.23b** *trans*-**5.24b**

Yellow solid. $^{31}P\{^1H\}$ NMR (162 MHz, $CD_2Cl_2$): $\delta_P$ (ppm) 42.8 (s, 25%, **5.23b**), 33.1 (s, 75%, *trans*-**5.24b**). $^1H$ NMR (400 MHz, $CD_2Cl_2$): $\delta_H$ (ppm) 8.65 (m, 2H, Py*H*), 7.82 (m, 2H, Py*H*), 7.67 (m, 3H, Py*H*), 7.46 (m, 1H, Py*H*), 7.30-7.25 (m, 2H, Py*H*), 7.23-7.18 (m, 1H, Py*H*), 7.17-7.08 (m, 1H, Py*H*), 2.31 (s, 2H, Cy*H*), 2.11 (br. s, 4H, Cy*H*), 1.90-1.61 (m, 24H, Cy*H*), 1.55-1.17 (m, 28H, Cy*H*), 1.12 (m, 7H, Cy*H*). HR-MS (ESI): m/z calcd. for *trans*-**5.24b** $C_{34}H_{52}ClN_2P_2Pd$ $[M\text{-}Cl]^+$ = 691.2333, obs. = 691.2333; for **5.23b** $C_{34}H_{54}Cl_3N_2P_2Pd_2$ $[M\text{-}Cl+H_2]^+$ = 869.0897, obs. = 869.0771.

### 7.5.21 Synthesis of *cis*- and *trans*-$[PdCl_2(L_{5.5})_2]$ (5.24c)

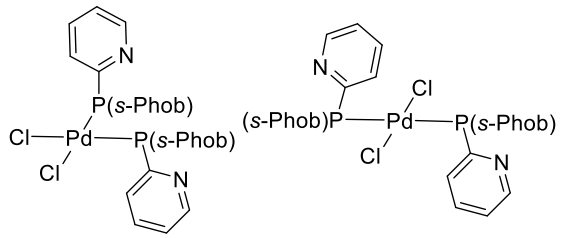


*cis*-**5.24c** *trans*-**5.24c**

Orange solid. Crystals of *cis*-**5.24c** suitable for analysis by single crystal X-ray diffraction were grown by slow diffusion of hexane into a saturated $CH_2Cl_2$ solution of the mixture of *cis*- and *trans*-**5.24c**. $^{31}P\{^1H\}$ NMR (162 MHz, $CD_2Cl_2$): $\delta_P$ (ppm) 15.8 (s, 90%, *cis*-**5.24c**), 10.3 (s, 10%, *trans*-**5.24c**). $^1H$ NMR (400 MHz, $CD_2Cl_2$): $\delta_H$ (ppm) 8.66 (d, $J_{H,H}$ = 4.9 Hz, 1H, Py*H*), 8.28 (t, $J_{H,H}$ = 6.8 Hz, 1H, Py*H*), 7.83 (m, 1H, Py*H*), 7.36 (t, $J_{H,H}$ = 5.2 Hz, 1H, Py*H*), 2.10-0.78 (m, 36H, Phob*H*). HR-MS (ESI): m/z calcd. for $C_{26}H_{38}ClN_2P_2Pd$ $[M\text{-}Cl+H_2]^+$ = 581.1, obs. = 581.1.

### 7.5.22 *In situ* synthesis of *cis*-$[PdCl(\kappa^2\text{-}L_{5.5})(\kappa^1\text{-}L_{5.5})][BF_4]$ (*cis*-5.25c$[BF_4]$)

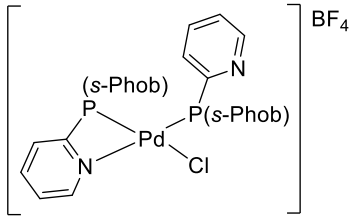


A solution of *cis*- and *trans*-**5.24c** (0.0120 g, 0.0194 mmol) in $CH_2Cl_2$ (1 mL) was added to $AgBF_4$ (0.004 g, 0.0194 mmol). Immediately a white precipitate formed. The reaction was monitored by $^{31}P\{^1H\}$ NMR spectroscopy. *In situ* $^{31}P\{^1H\}$ NMR (162 MHz, $CH_2Cl_2$): $\delta_P$ (ppm) 29.2 (d, $^2J_{P,P}$ = 8 Hz, $\kappa^1$-Phob*P*), -36.1 (d, $^2J_{P,P}$ = 9 Hz, $\kappa^2$-Phob*P*).

**General procedure for the synthesis of *trans*-$[RhCl(CO)L_2]$ complexes (5.26a-c)**

To a solution of $[Rh_2Cl_2(CO)_4]$ (0.0200 g, 0.0515 mmol) in $CH_2Cl_2$ (1 mL) was added a solution of ligand (0.206 mmol) in $CH_2Cl_2$ (1 mL). Upon completion, the product was

precipitated with hexane (*ca.* 10 mL). The solid was allowed to settle and the supernatant was removed; the precipitate was then washed with hexane (3 x 2 mL). Residual solvent was then removed from the solid under reduced pressure to yield the product.

### 7.5.23 Synthesis of *trans*-[RhCl(CO)($L_{5.3a}$)$_2$] (5.26a)

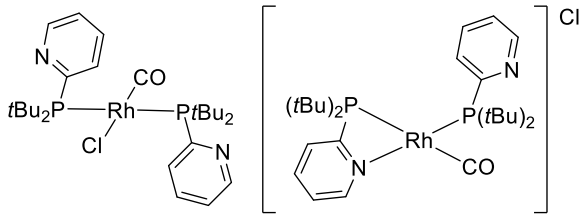


**5.26a** **5.26a'**

An equilibrium between complexes **5.26a** and **5.26a'** was established. Dark orange solid. $^{31}P\{^1H\}$ NMR (162 MHz, $CD_2Cl_2$): $\delta_P$ (ppm) 60.3 (br. d, $^1J_{P,Rh}$ = 124 Hz, **5.26a**), 43.3 (br. s, **5.26a'**), 39.5 (s, $\mathbf{L_{5.3a}}$), 35.5 (d, $^1J_{P,Rh}$ = 136 Hz, <5%, unidentified species). $^{31}P\{^1H\}$ NMR (162 MHz, $CD_2Cl_2$, -90 °C): $\delta_P$ (ppm) 66.5 (br. dd, $^2J_{P,P}$ = 242 Hz, $^1J_{P,Rh}$ = 128Hz, κ$^1$-*t*Bu$_2$*P* **5.26a'**), 16.7 (br. d, $^2J_{P,P}$ = 226 Hz, κ$^2$-*t*Bu$_2$*P* **5.26a'**). HR-MS (ESI): m/z calcd. for $C_{27}H_{44}N_2OP_2Rh$ $[M\text{-}Cl]^+$ = 577.2, obs. = 577.2. IR ($CH_2Cl_2$): ν(CO) = 1956 cm$^{-1}$.

### 7.5.24 Synthesis of *trans*-[RhCl(CO)($L_{5.4}$)$_2$] (5.26b)

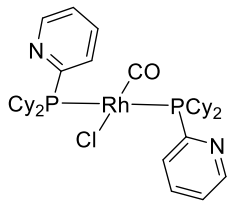


Light brown solid (0.0281 g, 76%). $^{31}P\{^1H\}$ NMR (162 MHz, $CD_2Cl_2$): $\delta_P$ (ppm) 41.2 (d, $^1J_{P,Rh}$ = 122 Hz). $^1H$ NMR (400 MHz, $CD_2Cl_2$): $\delta_H$ (ppm) 8.71 (d, $J_{H,H}$ = 4.7 Hz, 1H, Py*H*), 8.00 (d, $J_{H,H}$ = 7.3 Hz, 1H, Py*H*), 7.73 (t, $J_{H,H}$ = 7.8 Hz, 1H, Py*H*), 7.29 (dd, $J_{H,H}$ = 7.6, 4.9 Hz, 1H, Py*H*), 2.88 (m, 2H, Cy*H*), 2.15 (br. s, 2H, Cy*H*), 1.83-1.67 (m, 8H, Cy*H*), 1.35 (m, 8H, Cy*H*), 1.11 (m, 2H, Cy*H*). $^{13}C\{^1H\}$ NMR (101 MHz, $CD_2Cl_2$): $\delta_C$ (ppm) 221.8 (m, Rh-*C*O), 126.1 (vir. t, $J_{C,P}$ = 26 Hz, Py*C*), 149.6 (vir. t, $J_{C,P}$ = 5 Hz, Py*C*H), 135.1 (vir. t, $J_{C,P}$ = 5 Hz, Py*C*H), 133.7 (vir. t, $J_{C,P}$ = 14 Hz, Py*C*H), 124.3 (s, Py*C*H), 32.3 (vir. t, $J_{C,P}$ = 12 Hz, Cy*C*H$_2$), 29.3 (s, Cy*C*H$_2$), 29.2 (s, Cy*C*H$_2$), 27.7 (vir. t, $J_{C,P}$ = 7 Hz, Cy*C*H$_2$), 27.5 (vir. t, $J_{C,P}$ = 5 Hz, Cy*C*H$_2$), 27.1 (s, Cy*C*H$_2$). HR-MS (ESI): m/z calcd. for $C_{35}H_{52}N_2OP_2Rh$ $[M\text{-}Cl]^+$ = 681.2604, obs. = 681.2597. IR ($CH_2Cl_2$): ν(CO) = 1961 cm$^{-1}$.

### 7.5.25 Synthesis of *trans*-[RhCl(CO)($L_{5.5}$)$_2$] (5.26c)

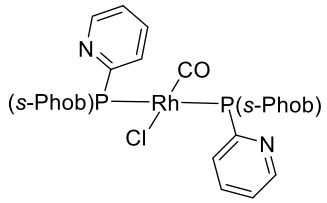


Only *ca.* 80% pure by $^{31}P\{^1H\}$ NMR; other unidentifiable Rh species present. $^{31}P\{^1H\}$ NMR (162 MHz, $CD_2Cl_2$): $\delta_P$ (ppm) 17.9 (d, $^1J_{P,Rh}$ = 120 Hz). HR-MS (ESI): m/z calcd. for $C_{27}H_{36}ClKN_2OP_2Rh$ $[M+K]^+$ = 643.1, obs. = 643.1. IR ($CH_2Cl_2$): ν(CO) = 1969 cm$^{-1}$.

### 7.5.26 Catalytic methoxycarbonylation of phenylacetylene and 3,3'-dimethylbutyne (Method A)

Adapted from a previously reported procedure.[34,35] Catalysis was performed using a Baskerville "Multi-Cell" autoclave. The ligand (0.11 mmol) was added to the autoclave and the system put under an atmosphere of $N_2$. Solutions of $Pd(OAc)_2$ ($5.5 \times 10^{-3}$ mmol) in MeOH (0.5 mL) and $TsOH.H_2O$ (0.22 mmol) in MeOH (0.5 mL) were added, followed by the substrate (5.5 mmol). This was then washed in using MeOH (0.5 mL) and the autoclave flushed with three cycles of CO (*ca.* 10 bar). The autoclave was then pressurised to 45 bar and heated to 60 °C. After either 1 h or 4.5 h, the autoclave was transferred to an ice bath and once cooled, the system was vented.

When using 3,3'-dimethylbutyne as the substrate, a small sample of the reaction mixture was dissolved in $CDCl_3$ and analysed by $^1H$ NMR spectroscopy. Conversion and selectivity were determined by integration of the 3,3'-dimethylbutyne alkynyl proton ($\delta_H$ 2.05 ppm) and the 4,4'-dimethyl-methylester ($\delta_H$ 7.10 and 6.02 ppm) and 3,3'-dimethyl-2-methylene-methylester ($\delta_H$ 5.87 and 5.48 ppm) alkenyl protons. For phenylacetylene, see below (Section 7.5.27).

### 7.5.27 Catalytic methoxycarbonylation of phenylacetylene (Method B)

Adapted from a previously reported procedure.[34,35] Catalysis was performed using a Baskerville "Multi-Cell" autoclave. The ligand ($5.5 \times 10^{-2}$ mmol) was added to the autoclave and the system was put under an atmosphere of $N_2$. Solutions of $Pd(OAc)_2$ ($2.8 \times 10^{-3}$ mmol) in MeOH (0.5 mL) and $TsOH.H_2O$ (0.11 mmol) in MeOH (0.5 mL) were added, followed by phenylacetylene (5.5 mmol). This was then washed in using MeOH (0.5 mL) and the autoclave was flushed with three cycle of CO (*ca.* 10 bar). The autoclave was then pressurised to 45 bar and heated to 60 °C. After 15 min or 1 h, the autoclave was transferred to an ice bath and once cooled, the system was vented.

When using phenylacetylene, for both methods A and B, a small sample of the reaction mixture was dissolved in $CDCl_3$ and analysed by $^1H$ NMR spectroscopy. Conversion and selectivity were determined by integration of the phenylacetylene alkynyl proton ($\delta_H$ 3.10 ppm) and the methyl atropate ($\delta_H$ 6.38 and 5.90 ppm) and methyl cinnamate ($\delta_H$ 7.71 and 6.42 ppm) alkenyl protons.

### 7.5.28 Catalytic methoxycarbonylation of phenylacetylene on a larger scale

The following procedure was performed and supplied by Dr M. Waugh and M. Nixon (at Lucite).[36] In a $N_2$ glove-box, [$Pd(OAc)_2$] (0.0370 g, 0.164 mmol) and the appropriate ligand (3.30 mmol for 0.1 mol% cat loading) were added to a schlenk flask. The schlenk flask was removed from the glove-box and put under an atmosphere of $N_2$. MeOH (200 mL) was then added, followed by $TsOH.H_2O$ (1.26 g, 6.60 mmol) in MeOH, and phenylacetylene (17.1 g, 167 mmol). The autoclave was put under vacuum for 30 min and the catalyst solution was then added. The autoclave was then pressurised to 45 bar of CO and heated to 60 °C. After 4 h, unless otherwise stated, the autoclave was cooled to ambient temperature and the system was vented.

A sample of the reaction mixture was dissolved in $CDCl_3$ and analysed by $^1H$ NMR spectroscopy: conversion and selectivity were determined by setting the integral area for the phenyl protons to 903 in this case ($\delta_H$ 7.38-7.30 ppm), because 903 mmol of phenyl protons were present in the reaction mixture at the start of the reaction, and integrating the relative methyl atropate alkenyl signal ($\delta_H$ 6.34 ppm) (which if 100% conversion was achieved would be equal to 165).[36]

### 7.5.29 Catalytic methoxycarbonylation of propyne

The following procedure was performed and supplied by Dr M. Waugh and M. Nixon (at Lucite).[36] In a $N_2$ glove-box, [$Pd(OAc)_2$] and the appropriate ligand were added to a schlenk flask. The schlenk flask was removed from the glove-box and put under an atmosphere of $N_2$. MeOH (200 mL) was then added, followed by $TsOH.H_2O$ in MeOH (100 mL). The autoclave was put under vacuum for 30 min and then the catalyst solution was added. Propyne was condensed into a pre-evacuated cooled pressure bomb and then added to the autoclave, which was then pressurised to 45 bar of CO and heated at 60 °C. The gas pressure of the autoclave was monitored throughout the reaction. After 4 h, unless otherwise stated, the autoclave was cooled to ambient temperature and the system was vented.

The reaction mixture was distilled under vacuum and the volatiles were collected in a liquid $N_2$ cooled flask. The volatiles were allowed to warm to ambient temperature and then weighed and analysed by Agilent GC. The % weight of methyl methacrylate (MMA) and methyl crotonate in the reaction volatiles were calculated from the GC analysis, and in combination with the mass of the reaction volatiles the mass of the products were

determined and therefore the selectivity and turnover number calculated (TON = mol of product produced per mol of Pd catalyst used).

## 7.6 Chapter 6

### 7.6.1 Synthesis of [Rh(acac)(cod*)] complexes (*(S,S)-*/*rac*-6.6)

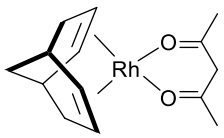


The following procedure was modified from the literature.[3] The following reaction was carried out in a $N_2$ glove-box. To a solution of [Rh(acac)($C_2H_4$)$_2$] (0.200 g, 0.774 mmol) in $CDCl_3$ (5 mL) was added *rac*-cod* (0.153 g, 0.929 mmol, 73% wt% soln in pentane).[3,37] The reaction vessel was open to the $N_2$ atmosphere in order to release the $C_2H_4$ that was generated. The reaction was monitored by $^1$H NMR spectroscopy and stirred for 30 h. Upon completion the volatiles were removed under reduced pressure (1 x$10^{-6}$ Torr) to yield the product as a yellow solid (0.161 g, 64%). $^1$H NMR (400 MHz, $CDCl_3$): $\delta_H$ (ppm) 5.32 (s, 1H, acac C*H*), 4.45 (m, 2H, cod* C*H*), 3.82 (m, 2H, cod* C*H*), 2.81 (dt, $J_{H,H}$ = 15.2, 4.2 Hz, 2H, cod* C*H*), 2.12 (m, 4H, cod* C$H_2$), 1.92 (d, $J_{H,H}$ = 0.6, 6H, acac C$H_3$), 1.16 (m, 2H, cod* C$H_2$). $^1$H NMR data agreed with the literature data.[3] The same procedure was used to prepare the enantiomerically pure complex *(S,S)*-**6.6**, but *(S,S)*-cod* was used instead of *rac*-cod*.

**General procedure for the synthesis of *cis*-[Rh(cod*)$L_2$][OTf] complexes (6.7a-e)**
To a solution of *rac*-**6.6** (0.0220 g, 0.0681 mmol) and the ligand (0.0280 g, 0.136 mmol) in $CH_2Cl_2$ (1 mL) was added $Me_3SiOTf$ (1.00 mL, 0.0681 mmol, 1.26 M in $CH_2Cl_2$). Upon completion of the reaction, the volatiles were removed under reduced pressure. The product was precipitated with hexane (*ca.* 10 mL). The solid was allowed to settle and the supernatant was removed; residual solvent was then removed from the solid under reduced pressure to yield the product. The same procedure was used to prepare the enantiomerically pure complexes **6.7a*** and **6.7b***, but *(S,S)*-**6.6** was used instead of *rac*-**6.6**.

### 7.6.2 Synthesis of *cis*-[Rh(*rac*-cod*)($L_{6.1}$)$_2$][OTf] (6.7a)

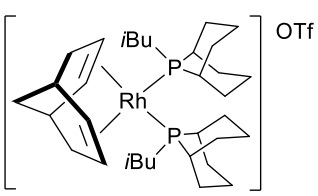


Orange solid (0.0370 g, 70%). Crystals of *δ-(S,S)*-**6.7a** suitable for analysis by single crystal X-ray diffraction were grown by slow diffusion of hexane into a saturated chlorobenzene solution of **6.7a**. $^{31}$P{$^1$H} NMR (162 MHz, $CD_2Cl_2$): $\delta_P$ (ppm) 9.5 (s, 2%), 2.0 (d, $^1J_{P,Rh}$ = 147 Hz, 95%), 1.7 (d, $^1J_{P,Rh}$ = 145 Hz, 5%, minor diastereomer).

$^{1}$H NMR (400 MHz, $CD_2Cl_2$): $\delta_H$ (ppm) 5.76 (d, $J_{H,H}$ = 7.5 Hz, 2H, cod* C*H*), 5.68 (m, 0.1H, cod* C*H* (minor diastereomer)), 4.47 (m, 2H, cod* C*H*), 4.28 (m, 0.1H, cod* C*H* (minor diastereomer)), 2.53 (s, 4H, cod* C$H_2$), 2.36-1.72 (m, 38H, C$H_2$, C*H*), 1.52 (m, 2H, C$H_2$), 1.16 (vir. t, $J_{H,H}$ = 5.8 Hz, 12H, *i*Bu-C$H_3$). $^{13}$C{$^{1}$H} NMR (101 MHz, $CD_2Cl_2$): $\delta_C$ (ppm) 94.7 (s, cod* *C*H), 94.0 (s, cod* *C*H), 40.6 (s, *C*$H_2$), 34.9 (m, *C*$H_2$), 32.5 (s, *C*$H_2$), 31.2 (s, *C*$H_2$), 31.1 (s, *C*$H_2$), 28.8 (s, *C*H), 28.0 (s, *C*H), 27.2 (m, *C*$H_2$), 27.0 (s, *C*H), 26.6 (s, *C*H), 26.4 (s, *i*Bu-(*C*$H_3$)$_2$), 24.4 (s, *i*Bu-(*C*$H_3$)$_2$), 22.3 (s, *C*$H_2$), 19.4 (s, *C*$H_2$). HR-MS (ESI): m/z calc. for $C_{33}H_{58}P_2Rh$ [M-OTf]$^+$ = 619.3069; obs = 619.3060.

### 7.6.3 Synthesis of *cis*-[Rh(*rac*-cod*)($L_{6.2}$)$_2$][OTf] (6.7b)

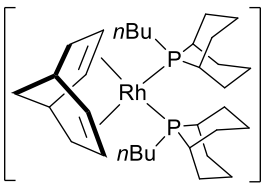


Orange solid (0.0320 g, 60%). Crystals of *δ-(S,S)-* and *λ-(R,R)-* **6.7b** suitable for analysis by single crystal X-ray diffraction were grown by slow diffusion of hexane into a saturated chlorobenzene solution of **6.7b**. $^{31}$P{$^{1}$H} NMR (162 MHz, $CD_2Cl_2$): $\delta_P$ (ppm) 4.2 (d, $^{1}J_{P,Rh}$ = 145 Hz, 4%, minor diastereomer), 0.4 (d, $^{1}J_{P,Rh}$ = 146 Hz, 96%). $^{1}$H NMR (400 MHz, $CD_2Cl_2$): $\delta_H$ (ppm) 5.56 (d, $J_{H,H}$ = 7.5 Hz, 2H, cod* C*H*), 5.29 (s, 0.1H, cod* C*H* (minor diastereomer)), 4.51 (t, $J_{H,H}$ = 6.6 Hz, 2H, cod* C*H*), 4.10 (br. s, 0.1H, cod* C*H* (minor diastereomer)), 2.51 (s, 4H, cod* C$H_2$), 2.36 (m, 4H), 2.19-1.41 (m, 48H, C$H_2$, C*H*), 1.01 (t, $^{3}J_{H,H}$ = 7.3 Hz, 6H, *n*Bu-C$H_3$). $^{13}$C{$^{1}$H} NMR (101 MHz, $CD_2Cl_2$): $\delta_C$ (ppm) 95.3 (s, cod* *C*H), 94.5 (s, cod* *C*H), 39.4 (s, *C*$H_2$), 30.5 (m, *C*$H_2$), 30.2 (s, *C*$H_2$), 28.5 (s, *C*$H_2$), 27.5 (m, *C*H), 26.7 (s, *C*H), 26.5 (s, *C*$H_2$), 25.3 (m, *C*$H_2$), 24.9 (m, *C*$H_2$), 21.6 (m, *C*$H_2$, *C*H), 18.2 (s, *C*$H_2$), 13.6 (s, *n*Bu-*C*$H_3$). HR-MS (ESI): m/z calc. for $C_{33}H_{58}P_2Rh$ [M-OTf]$^+$ = 619.3069; obs = 619.3058.

### 7.6.4 Synthesis of *cis*-[Rh(*rac*-cod*)($L_{6.3}$)$_2$][OTf] (6.7c)

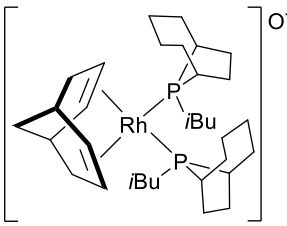


Orange solid (0.0240 g, 46%). $^{31}$P{$^{1}$H} NMR (162 MHz, $CD_2Cl_2$): $\delta_P$ (ppm) 41.8 (d, $^{1}J_{P,Rh}$ = 142 Hz, 90%), 40.3 (d, $^{1}J_{P,Rh}$ = 140 Hz, 10%). $^{1}$H NMR (400 MHz, $CD_2Cl_2$): $\delta_H$ (ppm) 6.05 (m, 0.2H, cod* C*H* (minor diastereomer)), 5.79 (m, 2H, cod* C*H*), 4.57 (m, 0.2H cod* C*H* (minor diastereomer)), 4.40 (m, 2H, cod* C*H*), 2.71 (m, 2H, cod* C*H*), 2.55-1.39 (m, 48H, C*H*, C$H_2$), 1.09 (d, $^{3}J_{H,H}$ = 6.6 Hz, 6H, *i*Bu-C$H_3$), 1.03 (d, $^{3}J_{H,H}$ = 6.5 Hz, 6H, *i*Bu-C$H_3$). HR-MS (ESI): m/z calc. for $C_{33}H_{58}P_2Rh$ [M-OTf]$^+$ = 619.3069; obs = 619.3049.

### 7.6.5 Synthesis of *cis*-[Rh(*rac*-cod*)($L_{6.4}$)$_2$][OTf] (6.7d)

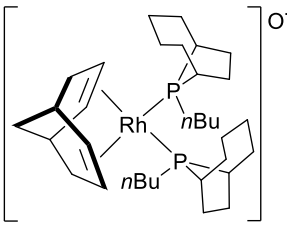


Orange solid (0.0280 g, 52%). $^{31}P\{^1H\}$ NMR (162 MHz, $CD_2Cl_2$): $\delta_P$ (ppm) 50.3 (d, $^1J_{P,Rh}$ = 145 Hz, 10%, unidentified species), 40.5 (d, $^1J_{P,Rh}$ = 141 Hz, 84%), 40.7 (d, $^1J_{P,Rh}$ = 142 Hz, 6%, minor diastereomer). $^1H$ NMR (400 MHz, $CD_2Cl_2$): $\delta_H$ (ppm) 6.05 (m, 0.2H, cod* C*H* (minor diastereomer)), 5.72 (d, $J_{H,H}$ = 7.4 Hz, 2H, cod* C*H*), 4.54 (t, $^3J_{H,H}$ = 5.9 Hz, 2H, cod* C*H*), 4.07 (br. s, 0.2H, cod* C*H* (minor diastereomer)), 2.44-1.40 (m, 90H, C$H_2$, C*H*), 1.25 (m, 10H, C*H*, C$H_2$), 0.94 (m, 10H, *n*Bu-C$H_3$), 0.85 (m, 14H, C$H_3$), mixture contained impurities. HR-MS (ESI): m/z calc. for $C_{33}H_{58}P_2Rh$ $[M\text{-}OTf]^+$ = 619.3069; obs = 619.3043.

### 7.6.6 Synthesis of *cis*-[Rh(*rac*-cod*)($L_{6.5}$)$_2$][OTf] (6.7e)

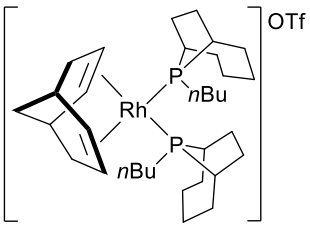


The workup described above yielded an oily residue, so the product was triturated with $Et_2O$ (10 mL). The solid was allowed to settle, and supernatant was removed; residual solvent was then removed from the solid under reduced pressure to yield the product as an orange solid (0.0150 g, 28%). $^{31}P\{^1H\}$ NMR (162 MHz, $CD_2Cl_2$): $\delta_P$ (ppm) 40.7 (d, $^1J_{P,Rh}$ = 142 Hz, 35%, minor diastereomer), 38.8 (d, $^1J_{P,Rh}$ = 140 Hz, 65%). $^1H$ NMR (400 MHz, $CD_2Cl_2$): $\delta_H$ (ppm) 5.36 (br. m, 1H, cod* C*H* (minor diastereomer)), 5.24 (br. m, 2H, cod* C*H*), 4.27 (br. s, 3H, cod* C*H*), 2.52-2.29 (m, 14H, C$H_2$, C*H*), 2.21-1.51 (m, 58H, C$H_2$, C*H*), 1.01 (vir. t, $J_{H,H}$ = 7.3 Hz, 9H, *n*Bu-C$H_3$). HR-MS (ESI): m/z calc. for $C_{33}H_{58}P_2Rh$ $[M\text{-}OTf]^+$ = 619.3069; obs = 619.3067.

### 7.6.7 Procedure for the kinetic study on the epimerisation of complexes 6.7a-e

At 0 °C, to a solution of *rac*-**6.6** (0.0110 g, 0.0341 mmol) and the ligand (0.0140 g, 0.069 mmol) in $CH_2Cl_2$ (0.5 mL) was added $Me_3SiOTf$ (0.5 mL, 0.0341 mmol, 1.26 M in $CH_2Cl_2$). The NMR sample was kept at 0 °C until the $^{31}P\{^1H\}$ NMR spectroscopic kinetic data was collected, at ambient temperature.

### 7.6.8 Catalytic asymmetric hydrogenation procedure

Catalysis was performed using a Baskerville "Multi-Cell" autoclave. Pre-prepared complexes **6.7a** or **6.7a*** and the appropriate substrate (0.200 mmol) were added to the autoclave and the system was put under a $N_2$ atmosphere. The appropriate solvent (3 or

5 mL) was then added and the reaction mixture stirred for 5 min to ensure the solutions were homogenised. For the runs conducted at lower temperatures, the autoclave was placed in the appropriate cooling bath and stirred for a further 10 min to reach the required temperature. The autoclave was then flushed with three cycles of $H_2$ (*ca.* 10 bar) and pressurised with $H_2$. After stirring the reaction mixture for the required time, the system was vented. A small sample (0.2 mL) of the reaction mixture was dissolved in $CH_2Cl_2$ and analysed by GC.

GC conditions for enantiomer resolution:

MAA: Varian CP-Chirasil-DEX CD (25 m) column. 90 °C for 1 min, then 5 °C/min to 140 °C for 11 min. Retention times: 7.71 (*S*), 7.89 (*R*).

MAC: Varian CP-Chirasil-DEX CD (25 m) column. 120 °C for 1 min, then 3 °C/ min to 175 °C for 15 min. Retention times: 18.50 (*R*), 18.65 (*S*).

## 7.7 References


1 W. M. Abdou and M. R. Mahran, *Phosphorus and Sulfur*, 1986, **26**, 119–127.

2 M. Poirier, M. Simard and J. D. Wuest, *Organometallics*, 1996, **15**, 1296–1300.

3 M. Mayr, C. J. R. Bataille, S. Gosiewska, J. A. Raskatov and J. M. Brown, *Tetrahedron Asymmetry*, 2008, **19**, 1328–1332.

4 J. X. McDermott, J. F. White and G. M. Whitesides, *J. Am. Chem. Soc.*, 1976, **98**, 6521–6528.

5 R. Bassan, K. H. Bryars, L. Judd, A. W. G. Platt and P. G. Pringle, *Inorg. Chim. Acta*, 1986, **121**, 41–42.

6 L. E. Crascall and J. L. Spencer, *Inorg. Synth.*, 1990, **28**, 126–129.

7 M. S. Kharasch, R. C. Seyler and F. R. Mayo, *J. Am. Chem. Soc.*, 1938, **60**, 882–884.

8 M. Carreira, M. Charernsuk, M. Eberhard, N. Fey, R. Van Ginkel, A. Hamilton, W. P. Mul, A. G. Orpen, H. Phetmung and P. G. Pringle, *J. Am. Chem. Soc.*, 2009, **131**, 3078–3092.

9 J. M. Lister, *PhD Thesis*, 2013, University of Bristol.

10 M. Moghadam, S. Tangestaninejad, V. Mirkhani, I. Mohammadpoor-Baltork and S. Gharaati, *Appl. Organomet. Chem.*, 2009, **23**, 446–454.

11 I. Neda, A. Fischer, T. Kaukorat, P. G. Jones and R. Schmutzler, *Chem. Ber.*, 1994, **127**, 1579–1586.

12 M. Al-Masri, D. Fritsch and H. R. Kricheldorf, *Macromolecules*, 2000, **33**, 7127–7135.

13 S. Wagner, M. Rakotomalala, Y. Bykov, O. Walter and M. Doring, *Heteroat. Chem.*, 2012, **25**, 216–222.

14 J. Coetzee, G. R. Eastham, A. M. Z. Slawin and D. J. Cole-Hamilton, *Org. Biomol. Chem.*, 2012, **10**, 3677–3688.

15 J. J. C. van Lier, R. J. M. Hermans and H. M. Buck, *Phosphorus Sulfur Relat. Elem.*, 1984, **19**, 173–188.

16 J. Gloede, U. Pieper and W. D. Habicher, *Zeitschrift für Anorg. und Allg. Chemie*, 2002, **628**, 877.

17 E. E. Nifant'ev, T. S. Kukhareva, I. A. Soldatova and T. G. Chukbar, *Zhurnal Obs.*

*Khimii*, 1986, **56**, 2487–2491.

18 E. E. Nifant'ev, T. S. Kukhareva, I. A. Soldatova, S. Belostotskaya, V. V Ershov and L. K. Vasyanina, *Zhurnal Obs. Khimii*, 1988, **58**, 2242–2246.

19 D. J. St-Cyr, M. S. Morin, F. B. Belanger-Gariepy, B. A. Arndtsen, E. H. Krenske and K. N. Houk, *J. Org. Chem.*, 2010, **75**, 4261–4273.

20 T. G. Meyer, A. Fischer, P. G. Jones and R. Schmutzler, *Zeitschrift fur Naturforschung, B*, 1993, **48**, 659–71.

21 L. M. Voropai, N. G. Ruchkina, E. E. Milliaresi and E. E. Nifant'ev, *J. Gen. Chem. USSR*, 1985, **55**, 55–62.

22 C. Crocker and R. J. Goodfellow, *J. Chem. Soc. Dalton Trans.*, 1977, 1687–1689.

23 P. B. Hitchcock, S. Morton and J. F. Nixon, *J. Chem. Soc. Dalton Trans.*, 1985, 1295–1301.

24 J. C. Shattuck, C. M. Shreve and S. E. Solomon, *Org. Lett.*, 2001, **3**, 3021–3023.

25 M. Jereb, *Tetrahedron*, 2012, **68**, 3861–3867.

26 L. C. Moores, D. Kaur, M. D. Smith and J. S. Poole, *J. Org. Chem.*, 2019, **84**, 3260–3269.

27 J. Schraml, M. Kvíčalová, V. Chvalovský, T. Elder and R. Brežný, *Magn. Reson. Chem.*, 1990, **28**, 973–978.

28 A. A. Bredikhin, Z. A. Bredikhina, L. Gaisina, E. L. Strunskaya and N. M. Azancheev, *Russ. Chem. Bull.*, 2000, **49**, 310–313.

29 P. Jiang, X. Guo, H. Fu, Y. Jiang and Y. Zhao, *Synlett*, 2005, 2537–2539.

30 L. Hintermann, T. T. Dang, A. Labonne, T. Kribber, L. Xiao and P. Naumov, *Chem. Eur. J. A*, 2009, **15**, 7167–7179.

31 P. G. Edwards, I. A. Fallis and B. S. Young, *GB Patent*, 2001, GB 2378182 A.

32 E. G. Bowes, D. D. Beattie and J. A. Love, *Inorg. Chem.*, 2019, **58**, 2925–2929.

33 D. Pingen, C. Müller and D. Vogt, *Angew. Chemie Int. Ed.*, 2010, **49**, 8130–8133.

34 M. L. Clarke, D. J. Cole-Hamilton, D. F. Foster, A. M. Z. Slawin and J. D. Woollins, *J. Chem. Soc. Dalton Trans.*, 2002, 1618–1624.

35 T. A. Shuttleworth, A. M. Miles-Hobbs, P. G. Pringle and H. A. Sparkes, *Dalton*

*Trans.*, 2016, **46**, 125–137.

36 M. Nixon, M. Waugh and G. R. Eastham, *Unpublished Work*, 2019, Lucite.

37 G. Mislin and M. Miesch, *Eur. J. Org. Chem.*, 2001, 1753–1759.

# Chapter 8

# Appendix

## 8.1 X-ray crystallography

All X-ray diffraction experiments were carried out at 100 K, with the exception of **2.10b** and $\mathbf{L}_{4.2}$ which were carried out at 200 K. All data were collected on a Bruker APEX II diffractometer using Mo-K$\alpha$ radiation ($\lambda$ = 0.71073 Å). Intensities were integrated in SAINT[1] and absorption corrections based on equivalent reflections were applied using SADABS.[2] All structures were solved using ShelXT,[3] ShelXS[4] and Superflip,[5,6] and refined by full matrix least squares against $F^2$ in ShelXL[4,7] using Olex2.[8] All of the non-hydrogen atoms were refined anisotropically. While all of the hydrogen atoms were located geometrically and refined using a riding model. Crystal structure and refinement data are given in Table 8.1.

**Table 8.1** Crystal data.

| Identification code | **2.7a** | **2.7b** | **2.7c** |
|---|---|---|---|
| Empirical formula | $C_{16}H_8F_2MoO_8P_2$ | $C_{24}H_{12}F_2MoO_8P_2$ | $C_{28}H_{16}F_2MoO_8P_2$ |
| Formula weight | 524.10 | 624.22 | 676.29 |
| Temperature/K | 100(2) | 100(2) | 100(2) |
| Crystal system | orthorhombic | orthorhombic | monoclinic |
| Space group | *Pnma* | *Fdd*2 | $P2_1/c$ |
| *a*/Å | 13.9152(3) | 43.6028(6) | 17.5271(6) |
| *b*/Å | 20.6660(4) | 9.9809(2) | 7.6758(3) |
| *c*/Å | 6.43140(10) | 10.58170(10) | 21.0653(7) |
| α/° | 90 | 90 | 90 |
| β/° | 90 | 90 | 111.373(2) |
| γ/° | 90 | 90 | 90 |
| Volume/Å$^3$ | 1849.49(6) | 4605.10(12) | 2639.11(17) |
| Z | 4 | 8 | 4 |
| $\varrho_{calc}$g/cm$^3$ | 1.882 | 1.801 | 1.702 |
| μ/mm$^{-1}$ | 0.946 | 0.776 | 0.684 |
| F(000) | 1032.0 | 2480.0 | 1352.0 |
| Crystal size/mm$^3$ | 0.344 × 0.325 × 0.199 | 0.294 × 0.288 × 0.126 | 0.402 × 0.258 × 0.252 |
| Radiation | MoKα (λ = 0.71073) | MoKα (λ = 0.71073) | MoKα (λ = 0.71073) |
| 2θ range for data collection/° | 3.942 to 55.988 | 5.688 to 55.826 | 3.99 to 55.946 |
| Index ranges | -18 ≤ h ≤ 18,<br>-26 ≤ k ≤ 27,<br>-8 ≤ l ≤ 8 | -57 ≤ h ≤ 57,<br>-13 ≤ k ≤ 13,<br>-13 ≤ l ≤ 11 | -23 ≤ h ≤ 22,<br>-9 ≤ k ≤ 10,<br>-27 ≤ l ≤ 27 |
| Reflections collected | 15356 | 10131 | 23439 |
| $R_{int}$ / $R_{sigma}$ | 0.0247 / 0.0151 | 0.0193 / 0.0170 | 0.0216 /0.0207 |
| Data/restraints/parameters | 2297/0/139 | 2624/1/168 | 6334/0/370 |
| Goodness-of-fit on F$^2$ | 1.109 | 1.112 | 1.028 |
| Final R indexes [I>=2σ (I)] | $R_1$ = 0.0205,<br>$wR_2$ = 0.0466 | $R_1$ = 0.0145,<br>$wR_2$ = 0.0375 | $R_1$ = 0.0211,<br>$wR_2$ = 0.0529 |
| Final R indexes [all data] | $R_1$ = 0.0232,<br>$wR_2$ = 0.0478 | $R_1$ = 0.0148,<br>$wR_2$ = 0.0376 | $R_1$ = 0.0249,<br>$wR_2$ = 0.0546 |
| Largest diff. peak/hole / e Å$^{-3}$ | 0.56/-0.39 | 0.25/-0.24 | 0.38/-0.39 |
| Flack parameter | - | -0.035(11) | - |

**Table 8.1** Crystal data (continued).

| Identification code | **2.7d** | **2.7e** | **2.8c** |
|---|---|---|---|
| Empirical formula | $C_{30}H_{20}F_2MoO_8P_2$ | $C_{26}H_{18}MoO_{10}P_2$ | $C_{24}H_{16}Cl_2F_2O_4P_2Pt$ |
| Formula weight | 704.34 | 648.28 | 734.30 |
| Temperature/K | 100(2) | 100(2) | 100(2) |
| Crystal system | triclinic | triclinic | triclinic |
| Space group | *P*-1 | *P*-1 | P-1 |
| *a*/Å | 9.0915(3) | 8.2570(2) | 8.9338(2) |
| *b*/Å | 12.3578(5) | 11.6685(3) | 9.8824(2) |
| *c*/Å | 13.8479(5) | 14.7840(4) | 15.4858(4) |
| α/° | 104.240(2) | 69.9560(10) | 99.689(2) |
| β/° | 98.951(3) | 76.9430(10) | 94.617(2) |
| γ/° | 100.618(3) | 83.4250(10) | 115.7300(10) |
| Volume/Å$^3$ | 1448.86(9) | 1302.45(6) | 1195.78(5) |
| Z | 2 | 2 | 2 |
| $\varrho_{calc}$g/cm$^3$ | 1.614 | 1.653 | 2.039 |
| μ/mm$^{-1}$ | 0.627 | 0.684 | 6.271 |
| F(000) | 708.0 | 652.0 | 704.0 |
| Crystal size/mm$^3$ | 0.256 × 0.231 × 0.15 | 0.297 × 0.279 × 0.216 | 0.259 × 0.145 × 0.08 |
| Radiation | MoKα (λ = 0.71073) | MoKα (λ = 0.71073) | MoKα (λ = 0.71073) |
| 2θ range for data collection/° | 4.664 to 55.98 | 2.992 to 55.934 | 4.698 to 55.9 |
| Index ranges | -11 ≤ h ≤ 11, -16 ≤ k ≤ 16, -18 ≤ l ≤ 18 | -10 ≤ h ≤ 10, -15 ≤ k ≤ 15, -19 ≤ l ≤ 19 | -11 ≤ h ≤ 11, -13 ≤ k ≤ 13, -19 ≤ l ≤ 20 |
| Reflections collected | 26861 | 24212 | 21890 |
| $R_{int}$ / $R_{sigma}$ | 0.0525 / 0.0495 | 0.0265 / 0.0245 | 5733 [$R_{int}$ = 0.0438, $R_{sigma}$ = 0.0416] |
| Data/restraints/parameters | 6977/0/388 | 6269/0/354 | 5733/0/316 |
| Goodness-of-fit on F$^2$ | 1.014 | 1.022 | 1.065 |
| Final R indexes [I>=2σ (I)] | $R_1$ = 0.0342, $wR_2$ = 0.0668 | $R_1$ = 0.0238, $wR_2$ = 0.0558 | $R_1$ = 0.0261, $wR_2$ = 0.0498 |
| Final R indexes [all data] | $R_1$ = 0.0484, $wR_2$ = 0.0719 | $R_1$ = 0.0278, $wR_2$ = 0.0577 | $R_1$ = 0.0336, $wR_2$ = 0.0516 |
| Largest diff. peak/hole / e Å$^{-3}$ | 0.47/-0.51 | 0.49/-0.36 | 1.16/-0.99 |
| Flack parameter | - | - | - |

**Table 8.1** Crystal data (continued).

| Identification code | **2.8e** | **2.10b**·$C_6H_5Cl$ | **2.10e** |
|---|---|---|---|
| Empirical formula | $C_{22}H_{18}Cl_2O_6P_2Pt$ | $C_{46}H_{29}ClF_4O_8P_4Pt$ | $C_{44}H_{36}O_{12}P_4Pt$ |
| Formula weight | 706.29 | 1140.11 | 1075.70 |
| Temperature/K | 100.0 | 200(2) | 99.98 |
| Crystal system | triclinic | tetragonal | triclinic |
| Space group | P-1 | *P*4/*n* | *P*-1 |
| a/Å | 8.2014(2) | 15.2985(4) | 11.8627(2) |
| b/Å | 9.8489(2) | 15.2985(4) | 12.1538(2) |
| c/Å | 14.7353(3) | 8.8050(3) | 15.4498(3) |
| α/° | 77.3976(10) | 90 | 83.6712(10) |
| β/° | 83.9807(9) | 90 | 77.7952(10) |
| γ/° | 75.1287(10) | 90 | 73.4378(10) |
| Volume/Å$^3$ | 1121.15(4) | 2060.76(13) | 2083.86(7) |
| Z | 2 | 2 | 2 |
| $\varrho_{calc}$g/cm$^3$ | 2.092 | 1.837 | 1.714 |
| μ/mm$^{-1}$ | 6.678 | 3.701 | 3.586 |
| F(000) | 680.0 | 1120.0 | 1068.0 |
| Crystal size/mm$^3$ | 0.376 × 0.292 × 0.058 | 0.379 × 0.117 × 0.102 | 0.449 × 0.293 × 0.084 |
| Radiation | MoKα (λ = 0.71073) | MoKα (λ = 0.71073) | MoKα (λ = 0.71073) |
| 2Θ range for data collection/° | 2.836 to 60.43 | 3.766 to 55.762 | 3.502 to 59.148 |
| Index ranges | -11 ≤ h ≤ 11, -13 ≤ k ≤ 13, -20 ≤ l ≤ 20 | -20 ≤ h ≤ 19, -18 ≤ k ≤ 20, -11 ≤ l ≤ 11 | -16 ≤ h ≤ 16, -16 ≤ k ≤ 16, -21 ≤ l ≤ 21 |
| Reflections collected | 25381 | 18431 | 45772 |
| Independent reflections | 6657 [$R_{int}$ = 0.0332, $R_{sigma}$ = 0.0304] | 0.0734 / 0.0435 | 0.0322 / 0.0286 |
| Data/restraints/parameters | 6657/360/391 | 2476/85/180 | 11692/0/554 |
| Goodness-of-fit on F$^2$ | 1.042 | 1.176 | 1.033 |
| Final R indexes [I>=2σ (I)] | $R_1$ = 0.0198, $wR_2$ = 0.0424 | $R_1$ = 0.0390, $wR_2$ = 0.0679 | $R_1$ = 0.0195, $wR_2$ = 0.0437 |
| Final R indexes [all data] | $R_1$ = 0.0230, $wR_2$ = 0.0433 | $R_1$ = 0.0587, $wR_2$ = 0.0724 | $R_1$ = 0.0219, $wR_2$ = 0.0445 |
| Largest diff. peak/hole / e Å$^{-3}$ | 1.25/-0.65 | 0.64/-0.78 | 0.95/-0.81 |
| Flack parameter | - | - | - |

**Table 8.1** Crystal data (continued).

| Identification code | **$L_{2.8}$** | **2.7h** | **$L_{4.2}$** |
|---|---|---|---|
| Empirical formula | $C_{12}H_{10}FO_2P$ | $C_{28}H_{20}F_2MoO_8P_2$ | $C_{30}H_{18}O_6P_2$ |
| Formula weight | 236.17 | 680.32 | 536.38 |
| Temperature/K | 100(2) | 100(2) | 200(2) |
| Crystal system | triclinic | monoclinic | triclinic |
| Space group | P-1 | $P2_1/c$ | P-1 |
| a/Å | 8.3229(2) | 7.8434(2) | 7.2434(2) |
| b/Å | 8.5875(2) | 18.9214(4) | 11.7049(3) |
| c/Å | 8.7858(3) | 18.5143(4) | 14.2729(4) |
| α/° | 68.494(2) | 90 | 84.8305(14) |
| β/° | 84.637(2) | 90.6770(10) | 88.0629(15) |
| γ/° | 65.826(2) | 90 | 81.1711(14) |
| Volume/Å$^3$ | 531.81(3) | 2747.48(11) | 1190.66(6) |
| Z | 2 | 4 | 2 |
| $\rho_{calc}$g/cm$^3$ | 1.475 | 1.645 | 1.496 |
| μ/mm$^{-1}$ | 0.252 | 0.658 | 0.230 |
| F(000) | 244.0 | 1368.0 | 552.0 |
| Crystal size/mm$^3$ | 0.301 × 0.25 × 0.16 | 0.474 × 0.371 × 0.206 | 0.509 × 0.349 × 0.25 |
| Radiation | MoKα (λ = 0.71073) | MoKα (λ = 0.71073) | MoKα (λ = 0.71073) |
| 2Θ range for data collection/° | 4.994 to 55.702 | 3.078 to 55.906 | 3.534 to 55.7 |
| Index ranges | -10 ≤ h ≤ 10, -11 ≤ k ≤ 11, -11 ≤ l ≤ 11 | -10 ≤ h ≤ 10, -24 ≤ k ≤ 24, -24 ≤ l ≤ 24 | -9 ≤ h ≤ 9, -15 ≤ k ≤ 15, -18 ≤ l ≤ 18 |
| Reflections collected | 8986 | 25012 | 21422 |
| Independent reflections | 2531 [$R_{int}$ = 0.0277, $R_{sigma}$ = 0.0266] | 6604 [$R_{int}$ = 0.0305, $R_{sigma}$ = 0.0283] | 5652 [$R_{int}$ = 0.0229, $R_{sigma}$ = 0.0209] |
| Data/restraints/parameters | 2531/0/147 | 6604/0/374 | 5652/0/343 |
| Goodness-of-fit on $F^2$ | 1.049 | 1.037 | 1.051 |
| Final R indexes [I>=2σ (I)] | $R_1$ = 0.0408, $wR_2$ = 0.1073 | $R_1$ = 0.0264, $wR_2$ = 0.0599 | $R_1$ = 0.0420, $wR_2$ = 0.1105 |
| Final R indexes [all data] | $R_1$ = 0.0543, $wR_2$ = 0.1160 | $R_1$ = 0.0346, $wR_2$ = 0.0632 | $R_1$ = 0.0500, $wR_2$ = 0.1153 |
| Largest diff. peak/hole / e Å$^{-3}$ | 0.56/-0.37 | 0.40/-0.33 | 0.29/-0.36 |
| Flack parameter | - | - | |

**Table 8.1** Crystal data (continued).

| Identification code | **4.10** | **$L_{5.2}$** | **5.14** |
|---|---|---|---|
| Empirical formula | $C_{32}H_{24}O_6P_2Pt$ | $C_{17}H_{13}ClNP$ | $C_{34}H_{26}Cl_4N_2P_2Pt$ |
| Formula weight | 761.54 | 297.70 | 861.40 |
| Temperature/K | 100(2) | 100(2) | 100(2) |
| Crystal system | monoclinic | monoclinic | monoclinic |
| Space group | $P2_1/c$ | $P2_1/c$ | $P2_1/n$ |
| a/Å | 12.9862(3) | 12.6658(3) | 10.9748(15) |
| b/Å | 14.8874(3) | 9.3254(3) | 18.760(2) |
| c/Å | 18.1010(3) | 12.6606(3) | 16.123(2) |
| α/° | 90 | 90 | 90 |
| β/° | 93.6582(11) | 97.254(2) | 98.839(9) |
| γ/° | 90 | 90 | 90 |
| Volume/Å$^3$ | 3492.35(12) | 1483.42(7) | 3280.2(7) |
| Z | 4 | 4 | 4 |
| $\varrho_{calc}$g/cm$^3$ | 1.448 | 1.333 | 1.744 |
| μ/mm$^{-1}$ | 4.146 | 0.354 | 4.729 |
| F(000) | 1488.0 | 616.0 | 1680.0 |
| Crystal size/mm$^3$ | 0.49 × 0.34 × 0.06 | 0.536 × 0.391 × 0.174 | 0.207 × 0.179 × 0.101 |
| Radiation | MoKα (λ = 0.71073) | MoKα (λ = 0.71073) | MoKα (λ = 0.71073) |
| 2Θ range for data collection/° | 3.142 to 60.264 | 3.242 to 55.862 | 4.206 to 55.89 |
| Index ranges | -18 ≤ h ≤ 18, -21 ≤ k ≤ 20, -25 ≤ l ≤ 25 | -16 ≤ h ≤ 16, -12 ≤ k ≤ 10, -16 ≤ l ≤ 16 | -14 ≤ h ≤ 14, -24 ≤ k ≤ 24, -19 ≤ l ≤ 21 |
| Reflections collected | 68905 | 12766 | 29519 |
| Independent reflections | 10292 [$R_{int}$ = 0.0472, $R_{sigma}$ = 0.0301] | 3556 [$R_{int}$ = 0.0374, $R_{sigma}$ = 0.0367] | 7788 [$R_{int}$ = 0.0765, $R_{sigma}$ = 0.0741] |
| Data/restraints/parameters | 10292/0/372 | 3556/0/181 | 7788/547/487 |
| Goodness-of-fit on $F^2$ | 1.041 | 1.026 | 1.017 |
| Final R indexes [I>=2σ (I)] | $R_1$ = 0.0213, $wR_2$ = 0.0490 | $R_1$ = 0.0361, $wR_2$ = 0.0791 | $R_1$ = 0.0407, $wR_2$ = 0.0730 |
| Final R indexes [all data] | $R_1$ = 0.0296, $wR_2$ = 0.0512 | $R_1$ = 0.0512, $wR_2$ = 0.0859 | $R_1$ = 0.0589, $wR_2$ = 0.0787 |
| Largest diff. peak/hole / e Å$^{-3}$ | 1.04/-0.98 | 0.45/-0.24 | 0.78/-1.11 |
| Flack parameter | - | - | - |

**Table 8.1** Crystal data (continued).

| Identification code | *cis*-**5.16** | **5.18** | **5.19a** |
|---|---|---|---|
| Empirical formula | $C_{34}H_{26}Cl_4N_2P_2Pd$ | $C_{35}H_{26}Cl_3N_2OP_2Rh$ | $C_{26}H_{44}Cl_4N_2P_2Pt_2$ |
| Formula weight | 772.71 | 761.78 | 978.55 |
| Temperature/K | 100(2) | 100(2) | 100(2) |
| Crystal system | monoclinic | orthorhombic | orthorhombic |
| Space group | $P2_1/n$ | Iba2 | $P2_12_12_1$ |
| a/Å | 10.9124(6) | 16.5553(4) | 9.6258(3) |
| b/Å | 18.6581(10) | 30.6526(7) | 11.4622(3) |
| c/Å | 16.1039(8) | 12.9723(3) | 14.8141(4) |
| α/° | 90 | 90 | 90 |
| β/° | 99.292(4) | 90 | 90 |
| γ/° | 90 | 90 | 90 |
| Volume/Å$^3$ | 3235.8(3) | 6583.0(3) | 1634.48(8) |
| Z | 4 | 8 | 2 |
| $\rho_{calc}$g/cm$^3$ | 1.586 | 1.537 | 1.988 |
| μ/mm$^{-1}$ | 1.031 | 0.891 | 8.993 |
| F(000) | 1552.0 | 3072.0 | 936.0 |
| Crystal size/mm$^3$ | 0.188 × 0.182 × 0.122 | 0.496 × 0.327 × 0.304 | 0.385 × 0.319 × 0.148 |
| Radiation | MoKα (λ = 0.71073) | MoKα (λ = 0.71073) | MoKα (λ = 0.71073) |
| 2Θ range for data collection/° | 3.366 to 52.742 | 2.796 to 56.012 | 4.494 to 55.848 |
| Index ranges | -13 ≤ h ≤ 13, -22 ≤ k ≤ 23, -20 ≤ l ≤ 19 | -21 ≤ h ≤ 21, -40 ≤ k ≤ 40, -16 ≤ l ≤ 17 | -12 ≤ h ≤ 12, -15 ≤ k ≤ 15, -19 ≤ l ≤ 19 |
| Reflections collected | 23407 | 30238 | 14684 |
| Independent reflections | 6616 [$R_{int}$ = 0.0965, $R_{sigma}$ = 0.1000] | 7668 [$R_{int}$ = 0.0378, $R_{sigma}$ = 0.0364] | 3905 [$R_{int}$ = 0.0313, $R_{sigma}$ = 0.0294] |
| Data/restraints/parameters | 6616/1193/521 | 7668/1/397 | 3905/0/169 |
| Goodness-of-fit on $F^2$ | 1.068 | 1.021 | 1.045 |
| Final R indexes [I>=2σ (I)] | $R_1$ = 0.0585, $wR_2$ = 0.1026 | $R_1$ = 0.0231, $wR_2$ = 0.0456 | $R_1$ = 0.0178, $wR_2$ = 0.0334 |
| Final R indexes [all data] | $R_1$ = 0.1034, $wR_2$ = 0.1154 | $R_1$ = 0.0260, $wR_2$ = 0.0466 | $R_1$ = 0.0189, $wR_2$ = 0.0336 |
| Largest diff. peak/hole / e Å$^{-3}$ | 0.73/-0.82 | 0.43/-0.23 | 0.49/-0.60 |
| Flack parameter | - | -0.003(12) | -0.020(4) |

**Table 8.1** Crystal data (continued).

| Identification code | **5.22a** | *trans*-**5.24a** | *cis*-**5.24c**·$CH_2Cl_2$ |
|---|---|---|---|
| Empirical formula | $C_{13}H_{22}Cl_2NPPd$ | $C_{26}H_{44}Cl_2N_2P_2Pd$ | $C_{26.7}H_{37.4}Cl_{3.4}N_2P_2Pd$ |
| Formula weight | 400.58 | 623.87 | 675.25 |
| Temperature/K | 100(2) | 100(2) | 100(2) |
| Crystal system | orthorhombic | monoclinic | monoclinic |
| Space group | Pbca | $P2_1/c$ | $P2_1/c$ |
| a/Å | 15.0320(3) | 10.9700(3) | 10.8894(3) |
| b/Å | 13.2243(3) | 8.2389(2) | 9.7232(3) |
| c/Å | 16.4720(3) | 16.4000(4) | 28.5291(8) |
| α/° | 90 | 90 | 90 |
| β/° | 90 | 106.542(2) | 90.719(2) |
| γ/° | 90 | 90 | 90 |
| Volume/Å$^3$ | 3274.43(12) | 1420.90(6) | 3020.42(15) |
| Z | 8 | 2 | 4 |
| $\rho_{calc}$g/cm$^3$ | 1.625 | 1.458 | 1.485 |
| μ/mm$^{-1}$ | 1.541 | 0.971 | 1.040 |
| F(000) | 1616.0 | 648.0 | 1382.0 |
| Crystal size/mm$^3$ | 0.527 × 0.287 × 0.215 | 0.366 × 0.313 × 0.136 | 0.368 × 0.184 × 0.111 |
| Radiation | MoKα (λ = 0.71073) | MoKα (λ = 0.71073) | MoKα (λ = 0.71073) |
| 2Θ range for data collection/° | 4.79 to 55.89 | 5.182 to 55.924 | 4.426 to 55.936 |
| Index ranges | -19 ≤ h ≤ 19, -15 ≤ k ≤ 17, -21 ≤ l ≤ 19 | -14 ≤ h ≤ 14, -10 ≤ k ≤ 10, -16 ≤ l ≤ 21 | -12 ≤ h ≤ 14, -12 ≤ k ≤ 12, -37 ≤ l ≤ 34 |
| Reflections collected | 28457 | 11970 | 27015 |
| Independent reflections | 3929 [$R_{int}$ = 0.0254, $R_{sigma}$ = 0.0148] | 3411 [$R_{int}$ = 0.0348, $R_{sigma}$ = 0.0330] | 7254 [$R_{int}$ = 0.0617, $R_{sigma}$ = 0.0618] |
| Data/restraints/parameters | 3929/0/169 | 3411/0/157 | 7254/144/379 |
| Goodness-of-fit on $F^2$ | 1.049 | 1.056 | 1.045 |
| Final R indexes [I>=2σ (I)] | $R_1$ = 0.0163, $wR_2$ = 0.0390 | $R_1$ = 0.0234, $wR_2$ = 0.0562 | $R_1$ = 0.0460, $wR_2$ = 0.1022 |
| Final R indexes [all data] | $R_1$ = 0.0185, $wR_2$ = 0.0397 | $R_1$ = 0.0286, $wR_2$ = 0.0586 | $R_1$ = 0.0698, $wR_2$ = 0.1111 |
| Largest diff. peak/hole / e Å$^{-3}$ | 0.38/-0.38 | 0.76/-0.55 | 1.32/-0.82 |
| Flack parameter | - | - | - |

**Table 8.1** Crystal data (continued).

| Identification code | *δ*-(*S*,*S*)**6.7a** | *rac*-**6.7b** |
|---|---|---|
| Empirical formula | $C_{34}H_{58}F_3O_3P_2RhS$ | $C_{34}H_{58}F_3O_3P_2RhS$ |
| Formula weight | 768.71 | 768.71 |
| Temperature/K | 100(2) | 100(2) |
| Crystal system | orthorhombic | monoclinic |
| Space group | $Pna2_1$ | $P2_1/c$ |
| a/Å | 19.8075(16) | 21.5264(4) |
| b/Å | 10.4794(8) | 16.5233(3) |
| c/Å | 16.7222(13) | 21.8522(4) |
| α/° | 90 | 90 |
| β/° | 90 | 114.6529(8) |
| γ/° | 90 | 90 |
| Volume/Å$^3$ | 3471.0(5) | 7064.1(2) |
| Z | 4 | 8 |
| $\varrho_{calc}$g/cm$^3$ | 1.471 | 1.446 |
| μ/mm$^{-1}$ | 0.694 | 0.682 |
| F(000) | 1616.0 | 3232.0 |
| Crystal size/mm$^3$ | 0.524 × 0.342 × 0.228 | 0.48 × 0.36 × 0.23 |
| Radiation | MoKα (λ = 0.71073) | MoKα (λ = 0.71073) |
| 2Θ range for data collection/° | 4.112 to 55.948 | 3.206 to 55.91 |
| Index ranges | -25 ≤ h ≤ 26, -13 ≤ k ≤ 13, -22 ≤ l ≤ 21 | -28 ≤ h ≤ 28, -21 ≤ k ≤ 21, -28 ≤ l ≤ 28 |
| Reflections collected | 30650 | 64116 |
| Independent reflections | 8233 [$R_{int}$ = 0.0230, $R_{sigma}$ = 0.0237] | 16956 [$R_{int}$ = 0.0395, $R_{sigma}$ = 0.0385] |
| Data/restraints/parameters | 8233/1/401 | 16956/97/814 |
| Goodness-of-fit on $F^2$ | 1.032 | 1.021 |
| Final R indexes [I>=2σ (I)] | $R_1$ = 0.0190, $wR_2$ = 0.0449 | $R_1$ = 0.0383, $wR_2$ = 0.0850 |
| Final R indexes [all data] | $R_1$ = 0.0203, $wR_2$ = 0.0455 | $R_1$ = 0.0540, $wR_2$ = 0.0932 |
| Largest diff. peak/hole / e Å$^{-3}$ | 0.51/-0.24 | 1.24/-0.55 |
| Flack parameter | 0.044(7) | - |

## 8.2 References

(1) Bruker. *SAINT+ v8.38A Integr. Engine, Data Reduct. Software, Bruker Anal. X-ray Instruments Inc., Madison, WI, USA* **2015**.

(2) Bruker. *SADABS 2014/5, Bruker AXS area Detect. scaling Absorpt. Correct. Bruker Anal. X-ray Instruments Inc., Madison, Wisconsin, USA*.

(3) Sheldrick, G. M. *Acta Crystallogr. Sect. A Found. Adv.* **2015**, *71*, 3–8.

(4) Sheldrick, G. M. *Acta Crystallogr. Sect. A Found. Crystallogr.* **2008**, *64*, 112–122.

(5) Palatinus, L.; Chapuis, G. *J. Appl. Crystallogr.* **2007**, *40*, 786–790.

(6) Palatinus, L.; Jagannatha Prathapa, S.; van Smaalen, S. *J. Appl. Crystallogr.* **2012**, *45*, 575–580.

(7) Sheldrick, G. M. *Acta Crystallogr. Sect. C Struct. Chem.* **2015**, *71*, 3–8.

(8) Dolomanov, O. V; Bourhis, L. J.; Gildea, R. J.; Howard, J. A. K.; Puschmann, H. *J. Appl. Crystallogr.* **2009**, *42*, 339–341.